

**BIO-BASED NON-ISOCYANATE POLYURETHANES AS  
THERMOPLASTICS AND HYBRID THERMOSETS**

by

Georges Roni Younes

Department of Chemical Engineering

McGill University, Montreal

February, 2022

A thesis submitted to McGill University  
In partial fulfillment of the requirements of  
the degree of Doctor of Philosophy

© Georges Roni Younes, 2022

## Abstract

Polyurethanes (PU) are versatile materials that find applications in many industries. However, there has been an increase in the awareness against the toxicity of isocyanates, which is a base monomer of PUs, on the environment and the public health, and investigations have led to the synthesis of non-isocyanate polyurethanes (NIPU) through different routes. Polyhydroxyurethanes (PHU) constitute one category of NIPUs, and their linear version is prepared from the polyaddition of cyclic dicarbonates and diamines, which are abundant monomers that can be synthesized from bio-based building blocks. Hence, this work investigates the synthesis of bio-sourced PHUs that could potentially replace PUs in the future. First, moisture-curable hybrid PHUs (HPHU) are prepared from diglycerol dicarbonate (DGC), derived from the bio-based glycerol, and various diamines. The method consists of end-capping the PHU prepolymers with moisture sensitive groups, so sealants and adhesives can be produced at ambient conditions, similarly to their preparation from end-capped conventional PUs. The HPHU films made from DGC and a long chain (5,000 g/mol) poly(dimethylsiloxane) (PDMS) diamine show high water resistance with a contact angle of  $109^\circ$  and acceptable mechanical properties relative to conventional PU benchmarks, in contrast to the HPHU films prepared from DGC and a long chain (2,000 g/mol) poly(propylene glycol) (PPG) diamine. After showing the proof of concept, new moisture-curable HPHU films are prepared from sugar-based cyclic dicarbonates: sorbitol and mannitol bicarbonates, and the same diamines. Interestingly, the PHU prepolymers are synthesized in bulk and moderate temperatures even though the sugar-based dicarbonates have high melting points ( $\sim 200^\circ\text{C}$ ). The PHU oligomers as well as their films seem to be highly affected by the long chain diamine being used, and the PDMS-based HPHUs are hydrophobic, anticorrosive, and brittle which make them good coatings candidates. The cheaper

PPG-based HPHUs were soft and hydrophilic in this case as well, which leads to the third study where a cyclic carbonate terminated DGC-PPG PHU (poly(DGC-PPG)) is synthesized and capped from both ends with hydrophobic PDMS diamines of different chain lengths and Priamine 1074, which is a bio-based diamine. The modified PHUs are end-capped with silane moisture-curing agents, and the final HPHU films exhibited a drop in water swelling index (4%) compared to the original poly(DGC-PPG) HPHUs (75%). Also, the Priamine 1074-modified HPHU revealed a higher storage modulus that is at least 12 times higher than that of the original films. After making HPHUs, the investigations continue to study bio-based thermoplastic PHUs (TPHU) synthesized from terpolymerizations between DGC and two diamines: Priamine 1074, as the base diamine, and a 1,000 g/mol PDMS diamine or 1,10-diaminodecane (DAD) as the second diamine. The segmented DGC/Priamine 1074/PDMS TPHUs are amorphous exhibiting nanophase separation and distinct rheological properties compared to conventional homopolymers. As for DAD, it introduces crystallinity (8%) and chain ordering into the TPHU structure. Some PDMS-based TPHUs are blended with poly(lactic acid) (PLA), and the blends are found to be partially miscible with the TPHUs finding potential applications as toughening agents and/or plasticizers for PLA. This study is the first to investigate the application of PHUs in melt-blending. In the last study, photocurable hydroxyurethane acrylates (HUA) are prepared from Priamine 1074-based hydroxyurethanes extended on both ends with caprolactone degradable moieties. These materials find potential applications in 3D printing and the biomedical field. This last study, along with the others, demonstrates the versatility of PHUs as a platform for different types of polymeric materials that can be applied in different areas and replace conventional PU products.

## Résumé

Les polyuréthanes (PU) sont des matériaux polyvalents. Mais vu la toxicité des isocyanates, étant des monomères de base des PU, sur l'environnement et la santé publique, on a exploré la synthèse de polyuréthanes non isocyanates (NIPU) par différentes voies. Les polyhydroxyuréthanes (PHU) en sont une catégorie, et ils sont préparés par la polyaddition de dicarbonates cycliques et de diamines qui sont des monomères abondants pouvant être synthétisés à partir de matières biosourcées. Ainsi, ce travail vise à la synthèse de PHU biosourcés qui pourraient remplacer les PU dans le futur. Premièrement, les PHU hybrides (HPHU) réticulables par l'humidité sont préparés à partir de dicarbonate de diglycérol (DGC) et de diverses diamines. La méthode consiste à réagir des deux bouts les chaînes des PHU avec des groupes sensibles à l'humidité de sorte que des isolants et des adhésifs peuvent être produits à des conditions ambiantes, comme il en est le cas des PU conventionnels. Les HPHU fabriqués à partir de DGC et d'une diamine de 5,000 g/mol, à base de poly(diméthylsiloxane) (PDMS), présentent une haute résistance à l'eau avec un angle de contact de 109° et des propriétés mécaniques acceptables par référence aux PU et cela contrairement aux HPHU préparés à partir de DGC et d'une diamine de 2,000 g/mol, à base de poly(propylène glycol) (PPG). Puis, de nouveaux HPHU réticulables par l'humidité sont préparés à partir de dicarbonates cycliques à base de sucres : bicarbonates de sorbitol et de mannitol, et les mêmes diamines. Les prépolymères sont synthétisés en masse et à des températures modérées même si les bicarbonates ont des points de fusion élevés (~200 °C). Les oligomères ainsi que leurs pellicules semblent être influencés par la diamine utilisée. Les HPHU à base de PDMS démontrent des propriétés hydrophobes et anticorrosifs, ce qui en fait d'eux des revêtements alors que les HPHU à base de PPG, qui sont moins chers, présentent des traits mous et hydrophiles, ce qui conduit à l'étude

suivante. Dans cette troisième étude, un PHU de DGC-PPG (poly(DGC-PPG)), ayant des carbonates cycliques comme groupes terminaux, est réagi des deux extrémités avec des diamines hydrophobes à base de PDMS et Priamine 1074, une diamine biosourcée. Les PHU sont modifiés avec des agents de silane sensibles à l'humidité, et les pellicules finales présentent une baisse de l'indice de gonflement de l'eau (4 %) par rapport aux HPHU constitués du polymère d'origine (75 %). De plus, le HPHU modifié par Priamine 1074 révèle un module de stockage plus élevé : au moins 12 fois supérieur à celui des pellicules d'origine. Après la fabrication des HPHU, les investigations se poursuivent pour étudier des PHU thermoplastiques biosourcés (TPHU) synthétisés à partir des terpolymérisations entre DGC et deux diamines : Priamine 1074, comme diamine de base, et une diamine de 1,000 g/mol à base de PDMS ou 1,10-diaminodécane (DAD), comme deuxième diamine. Les TPHU segmentés DGC/Priamine 1074/PDMS sont amorphes et présentent une séparation nanophasique et des propriétés rhéologiques distinctes par rapport aux homopolymères conventionnels. DAD, par contre, a introduit une cristallinité (8%) et une ordonnance de chaînes des TPHU. Certains TPHU à base de PDMS sont mélangés avec du poly(acide lactique) (PLA), et les mélanges s'avèrent partiellement miscibles avec les TPHU trouvant des applications potentielles comme durcisseurs et/ou plastifiants pour le PLA. Cette étude est la première à étudier l'application des PHU dans un mélange de polymères. Dans la dernière étude, des acrylates photoréticulables sont préparés à partir d'hydroxyuréthanes (HUA), à base de Priamine 1074, réagis avec des espèces dégradables de caprolactone. Ces matériaux trouvent des applications dans l'impression 3D et le domaine biomédical. Cette dernière étude, ainsi que les autres, démontrent la polyvalence des PHU pouvant être appliqués dans des domaines variés afin de remplacer les produits à base de PU.

## Acknowledgements

I would first like to thank Prof. Milan Maric for giving me the opportunity to work on an industrial project during my PhD. I am grateful for his supervision, guidance, and support during the last three years, as he mentored me and gave me room to grow as a researcher. I would like to acknowledge the research and development team at ADFAST Corp. and especially Yves Dandurand, their CEO, for providing the necessary resources for my project. I would also like to thank Dr. Robin Stein for running countless NMR samples for me due to limited access during COVID. As well, I would like to thank Petr Fiurasek for his training and guidance in using the DSC, TGA, and FTIR instruments, and Dr. Hatem Titi, who became a great friend, for his help in running samples on SAXS and WAXS.

Special thanks to Sharmaine Luk, who became more than a friend. I am grateful for her continuous support and patience through the hard times I faced before and during my PhD. I am happy we got to overlap again at McGill after we were in the same research group at Queen's University. I am grateful for the NIPU group members: Mohammad, Carlee, Louis-Paul, and Noushin for making the second half of my PhD memorable with nice scientific and non-scientific conversations in and out of school. I am thankful for my McGill friends who helped me come that far: Maru, Julia, Mike, Laura, Matt, and Farhad. I would also like to thank Frank Caporuscio for his expertise that allowed me to do my research safely and effectively.

For my best friends in Lebanon: Stéphanie, Cynthia and Chadi, and those who left the country: Sarah, Sandra, Fares, and Ingrid, thank you for always keeping in touch and for being there whenever I sought comfort. For my two Queen's partners in crime: Jaime and Loretta, I was sure we were going to keep our friendship tight despite the distance that separated us after I left Kingston. Thank you for always checking and encouraging me throughout my PhD. I am

also thankful for Rania, a devoted friend, whose presence made my life much easier. Besides, I am grateful to Mario for the emotional support he has provided me. I am very lucky to have met such an amazing person along this journey.

I would like to acknowledge the huge support both my siblings, Julien and Gloria, provided during this phase. Living with Julien was not always easy, but was exceptional on different levels. Gloria, on the other hand, had two babies to commemorate the beginning and the end of my PhD, and she used every free second she had to assist in my daily errands. I am grateful that my mom, Antoinette, got to join us in Montreal during my PhD. Her presence was indeed an inspiration for me to stand up and fight for my goals. As well, I would like to remember my father, Roni, who has been my guardian angel all along. I know that he is watching over me, and I hope that he is proud of this accomplishment. I would like to end by thanking our big family, especially my uncles Joseph and Rachid, my aunt Fadia, and my grandmother Thérèse, for their continuous support and encouragement for my mother, my siblings, and myself.

## **Contribution to Original Knowledge**

The three studies on bio-based moisture-curable hybrid polyhydroxyurethanes, presented in Chapters 3, 4, and 5, are the first to cure the functionalized polymers at ambient conditions and without the use of external heating, like it was previously done in the literature. Also, Chapter 5 benefits from end-chain capping with hydrophobic diamines to increase the water resistance of the base polymer which discerns it from other studies focusing on water resistant polyhydroxyurethanes. Chapter 6 deepened the understanding of the nanophase separation and the rheology exhibited by segmented thermoplastic polyhydroxyurethanes, and these polymers were applied for the first time in melt-blending with other polymers. The effects of their addition on the poly(lactic acid) matrix were investigated, and recommendations were drawn for the eventual replacement of conventional thermoplastic polyurethane additives with non-toxic and bio-based thermoplastic polyhydroxyurethanes. Finally, Chapter 7 uses bio-based hydroxyurethanes as initiators for the living radical polymerization of biodegradable caprolactone moieties. The macromolecules were acrylated to prepare photocurable macromonomers affording final bio-based and biodegradable films, which distinguishes Chapter 7 from other studies conducted on photocurable hydroxyurethane methacrylates and acrylates.

## **Contribution of Authors**

Professor Milan Maric is a coauthor on every manuscript-based chapter in this thesis. As the principle investigator, he conceptualized the idea and advised the progress of research since the beginning, especially on the industrial-oriented projects in Chapters 3, 4, and 5. He helped me gain confidence in myself by giving me the chance to come up with academic projects presented in Chapters 6 and 7, and on which he provided continuous guidance, especially in Chapter 6 while I was working on the melt-blending part. Besides, Gareth Price, who was hired as an undergraduate researcher during Summer 2019, helped me optimize the formulation of the poly(dimethylsiloxane)/diglycerol dicarbonate-based hybrid polyhydroxyurethanes of Chapter 3.

## Table of Contents

Abstract .....	ii
Résumé.....	iv
Acknowledgements.....	vi
Contribution to Original Knowledge .....	viii
Contribution of Authors.....	ix
List of Figures .....	xiv
List of Schemes.....	xxvi
List of Tables .....	xxviii
List of Abbreviations .....	xxxii
Chapter 1 Introduction .....	1
Chapter 2 Literature Review.....	6
2.1 Polyhydroxyurethanes synthesized from vegetable oils and their fatty acids.....	22
2.2 Polyhydroxyurethanes synthesized from plant-based materials and fatty acids.....	23
2.3 Polyhydroxyurethanes synthesized from glycerol and its derivatives .....	24
2.4 Polyhydroxyurethanes synthesized from sugar derived materials .....	25
2.5 Conclusion and thesis work considerations .....	26
Chapter 3 Study of moisture-curable hybrid NIPUs based on glycerol with various diamines: emergent advantages of PDMS-diamines.....	29
3.1 Abstract .....	30
3.2 Introduction .....	31
3.3 Results and Discussion.....	34
3.3.1 DGC reaction and kinetics.....	34
3.3.2 Characterization and screening of PHU prepolymers .....	37
3.3.3 End-capping of prepolymers .....	46
3.3.4 HPHUs-Water interaction and chemical stability .....	56
3.4 Conclusion.....	58
3.5 Materials and Methods.....	60
3.5.1 Materials .....	60
3.5.2 Experimental methods .....	61

3.5.3 Characterization methods .....	64
3.6 References .....	68
Chapter 4 Moisture-curable hybrid polyhydroxyurethanes from sugar-derived dicarbonates .....	75
4.1 Abstract .....	76
4.2 Introduction .....	76
4.3 Results and Discussion.....	80
4.3.1 SBC and MBC reactions.....	80
4.3.2 Characterization and screening of PHU prepolymers .....	81
4.3.3 End-capping and crosslinking of prepolymers .....	87
4.3.4 HPHUs-water interaction and chemical stability .....	97
4.3.5 HPHUs microstructure from WAXS and SAXS .....	99
4.4 Conclusion.....	103
4.5 Materials and Methods .....	104
4.5.1 Materials .....	104
4.5.2 Experimental methods .....	105
4.5.3 Characterization methods .....	109
4.6 References .....	112
Chapter 5 Increasing the hydrophobicity of hybrid poly(propylene glycol)-based polyhydroxyurethanes by capping with hydrophobic diamine.....	117
5.1 Abstract .....	118
5.2 Introduction .....	118
5.3 Materials and Methods .....	122
5.3.1 Materials .....	122
5.3.2 Experimental methods .....	122
5.3.3 Characterization methods .....	125
5.4 Results and Discussion.....	129
5.4.1 Characterization of the DGC-PPG/HydrophobicDiamine PHUs.....	129
5.4.2 End-capping of the modified poly(DGC-PPG) .....	140
5.4.3 Swelling of DGC-PPG/HydrophobicDiamine HPHUs .....	144
5.5 Conclusion.....	149
5.6 References .....	150

Chapter 6 Bio-based thermoplastic polyhydroxyurethanes synthesized from the terpolymerization of a dicarbonate and two diamines: design, rheology, and application in melt blending.....	157
6.1 Abstract .....	158
6.2 Introduction .....	158
6.3 Materials and Methods .....	161
6.3.1 Materials .....	161
6.3.2 Experimental methods .....	162
6.3.3 Characterization methods .....	163
6.4 Results and Discussion.....	168
6.4.1 Characterization of the PDMS containing TPHUs.....	168
6.4.2 Characterization of DAD containing TPHUs.....	182
6.4.3 Blends of PLA with bio-based TPHUs.....	188
6.5 Conclusion.....	195
6.6 References .....	197
Chapter 7 Bio-based and hydrolytically degradable hydroxyurethane acrylates as photocurable thermosets .....	207
7.1 Abstract .....	208
7.2 Introduction .....	208
7.3 Results and Discussion.....	210
7.3.1 Synthesis of HU-CL <sub>5</sub> -A.....	210
7.3.2 Photocurable Thermosets and Degradation Study.....	218
7.4 Conclusion.....	224
7.5 Experimental Section .....	225
7.6 References .....	230
Chapter 8 Conclusions and future work.....	232
References.....	235
Appendix A Supporting information for “Study of moisture-curable hybrid NIPUs based on glycerol with various diamines: emergent advantages of PDMS-diamines” .....	265
Appendix B Supporting information for “Moisture-curable hybrid polyhydroxyurethanes from sugar-derived dicarbonates” .....	282

Appendix C Supporting information for “Increasing the hydrophobicity of hybrid poly(propylene glycol)-based polyhydroxyurethanes by capping with hydrophobic diamine” .....	303
Appendix D Supporting information for “Bio-based thermoplastic polyhydroxyurethanes synthesized from the terpolymerization of a dicarbonate and two diamines: design, rheology, and application in melt blending” .....	319
Appendix E Supporting information for “Bio-based and hydrolytically degradable hydroxyurethane acrylates as photocurable thermosets” .....	346

## List of Figures

Figure 3.1 - Kinetic study tracking the evolution of the reaction between DIG and DMC to get DGC, the renewable monomer of this study.....	36
Figure 3.2 - Molecular weight evolution of PHU 6 (DGC + Jeffamine D-2000) polymerization at 140 °C for 48 h (based on PS standards) .....	42
Figure 3.3 - <sup>1</sup> H-NMR spectrum of PHU 4 (DGC + Jeffamine D-2000) with all protons labelled) in CDCl <sub>3</sub> at 25°C. Protons denoted by c belong to the diamine backbone (R <sup>1</sup> ) whereas protons denoted by e belong to the opened cyclic carbonate ring and what belonged to DGC. The rest of the peaks are predicted.....	43
Figure 3.4 - Molecular weight evolution of PHU 11 polymerization at 80 °C for 48 h (measured by SEC relative to PS standards). .....	44
Figure 3.5 - <sup>1</sup> H-NMR spectrum of PHU 10 (DGC + PDMS-5k-(NH <sub>2</sub> ) <sub>2</sub> ) in CDCl <sub>3</sub> at 25°C. Protons denoted by c belong to the diamine backbone (R <sup>1</sup> ) whereas protons denoted by e belong to the opened cyclic carbonate ring and what belonged to DGC. The rest of the peaks are predicted.....	45
Figure 3.6 - Labelled FTIR spectrum of PHU 4 (C=O stretch of carbonate end-groups at 1800 cm <sup>-1</sup> ) .....	47
Figure 3.7 - Labelled FTIR spectrum of PHU 10 (absence of C=O stretch of carbonate end-groups) .....	48
Figure 3.8 - Comparison of FTIR spectra (PHU 4-1 (black) and PHU 4-2 (red)) between successful and unsuccessful end-capping reactions of PHU-4 with DAMO (red) and GLYMO (black). Disappearance of the 1800 cm <sup>-1</sup> C=O stretch observed with the DAMO end-capper compared to the GLYMO one. ....	51
Figure 3.9 - PHU 4 end-capping reaction summary: PHU 4-1 with excess DAMO resulting in brittle films, PHU 4-2 with excess GLYMO resulting in noncured materials, and PHU 4-4 resulting in smooth HPHU 4 films.....	52
Figure 3.10 - Curing kinetics of end-capped PHU 4 by following the storage (G') and loss (G'') moduli (Pa) at a frequency of 1 Hz and a strain of 1% for 20 h. Measurements were done at 22 °C and 40-50% humidity. ....	53

Figure 3.11 - Curing kinetics of end-capped PHU 10 by following the storage ( $G'$ ) and loss ( $G''$ ) moduli (Pa) at a frequency of 1 Hz and a strain of 1% for 7 h. Measurements were done at 22 °C and 40-50% humidity.....	55
Figure 3.12 - PHU 10 end-capping reaction summary: PHU 10-1 with excess GLYMO resulting in brittle films, PHU 10-2 with excess DAMO resulting in non-curing materials, and PHU 10-4 resulting in smooth HPHU 10 films.....	56
Figure 3.13 - Summary of the method followed to synthesize moisture curable HPHU sealants and adhesives .....	59
Figure 4.1 - Labelled FTIR spectrum of SBC-PHU 1 or MBC-PHU 1 ( $C=O$ stretch of carbonate end-groups at $1800\text{ cm}^{-1}$ ) .....	88
Figure 4.2 - Labelled FTIR spectrum of SBC-PHU 3 or MBC-PHU 3 (absence of $C=O$ stretch of carbonate end-groups).....	88
Figure 4.3 - Comparison of FTIR spectra showing the successful end-capping of SBC-PHU 1 or MBC-PHU 1 with DAMO. Disappearance of the $1800\text{ cm}^{-1}$ $C=O$ stretch observed with the DAMO end-capper.....	91
Figure 4.4 - Smooth HPHU films resulting from trials SBC-PHU 1-3 and MBC-PHU 1-1 presented in Table 4.4 and Table 4.5 .....	91
Figure 4.5 - Crosslinked HPHU products obtained from different end-capping trials with SBC-PHU 3 and MBC-PHU 3: in the cases of SBC-PHU 3-2 and MBC-PHU 3-2, the crosslinking occurred in the reactors contrary to trial MBC-PHU 3-1 in which crosslinking occurred under moisture resulting in a smooth film. ....	93
Figure 4.6 - Curing kinetics of end-capped SBC-PHU 1 and MBC-PHU 1 by following the storage ( $G'$ ) and loss ( $G''$ ) moduli (Pa) at a frequency of 1 Hz and a strain of 1% for 24 h. 0.5 wt.% of the proprietary catalyst was added to end-capped SBC-PHU 1 to accelerate the curing. Measurements were done at 22 °C and 20-30% humidity.....	94
Figure 4.7 - Curing kinetics of end-capped SBC-PHU 3 and MBC-PHU 3 by following the storage ( $G'$ ) and loss ( $G''$ ) moduli (Pa) at a frequency of 1 Hz and a strain of 1% for 24 h. Measurements were done at 22 °C and 20-30% humidity.....	95

Figure 4.8 - Swelling of SBC-HPHU 1 and MBC-HPHU 1 in pure H<sub>2</sub>O after one week. Swollen MBC-HPHU 1 films broke down into smaller pieces in the water medium. .... 98

Figure 4.9 - WAXS spectra of DGC- PDMS-5k-(NH<sub>2</sub>)<sub>2</sub> HPHU, SBC-HPHU 3, and MBC-HPHU 3 showing the clear peak of PDMS chain distinctly appearing at 2θ of 12.3 to 12.65° proving that the hydroxyurethane units are spread in the PDMS matrix. The intensity is given in logarithmic scale..... 101

Figure 5.1 - Labelled <sup>1</sup>H-NMR spectra of PDMS-poly(DGC-PPG)-PDMS of this work (2 molar equivalents of PDMS-(NH<sub>2</sub>)<sub>2</sub> per polymer) showing the main signals of the diamines used in this work. The Si-(CH<sub>3</sub>)<sub>2</sub>-O methyl protons signal (at 0.05 ppm) increases with respect to PPG-CH<sub>3</sub> (at 1.15 ppm) with increase in the PDMS-(NH<sub>2</sub>)<sub>2</sub> molecular weight used to cap poly(DGC-PPG) from both ends. .... 130

Figure 5.2 - FTIR spectra of poly(DGC-PPG) (black), PDMS-1k-poly(DGC-PPG)-1k-PDMS-1k (red) and Priamine-poly(DGC-PPG)-Priamine (blue) showing the disappearance of the carbonyl stretch at 1800 cm<sup>-1</sup> for the extended PHUs compared to the FTIR spectrum of poly(DGC-PPG). .... 133

Figure 5.3 - WAXS spectra of extended poly(DGC-PPG) from both ends with PDMS-1k-(NH<sub>2</sub>)<sub>2</sub> (black), PDMS-3k-(NH<sub>2</sub>)<sub>2</sub> (red), PDMS-5k-(NH<sub>2</sub>)<sub>2</sub> (blue), and PDMS-7k-(NH<sub>2</sub>)<sub>2</sub> (green) (2 molar equivalents of hydrophobic diamine per polymer) showing an increase of the PDMS chains peak at 2θ of 12.5° with increase in molecular weight of the PDMS-(NH<sub>2</sub>)<sub>2</sub> hydrophobic diamine. The intensity is given in logarithmic scale..... 138

Figure 5.4 - Derivative of weight percentage with respect to temperature traces of poly(DGC-PPG) (grey) and extended poly(DGC-PPG) from both ends with PDMS-1k-(NH<sub>2</sub>)<sub>2</sub> (black), PDMS-3k-(NH<sub>2</sub>)<sub>2</sub> (red), PDMS-5k-(NH<sub>2</sub>)<sub>2</sub> (blue), and PDMS-7k-(NH<sub>2</sub>)<sub>2</sub> (green) used in this work (2 molar equivalents of hydrophobic diamine per polymer). .... 140

Figure 5.5 - Curing kinetics of the end-capped poly(DGC-PPG) (black), PDMS-7k-poly(DGC-PPG)-7k-PDMS (red), and Priamine-poly(DGC-PPG)-Priamine (blue) by following the storage (G', full lines) and loss (G'', dashed lines) moduli (Pa) at a frequency of 1 Hz and a strain of 1% for 24 h. 0.5 wt.% of the proprietary catalyst was added to accelerate the curing of PDMS-7k-poly(DGC-PPG)-7k-PDMS and Priamine-poly(DGC-PPG)-Priamine. Measurements were done at 22 °C and 40-50% humidity. .... 143

Figure 5.6 - WAXS spectra of the poly(DGC-PPG) (black), PDMS-7k-poly(DGC-PPG)-7k-PDMS (red), and Priamine-poly(DGC-PPG)-Priamine (blue) HPHUs. The distinct sharp peak at  $2\theta$  of  $12.5^\circ$  proving the presence of a distinct PDMS phase in the microstructure of the PDMS-7k-poly(DGC-PPG)-7k-PDMS HPHU film. The intensity is given in logarithmic scale. .... 148

Figure 6.1 - Summary of structural phenomena observed in this study: A and B-segmented block and statistical copolymers, respectively formed during the terpolymerization of Priamine 1074 and PDMS-1k-(NH<sub>2</sub>)<sub>2</sub> with excess and equimolar amounts of DGC, respectively, and C-segmented lamellae-like microstructure of DAD-4040 TPHU. .... 171

Figure 6.2 - WAXS spectra of PDMS-0025, PDMS-2025, and PDMS-4025. The distinct shoulder peak at  $2\theta$  of  $9^\circ$  proving the presence of a PDMS phase in the microstructure of the TPHUs. The intensity is given in logarithmic scale. .... 174

Figure 6.3 - Storage modulus of the PDMS-based TPHUs collected from amplitude sweeps conducted at 22 °C and a frequency of 10 Hz. .... 175

Figure 6.4 - Dynamic mechanical frequency sweep data for PDMS-0040 ( $G''$  curve is shifted by a factor of 5) at 0.5% shear strain. The solid line is a fit to the Generalized Maxwell model. The inset shows the shift factors used for time-temperature superposition. The solid and dashed lines in the inset are the WLF and Arrhenius law fit equations, respectively. .... 179

Figure 6.5 - Dynamic mechanical frequency sweep data for PDMS-2040 ( $G''$  curve is shifted by a factor of 5) at 0.5% shear strain. The solid line is a fit to the Generalized Maxwell model. The inset shows the shift factors used for time-temperature superposition. The solid and dashed lines in the inset are the WLF and Arrhenius law fit equations, respectively. .... 180

Figure 6.6 - Dynamic mechanical frequency sweep data for PDMS-4040 ( $G''$  curve is shifted by a factor of 5) at 0.5% shear strain. The solid line is a fit to the Generalized Maxwell model. The inset shows the shift factors used for time-temperature superposition. The solid and dashed lines in the inset are the WLF and Arrhenius law fit equations, respectively. .... 181

Figure 6.7 - SAXS spectra of DAD-based TPHUs showing ordering in their microstructure. The intensity is given in logarithmic scale. .... 185

Figure 6.8 - Tensile test results of the semi-crystalline DAD-2040 and DAD-3040 showing the stretching of the amorphous phase first followed by the crystalline phase before yielding and breaking.....	186
Figure 6.9 - Storage modulus of the DAD-based TPHUs collected from amplitude sweeps conducted at 22 °C and a frequency of 10 Hz. ....	187
Figure 6.10 - Stress-strain curves of the PLA/TPHU blends of this study (80/20 wt.%/wt.%).	193
Figure 6.11 - SEM of cryogenically fractured surfaces of PLA/TPHUs blends (80/20 wt.%/wt.%) untreated and treated with THF to remove the TPHUs phase solely (5000× magnification).....	195
Figure 7.1 - Conversion of CL tracked from <sup>1</sup> H-NMR using signals of two different proton sets (the disappearance and appearance of protons at 4.23 and 3.65/4.07 ppm (Method 1), respectively, and those of 2.64 and 2.33 ppm (Method 2), respectively). Conversion of HU tracked using the disappearance of the signal at 3.79 ppm with the signal at 3.17 ppm being the reference (Figure E.2). ....	216
Figure 7.2 - Labelled <sup>1</sup> H-NMR of the bio-based HU-CL <sub>5</sub> -A of this work in CDCl <sub>3</sub> at 25 °C. (500 MHz, CDCl <sub>3</sub> , δ): 6.4 (k), 6.13 (i), 5.83 (j), 4.26 (b, c), 4.17 (end d), 4.07 (middle d), 3.17 (a), 2.32 (h), 1.66 (e, g), 1.40 (f), 1.50/1.27/0.89 (R). ....	217
Figure 7.3 - FTIR spectra showing the changes in the functional groups during the step-wise synthesis of bio-based and degradable HU-CL <sub>5</sub> -A of this work.....	218
Figure 7.4 - Photocurable films accelerated degradation study with initial and final films SEM images (1000 magnification) and their FTIR spectra in the range of 1800 and 1550 cm <sup>-1</sup> proving the hydrolysis of CL units resulting in the cleaving of film parts. ....	220
Figure 7.5 - Proposed degradation mechanism of accelerated hydrolysis of the photocurable thermosets of this work leading to the final water-soluble degradation products detected from <sup>1</sup> H-NMR (Figure E.8).....	223
Figure A.1 - FTIR spectra of DGC molecule at room temperature (C=O stretch is at 1780 cm <sup>-1</sup> ) .....	265
Figure A.2 - Labelled DGC <sup>1</sup> H-NMR spectrum in DMSO-d <sub>6</sub> at 25 °C.....	266

Figure A.3 - GPC signals showing chain scission occurring after 18 h of PHU 6 polymerization reaction at 140 °C .....	266
Figure A.4 - DSC traces of the second heating run of PHUs 2 and 4.....	269
Figure A.5 - TGA traces of PHUs 2, 4, and 10.....	269
Figure A.6 - Curing kinetics of PHU 4 by following the complex viscosity ( $\eta^*$ ) (Pa.s) at a frequency of 1 Hz and a strain of 1% for 20 h. Measurements were done at 22 °C and 40-50% humidity. ....	272
Figure A.7 - Curing kinetics of PHU 4 by following the damping factor ( $\tan\delta$ ) at a frequency of 1 Hz and a strain of 1% for 20 h. Measurements were done at 22 °C and 40-50% humidity. ....	273
Figure A.8 - Curing kinetics of PHU 10 by following the complex viscosity ( $\eta^*$ ) (Pa.s) at a frequency of 1 Hz and a strain of 1% for 7 h. Measurements were done at 22 °C and 40-50% humidity. ....	274
Figure A.9 - Curing kinetics of PHU 10 by following the damping factor ( $\tan\delta$ ) at a frequency of 1 Hz and a strain of 1% for 7 h. Measurements were done at 22 °C and 40-50% humidity. ....	275
Figure A.10 - $^1\text{H-NMR}$ spectrum on HPHU 4 degradation residuals in $\text{D}_2\text{O}$ at 25 °C showing possible leaching occurring from HPHU 4 films in pure $\text{H}_2\text{O}$ .....	277
Figure A.11 - $^1\text{H-NMR}$ spectrum on HPHU 10 degradation residuals in $\text{D}_2\text{O}$ at 25 °C showing no leaching occurring from HPHU 10 films in pure $\text{H}_2\text{O}$ .....	278
Figure A.12 - Tensile tests data for the dog-bone samples cured for one week under moisture at ambient conditions .....	279
Figure A.13 - Tensile tests data for the dog-bone samples cured for one week at ambient conditions and another week in pure $\text{H}_2\text{O}$ .....	280
Figure A.14 - Dynamic mechanical thermal analysis on the sample cured at ambient conditions for one week and the ones cured at ambient conditions for one week and in water for an extra week at a strain of 0.5% and a frequency of 1 Hz from 25 °C to 120 °C at a rate of 5 °C/min .	281
Figure B.1 - Labelled SBC $^1\text{H-NMR}$ spectrum in $\text{DMSO-d}_6$ at 25 °C.....	282
Figure B.2 - Labelled MBC $^1\text{H-NMR}$ spectrum in $\text{DMSO-d}_6$ at 25 °C .....	283
Figure B.3 - FTIR spectra of SBC or MBC molecule at room temperature ( $\text{C=O}$ stretch is at $1780\text{ cm}^{-1}$ ).....	283

Figure B.4 - <sup>1</sup>H-NMR spectrum of SBC-PHU 1 (SBC + Jeffamine D-2000) in CDCl<sub>3</sub> at 25°C. Protons denoted by c belong to the diamine backbone (R<sup>1</sup>) whereas protons denoted by e belong to the opened cyclic carbonate ring and what belonged to SBC. The rest of the peaks are predicted..... 284

Figure B.5 - <sup>1</sup>H-NMR spectrum of MBC-PHU 1 (MBC + Jeffamine D-2000) in CDCl<sub>3</sub> at 25°C. Protons denoted by c belong to the diamine backbone (R<sup>1</sup>) whereas protons denoted by e belong to the opened cyclic carbonate ring and what belonged to MBC. The rest of the peaks are predicted..... 285

Figure B.6 - GPC traces of SBC-PHU 3 and SBC-PHU 4 showing the broad distribution of the latter compared to the former..... 286

Figure B.7 - GPC traces of MBC-PHU 3 and MBC-PHU 6 showing the broad distribution of the latter compared to the former..... 286

Figure B.8 - <sup>1</sup>H-NMR spectrum of SBC-PHU 3 (SBC + PDMS-5k-(NH<sub>2</sub>)<sub>2</sub>) in CDCl<sub>3</sub> at 25°C (note that the signal shown at 0 ppm is the proton from the -O-Si(CH<sub>3</sub>)<sub>2</sub> groups). Protons denoted by c belong to the diamine backbone (R<sup>1</sup>) whereas protons denoted by e belong to the opened cyclic carbonate ring and what belonged to SBC. The rest of the peaks are predicted. .... 287

Figure B.9 - <sup>1</sup>H-NMR spectrum of MBC-PHU 3 (MBC + PDMS-5k-(NH<sub>2</sub>)<sub>2</sub>) in CDCl<sub>3</sub> at 25°C (note that the signal shown at 0 ppm is the proton from the -O-Si(CH<sub>3</sub>)<sub>2</sub> groups). Protons denoted by c belong to the diamine backbone (R<sup>1</sup>) whereas protons denoted by e belong to the opened cyclic carbonate ring and what belonged to MBC. The rest of the peaks are predicted. .... 288

Figure B.10 - DSC traces of the second heating run of SBC-PHU 1 and MBC-PHU 1 ..... 289

Figure B.11 - TGA traces of selected sugar-based PHUs..... 289

Figure B.12 - Curing kinetics of SBC-PHU 1 and MBC-PHU 1 by following the complex viscosity ( $\eta^*$ ) (Pa.s) at a frequency of 1 Hz and a strain of 1% for 24 h. 0.5 wt.% of the proprietary catalyst was added to end-capped SBC-PHU 1 to accelerate the curing. Measurements were done at 22 °C and 20-30% humidity..... 291

Figure B.13 - Curing kinetics of SBC-PHU 1 and MBC-PHU 1 by following the damping factor ( $\tan\delta$ ) at a frequency of 1 Hz and a strain of 1% for 24 h. 0.5 wt.% of the proprietary catalyst was added to end-capped SBC-PHU 1 to accelerate the curing. Measurements were done at 22 °C and 20-30% humidity. .... 292

Figure B.14 - Curing kinetics of SBC-PHU 3 and MBC-PHU 3 by following the complex viscosity ( $\eta^*$ ) (Pa.s) at a frequency of 1 Hz and a strain of 1% for 24 h. Measurements were done at 22 °C and 20-30% humidity. ....	293
Figure B.15 - Curing kinetics of SBC-PHU 3 and MBC-PHU 3 by following the damping factor ( $\tan\delta$ ) at a frequency of 1 Hz and a strain of 1% for 24 h. Measurements were done at 22 °C and 20-30% humidity. ....	294
Figure B.16 - $^1\text{H-NMR}$ spectrum on SBC-HPHU 1 degradation residuals in $\text{D}_2\text{O}$ at 25 °C showing possible leaching occurring from SBC-HPHU 1 films in pure $\text{H}_2\text{O}$ .....	297
Figure B.17 - $^1\text{H-NMR}$ spectrum on MBC-HPHU 3 degradation residuals in $\text{D}_2\text{O}$ at 25 °C showing no leaching occurring from MBC-HPHU 3 films in pure $\text{H}_2\text{O}$ .....	297
Figure B.18 - $^1\text{H-NMR}$ spectrum on MBC-HPHU 1 degradation residuals in $\text{D}_2\text{O}$ at 25 °C showing possible leaching occurring from MBC-HPHU 1 films in pure $\text{H}_2\text{O}$ .....	298
Figure B.19 - $^1\text{H-NMR}$ spectrum on MBC-HPHU 3 degradation residuals in $\text{D}_2\text{O}$ at 25 °C showing no leaching occurring from MBC-HPHU 3 films in pure $\text{H}_2\text{O}$ .....	298
Figure B.20 - SAXS spectra of DGC- PDMS-5k-( $\text{NH}_2$ ) $_2$ HPHU, SBC-HPHU 3, and MBC-HPHU 3 showing peaks at $q_{\text{max}}$ used to calculate the mean interdomain spacing of the films. The intensity is given in logarithmic scale.....	301
Figure C.1 - Labelled DGC $^1\text{H-NMR}$ spectrum in $\text{DMSO-d}_6$ at 25 °C. $\delta$ (ppm): 4.93 (m, 2H, $\text{H}_2$ ), 4.52 (t, 2H, $\text{H}_1^{\text{cis or trans}}$ ), 4.25 (ddd, 2H, $\text{H}_1^{\text{cis or trans}}$ ), 3.79-3.65 (m, 4H, $\text{H}_3$ ). ....	303
Figure C.2 - FTIR spectra of decanted poly(DGC-PPG) (black) and filtered poly(DGC-PPG) to verify that the DGC monomer was fully removed from the polymer medium. The carbonyl stretch $1800\text{ cm}^{-1}$ area remained unchanged relatively to that of the carbonyl stretch of the urethane linkage at $1720\text{ cm}^{-1}$ . DGC has a carbonyl stretch at $1780\text{ cm}^{-1}$ that would have overlapped with the one at $1800\text{ cm}^{-1}$ and increased its intensity if it were present in the PHU medium. ....	304
Figure C.3 - FTIR spectra of poly(DGC-PPG) (black) and extended poly(DGC-PPG) with PDMS-3k-( $\text{NH}_2$ ) $_2$ (red), PDMS-5k-( $\text{NH}_2$ ) $_2$ (blue), and PDMS-7k-( $\text{NH}_2$ ) $_2$ (green) (2 molar equivalents of hydrophobic diamine per polymer) showing the disappearance of the carbonyl	

stretch at 1800 cm <sup>-1</sup> for the extended polymers from both ends compared to poly(DGC-PPG) FTIR spectrum. ....	306
Figure C.4 - SEC traces of poly(DGC-PPG) (black-discontinuous) and extended poly(DGC-PPG) with PDMS-1k-(NH <sub>2</sub> ) <sub>2</sub> (black) and PDMS-3k-(NH <sub>2</sub> ) <sub>2</sub> (red) (2 molar equivalents of hydrophobic diamine per polymer).....	307
Figure C.5 - SEC traces of poly(DGC-PPG) (black-discontinuous) and extended poly(DGC-PPG) with PDMS-5k-(NH <sub>2</sub> ) <sub>2</sub> (blue) and PDMS-7k-(NH <sub>2</sub> ) <sub>2</sub> (green) (2 molar equivalents of hydrophobic diamine per polymer).....	308
Figure C.6 - SEC traces of poly(DGC-PPG) (black-discontinuous) and Priamine-poly(DGC-PPG)-Priamine (black).....	308
Figure C.7 - SAXS spectra of extended poly(DGC-PPG) from both ends with PDMS-1k-(NH <sub>2</sub> ) <sub>2</sub> (black), PDMS-3k-(NH <sub>2</sub> ) <sub>2</sub> (red), PDMS-5k-(NH <sub>2</sub> ) <sub>2</sub> (blue), and PDMS-7k-(NH <sub>2</sub> ) <sub>2</sub> (green) (2 molar equivalents of hydrophobic diamine per polymer) showing peaks at q <sub>max</sub> used to calculate the mean interdomain spacing of the gel-like samples. The intensity is given in logarithmic scale. ....	309
Figure C.8 - TGA traces of poly(DGC-PPG) (black-discontinued) and extended poly(DGC-PPG) from both ends with PDMS-1k-(NH <sub>2</sub> ) <sub>2</sub> (black), PDMS-3k-(NH <sub>2</sub> ) <sub>2</sub> (red), PDMS-5k-(NH <sub>2</sub> ) <sub>2</sub> (blue), and PDMS-7k-(NH <sub>2</sub> ) <sub>2</sub> (green) used in this work (2 molar equivalents of hydrophobic diamine per polymer).....	310
Figure C.9 - TGA traces of poly(DGC-PPG) (black-discontinuous) and Priamine-poly(DGC-PPG)-Priamine (black).....	311
Figure C.10 - Derivative of weight percentage with respect to temperature traces of poly(DGC-PPG) (grey) and Priamine-poly(DGC-PPG)-Priamine (black).....	312
Figure C.11 - Curing kinetics of the end-capped poly(DGC-PPG) (black), PDMS-7k-poly(DGC-PPG)-7k-PDMS (red), and Priamine-poly(DGC-PPG)-Priamine (blue) by following the complex viscosity (η*) (Pa.s) at a frequency of 1 Hz and a strain of 1% for 24 h. 0.5 wt.% of the proprietary catalyst was added to accelerate the curing of PDMS-7k-poly(DGC-PPG)-7k-PDMS, and Priamine-poly(DGC-PPG)-Priamine. Measurements were done at 22 °C and 40-50% humidity. ....	314
Figure C.12 - Curing kinetics of the end-capped poly(DGC-PPG) (black), PDMS-7k-poly(DGC-PPG)-7k-PDMS (red), and Priamine-poly(DGC-PPG)-Priamine (blue) by following the damping	

factor ( $\tan\delta$ ) at a frequency of 1 Hz and a strain of 1% for 24 h. 0.5 wt.% of the proprietary catalyst was added to accelerate the curing of PDMS-7k-poly(DGC-PPG)-7k-PDMS, and Priamine-poly(DGC-PPG)-Priamine. Measurements were done at 22 °C and 40-50% humidity. .... 315

Figure C.13 - FTIR spectra of PDMS-7k-poly(DGC-PPG)-7k-PDMS-7k before (black) and after (red) end-capping showing the decrease of the carbonyl stretch at  $1800\text{ cm}^{-1}$  in the end-capped prepolymer spectrum. .... 316

Figure D.1 - Labelled DGC  $^1\text{H-NMR}$  spectrum in  $\text{DMSO-d}_6$  at 25 °C.  $\delta$  (ppm): 4.93 (m, 2H,  $\text{H}_2$ ), 4.52 (t, 2H,  $\text{H}_1^{\text{cis or trans}}$ ), 4.25 (ddd, 2H,  $\text{H}_1^{\text{cis or trans}}$ ), 3.79-3.65 (m, 4H,  $\text{H}_3$ ). .... 319

Figure D.2 - FTIR spectra showing the decrease in the carbonyl stretch related to the cyclic carbonate end-groups and unreacted carbonates (at  $1780\text{ cm}^{-1}$ ) with respect to that of the carbonyl stretch of the urethane linkages (at  $1695\text{ cm}^{-1}$ ) after purifying PDMS-2040. .... 320

Figure D.3 - Stacked  $^1\text{H-NMR}$  spectra of unpurified PDMS-0040 (black), PDMS-2040 (red), and PDMS-4040 (blue) in  $\text{CDCl}_3$  at 25 °C. .... 321

Figure D.4 - Stacked  $^1\text{H-NMR}$  spectra of unpurified PDMS-0025 (black), PDMS-2025 (red), and PDMS-4025 (blue) in  $\text{CDCl}_3$  at 25 °C. .... 322

Figure D.5 - TGA traces of the PDMS containing TPHUs ..... 326

Figure D.6 - WAXS spectra of PDMS-0040, PDMS-2040, and PDMS-4040. The distinct shoulder peak at  $2\theta$  of  $9^\circ$  proving the presence of a PDMS phase in the microstructure of the TPHUs. The intensity is given in logarithmic scale. .... 327

Figure D.7 - Loss modulus of the PDMS containing TPHUs collected from amplitude sweeps conducted at 22 °C and a frequency of 10 Hz. .... 328

Figure D.8 - Dynamic mechanical frequency sweep data for PDMS-0025 ( $G''$  curve is shifted by a factor of 5) at 0.5% shear strain. The solid line is a fit to the Generalized Maxwell model. The inset shows the shift factors used for time-temperature superposition. The solid and dashed lines in the inset are the WLF and Arrhenius law fit equations, respectively. .... 329

Figure D.9 - Dynamic mechanical frequency sweep data for PDMS-2025 ( $G''$  curve is shifted by a factor of 5) at 0.5% shear strain. The solid line is a fit to the Generalized Maxwell model. The

inset shows the shift factors used for time-temperature superposition. The solid and dashed lines in the inset are the WLF and Arrhenius law fit equations, respectively. ....	330
Figure D.10 - Dynamic mechanical frequency sweep data for PDMS-4025 ( $G''$ curve is shifted by a factor of 5) at 0.5% shear strain. The solid line is a fit to the Generalized Maxwell model. The inset shows the shift factors used for time-temperature superposition. The solid and dashed lines in the inset are the WLF and Arrhenius law fit equations, respectively. ....	331
Figure D.11 - FTIR spectra of the unpurified DAD containing TPHUs. ....	332
Figure D.12 - Stacked $^1\text{H-NMR}$ spectra of unpurified DAD-0040 (black), DAD-2040 (red), and DAD-4040 (blue) in $\text{CDCl}_3$ at 25 °C. ....	333
Figure D.13 - TGA traces of the DAD containing TPHUs.....	334
Figure D.14 - WAXS spectra of DAD-0040, DAD-2040, and DAD-4040. The distinct sharp peak at $2\theta$ of $14.8^\circ$ proving the presence of crystallinity in the microstructure of the TPHUs having an amorphous phase constituted of Priamine 1074. The intensity is given in logarithmic scale.....	335
Figure D.15 - Loss modulus of the DAD containing TPHUs collected from amplitude sweeps conducted at 22 °C and a frequency of 10 Hz. ....	336
Figure D.16 - Storage and loss moduli of the PLA/TPHUs blends (80/20 wt.%/wt.%) collected from amplitude sweeps conducted at 22 °C and a frequency of 1 Hz. ....	337
Figure D.17 - Storage and loss moduli of the PLA/TPHUs blends (80/20 wt.%/wt.%) collected from amplitude sweeps conducted at 150 °C and a frequency of 1 Hz. ....	338
Figure D.18 - Storage modulus data of the PLA/TPHUs blends (80/20 wt.%/wt.%) collected from dynamic mechanical thermal analysis conducted at frequency of 1 Hz and 0.01% shear strain.....	339
Figure D.19 - Loss modulus data of the PLA/TPHUs blends (80/20 wt.%/wt.%) collected from dynamic mechanical thermal analysis conducted at frequency of 1 Hz and 0.01% shear strain.....	340
Figure D.20 - Loss factor data of the PLA/TPHUs blends (80/20 wt.%/wt.%) collected from dynamic mechanical thermal analysis conducted at frequency of 1 Hz and 0.01% shear strain.....	341
Figure D.21 - Portion of the FTIR spectra of some TPHUs showing the distinct $\text{C=O}$ stretch at $1790\text{ cm}^{-1}$ proving the abundance of carbonate end-groups in the chains of PDMS-0040 and PDMS-2040. ....	342

Figure D.22 - Portion of the FTIR spectra of the blends (80/20 wt.%/wt.%) showing the broadening of the C=O stretch of PLA at  $1760\text{ cm}^{-1}$  proving the presence of hydrogen bonding. .... 342

Figure D.23 - Portion of the FTIR spectra of the blends (80/20 wt.%/wt.%) showing the appearance of the broad hydroxyl groups band proving the presence of hydrogen bonding (intermolecular interactions). .... 343

Figure E.1 - Labelled  $^1\text{H-NMR}$  of the bio-based HU of this work in  $\text{CDCl}_3$  at  $25\text{ }^\circ\text{C}$ . (500 MHz,  $\text{CDCl}_3$ ,  $\delta$ ): 7.58 (g), 6.87/6.78 (g), 5.23 (f), 4.50 (a), 4.15 (d), 3.75 (e), 3.39 (f), 3.13 (c), 2.65 (b), 2.6-0.6 (R). .... 346

Figure E.2 - Labelled  $^1\text{H-NMR}$  of the kinetic study of trial 4 (Table 7.1) at  $t = 5, 30,$  and  $90\text{ min}$  of forming the bio-based and degradable HU- $\text{CL}_5$  of this work in  $\text{CDCl}_3$  at  $25\text{ }^\circ\text{C}$ . (500 MHz,  $\text{CDCl}_3$ ,  $\delta$ ): 4.26 (b', c'), 4.24 (d), 4.19 (b), 4.07 (middle d'), 3.79 (c), 3.65 (end d'), 3.17 (a), 2.64 (h), 2.33 (h'), 1.86 (g), 1.77 (e, f), 1.66/1.59 (e', g'), 1.40 (f'), 1.49/1.28/0.88 (R). .... 347

Figure E.3 - Plot of  $\ln(1/(1-X))$  using the CL conversion data of trial 4 (Table 7.1) with the linear fitting of Eq. (E.7) and the smooth fitting of the data (dashed and solid, respectively) added... 349

Figure E.4 - SEC traces of aliquots withdrawn during the kinetic study of trial 4 (Table 7.1) at specific time intervals ..... 350

Figure E.5 - Labelled  $^1\text{H-NMR}$  of the bio-based and degradable HU- $\text{CL}_5$  of this work in  $\text{CDCl}_3$  at  $25\text{ }^\circ\text{C}$ . (500 MHz,  $\text{CDCl}_3$ ,  $\delta$ ): 4.88 (i), 4.25 (b, c), 4.06 (middle d), 3.64 (end d), 3.16 (a), 2.31 (h), 1.65/1.58 (e, g), 1.39 (f), 1.49/1.26/0.87 (R). .... 351

Figure E.6 - Unadjusted TGA traces of photocurable thermosets before and after degradation 352

Figure E.7 - Adjusted TGA traces of photocurable thermosets before and after degradation.... 353

Figure E.8 - Water-soluble degradation products caused by the accelerated hydrolysis of the degradable photocurable thermosets (details about the peaks given in Table E.2). .... 353

## List of Schemes

Scheme 1.1 - Polyurethane synthesis via isocyanate- and phosgene-free routes: (1) the polyaddition of bifunctional cyclic carbonate and diamine; (2) the polycondensation of ethylene carbonate, diamines and diols; (3) the copolymerization of substituted aziridines with carbon dioxide; (4) the rearrangement reaction (case of Curtius rearrangement of acyl azides) in the presence of diols. ....	3
Scheme 2.1 - Synthesis of amino-telechelic oligoamide based on dimer fatty acids .....	6
Scheme 3.1 - Moisture-curing method based on end-capping the carbonate and diamine end-groups of PHU prepolymers (proposed in this work).....	34
Scheme 3.2 - Synthesis of DGC from DIG and DMC transesterification reaction .....	35
Scheme 3.3 - Polyaddition reaction for DGC-based PHUs synthesis including the diamines investigated in this work.....	38
Scheme 4.1 - D-sorbitol and D-mannitol molecular structures .....	80
Scheme 4.2 - GLYMO and DAMO silane curing agent molecular structures .....	80
Scheme 4.3 - Synthesis of sugar-derived alcohol dicarbonates from D-sorbitol and D-mannitol and DMC transesterification reaction .....	81
Scheme 4.4 - Polyaddition reaction for sugar-based PHUs synthesis .....	82
Scheme 4.5 - Chemical structures of the diamines used in this work.....	83
Scheme 5.1 - The step-wise synthesis method proposed in this work to increase the hydrophobicity of the DGC-PPG HPHUs .....	121
Scheme 5.2 - Series of products obtained from reacting the hydrophobic diamines with poly(DGC-PPG). The hydrophobic diamines are more inclined to cap poly(DGC-PPG) from both ends by reacting with its cyclic carbonate end-groups. ....	135

Scheme 7.1 - Reaction pathway for the preparation of bio-based and hydrolytically degradable hydroxyurethane acrylates (HUAs) ..... 212

## List of Tables

Table 2.1 - Vegetable oil-based polyhydroxyurethanes (fatty acids derived from vegetable oils inclusive).....	7
Table 2.2 - Plant-based polyhydroxyurethanes (fatty acids derived from plants inclusive).....	13
Table 2.3 - Glycerol-based polyhydroxyurethanes (polyoyl belonging to the same family inclusive).....	16
Table 2.4 - Sugar-based polyhydroxyurethanes (fatty acids derived from sugars inclusive).....	20
Table 3.1 - Physical properties of the synthesized PHU prepolymers of this work derived from diglycerol dicarbonate (DGC) and various amines based on a 1/1 molar equivalent formulation	41
Table 3.2 - Thermal properties of selected PHU prepolymers as potential sealant candidate (data of PHU 2 are also included although the polymer is not considered for end-capping) <sup>a</sup> .....	46
Table 3.3 - Prepolymer information necessary for preparing end-capped PHUs (HPHUs).....	48
Table 3.4 - End-capping experiments of PHU 4.....	49
Table 3.5 - End-capping experiments of PHU 10.....	50
Table 3.6 - Comparison of tensile and rheological tests results for HPHU 10 samples cured under lab conditions for one week and HPHU 10 samples cured for one week under lab conditions and another week in pure H <sub>2</sub> O.....	58
Table 4.1 - Physical properties of the synthesized PHU prepolymers of this work derived from SBC and MBC and various amines based on a 1/1 molar equivalent formulation.....	84
Table 4.2 - Thermal properties of selected sugar-based PHU prepolymers as potential sealant candidates <sup>a</sup> ).....	86
Table 4.3 - Prepolymer information necessary for preparing end-capped PHUs (HPHUs).....	89
Table 4.4 - End-capping experiments of SBC-based PHU prepolymers.....	89
Table 4.5 - End-capping experiments of MBC-based PHU prepolymers .....	90
Table 4.6 - Swelling in THF and pure H <sub>2</sub> O experimental results for the sugar-based HPHUs synthesized in this work.....	97

Table 4.7 - Mean interdomain spacing, $d$ , calculated from SAXS spectra (Figure B.20 of the supporting information) and Eq. (4.5), of DGC-PDMS-5k-(NH <sub>2</sub> ) <sub>2</sub> and the sugar-based PDMS HPHUs of this work.....	102
Table 5.1 - Si-(CH <sub>3</sub> ) <sub>2</sub> -O to PPG-CH <sub>3</sub> unit ratios estimated and predicted from <sup>1</sup> H-NMR for PDMS-poly(DGC-PPG)-PDMS of this work (2 molar equivalents of PDMS-(NH <sub>2</sub> ) <sub>2</sub> per polymer).....	131
Table 5.2 - Structural and thermal properties of the extended poly(DGC-PPG) from both ends with the hydrophobic diamines of this work (2 molar equivalents of hydrophobic diamine per polymer).....	137
Table 5.3 - Prepolymer information necessary for end-capping the PHUs of this work to afford HPHUs. The gel times for the PDMS-7k-poly(DGC-PPG)-7k-PDMS and Priamine-poly(DGC-PPG)-Priamine were measured after addition of 0.5 wt.% of the proprietary catalyst.....	142
Table 5.4 - Swelling experimental results of the synthesized HPHUs of this work in different solvents. ....	146
Table 6.1 - Structural and thermal properties of the PDMS containing TPHUs .....	170
Table 6.2 - Structural and thermal properties of the DAD containing TPHUs.....	184
Table 6.3 - Thermal transitions of the blends of this study (80/20 wt.%/wt.%).....	189
Table 6.4 - Structural, mechanical, and miscibility properties of the blends of this study (80/20 wt.%/wt.%) .....	192
Table 7.1 - Trials of ROP of CL using bio-based HU macroinitiator and SEC results .....	213
Table A.1 - Data of molecular weight and dispersity evolution during PHU 6 polymerization at 140 °C (the initial data is that of Jeffamine D-2000).....	267
Table A.2 - Data of molecular weight and dispersity evolution during PHU 11 polymerization at 80 °C (the initial data is that of PDMS-(NH <sub>2</sub> ) <sub>2</sub> , M <sub>n</sub> = 5,000 g/mol).....	268
Table A.3 - Swelling experiment data HPHU 4 samples in pure H <sub>2</sub> O .....	276
Table A.4 - Swelling experiment data of HPHU 10 samples in pure H <sub>2</sub> O.....	276

Table A.5 - Sessile drop tests of Milli-Q water on HPHU 10 films .....	277
Table A.6 - Degradation experiment data of HPHU 10 films in acid medium pH = 3 .....	278
Table A.7 - Tensile properties for the dog-bone samples cured for one week under moisture at ambient conditions .....	279
Table A.8 - Tensile properties for the dog-bone samples cured for one week at ambient conditions and another week in pure H <sub>2</sub> O .....	280
Table B.1 - Swelling experiment data of SBC-HPHU 1 samples in THF and pure H <sub>2</sub> O.....	295
Table B.2 - Swelling experiment data of MBC-HPHU 1 samples in THF and pure H <sub>2</sub> O.....	295
Table B.3 - Swelling experiment data of SBC-HPHU 3 samples in THF and pure H <sub>2</sub> O.....	296
Table B.4 - Swelling experiment data of MBC-HPHU 3 samples in THF and pure H <sub>2</sub> O.....	296
Table B.5 - Degradation experiment data of SBC-HPHU 3 films in acid medium pH = 3.....	299
Table B.6 - Degradation experiment data of MBC-HPHU 3 films in acid medium pH = 3 .....	299
Table B.7 - Sessile drop tests of Milli-Q water on SBC-HPHU 3 films .....	300
Table B.8 - Sessile drop tests of Milli-Q water on MBC-HPHU 3 films .....	300
Table B.9 - SBC and MBC experimental trials for reaction optimization.....	302
Table C.1 - Swelling experiment data of the poly(DGC-PPG) HPHU samples in different solvents .....	317
Table C.2 - Swelling experiment data of the PDMS-7k-poly(DGC-PPG)-7k-PDMS HPHU samples in different solvents.....	317
Table C.3 - Swelling experiment data of the Priamine-poly(DGC-PPG)-Priamine HPHU samples in different solvents.....	318
Table D.1 - Parameters analyzed from the <sup>1</sup> H-NMR of PDMS containing TPHUs.....	323
Table D.2 - Calculation of solubility parameters using the Hoftyzer-Van Krevelen group contribution method of the PDMS containing TPHUs.....	324
Table D.3 - Parameters analyzed from the <sup>1</sup> H-NMR of DAD containing TPHUs.....	333
Table D.4 - Calculation of solubility parameters using the Hoftyzer-Van Krevelen group contribution method of PLA (those of the TPHUs found in the previous sections).....	343

Table D.5 - Solubility parameters used to calculate the RED. The solubility parameters of the TPHUs were calculated from the linear mixing rule based on the ones estimated for the Priamine and PDMS hydroxyurethane linkages. ....	344
Table E.1 - Swelling experiment data of the photocurable thermoset in different solvents .....	352
Table E.2 - Information of the peak assignments of the water-soluble degradation products complementing Figure E.8.....	354

## List of Abbreviations

Acronym/symbol	Definition
$a_T$	Shift factor
ACMO	4-Acryloylmorpholine
CL	$\epsilon$ -Caprolactone
$CDCl_3$	Deuterated chloroform
d	Interdomain spacing
DAD	1,10-diaminodecane
DGC	Diglycerol dicarbonate
DIG	Diglycerol
DMF	Dimethylformamide
DMC	Dimethyl carbonate
$DMSO-d_6$	Deuterated dimethyl sulfoxide
DMTA	Dynamic mechanical thermal analysis
$DP_n$	Degree of polymerization
DSC	Differential scanning calorimetry
$D_2O$	Deuterium oxide
E	Young's modulus
$E_A$	Activation Energy
EB%	Elongation at break percentage
EC	Ethylene carbonate
ESI-MS	Electrospray ionization mass spectroscopy
EWA	Equilibrium water absorption

EWC	Equilibrium water content
$f_{\text{C=O}}^{\text{b}}$	Fraction of hydrogen bonded carbonyl groups
FTIR	Fourier-Transform infrared spectroscopy
GC	Gel content
GPC	Gel permeation chromatography
G'	Storage moduli
G''	Loss moduli
HPHU	Hybrid polyhydroxyurethane
HU	Hydroxyurethane
H <sub>2</sub> O	Water
HUA	Hydroxyurethane acrylate
HUMA	Hydroxyurethane methacrylate
$k_p$	Rate of propagation coefficient
$M_n$	Number-average molecular weight
$M_w$	Weight-average molecular weight
MBC	Mannitol bicarbonate
MWD	Molecular weight distribution
NMR	Nuclear magnetic resonance
PCL	Poly(caprolactone)
PDMS-(NH <sub>2</sub> ) <sub>2</sub>	Poly(dimethylsiloxane) diamine
PHU	Polyhydroxyurethane
PLA	Poly(lactic acid)
PMMA	Poly(methyl methacrylate)

PPG	Poly(propylene glycol)
PS	Poly(styrene)
PU	Polyurethane
[P*]	Concentration of active species
$q_{\max}$	Scattering vector at maximum signal
RED	Relative energy difference
$R_{C=O}^{\text{TPHU}}$	Ratio of carbonyl end-groups to carbonyl urethane
SAXS	Small angle X-ray scattering
SBC	Sorbitol bicarbonate
SEC	Size exclusion chromatography
SEM	Scanning electron microscopy
SI	Swelling index
$T_{d,10\%}$	Temperature at 10 wt.% degradation
$T_c$	Crystallization temperature
$T_g$	Glass transition temperature
$T_m$	Melting temperature
TGA	Thermogravimetric analysis
THF	Tetrahydrofuran
TPHU	Thermoplastic polyhydroxyurethane
TPU	Thermoplastic polyurethane
WAXS	Wide-angle X-ray scattering
$\Delta H_c$	Crystallization enthalpy
$\Delta H_m$	Melting enthalpy

$X_c$	Crystallinity fraction
$X_i$	Conversion of component i
$\bar{D}$	Dispersity ( $M_w/M_n$ )
$\tan\delta$	Damping factor ( $G''/G'$ )
$\eta_i$	Viscosity of polymer i
$\delta_i$	Solubility parameter of polymer i
$\delta_{d,i}$	Solubility parameter of i - dispersion forces
$\delta_{p,i}$	Solubility parameter of i - polar forces
$\delta_{h,i}$	Solubility parameter of i - hydrogen bonding
$\sigma_{max}$	Tensile strength
$2\theta$	X-ray diffraction angle
$\nu_e$	Crosslink density

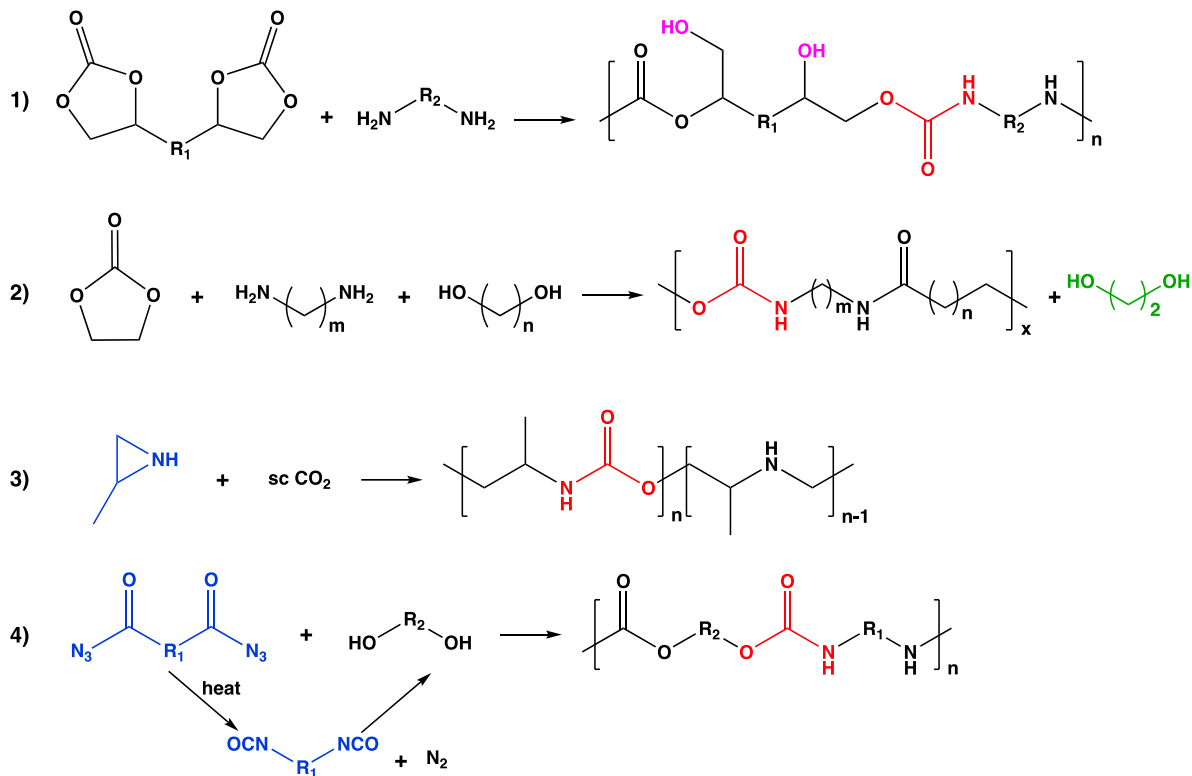
# Chapter 1

## Introduction

Polyurethanes (PU) constitute a special class of polymers as, unlike other commercial plastics, they find a wide range of application in building and construction, automotive, coatings, marine, medical, apparels, wood composites, appliances, flooring, and packaging.<sup>1</sup> This versatility in application is owed to the different types of PUs including rigid and flexible foams, thermoplastics, ionomers, binders, waterborne dispersions, elastomers, coatings, sealants, and adhesives.<sup>1-2</sup> With an estimated global production of 24 billion tons in 2020, PUs rank 6<sup>th</sup> in the worldwide consumption of polymers.<sup>1,3</sup> The chemistry of PUs goes back to 1937 when Bayer et al. synthesized the first PU from the polyaddition of diisocyanates (hard segments) and diols (soft segments),<sup>4</sup> and since then, researchers have investigated numerous poly(isocyanates)/polyols couples for new PU formulations achieving high end properties to meet industrial needs. However, conventional PUs present many hazards to the environment and human health, and that at different stages of their production going from their monomer synthesis (isocyanates) to their polymerization and finally their disposal. In fact, isocyanates are synthesized from phosgene, which is a lethal gas, at critical conditions.<sup>5</sup> Moreover, common isocyanates, such as methyl isocyanate and tolylene diisocyanate, cause several health risks, such as asthma and skin irritation,<sup>6-9</sup> when prolongedly exposed to them, and they have been classified as CMR; carcinogenic, mutagenic, and reprotoxic.<sup>10-12</sup> Finally, at their end life, PUs are incinerated, and they decompose by releasing isocyanates and other poisonous derivatives, like hydrogen cyanide and toxic amines<sup>13-14</sup> Owing to these environmental and health concerns along with other industrial considerations, mainly the moisture sensitivity, poor chemical

resistance, and weakness in weatherability of conventional PUs, <sup>15-16</sup> researchers investigated different routes to obtain PUs free of isocyanates, known as non-isocyanate polyurethanes (NIPU). <sup>3, 15-21</sup>

NIPUs have been the subject of interest of different research groups across the world in the last decade. They can be synthesized as linear chains from four different isocyanate and phosgene-free routes: (1) the polyaddition of bifunctional cyclic carbonate and diamine, (2) the polycondensation of ethylene carbonate, diamines and diols (transurethanization), (3) the copolymerization of substituted aziridines with carbon dioxide, and (4) the rearrangement reactions in the presence of diols, summarized in Scheme 1.1. <sup>3, 17-18, 20-21</sup> Among these pathways, the first two have the greenest and safest reagents, as aziridine and acyl azides are harmful substances with the latter forming an in-situ diisocyanate, via Curtius rearrangements, that further reacts with the diol to give carbamates or urethane linkages (highlighted in red in Scheme 1.1). <sup>17, 20</sup> While the polyaddition of cyclic dicarbonates and diamines occur in one step, the polycondensation goes over two; ethylene carbonate reacts first with the diamine to obtain a dicarbamate, and then the polycondensation follows between the latter and the diols. Also, the transurethanizations are conducted in solvents with catalysts, and they form alcohols as by-products which must be removed and might cause issues when scaling up their processes. The polyaddition route, on the other hand, does not form any lower molecular weight by-products or volatile organic compounds and can be performed in bulk and without catalysts. <sup>22</sup> Consequently, the NIPUs deriving from the polyaddition of cyclic dicarbonates and diamines were extensively studied, in the last decade, by academic and industrial researchers, and they were also selected as the main focus of this thesis. This category of NIPUs is known by polyhydroxyurethanes (PHU) since the resulting polymer chains contain pendent secondary and primary hydroxyl groups.



**Scheme 1.1 - Polyurethane synthesis via isocyanate- and phosgene-free routes: (1) the polyaddition of bifunctional cyclic carbonate and diamine; (2) the polycondensation of ethylene carbonate, diamines and diols; (3) the copolymerization of substituted aziridines with carbon dioxide; (4) the rearrangement reaction (case of Curtius rearrangement of acyl azides) in the presence of diols.**

PHUs present many differences when compared to conventional PUs. The cyclic carbonates (hard segments) are non-toxic and non-moisture sensitive, unlike isocyanates that are toxic and that easily react with water to form carbon dioxide (CO<sub>2</sub>) and urea side products.<sup>16, 20</sup> Moreover, the presence of hydroxyl groups in the PHU chains provide structural differences with respect to conventional PUs. The hydroxyl groups can participate in inter and intramolecular hydrogen bonding with the urethane groups, improving the chemical resistance against non-protic solvents.<sup>16, 20</sup> While there is a disagreement about their effects on the thermal stability

and the water resistance of PHUs, the hydroxyl groups provide sites of chain post-functionalization with chemical and biological moieties.<sup>23</sup>

Interestingly, the monomers, the cyclic dicarbonates and the diamines, of PHUs are abundant and can be obtained from bio-based sources. Cyclic dicarbonates were synthesized from vegetable oils, terpenes, glycerol, sugars, tannin, and lignin.<sup>24-32</sup> While diglycerol dicarbonate (DGC) and sugar-based D-sorbitol and D-mannitol biscarbonates (SBC and MBC, respectively) were directly prepared from the intramolecular etherifications or transesterifications of dimethyl carbonate (DMC) with their raw materials,<sup>33-35</sup> vegetable oils and limonene, for example, containing natural double bonds in their structures were first epoxidized,<sup>36-39</sup> and then carbonated through the chemical fixation of CO<sub>2</sub>.<sup>36, 40-47</sup> Different catalysts have been developed to optimize the latter carbonation reaction.<sup>48-61</sup> Bioderived diamines were investigated as well from several renewable sources, such as plant-based fatty acids, lysine, and sugars.<sup>62-63</sup>

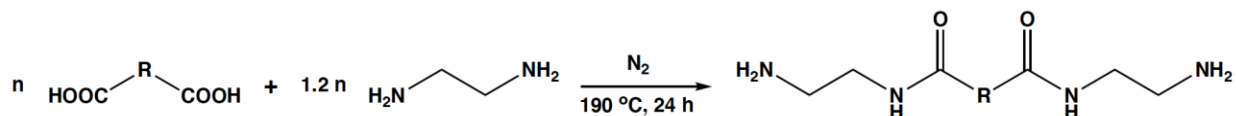
Seeing the green and industrial prospects of PHUs, many studies have relied on the kinetics of the aminolysis reaction between cyclic carbonates and amines<sup>64-87</sup> to synthesize thermoplastic, hybrid thermosets, and waterborne PHU dispersions (TPHU, HPHU, and WPHU, respectively).<sup>88-91</sup> Even though studies agree that high molecular weight PHUs are hard to achieve due to hydrogen bonding and side reactions,<sup>92-93</sup> that did not prevent researchers from developing PHUs with advanced features, like self-healing, reprocessability, shape memory, and composites, and for several applications, for example, coatings, adhesives, foams, and biomedical materials.<sup>94-97</sup> Among these types and features, partially/fully sustainable moisture-curable HPHUs, TPHUs, and UV-curable hydrolytically degradable hydroxyurethane acrylates (HUA) are investigated in this work.

As it was previously mentioned, linear bio-based PHUs, derived from renewable sources in making the cyclic dicarbonates or the diamines, constitute the heart of this thesis. Hence, the next chapter (Chapter 2) will examine in depth the different partially and fully sustainable PHUs while focusing on their types (thermoplastic, thermosets, or hybrid thermosets), special features, and intended applications. The choice of the bio-based dicarbonates, DGC, SBC, and MBC, adopted in the following manuscript-based chapters will be also discussed along with the special features and applications targeted in this work, which are: moisture-curable HPHUs advanced to make promising non-toxic and partially sustainable sealants and adhesives (Chapters 3, 4, and 5), fully/partially bio-based TPHUs made from terpolymerizations and their application in melt blending (Chapter 6), and UV-curable bio-based and hydrolytically degradable hydroxyurethane acrylates (HUA) to be applied in 3D Printing and biomedical applications (Chapter 7). Finally, Chapter 8 provides an overall summary that emphasizes on the power of PHUs, which are proven to be versatile materials, while giving recommendations for future investigations.

## Chapter 2

### Literature Review

The investigations on bio-based raw materials for PHU synthesis have started in 2004 with Tamami et al., who used soybean oil as a precursor for cyclic carbonates.<sup>98</sup> However, it is not until 2012 that this topic really caught the attention of many research groups around the world. After soybean oil, other vegetable oils were investigated as precursors for cyclic carbonates along with terpenes, glycerol, and glucose-derived materials, as it is presented in the following sub-sections. While bio-based cyclic carbonates have been widely studied, less effort has been put towards synthesizing bio-based diamines. Still, the latter can be easily derived from fatty acids through basic organic chemistry by reacting dimer fatty acids with short chain diamines to afford oligoamides, as presented in Scheme 2.1.<sup>99</sup> Commercialized bio-based diamine products from Croda, such as Priamine 1074 and 1075, were used in different studies to synthesize fully bio-based PHU products, as presented in Table 2.1 through Table 2.4. These tables also summarize the precursors, the types, and the special features of the fully/partially bio-based PHUs found in the literature. The bio-based renewable sources were grouped under four main categories: vegetable oils and their fatty acids (Table 2.1), plant-based materials and their fatty acids (Table 2.2), glycerol and its derived polyols (Table 2.3), and sugars and their fatty acids (Table 2.4).



**Scheme 2.1 - Synthesis of amino-telechelic oligoamide based on dimer fatty acids**

**Table 2.1 - Vegetable oil-based polyhydroxyurethanes (fatty acids derived from vegetable oils inclusive)**

<b>Authors (year)<sup>reference</sup></b>	<b>Cyclic Carbonates</b>	<b>Amines</b>	<b>Type</b>	<b>Special feature/ Application</b>
<b>Tamami et al. (2004)<sup>98</sup></b>	Carbonated soybean oil	Ethylenediamine, 1,6-hexamethylenediamine, and tris(2-aminoethyl)amine	Thermosets	-
<b>Javni et al. (2008)<sup>100</sup></b>	Carbonated soybean oil	Ethylenediamine, 1,4-butylenediamine, and 1,6- hexamethylenediamine	Thermosets	-
<b>Li et al. (2008)<sup>101</sup></b>	Carbonated soybean oil	Ethylenediamine	Thermosets	-
<b>Türünç et al. (2008)<sup>102</sup></b>	Carbonated soybean oil with carbonated polypropylene glycol	1,4-Butylenediamine	Thermosets with silica nanoparticles	Nanocomposites/ Coatings
<b>Boyer et al. (2010)<sup>103</sup></b>	Dicarbonated fatty acid diester (from pecan oil)	Ethylenediamine and isophoronediamine	Linear thermoplastics	-
<b>Bähr et al. (2012)<sup>104</sup></b>	Carbonated soybean oil and carbonated linseed oil	Ethylenediamine, 1,4-butylenediamine, and isophoronediamine	Thermosets	-
<b>Javni et al. (2013)<sup>105</sup></b>	Carbonated soybean oil	m-Xylene diamine, p-xylene diamine, and isophoronediamine	Thermosets	-
<b>Hambali et al. (2013)<sup>106</sup></b>	Carboxylated linoleic acid from rubber seed oil	Ethylenediamine	Linear thermoplastic and thermosets	-
<b>Camara et al. (2014)<sup>107</sup></b>	Resorcinol dicarbonate (from argan oil)	Tetraethylenepentamine	Linear thermoplastics and thermosets	-

<b>Carré et al. (2014)<sup>108</sup></b>	Sebacic cyclic dicarbonate (from castor oil)	Two bio-based Priamine grades from Croda	Linear thermoplastics and thermosets	-
<b>Kathalewar et al. (2014)<sup>109</sup></b>	Carbonated cashew nut shell liquid	1,6-Hexamethylenediamine and isophoronediamine	Linear thermoplastics and thermosets	Coatings
<b>Mahendran et al. (2014)<sup>110-111</sup></b>	Carbonated linseed oil	Phenylkamine (from cashew nut shell liquid)	Thermosets	Coatings <sup>111</sup>
<b>Maisonneuve et al. (2014)<sup>112-113</sup></b>	Carbonated fatty acids derived from ricinoleic acid (contained in castor oil)	1,4-Butylenediamine, isophoronediamine, Jeffamine 400, and Priamine 1075	Linear thermoplastics and chemical gel formation <sup>113</sup>	-
<b>Jalilian et al. (2015)<sup>114</sup></b>	Carbonated soybean oil	Ethylenediamine and biodegradable amine based on polyethylene glycol	Thermosets	Biodegradable and cytocompatibility
<b>Bigot et al. (2016)<sup>115</sup></b>	Carbonated fatty acids derived from ricinoleic acid (contained in castor oil)	1,6-Hexamethylenediamine and isophoronediamine	Linear thermoplastics	-
<b>Carré et al. (2016)<sup>116</sup></b>	Turpentine oil-based cyclic dicarbonate	Jeffamine D-2000, Priamine 1075, 1,4-butylenediamine, and m-xylene diamine	Linear thermoplastics	-
<b>Duval et al. (2016)<sup>117</sup></b>	Sebacic cyclic dicarbonate (from castor oil)	1,6-Hexamethylenediamine, Primanie 1074, and methyl ricinoleate-based diamine (from castor oil)	Linear and branched thermoplastics	-

<b>Poussard et al. (2016)<sup>118</sup></b>	Carbonated soybean oil	Bio-based Amino-telechelic oligoamides (from dimer fatty acid Pripol 1013), 1,4-butylenediamine, and isophoronediamine	Branched thermoplastics and thermosets	-
<b>Samanta et al. (2016)<sup>119</sup></b>	Carbonated soybean oil derived poly(vinyl ether) and carbonated soybean oil	1,6-Hexamethylenediamine, 1,9-nonanediamine, and 1,13-tridecanediamine	Thermosets	-
<b>Cheng et al. (2017)<sup>120</sup></b>	Eugenol-based carbonate (from clove oil)	4,4'-Diaminodiphenylmethane, p-xylene diamine, and 1,6-hexamethylenediamine	Lineay thermoplastics	-
<b>Haniffa et al. (2017)<sup>121</sup></b>	Carbonated jatropha curcas oil	Isophoronediamine and 1,3-diaminopropane	Thermosets	-
<b>Doley et al. (2018)<sup>122</sup></b>	Carbonated sunflower oil	Isophoronediamine	Thermosets with Multiwalled Carbon Nanotube	Composites
<b>Doley et al. (2018)<sup>123</sup></b>	Carbonated sunflower oil	Ethylenediamine, isophoronediamine, and diethylenetriamine	Thermosets	Coatings
<b>Doley et al. (2018)<sup>124</sup></b>	Carbonated sunflower oil	Isophoronediamine	Hybrid thermosets/epoxy blending with graphene oxide	Nanocomposites
<b>Farhadian et al. (2018)<sup>125</sup></b>	Carbonated sunflower oil	New synthesized vegetable oil-based di/polyamines	Thermosets	Low water degradation/ medical field

<b>He et al. (2018)<sup>126</sup></b>	Sapium sebiferum oil-derived dimer acid cyclic carbonate	Ethylenediamine, 1,6-hexamethylenediamine, diethylenetriamine, triethylenetetramine, and tetraethylenepentamine	Linear thermoplastics	-
<b>Levina et al. (2018)<sup>80</sup></b>	Carbonated soybean oil	n-Butylamine	Thermosets	-
<b>Malik et al. (2018)<sup>127</sup></b>	Carbonated canola oil	Ethylenediamine, 1,6-hexamethylenediamine, paraphenylenediamine, and isophoronediamine	Thermosets	-
<b>Panchireddy et al. (2018)<sup>128</sup></b>	Carbonated soybean oil	1,6-hexamethylenediamine, m-xylene diamine, and isophoronediamine	Thermosets with silica and zinc oxide fillers	Nanocomposites/ Adhesives
<b>Farid et al. (2019)<sup>129</sup></b>	Carbonated sunflower oil	1,4-Phenylenediamine	Thermosets with zirconia at silica fillers	Flame retardant nanocomposites/ Coatings
<b>Gharibi et al. (2019)<sup>130</sup></b>	Carbonated soybean oil	3-Aminopropyl trimethoxysilane	Thermosets	Antimicrobial/ Coatings
<b>Hu et al. (2019)<sup>131</sup></b>	Carbonated soybean oil	Priamine 1074 and Diethylene glycol bis(3-aminopropyl) ether	Thermosets	Reprocessable networks
<b>Mokhtari et al. (2019)<sup>132</sup></b>	Carbonated jujuba and castor oils	1,4-Butylenediamine and m-xylene diamine	Linear thermoplastics and thermosets	-
<b>Quérette et al. (2019)<sup>133</sup></b>	Sebacic cyclic dicarbonate (from castor oil)	1,6-Hexamethylenediamine and tetramethylene diamine	Nanoparticles	-

<b>Bizet et al. (2020)<sup>134</sup></b>	Sebacic cyclic dicarbonate (from castor oil)	Priamine 1075	Hybrid waterborne dispersions	Coatings and adhesives
<b>Das et al. (2020)<sup>135</sup></b>	Carbonated soybean oil	Natural chitosan-based amine	Thermosets	Chemical resistant/ Coatings, sealants, and inorganic plant growth substrates
<b>Gomez-Lopez et al. (2020)<sup>136</sup></b>	Resorcinol dicarbonate (from argan oil)	Priamine 1074	Hybrid thermosets	Moisture-curable/ Adhesives
<b>Laprise et al. (2020)<sup>137</sup></b>	Waste-derived fish oil carbonate	Cardolite phenalkamine NC-540 and triamine derived from cardanol	Thermosets	-
<b>Mokhtari &amp; Malek (2020)<sup>138</sup></b>	Carbonated Jojoba oil	1,5-Pentanediamine	Thermosets	-
<b>Doley et al. (2021)<sup>139</sup></b>	Glycerol derived carbonate blended with carbonated soybean oil	Polyamidoamine	Thermosets	-
<b>Dong et al. (2021)<sup>87</sup></b>	Carbonated soybean oil and carbonated linseed oil	1,4-Butylenediamine, 1,5-pentanediamine, 1,6-hexamethylenediamine, 1,8-octanediamine	Thermosets	Foams
<b>Gholami et al. (2021)<sup>140</sup></b>	Carbonated soybean oil	Tetraethylenepentamine	Hybrid thermosets	Antibacterial/ Wound dressing
<b>Hambali et al. (2021)<sup>141</sup></b>	Carbonated rubber seed oil	Ethylenediamine	Thermosets	-

<b>Liu et al. (2021)<sup>142</sup></b>	Carbonated soybean oil	1,8-Menthanediamine (derived from turpentine)	Thermosets	Self-healable, recyclable, and shape memory
<b>Ren et al. (2021)<sup>143</sup></b>	Oligomeric ricinoleic acid derived carbonate	1,6-Hexamethylene diamine and isophoronediamine	Thermosets	-
<b>Sessini et al. (2021)<sup>144</sup></b>	Resorcinol dicarbonate (from argan oil)	Cadaverine, putrescine, and amino-telechelic oligoamide	Linear thermoplastics	Ferroelectric/ Sensors
<b>Yang et al. (2021)<sup>145-146</sup></b>	Carbonated soybean oil	4,4-Diaminodiphenyl methane and 4,4'-diaminodiphenyldisulfide	Thermosets	Recyclable, shape memory, and self-healable

**Table 2.2 - Plant-based polyhydroxyurethanes (fatty acids derived from plants inclusive)**

<b>Authors (year)<sup>reference</sup></b>	<b>Cyclic Carbonates</b>	<b>Amines</b>	<b>Type</b>	<b>Special feature/ Application</b>
<b>Bähr et al. (2012)<sup>147</sup></b>	Cyclic limonene dicarbonate	1,4-Butylenediamine, 1,6-hexamethylenediamine, 1,12-dodecanediamine, isophoronediamine, and tris(N-2-aminoethyl)amine	Linear thermoplastics and thermosets	-
<b>Liu et al. (2015)<sup>148</sup></b>	Gallic acid-based cyclic carbonate	Ethylenediamine, 1,6-hexamethylenediamine, isophoronediamine, and Jeffamine D230	Hybrid thermosets with polyhedral oligomeric silsesquioxanes	Coatings
<b>Liu et al. (2016)<sup>149</sup></b>	Rosin acid-based cyclic carbonate	Ethylenediamine, 1,6-hexamethylenediamine, isophoronediamine, and triethylenetetramine	Hybrid thermosets with polyhedral oligomeric silsesquioxanes	Coatings
<b>Janvier et al. (2017)<sup>150</sup></b>	Syringaresinol-based cyclic carbonate	Isophoronediamine and 1,10-diaminodecane	Linear thermoplastics	-
<b>Ménard et al. (2017)<sup>151</sup></b>	Ferulic acid-based carbonate	Isophoronediamine and 1,10-diaminodecane	Linear thermoplastics and thermosets	-

<b>Schimpf et al. (2017)</b> <sup>152</sup>	Cyclic limonene dicarbonate and polyfunctional carbonated pentaerythritol glycidyl ether	Priamine 1074 and 1,5-pentanediamine	Thermoplastics and thermosets	Coatings
<b>Esmacili et al. (2018)</b> <sup>153</sup>	Carbonated tannic acid	Diethylenetriamine and 4,4'-diaminodiphenylmethane	Thermosets	Cytocompatibility/ Biomaterials
<b>Santiago-Medina et al. (2018)</b> <sup>154</sup>	Lignin and dimethyl carbonate	1,6-Hexamethylenediamine	Linear thermoplastics	-
<b>Mimini et al. (2019)</b> <sup>155</sup>	Carbonated lignin	1,6-Hexamethylenediamine	Linear thermoplastics	-
<b>Blažek et al. (2020)</b> <sup>156</sup>	Diacarbonate derived from fatty acids	Priamine 1071, 1073, 1074, and 1075	Linear thermoplastics	-
<b>Capar et al. (2020)</b> <sup>157</sup>	Carbonated glycidyl ethers	Priamine 1071, branched polyethyleneimine, and Tris(2-aminoethyl)amine	Thermosets	Fast curing
<b>Chen et al. (2020)</b> <sup>158</sup>	Tannin dicyclic carbonate	1,6-Hexamethylenediamine	Thermosets	Rigid foams
<b>Chen et al. (2020)</b> <sup>159</sup>	Mix of glucose-based carbonates and tannin-based carbonate	1,6-Hexamethylenediamine	Thermosets with glucose fillers	Composites/ bio-foams

<b>Chen et al. (2020)<sup>160</sup></b>	Carbonated bark oil	Ethylenediamine, 1,6-hexamethylenediamine, isophoronediamine, diethylenetriamine, and tris(2-aminoethyl)amine	Thermosets	-
<b>Sternberg &amp; Pilla (2020)<sup>161</sup></b>	Carbonated lignin	Priamine 1074	Thermosets	Shape memory/ foams
<b>Zhang et al. (2020)<sup>162</sup></b>	Bisphenol A cyclic carbonate	Priamine 1075	Hybrid thermosets	Anticorrosive/ Coatings
<b>Chen et al. (2021)<sup>163</sup></b>	Tannin-based carbonates	1,6-Hexamethylenediamine	Thermosets with non-furanic humins	Adhesives
<b>Dong et al. (2021)<sup>87</sup></b>	Thrive culinary algae oil and high PUFA algal oil carbonates	1,4-Butylenediamine, 1,5-pentanediamine, 1,6-hexamethylenediamine, 1,8-octanediamine	Thermosets	Foams
<b>Liu et al. (2021)<sup>142</sup></b>	Carbonated soybean oil	1,8-Menthanediamine (derived from turpentine)	Thermosets	Self-healable and shape memory
<b>Zhao et al. (2021)<sup>164</sup></b>	Dimethylpropane carbonate	Priamine 1074	Thermosets with lignin additives	Recyclable, shape memory, self-healing, and composites /Smart packaging label and paper composite laminate

**Table 2.3 - Glycerol-based polyhydroxyurethanes (polyoyl belonging to the same family inclusive)**

<b>Authors (year)<sup>reference</sup></b>	<b>Cyclic Carbonates</b>	<b>Amines</b>	<b>Type</b>	<b>Special feature/ Application</b>
<b>Benyahya et al. (2011)<sup>165</sup></b>	Dicyclic carbonates synthesized from glycerol carbonate	1,10-Diaminodecane	Linear thermoplastics	-
<b>Fleischer et al. (2013)<sup>166</sup></b>	Glycerol cyclic carbonate blend with other polyoyls	1,6-Hexamethylenediamine and citric acid amino amides	Thermosets with cellulose carbonate fillers	Composites
<b>Carré et al. (2015)<sup>167</sup></b>	Carbonate based on glycerol carbonate and dimeric fatty acid	Priamine 1071 and 1075	Linear thermoplastics and thermosets	-
<b>Tryznowski et al. (2015)<sup>168</sup></b>	Diglycerol carbonate-based cyclic carbonate	Various diamines (ten different kinds)	Linear thermoplastics	-
<b>Van Velthoven et al. (2015)<sup>169</sup></b>	Diglycerol dicarbonate	1,4-Butylenediamine, 1,5-pentanediamine, isoidide diamine, 1,9-nonanediamine, and Priamine 1075	Linear thermoplastics	-
<b>Blattmann et al. (2016)<sup>170</sup></b>	Carbonated trimethyloxypropane glycidylether	1,6-Hexamethylenediamine	Thermosets	Flexible foams
<b>Blattmann et al. (2016)<sup>171</sup></b>	Carbonated polyoyls	1,6-Hexamethylenediamine and isophoronediamine	Hybrid thermosets	Casting and coatings

<b>Blattmann et al. (2016)</b> <sup>172</sup>	Carbonated polyoyls	Biobased diamines from polyoyls and limonene and 1,6-hexamethylenediamine	Thermosets	-
<b>Lamarzelle et al. (2016)</b> <sup>173</sup>	Glycerol-based cyclic carbonates	1,10-Diaminodecane and 1,3-cyclohexanedi(methylamine)	Linear thermoplastics	-
<b>Hibert et al. (2016)</b> <sup>174</sup>	Glycerol-based cyclic carbonates	Bioalcohol-based primary amine and 1,10-Diaminodecane	Linear thermoplastics	-
<b>Nohra et al. (2016)</b> <sup>175</sup>	Glycerol-based cyclic carbonate	Ethylenediamine, 1,6-hexamethylenediamine, and triethylenetetramine	Linear thermoplastics and thermosets	-
<b>Rix et al. (2016)</b> <sup>176</sup>	Carbonate based on glycerol carbonate and fatty acid	Priamine 1075	Waterborne latexes	-
<b>Schmidt et al. (2016)</b> <sup>177</sup>	Glycerol-based sorbitol tricarboxylate	Priamine 1074 and isophoronediamine	Thermosets	Cure at ambient temperature/ Coatings
<b>He et al. (2017)</b> <sup>178</sup>	Carbonate based on glycerol carbonate and fatty acid	Triethylenetetramine and diethylenetriamine	Hybrid thermosets	Coatings
<b>Karami et al. (2017)</b> <sup>179</sup>	Furfuryl glycidyl ether derived from glycerol	Diethylenetriamine	Thermosets	Thermo-healable
<b>Lamarzelle et al. (2017)</b> <sup>180</sup>	Thioglycerol-based cyclic carbonate	1,10-Diaminodecane, isophoronediamine, and Primanie 1075	Linear thermoplastics	-
<b>Bossion et al. (2018)</b> <sup>181</sup>	Diglycerol dicarbonate	1,12-Dodecanediamine and Jeffamine ED 2003	Linear thermoplastics	Segmented poly(hydroxyurea-urethanes)

<b>Tryznowski et al. (2018)</b> <sup>81</sup>	Diglycerol dicarbonate	1,4-Butylenediamine	Linear thermoplastics	-
<b>Bossion et al. (2019)</b> <sup>182</sup>	Diglycerol dicarbonate	Aminoalkyl-terminated poly(dimethylsiloxane)	Waterborne dispersions	Networks formation by ionic interaction and self-healable
<b>Karami et al. (2019)</b> <sup>183</sup>	Carbonate based on glycerol	Diethylenetriamine	Thermosets	Antibacterial networks
<b>Magliozzi et al. (2019)</b> <sup>184</sup>	Diglycerol dicarbonate	1,6-Hexamethylenediamine and 1,10-diaminodecane	Linear thermoplastics	-
<b>Peixoto et al. (2019)</b> <sup>185</sup>	Diglycerol dicarbonate	Lysine and protein-based amines	Linear thermoplastics	-
<b>Schimpf et al. (2019)</b> <sup>186</sup>	Glycerol carbonate methacrylate	Several diamines were used	Hydroxyurethane methacrylate	Photocurable films/ 3D Printing
<b>Magliozzi et al. (2020)</b> <sup>187</sup>	Diglycerol dicarbonate	Tris(2-aminoethyl)amine and tris(2-(methylamino)ethyl)amine)	Thermosets	Hydrolysable and shape memory
<b>Wang et al. (2020)</b> <sup>188-189</sup>	Diglycerol dicarbonate	Isophoronediamine, furfurylamine, furan methylamine and trimethylolpropane tris(poly[propylene glycol], amine terminated) ether, or tris(2-aminoethyl) amine	Thermosets	Self-healable
<b>Younes et al. (2020)</b> <sup>190</sup>	Diglycerol dicarbonate	Jeffamine D-2000, Priamine 1074, and aminopropyl-terminated polydimethylsiloxane	Hybrid thermosets	Moisture-curable/ Adhesives and sealants
<b>Zhang et al. (2020)</b> <sup>191</sup>	Diglycerol dicarbonate	Priamine 1075	Hybrid waterborne	Coatings

<b>Blázquez et al. (2021)<sup>192</sup></b>	Cyclic dicarbonates based on polyether polyol	Priamine 1071	Thermosets	-
<b>Buchheit et al. (2021)<sup>193</sup></b>	Glycerol carbonate methacrylate	1,5-pentanediamine, Jeffamine EDR-148, and Jeffamine THF-170	Functionalized hydroxyurethane methacrylate	Photocurable/ 3D Printing
<b>Doley et al. (2021)<sup>139</sup></b>	Glycerol derived carbonate blended with carbonated soybean oil	Polyamidoamine	Thermosets	-
<b>Magliozzi et al. (2021)<sup>35</sup></b>	Diglycerol dicarbonate	1,6-Hexamethylenediamine, 1,10-diaminodecane, and m-xylene diamine	Linear thermoplastics	-
<b>Pronoitis et al. (2021)<sup>194</sup></b>	Diglycerol dicarbonate	2,2'-(Ethylenedioxy)bis (ethylamine)	Grafted linear thermoplastic	-
<b>Younes &amp; Maric (2021)<sup>195</sup></b>	Diglycerol dicarbonate	Jeffamine D-2000, Priamine 1074, and aminopropyl-terminated polydimethylsiloxane	Hybrid thermosets	Increased hydrophobicity and moisture-curable/ Adhesives and sealants
<b>Younes &amp; Maric (2021)<sup>196</sup></b>	Diglycerol dicarbonate	1,10-diaminodecane, Priamine 1074, and aminopropyl-terminated polydimethylsiloxane	Linear thermoplastics	Terpolymerizations/ plasticizers and toughening agents

**Table 2.4 - Sugar-based polyhydroxyurethanes (fatty acids derived from sugars inclusive)**

<b>Authors (year)<sup>reference</sup></b>	<b>Cyclic Carbonates</b>	<b>Amines</b>	<b>Type</b>	<b>Special feature/ Application</b>
<b>Besse et al. (2013)<sup>197</sup></b>	Isosorbide cyclic dicarbonate (from glucose)	Jeffamine D-400, 1,10-diaminodecane, diethylenetriamine and isophoronediamine	Linear thermoplastics	-
<b>Mazurek-Budzyńska et al. (2016)<sup>198</sup></b>	Mannitol and sorbitol cyclic dicarbonate (from glucose)	1,4-Butylenediamine and 1,6-hexamethylenediamine	Thermosets	-
<b>Ma et al. (2017)<sup>199</sup></b>	Diphenolic acid-based cyclic carbonate (derived from cellulose)	Ethylenediamine, diethylenetriamine, and isophoronediamine	Linear thermoplastics, thermosets and waterborne dispersions	Coatings
<b>Schmidt et al. (2017)<sup>200</sup></b>	Erythritol dicarbonate	Isophoronediamine, 1,6-hexamethylenediamine, and Pripol 1009	Linear thermoplastics	-
<b>Schmidt et al. (2017)<sup>201</sup></b>	Sorbitol ether carbonate and sorbitol tricarboxylate	Priamine 1074, 1,6-hexamethylenediamine, isophoronediamine, and Jeffamine DT403	Thermosets	-
<b>Zhang et al. (2017)<sup>202</sup></b>	2,5-Furandicarboxylic acid-based cyclic dicarbonate (derived from cellulose)	1,6-Hexamethylenediamine, 1,8-octanediamine, and isophoronediamine	Linear thermoplastics	-
<b>Clark et al. (2018)<sup>203</sup></b>	Sorbitol cyclic dicarbonate	Pentamethylene diamine (obtained from lysine) and 1,6-hexamethylenediamine	Linear thermoplastics	Self-blowing foams

<b>Furtwengler et al. (2018)</b> <sup>204</sup>	Sorbitol cyclic dicarbonate	1,4-Butylenediamine and Priamine 1075	Linear thermoplastics	-
<b>Wu et al. (2018)</b> <sup>205</sup>	Sorbitol polycarbonate	Ethylenediamine, 1,4-butylenediamine, 1,6-hexamethylenediamine, isophoronediamine, and 1,8-octanediamine	Waterborne dispersions	Coatings
<b>Xi et al. (2018)</b> <sup>206</sup>	Glucose and sucrose with dimethyl carbonate	1,6-Hexamethylenediamine	Thermosets	Adhesives and coatings
<b>Yu et al. (2018)</b> <sup>207</sup>	Sucrose soyate polycarbonate	Tris(2-aminoethyl)amine	Thermosets	Coatings
<b>Hu et al. (2019)</b> <sup>131</sup>	Sorbitol polycarbonate	Priamine 1074 and diethylene glycol bis(3-aminopropyl) ether	Thermosets	Reprocessable networks
<b>Xi et al. (2019)</b> <sup>208-209</sup>	Glucose with dimethyl carbonate	1,6-Hexamethylenediamine	Thermosets	Flame retardant/ Rigid foams
<b>Xi et al. (2019)</b> <sup>210</sup>	Sucrose with dimethyl carbonate	1,6-Hexamethylenediamine	Thermosets	Adhesives
<b>Choong et al. (2021)</b> <sup>211-212</sup>	Furan-based dicarbonates	Furan-based diamines	Thermosets	Thermo-healable, moisture-healable and self-healable/ Coatings
<b>Younes &amp; Maric (2021)</b> <sup>213</sup>	Sorbitol and mannitol dicarbonates	Jeffamine D-2000 and aminopropyl-terminated polydimethylsiloxane	Hybrid thermosets	Moisture-curable/ Adhesives and sealants

## 2.1 Polyhydroxyurethanes synthesized from vegetable oils and their fatty acids

Vegetable oils and triglycerides are diverse and abundant because they chemically and physically differ from one source to another. Many have served as precursors for cyclic carbonates, as revealed in Table 2.1, and because their final molecular structure contains more than two cyclic carbonates, they lead in most cases to crosslinked polymeric networks. PHUs from carbonated soybean oil (CSBO) were mostly studied for potential applications as coatings,<sup>102, 130, 135</sup> scaffolds,<sup>114</sup> adhesives,<sup>128</sup> wound dressings,<sup>140</sup> and foams.<sup>87</sup> Also, Lee et al. created hydroxyurethane bridges from CSBO molecules with silane coupling agents to attach lignin,<sup>214</sup> and recently, self-healable, reprocessable, recyclable, and shape memory PHU networks from CSBO were developed.<sup>131, 142, 145-146</sup> Among these studies, Liu et al. prepared a fully bio-based PHU dynamic networks from CSBO and a turpentine sourced diamine.<sup>142</sup>

Besides, other vegetable oils, such as linseed and sunflower oils, were investigated for the preparation of PHU thermosets suitable as composite coatings<sup>111, 122-124, 129</sup> and for the medical field.<sup>125</sup> However, side reactions might occur when CSBO and other carbonated vegetable oils are involved since the ester groups, present in their molecular structures, are subject to cleavage during the polyaddition reaction causing amide formation and polyoyl emission. Polyoyls negatively affect the network formation by plasticizing the final PHU networks.<sup>100, 105</sup> Hence, many have started to switch to carbonated fatty acids and phenols derived from vegetable oils, summarized in Table 2.1, to avoid these side reactions. In fact, Bizet et al. were successful in preparing waterborne PHUs (WPHU) coatings and adhesives from sebacic acid cyclic carbonates,<sup>134</sup> and Gomez-Lopez et al. developed moisture-curable hybrid PHUs (HPHU) from resorcinol dicarbonates, derived from argan oil, to be applied as adhesives.<sup>136</sup>

## 2.2 Polyhydroxyurethanes synthesized from plant-based materials and fatty acids

Similarly to carbonated fatty acids, cyclic carbonates obtained from compounds derived from plants do not contain ester groups; hence, their polyaddition with diamines does not involve side reactions.<sup>147</sup> If not cured, the resulting PHUs are linear and do not have branches and/or crosslinks, contrary to those obtained from carbonated vegetable oils. Among the PHUs listed in Table 2.2, the ones made from cyclic limonene dicarbonates (CLD) seem to be very popular, as limonene can be extracted from orange peels, a daily organic waste derived from orange juice manufacture,<sup>152</sup> contrary to other bio-based raw materials that are extracted from important resources for the food and nutrition industries, such as living plants, seeds, and vegetable oils.<sup>24</sup> Moreover, effort has been lately put towards optimizing the epoxidation and carbonation reactions of limonene by developing new catalysts.<sup>27, 37, 39, 41-42, 59, 215-219</sup> It was found that epoxidized limonene affords much higher CO<sub>2</sub> fixation than epoxidized vegetable oils, which is better from a green chemistry point of view.<sup>147</sup> In terms of applications, CLD-based PHU coatings were synthesized by Schimpf et al. using Priamine 1074, a diamine derived from dimer fatty acids, to afford 100% bio-based thermosets.<sup>152</sup>

Furthermore, cyclic carbonate monomers derived from plant-derived fatty acids, such as gallic,<sup>148</sup> rosin,<sup>149</sup> and tannin acids<sup>153, 158-159, 163</sup> were polymerized with different diamines to make PHU thermosets, hybrids, and composites seen as potential coatings, rigid foams, biomaterials, and adhesives. Interestingly, carbonated lignin and algae oils were recently prepared, and their respective PHUs had promising properties for a foam and shape memory foam application, respectively.<sup>87, 161</sup> Also, Priamine 1074, Priamine 1075, and 1,8-menthane diamine, which are derived from fatty acids and turpentine, respectively, were polymerized with synthetic cyclic dicarbonates and then cured with their final PHU thermosets

showing interesting anticorrosive,<sup>162</sup> self-healable, and shape memory<sup>142, 164</sup> features to be used in the coatings and packaging industries.

### **2.3 Polyhydroxyurethanes synthesized from glycerol and its derivatives**

Glycerol is a renewable source generated as byproduct from different processes converting vegetable oils to soap, fatty acids, and fatty esters. It can also be obtained from biomass conversion via triglyceride hydrolysis or methanolysis and from biodiesel production processes.<sup>24</sup> Its worldwide annual production has increased over 200% between the years 2000 and 2010, and it was predicted that by the year 2020, its production would be 6 times more than the demand,<sup>24, 220</sup> which makes it an abundant raw material for the preparation of PHUs.

The glycerol derivative that has been mostly investigated in the literature is diglycerol dicarbonate (DGC), as observed from Table 2.3. DGC is synthesized from diglycerol via a simple transesterification reaction with dimethyl carbonate (DMC), and it was found to have a low melting point of 65 °C which allowed the polyadditions to be conducted in bulk, moderate temperatures, and without any catalyst.<sup>169</sup> Hence, PHUs of different types and features were synthesized from this cyclic dicarbonate starting with simple linear thermoplastics to more complex self-healable WPHU,<sup>182</sup> hybrid WPHU coatings,<sup>191</sup> shape memory and self-healable PHU thermosets,<sup>187-189</sup> and moisture-curable HPHUs to be eventually applied as sealants and adhesives.<sup>190, 195</sup>

Nevertheless, many other di and poly(carbonates) were synthesized from glycerol as the starting material, such as glycidyl ether-based carbonates and sorbitol tricarboxylate, and they were polymerized with different diamines to afford PHU composites<sup>166</sup> as well as thermosets and hybrids that are thermo-healable<sup>179</sup> and antibacterial.<sup>183</sup> In terms of applications, these thermosets were designed to fit in as coatings<sup>171, 177-178</sup> and flexible foams.<sup>170</sup> Interestingly, the

studies by Schimpf et al. and Buchheit et al. used a carbonated glycerol methacrylate to prepare hydroxyurethane methacrylate (HUMA) that are photocurable and can be applied in 3D printing.

186, 193

## 2.4 Polyhydroxyurethanes synthesized from sugar derived materials

Among the sugar-based cyclic carbonates presented in Table 2.4, sorbitol bicarbonates (SBC) and poly(carbonates) were mostly used in the synthesis of PHUs. Sorbitol is an abundant and cheap sugar that is added as a sweetener to many commercialized edible products. It is primarily extracted from cellulose and can be obtained from the decomposition of polysaccharides, such as starch, dextrin, and malt dust.<sup>221</sup> Similar to the synthesis of DGC, SBC is prepared from the transesterification of sorbitol and DMC.<sup>198</sup> The polymerization of SBC with a lysine derived diamine formed CO<sub>2</sub> that was responsible of obtaining fully bio-based self-blowing foam PHUs.<sup>203</sup> Also, SBC along with its diastereomer mannitol bicarbonate (MBC) were polymerized with long chain diamines to prepare PHUs that were reacted afterwards with silane agents so that the final HPHUs were moisture-curable.<sup>213</sup> One difference between SBC and DGC is its high melting point which is close to 200 °C, making it harder to conduct the polyadditions in bulk and moderate temperatures. Solution or melt polymerizations are usually adopted in such cases.<sup>198,</sup><sup>200</sup> Besides, reprocessable PHU and WPHUs coatings were prepared from sorbitol poly(carbonates).<sup>131, 205</sup>

Moreover, Yu et al. synthesized poly(carbonates) from sucrose soyate and crosslinked them with triamine to prepare PHU coatings,<sup>207</sup> whereas Choong et al. used furan-based dicarbonates and diamines to make thermo, moisture, and self-healable coatings which they recently patented.<sup>211-212</sup> On the other hand, Xi et al. reacted sucrose and glucose with DMC and blended them with 1,6-hexamethylenediamine to afford PHUs that can be used as coatings,

adhesives, and rigid foams.<sup>206, 208-210</sup> Finally, fatty acids derived from sugars, like diphenolic acid from cellulose, were carbonated, and they were incorporated in a WPHU coatings system.

199

## **2.5 Conclusion and thesis work considerations**

While CSBO was the first renewable cyclic carbonate to be investigated in the preparation of PHUs, numerous bio-sourced cyclic di and poly(carbonates) have followed in the last decade. As any research topic, the early renewable PHUs focused merely on preparing and characterizing the obtained thermoplastics and thermosets, but after 2017, an advancement in the field was obvious with the research and development focusing on making HPHUs and WPHUs for specific industrial applications, like coatings, adhesives, and foams, and creating smart PHU materials that can moisture-cure, self-heal, and photocure.

To prepare linear PHUs, one has to be content with renewable cyclic dicarbonates and diamines. Among the bio-based sources, it seems that diglycerol, sorbitol/mannitol, and limonene present an abundant platform of sustainable dicarbonates. However, the epoxidation and carbonation of limonene are still under investigation, as higher yields and better selectivity still have to be achieved. The transesterification reactions of diglycerol and the sugars present a reasonably straightforward alternative that is more economically viable from an industrial perspective. Therefore, the work in this thesis focuses on diglycerol, sorbitol, and mannitol as the bio-based building blocks to prepare the cyclic dicarbonates. On the other hand, Priamine 1074, commercialized by Croda, is a cheaper bio-based diamine with a high purity; hence, it was selected as the sustainable diamine building block in this work.

The different projects of this manuscript-based thesis can be divided into two categories; industrial and academic. The industrial projects are presented in the first three chapters in which

moisture-curable HPHUs were synthesized,<sup>190, 195, 213</sup> and it was shown for the first time that the films can cure within a 24 h window at ambient conditions without using an external heating source to accelerate the curing, like Gomez-Lopez et al. and Deconstanzi et al. did in their studies.<sup>136, 222</sup> ADFAST Corp., the partner on the industrial projects, shared their isocyanate-based formulation which was used as a benchmark while making the non-isocyanate analogs. Chapter 3 and Chapter 4 discuss the preparation of DGC and sugar-based moisture-curable HPHUs, respectively, with an intention to applying them as sealants and adhesives. Chapter 5 uses a PHU extension method to make moisture-curable HPHUs with increased hydrophobicity based on a PHU made from DGC and a poly(propylene glycol) (PPG)-based diamine. This chapter is important as PPG-based diols have been used in the formulation of conventional PU sealants and adhesives, as it is going to be discussed later in the concluding sections of the thesis.

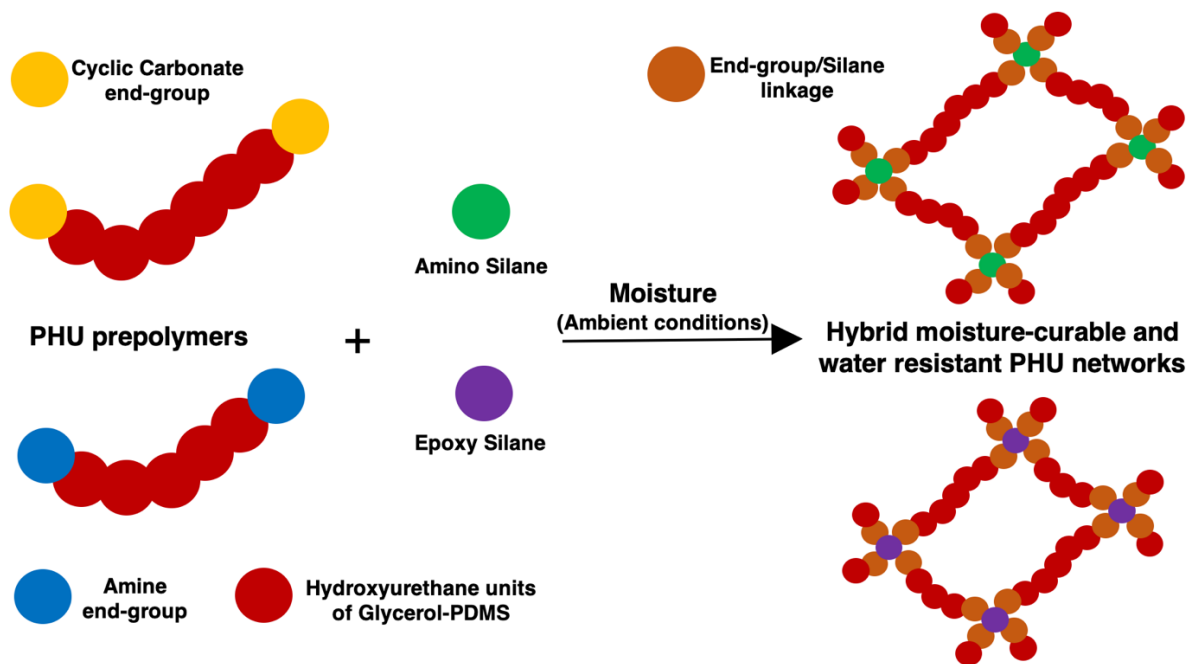
As for the academic projects, the first one presented in Chapter 6 deals with the synthesis of partially and fully bio-based thermoplastic PHUs (TPHU) using a terpolymerization system. The segmented microstructure of the TPHUs was characterized and rheologically studied. Additionally, the TPHUs were blended with poly(lactic acid) (PLA) to study their role as plasticizers and toughening agents on the biopolymer matrix. The melt-blending of PHUs into PLA is studied for the first time, to the best of our knowledge, in Chapter 6. Furthermore, Chapter 7 mainly focuses on the synthesis of bio-based and hydrolytically degradable photocurable hydroxyurethane acrylates (HUA). Priamine 1074 is used as the building block for the hydroxyurethanes from which degradable caprolactone moieties were grown. The final macromolecules were acrylated from both ends to make a novel, telechelic photocurable macromonomer which is distinct from previously published studies on nondegradable HUMA.

<sup>186, 193</sup> Seeing that this thesis is manuscript-based, Chapter 3 to Chapter 7 were submitted to peer-reviewed journals, and they are published.

## Chapter 3

### Study of moisture-curable hybrid NIPUs based on glycerol with various diamines: emergent advantages of PDMS-diamines

The manuscript of this chapter was published in *ACS Omega* in 2020 (Younes, G. R.; Price, G.; Dandurand, Y.; Maric, M., Study of Moisture-Curable Hybrid NIPUs Based on Glycerol with Various Diamines: Emergent Advantages of PDMS Diamines. *ACS Omega* **2020**, 5 (47), 30657-30670).<sup>190</sup> This chapter constitutes the proof of concept for the preparation of partially bio-based HPHUs from DGC and long chain diamines derived from PPG and poly(dimethyl siloxane) (PDMS). This manuscript achieves, for the first time, moisture (or sol/gel) curing of the PHUs at ambient lab conditions and provides guidelines on the development of such materials in bulk. The supporting information of this manuscript is included in Appendix A.



### 3.1 Abstract

A sol/gel curing method is used in this work to synthesize hybrid partially bio-based polyhydroxyurethanes (PHUs) from dicarbonates derived from glycerol and various diamines. The method consists of end-capping the PHU prepolymers with moisture sensitive groups, so sealants and adhesives can be produced from partially sustainable hybrid PHUs (HPHUs), similarly to their preparation from end-capped conventional polyurethanes. Diglycerol dicarbonate (DGC) is synthesized and polymerized with different diamines of various chain lengths, and the resulting PHU structural and thermal properties are qualitatively and quantitatively characterized. This characterization led to two potential candidates; PHU 4, made of DGC and a poly(propylene glycol) diamine, and PHU 10, prepared from DGC and a poly(dimethylsiloxane) diamine. These polymers, with respective relative average number molecular weights of 3,200 and 7,400 g/mol, are end-capped and left to cure at ambient lab conditions (22 °C and 40-50% humidity), and the curing processes are monitored rheologically. Notably, the moisture curing does not require any catalyst. The chemical stability of the resulting hybrid PHUs, HPHUs 4 and 10, in pure water is investigated to check the viability of applying them under outdoor conditions. Only HPHU 10 is found to be resistant to water and shows hydrophobicity with contact angles of 109°. Tensile tests are conducted on HPHU 10 samples cured under lab conditions for a week and others cured for another week while being immersed in water. The mechanical properties: tensile strength and elongation at break; improve with the samples cured in water, indicating the high water repellency of HPHU 10.

### 3.2 Introduction

Polyurethanes (PUs) have become one of the most widely used industrial polymers since they were first discovered by Bayer et al. in 1937.<sup>1-4</sup> More specifically, PU sealants are known to be cheap, having long shelf and pot lives, resisting aging, having good anti-flammability properties and a wide range of applications in indoor and outdoor conditions as well as in porous and non-porous materials.<sup>4</sup> As any conventional PU, they are synthesized from the polyaddition of diisocyanates with diols, and the resulting PU prepolymers are cured using moisture-curable agents to get the final sealants.<sup>2-4</sup> Since the –NCO end-groups in the prepolymer chain are very reactive, it is common to end-cap the oligomers with moisture-curable silane terminated groups to produce self-crosslinkable PUs in presence of moisture.<sup>5-11</sup>

However, many environmental and health issues are associated with the synthesis of conventional PUs, as the diisocyanates are produced from phosgene, which is known to be a lethal gas.<sup>3, 12-14</sup> Besides, conventional PUs are too moisture-sensitive, and hence chemically unstable.<sup>12</sup> Thus, new routes have been developed for non-isocyanate polyurethanes (NIPUs) synthesis<sup>15</sup> with the step-growth polyaddition of five-membered cyclic dicarbonates with diamines investigated the most because it does not form lower molecular weight byproducts and its precursors are abundant.<sup>3, 12-19</sup> These NIPUs are also known as poly(hydroxyurethane)s (PHUs) because hydroxyl pendant groups are present in the resulting polymer backbone. As summarized by Maisonneuve et al., cyclic carbonates can be synthesized via different ways leading to five-membered, six-membered, and seven-membered mono/polycyclic carbonates.<sup>17</sup> More specifically, the route involving the chemical fixation of carbon dioxide (CO<sub>2</sub>) into epoxy (or oxirane) groups received most researchers' attention, seeing its importance from a green chemistry perspective.<sup>16, 20-23</sup> With the many commercially available diamines, various cyclic

dicarbonate/diamine couples were studied, and their respective PHUs showed similar mechanical properties, chemical resistance, and thermal stability as well as lower permeability compared to conventional PUs. PHUs were also investigated for the preparation of sealants by Figovsky et al., who synthesized acrylic-modified petrochemical PHUs that cure under ultraviolet radiation to give hybrid PHU (HPHU) sealants with high performance.<sup>24, 25</sup>

While HPHUs have not been extensively studied, there exist different methods to synthesize them.<sup>3, 26</sup> For the synthesis of HPHU sealants and adhesives, the sol/gel or moisture-curing method is considered to be the best. Hence, this work uses sol/gel curing method, as shown in Scheme 3.1, to synthesize new partially bio-based HPHUs by end-capping the PHU prepolymers with moisture curable agents. These agents can be either silane terminated amines, such as N-(2-aminoethyl)-3-aminopropyltrimethoxysilane (termed DAMO), when the end-group is a cyclic carbonate or silane terminated epoxies, like [3-(2,3-epoxypropoxy)-propyl]-trimethoxysilane (termed GLYMO), when the end-group is an amine. Once this is done, the resulting end-capped prepolymers would be ready to self-link through a moisture curing mechanism, leading to HPHUs, similarly to an end-capped conventional PU sealants and adhesives.

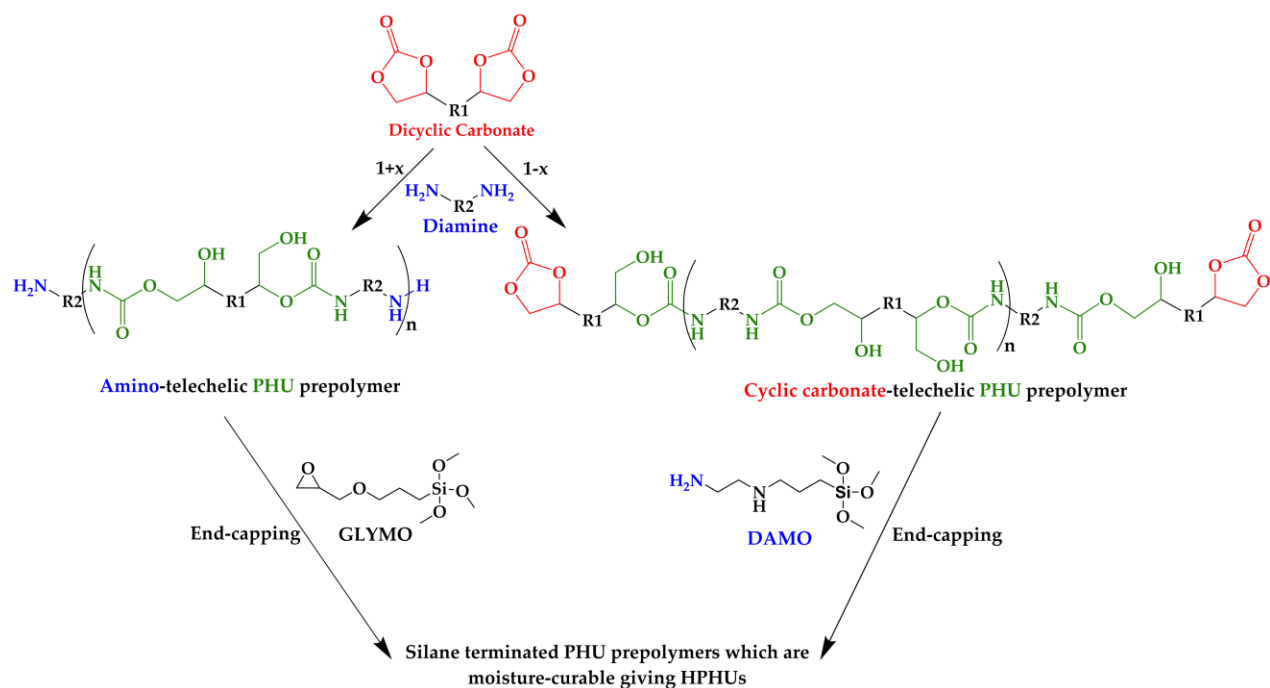
Similar studies were conducted by Gomez-Lopez et al., who recently synthesized moisture curable PHUs from resorcinol and poly(propylene glycol) (PPG) dicarbonates, with DAMO as the moisture curable agent. However, in order to obtain faster curing of their samples they had to increase the temperature to 100 °C and add acetic acid as catalyst,<sup>27</sup> which were issues overcome in the present study. Moisture curable HPHUs were achieved at ambient conditions and without the use of a catalyst. Additionally, Deconstanzi et al. reacted DAMO with poly(propylene oxide) dicarbonate as well as carbonate propyltrimethoxysilane with Priamine

1075, a bio-based diamine, or aminopropyl terminated poly(dimethylsiloxane) (PDMS) with  $M_n = 2,500$  g/mol, and they observed lower swelling index within their PPG based HPHUs, compared to the other materials, when immersed in THF for 24 h.<sup>28</sup> Sol/gel HPHUs were also investigated by Rossi de Aguiar et al. using PDMS-based cyclic dicarbonate with isophorone diamine and DAMO. The resulting hybrid polymer coatings had high thermal stability.<sup>29</sup>

This work, on the other hand, uses the chemistry described in Scheme 3.1 to make partially bio-based HPHUs. Diglycerol (DIG) is used as precursor of the cyclic dicarbonates of this work. Among the bio-renewable sources studied in the last decade,<sup>16, 24, 30-33</sup> researchers have shown interest in glycerol since it can be obtained from biomass wastes via hydrolysis or methanolysis of triglycerides and from biodiesel processes. Its worldwide annual production has increased over 200% between the years 2000 and 2010, and it was predicted that by the year 2020 its production would be six times more than demand,<sup>24, 34</sup> which makes it an abundant raw material for the preparation of the new sustainable HPHU sealants and adhesives. Many studies have prepared and characterized diglycerol dicarbonate (DGC)-based PHUs prepared from diamines of different chain lengths.<sup>35-42</sup> As for the diamines bio-based and petrochemical ones are available, and this work uses both with more attention given to poly(dimethylsiloxane) diamines expected to make PHUs of high value-added end properties.<sup>29</sup>

In this work, a different chemistry path is used to afford PDMS or PPG/DGC moisture curable HPHU sealants and adhesives, compared to previously cited studies. DGC is first reacted with diamines of different chain lengths, including bio-derived ones, PPG, and PDMS diamines, after which a screening of the resulting PHUs depending on their molecular weight, viscosity, texture, color, and thermal properties is conducted to select the potential DGC/diamine candidates for end-capping, presented in Scheme 3.1. The curing kinetics, at ambient conditions

and without the use of a catalyst, are studied to identify the gel time needed to form the HPHU films. Interaction of the cured polymers with water is also studied to ensure that they are chemically stable and exhibit resistance to water.

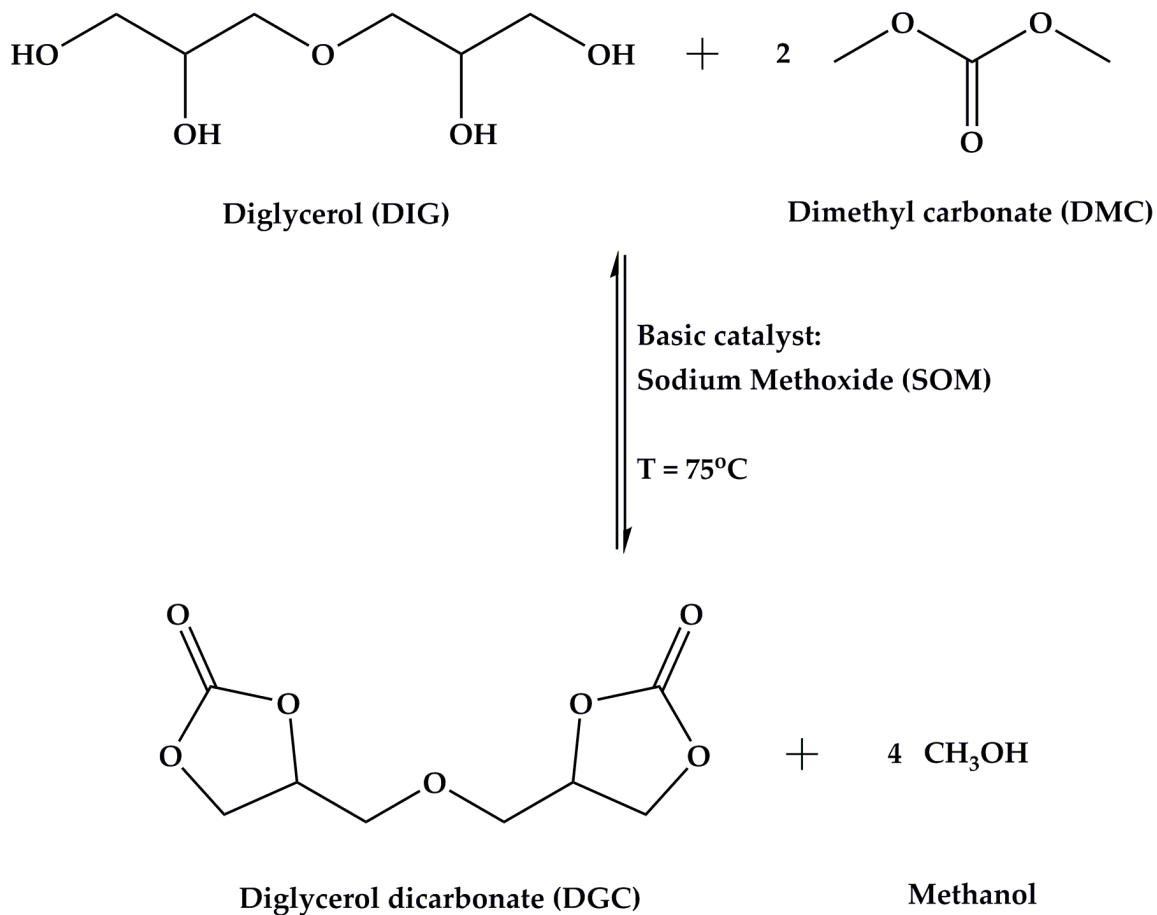


**Scheme 3.1 - Moisture-curing method based on end-capping the carbonate and diamine end-groups of PHU prepolymers (proposed in this work)**

### 3.3 Results and Discussion

#### 3.3.1 DGC reaction and kinetics

The evolution of the reaction between DIG and DMC was tracked to understand the mechanism underlying it and hopefully optimize the synthesis. It is considered to be a complex reaction since it is reversible and has to go through three intermediates before obtaining DGC. Scheme 3.2 gives the overall reaction scheme, and Figure 3.1 summarizes the evolution of the reactants' consumption and products' formation during 24 h.



**Scheme 3.2 - Synthesis of DGC from DIG and DMC transesterification reaction**

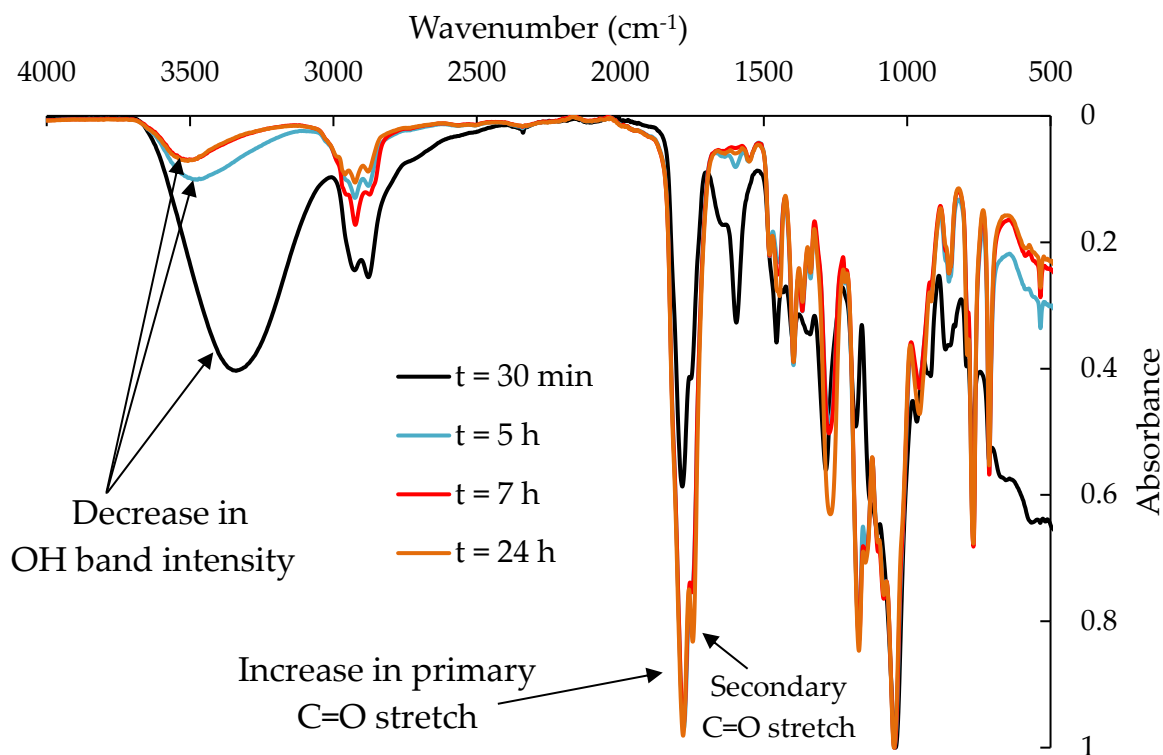


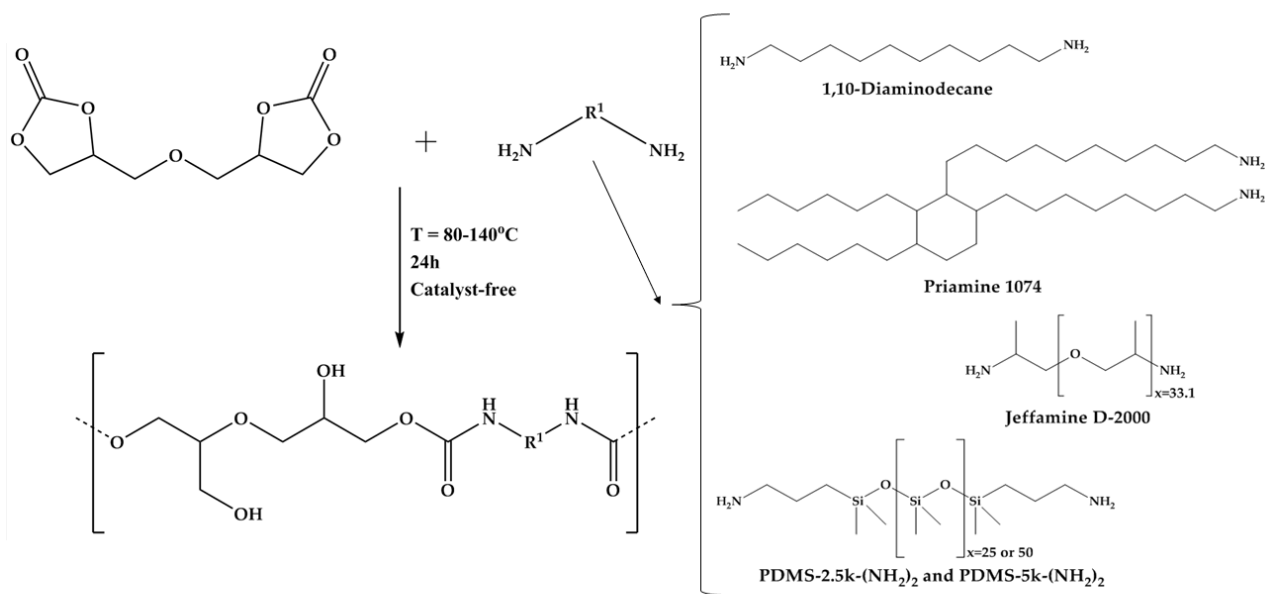
**Figure 3.1 - Kinetic study tracking the evolution of the reaction between DIG and DMC to get DGC, the renewable monomer of this study.**

As expected and shown in the FTIR spectra of Figure 3.1, the intensity of the OH band decreases with the consumption of DIG while the primary C=O stretch at  $1780\text{ cm}^{-1}$  increases with the formation of DGC (see Figure A.1). These changes are observed until 7 h of the reaction were reached, after which the FTIR spectra quasi-overlapped. The only difference between the spectra taken at 7 h and 24 h is the increase in the secondary C=O stretch at  $1750\text{ cm}^{-1}$ , which can be either that of the intermediates which form before obtaining DGC or that of the byproducts produced throughout the reaction as the DIG sample has originally up to 20 wt.% of impurities. Also, the fact that the OH band intensity stopped decreasing after 7 h can be attributed to one of the following factors; the impurities in the original DIG batch, the reaction reaching equilibrium, or both.

To complement the kinetic study, two DGC synthesis reactions were allowed to proceed for 8 h and 24 h, and both gave similar DGC yields of 51% and 47%, respectively. Additionally, the residual product from the latter, after the evaporation of DMC and methanol, was brown leading to addition of more EtAc compared to the former, and the purification was given more time to obtain the final product. Perhaps the increase in the reaction byproducts and/or DGC intermediates, during the 24 h reaction, could have caused this darker brown color, compared to the 8 h reaction. Finally, a white DGC powder was obtained at the end of both reactions with the <sup>1</sup>H-NMR and FTIR spectra given in the supporting information as Figure A.1 and Figure A.2.

### **3.3.2 Characterization and screening of PHU prepolymers**

The polyaddition between DGC and the diamines is presented in Scheme 3.3. Seeing that DGC has a melting point at around 65 °C, <sup>35, 36</sup> it was possible to conduct the polyadditions at moderate temperatures and in bulk, while obtaining high monomer conversions. Besides and as mentioned in previous studies, no catalyst was needed to synthesize the PHU prepolymers. <sup>35, 36</sup>



**Scheme 3.3 - Polyaddition reaction for DGC-based PHUs synthesis including the diamines investigated in this work**

The physical properties of the synthesized PHU prepolymers were analyzed qualitatively and quantitatively, and they are summarized in Table 3.1. PHUs 1 and 2 can be considered fully bio-based prepolymers, as 1,10-diaminodecane can be obtained from bio-based sources and Priamine 1074 is bio-sourced.<sup>43</sup> However, these diamines are low/medium chain length diamines resulting in brittle and rubbery polymers at room temperature, which means that PHUs 1 and 2 were not further investigated in the end-capping process.

In contrast, PHUs 3 through 6 were made of Jeffamine D-2000, a poly(propylene glycol) (PPG) derivative with telechelic amine functionality, which is relevant as PPG with telechelic hydroxy groups is used as the diol in the synthesis of many conventional PU sealants and adhesives. Their molecular weights can be easily tailored to a few hydroxyurethane units and they are liquid-like at room temperature, making them good candidates for subsequent end-

capping reactions. A kinetic study conducted at 140 °C to study the evolution of the molecular weight of DGC-Jeffamine D-2000 based polymers showed a decrease in average molecular weights when running the reaction beyond 18 h, as shown in Figure 3.2 and Figure A.3. This is equivalent to a  $DP_n$  decrease from, approximately, 3 to 2. This unit cleavage can be due to the reaction temperature that was used or it can be attributed to inter-molecular side reactions (transurethanization or urea formation) as observed in previous studies lead by Besse et al.<sup>44</sup> and Maisonneuve et al..<sup>45</sup> Seeing that 140 °C is causing this phenomenon to occur, PHUs 3 and 4 were synthesized at 100 °C and 120 °C for 24 h to investigate the effect of temperature on the end product. The formulation leading to PHU 4, whose <sup>1</sup>H-NMR spectrum is presented in Figure 3.3, proved to be the most desirable since its  $M_n$  value is in the maximum range observed in Figure 3.2 and the product was liquid-like at room temperature.

As for the PHUs made from DGC and the PDMS-(NH<sub>2</sub>)<sub>2</sub> diamines, chain scission might have occurred at 120 °C if comparing the molecular weights and dispersities ( $\mathcal{D}$ ) of PHU 9 with PHUs 7 and 8 as well as PHU 13 with PHUs 11 and 12. This might be due to the activation of side reactions at 120 °C that led to lower average molecular weights, as discussed in the previous case. Optimistically, the PDMS-(NH<sub>2</sub>)<sub>2</sub> had a positive impact on the color as most of the prepolymers were white and clear. Unlike the reaction of DGC with Jeffamine D-2000, the polyadditions leading to PHUs 7 to 13 have to be tailored as most of them gave high molecular weights and highly viscous materials.

The polyaddition leading to PHU 11 was the easiest to control since the reaction was the slowest at 80 °C, resulting in high molecular weights after 24 h as Figure 3.4 shows. At 16 h, the molecular weight was around 6,300 g/mol, which is equivalent to two hydroxyurethane linkages as the PDMS-(NH<sub>2</sub>)<sub>2</sub> with  $M_n = 5,000$  g/mol has a relative number average molecular weight of

2,800 g/mol ( $DP_n \approx 2$ ). Hence, PHU 10 ( $^1\text{H-NMR}$  spectrum given as Figure 3.5) was synthesized to obtain a liquid-like and clear prepolymer with  $M_n = 7,400$  g/mol, making it a potential sealant or adhesive candidate.

**Table 3.1 - Physical properties of the synthesized PHU prepolymers of this work derived from diglycerol dicarbonate (DGC) and various amines based on a 1/1 molar equivalent formulation**

<b>Prepolymer</b>	<b>Diamine, Temperature (°C)/Time (h)</b>	<b>M<sub>n</sub> (g/mol)<sup>a</sup></b>	<b><math>\bar{D} =</math> M<sub>w</sub>/M<sub>n</sub><sup>a</sup></b>	<b>Color</b>	<b>Physical state</b>
<b>PHU 1</b>	1,10-diaminododecane 80/2	10,500	1.7	Light yellow	Brittle
<b>PHU 2</b>	Priamine 1074 80/16	12,700	2.0	Yellow	Rubbery
<b>PHU 3</b>	Jeffamine D-2000 100/24	2,700	2.0	Clear orange	Liquid
<b>PHU 4</b>	Jeffamine D-2000 120/24	3,200	2.8	Dark red	Liquid
<b>PHU 5</b>	Jeffamine D-2000 140/18	3,300	2.1	Dark red	Liquid
<b>PHU 6</b>	Jeffamine D-2000 140/48	2,000	1.9	Dark brown	Liquid
<b>PHU 7</b>	PDMS-2.5k-(NH <sub>2</sub> ) <sub>2</sub> 80/24	26,300	1.8	Cloudy white	Sticky liquid
<b>PHU 8</b>	PDMS-2.5k-(NH <sub>2</sub> ) <sub>2</sub> 100/24	33,100	2.0	Cloudy white	Sticky liquid
<b>PHU 9</b>	PDMS-2.5k-(NH <sub>2</sub> ) <sub>2</sub> 120/24	21,500	3.3	Clear yellow	Sticky liquid
<b>PHU 10</b>	PDMS-5k-(NH <sub>2</sub> ) <sub>2</sub> 80/16	7,400	2.5	Clear colorless	Liquid
<b>PHU 11</b>	PDMS-5k-(NH <sub>2</sub> ) <sub>2</sub> 80/48	31,300	1.8	Clear colorless	Sticky Liquid
<b>PHU 12</b>	PDMS-5k-(NH <sub>2</sub> ) <sub>2</sub> 100/24	35,500	2.3	Clear yellow	Sticky Liquid
<b>PHU 13</b>	PDMS-5k-(NH <sub>2</sub> ) <sub>2</sub> 120/24	28,100	3.9	Cloudy yellow	Rubbery

a. Molecular weight distributions were estimated from GPC with THF (DMF for PHU 1 only) eluent at 40 °C and average molecular weights reported relative to poly(styrene) standards.

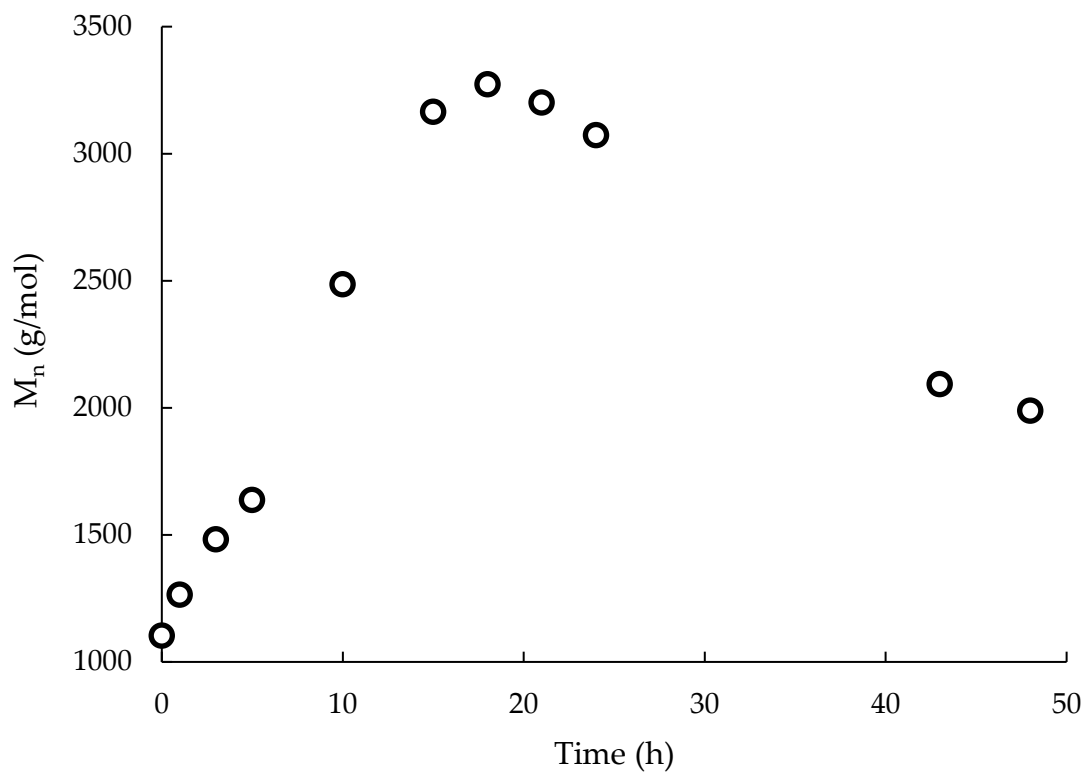


**Figure 3.2 - Molecular weight evolution of PHU 6 (DGC + Jeffamine D-2000) polymerization at 140 °C for 48 h (based on PS standards).**

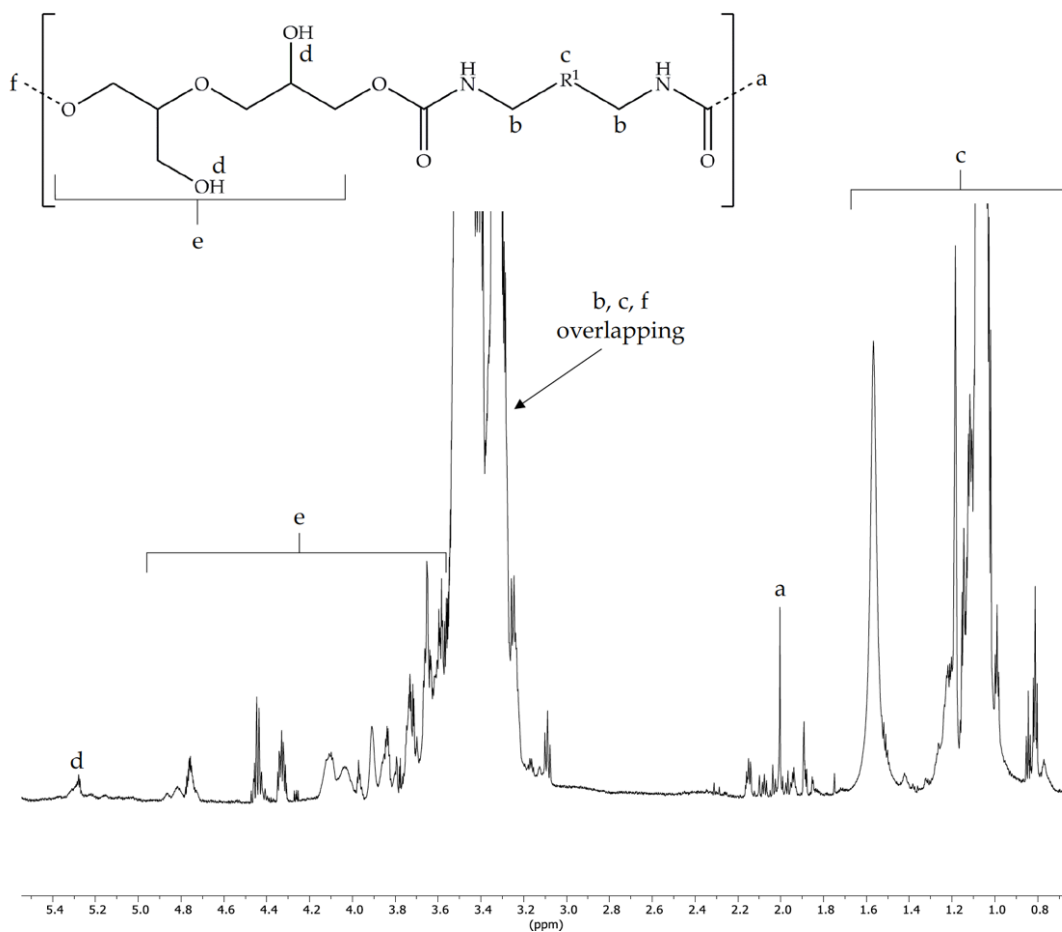


**Figure 3.3 - <sup>1</sup>H-NMR spectrum of PHU 4 (DGC + Jeffamine D-2000) with all protons labelled) in CDCl<sub>3</sub> at 25°C. Protons denoted by c belong to the diamine backbone (R<sup>1</sup>) whereas protons denoted by e belong to the opened cyclic carbonate ring and what belonged to DGC. The rest of the peaks are predicted.**

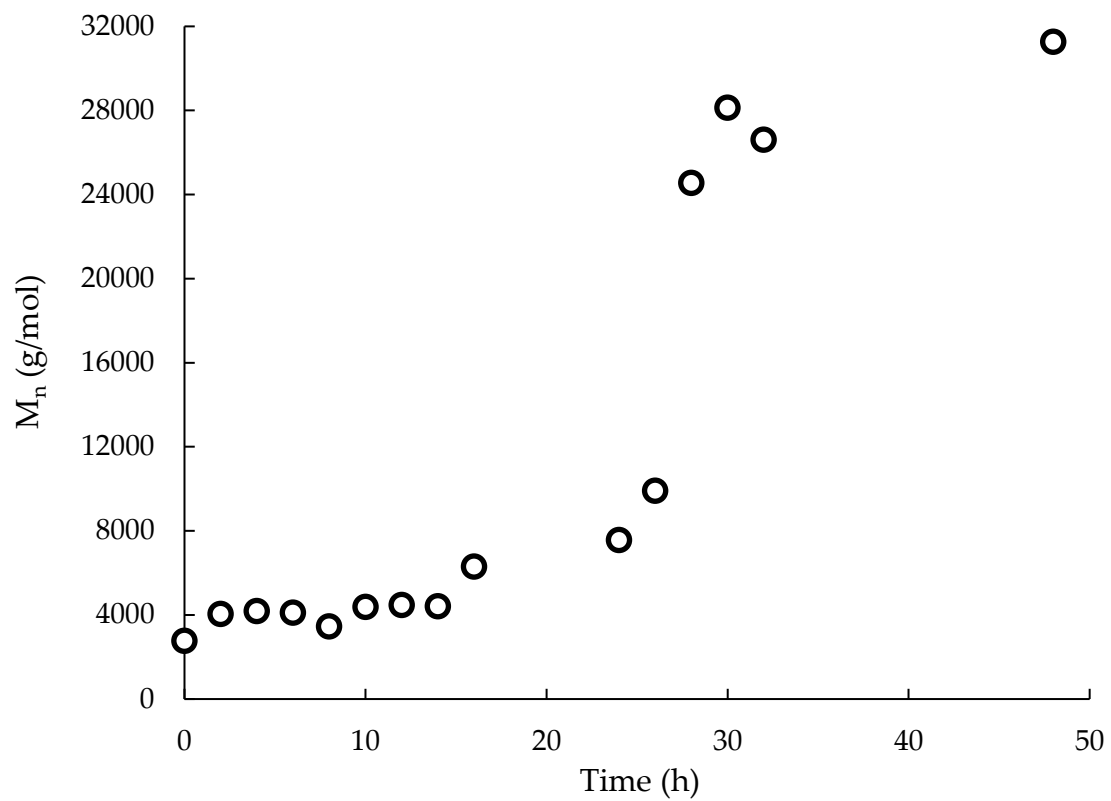


**Figure 3.4 - Molecular weight evolution of PHU 11 polymerization at 80 °C for 48 h (measured by SEC relative to PS standards).**

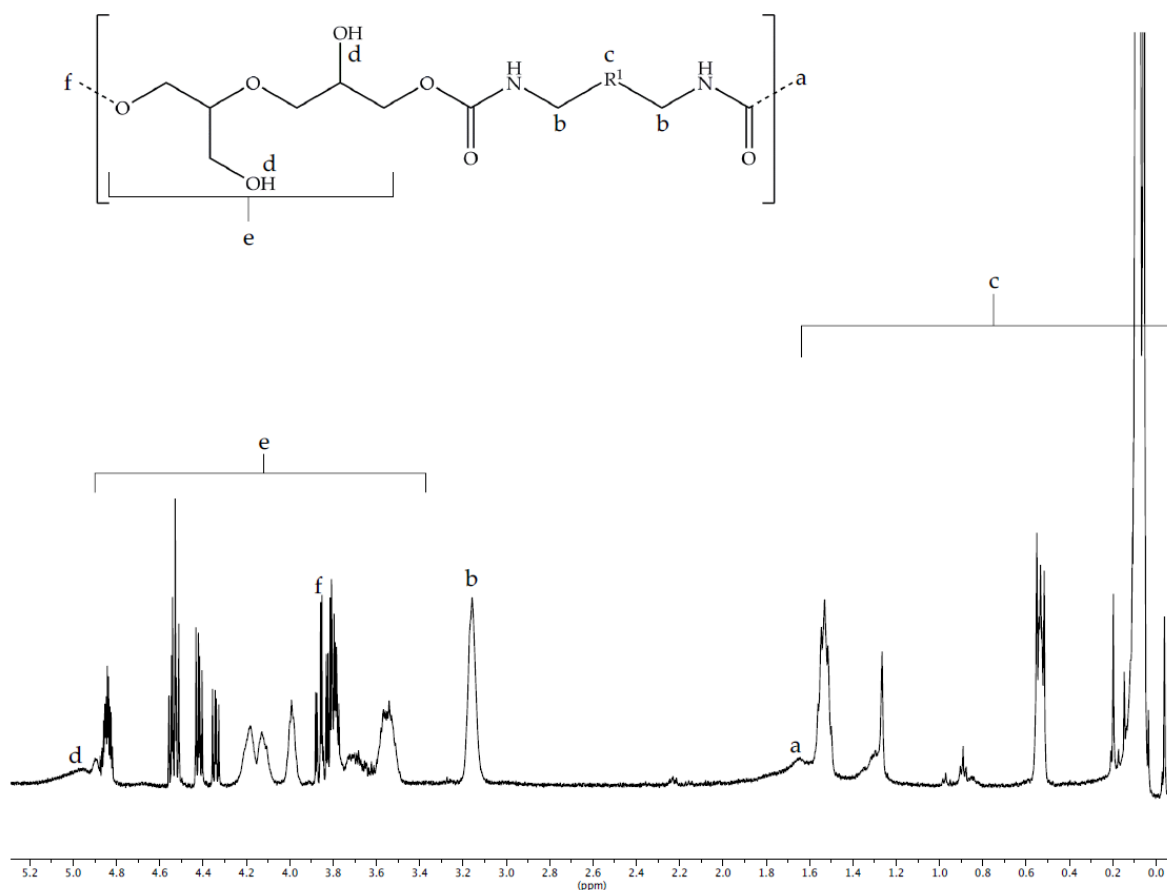


**Figure 3.5 -  $^1\text{H-NMR}$  spectrum of PHU 10 (DGC + PDMS-5k-( $\text{NH}_2$ ) $_2$ ) in  $\text{CDCl}_3$  at  $25^\circ\text{C}$ . Protons denoted by c belong to the diamine backbone ( $\text{R}^1$ ) whereas protons denoted by e belong to the opened cyclic carbonate ring and what belonged to DGC. The rest of the peaks are predicted.**

Besides checking for the prepolymers' physical properties, it is important to assess their thermal properties, which are summarized in Table 3.2. PHUs 4 and 10 have both very low  $T_g$ s, as they are both made of long chain length diamines which provide their chains with more flexibility, and hence a lower  $T_g$  compared to PHU 2 which was synthesized using a medium chain length diamine. The  $T_g$  of PHU 10 was not measured due to instrument limitation that did not allow cooling less than  $-90^\circ\text{C}$ ; however, this parameter was measured by Bossion et al. for a

similar system, and the value is included in Table 3.2.<sup>38</sup> Moreover, PHUs 4 and 10 show high thermal stability compared to other DGC-based PHUs studied in the literature.<sup>35, 36</sup> In fact, the chemical structure of both PDMS-5k-(NH<sub>2</sub>)<sub>2</sub> and Jeffamine D-2000 have ether bonds known to increase the thermal stability of PHUs.<sup>46</sup> Finally, and in addition to the properties discussed previously, seeing that both PHUs 4 and 10 exhibit viscosities allowing them to flow easily at ambient conditions, it is confirmed at this stage that these prepolymers can be considered for the next step.

**Table 3.2 - Thermal properties of selected PHU prepolymers as potential sealant candidate (data of PHU 2 are also included although the polymer is not considered for end-capping)<sup>a</sup>**

<b>Prepolymer</b>	<b>T<sub>g</sub> (°C)</b>	<b>T<sub>d,onset</sub> (°C)</b>	<b>T<sub>d,10%</sub> (°C)</b>	<b>η (Pa.s)<sup>b</sup></b>
<b>PHU 2</b>	-9	200	232	-
<b>PHU 4</b>	-60	205	300	11.5
<b>PHU 10</b>	-120 <sup>38</sup>	250	369	21.5

a. The formulations of the polymers are given in Table 3.1.

b. Viscosities are measured at room temperature (~22 °C).

### 3.3.3 End-capping of prepolymers

To proceed with this step, it is important to characterize the end-groups of the prepolymers as it determines the functionality of capping agent required. The FTIR spectra of both PHUs 4 and 10 are given as Figure 3.6 and Figure 3.7. The second C=O stretch appearing at around 1800 cm<sup>-1</sup> proves the presence of carbonate end-groups, whereas its absence implies that the prepolymers have amine end-groups. In fact, any nonreacted DGC, whose melting point is at 65 °C, precipitated at the bottom of the reactor after bringing the reaction mixture to room

temperature, so the C=O stretch appearing at 1800  $\text{cm}^{-1}$  in Figure 3.6 had to be that of the carbonate end-groups. As a result, PHUs 4 and 10 were found to possess carbonate and amine end-groups, respectively, as mentioned in Table 3.3. The necessary information to conduct these reactions are given in Table 3.3 (more information regarding the estimation of the absolute molecular weights of the PHUs in this work is given in Appendix A), and the different trials with PHUs 4 and 10 are summarized in Table 3.4 and Table 3.5, respectively.

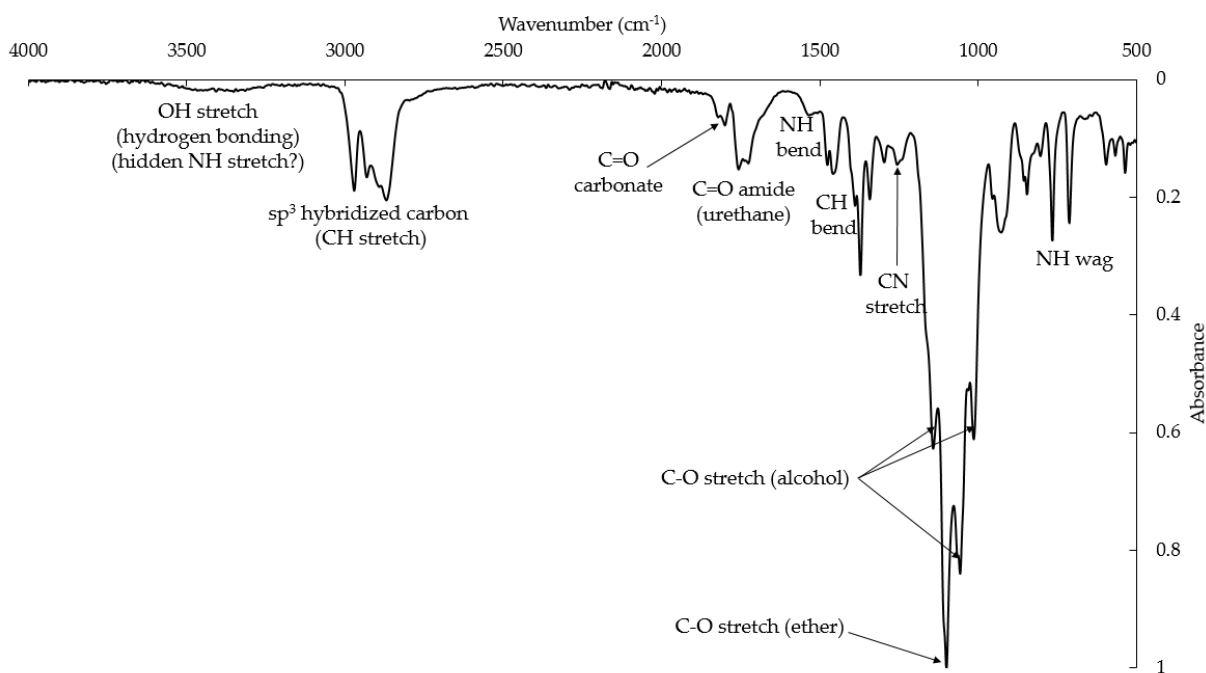


**Figure 3.6 - Labelled FTIR spectrum of PHU 4 (C=O stretch of carbonate end-groups at 1800  $\text{cm}^{-1}$ )**

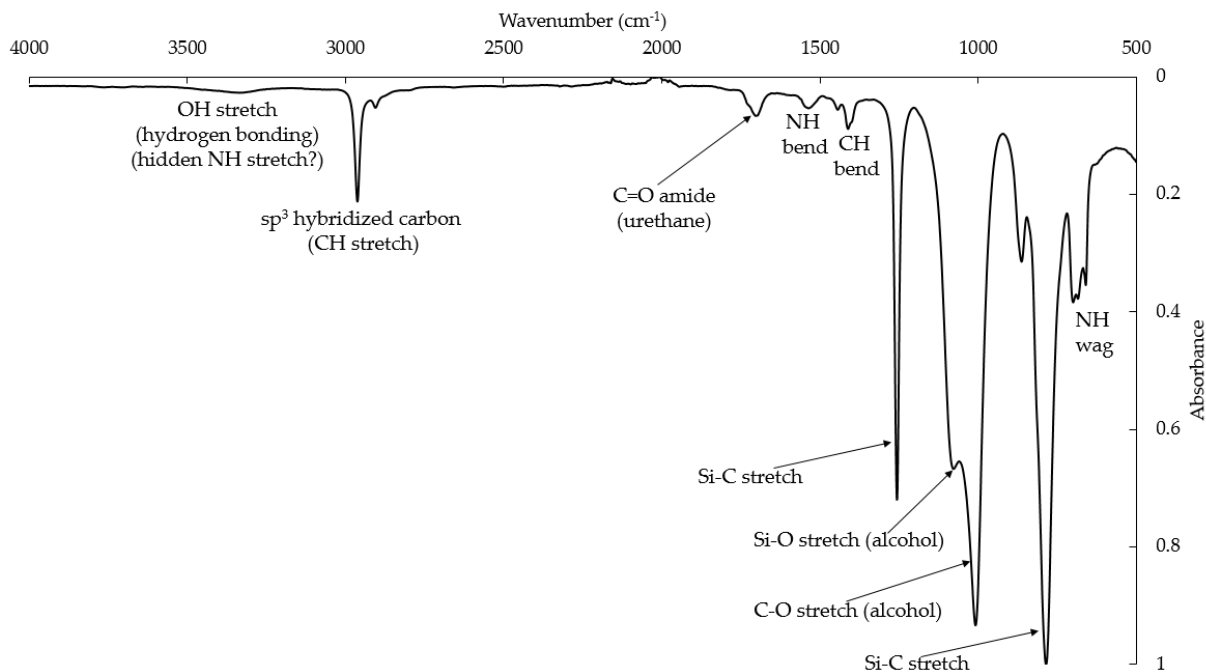


**Figure 3.7 - Labelled FTIR spectrum of PHU 10 (absence of C=O stretch of carbonate end-groups)**

**Table 3.3 - Prepolymer information necessary for preparing end-capped PHUs (HPHUs)**

Prepolymer	End-group	Compatible end-capper	Number of hydroxyurethane linkages	Estimated molecular weight (g/mol)
PHU 4	Carbonate	DAMO	6	6,872
PHU 10	Amine	GLYMO	2	10,218

**Table 3.4 - End-capping experiments of PHU 4**

<b>Trial</b>	<b>End-capper</b>	$n_{\text{capper}}/n_{\text{polymer}}$	<b>Temperature (°C), time (h)</b>	<b>Curing information</b>
<b>PHU 4-1</b>	DAMO	3	120, 5	Curing in the reactor, resulting in brittle material
<b>PHU 4-2</b>	GLYMO	3	120, 5	No curing even after one week
<b>PHU 4-3</b>	DAMO	2	120, 2	Curing started in the reactor and continued under moisture, resulting in smooth film
<b>PHU 4-4</b>	DAMO	2	120, 1 h 15 min	Curing after 24 h under moisture, resulting in smooth film
<b>PHU 4-5</b>	DAMO	4	120, 1 h 15 min	Curing after 24 h under moisture, resulting in brittle film
<b>PHU 4-6</b>	DAMO	6	120, 1 h 15 min	Curing after 24 h under moisture, resulting in brittle film
<b>PHU 4-7</b>	DAMO	2	22, 14	No curing even after one week

**Table 3.5 - End-capping experiments of PHU 10**

<b>Trial</b>	<b>End-capper</b>	<b><math>n_{\text{capper}}/n_{\text{polymer}}</math></b>	<b>Temperature (°C), time (h)</b>	<b>Curing information</b>
<b>PHU 10-1</b>	GLYMO	6	80, 4	Curing in the reactor, resulting in brittle material
<b>PHU 10-2</b>	DAMO	6	80, 4	No curing even after one week
<b>PHU 10-3</b>	GLYMO	6	80, 2	Curing after 24 h under moisture, resulting in brittle film
<b>PHU 10-4</b>	GLYMO	2	80, 2	Curing after 24 h under moisture, resulting in smooth film
<b>PHU 10-5</b>	GLYMO	3	22, 14	Curing after 24 h under moisture, resulting in brittle film
<b>PHU 10-6</b>	GLYMO	2	22, 14	Curing after 24 h under moisture, resulting in smooth film
<b>PHU 10-7</b>	GLYMO	1	22, 14	Partial curing after one week, resulting in softer film

Since the PHU 4 prepolymer chain has carbonate end-groups, the end-capping reaction with GLYMO did not work (PHU 4-2 in Table 3.4), and no curing occurred with moisture when exposed to air afterwards. On the other hand, the end-capping with DAMO (PHU 4-1, and PHU 4-3 to PHU 4-6 in Table 3.4) led to moisture sensitive HPHUs, which is proven by the disappearance of the C=O stretch at  $1800\text{ cm}^{-1}$ , as shown in Figure 3.8. DAMO content was varied (PHU 4-3 to PHU 4-6), and a capper equivalent molar ratio of two seems to be forming the best film, as the film is smooth and not brittle. Figure 3.9 presents different cases discussed previously. All the films formed using PHU 4-DAMO had a sticky surface, meaning that HPHU 4 could be possibly used as a sealant-adhesive. The curing kinetics of this polymer were rheologically followed for 24 h under ambient lab conditions (22 °C and 40-50% humidity), as

shown in Figure 3.10, Figure A.6, and Figure A.7. A gel time of 7.5 h was measured, which proves the qualitative observations discussed previously.

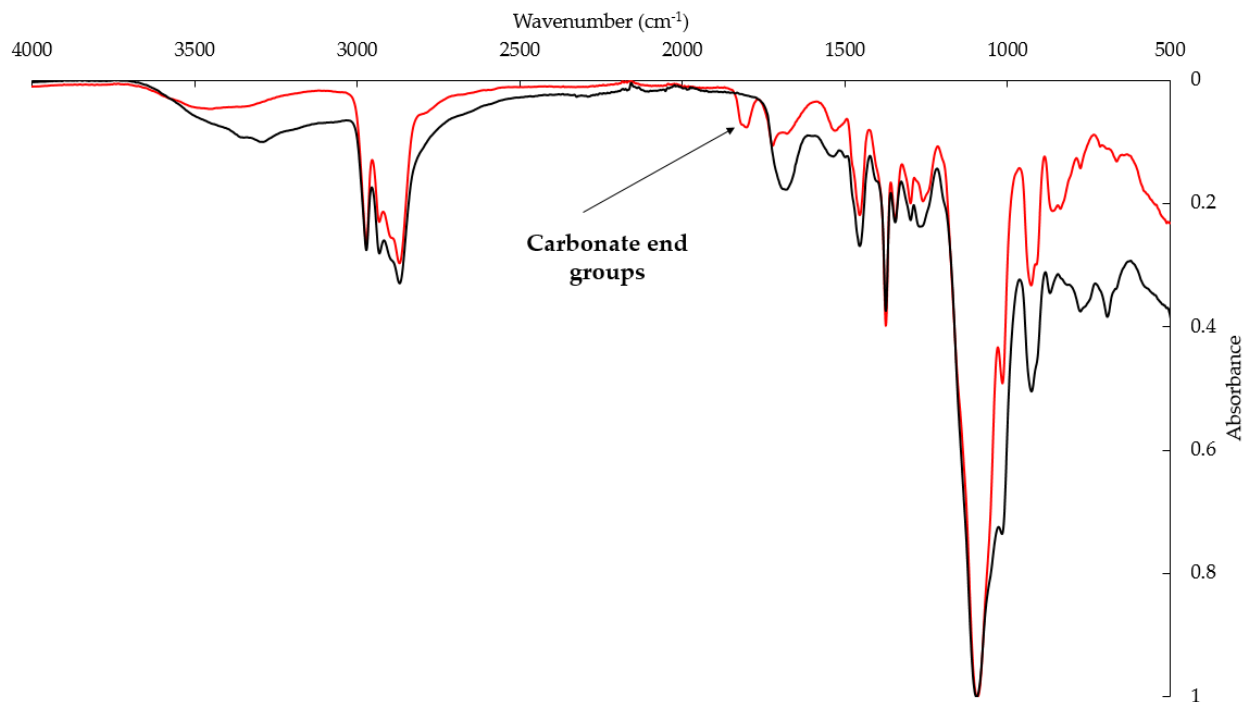


**Figure 3.8 - Comparison of FTIR spectra (PHU 4-1 (black) and PHU 4-2 (red)) between successful and unsuccessful end-capping reactions of PHU-4 with DAMO (red) and GLYMO (black). Disappearance of the 1800 cm<sup>-1</sup> C=O stretch observed with the DAMO end-capper compared to the GLYMO one.**



PHU 4-1

PHU 4-2

PHU 4-4

**Figure 3.9 - PHU 4 end-capping reaction summary: PHU 4-1 with excess DAMO resulting in brittle films, PHU 4-2 with excess GLYMO resulting in noncured materials, and PHU 4-4 resulting in smooth HPHU 4 films.**

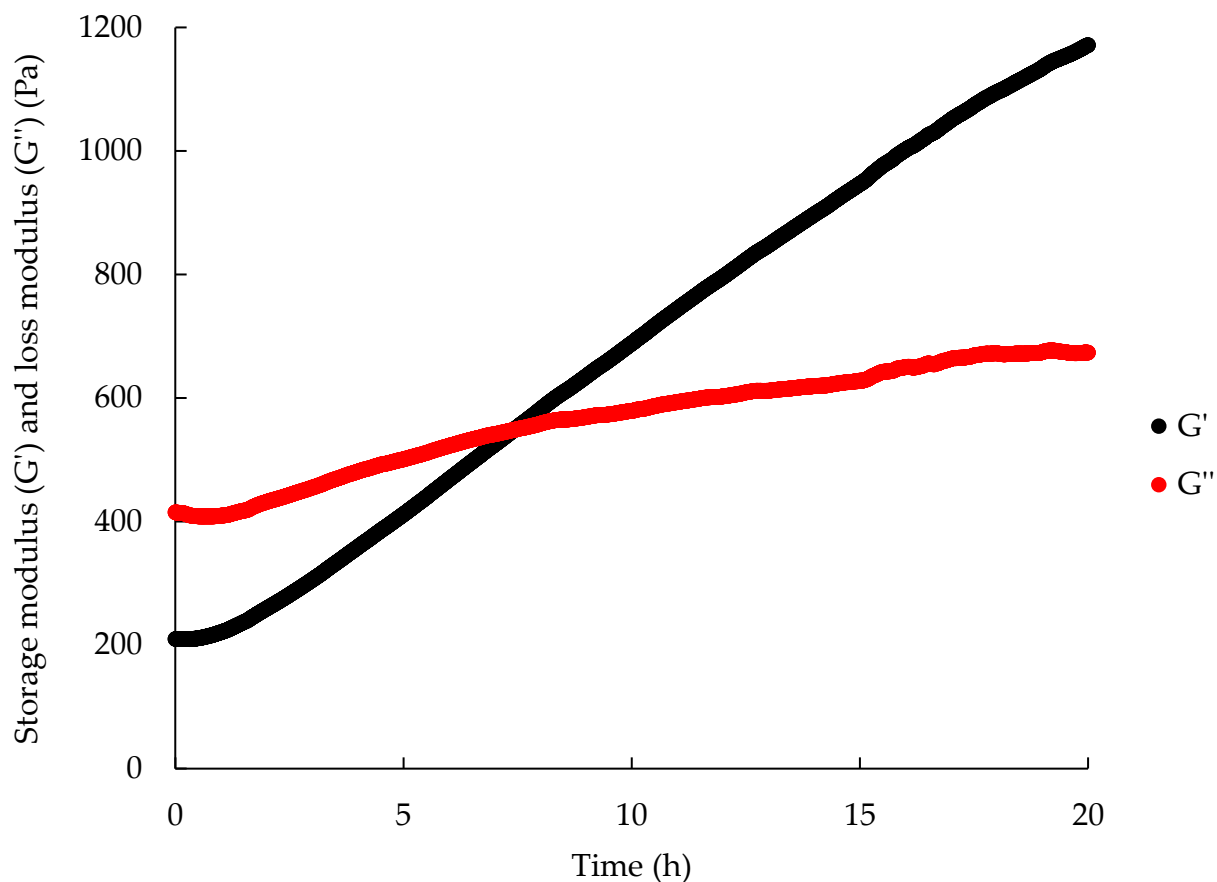


**Figure 3.10 - Curing kinetics of end-capped PHU 4 by following the storage ( $G'$ ) and loss ( $G''$ ) moduli (Pa) at a frequency of 1 Hz and a strain of 1% for 20 h. Measurements were done at 22 °C and 40-50% humidity.**

Nevertheless, the end-capping reaction of PHU 10 with GLYMO was performed at lower temperatures and proved to work at ambient conditions, as shown elsewhere.<sup>47</sup> Since the polyaddition of PHU 10 is very sensitive to temperature (shown previously in Section 3.3.2 and Figure 3.4), it is convenient to have the end-capping reaction performed at room temperature to inhibit the increase of the prepolymer molecular weight at higher temperatures, like 80 °C. A curing kinetics study on the end-capped PHU 10 proved that polymeric films start forming after 3 h when exposed to moisture at ambient conditions, as shown in Figure 3.11, Figure A.8, and

Figure A.9. Similarly to PHU 4, increasing the end-capper stoichiometric content more than two-fold resulted in brittle HPHU 10 films (PHU 10-1, PHU 10-3, and PHU 10-5 in Table 3.5), whereas a lower amount led to soft films as crosslinking was incomplete (PHU 10-7 in Table 3.5). An end-capper stoichiometric content twice that of the polymer end groups gave smooth films with a non-sticky surface, making HPHU-10 materials viable as potential sealant coatings. End-capping PHU 10 was also tried with DAMO, but no curing occurred after one week, proving further that the end-groups are amines and not carbonates (PHU 10-2 in Table 3.5). Figure 3.12 summarizes the different HPHU 10 materials formed under the conditions discussed earlier herein.

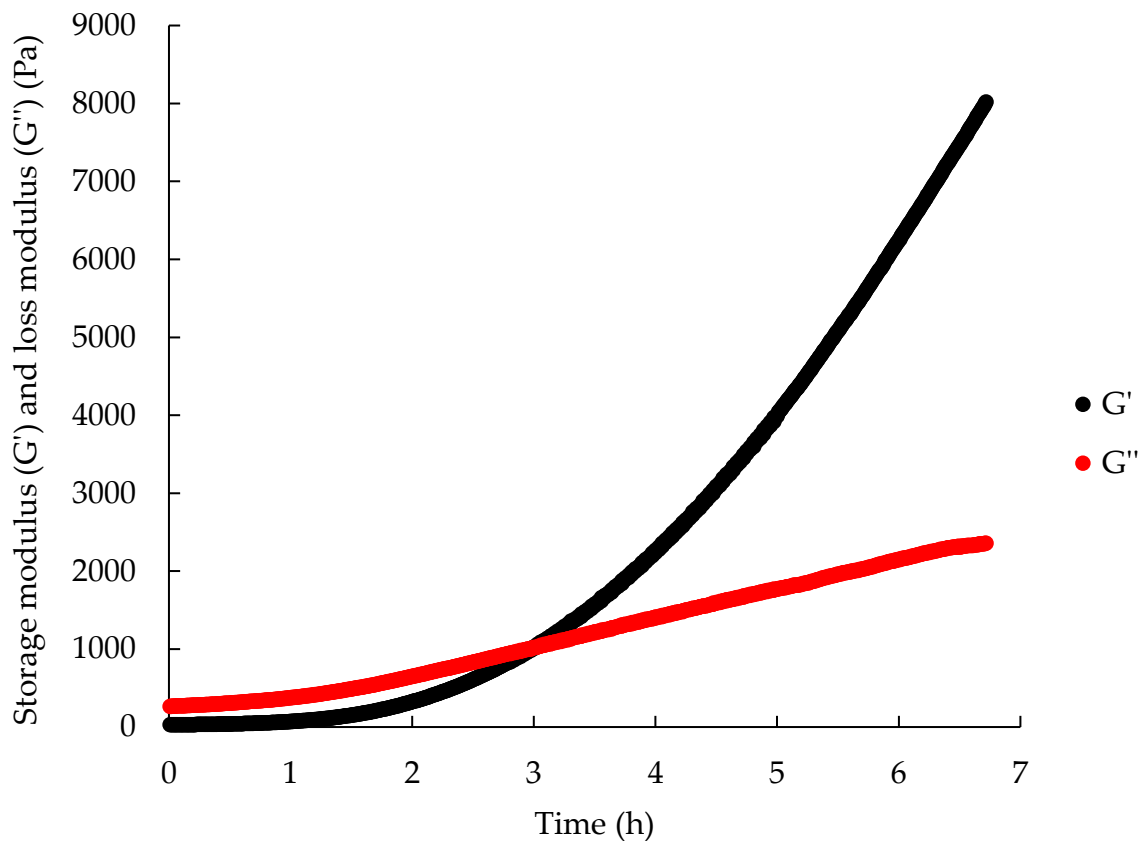


**Figure 3.11 - Curing kinetics of end-capped PHU 10 by following the storage ( $G'$ ) and loss ( $G''$ ) moduli (Pa) at a frequency of 1 Hz and a strain of 1% for 7 h. Measurements were done at 22 °C and 40-50% humidity.**



PHU 10-1

PHU 10-2

PHU 10-6

**Figure 3.12 - PHU 10 end-capping reaction summary: PHU 10-1 with excess GLYMO resulting in brittle films, PHU 10-2 with excess DAMO resulting in non-curing materials, and PHU 10-4 resulting in smooth HPHU 10 films.**

### 3.3.4 HPHUs-Water interaction and chemical stability

Swelling experiments in purified H<sub>2</sub>O were conducted on films of both HPHUs 4 and 10 to check for possible interactions between the synthesized materials and water. The data for these experiments are summarized in Table A.3 and Table A.4. HPHU 4 was found to swell in the presence of water with an EWC (%) =  $62.97 \pm 3.54$ , EWA (%) =  $38.62 \pm 1.35$ , and GC (%) =  $66.70 \pm 0.97$ , making these materials sensitive to water, and thus could be problematic in outdoor applications. In fact, the PPG co-monomer is polar and is expected to be water-swellaible.<sup>48</sup> Therefore, these materials are limited to indoor applications only, unless the resin is blended with other additives and reagents. Conversely, HPHU 10 did not swell in the presence of water, and the weights of the samples were the same after one week. Sessile drop tests on these films showed that they are hydrophobic with an average contact angle with Milli-Q water of  $109^\circ \pm 2.1$

(Table A.5), which is expected as PDMS is known to be hydrophobic with a contact angle around 140°. <sup>49</sup>

Moreover, after drying pure H<sub>2</sub>O and collecting the residuals (if any), <sup>1</sup>H-NMR analysis in D<sub>2</sub>O showed materials being leached from the HPHU 4 samples when they were immersed in water while no leaching occurred from the HPHU 10 films (Figure A.10 and Figure A.11, respectively). As a result, it can be implied that HPHU 10 films are suitable for both indoor and outdoor applications, as they are resistant to water. They also exhibited resistance to the acid medium they were immersed in, as HPHU 10 samples' weights remained unchanged during that degradation study (Table A.6).

Additionally, it was possible to cut dog-bone shapes from the HPHU 10 films formed previously because they were firm and easier to handle than the HPHU 4 ones. The tensile test results for the samples cured under lab conditions for one week only and those cured in pure H<sub>2</sub>O for another week afterwards are presented in Table 3.6 (refer to Table A.7, Table A.8, Figure A.12, and Figure A.13 where the results of the tests are summarized). These results suggest that the latter were exposed to more “moisture” than the former, making their crosslinking easier. In fact, they exhibited higher EB% and  $\sigma_{\max}$ , which proves that these samples achieved higher crosslinking density than the samples cured under lab conditions only, also confirmed from the DMTA tests results from which the crosslinking density,  $v_e$ , was calculated at 30 °C and given in Table 3.6 (refer to Figure A.14 where the full storage modulus, G', variation with temperature is combined for all samples). Lower E was measured for those samples, but that is expected since E and EB% follow opposite trends. However, the HPHU 10 films herein are still weak and soft, which is not a problem as the film is made from the base resin only. Finally, the results in Table

3.6 also underscore the water resistance of HPHU 10 as the mechanical properties improved when the samples were immersed in water prior to being dried and tested.

**Table 3.6 - Comparison of tensile and rheological tests results for HPHU 10 samples cured under lab conditions for one week and HPHU 10 samples cured for one week under lab conditions and another week in pure H<sub>2</sub>O**

Samples	E (MPa)	EB%	$\sigma_{\max}$ (MPa)	$V_{e,30^{\circ}\text{C}}$ (mol/m <sup>3</sup> )
Cured under lab conditions for one week	1.2±0.2	54±11	0.30±0.07	142±55
Cured under lab conditions for one week and in pure H <sub>2</sub> O for another week	0.75±0.25	100±8	0.42±0.04	311±11

### 3.4 Conclusion

A sol/gel curing method was taken advantage of in this work, and new hybrid partially bio-based PHUs were developed by end-capping the prepolymers with moisture curable groups, such as epoxy or amino silanes, depending on the type of end-groups in the prepolymer chains. This type of curing would be crucial in developing new PHU sealants and adhesives, as the conventional PU counterparts are moisture sensitive and crosslink when in contact with air at ambient conditions. A bio-based dicarbonate, DGC based on glycerol, was targeted in this work. DGC was synthesized and polymerized with diamines of different chain lengths; however, only the long chain diamines proved to be suitable for this work, as the resulting prepolymers were liquid-like at room temperature. PHU 4, based on DGC and PPG diamine (Jeffamine D-2000), and PHU 10, prepared from DGC and PDMS diamine (PDMS-5k-(NH<sub>2</sub>)<sub>2</sub>), were found to be good candidates for end-capping. The end-capping reactions to place the appropriate silane moisture

curable groups was dictated by the nature of the terminal groups and were effective at the ambient conditions without the use of catalyst, marking one of the first times that hybrid moisture curable HPHUs are possible at such conditions. The curing kinetics of some HPHUs were studied and typical gel times of 3 and 7.5 h were measured at 22 °C and 40-50% humidity under lab conditions. The steps followed to make the HPHUs of this work are summarized in Figure 3.13.

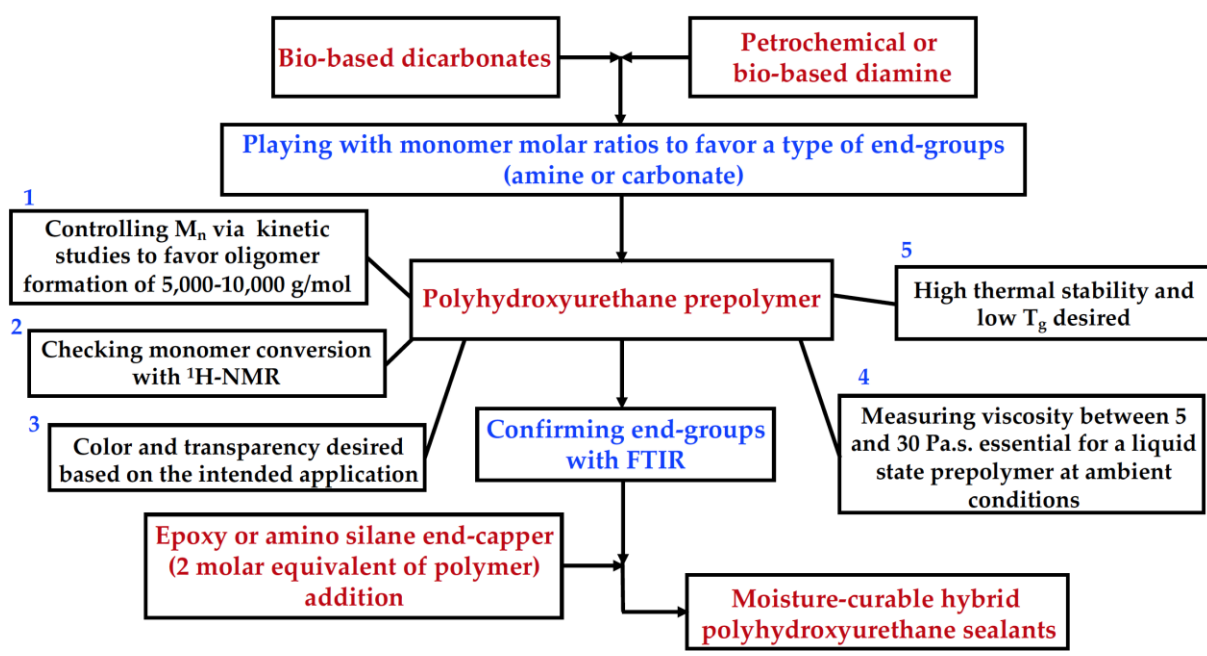


**Figure 3.13 - Summary of the method followed to synthesize moisture curable HPHU sealants and adhesives.**

Degradation and swelling studies in H<sub>2</sub>O were then conducted to ensure that the new films are resistant to water when used in outdoor applications. HPHU 4 films were swollen when immersed in H<sub>2</sub>O for a week, whereas HPHU 10 films were water resistant as weight loss was negligible. Further, the <sup>1</sup>H-NMR spectrum of the residual solvent HPHU 10 study indicated no significant leaching. The latter films were hydrophobic, exhibiting a water contact angle of 109°.

The HPHU 10 mechanical properties improved (EB% and  $\sigma_{\max}$ ) after the samples were immersed in H<sub>2</sub>O as the curing process was more effective in that medium compared to that with the samples exposed to ambient conditions only. This proves again the water repellency of the PDMS-based derived HPHUs.

### 3.5 Materials and Methods

#### 3.5.1 Materials

Diglycerol (DIG,  $\geq 80\%$   $\alpha,\alpha$ , impurities consist of mono-,  $\alpha,\beta$ -di-,  $\beta,\beta$ -di-, and triglycerol) was obtained from Tokyo Chemical Industry (TCI). Dimethyl carbonate (DMC,  $\geq 99\%$ , anhydrous), and sodium methoxide (SOM, 95%, anhydrous powder) were purchased from Sigma Aldrich and Acros, respectively. Ethyl acetate (EthAc, certified grade), tetrahydrofuran (THF, HPCL grade), and dimethyl formamide (DMF, HPLC grade) were purchased from Fischer Chemical. Water purified by a reverse osmosis process (pure H<sub>2</sub>O) was provided by the McGill Chemical Engineering Department. The diamines used in this work are 1,10-diaminodecane (Aldrich), Jeffamine D-2000 or poly(propylene glycol) bis(2-aminopropyl ether) with  $M_n = 2,000$  g/mol (Aldrich), and PDMS-(NH<sub>2</sub>)<sub>2</sub> or aminopropyl terminated polydimethylsiloxane with  $M_n = 2,500$  g/mol (PDMS-2.5k-(NH<sub>2</sub>)<sub>2</sub>) (Aldrich), PDMS-(NH<sub>2</sub>)<sub>2</sub> with  $M_n = 5,000$  g/mol (PDMS-5k-(NH<sub>2</sub>)<sub>2</sub>) from Gelest, and Priamine 1074 from Croda. Deuterated dimethyl sulfoxide (DMSO-d<sub>6</sub>) and deuterated chloroform (CDCl<sub>3</sub>) were provided from Sigma Aldrich. Deuterium oxide (D<sub>2</sub>O, 99.9% D) was purchased from Cambridge Isotope Laboratories, whereas GLYMO or [3-(2,3-epoxypropoxy)-propyl]-trimethoxysilane, DAMO or N-(2-aminoethyl)-3-aminopropyltrimethoxysilane were purchased from Sigma Aldrich. Acid buffer solution of pH = 3 at 20-25 °C was purchased from Fischer. All the chemicals were used as received.

### 3.5.2 Experimental methods

**Kinetic study of DGC reaction:** DIG (6.05 g, 36.4 mmol) and SOM (184 mg, molar ratio of DIG to SOM of 10) were introduced into a 50 mL round-bottom flask having a stir bar in it. The reactor was set on the stirrer in an oil bath controlled by a thermostat equipped with a temperature sensor and the temperature was adjusted to 75 °C. Meanwhile, the reactor mixture was purged with nitrogen (N<sub>2</sub>) for 15 min, after which 30 mL of DMC (364 mmol) were added to the mixture, and the reaction was allowed to proceed for 24 h. Aliquots were collected throughout the reaction at 30 min, 1 h, 3 h, 5 h, 7 h, 9 h, and 24 h. The collected samples were allowed to cool down to room temperature before drying them under air for two days to make sure DMC and methanol had totally evaporated.

**DGC synthesis and purification:** DIG (30.0 g, 181 mmol) and SOM (970 mg, molar ratio of DIG to SOM of 10) were introduced into a 250 mL round-bottom flask having a stir bar in it. 152 mL of DMC (1810 mmol) were then added before purging the reaction mixture with N<sub>2</sub> for 15 min. The reactor was set on the stirrer in an oil bath controlled by a thermostat equipped with a temperature sensor and the temperature was adjusted to 75 °C. The reaction was allowed to proceed for 8 h after which the colorless mixture turned light brown. The mixture was allowed to cool down to room temperature and it was filtered to remove SOM (the catalyst). Unreacted DMC along with the formed methanol were evaporated and the light brown residue was soaked for 2 h in 100 mL of pure H<sub>2</sub>O in an Erlenmeyer flask in which a stir bar was set to slowly rotate. After 2 h, the light brown colored was transferred to water, and a beige solid precipitated. The residue was collected via filtration and dried overnight in a vacuum oven at room temperature. Then, the brown H<sub>2</sub>O solution was purged with air for 2 h, after which more beige residues precipitated, then filtered and dried under vacuum like the previous sample. The process of

purging the brown H<sub>2</sub>O solution with air and residue filtration was repeated for three times until no residues were observed to precipitate from H<sub>2</sub>O solution anymore. The collected product was then soaked in 50 mL of EthAc for 30 min to remove the rest of the impurities coming from the byproducts originally found in the DIG sample. The resulting white solids were then filtered and dried overnight in the vacuum oven at room temperature. At the end of the process, 20.0 g of DGC were weighed corresponding to 51% yield based on the total amount of DIG originally loaded. The same procedure was repeated, but in that case the reaction was allowed to proceed for 24 h. The final DGC yield achieved in this latter case was 47%.

**Polyaddition of DGC with Diamines (1/1 molar equivalent with AHEW and CEW given below):** 2.0 g (9.17 mmol) of DGC were reacted in separate 25 mL round bottom flasks with 1.6 g (9.29 mmol) of 1,10-Diaminodecane (PHU 1) or 4.9 g (9.18 mmol) of Priamine 1074 (PHU 2). The reactions were allowed to react at 80 °C until no stirring could be achieved in the reactor anymore (around 2 h for the former and 16 h for the latter). 1.0 g (4.59 mmol) of DGC was reacted in separate 50 mL round bottom flasks with 9.2 g (4.60 mmol) of Jeffamine D-2000, and the mixtures were allowed to react at 100 °C (PHU 3) and 120 °C (PHU 4) for 24 h and at 140 °C for 18 h (PHU 5) and 48 h (PHU 6). 0.50 g (2.29 mmol) of DGC was reacted in separate 50 mL round bottoms flasks with 5.8 g (2.32 mmol) of PDMS-2.5k-(NH<sub>2</sub>)<sub>2</sub>, and the polyadditions were allowed to proceed for 24 h at 80 °C (PHU 7), 100 °C (PHU 8), and 120 °C (PHU 9) and then the same amount of DGC was reacted with 11.3 g (2.26 mmol) of PDMS-5k-(NH<sub>2</sub>)<sub>2</sub>, and the mixtures were left for 16 h (PHU 10) and 48 h (PHU 11) at 80 °C and 24 h at 100 °C (PHU 12) and 120 °C (PHU 13). All the batches were purged with N<sub>2</sub> for 15 min prior to heating them in the oil bath to the specified temperatures, and every reactor was equipped with a high viscosity stir bar allowing good mixing of the monomers throughout the polyaddition reaction.

Table 3.1 summarizes the PHU formulations described herein. The amine hydrogen equivalent weight (AHEW) is calculated by dividing the diamine molecular weight by the number of amine hydrogens. For the diamines used herein, the AHEW are as follows: 43 g/eq for 1,10-Diaminodecane, 134 g/eq for Priamine 1074, 500 g/eq for Jeffamine D-2000, 625 g/eq for PDMS-2.5k-(NH<sub>2</sub>)<sub>2</sub>, and 1250 g/eq for PDMS-5k-(NH<sub>2</sub>)<sub>2</sub>. For DGC, the carbonate equivalent weight (CEW) is calculated to be 109 g/eq after dividing DGC molecular weight by the number of cyclic carbonates in the molecules.

**Tailoring PHU molecular weights for sealant and adhesives applications:** The polymerizations leading to PHU 6 and PHU 11 were kinetically studied during which aliquots from the reactor were taken to track the progress of the PHU molecular weights. Aliquots at 1 h, 2 h, 3 h, 5 h, 10 h, 15 h, 18 h, 21 h, 24 h, 43 h, and 48 h were taken from PHU 6 polymerization batch, whereas aliquots were taken from PHU 10 batch every 2 h up to 16 h, then every 2 h between 24 h and 32 h, and at 48 h. The evolution of the reaction was monitored by estimating the number average degree of polymerization (DP<sub>n</sub>) using Carothers equations for linear polymers in stoichiometric ratios<sup>49</sup>:

$$DP_n = \frac{M_n}{M_0} = \frac{1}{1-p} \quad \text{Eq. (3.1)}$$

Here, M<sub>n</sub> is the relative average number molecular weight measured from gel permeation chromatography (discussed in the next section), M<sub>0</sub> is the relative average number molecular weight of the diamines in question (the diamines having a much higher molecular weight than DGC), and p is the extent of the reaction that could be found by recovering the unreacted DGC that precipitates in the bottom of the reaction medium.

**End-capping of PHU prepolymers:** PHU 4 and PHU 10 were selected for end-capping. An estimate of their absolute molecular weights was made based on their relative molecular weights

and those of their respective diamines found from the gel permeation chromatography (GPC) technique discussed below. From the estimated absolute molecular weights, the amount of end-cappers to be used, which is ideally set at 2 molar equivalents per mol of polymer, was calculated. 2-3 g of the polymers was mixed with 1, 2, 3, 4, and 6 molar equivalent of GLYMO or DAMO, depending on the end-groups of the prepolymer chains. The end-capping reactions with PHU 4 were run at 120 °C from 75 min to 5 h, and those with PHU 10 were conducted at room temperature (22 °C) and 80 °C from 2 h to 14 h. The polymer was purged with N<sub>2</sub> for 15 min prior to adding the end-capper.

### 3.5.3 Characterization methods

**Proton nuclear magnetic resonance (<sup>1</sup>H-NMR) spectroscopy:** Solution-phase NMR spectra were recorded on a Bruker 500 MHz instrument (16 scans) at ambient temperature. DGC was dissolved in DMSO-d<sub>6</sub>, whereas the PHU prepolymers were dissolved in CDCl<sub>3</sub> to be analyzed.

**Fourier transform infrared (FTIR) spectroscopy:** FTIR measurements were carried out on a PerkinElmer instrument equipped with a single bounce diamond attenuated transmission reflectance (ATR) for solids and zinc selenide (ZnSe) holder for liquids. 32 scans were recorded for each sample over the range 4000-500 cm<sup>-1</sup> with a normal resolution of 4 cm<sup>-1</sup>. DGC, the PHU prepolymers, and the HPHUs structures were recorded on the machine. The collected samples from DGC reaction kinetic studies were also analyzed on this machine by tracking the disappearance of the hydroxyl (OH) broad band in the 3200 cm<sup>-1</sup> range and the appearance of the carbonyl (C=O) stretch in the 1700-1800 cm<sup>-1</sup> range.

**Gel permeation chromatography (GPC):** Number average molecular weight (M<sub>n</sub>) and dispersity (Đ = M<sub>w</sub>/M<sub>n</sub>) of prepolymer samples were measured using this technique on a Waters Breeze instrument with HPLC grade THF as an eluent at a flow rate of 0.3 mL/min. Only PHU 1

was measured using DMF HPLC grade as the eluent because it was not soluble in THF HPLC grade. The GPC has three Waters Styragel HR columns (HR1 with a molecular weight measurement range of  $10^2$  to  $5 \times 10^3$  g/mol, HR2 with a molecular weight measurement range of  $5 \times 10^2$  to  $2 \times 10^4$  g/mol, and HR4 with a molecular weight measurement range of  $5 \times 10^3$  to  $6 \times 10^5$  g/mol), a guard column, and a refractive index (RI 2414) detector. The columns were heated to 40 °C during analysis. The molecular weights were determined relative to polystyrene (PS) calibration standards from Varian Inc. (ranging from 682 to 2,520,000 g/mol). The reported molecular weights were all relative to the PS standards and not adjusted with Mark-Houwink parameters. The PHU prepolymers' molecular weights were analyzed using this instrument in addition to the samples collected from the polyaddition kinetic studies of PHUs 6 and 10.

**Thermogravimetric analysis (TGA):** TGA was performed on a Q500 from TA Instruments system. The thermal degradation of the synthesized PHU prepolymers was measured at a heating rate of 10 °C/min over the temperature range of 25-600 °C under a nitrogen atmosphere. The onset degradation temperature ( $T_{d,onset}$ ) and the 10% degradation temperature ( $T_{d,10\%}$ ) were calculated using this method.

**Differential scanning calorimetry (DSC):** DSC was performed using a Q2000 TA Instruments calorimeter using standard hermetic aluminum pans, calibrated with indium and nitrogen as purge gas. The samples were analyzed at a heating rate of 10 °C/min over a temperature range of -80 °C to 120 °C under a nitrogen atmosphere. Glass transition temperatures ( $T_g$ s) were calculated from the second heating ramp.

**Rheology:** Viscosities of PHUs 4 and 10 were measured on an Anton Paar Instruments rheometer (MCR 302) operated in the parallel plate steady shear mode (gap 1 mm). The samples were placed symmetrically in the center of the plate. The shear stress was measured at different

shear rates ranging from  $0.01 \text{ s}^{-1}$  to  $10 \text{ s}^{-1}$  in 19 measurements during 3 min. All the measurements were conducted at ambient conditions.

The curing kinetics of the end-capped PHUs was carried out on the same instrument equipped with two parallel plate geometries at a frequency of 1 Hz, a strain of 1%, and the measurements were carried out at room temperature (around  $22 \text{ }^{\circ}\text{C}$ ) with a humidity range of 40-50%. The evolutions of storage modulus ( $G'$ ), loss modulus ( $G''$ ), damping factor ( $\tan\delta = G''/G'$ ), and complex viscosity ( $\eta^*$ ) were monitored as a function of time for 20 h and 7 h with PHUs 4 and 10, respectively. End-capped PHU 4 was allowed to cool down to room temperature before proceeding with these measurements.

**Water swelling:** Water swelling of PHUs 4 and 10 (in the form of films) was evaluated using water content and absorption measurements at room temperature. Film samples with dimensions of 0.5 cm length, 0.5 cm width, and 0.1 cm thickness were immersed in 7 mL pure  $\text{H}_2\text{O}$  at room temperature. The water uptake was measured every 24 h for one week from immersing the samples. The equilibrium water content (EWC) and equilibrium water absorption (EWA) were estimated using Eq. (3.2) and Eq. (3.3). Afterwards, the samples were dried in a vacuum oven overnight at  $40 \text{ }^{\circ}\text{C}$ , and the gel content was measured using Eq. (3.4).

$$EWC (\%) = \left( \frac{W_s - W_d}{W_d} \right) \times 100 \quad \text{Eq. (3.2)}$$

$$EWA (\%) = \left( \frac{W_s - W_d}{W_s} \right) \times 100 \quad \text{Eq. (3.3)}$$

$$GC (\%) = \left( \frac{W_f}{W_i} \right) \times 100 \quad \text{Eq. (3.4)}$$

Here,  $W_s$  is the weight of the swollen sample,  $W_d$  is the weight of the dried sample,  $W_i$  is the initial weight, and  $W_f$  is the final weight of the dried sample.

**HPHUs degradation in water:** The samples from the water swelling study were used herein afterwards. The water was dried under air flow overnight, and the residuals, if any, were dissolved in D<sub>2</sub>O to be analyzed using <sup>1</sup>H-NMR. The degradation of HPHU 10 was also assessed in water with a pH adjusted to 3. Three samples of the films were taken and weighed over a week to check for any mass loss.

**Water contact angle:** Contact angle measurements were performed on an OCA 150 apparatus (Dataphysics Instrument GmbH) in the sessile drop configuration by the deposition of a 10 μL droplet of Milli-Q water at the rate of 2.0 μL/s with a 0.5 mL GASTIGHT #1750 syringe. The mean contact angle value on the HPHU 10 film was determined using SCA20 software from five repeated measurements conducted on different locations of the film.

**Tensile testing:** Tensile properties were determined at ambient temperature using an EZ Test (Shimadzu) tensile machine at a speed of 20 mm/min with a load capacity of 10,000 N. Young's modulus (E), tensile strength ( $\sigma_{\max}$ ), and elongation at break (EB%) were estimated by the average of at least three repeated film samples of cured HPHU 10 films. Five samples were tested after one week of curing at ambient conditions and three others were tested after curing in ambient conditions for one week then in pure H<sub>2</sub>O for a second week. Free standing dog bone shaped HPHU-10 samples were prepared using Teflon molds with the following dimensions: length of 50 mm, width of 3 mm, thickness of 1 mm, and gauge length of 25 mm. The tensile properties were monitored on WinAGS Lite software.

**Dynamic mechanical thermal analysis (DMTA):** This test was performed on an Anton Paar Instruments rheometer (MCR 302) using rectangular HPHU 10 films prepared using Teflon molds with the following dimensions: length 50 mm (length cut to 45 mm when running the tests), width of 10 mm, thickness of 1 mm, and gauge length of 36 mm. Samples were loaded in

tension and a temperature ramp was performed from 25 °C to 120 °C at a rate of 5 °C/min, with an oscillation strain of 0.5% and a frequency of 1 Hz, and the evolutions of storage modulus ( $G'$ ), loss modulus ( $G''$ ), and damping factor ( $\tan\delta = G''/G'$ ) were monitored for each sample. Three samples were tested after one week of curing at ambient conditions and three others were tested after curing in ambient conditions for one week then in pure H<sub>2</sub>O for a second week. The considered temperature range in this test corresponded to the rubbery plateau of HPHU 10 films. Hence, this test allowed the calculation of the crosslink density ( $\nu_e$ ) given by the equation below:

50

$$\nu_e = \frac{G'_\alpha}{3RT_\alpha}. \quad \text{Eq. (3.5)}$$

Here,  $\nu_e$  is the crosslink density in mol/m<sup>3</sup>,  $G'_\alpha$  is the rubbery plateau modulus at time  $\alpha$  in Pa,  $R$  is the gas constant given in this case as 8.314 J/mol.K, and  $T_\alpha$  is the temperature at time  $\alpha$  in K.

### 3.6 References

1. Bayer, O.; Siefken, W.; Rinke, H.; Orthner, L.; Schild, H. A process for the production of polyurethanes and polyureas. German Patent DRP 728981, 1937.
2. Engels, H. W.; Pirkl, H. G.; Albers, R.; Albach, R. W.; Krause, J.; Hoffmann, A.; Casselmann, H.; Dormish, J. Polyurethanes: versatile materials and sustainable problem solvers for today's challenges. *Angew. Chem., Int. Ed. Engl.* **2013**, *52*, 9422–9441.
3. Cornille, A.; Auvergne, R.; Figovsky, O.; Boutevin, B.; Caillol, S. A perspective approach to sustainable routes for non-isocyanate polyurethanes. *Eur. Polym. J.* **2017**, *87*, 535–552.
4. Kozakiewicz, J. Moisture-Curable Polyurethane Adhesives And Sealants For Civil Engineering And Construction Applications. In 26th annual conference on Adhesion and

Adhesives, The City University, London, UK, Allen, K. W., Ed; Elsevier Science Publishers LTD: The City University, London, UK, 1989; pp 114–141.

5. Berger, M. H.; Mayer, W. P.; Ward, R. J. Silane-containing isocyanate-terminated polyurethane polymers. 4,374,237, February 15, 1983.
6. Jiang, H. M.; Zheng, Z.; Song, W. H.; Li, Z. M.; Wang, X. L. Alkoxysilane functionalized polyurethane/polysiloxane copolymers: Synthesis and the effect of end-capping agent. *Polym. Bull.* **2007**, *59*, 53–63.
7. Nomura, Y.; Sato, A.; Sato, S.; Mori, H.; Endo, T. Synthesis of novel moisture-curable polyurethanes end-capped with trialkoxysilane and their application to one-component adhesives. *J. Polym. Sci., Part A: Polym. Chem.* **2007**, *45*, 2689–2704.
8. Nomura, Y.; Sato, A.; Sato, S.; Mori, H.; Endo, T. Synthesis of novel moisture-curable polyurethanes end-capped with alkoxysilane and use as solvent-free elastic adhesives. *J. Appl. Polym. Sci.* **2008**, *108*, 236–244.
9. Cao, C. L.; Cheng, J.; Di Liu, X.; Wang, R.; Zhang, J. Y.; Qu, J.; Jaeger, U. Study of Properties of One-Component Moisture-Curable Polyurethane and Silane Modified Polyurethane Adhesives. *J. Adhes. Sci. Technol.* **2012**, *26*, 1395–1405.
10. Yuan, Y.; Zhang, Y. Y.; Fu, X. W.; Jiang, L.; Liu, Z. M.; Hu, K.; Wu, B.; Lei, J. X.; Zhou, C. L. Silane-terminated polyurethane applied to a moisture-curable pressure-sensitive adhesive using triethoxysilane. *RSC Adv.* **2016**, *6*, 83688–83696.
11. Yuan, Y.; Zhang, Y. Y.; Fu, X. W.; Kong, W. B.; Liu, Z. M.; Hu, K.; Jiang, L.; Lei, J. X. Molecular design for silane-terminated polyurethane applied to moisture-curable pressure-sensitive adhesive. *J. Appl. Polym. Sci.* **2017**, *134*, 45292.

12. Kathalewar, M. S.; Joshi, P. B.; Sabnis, A. S.; Malshe, V. C. Non-isocyanate polyurethanes: from chemistry to applications. *RSC Adv.* **2013**, *3*, 4110–4129.
13. Guan, J.; Song, Y.; Lin, Y.; Yin, X.; Zuo, M.; Zhao, Y.; Tao, X.; Zheng, Q. Progress in Study of Non-Isocyanate Polyurethane. *Ind. Eng. Chem. Res.* **2011**, *50*, 6517–6527.
14. Rokicki, G.; Parzuchowski, P. G.; Mazurek, M. Non-isocyanate polyurethanes: Synthesis, properties, and applications. *Polym. Adv. Technol.* **2015**, *26*, 707–761.
15. Kreye, O.; Mutlu, H.; Meier, M. A. R. Sustainable routes to polyurethane precursors. *Green Chem.* **2013**, *15*, 1431–1455.
16. Blattmann, H.; Fleischer, M.; Bahr, M.; Mulhaupt, R. Isocyanate- and Phosgene-Free Routes to Polyfunctional Cyclic Carbonates and Green Polyurethanes by Fixation of Carbon Dioxide. *Macromol. Rapid Commun.* **2014**, *35*, 1238–1254.
17. Maisonneuve, L.; Lamarzelle, O.; Rix, E.; Grau, E.; Cramail, H. Isocyanate-Free Routes to Polyurethanes and Poly(hydroxy Urethane)s. *Chem. Rev.* **2015**, *115*, 12407–12439.
18. Abitha, V. K.; Jadhav, S. A.; Rane, A. V. Non-Isocyanate Polyurethane Systems: A Review. *Moroccan J. Chem.* **2016**, *4*, 361–383.
19. Figovsky, O.; Shapovalov, L.; Leykin, A.; Birukova, O. Potashnikova, R. Advances In The Field Of Nonisocyanate Polyurethanes Based On Cyclic Carbonates. *Chem. Chem. Technol.* **2013**, *7*, 79–87.
20. Verma, S.; Kumar, G.; Ansari, A.; Kureshy, R. I.; Khan, N. U. A nitrogen rich polymer as an organo-catalyst for cycloaddition of CO<sub>2</sub> to epoxides and its application for the synthesis of polyurethane. *Sustainable Energy Fuels* **2017**, *1*, 1620–1629.

21. Verma, S.; Nazish, M.; Kureshy, R. I.; Khan, N. U. Bi-functional heterogeneous iron complexes for catalytic conversion of epoxides to cyclic carbonates and their application in the synthesis of polyurethane. *Sustainable Energy Fuels* **2018**, *2*, 1312–1322.
22. Liang, H.; Wang, J.; Wang, F.; Feng, Y.; Kang, M.; Wang, Z. An efficient heterogeneous LiBr/-Al<sub>2</sub>O<sub>3</sub> catalyst for the cycloaddition of CO<sub>2</sub> with diglycidyl ethers. *J. Chem. Technol. Biotechnol.* **2018**, *93*, 2271–2280.
23. Bobbink, F. D.; van Muyden, A. P.; Dyson, P. J. En route to CO<sub>2</sub>-containing renewable materials: catalytic synthesis of polycarbonates and non-isocyanate polyhydroxyurethanes derived from cyclic carbonates. *Chem. Commun.* **2019**, *55*, 1360–1373.
24. Nohra, B.; Candy, L.; Blanco, J. F.; Guerin, C.; Raoul, Y.; Mouloungui, Z. From Petrochemical Polyurethanes to Biobased Polyhydroxyurethanes. *Macromolecules* **2013**, *46*, 3771–3792.
25. Figovsky, O. L.; Shapovalov, L.; Axenov, O. Advanced coatings based upon non-isocyanate polyurethanes for industrial applications. *Surf. Coat. Int., Part B* **2004**, *87*, 83–90.
26. Ecochard, Y.; Caillol, S. Hybrid polyhydroxyurethanes: How to overcome limitations and reach cutting edge properties? *Eur. Polym. J.* **2020**, *137*, 109915.
27. Gomez-Lopez, A.; Grignard, B.; Calvo, I.; Detrembleur, C.; Sardón, H. Monocomponent Non-Isocyanate Polyurethane Adhesives Based on a Sol-Gel Process. *ACS Appl. Polym. Mater.* **2020**, *2*, 1839–1847.
28. Decostanzi, M.; Ecochard, Y.; Caillol, S. Synthesis of sol-gel hybrid polyhydroxyurethanes. *Eur. Polym. J.* **2018**, *109*, 1–7.
29. Rossi de Aguiar, K. M. F.; Ferreira-Neto, E. P.; Blunk, S.; Schneider, J. F.; Picon, C. A.; Lepienski, C. M.; Rischka, K.; Rodrigues-Filho, U. P. Hybrid urethanesil coatings for inorganic

surfaces produced by isocyanate-free and sol–gel routes: synthesis and characterization. *RSC Adv.* **2016**, *6*, 19160–19172.

30. Meier, M. A. R. Plant-Oil-Based Polyamides and Polyurethanes: Toward Sustainable Nitrogen-Containing Thermoplastic Materials. *Macromol. Rapid Commun.* **2019**, *40*, 1800524.

31. Ghasemlou, M.; Daver, F.; Ivanova, E. P.; Adhikari, B. Bio-based routes to synthesize cyclic carbonates and polyamines precursors of non-isocyanate polyurethanes: A review. *Eur. Polym. J.* **2019**, *118*, 668–684.

32. Błażek, K.; Datta, J. Renewable natural resources as green alternative substrates to obtain bio-based non-isocyanate polyurethanes-review. *Crit. Rev. Environ. Sci. Technol.* **2019**, *49*, 1–39.

33. Carré, C.; Ecochard, Y.; Caillol, S.; Averous, L. From the Synthesis of Biobased Cyclic Carbonate to Polyhydroxyurethanes: A Promising Route towards Renewable Non-Isocyanate Polyurethanes. *ChemSusChem* **2019**, *12*, 3410–3430.

34. Christoph, R.; Schmidt, B.; Steinberner, U.; Dilla, W.; Karinen, R. Glycerol. *Ullmann's Encycl. Ind. Chem.* **2006**, *17*, 67–82.

35. van Velthoven, J. L. J.; Gootjes, L.; van Es, D. S.; Noordover, B. A. J.; Meuldijk, J. Poly(hydroxy urethane)s based on renewable diglycerol dicarbonate. *Eur. Polym. J.* **2015**, *70*, 125–135.

36. Tryznowski, M.; Swiderska, A.; Zolek-Tryznowska, Z.; Golofit, T.; Parzuchowski, P. G. Facile route to multigram synthesis of environmentally friendly non-isocyanate polyurethanes. *Polymer* **2015**, *80*, 228–236.

37. Bossion, A.; Aguirresarobe, R. H.; Irusta, L.; Taton, D.; Cramail, H.; Grau, E.; Mecerreyes, D.; Su, C.; Liu, G. M.; Muller, A. J.; Sardon, H. Unexpected Synthesis of

Segmented Poly(hydroxyurea-urethane)s from Dicyclic Carbonates and Diamines by Organocatalysis. *Macromolecules* **2018**, *51*, 5556–5566.

38. Bossion, A.; Olazabal, I.; Aguirresarobe, R. H.; Marina, S.; Martín, J.; Irusta, L.; Taton, D.; Sardon, H. Synthesis of self-healable waterborne isocyanate-free poly(hydroxyurethane)-based supramolecular networks by ionic interactions. *Polym. Chem.* **2019**, *10*, 2723–2733.

39. Magliozzi, F.; Chollet, G.; Grau, E.; Cramail, H. Benefit of the Reactive Extrusion in the Course of Polyhydroxyurethanes Synthesis by Aminolysis of Cyclic Carbonates. *ACS Sustainable Chem. Eng.* **2019**, *7*, 17282–17292.

40. Peixoto, C.; Soares, A. M. S.; Araujo, A.; Olsen, B. D.; Machado, A. V. Non-isocyanate urethane linkage formation using l-lysine residues as amine sources. *Amino Acids* **2019**, *51*, 1323–1335.

41. Zhang, C.; Wang, H.; Zhou, Q. Waterborne isocyanate-free polyurethane epoxy hybrid coatings synthesized from sustainable fatty acid diamine. *Green Chem.* **2020**, *22*, 1329–1337.

42. Magliozzi, F.; Scali, A.; Chollet, G.; Montarnal, D.; Grau, E.; Cramail, H. Hydrolyzable Biobased Polyhydroxyurethane Networks with Shape Memory Behavior at Body Temperature. *ACS Sustainable Chem. Eng.* **2020**, *8*, 9125–9135.

43. Froidevaux, V.; Negrell, C.; Caillol, S.; Pascault, J. P.; Boutevin, B. Biobased Amines: From Synthesis to Polymers; Present and Future. *Chem. Rev.* **2016**, *116*, 14181–14224.

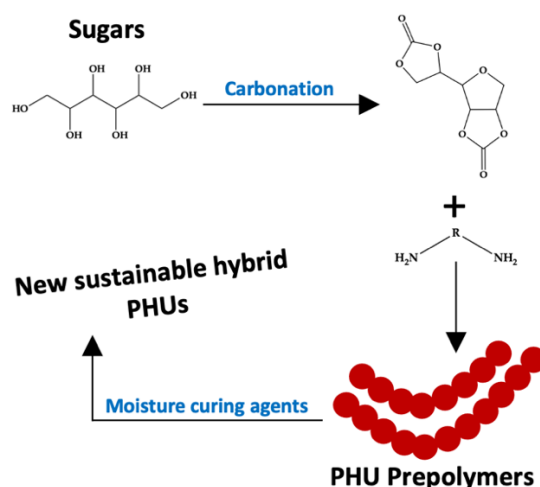
44. Besse, V.; Camara, F.; Mechin, F.; Fleury, E.; Caillol, S.; Pascault, J. P.; Boutevin, B. How to explain low molar masses in PolyHydroxyUrethanes (PHUs). *Eur. Polym. J.* **2015**, *71*, 1–11.

45. Maisonneuve, L.; Wirotius, A. L.; Alfos, C.; Grau, E.; Cramail, H. Fatty acid-based (bis) 6-membered cyclic carbonates as efficient isocyanate free poly(hydroxyurethane) precursors. *Polym. Chem.* **2014**, *5*, 6142–6147.
46. Wloch, M.; Datta, J. Nonisocyanate Polyurethanes. In *Polyurethane Polymers: Blends and Interpenetrating Polymer Networks*, 1st ed.; Thomas, S.; Datta, J.; Haponiuk, J. T.; Reghunadhan, A., Eds.; Elsevier: Oxford, 2017; pp 169–202.
47. Lee, H.; Sung, D.; Kim, J.; Kim, B. T.; Wang, T.; An, S. S.; Seo, S. W.; Yi, D. K. Silica nanoparticle-based dual imaging colloidal hybrids: cancer cell imaging and biodistribution. *Int. J. Nanomed.* **2015**, *10*, 215–225.
48. Loh, X. J.; Colin Sng, K. B.; Li, J. Synthesis and water-swelling of thermo-responsive poly(ester urethane)s containing poly(epsilon-caprolactone), poly(ethylene glycol) and poly(propylene glycol). *Biomaterials* **2008**, *29*, 3185–3194.
49. Jones, A.; Lamb, R. N.; Zhang, H. Hydrophobic Material. US 6,743,467 B1, June 1, 2004.
50. Rudin, A.; Choi, P. *The Elements of Polymer Science & Engineering*. 3rd ed.; Academic Press: Oxford, United Kingdom, 2013.

## Chapter 4

### Moisture-curable hybrid polyhydroxyurethanes from sugar-derived dicarbonates

After successful synthesis of moisture-curable HPHUs from DGC, the next step was to prepare similar materials from cheaper sugar derived cyclic dicarbonates. Unlike diglycerol that has to be produced from glycerol, sorbitol and mannitol can be readily used to make SBC and MBC, respectively. A conducted price estimation, based on the cost of raw materials received from suppliers, showed that DGC would cost 28 \$US/kg, whereas SBC and MBC 18 and 13 \$US/kg, respectively. The price of diglycerol (8 US\$/kg) is the main factor driving up the cost of DGC while the market price of sorbitol and mannitol is 2 US\$/kg. This chapter was published in *Macromolecular Materials & Engineering* in 2021 (Younes, G. R.; Maric, M., Moisture Curable Hybrid Polyhydroxyurethanes from Sugar-Derived Dicarbonates. *Macromol. Mater. Eng.* **2021**, *306* (4), 2000715), <sup>213</sup> and it demonstrates the preparation of SBC and MBC-based moisture-curable PHUs using green chemistry principles. The supporting information of this publication is given in Appendix B.



## 4.1 Abstract

A new set of polyhydroxyurethanes (PHUs) is synthesized from bio-based sorbitol bicarbonate (SBC) and mannitol bicarbonate (MBC). Those dicarbonates are synthesized and polymerized with two long chain diamines, telechelic amine terminated poly(propylene glycol) (PPG) and poly(dimethylsiloxane) (PDMS). Despite the high melting points of SBC and MBC, PHU prepolymers are prepared in bulk and at moderate temperatures of 60-100 °C. The structural and thermal properties of the resulting PHUs are qualitatively and quantitatively characterized with the goal of evaluating them as potential sealants and adhesives, and they are end-capped with moisture curing agents and left to cure at ambient conditions (22 °C and 20-30% humidity) with the curing processes monitored rheologically. The chemical stability of the novel partially sustainable hybrid PHUs (HPHUs) in pure water is investigated to check the viability of applying them outdoors. Only the SBC or MBC-PDMS HPHUs are found to be hydrophobic with water contact angles of 105 and 109°, respectively, but they were brittle. Small and wide-angle X-ray scattering of these water-resistant films showed that they are potentially composed of three different phases due to microphase separation: the PDMS matrix, a hard segments phase, and a third phase mixing the PDMS diamine end-segments and some dissolved hard segments.

## 4.2 Introduction

Due to the environmental and health issues associated with isocyanates, one of the main components of conventional polyurethanes (PUs), researchers have been focusing on the synthesis of non-isocyanate polyurethanes (NIPUs) in the last decade.<sup>1</sup> This is critical as polyurethanes are the 6<sup>th</sup> most used polymer (8% of all plastics), with a market valued at ~ \$60 billion US in 2016.<sup>1-5</sup> From all possible routes to make NIPUs, the step-growth polymerization

of five-membered cyclic dicarbonates with diamines has become most prominent because it does not form lower molecular weight byproducts and its precursors are abundant.<sup>6-10</sup> The cyclic dicarbonates used in preparing these NIPUs, also known as polyhydroxyurethanes (PHUs), can be synthesized in different ways, but the pathway involving the chemical fixation of carbon dioxide (CO<sub>2</sub>) into epoxy (oxirane) groups has received most attention.<sup>11-20</sup> Further, bio-based and bio-renewable sources, such as vegetable oils, bio-polyols, and terpenes, can be used as raw materials in formulating the monomers, and thus embodies many green chemistry principles, particularly those aiming at replacing non-renewable fossil fuel-based building blocks with alternatives.<sup>6, 21-25</sup> With the many commercially available diamines, various cyclic dicarbonate/diamine couples have been studied so far, and their respective PHUs showed similar mechanical properties, chemical resistance, and thermal stability as well as lower permeability compared to conventional polyurethanes (PUs).<sup>1</sup>

In the past five years, different studies have examined PHU thermosets to serve ultimately as adhesives.<sup>26-31</sup> All of these studies emphasized that PHU thermosets have comparable mechanical properties to those of conventional PUs, making them potential products to replace the latter which are based on isocyanates.<sup>28, 29, 31</sup> However, these PHUs were mostly efficient when cured at high temperatures and could not achieve the same adhesion properties of the commercialized PU adhesives at ambient conditions. Hence, it was important to develop new hybrid PHUs (HPHUs) that would crosslink effectively at ambient conditions similarly to the conventional PU adhesives on the market. Recently, HPHUs have gained much attention,<sup>32, 33</sup> especially the ones employing sol/gel crosslinking.<sup>34-40</sup> The studies by Kathelawar et al.<sup>34</sup> and Decostanzi et al.<sup>36</sup> made their sol/gel samples by reacting their diamines and cyclic dicarbonates with silane terminated carbonate and amine, respectively, whereas other studies reacted the

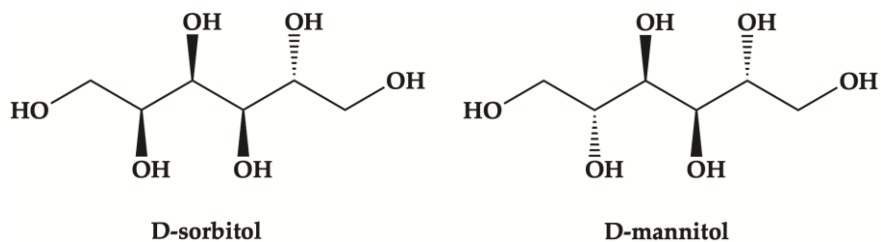
silane agent while running the polyaddition between the cyclic dicarbonate and the diamine.<sup>35, 39</sup> Gomez-Lopez et al. recently made moisture curable HPHUs by end-capping their carbonate terminated-PHUs with amino silanes, but they had to add a catalyst and increase the temperature to aid the sol/gel curing process of their samples.<sup>37, 38</sup>

We previously synthesized new moisture curable hybrid PHUs (HPHUs) from diglycerol dicarbonate (DGC) as the carbonate counterpart.<sup>40</sup> Different diamines were coupled with DGC to prepare the PHUs; however, Jeffamine D-2000 (or poly(propylene glycol) bis(2-aminopropyl ether)), based on poly(propylene glycol) (PPG) with  $M_n = 2,000 \text{ g.mol}^{-1}$ , and PDMS-5k-(NH<sub>2</sub>)<sub>2</sub> (or aminopropyl terminated poly(dimethylsiloxane)), based on poly(dimethylsiloxane) (PDMS) with  $M_n = 5,000 \text{ g.mol}^{-1}$ , proved to give resins suitable for sealants and adhesives applications.<sup>40</sup> The PDMS diamine added the needed hydrophobicity and mechanical properties for these applications, which was noted by Panchireddy et al. who added PDMS into their PHU thermoset structures to prevent the water swelling of the films and delamination of the coatings from the aluminum surface.<sup>[28]</sup> Furthermore, the samples were cured at ambient conditions and without the use of a catalyst, unlike Gomez-Lopez et al.'s studies.<sup>37, 38</sup>

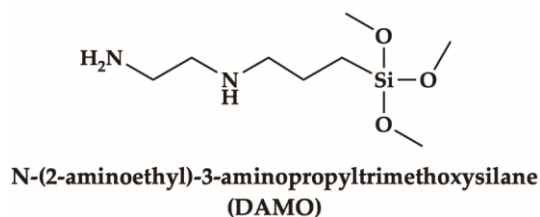
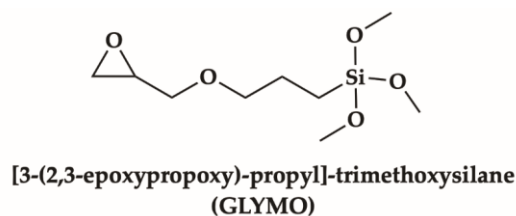
In this study, a different set of dicarbonates prepared from D-sorbitol and D-mannitol is investigated. D-sorbitol and D-mannitol are sugar-derived alcohols obtained from glucose processing, an abundant renewable feedstock. D-Sorbitol and D-mannitol are diastereomers, and their molecular structures are given in Scheme 4.1. They both have high melting points, 98-100 °C and 167-170 °C, respectively, which apparently might be considered a drawback for the synthesis of their dicarbonate counterparts, sorbitol and mannitol bicarbonate (SBC and MBC, respectively). In fact, SBC and MBC were first synthesized from the sugars and dimethyl carbonate (DMC) using organic solvents<sup>41-43</sup> achieving 40 and 60% yield of the dicarbonates,

respectively. Only Furtwengler and Avérous prepared SBC without the use of a solvent. They added D-sorbitol to 7 to 9 molar equivalents of DMC and 5 mol.% of 1.3.5-triazabicyclo[4.4.0]dec-5-ene (TBD) as the catalyst to get SBC with 40 to 45% yield within 16 h at 75 °C. In that work, SBC was recovered using water which is considered a greener way of preparing the dicarbonate according to the authors.<sup>44</sup>

Even if SBC and MBC can be prepared without organic solvents, their melting points of 214-216 °C and 181-183 °C, respectively,<sup>42</sup> are considerably higher than the melting point of DGC of 65 °C.<sup>45, 46</sup> Therefore, their polyadditions will most likely require the use of organic solvents if conducted at moderate temperatures, as it was done previously.<sup>42-44</sup> However, this study tries to avoid using organic solvents, and the reactions with the long chain diamines, Jeffamine D-2000 and PDMS-5k-(NH<sub>2</sub>)<sub>2</sub>, were investigated in bulk, at moderate temperatures, and without a catalyst. This approach was feasible because we targeted short chain PHU prepolymers (oligomers) that were subsequently end-capped to prepare the final moisture curable HPHUs. Depending on the oligomer end groups, either amine or carbonate, the requisite moisture curing agent was added, [3-(2,3-epoxypropoxy)-propyl]-trimethoxysilane (known as GLYMO) or N-(2-aminoethyl)-3-aminopropyltrimethoxysilane (known as DAMO), respectively, whose chemical structure are given in Scheme 4.2. The guidelines, summarized in Figure 3.13 of our previous work, on moisture curable DGC-based HPHUs,<sup>40</sup> were followed herein to synthesize new partially sustainable hybrid materials.



**Scheme 4.1 - D-sorbitol and D-mannitol molecular structures**



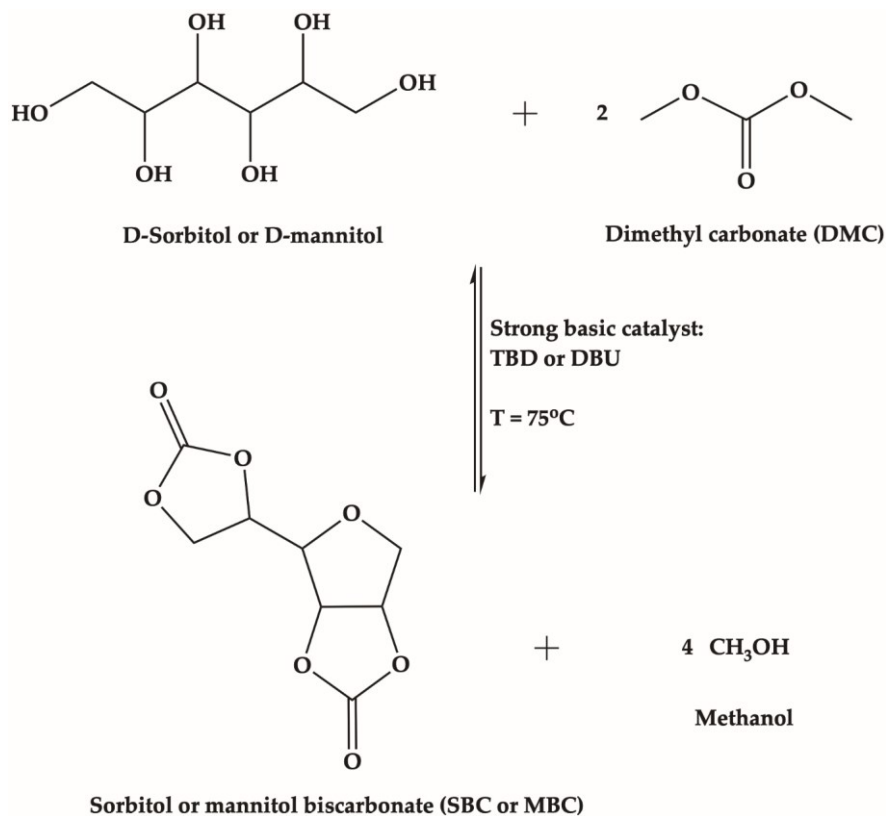
**Scheme 4.2 - GLYMO and DAMO silane curing agent molecular structures**

## 4.3 Results and Discussion

### 4.3.1 SBC and MBC reactions

Our synthesis of the sugar-derived dicarbonates, presented in Scheme 4.3, was notable because we used DMC as both reactant and solvent and water as the only crystallizing and purifying agent. The final yields of 41% and 55% of SBC and MBC, respectively, comply with those reported in the literature using similar and different synthesis procedures.<sup>41, 42, 44</sup> The difference in the yields is most likely caused by the differences in the stereochemistry of D-sorbitol and D-mannitol, leading to different chemical reactivities with DMC. The <sup>1</sup>H-NMR and FTIR spectra

of both sugar-based alcohol dicarbonates are given in the supporting information as Figure B.1 to Figure B.3, and comply with spectra reported elsewhere.<sup>42, 44</sup>

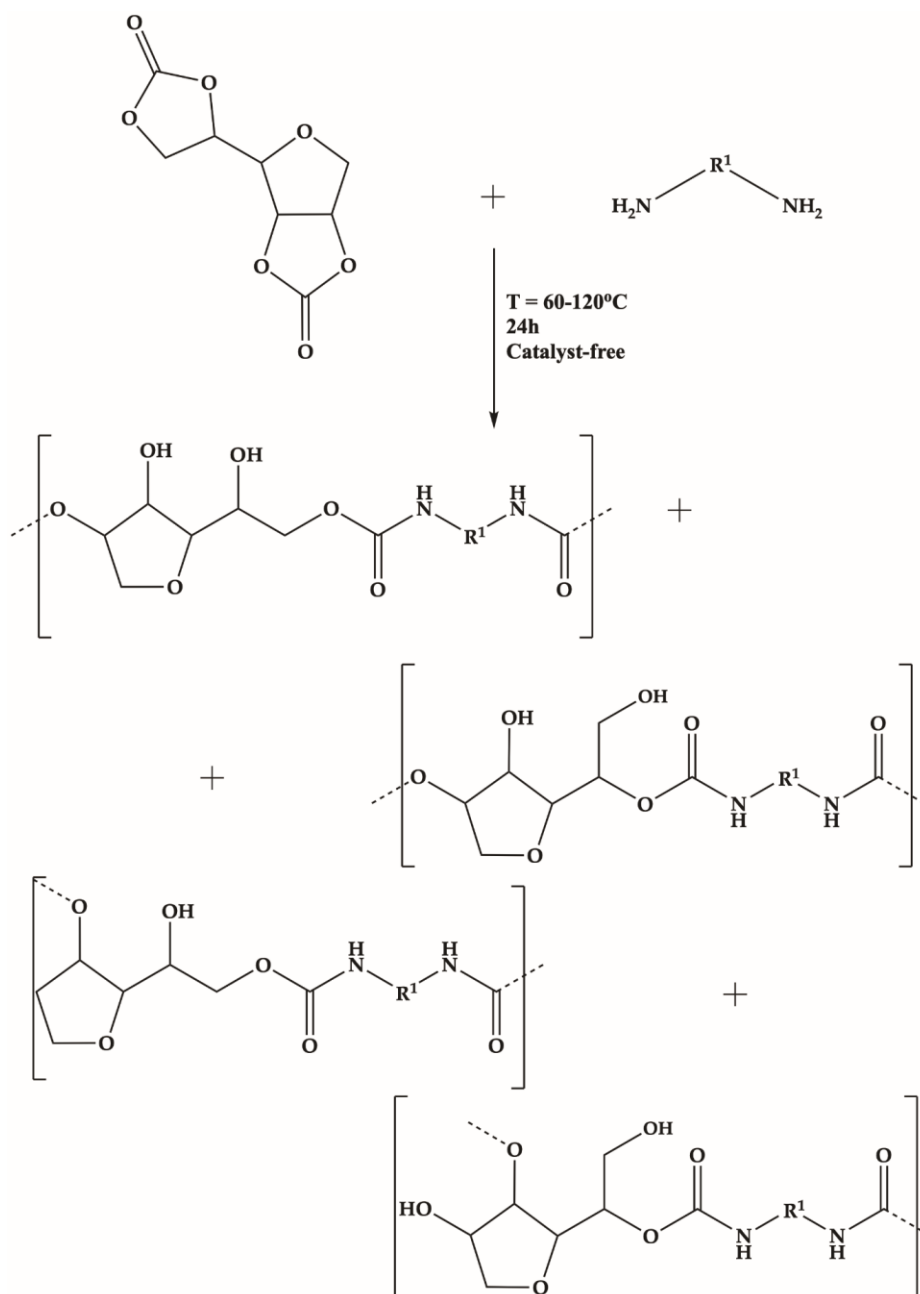


**Scheme 4.3 - Synthesis of sugar-derived alcohol dicarbonates from D-sorbitol and D-mannitol and DMC transesterification reaction**

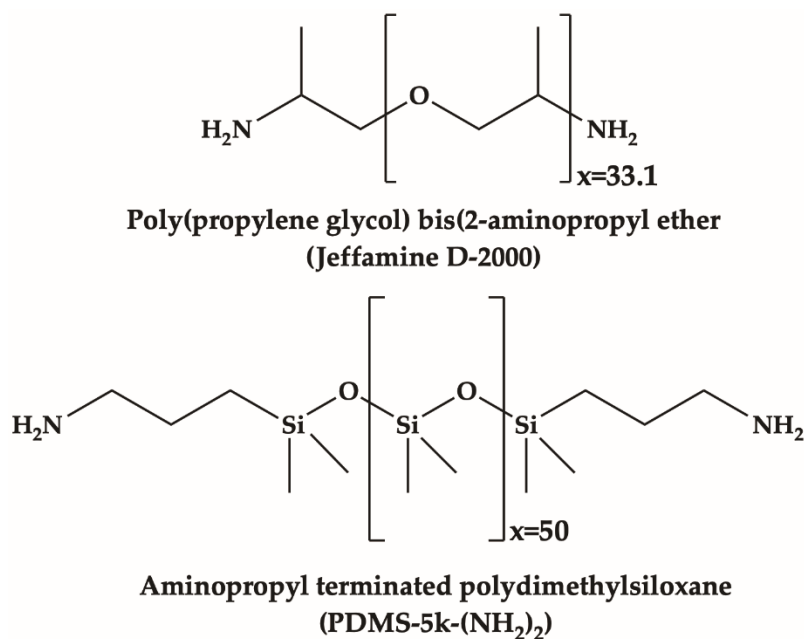
#### 4.3.2 Characterization and screening of PHU prepolymers

The polyaddition between SBC/MBC and a generic diamine is presented in Scheme 4.4. Even though SBC and MBC have high melting points of 214-216 °C and 181-183 °C,<sup>42</sup> respectively, the reactions led to sugar-based PHU oligomers with number average degrees of polymerization ( $DP_n$ ) of 2 to 4 when prepared from the diamines presented in Scheme 4.5. Therefore, it was possible to conduct the polyadditions in bulk and moderate temperatures while obtaining monomer conversions between 50 and 75%. The  $DP_n$  and conversions were calculated from

Carothers equations presented of Eq. (4.1) in Section 4.5.2. At the end of the polyaddition, the remaining unreacted SBC and MBC settled at the bottom of the solution, which makes their separation from the PHU prepolymers facile. Furthermore, no catalyst was needed to synthesize the sugar-based PHU prepolymers.



**Scheme 4.4 - Polyaddition reaction for sugar-based PHUs synthesis**



**Scheme 4.5 - Chemical structures of the diamines used in this work**

The physical properties of the synthesized PHU prepolymers were analyzed and summarized in Table 4.1. Jeffamine D-2000, a poly(propylene glycol) (PPG) derivative with telechelic amine functionality, was used with SBC and MBC to prepare SBC-PHU 1 and MBC-PHU 1, respectively. This particular diamine was studied as it is similar to the PPG-based diols often used as the soft segment in the formulation of conventional polyurethane sealants and adhesives.<sup>40</sup> SBC-PHU 1 and MBC-PHU 1 oligomers consist of a few hydroxyurethane units and these oligomers are liquid-like at room temperature, making them good candidates to be considered for end-capping in bulk. Besides, the same formulation of SBC/MBC and Jeffamine D-2000 led to PHUs with similar  $M_n$ , and this is most likely caused by the low reactivity of the diamine. That is, higher temperatures were required with Jeffamine D-2000 compared to PDMS-5k-(NH<sub>2</sub>)<sub>2</sub> to get similar  $DP_n$  of the corresponding PHUs. The <sup>1</sup>H-NMR spectra of these PHUs are presented in Figure B.4 and Figure B.5.

**Table 4.1 - Physical properties of the synthesized PHU prepolymers of this work derived from SBC and MBC and various amines based on a 1/1 molar equivalent formulation**

<b>Prepolymer</b>	<b>Diamine, Temperature (°C)/Time (h)</b>	<b><math>M_n</math> (g.mol<sup>-1</sup>)<sup>a)</sup></b>	<b><math>\bar{D} =</math> <math>M_w/M_n</math><sup>a)</sup></b>	<b>Color</b>	<b>Physical state</b>
<b>SBC-PHU 1</b>	Jeffamine D-2000 120/24	3,400	2.0	Dark red	Viscous liquid
<b>SBC-PHU 2</b>	PDMS-5k-(NH <sub>2</sub> ) <sub>2</sub> 80/24	6,000	2.8	Clear colorless	Low viscosity liquid
<b>SBC-PHU 3</b>	PDMS-5k-(NH <sub>2</sub> ) <sub>2</sub> 90/24	11,000	2.7	Cloudy yellow	Viscous liquid
<b>SBC-PHU 4</b>	PDMS-5k-(NH <sub>2</sub> ) <sub>2</sub> 100/24	13,000	5.5	Cloudy orange	Solid-like
<b>MBC-PHU 1</b>	Jeffamine D-2000 120/24	3,900	2.5	Dark red	Viscous Liquid
<b>MBC-PHU 2</b>	PDMS-5k-(NH <sub>2</sub> ) <sub>2</sub> 50/24	6,600	2.4	Clear colorless	Low viscosity liquid
<b>MBC-PHU 3</b>	PDMS-5k-(NH <sub>2</sub> ) <sub>2</sub> 60/24	7,500	2.8	Clear colorless	Viscous liquid
<b>MBC-PHU 4</b>	PDMS-5k-(NH <sub>2</sub> ) <sub>2</sub> 70/24	11,500	4.0	Clear light yellow	Highly viscosity liquid
<b>MBC-PHU 5</b>	PDMS-5k-(NH <sub>2</sub> ) <sub>2</sub> 80/24	6,900	6.5	Clear dark yellow	Highly viscosity liquid
<b>MBC-PHU 6</b>	PDMS-5k-(NH <sub>2</sub> ) <sub>2</sub> 90/24	9,200	5.9	Clear dark yellow	Highly viscosity liquid

<sup>a)</sup>Molecular weight distributions were estimated from GPC with THF eluent at 40 °C and average molecular weights reported relative to poly(styrene) standards.

As for the PHUs prepared from PDMS-5k-(NH<sub>2</sub>)<sub>2</sub>, the polyaddition manifold was mostly dependent on the diastereomer of the dicarbonate. Table 4.1 shows that lower temperatures were needed with MBC than with SBC to achieve the desired  $M_n$  of the PHUs. For instance, the polyaddition conducted at 50 °C with MBC for 24 h led to a PHU with similar  $M_n$  as the polyaddition conducted at 80 °C with SBC for a similar reaction time. Therefore, the differences

in chemical properties between SBC and MBC are fairly pronounced when it comes to PDMS-5k-(NH<sub>2</sub>)<sub>2</sub>, which reacted faster compared to Jeffamine D-2000. Similar trends in the reactivities of similar diamines were observed in our previous DGC study.<sup>40</sup>

We notice an increase in dispersity with both dicarbonates and PDMS-5k-(NH<sub>2</sub>)<sub>2</sub> when increasing the polymerization temperature. The dispersity of the PHUs drastically increased from 2.7 to 5.5 between SBC-PHU 3 (90 °C, 24 h) and SBC-PHU 4 (100 °C, 24 h) and from 2.8 to 5.9 between MBC-PHU 3 (60 °C, 24 h) and MBC-PHU 6 (90 °C, 24 h). It seems some of the oligomers reacted with each other at higher temperatures, forming longer chains, while others did not, leading to broad molecular weight distributions, as shown in Figure B.6 and Figure B.7. This increase in dispersity is not surprising as this work is targeting oligomers and PDMS-5k-(NH<sub>2</sub>)<sub>2</sub> is already a short chain polymer on its own, so any small changes in the  $DP_n$  will greatly affect the dispersity of the PHUs. In contrast, SBC-PHU 2 and MBC-PHU 2 had the lowest viscosities close to 0.5 Pa.s at room temperature, whereas SBC-PHU 3 and MBC-PHU 3 were more viscous but still liquid-like and fairly sticky under similar conditions. Hence, SBC-PHU 3 and MBC-PHU 3, whose <sup>1</sup>H-NMR spectra are given as Figure B.8 and Figure B.9, were selected for end-capping since they have relatively narrow molecular weight distributions, they are liquid-like at ambient conditions, and they have apparent stickiness to ensure adhesive-like behavior of the polymer resins.

It is also important to assess the PHU thermal properties summarized in Table 4.2. SBC-PHU 1 and MBC-PHU 1 have both comparatively low glass transition temperatures,  $T_{gs}$ , ~ -60 °C, as they are both made of long chain length PPG-based diamines which provide more flexibility to the final PHU. The  $T_g$  of SBC-PHU 3 and MBC-PHU 3 were not measured as the DSC used did not allow cooling to temperatures less than -90 °C; however,  $T_g$  was measured by

Bossion et al. for a similar system with DGC, and the value is denoted in Table 4.2.<sup>47</sup> This is reasonable as PDMS has a literature  $T_g$  of -120 °C. In our previous study on DGC coupled with Jeffamine D-2000, the resulting PHU had  $T_g$  governed by the that of the flexible long-chain diamine, which was approximately -60 °C.<sup>40</sup> From our examinations, it seems that the type of long chain diamine governs the thermal properties of the PHUs, regardless of the dicarbonates being used.

**Table 4.2 - Thermal properties of selected sugar-based PHU prepolymers as potential sealant candidates<sup>a)</sup>**

Prepolymer	$T_g$ (°C)	$T_{d,onset}$ (°C)	$T_{d,10\%}$ (°C)	$\eta$ (Pa.s) <sup>b)</sup>
<b>SBC-PHU 1</b>	-63	150	304	3.70
<b>SBC-PHU 3</b>	-120 <sup>[27]</sup>	165	344	67.2
<b>MBC-PHU 1</b>	-59	175	287	7.80
<b>MBC-PHU 3</b>	-120 <sup>[27]</sup>	150	353	83.3

<sup>a)</sup>The formulations of the polymers are given in Table 4.1; <sup>b)</sup>Viscosities are measured at room temperature (~22 °C steady shear mode).

In addition to the  $T_g$ , the temperature at 10 wt.% degradation,  $T_{d,10\%}$ , values for SBC-PHU 1 and MBC-PHU 1 (~300 °C) were similar to the one reported for DGC-Jeffamine D-2000, and those for SBC-PHU 3 and MBC-PHU 3 (the PHUs with the long PDMS chains) were similar to that of DGC-PDMS-5k-(NH<sub>2</sub>)<sub>2</sub> (369 °C).<sup>40</sup> Hence, the sugar-based PHUs showed high thermal stabilities seeing that both PDMS-5k-(NH<sub>2</sub>)<sub>2</sub> and Jeffamine D-2000 have ether bonds known to increase the thermal stability of PHUs.<sup>48</sup> Besides, PDMS is known to have high thermal stability because of the Si-O bond strength, which explains the higher degradation temperatures the PDMS-5k-(NH<sub>2</sub>)<sub>2</sub>-based polymers exhibit compared to their Jeffamine D-2000-based

counterparts.<sup>49</sup> Finally, the selected sugar-based PHUs exhibited viscosities allowing them to mix easily with the moisture curing agents (Table 4.2), making them promising candidates for end-capping.

### **4.3.3 End-capping and crosslinking of prepolymers**

To proceed with this step, it is important to characterize the end-groups of the prepolymers as it determines the functionality of the end-capping agent required. The FTIR spectra of the selected sugar-based PHUs are given as Figure 4.1 and Figure 4.2. The second C=O stretch appearing at around  $1800\text{ cm}^{-1}$  proves the presence of carbonate end-groups, whereas its absence implies that the prepolymers have amine end-groups. In fact, any unreacted SBC or MBC precipitated at the bottom of the reactor after bringing the reaction mixture to room temperature, so the C=O stretch appearing at  $1800\text{ cm}^{-1}$  in Figure 4.1 is definitely that of the carbonate end-groups. As a result, SBC-PHU 1 and MBC-PHU 1 were found to possess carbonate end-groups whereas SBC-PHU 3 and MBC-PHU 3 prepolymers had amine end-groups, as presented in Table 4.3. The necessary information to conduct these reactions are given in Table 4.3 (more information regarding the estimation of the average molecular weights of the PHUs of this work is given in the supporting information of Appendix B), and the different trials with SBC and MBC-based PHUs are summarized in Table 4.4 and Table 4.5, respectively.

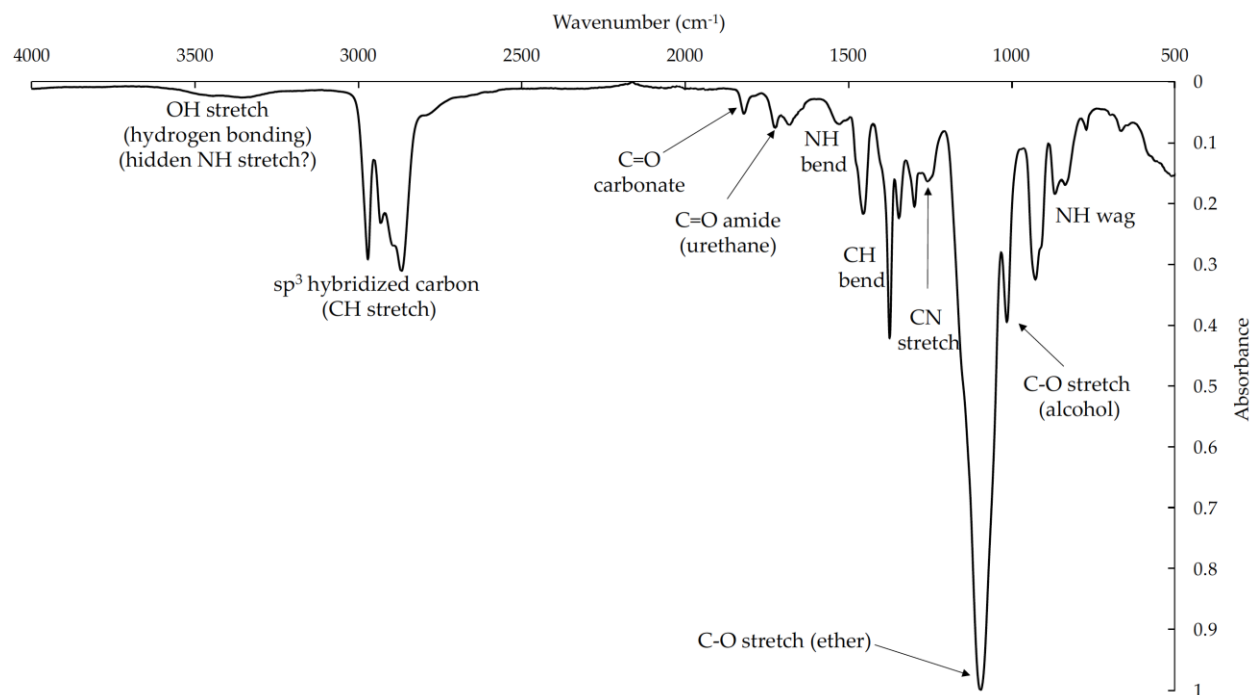


**Figure 4.1 - Labelled FTIR spectrum of SBC-PHU 1 or MBC-PHU 1 (C=O stretch of carbonate end-groups at 1800 cm<sup>-1</sup>).**

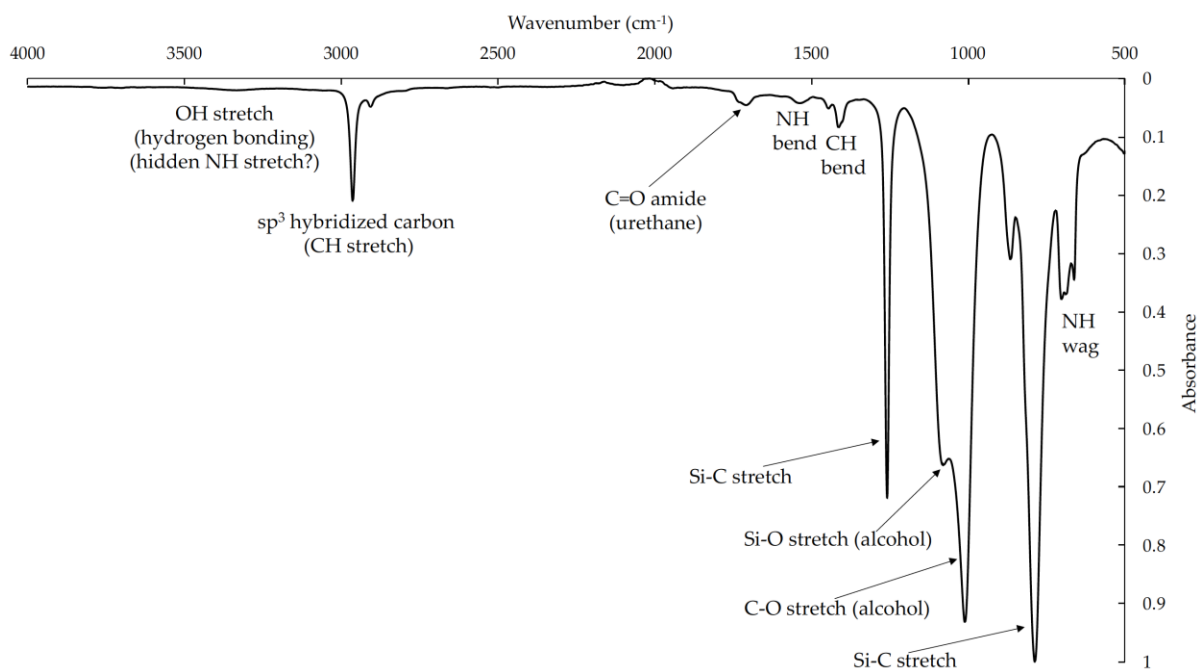


**Figure 4.2 - Labelled FTIR spectrum of SBC-PHU 3 or MBC-PHU 3 (absence of C=O stretch of carbonate end-groups).**

**Table 4.3 - Prepolymer information necessary for preparing end-capped PHUs (HPHUs)**

Prepolymer	End-group	Compatible end-capper	Number of hydroxyurethane linkages	Estimated average molecular weight (g/mol) <sup>1</sup>
<b>SBC-PHU 1</b>	Carbonate	DAMO	4	4,600
<b>SBC-PHU 3</b>	Amine	GLYMO	4	15,400
<b>MBC-PHU 1</b>	Carbonate	DAMO	6	6,900
<b>MBC-PHU 3</b>	Amine	GLYMO	2	10,200

**Table 4.4 - End-capping experiments of SBC-based PHU prepolymers**

Trial	End-capper	$n_{\text{capper}}/n_{\text{polymer}}$	Temperature (°C), time (h)	Curing information
<b>SBC-PHU 1-1</b>	DAMO	2	120, 0.5	No curing even after one week
<b>SBC-PHU 1-2</b>	DAMO	2	120, 1	Incomplete curing even after one week
<b>SBC-PHU 1-3</b>	DAMO	2	120, 1 (with 0.5 wt.% catalyst)	Curing after 24 h under moisture, resulting in smooth film
<b>SBC-PHU 3-1</b>	GLYMO	2	22, 2	Curing after 24 h under moisture, resulting in smooth film
<b>SBC-PHU 3-2</b>	GLYMO	2	22, 16	Curing occurred in the reactor

<sup>1</sup>More information regarding the estimation of the average molecular weights of the PHUs in this work is given in the supporting information of Appendix B. The values reported in Table 4.3 are rounded values of the estimated average molecular weights.

**Table 4.5 - End-capping experiments of MBC-based PHU prepolymers**

<b>Trial</b>	<b>End-capper</b>	<b>n<sub>capper</sub>/n<sub>polymer</sub></b>	<b>Temperature (°C), time (h)</b>	<b>Curing information</b>
<b>MBC-PHU 1-1</b>	DAMO	2	120, 0.25	Curing after 24 h under moisture, resulting in smooth film
<b>MBC-PHU 1-2</b>	DAMO	2	120, 1	Curing started in the reactor and continued under moisture
<b>MBC-PHU 3-1</b>	GLYMO	2	22, 2	Curing after 24 h under moisture, resulting in smooth film
<b>MBC-PHU 3-2</b>	GLYMO	2	22, 16	Curing occurred in the reactor

Since the SBC-PHU 1 and MBC-PHU 1 prepolymers have carbonate end-groups, the end-capping reactions were conducted with DAMO only. It was found that MBC-PHU 1 (0.25 h at 120 °C) was more reactive with DAMO and curing occurred under ambient conditions without the use of a catalyst, contrary to SBC-PHU 1 (1 h at 120 °C) which needed the catalyst to accelerate the curing in the 24 h timeframe. The success of the end-capping of these PHUs with DAMO was revealed by the disappearance of the C=O stretch at 1800 cm<sup>-1</sup>, as shown in Figure 4.3. DAMO content was set to two stoichiometric amounts with respect to the polymer based on our earlier study conducted on DGC-based PHUs.<sup>40</sup> Figure 4.4 presents the final SBC-HPHU 1 and MBC-HPHU 1 thermosets prepared following the formulations presented in in Table 4.4 and Table 4.5 (SBC-PHU 1-3 and MBC-PHU 1-1), respectively. However, all the prepared

thermosets, although presenting a sticky surface necessary for sealants and adhesives applications, were very soft and not easy to handle.

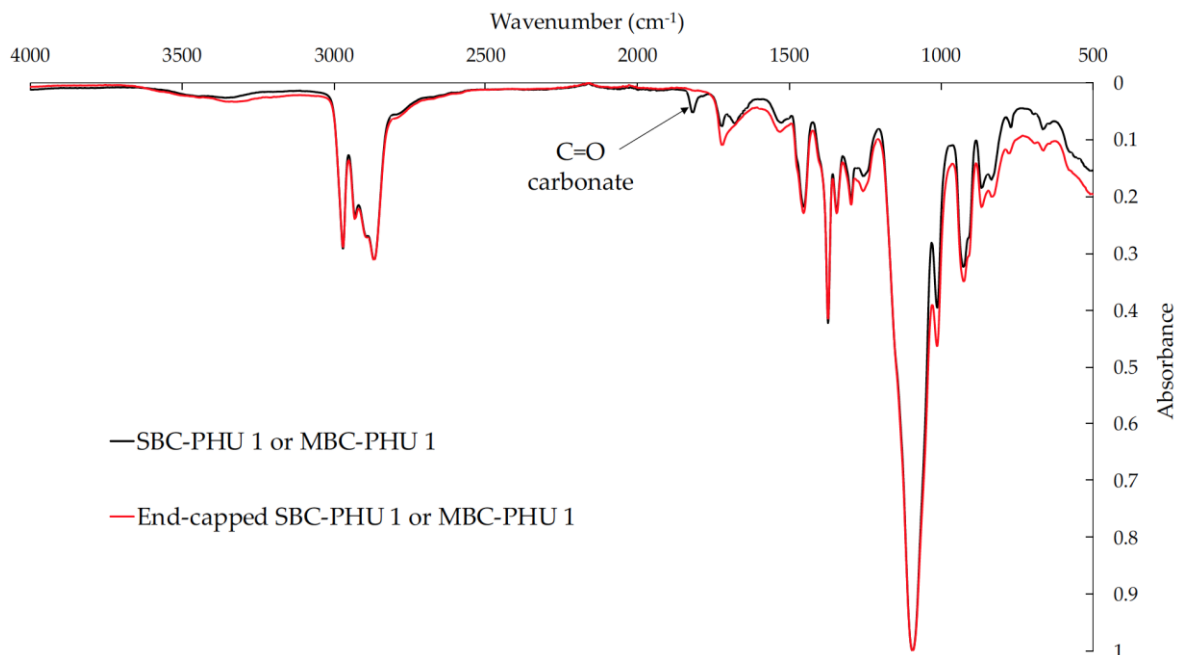


**Figure 4.3 - Comparison of FTIR spectra showing the successful end-capping of SBC-PHU 1 or MBC-PHU 1 with DAMO. Disappearance of the 1800 cm<sup>-1</sup> C=O stretch observed with the DAMO end-capper.**

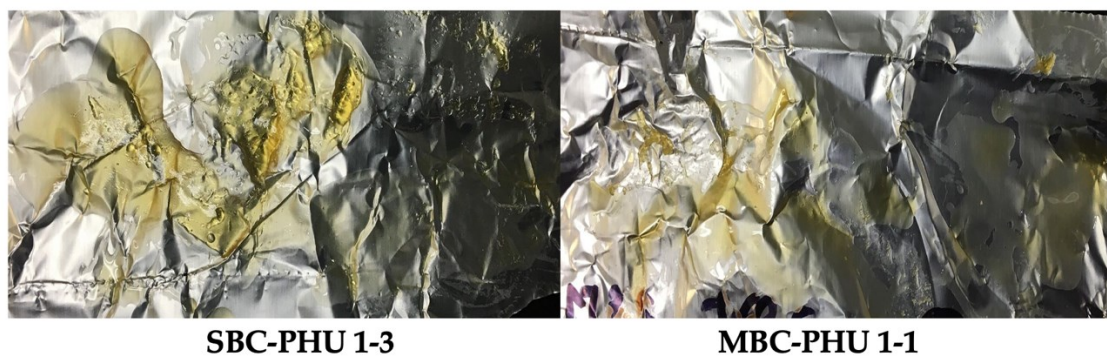


**Figure 4.4 - Smooth HPHU films resulting from trials SBC-PHU 1-3 and MBC-PHU 1-1 presented in Table 4.4 and Table 4.5.**

By comparison, the end-capping reaction of SBC-PHU 3 and MBC-PHU 3 with GLYMO were performed at lower temperatures and proved to work at ambient conditions, as shown elsewhere.<sup>50</sup> Since the polyaddition of SBC-PHU 3 and MBC-PHU 3 were conducted at moderate temperatures of 60 °C and 90 °C, respectively, as shown in Table 4.2, it is convenient to have the end-capping reactions performed at room temperature to inhibit the increase of the prepolymer molecular weight at higher temperatures, such as 120 °C. Unfortunately, the curing of these PHUs seem to be triggered and accelerated by temperatures as low as 22 °C (Trials SBC-PHU 3-2 and MBC-PHU 3-2), which was the ambient lab temperature when running the end-capping reactions. This sheds light on the chemical stability of the end-capped SBC-PHU 3 and MBC-PHU 3 prepolymers, which seems to be compromised even at room temperature. Figure 4.5 shows the different products obtained from trials SBC-PHU 3-2 and MBC-PHU 3-2, in which the polymers crosslinked in the reactor, and trial MBC-PHU 3-1, in which the polymer crosslinked under ambient conditions leading to a smooth film. It is important to mention that the end-capping reactions of the four PHUs were conducted with the counter silane agents, and no curing was observed even after weeks of letting the samples cure under ambient conditions. This is in agreement with the results reported in our previous study.<sup>40</sup>

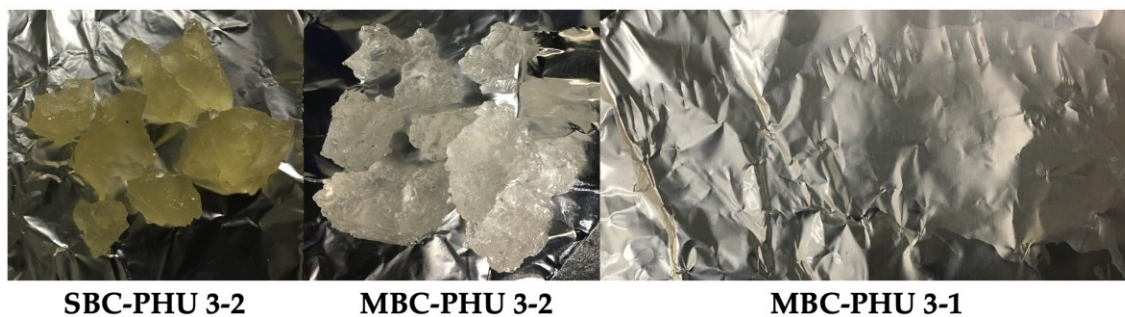


**Figure 4.5 - Crosslinked HPHU products obtained from different end-capping trials with SBC-PHU 3 and MBC-PHU 3: in the cases of SBC-PHU 3-2 and MBC-PHU 3-2, the crosslinking occurred in the reactors contrary to trial MBC-PHU 3-1 in which crosslinking occurred under moisture resulting in a smooth film.**

Curing kinetic studies on the end-capped PHUs were conducted, and combined results of SBC-PHU 1/MBC-PHU 1 and SBC-PHU 3/MBC-PHU 3 are summarized in Figure 4.6, Figure B.12, and Figure B.13 and Figure 4.7, Figure B.14, and Figure B.15, respectively. The importance of these tests is to measure the time needed for the end-capped polymers to crosslink under ambient conditions. When exposed to these conditions, 20-30% humidity and 22 °C, SBC-HPHU 1 and MBC-HPHU 1 films started forming around 30 min and 8 h, respectively, which constitute the gel times of both systems. SBC-PHU 1 cured much faster than its MBC analog due to the addition of the proprietary catalyst, but at the end of the study and even after waiting for a week, both HPHU films were still qualitatively soft. On the other hand, SBC-PHU 3 and MBC-PHU 3 presented similar trends of the moduli and complex viscosities, and gel times of 8 h and 9 h, respectively, were measured. After a week, SBC-HPHU 3 and MBC-HPHU 3 films exhibited good strength with the latter, being clear and colorless, as shown in Figure 4.5.

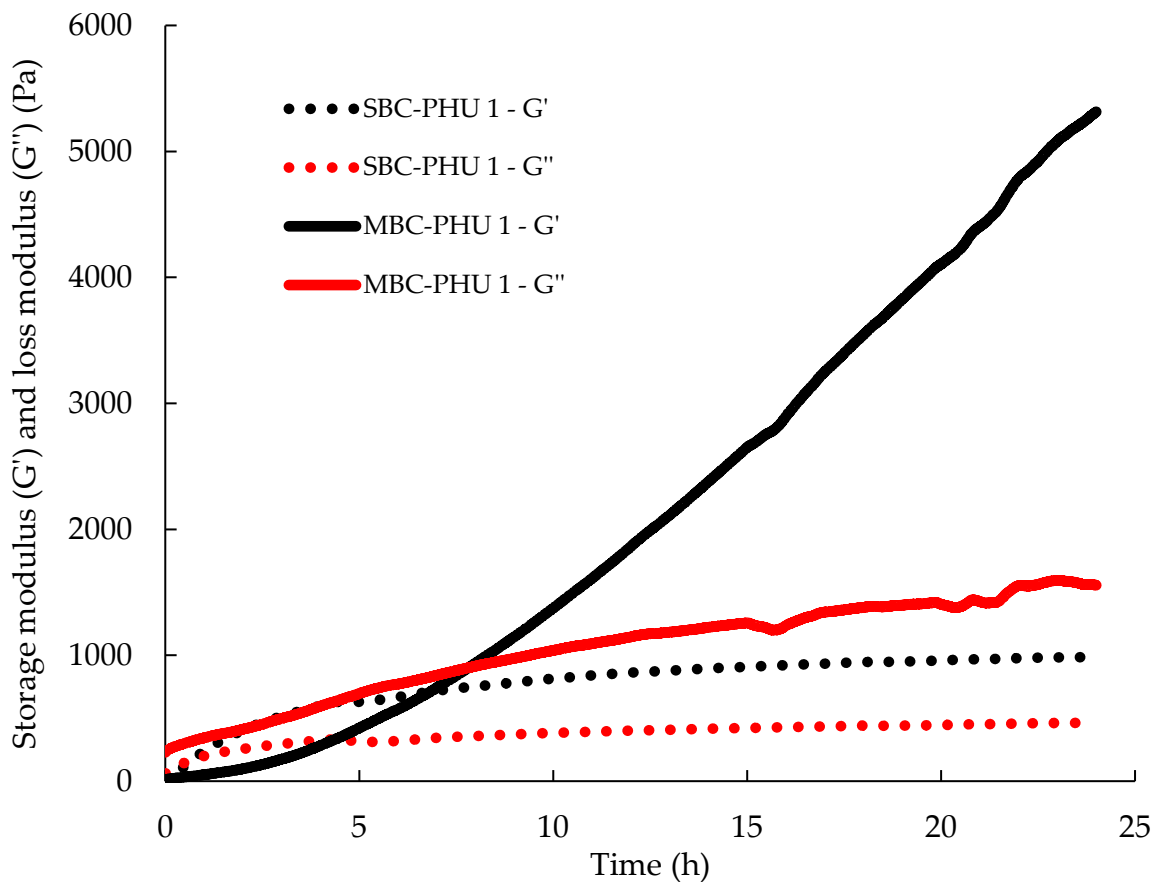


**Figure 4.6 - Curing kinetics of end-capped SBC-PHU 1 and MBC-PHU 1 by following the storage ( $G'$ ) and loss ( $G''$ ) moduli (Pa) at a frequency of 1 Hz and a strain of 1% for 24 h. 0.5 wt.% of the proprietary catalyst was added to end-capped SBC-PHU 1 to accelerate the curing. Measurements were done at 22 °C and 20-30% humidity.**

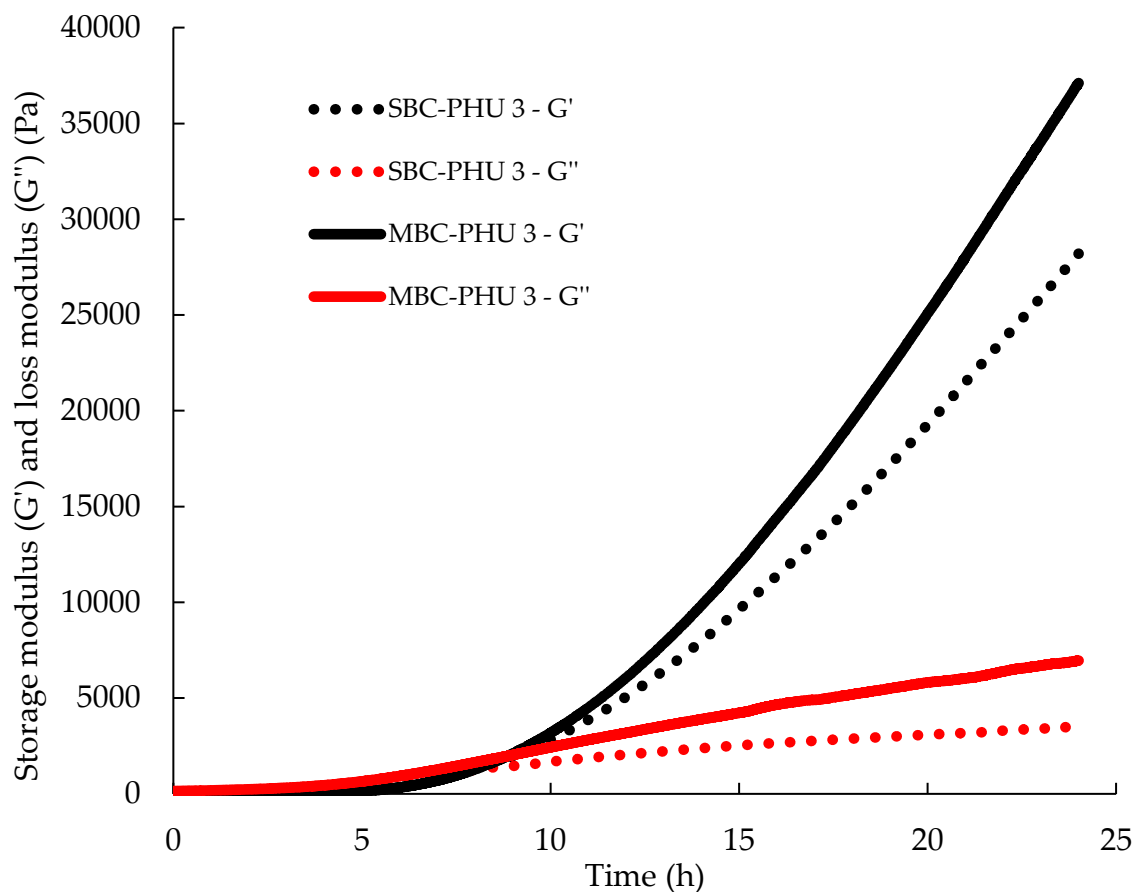


**Figure 4.7 - Curing kinetics of end-capped SBC-PHU 3 and MBC-PHU 3 by following the storage ( $G'$ ) and loss ( $G''$ ) moduli (Pa) at a frequency of 1 Hz and a strain of 1% for 24 h.**

**Measurements were done at 22 °C and 20-30% humidity.**

Surprisingly, the resulting HPHU films did not exhibit any bubble defects in them unlike what was reported in Clark et al.'s study, in which renewable self-blowing PHUs were synthesized from SBC and a lysine derived diamine.<sup>43</sup> The authors reported the formation of  $\text{CO}_2$  through a side reaction during the polymerization, and the gas served as a foaming agent in the final PHU material. During the polyadditions of SBC and MBC conducted in this study, there was no sign of  $\text{CO}_2$  formation, as neither of the HPHU films presented bubbles after crosslinking, as observed from the HPHU films in Figure 4.4 and Figure 4.5.

Moreover, the swelling index (*SI*) and the gel content (*GC*) were measured in THF, which is a solvent the original PHUs dissolved in. *SI* gives insight into the crosslink density of a given HPHU with a lower value corresponding to higher crosslink density. In fact, less solvent can penetrate when the space between the crosslinking nodes is smaller, and that is directly related to a smaller average molecular weight between the crosslinked segments or higher crosslink density. Table 4.6 reports *SI* values between 300 and 400%, implying that all HPHUs of this study have similar crosslink densities. These values are similar to the ones reported for DGC-PPG and DGC-PDMS-5k-(NH<sub>2</sub>)<sub>2</sub> HPHUs synthesized in our previous study (315±22 and 343±8.8, respectively).<sup>40</sup> In contrast, the *GC* data report indirectly the fraction of non-crosslinked species in the HPHU samples. Similarly to the DGC-based samples, the sugar-based PPG HPHUs had much lower *GC* than the PDMS analogues (25% versus 70%, respectively), which agrees with the observations made when qualitatively comparing the mechanical strengths of the films. However, the DGC-based HPHU samples showed higher *GC* values (36.6±3.9 for the PPG-based HPHU and 96.0±0.74 for the PDMS-based one) although a similar synthesis method was adapted for all samples. Higher *GC* values implies higher conversion during the curing process, and hence better final mechanical properties of the films. Previously, the THF *GC* values reported were around 90%,<sup>36</sup> 70%,<sup>37</sup> and >99%,<sup>38</sup> but these samples were cured at high temperatures (at least 100 °C) and some used a catalyst,<sup>37</sup> unlike the moisture-curable HPHU films prepared herein at ambient conditions without a catalyst (except of SBC-HPHU 1).

**Table 4.6 - Swelling in THF and pure H<sub>2</sub>O experimental results for the sugar-based HPHUs synthesized in this work**

HPHUs	THF			Water	
	SI (%)	GC (%)	EWC (%)	EWA (%)	GC (%)
<b>SBC-PHU 1</b>	-	24.8±3.6	-	-	39.1±3.9
<b>MBC-PHU 1</b>	317±26	25.2±2.8	-	-	54.8±3.8
<b>SBC-PHU 3</b>	372±18	63.1±3.1	4.4±1.7	4.2±1.5	99.5±0.44
<b>MBC-PHU 3</b>	303±5.6	76.8±0.97	4.3±0.37	4.1±0.34	98.5±0.08

#### **4.3.4 HPHUs-water interaction and chemical stability**

Swelling experiments in purified H<sub>2</sub>O were conducted on the films of the four different sugar-based HPHU materials. This is done to check for possible interactions between the synthesized materials and water. The data for these experiments is summarized in Table B.1 through Table B.4, and the final results are presented in Table 4.6. EWA and EWC could not be measured for the SBC-HPHU 1 and MBC-HPHU 1 because they became very soft in water, after penetration of water, to be recovered for daily measurements, as shown in Figure 4.8. Also, swollen MBC-HPHU 1 samples broke down into smaller pieces in the water medium due to their low mechanical strength, making these measurements difficult to complete. Similar phenomenon occurs in drug delivery systems in which the polymer carrier swells in the given medium and degrades to release the therapeutic in the targeted site. In fact, PPG co-monomers have been extensively investigated for biomedical applications since they are hydrophilic and water-swella-<sup>51</sup>

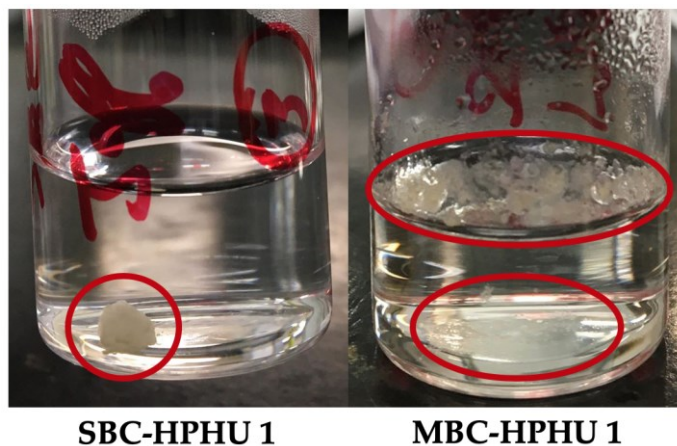


**Figure 4.8 - Swelling of SBC-HPHU 1 and MBC-HPHU 1 in pure H<sub>2</sub>O after one week.**

**Swollen MBC-HPHU 1 films broke down into smaller pieces in the water medium.**

Nevertheless, SBC-HPHU 3 and MBC-HPHU 3, made from PDMS-5k-(NH<sub>2</sub>)<sub>2</sub>, had low *EWC* and *EWA* ~ 4% each, coupled with high gel contents, *GC*, in water of 98-100% after one week, which confirms their hydrophobicity. There was minimal water swelling and penetration between the crosslinking nodes of these samples, which is in agreement with the low *EWC* values. PDMS was extensively studied and was found to be hydrophobic,<sup>49</sup> which correlates with the results obtained herein and that is not surprising considering the low surface energy of silicones. Hence, both PDMS-based HPHUs are considered to be promising materials for exterior sealants and adhesives particularly. Their Jeffamine D-2000-based analogs have to be blended with other additives or reacted with chain extenders to make the resins more hydrophobic.

After drying H<sub>2</sub>O, the residuals (if any) were collected and dissolved in D<sub>2</sub>O and analyzed using <sup>1</sup>H-NMR. This analysis showed materials being leached from the SBC-HPHU 1 and MBC-HPHU 1 samples into the water media while no leaching occurred from the SBC-HPHU 3 and MBC-HPHU 3 films (Figure B.16 and Figure B.19). This result is in agreement with the water *GC* values reported in Table 4.6. As a matter of fact, the lower *GC* of the former

HPHUs (around 40-50%) implies that a part of the films, likely the noncrosslinked PHU chains, dissolved in water, whereas *GC* values of almost 100% were reported for the latter HPHUs. As a result, it can be implied that PDMS-based films are suitable for both indoor and outdoor applications, as they are resistant to water. They also exhibited resistance to the acid medium they were immersed in, as SBC-HPHU 3 and MBC-HPHU 3 samples' weights remained quasi-unchanged during that degradation study with  $99.85\% \pm 0.27$  and  $97.69\% \pm 0.62$  recovery of the initial mass of the films, respectively (Table B.5 and Table B.6, respectively).

Sessile drop tests on SBC-HPHU 3 and MBC-HPHU 3 films showed that they are hydrophobic with an average contact angle with Milli-Q water of  $105^\circ \pm 4.5$  and  $109^\circ \pm 1.2$ , respectively, (Table B.7 and Table B.8). This result is expected as PDMS is known to be hydrophobic.<sup>49</sup> Similar water contact angles were obtained with DGC-PDMS-5k-(NH<sub>2</sub>)<sub>2</sub> HPHU synthesized previously,<sup>40</sup> but the new sugar-based PDMS HPHUs did show a similar elasticity to the DGC-based sample, making them difficult to handle when preparing samples for mechanical and rheological testing. In addition to the difference of the THF *GC* values discussed in the previous section, this can be due to the cycloaliphatic ring present in SBC and MBC. Hence, SAXS and WAXS were conducted on DGC-PDMS-5k-(NH<sub>2</sub>)<sub>2</sub> HPHU, SBC-HPHU 3, and MBC-HPHU 3 films to unveil an explanation for the mechanical performance.

#### **4.3.5 HPHUs microstructure from WAXS and SAXS**

Figure 4.9 shows the WAXS spectra of the polymeric films considered herein. These spectra show neat sharp PDMS peaks in the  $2\theta = 12.5^\circ$  region along with broad peaks centered at  $2\theta = 21.5^\circ$  which is related to the segmented PHU units and the hard segments constituted of the DGC, SBC or MBC alkyl chains. This is similar to the WAXS results obtained with

conventional polyurethanes (PUs) prepared from PDMS diols with the PDMS sharp peak appearing at  $2\theta = 12^\circ$ , and the second broad peak of segmented PUs showing at  $2\theta = 20^\circ$ .<sup>52</sup> These results suggested that these systems of conventional PUs exhibited distinct microphase separated structures. The PDMS soft segments form one phase, seeing their neat peak appearing in the WAXS spectra, while the hard segments, made of the diisocyanates, form the second one, and the third phase is formed from a mixture of the PDMS end-group segments and some dissolved short hard chains.<sup>52-54</sup> Since the WAXS results of Figure 4.9 show similar patterns to those previously discussed,<sup>52-54</sup> the analogy can be applied to the present PHU systems. Therefore, the HPHU films of this work may consist of a PDMS matrix phase, hard domains made of DGC, SBC or MBC alkyl chains, and a mixed phase containing the PDMS end-group segments (propyl chains) and dissolved short hard segments.

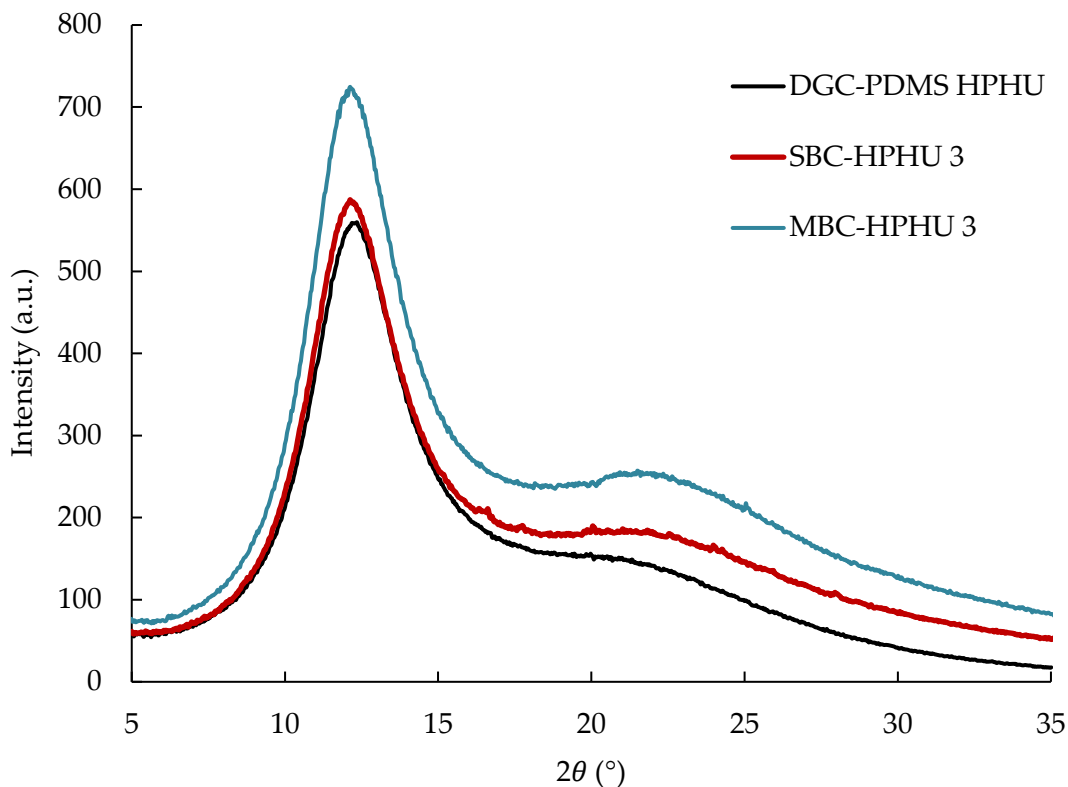


**Figure 4.9 - WAXS spectra of DGC- PDMS-5k-(NH<sub>2</sub>)<sub>2</sub> HPHU, SBC-HPHU 3, and MBC-HPHU 3 showing the clear peak of PDMS chain distinctly appearing at  $2\theta$  of 12.3 to 12.65° proving that the hydroxyurethane units are spread in the PDMS matrix. The intensity is given in logarithmic scale.**

This microphase separation is also observed from the SAXS spectra of Figure B.20, showing a single peak for the PDMS-HPHU films with no higher order reflections, suggesting a relatively weakly disordered morphology of the hard mannitol/sorbitol and hydroxyurethane segments in the PDMS matrix. The mean interdomain spacings,  $d$ , were calculated using these spectra, and the DGC film showed the lowest  $d$  value followed by SBC-HPHU 3, then MBC-HPHU 3, as summarized in Table 4.7. In fact, the structure of DGC is linear whereas SBC and MBC contain a bulky ethoxy cycloaliphatic ring in their structure, which leads to higher  $d$  in

their HPHUs (6.5 and 7.0 nm, respectively). As to the difference between  $d$  of both sugar-based cyclic dicarbonates products with the diamines, it may be caused by the spatial orientations of the bonds forming their cycloaliphatic rings. The lower  $d$  in the DGC film (5.7 nm) might be responsible for the higher elasticity this film exhibits when compared to the sugar-based HPHU films (taking that smaller disperse phase sizes lead to softer materials). A similar trend was found in Beniah et al.'s study on bisphenol A dicarbonate and resorcinol bicarbonate which have similar structures, but the structure of the former has two aromatic rings compared to one in the latter structure. Cured PHU samples of bisphenol A dicarbonate had higher  $d$  and Young's modulus but lower elongation at break and hence lower elasticity compared to their analogous resorcinol bicarbonate samples.<sup>55</sup>

**Table 4.7 - Mean interdomain spacing,  $d$ , calculated from SAXS spectra (Figure B.20 of the supporting information) and Eq. (4.5), of DGC-PDMS-5k-(NH<sub>2</sub>)<sub>2</sub> and the sugar-based PDMS HPHUs of this work**

HPHUs	$q_{\max}$ (nm <sup>-1</sup> )	$d$ (nm)
DGC-PDMS-5k-(NH <sub>2</sub> ) <sub>2</sub>	1.11	5.66
SBC-HPHU 3	0.97	6.48
MBC-HPHU 3	0.90	6.98

Finally, since these hybrid materials do not exhibit the elasticity necessary for the adhesives and sealants, they should be investigated for different industrial applications, such as coatings for example. In fact, Rossi de Aguiar et al. designed moisture curable HPHU coatings from PDMS cyclic carbonates and isophorone diamine which exhibited good adhesion strengths to glass and metallic surfaces and were very effective in protecting steel surfaces against

corrosion processes in acidic and basic media,<sup>35, 39</sup> two properties that were observed in the PDMS-HPHUs of this work.

#### 4.4 Conclusion

The synthesis of new PHUs based on D-sorbitol and D-mannitol, derivatives of glucose processing, was conducted. Despite the high melting points of the sugar-derived dicarbonates, SBC and MBC, PHU oligomers of  $DP_n$  of 2-4 were prepared with long chain diamines, Jeffamine D-2000 and PDMS-5k-(NH<sub>2</sub>)<sub>2</sub>, at moderate temperatures of 60 to 100 °C, in bulk, and without a catalyst compared to previous studies on SBC-based PHUs. Different physical and chemical properties of the resulting PHUs were measured before end-capping them with the corresponding moisture curing agent to afford new partially sustainable sugar-based HPHUs. The curing kinetics of the end-capped PHU prepolymers, SBC-PHU 1 and MBC-PHU 1 based on Jeffamine D-2000 and SBC-PHU 3 and MBC-PHU 3 based on PDMS-5k-(NH<sub>2</sub>)<sub>2</sub>, were monitored, and gel times of less than 10 h were measured at ambient conditions of 22 °C and 20-30% humidity. The end films exhibited gel contents in THF of 25% and 60-80% (for SBC/MBC-HPHU 1 and SBC/MBC-HPHU 3, respectively).

Degradation and swelling studies in H<sub>2</sub>O were then conducted to ensure that the new films are not sensitive to moisture in outdoor conditions. SBC-HPHU 1 and MBC-HPHU 1 films were swollen when immersed in H<sub>2</sub>O for a week, whereas SBC-HPHU 3 and MBC-HPHU 3 films were water resistant as weight loss and swelling were negligible. Further, the <sup>1</sup>H-NMR spectra of the residual solvent from the SBC-HPHU 3 and MBC-HPHU 3 immersion studies indicated no significant leaching from these films. These films were hydrophobic, exhibiting water contact angles of 105° and 109°, respectively; however, they were too brittle to handle so mechanical and rheological properties could not be measured. This brittleness is caused by the

rigidity of SBC and MBC, when compared to DGC, which constitute the hard segments of the PHUs in hand. The microstructure of the PDMS-based films was also investigated, and microphase separation was obvious from the SAXS and WAXS spectra. It is suggested that the films are made of three different phases: a PDMS matrix phase, hard segments phase, and a third phase mixing the PDMS-5k-(NH<sub>2</sub>)<sub>2</sub> end-segments and some dissolved hard segments.

Although this study targeted the synthesis of new sealants and adhesives hybrid materials, the final sugar-based HPHUs still require more work before being applied in such industrial applications. The new hybrid HPHUs were soft or brittle depending on the diamine used, Jeffamine D-2000 or PDMS-5k-(NH<sub>2</sub>)<sub>2</sub>, respectively. However, other applications, such as targeted drug delivery carriers (for SBC/MBC-PHU 1) and coatings (for SBC/MBC-PHU 3), can be investigated in the future.

## 4.5 Materials and Methods

### 4.5.1 Materials

D-Sorbitol ( $\geq 98\%$  powder) and D-mannitol ( $\geq 98\%$  powder), dimethyl carbonate (DMC,  $\geq 99\%$ , anhydrous), 1,5,7,5-triazabicyclo[4.4.0]dec-5-ene (TBD, 98%), and 1,8-Diazabicyclo[5.4.0]undec-7-ene (DBU, 98%) were purchased from Sigma Aldrich. Tetrahydrofuran (THF, HPCL and Certified grades) was obtained from Fisher. Water purified by a reverse osmosis process (pure H<sub>2</sub>O) was provided by the McGill Chemical Engineering Department. The diamines used in this work are Jeffamine D-2000 (poly(propylene glycol) bis(2-aminopropyl ether) with  $M_n = 2,000 \text{ g}\cdot\text{mol}^{-1}$ ) (Huntsman Corp.) and PDMS-(NH<sub>2</sub>)<sub>2</sub>, an aminopropyl terminated polydimethylsiloxane with  $M_n = 5,000 \text{ g}\cdot\text{mol}^{-1}$  (PDMS-5k-(NH<sub>2</sub>)<sub>2</sub>) which was purchased from Gelest. Deuterated dimethyl sulfoxide (DMSO-d<sub>6</sub>) and deuterated

chloroform ( $\text{CDCl}_3$ ) were provided from Sigma Aldrich. Deuterium oxide ( $\text{D}_2\text{O}$ , 99.9% D) was purchased from Cambridge Isotope Laboratories, whereas GLYMO or [3-(2,3-epoxypropoxy)-propyl]-trimethoxysilane, DAMO or N-(2-aminoethyl)-3-aminopropyltrimethoxysilane, and a proprietary silane blend catalyst were purchased from Sigma Aldrich. Acid buffer solution of  $\text{pH} = 3$  at 20-25 °C was bought from Fischer. All the chemicals were used as received. Diglycerol dicarbonate (DGC)-PDMS-5k-( $\text{NH}_2$ )<sub>2</sub> and DGC-PPG were synthesized according to the method detailed in our previous work.<sup>40</sup>

#### 4.5.2 Experimental methods

*SBC synthesis and purification:* D-Sorbitol (10.0 g, 54.9 mmol) and 3 mol.% of TBD with respect to D-sorbitol (234 mg or 1.65 mmol) were introduced into a 100 mL round-bottom flask having a stir bar in it. DMC (32.4 mL, 384 mmol or 7 molar equivalents with respect to D-sorbitol) was then added before purging the reaction mixture with  $\text{N}_2$  for 15 min. The reactor, having an outlet needle in its septum, was set on the stirrer in an oil bath controlled by a thermostat equipped with a temperature sensor and the temperature was adjusted to 75 °C. D-Sorbitol dissolved in DMC within 1 h of the start of the reaction. The reaction was allowed to proceed for 19 h after which the reactor was allowed to cool down to ambient temperatures. Unreacted DMC along with the formed methanol were evaporated from the reaction medium and the light brown residue was soaked for 2 h in pure  $\text{H}_2\text{O}$  (60 mL) in an Erlenmeyer flask containing a stir bar for mixing. After 2 h, the white SBC powder that precipitated was filtered and dried overnight in a vacuum oven at room temperature. At the end of the process, SBC (4.85 g) was weighed, corresponding to 41% yield based on the total amount of D-sorbitol originally loaded. This synthesis method and formulation were obtained following many trials presented in Table B.9 in the supporting information.

*MBC synthesis and purification:* D-Mannitol (10.0 g, 54.9 mmol) and 5 mol.% of TBD with respect to D-mannitol (382 mg or 2.75 mmol) were introduced into a 100 mL round-bottom flask having a stir bar in it. DMC (32.4 mL, 384 mmol or 7 molar equivalents with respect to D-mannitol) was then added before purging the reaction mixture with N<sub>2</sub> for 15 min. The reactor, having an outlet needle in its septum, was set on the stirrer in an oil bath controlled by a thermostat equipped with a temperature sensor and the temperature was adjusted to 75 °C. D-Mannitol dissolved in DMC within 1 h of the start of the reaction. The reaction was allowed to proceed for 16 h after which the reactor was allowed to cool down to ambient temperatures. Unreacted DMC along with the formed methanol were evaporated from the reaction medium and the light brown residue was soaked for 2 h in pure H<sub>2</sub>O (60 mL) in an Erlenmeyer flask containing a stir bar for mixing. After 2 h, the white MBC powder that precipitated was filtered and dried overnight in a vacuum oven at room temperature. At the end of the process, MBC (6.47 g) was weighed corresponding to 55% yield based on the total amount of D-mannitol originally loaded. This synthesis method and formulation were obtained following many trials presented in Table B.9 in the supporting information of Appendix B.

*Polyaddition of SBC with Diamines (1/1 molar equivalent):* SBC (1.0 g, 4.63 mmol) was reacted in a 50 mL round bottom flask with Jeffamine D-2000 (9.3 g, 4.63 mmol), and the mixtures were allowed to react at 120 °C (SBC-PHU 1) for 24 h. SBC (0.50 g, 2.32 mmol) was reacted in separate 50 mL round bottom flasks with PDMS-5k-(NH<sub>2</sub>)<sub>2</sub> (11.6 g, 2.32 mmol), and the mixtures were left for 24 h at 80 °C (SBC-PHU 2), 90 °C (SBC-PHU 3), and 100 °C (SBC-PHU 4). All the batches were purged with N<sub>2</sub> for 15 min prior to heating on a mantle, controlled by a thermostat equipped with a temperature sensor, to the specified temperatures, and every reactor

was equipped with a high viscosity stir bar allowing good mixing of the monomers throughout the polyaddition reaction. Table 4.1 summarizes the SBC-PHU formulations described herein.

*Polyaddition of MBC with Diamines (1/1 molar equivalent):* MBC (1.0 g, 4.63 mmol) was reacted in a 50 mL round bottom flask with Jeffamine D-2000 (9.3 g, 4.63 mmol), and the mixtures were allowed to react at 120 °C (MBC-PHU 1) for 24 h. MBC (0.50 g, 2.32 mmol) was reacted in separate 50 mL round bottom flasks with PDMS-5k-(NH<sub>2</sub>)<sub>2</sub> (11.6 g, 2.32 mmol), and the mixtures were left for 24 h at 50 °C (MBC-PHU 2), 60 °C (MBC-PHU 3), 70 °C (MBC-PHU 4), 80 °C (MBC-PHU 5), and 90 °C (MBC-PHU 6). All the batches were purged with N<sub>2</sub> for 15 min prior to heating on a mantle, controlled by a thermostat equipped with a temperature sensor, to the specified temperatures, and every reactor was equipped with a high viscosity stir bar allowing good mixing of the monomers throughout the polyaddition reaction. Table 4.1 summarizes the MBC-PHU formulations described herein. For all SBC and MBC polyadditions, estimates of the number average degree of polymerization ( $DP_n$ ) and extents of reactions were calculated using Carothers equations for linear polymers in stoichiometric ratios:<sup>56</sup>

$$DP_n = \frac{M_n}{M_0} = \frac{1}{1-p} \quad \text{Eq. (4.1)}$$

Here,  $M_n$  is the relative average number molecular weight measured from gel permeation chromatography (discussed in the next section),  $M_0$  is the relative average number molecular weight of the diamines in question (the diamines having a much higher molecular weight than the dicarbonates), and  $p$  is the conversion of the reaction.

*End-capping of SBC-PHU prepolymers:* SBC-PHU 1 and SBC-PHU 3 were selected for end-capping as their respective viscosities allowed for further reactions to occur in bulk. An estimate of their average molecular weights was made based on their relative molecular weights and those of their respective diamines found from the gel permeation chromatography (GPC) technique

discussed below. From the estimated average molecular weights, the amount of end-cappers to be used, which is ideally set at 2 molar equivalents per mol of polymer, was calculated. 2-3 g of the polymers was mixed with 2 molar equivalents of GLYMO or DAMO, depending on the end-groups of the prepolymer chains. The end-capping reactions with SBC-PHU 1 were run at 120 °C for 30 min and 1 h, and those with SBC-PHU 3 were conducted at room temperature (22 °C) from 2 h and 16 h. The polymer was purged with N<sub>2</sub> for 15 min prior to adding the end-capper. The proprietary catalyst was added when needed at 0.5 wt.% relative to the end-capped polymer mixture. The resulting HPHUs are given the same notation as the PHUs they derive from, and hence PHU is replaced by HPHU in the naming of the samples.

*End-capping of MBC-PHU prepolymers:* MBC-PHU 1 and MBC-PHU 3 were selected for end-capping as their respective viscosities allowed for further reactions to occur in bulk. An estimate of their average molecular weights was made based on their relative molecular weights and those of their respective diamines found from the gel permeation chromatography (GPC) technique discussed below. From the estimated average molecular weights, the concentration of end-cappers to be used, which is ideally set at 2 molar equivalents per mol of polymer, was calculated. 2-3 g of the polymers was mixed with 2 molar equivalents of GLYMO or DAMO, depending on the end-groups of the prepolymer chains. Similar procedures to end-capping the SBC-PHUs were applied. The end-capping reactions with MBC-PHU 1 were run at 120 °C for 15 min and 1 h, and those with MBC-PHU 3 were conducted at room temperature (22 °C) for 2 h and 16 h. The polymer was purged with N<sub>2</sub> for 15 min prior to adding the end-capper. The proprietary catalyst was added when needed at 0.5 wt.% relative to the end-capped polymer mixture. The resulting HPHUs are given the same notation as the PHUs they derive from, and hence PHU is replaced by HPHU in the naming of the samples.

### 4.5.3 Characterization methods

*Proton nuclear magnetic resonance ( $^1\text{H-NMR}$ ) spectroscopy:* Solution-phase NMR spectra were recorded on a Bruker 500 MHz instrument (16 scans) at ambient temperature. SBC and MBC were dissolved in DMSO- $d_6$ , whereas the PHU prepolymers were dissolved in  $\text{CDCl}_3$  to be analyzed.

*Fourier transform infrared (FTIR) spectroscopy:* FTIR measurements were carried out on a PerkinElmer instrument equipped with a single bounce diamond attenuated transmission reflectance (ATR) for solids and zinc selenide (ZnSe) holder for liquids. 32 scans were recorded for each sample over the range 4000-500  $\text{cm}^{-1}$  with a normal resolution of 4  $\text{cm}^{-1}$ . SBC, MBC, their respective PHU prepolymers, and the HPHUs structures were recorded on the machine.

*Gel permeation chromatography (GPC):* The PHU prepolymers' molecular weights were analyzed via GPC. Number average molecular weight ( $M_n$ ) and dispersity ( $D = M_w/M_n$ ) of prepolymer samples were measured using this technique on a Waters Breeze instrument with HPLC grade THF as an eluent at a flow rate of 0.3  $\text{mL}\cdot\text{min}^{-1}$ . The GPC has three Waters Styragel HR columns (HR1 with a molecular weight measurement range of  $10^2$  to  $5 \times 10^3$   $\text{g}\cdot\text{mol}^{-1}$ , HR2 with a molecular weight measurement range of  $5 \times 10^2$  to  $2 \times 10^4$   $\text{g}\cdot\text{mol}^{-1}$ , and HR4 with a molecular weight measurement range of  $5 \times 10^3$  to  $6 \times 10^5$   $\text{g}\cdot\text{mol}^{-1}$ ), a guard column, and a refractive index (RI 2414) detector. The columns were heated to 40  $^\circ\text{C}$  during analysis. The molecular weights were determined relative to polystyrene (PS) calibration standards from Varian Inc. (ranging from 682 to 2,520,000  $\text{g}\cdot\text{mol}^{-1}$ ). The reported molecular weights were all relative to the PS standards and not adjusted with Mark-Houwink parameters.

*Thermogravimetric analysis (TGA):* TGA was performed on a Q500 system from TA Instruments. The thermal degradation of the synthesized PHU prepolymers was measured at a

heating rate of  $10\text{ }^{\circ}\text{C}\cdot\text{min}^{-1}$  over the temperature range of  $25\text{-}700\text{ }^{\circ}\text{C}$  under a nitrogen atmosphere. The onset degradation temperature ( $T_{d,onset}$ ) and the 10% degradation temperature ( $T_{d,10\%}$ ) were calculated using this method.

*Differential scanning calorimetry (DSC):* DSC was performed using a Q2000 TA Instruments calorimeter employing standard hermetic aluminum pans, calibrated with indium and nitrogen as purge gas. The samples were analyzed at a heating rate of  $10\text{ }^{\circ}\text{C}\cdot\text{min}^{-1}$  over a temperature range of  $-90\text{ }^{\circ}\text{C}$  to  $120\text{ }^{\circ}\text{C}$  under a nitrogen atmosphere. Glass transition temperatures ( $T_{gs}$ ) were calculated from the second heating ramp.

*Rheology:* Viscosities of SBC-PHUs 1 and 3 and MBC-PHUs 1 and 3 were measured on an Anton Paar Instruments rheometer (MCR 302) operated in the parallel plate steady shear mode (gap 1 mm). The samples were placed symmetrically in the center of the plate. The shear stress was measured at different shear rates ranging from  $0.01\text{ s}^{-1}$  to  $10\text{ s}^{-1}$  in 19 measurements during 3 min. All the measurements were conducted at ambient conditions.

The curing kinetics of the end-capped PHUs was carried out on the same instrument equipped with two parallel plate geometry at a frequency of 1 Hz, a strain of 1%, and the measurements were carried out at room temperature (around  $22\text{ }^{\circ}\text{C}$ ) with a humidity range of 20-30%. The evolutions of storage modulus ( $G'$ ), loss modulus ( $G''$ ), damping factor ( $\tan\delta = G''/G'$ ), and complex viscosity ( $\eta^*$ ) were monitored as a function of time for 24 h. Before running these measurements, the samples were allowed to cool down to room temperature.

*Swelling:* Swelling of the HPHUs in THF and water was conducted at room temperature. THF swelling of the HPHUs was evaluated using the swelling index ( $SI$ ) and gel content ( $GC$ ). Water swelling of SBC-PHUs 1 and 3 and MBC-PHUs 1 and 3 (in the form of films) was evaluated using water content and absorption measurements. Film samples of random sizes were immersed

in 7 mL pure H<sub>2</sub>O or THF at room temperature. A period of a week was adapted with all samples in both solvents to make sure they reached their swelling equilibrium state. In fact, the weights of the PDMS-based samples immersed in water were measured every day, and after 5 days the weight stopped changing, and hence a period of a week was chosen for the rest of the samples. The swelling index (*SI*), equilibrium water content (*EW**C*) and equilibrium water absorption (*EW**A*) were estimated using Eq. (4.2) and Eq. (4.3). After swelling measurements, the samples were dried in a vacuum oven overnight at 40 °C, and the gel content was measured using Eq. (4.4).<sup>57</sup>

$$SI(\%) = EW\text{C}(\%) = \left( \frac{W_s - W_d}{W_d} \right) \times 100 \quad \text{Eq. (4.2)}$$

$$EW\text{A}(\%) = \left( \frac{W_s - W_d}{W_s} \right) \times 100 \quad \text{Eq. (4.3)}$$

$$GC(\%) = \left( \frac{W_f}{W_i} \right) \times 100 \quad \text{Eq. (4.4)}$$

Here, *W<sub>s</sub>* is the weight of the swollen sample, *W<sub>d</sub>* is the weight of the dry sample, *W<sub>i</sub>* is the initial weight, and *W<sub>f</sub>* is the final weight of the dried sample. The swelling in THF of the DGC-based HPHUs synthesized previously<sup>40</sup> were also assessed herein for comparison purposes.

*HPHUs degradation in water:* The samples from the water swelling study were used herein afterwards. The water was dried under air flow overnight, and the residuals, if any, were dissolved in D<sub>2</sub>O to be analyzed using <sup>1</sup>H-NMR. The degradation of SBC-HPHU 3 and MBC-HPHU 3 films was also assessed in a buffer solution of water with the pH adjusted to 3. Three samples of random sizes of each of the films were taken and weighed over a week to check for any mass losses.

*Water contact angle:* Contact angle measurements were performed on an OCA 150 apparatus (Dataphysics Instrument GmbH) in the sessile drop configuration by the deposition of a 10 μL

droplet of Milli-Q water at the rate of  $2.0 \mu\text{L}\cdot\text{s}^{-1}$  with a 0.5 mL GASTIGHT #1750 syringe. The mean contact angle values on the SBC-HPHU 3 and MBC-HPHU 3 films were determined using SCA20 software from five repeated measurements conducted on different locations of the film.

*Small and Wide Angle X-ray Scattering (SAXS and WAXS):* SAXS and WAXS spectroscopy measurements were recorded on a SAXSpoint 2.0 (Anton Paar, Austria) equipped with a  $\text{CuK}\alpha$  radiation source (wavelength,  $\lambda = 1.54 \text{ \AA}$ ), using a detector of Eiger R 1M (Horizontal) at SAXS and WAXS distances of 1075.9 and 113.1 mm, respectively. The hybrid polymers DGC-PDMS-5k-( $\text{NH}_2$ )<sub>2</sub> HPHU (synthesized in our previous study),<sup>40</sup> SBC-HPHU 3, and MBC-HPHU with thickness of 1 mm were placed on a sample holder for solids (10 by 10 mm) provided by Anton Paar, which was further secured by tape. X-ray exposure times were 30 min per frame for a total of 4 frames for every experiment. The obtained SAXS profiles were corrected and shown as function of scattering vector ( $q = (4\pi/\lambda)\cdot\sin\theta$ , where  $2\theta$  is the scattering angle in  $^\circ$  and  $q$  in  $\text{nm}^{-1}$ ). The mean interdomain spacing,  $d$  (nm), was calculated from the obtained SAXS spectra using the following formula:

$$d = 2\pi/q_{max} \quad \text{Eq. (4.5)}$$

with  $q_{max}$  ( $\text{nm}^{-1}$ ) is the value of  $q$  at maximum peak position read from SAXS spectra.

#### 4.6 References

1. J. Guan, Y. Song, Y. Lin, X. Yin, M. Zuo, Y. Zhao, X. Tao, Q. Zheng, *Ind. Eng. Chem. Res.* **2011**, *50*, 6517.
2. M. S. Kathalewar, P. B. Joshi, A. S. Sabnis, V. C. Malshe, *RSC Adv.* **2013**, *3*, 4110.
3. G. Rokicki, P. G. Parzuchowski, M. Mazurek, *Polym. Adv. Technol.* **2015**, *26*, 707.

4. A. Cornille, R. Auvergne, O. Figovsky, B. Boutevin, S. Caillol, *Eur. Polym. J.* **2017**, *87*, 535.
5. O. Kreye, H. Mutlu, M. A. R. Meier, *Green Chem.* **2013**, *15*, 1431.
6. H. Blattmann, M. Fleischer, M. Bahr, R. Mulhaupt, *Macromol. Rapid Commun.* **2014**, *35*, 1238.
7. L. Maisonneuve, O. Lamarzelle, E. Rix, E. Grau, H. Cramail, *Chem. Rev.* **2015**, *115*, 12407.
8. V. K. Abitha, S. A. Jadhav, A. V. Rane, *Moroccan J. Chem.* **2016**, *4*, 361.
9. V. Kestelman, O. Figovsky, D. Beilin, in *Advanced Polymer Concretes and Compounds*, CRC Press Taylor & Francis Group, 2014, Ch. 4.
10. O. Figovsky, L. Shapovalov, A. Leykin, O. Birukova, R. Potashnikova, *Chem. Chem. Technol.* **2013**, *7*, 79.
11. S. Verma, G. Kumar, A. Ansari, R. I. Kureshy, N. U. Khan, *Sustainable Energy Fuels* **2017**, *1*, 1620.
12. S. Verma, M. Nazish, R. I. Kureshy, N. U. Khan, *Sustainable Energy & Fuels* **2018**, *2*, 1312.
13. H. Liang, J. Wang, F. Wang, Y. Feng, M. Kang, Z. Wang, *J. Chem. Technol. Biotechnol.* **2018**, *93*, 2271.
14. F. D. Bobbink, A. P. van Muyden, P. J. Dyson, *Chem. Commun.* **2019**, *55*, 1360.
15. H. Büttner, L. Longwitz, J. Steinbauer, C. Wulf, T. Werner, *Top. Curr. Chem.* **2017**, *375*, 50.
16. M. Alves, B. Grignard, R. Mereau, C. Jerome, T. Tassaing, C. Detrembleur, *Catal. Sci. Technol.* **2017**, *7*, 2651.

17. M. North, R. Pasquale, C. Young, *Green Chem.* **2010**, *12*, 1514.
18. J. W. Comerford, I. D. V. Ingram, M. North, X. Wu, *Green Chem.* **2015**, *17*, 1966.
19. G. Fiorani, W. Guo, A. W. Kleij, *Green Chem.* **2015**, *17*, 1375.
20. C. Martín, G. Fiorani, A. W. Kleij, *ACS Catal.* **2015**, *5*, 1353.
21. B. Nohra, L. Candy, J. F. Blanco, C. Guerin, Y. Raoul, Z. Mouloungui, *Macromolecules* **2013**, *46*, 3771.
22. M. A. R. Meier, *Macromol. Rapid Commun.* **2019**, *40*, 1800524.
23. M. Ghasemlou, F. Daver, E. P. Ivanova, B. Adhikari, *Eur. Polym. J.* **2019**, *118*, 668.
24. K. Błażek, J. Datta, *Cri. Rev. Environ. Sci. Technol.* **2019**, *49*, 173.
25. C. Carré, Y. Ecochard, S. Caillol, L. Averous, *ChemSusChem* **2019**, *12*, 3410.
26. A. Cornille, G. Michaud, F. Simon, S. Fouquay, R. Auvergne, B. Boutevin, S. Caillol, *Eur. Polym. J.* **2016**, *84*, 404.
27. M. Tryznowski, A. Swiderska, T. Golofit, Z. Zolek-Tryznowska, *RSC Adv.* **2017**, *7*, 30385.
28. S. Panchireddy, J. M. Thomassin, B. Grignard, C. Damblon, A. Tatton, C. Jerome, C. Detrembleur, *Polym. Chem.* **2017**, *8*, 5897.
29. S. Panchireddy, B. Grignard, J. M. Thomassin, C. Jerome, C. Detrembleur, *Polym. Chem.* **2018**, *9*, 2650.
30. M. Tryznowski, T. Golofit, A. Swiderska, *Polymer* **2018**, *144*, 1.
31. S. Panchireddy, B. Grignard, J.-M. Thomassin, C. Jerome, C. Detrembleur, *ACS Sustainable Chem. Eng.* **2018**.
32. R. H. Lambeth, *Polym. Int.* **2020**, <https://doi.org/10.1002/pi.6078>.
33. Y. Ecochard, S. Caillol, *Eur. Polym. J.* **2020**, *137*, 109915.

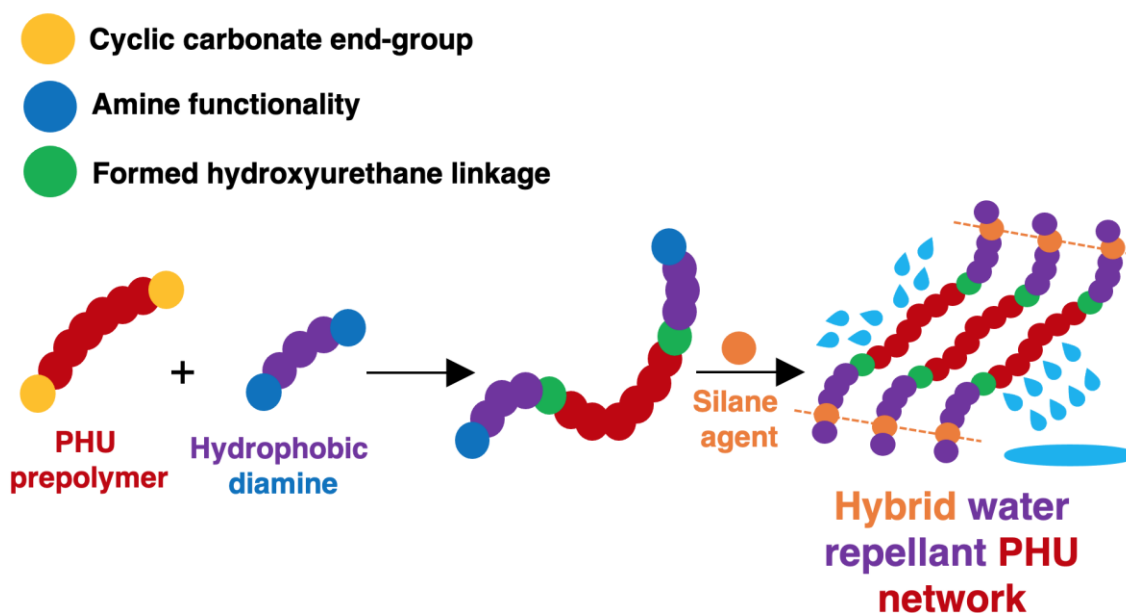
34. M. Kathalewar, A. Sabnis, *Int. J. Sci. Eng. Res.* **2012**, 3, 1.
35. K. M. F. Rossi de Aguiar, E. P. Ferreira-Neto, S. Blunk, J. F. Schneider, C. A. Picon, C. M. Lepienski, K. Rischka, U. P. Rodrigues-Filho, *RSC Adv.* **2016**, 6, 19160.
36. M. Decostanzi, Y. Ecochard, S. Caillol, *Eur. Polym. J.* **2018**, 109, 1.
37. A. Gomez-Lopez, B. Grignard, I. Calvo, C. Detrembleur, H. Sardon, *ACS Appl. Polym. Mater.* **2020**, 2, 1839.
38. A. Gomez-Lopez, B. Grignard, I. Calvo, C. Detrembleur, H. Sardon, *Macromol. Rapid Commun.* **2020**, 2000538.
39. F. Günther, E. F. S. Lima, K. M. F. Rossi de Aguiar, J. R. Bearzi, M. B. Simões, R. Schneider, R. A. Bini, S. J. L. Ribeiro, M. W. C. Man, K. Rischka, F. H. B. Aguiar, R. Pereira, M. d. C. A. J. Mainardi, M. C. Rocha, I. Malavazi, T. A. Passeti, M. L. Santos, H. Imasato, U. P. Rodrigues-Filho, *J. Sol-Gel Sci. Technol.* **2020**, 95, 693.
40. G. R. Younes, G. Price, Y. Dandurand, M. Maric, *ACS Omega* **2020**, 5, 30657.
41. K. M. Tomczyk, P. A. Guńka, P. G. Parzuchowski, J. Zachara, G. Rokicki, *Green Chem.* **2012**, 14, 1749.
42. M. M. Mazurek-Budzyska, G. Rokicki, M. Drzewicz, P. A. Guka, J. Zachara, *Eur. Polym. J.* **2016**, 84, 799.
43. J. H. Clark, T. J. Farmer, I. D. V. Ingram, Y. Lie, M. North, *Eur. J. Org. Chem.* **2018**, 2018, 4265.
44. P. Furtwengler, L. Averous, *Sci. Rep.* **2018**, 8, 1.
45. J. L. J. van Velthoven, L. Gootjes, D. S. van Es, B. A. J. Noordover, J. Meuldijk, *Eur. Polym. J.* **2015**, 70, 125.

46. M. Tryznowski, A. Swiderska, Z. Zolek-Tryznowska, T. Golofit, P. G. Parzuchowski, *Polymer* **2015**, *80*, 228.
47. A. Bossion, I. Olazabal, R. H. Aguirresarobe, S. Marina, J. Martín, L. Irusta, D. Taton, H. Sardon, *Polym. Chem.* **2019**, *10*, 2723.
48. M. Wloch, J. Datta, in *Polyurethane Polymers: Blends and Interpenetrating Polymer Networks*, (Eds: S. Thomas; J. Datta; J. T. Haponiuk, A. Reghunadhan), Elsevier, 2017, Ch. 7.
49. A. Jones, R. N. Lamb, H. Zhang (Unisearch Limited), US 6,743,467 B1, **2004**.
50. H. Lee, D. Sung, J. Kim, B. T. Kim, T. Wang, S. S. An, S. W. Seo, D. K. Yi, *Int. J. Nanomed.* **2015**, *10 Spec Iss*, 215.
51. X. J. Loh, K. B. Colin Sng, J. Li, *Biomaterials* **2008**, *29*, 3185.
52. T. Choi, J. Weksler, A. Padsalgikar, J. Runt, *Polymer* **2010**, *51*, 4375.
53. R. Hernandez, J. Weksler, A. Padsalgikar, J. Runt, *Macromolecules* **2007**, *40*, 5441.
54. T. Choi, J. Weksler, A. Padsalgikar, J. Runt, *Polymer* **2009**, *50*, 2320.
55. G. Beniah, X. Chen, B. E. Uno, K. Liu, E. K. Leitsch, J. Jeon, W. H. Heath, K. A. Scheidt, J. M. Torkelson, *Macromolecules* **2017**, *50*, 3193.
56. A. Rudin, P. Choi, *The Elements of Polymer Science & Engineering*, Academic Press, Oxford, UK **2013**.
57. S. Gennen, B. Grignard, J. M. Thomassin, B. Gilbert, B. Vertruyen, C. Jerome, C. Detrembleur, *Eur. Polym. J.* **2016**, *84*, 849.

## Chapter 5

### Increasing the hydrophobicity of hybrid poly(propylene glycol)-based polyhydroxyurethanes by capping with hydrophobic diamine

While making the HPHUs from the bio-based dicarbonates, the PHUs prepared using Jeffamine D-2000 or the poly(propylene glycol) (PPG) diamine had weaker tensile strength and were less resistant to water compared to the PHUs made from the poly(dimethylsiloxane) (PDMS) diamine. However, the latter was estimated to be cheaper than the former with a cost of 9 US\$/kg versus 39 US\$/kg, respectively. Consequently, cost dilution of the poly(DGC-PPG) PHU while still maintaining desirable mechanical properties and water resistance was the focus of this chapter published in *Industrial & Engineering Chemistry Research* in 2021 (Younes, G. R.; Maric, M., Increasing the Hydrophobicity of Hybrid Poly(propylene glycol)-Based Polyhydroxyurethanes by Capping with Hydrophobic Diamine. *Ind. Eng. Chem. Res.* **2021**, *60* (22), 8159-8171).<sup>195</sup>



## 5.1 Abstract

Hydrophobicity of hybrid polyhydroxyurethane (HPHU), via sol/gel curing of a PHU made from diglycerol dicarbonate (DGC) and a poly(propylene glycol) (PPG)-based diamine, is increased by reacting the carbonate-terminated PHU with diamines based on poly(dimethylsiloxane) (PDMS) and the fatty acid-derived Priamine 1074. The modified PHUs were end-capped with silane moisture-curing agents, and swelling of the HPHUs was studied in water and other solvents over one week. These films exhibited a drop in water swelling index (4%) compared to the original poly(DGC-PPG) HPHUs (75%). The PDMS-modified HPHU has a dominant PDMS phase, due to its comparatively longer chain length relative to the PHU, thereby increasing water repellency. Besides an increase in hydrophobicity, the Priamine 1074-modified HPHU revealed a higher storage modulus that is at least 12 times higher than that of the original films. Consequently, Priamine 1074 is regarded as a promising bio-based reactive additive when formulating hydrophobic PHU resins.

## 5.2 Introduction

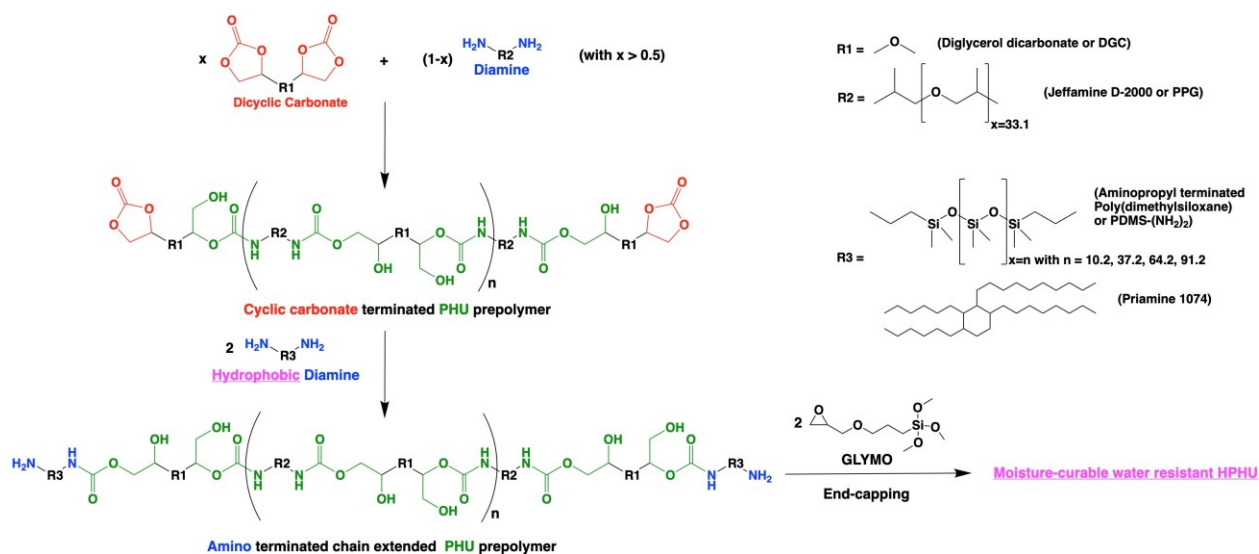
In the last decade, different routes for non-isocyanate poly(urethanes) (NIPUs) have been developed to eliminate the use of isocyanates, a dangerous and lethal main component of conventional poly(urethanes) (PUs). This is critical as PUs are the 6<sup>th</sup> most used polymer (8% of all plastics), with a market valued at ~ \$70 billion US.<sup>1-3</sup> Among the different routes, the step-growth polymerization of cyclic (poly)carbonates with (poly)amines has become the most prominent because it does not form lower molecular weight byproducts and its precursors are abundant.<sup>4-7</sup> These NIPUs are known as poly(hydroxyurethanes) (PHUs) because the resulting polymer chains contain hydroxyl pendant groups. Furthermore, the cyclic carbonate precursors used to prepare these PHUs can be synthesized from reactions involving the chemical fixation of

carbon dioxide (CO<sub>2</sub>) with epoxy (oxirane) groups, which has received most attention from researchers.<sup>8</sup> The cyclic dicarbonates and diamines, and therefore the respective PHUs, were also synthesized from bio-based and bio-renewable sources, such as vegetable oils, bio-polyols, and terpenes, which targets different green chemistry principles, particularly those aiming at substituting non-renewable fossil fuel-based building blocks with greener ones.<sup>9-13</sup>

Increasingly more attention has been given to the preparation of petrochemical and bio-based hybrid PHUs (HPHU) for specific applications, such as adhesives, sealants, coatings, and rigid foams.<sup>14, 15</sup> Specifically, moisture-curable or sol/gel HPHUs were developed by making PHUs with alkoxy silane functional groups<sup>16</sup> or by reacting the PHU end-groups with the appropriate silane curing agent.<sup>17-23</sup> Among these studies, we were able to cure our partially bio-based PHUs at ambient conditions and without the use of any catalyst.<sup>21</sup>

In our last study, moisture-curable HPHUs from diglycerol dicarbonate (DGC), as the bio-based cyclic carbonate counterpart, were synthesized.<sup>21</sup> DGC was coupled with different diamines, and sol/gel HPHUs made of DGC and poly(dimethyl siloxane) diamine with  $M_n = 5,000$  g/mol (PDMS-5k-(NH<sub>2</sub>)<sub>2</sub>) were found as promising sealants and adhesives; however, the relatively high cost of the PDMS diamine might be commercially prohibitive. In contrast, a poly(propylene glycol) bis(2-aminopropyl ether) with  $M_n = 2,000$  g/mol diamine, known as Jeffamine D-2000, was also coupled with DGC. The resulting poly(propylene glycol) (PPG)-based HPHUs are cheaper to produce, but they showed poor mechanical properties and low water resistance when immersed in pure water for a week, with an equilibrium water content (EWC) of 62.97%±3.54. This restricted us from further investigating these materials in sealant and adhesive applications.

This work explores a new method to dilute the cost of the previously synthesized HPHUs by proposing the following. Since the DGC/PPG HPHUs are cheaper to produce, it would be beneficial to overcome their swelling when exposed to water, especially that PPG diol soft segments have been commonly used in the formulation of conventional PU sealants and adhesives because they provide good adhesion of the resin to different substrates.<sup>19</sup> Hence, the objective of this work is to increase the hydrophobicity of the cheaper DGC-Jeffamine D-2000 (PPG-based diamine) HPHUs, previously investigated.<sup>21</sup> It takes advantage of a step-wise synthesis method and uses different hydrophobic diamines as the soft segments to increase the water repellency of the targeted HPHUs. First, cyclic carbonate terminated prepolymers are prepared after which the cyclic carbonate end-groups are reacted with the oily Priamine 1074 and the hydrophobic PDMS-based diamines (PDMS-(NH<sub>2</sub>)<sub>2</sub>) of different chain length (M<sub>n</sub> ranging from 1,000 to 7,000 g/mol). The modified PHUs are then functionalized with silane moisture-curing agents, GLYMO or [3-(2,3-epoxypropoxy)-propyl]-trimethoxysilane and DAMO or N-(2-aminoethyl)-3-aminopropyltrimethoxysilane, to prepare the final HPHUs whose curing kinetics and water repellency are studied. Scheme 5.1 summarizes the proposed idea of this study.



**Scheme 5.1 - The step-wise synthesis method proposed in this work to increase the hydrophobicity of the DGC-PPG HPHUs**

Previously, many studies have acknowledged the increase in hydrophobicity of their PHUs and HPHUs containing Priamine 1074 or other bio-based dimer fatty acid-derived diamines, as well as vegetable and plant oil-based derived cyclic carbonates.<sup>24-34</sup> Moreover, others have incorporated poly(dimethylsiloxane) (PDMS), present in either the carbonate or the diamine component,<sup>22, 35-39</sup> into their PHU structure or functionalized the polymer chains with polyhedral oligomeric silsesquioxanes (POSS),<sup>40</sup> starch additives,<sup>41</sup> fluorine,<sup>42</sup> silica nanoparticles and functional groups,<sup>43, 44</sup> n-alkyl side chains,<sup>45</sup> or diethyl tartrate<sup>46</sup> to increase the water resistance of their PHU materials. Interestingly, Li et al. reacted their amine-terminated PHU prepolymers from both ends with isocyanate-terminated conventional PU to make water and solvent resistant coatings.<sup>47</sup> A similar method is adopted herein, but the carbonate-terminated PHUs are reacted with different hydrophobic diamines, constituting a novel step-wise synthesis method toward engineering cheaper relatively hydrophobic PPG-based HPHUs.

## 5.3 Materials and Methods

### 5.3.1 Materials

Diglycerol (DIG,  $\geq 80\%$   $\alpha,\alpha$ , impurities consist of mono-,  $\alpha,\beta$ -di-,  $\beta,\beta$ -di-, and triglycerol) was obtained from Tokyo Chemical Industry (TCI). Dimethyl carbonate (DMC,  $\geq 99\%$ , anhydrous) and potassium carbonate ( $K_2CO_3$ , 98%, anhydrous powder) were purchased from Acros. Ethyl acetate (EtOAc, certified grade), tetrahydrofuran (THF, HPCL and certified grades), toluene (certified grade), and chloroform (stabilized with ethanol) were purchased from Fischer Chemical. Water purified by a reverse osmosis process (pure  $H_2O$ ) was provided by the McGill Chemical Engineering Department. The diamines used in this work are Jeffamine D-2000 or poly(propylene glycol) bis(2-aminopropyl ether) with  $M_n = 2,000$  g/mol (PPG) and Priamine 1074 which were provided by Huntsman and Croda, respectively. The PDMS-( $NH_2$ )<sub>2</sub> or aminopropyl terminated polydimethylsiloxane with  $M_n = 1,000$  g/mol (PDMS-1k-( $NH_2$ )<sub>2</sub>),  $M_n = 3,000$  g/mol (PDMS-3k-( $NH_2$ )<sub>2</sub>), and  $M_n = 5,000$  g/mol (PDMS-5k-( $NH_2$ )<sub>2</sub>) were provided by Gelest, and PDMS-7k-( $NH_2$ )<sub>2</sub> with  $M_n = 7,000$  g/mol was provided by Genesee. Deuterated dimethyl sulfoxide ( $DMSO-d_6$ ), deuterated chloroform ( $CDCl_3$ ), GLYMO or [3-(2,3-epoxypropoxy)-propyl]-trimethoxysilane, and DAMO or N-(2-aminoethyl)-3-aminopropyltrimethoxysilane and a proprietary silane blend catalyst were purchased from Sigma Aldrich. All the chemicals were used as received.

### 5.3.2 Experimental methods

**DGC synthesis and purification:** The DGC reaction and purification were performed similarly to our previous study.<sup>21</sup> At the end of the synthesis, a DGC yield of 58% was achieved. The labelled  $^1H$ -NMR spectrum of DGC is given as Figure C.1 of the supporting information.

**Polyaddition of DGC with PPG-based diamine (55 mol.% to 45 mol.%, respectively):** The polyaddition was conducted following the same method described in our previous study at 120 °C for 24 h.<sup>21</sup> The resulting DGC-PPG PHU prepolymer, abbreviated as poly(DGC-PPG), had carbonate terminated oligomer chains whose carbonyl stretch was observed from Fourier transform infrared (FTIR) spectroscopy measurements discussed in the next section. Before using the PHU in further steps, the unreacted DGC was allowed to settle down at the bottom of the flask over a period of 48 h, and the polymer was decanted. This ensured that the unreacted DGC does not participate in future polymerization with the hydrophobic diamines. The absence of DGC in the PHU was further verified by dissolving the polymer in chloroform, in which DGC is insoluble, and the solution was filtered before evaporating chloroform and further drying the PHU in a vacuum oven at 40 °C overnight. The new FTIR showed a similar carbonyl stretch area of the carbonate end-group (at 1800 cm<sup>-1</sup>) relative to that of the urethane linkage (at 1720 cm<sup>-1</sup>) proving that there was no DGC in the decanted polymer (Figure C.2).

**Sequential addition of the hydrophobic diamine to poly(DGC-PPG):** Poly(DGC-PPG) had a sufficiently low viscosity, allowing the reactions to be carried out in bulk. An estimate of its molecular weight was made based on its relative molecular weight and that of Jeffamine D-2000 found from the size exclusion chromatography (SEC) technique discussed below (see Appendix C). We acknowledge that these molecular weights are only estimates and do not represent the actual absolute molecular weights. However, since we are working with oligomers of four to six hydroxyurethane linkages, this method does not give erroneous estimates. From the estimated molecular weights, the amount of hydrophobic diamine to be used, which is set at 2 molar equivalents per mol of polymer (to account for each chain end of the linear polymer), was calculated. Typically, 2-3 g of the polymers were mixed with 2 molar equivalents of each of the

different chain length PDMS-(NH<sub>2</sub>)<sub>2</sub> or Priamine 1074. The reaction media were purged with N<sub>2</sub> for 15 min prior to starting the reaction, which was allowed to proceed for 24 h at 100 °C. A preliminary reaction of poly(DGC-PPG) at these conditions was conducted to ensure that no chain scission of the prepolymer would occur while chain extending it. All the synthesized PHUs, denoted by HydrophobicDiamine-poly(DGC-PPG)-HydrophobicDiamine, had amine terminated chains, except for one sample that was reacted with only 0.5 molar equivalents of PDMS-7k-(NH<sub>2</sub>)<sub>2</sub> per mol of polymer to afford PDMS-7k-poly(DGC-PPG)-7k-PDMS with a suitable viscosity to run the end-capping reaction in bulk. In fact, all PDMS-poly(DGC-PPG)-PDMS led to gel-like materials that could not be end-capped in bulk, and this work tried to minimize the use of organic solvents as much as possible.

**End-capping of modified PHUs:** Priamine-poly(DGC-PPG)-Priamine and PDMS-7k-poly(DGC-PPG)-PDMS-7k had viscosities low enough to allow the end-capping reactions to proceed in bulk. An estimate of their molecular weights was made based on the sum of the estimated molecular weight of poly(DGC-PPG) with the molecular weight of the diamine added multiplied by the number of molar equivalents added (2 or 0.5) (refer to Appendix C). From the estimated molecular weights, the concentration of end-cappers to be used, which is set at 2 molar equivalents per mol of chain extended polymer, was calculated. Typically, 2-3 g of poly(DGC-PPG) or Priamine-poly(DGC-PPG)-Priamine was mixed with 2 molar equivalents of DAMO or GLYMO, respectively, and the reactions were allowed to proceed at 120 °C or 100 °C, respectively, for 1 h. The end-capping reaction of PDMS-7k-poly(DGC-PPG)-PDMS-7k was conducted after mixing the chain extended prepolymer with 1.5 molar equivalents of DAMO and then 0.5 molar equivalent of GLYMO per chain extended polymer, and the reaction was allowed to proceed for 1 h at 100 °C. DAMO was added first and was allowed to react with the PHU for

30 min before adding GLYMO to complete the total 1 h for the reaction. This step-wise addition of the end-cappers was performed to limit the possible reaction between DAMO and GLYMO. All reaction media were purged with N<sub>2</sub> for 15 min prior to adding the end-cappers. The proprietary catalyst was added, when needed, at a load of 0.5 wt.% with respect to the reaction mixtures after the reactions were complete, and everything was mixed for 2-3 min before pouring the samples on aluminum foil to cure under ambient conditions (22 °C and 40-50% humidity). Note that preliminary reactions on similar systems showed that the reaction conditions used herein do not favor at all the interaction between the epoxy group of GLYMO and the hydroxyl pendant groups in the PHU chains.

### 5.3.3 Characterization methods

**Proton nuclear magnetic resonance (<sup>1</sup>H-NMR) spectroscopy:** Solution-phase NMR spectra were recorded on a Bruker 500 MHz instrument (16 scans) at ambient temperature. DGC was dissolved in DMSO-d<sub>6</sub>, whereas poly(DGC-PPG) and the modified PHUs were dissolved in CDCl<sub>3</sub> to be analyzed.

**Fourier transform infrared (FTIR) spectroscopy:** FTIR measurements were carried out on a Perkin Elmer instrument (Spectrum two series) equipped with a single bounce diamond attenuated transmission reflectance (ATR) for solids and zinc selenide (ZnSe) holder for liquids. 32 scans were recorded for each sample over the range 4000-500 cm<sup>-1</sup> with a normal resolution of 4 cm<sup>-1</sup>. Poly(DGC-PPG), the modified poly(DGC-PPG) with the hydrophobic diamines, and the prepared HPHU structures were recorded on the machine.

**Size exclusion chromatography (SEC):** Poly(DGC-PPG) and the modified poly(DGC-PPG) with the hydrophobic diamines molecular weights were analyzed via SEC. Number average molecular weight (M<sub>n</sub>), weight average molecular weight (M<sub>w</sub>), and dispersity (Đ = M<sub>w</sub>/M<sub>n</sub>) of

prepolymer samples were measured using this technique on a Waters Breeze instrument with HPLC grade THF as an eluent at a flow rate of 0.3 mL/min. The SEC has three Waters Styragel HR columns (HR1 with a molecular weight measurement range of  $10^2$  to  $5 \times 10^3$  g/mol, HR2 with a molecular weight measurement range of  $5 \times 10^2$  to  $2 \times 10^4$  g/mol, and HR4 with a molecular weight measurement range of  $5 \times 10^3$  to  $6 \times 10^5$  g/mol), a guard column, and a refractive index (RI 2414) detector. The columns were heated to 40 °C during analysis. The molecular weights were determined relative to poly(methylmethacrylate) (PMMA) calibration standards from Varian Inc. (ranging from 875 to 1,677,000 g/mol). The reported molecular weights were all relative to the PMMA standards and not adjusted with Mark-Houwink parameters.

**Thermogravimetric analysis (TGA):** TGA was performed on a Q5500 system from TA Instruments. The thermal degradation of the synthesized PHU prepolymers was measured at a heating rate of 10 °C/min over the temperature range of 25-800 °C under a nitrogen atmosphere. The onset degradation temperature ( $T_{d,onset}$ ) as well as the 10% and 50% degradation temperatures ( $T_{d,10\%}$  and  $T_{d,50\%}$ ) were calculated using this method.

**Differential scanning calorimetry (DSC):** DSC was performed using a Q2000 TA Instruments calorimeter employing standard hermetic aluminum pans, calibrated with indium and nitrogen as purge gas. The instrument is equipped with a cryogenic unit operating with liquid nitrogen. The samples were analyzed at a heating rate of 10 °C/min over a temperature range of -140 °C to 120 °C under a nitrogen atmosphere. Glass transition temperatures ( $T_{gs}$ ) were calculated from the second heating ramp.

**Small and Wide Angle X-ray Scattering (SAXS and WAXS):** SAXS and WAXS spectroscopy measurements were recorded on a SAXSpoint 2.0 (Anton Paar, Austria) equipped

with a CuK $\alpha$  radiation source (wavelength,  $\lambda = 1.54 \text{ \AA}$ ), using a detector of Eiger R 1M (Horizontal) at SAXS and WAXS distances of 1075.9 and 113.1 mm, respectively. The gel-like modified PHU prepolymers were dissolved in methanol at a concentration of 20 mg/mL and placed in a sealed cell, whereas the hybrid polymeric films, with thickness of 1 mm, were placed on a sample holder for solids (10 by 10 mm) provided by Anton Paar, which was further secured by tape. X-ray exposure times were 30 min per frame for a total of 4 frames for every experiment. The obtained SAXS profiles were corrected and shown as function of scattering vector ( $q = (4\pi/\lambda) \sin\theta$ , where  $2\theta$  is the scattering angle in  $^\circ$  and  $q$  in  $\text{nm}^{-1}$ ). The mean interdomain spacing,  $d$  (nm), was calculated from the obtained SAXS spectra using the following formula:

$$d = 2\pi/q_{max} \quad \text{Eq. (5.1)}$$

with  $q_{max}$  ( $\text{nm}^{-1}$ ) is the value of  $q$  at maximum peak position read from SAXS spectra.

**Rheology:** Viscosities of poly(DGC-PPG) and Priamine-poly(DGC-PPG)-Priamine were measured on an Anton Paar Instruments rheometer (MCR 302) operated in the parallel plate (25 mm diameter) steady shear mode (gap 1 mm). The samples were placed symmetrically in the center of the plate. The shear stress was measured at different shear rates ranging from  $0.01 \text{ s}^{-1}$  to  $10 \text{ s}^{-1}$  in 21 measurements during 3 min. All the measurements were conducted at ambient conditions ( $\sim 22 \text{ }^\circ\text{C}$ ).

The curing kinetics of the end-capped PHUs were carried out on the same instrument equipped with two parallel plate geometry (25 mm diameter) at a frequency of 1 Hz, a strain of 1%, and the measurements were carried out at room temperature (around  $22 \text{ }^\circ\text{C}$ ) with a humidity range of 40-50%. The evolutions of the storage modulus ( $G'$ ), loss modulus ( $G''$ ), damping factor

( $\tan\delta = G''/G'$ ), and complex viscosity ( $\eta^*$ ) were monitored as a function of time for 24 h, which was sufficient to measure the gel time for these samples.

**Swelling:** After allowing poly(DGC-PPG), Priamine-poly(DGC-PPG)-Priamine, and PDMS-7k-poly(DGC-PPG)-PDMS-7k HPHU films to cure at ambient conditions for five months, their swelling was tested in THF, pure H<sub>2</sub>O, and toluene. Film samples of 10-20 mg were immersed in 7 mL of solvent at room temperature for a week, after which the swelling index (SI) was calculated using Eq. (5.2), after which the samples were dried in a vacuum oven overnight at 40 °C to find their gel content (GC) by applying Eq. (5.3).

$$SI(\%) = \left( \frac{W_s - W_d}{W_d} \right) \times 100 \quad \text{Eq. (5.2)}$$

$$GC(\%) = \left( \frac{W_f}{W_i} \right) \times 100 \quad \text{Eq. (5.3)}$$

Here,  $W_s$  is the weight of the swollen sample,  $W_d$  is the weight of the dry sample,  $W_i$  is the initial weight (same as  $W_d$  in this case), and  $W_f$  is the final weight of the dried sample. The samples were left for a week in the solvents to ensure that equilibrium is reached. This period was determined after running some preliminary measurements. Besides, these tests were conducted after five months to ensure that the films had reached their maximum level of curing and hence accurate SI and GC measurements (for the case of water, SI is similar to the equilibrium water content (EWC)).

## 5.4 Results and Discussion

### 5.4.1 Characterization of the DGC-PPG/HydrophobicDiamine PHUs

As mentioned earlier, the purpose of reacting the cyclic carbonate terminated poly(DGC-PPG) with PDMS-(NH<sub>2</sub>)<sub>2</sub> and Priamine 1074 is to increase the water resistance of the final HPHU products prepared via the sol/gel curing method. In the present section, poly(DGC-PPG) is mixed with 2 molar equivalent diamines per polymer to cap the cyclic carbonates on both ends of the prepolymer chain with amine groups. The added amount of hydrophobic diamine was calculated based on an estimation of the molecular weight of poly(DGC-PPG) done using the relative molecular weights of the polymer to that of Jeffamine D-2000. To confirm our estimated values, <sup>1</sup>H-NMR was conducted on poly(DGC-PPG) and the PDMS-poly(DGC-PPG)-PDMS to analyze the PPG to dimethylsiloxane segment ratios and compare them to the ratios found from the estimated molecular weight value of poly(DGC-PPG). This was done by tracking the increase in the integration of the dimethylsiloxane, Si-(CH<sub>3</sub>)<sub>2</sub>-O, protons' signal (at 0.05 ppm) of the PHUs with respect to the methyl group found in the propylene glycol repeating unit (PPG-CH<sub>3</sub>) (at 1.15 ppm). This trend can be observed from the stacked <sup>1</sup>H-NMR spectra of Figure 5.1 where the integrations of the distinct peaks are provided. The increase in the molecular weight of the PDMS-(NH<sub>2</sub>)<sub>2</sub>, used to cap both ends of poly(DGC-PPG), leads to an increase in the dimethylsiloxane segments with respect to the PPG ones (note the ~1/1 ratio obtained with PDMS-3k-(NH<sub>2</sub>)<sub>2</sub>). Estimations of the Si-(CH<sub>3</sub>)<sub>2</sub>-O to PPG-CH<sub>3</sub> unit ratios for the different PDMS-(NH<sub>2</sub>)<sub>2</sub> were conducted, and the results matched those analyzed from <sup>1</sup>H-NMR, especially for the PDMS-5k-(NH<sub>2</sub>)<sub>2</sub> and PDMS-7k-(NH<sub>2</sub>)<sub>2</sub> cases, as shown in Table 5.1. The other peaks related to the hydroxyurethane linkages are not assigned in these spectra because we were specifically interested in the ratios of the dimethylsiloxane to the PPG segments in the

PHUs. Those peaks can be obtained after increasing the intensity of the stacked spectra of Figure 5.1, but peak assignment and integration remained difficult to do and inaccurate, respectively. The peaks highlighted in green were not used in this comparison because they contain overlapping peaks. More information about the estimates can be found in Appendix C, as well as in the footnotes of Table 5.1. The  $^1\text{H-NMR}$  of poly(DGC-PPG) was reported in our previous study.<sup>21</sup>

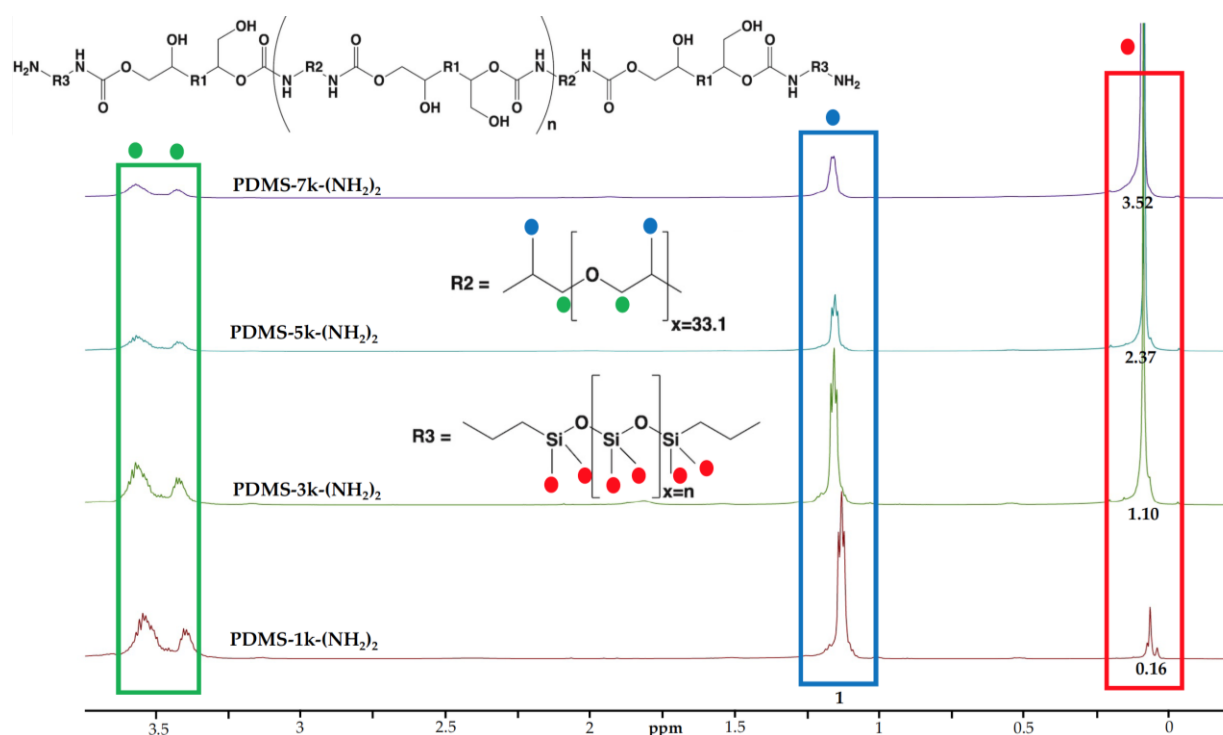


**Figure 5.1 - Labeled  $^1\text{H-NMR}$  spectra of PDMS-poly(DGC-PPG)-PDMS of this work (2 molar equivalents of PDMS-(NH<sub>2</sub>)<sub>2</sub> per polymer) showing the main signals of the diamines used in this work. The Si-(CH<sub>3</sub>)<sub>2</sub>-O methyl protons signal (at 0.05 ppm) increases with respect to PPG-CH<sub>3</sub> (at 1.15 ppm) with increase in the PDMS-(NH<sub>2</sub>)<sub>2</sub> molecular weight used to cap poly(DGC-PPG) from both ends.**

**Table 5.1 - Si-(CH<sub>3</sub>)<sub>2</sub>-O to PPG-CH<sub>3</sub> unit ratios estimated and predicted from <sup>1</sup>H-NMR for PDMS-poly(DGC-PPG)-PDMS of this work (2 molar equivalents of PDMS-(NH<sub>2</sub>)<sub>2</sub> per polymer)<sup>2</sup>**

Hydrophobic diamine	n <sup>a</sup>	Total methyl groups in Si-(CH <sub>3</sub> ) <sub>2</sub> -O units <sup>a</sup>	Total methyl groups in PPG-CH <sub>3</sub> units <sup>b</sup>	Estimated Si-(CH <sub>3</sub> ) <sub>2</sub> -O/PPG-CH <sub>3</sub>	NMR Si-(CH <sub>3</sub> ) <sub>2</sub> -O/PPG-CH <sub>3</sub>
PDMS-1k-(NH <sub>2</sub> ) <sub>2</sub>	10.2	48.8	104.7	0.47	0.16
PDMS-3k-(NH <sub>2</sub> ) <sub>2</sub>	37.2	156.8	104.7	1.50	1.10
PDMS-5k-(NH <sub>2</sub> ) <sub>2</sub>	64.2	264.8	104.7	2.53	2.37
PDMS-7k-(NH <sub>2</sub> ) <sub>2</sub>	91.2	372.8	104.7	3.56	3.52

a. n is the number of Si-(CH<sub>3</sub>)<sub>2</sub>-O repeating units. The total number of methyl groups in Si-(CH<sub>3</sub>)<sub>2</sub>-O units is found by multiplying (n+2) (two groups are outside of the brackets) by 4 since there are two methyl groups and two PDMS-(NH<sub>2</sub>)<sub>2</sub> are getting attached on each side of the chains of poly(DGC-PPG).

b. The total number of PPG-CH<sub>3</sub> units includes the 33.1 methyl groups plus the one outside that is not part of the propylene glycol repeating unit. This number is multiplied by 3.07 which is the estimated average number of Jeffamine D-2000 in the chains of poly(DGC-PPG).

The reactions of the cyclic carbonate terminated poly(DGC-PPG) with the different hydrophobic diamines were confirmed by the disappearance of the carbonyl stretch (C=O) of the carbonate observed at 1800 cm<sup>-1</sup> in the FTIR spectrum of poly(DGC-PPG), as shown in Figure 5.2. By reacting both cyclic carbonates with the amine groups of the chain extenders, this carbonyl stretch decreases until total disappearance in some cases, while it remained weak in some others with respect to the carbonyl stretch of the hydroxyurethane linkage at 1700 cm<sup>-1</sup>, as observed from the FTIR spectra of the reacted poly(DGC-PPG) with both PDMS-1k-(NH<sub>2</sub>)<sub>2</sub> and Priamine 1074 in Figure 5.2. The rest of the FTIR spectra with the other PDMS-(NH<sub>2</sub>)<sub>2</sub> are provided in Figure C.3 of the supporting information. This carbonyl stretch's disappearance

<sup>2</sup> More information regarding the estimation presented in Table 5.1 is given in Appendix C.

confirms the attachment of the diamines on both ends of the cyclic carbonate terminated poly(DGC-PPG), and it indicates that the concentration of hydrophobic diamine calculated from the estimated molecular weight of poly(DGC-PPG) was not far from the actual one. This latter point was expected as this work targets oligomers with relatively few hydroxyurethane linkages  $\sim$  six, so approximations of the number of Jeffamine D-2000 units using relative molecular weights were viable. As for the weak carbonyl stretch remaining at  $1800\text{ cm}^{-1}$  in some cases, such as after reaction with PDMS-1k-(NH<sub>2</sub>)<sub>2</sub>, means that there are a few unreacted cyclic carbonate end-groups. This implies that few poly(DGC-PPG) chains either did not react or partially reacted with the hydrophobic diamines. While this could result from a minor deficiency in the added amount of hydrophobic diamines, as the latter was based on an estimation of poly(DGC-PPG) molecular weight, we believe that there are other aspects leading to unreacted cyclic carbonate end-groups in the reaction medium, seeing that these groups did fully react in some cases. One plausible explanation for this observation could be related to a limitation in the diffusion of the hydrophobic diamines which was caused by the increase of the viscosity of the reaction medium. In fact, the reactions of the PDMS-(NH<sub>2</sub>)<sub>2</sub> and poly(DGC-PPG) gave gel-like products. More details on the effects of this phenomenon are presented in the next section while discussing the results obtained from the size exclusion chromatography (SEC).

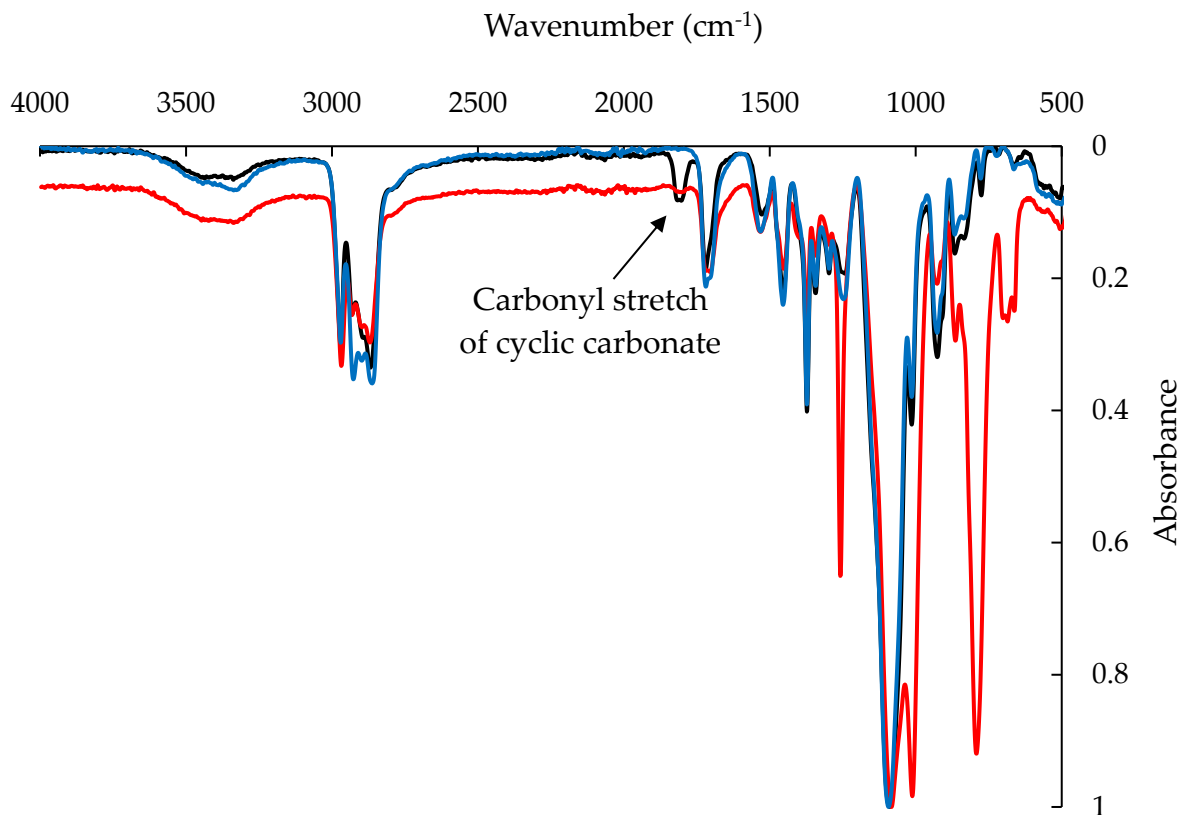
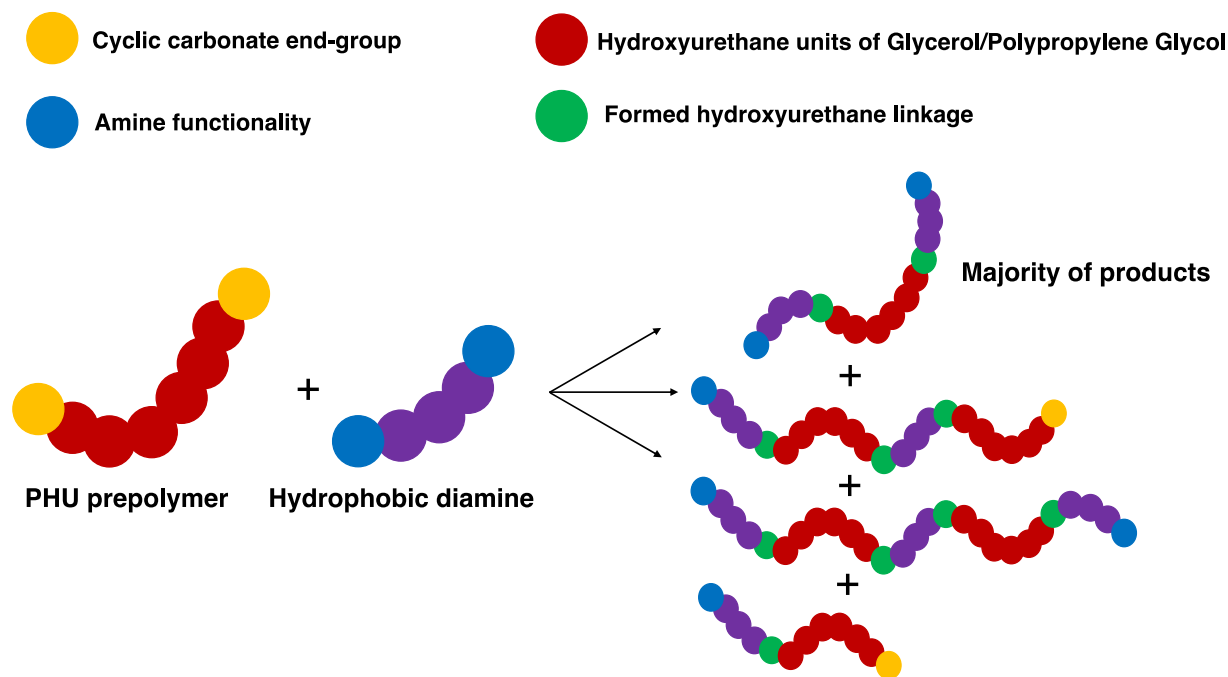


**Figure 5.2 - FTIR spectra of poly(DGC-PPG) (black), PDMS-1k-poly(DGC-PPG)-1k-PDMS-1k (red) and Priamine-poly(DGC-PPG)-Priamine (blue) showing the disappearance of the carbonyl stretch at  $1800\text{ cm}^{-1}$  for the extended PHUs compared to the FTIR spectrum of poly(DGC-PPG).**

The modified poly(DGC-PPG) PHUs were also characterized using the SEC analysis to observe the increase in their molecular weights with respect to the initial poly(DGC-PPG) (Figure C.4 to Figure C.6). The number average molecular weight,  $M_n$ , in Table 5.2 gradually increased when reacting poly(DGC-PPG) with PDMS-1k-(NH<sub>2</sub>)<sub>2</sub> and PDMS-3k-(NH<sub>2</sub>)<sub>2</sub> (5,400 and 8,300 g/mol, respectively, versus 4,600 g/mol for poly(DGC-PPG)), but it fell back to 5,900 g/mol for the 5k and 7k PDMS diamine cases while remaining higher than 4,600 g/mol. Since one would expect that the molecular weight would continue to increase when reacting poly(DGC-PPG) with the 5k and 7k PDMS diamines, it was necessary to look for a reasonable cause for this phenomenon. By looking at the dispersity values of Table 5.2, the drop in  $M_n$  was countered by an increase in the dispersity of these two PHUs to 3.0 while it was 2.1 and 2.5 for PDMS-1k-poly(DGC-PPG)-1k-PDMS and PDMS-3k-poly(DGC-PPG)-3k-PDMS, respectively. The low dispersity suggests that most of the poly(DGC-PPG) chains, having a dispersity of 2.0, reacted from both ends with the 1k and 3k PDMS diamines and grew simultaneously. The Diamine-poly(DGC-PPG)-Diamine had a low dispersity of 2.3 as well. The higher dispersity, on the other hand, implies that not all of the poly(DGC-PPG) chains participated in the reaction with the 5k and 7k PDMS diamines. These reactions could have been limited by the viscosity of the reaction medium, as they gave gel-like products that are more viscous than those obtained with the 1k and 3k PDMS diamines. While the viscosity factor could have limited the diffusion of the hydrophobic diamines and their interaction with the chains of poly(DGC-PPG), as explained previously, we believe that the high dispersities resulted as well from the reaction of these diamines with two different poly(DGC-PPG) chains instead of each diamine getting attached to the same poly(DGC-PPG) chain via its two cyclic carbonate end-groups. The SEC traces of PDMS-5k-poly(DGC-PPG)-5k-PDMS and PDMS-7k-poly(DGC-PPG)-7k-PDMS

PHUs of Figure C.5 show tails towards higher molecular weights which proves that such phenomenon might have occurred. This latter reasoning matches the explanation given above when discussing the FTIR results and is illustrated in Scheme 5.2. However, it seems that the hydrophobic diamines are more inclined to react with the poly(DGC-PPG) chains by capping them from both ends, seeing the low dispersity of the resulting PHUs extended with the lower molecular weight diamines and their bimodal SEC traces that is similar to the trace of poly(DGC-PPG). As for the SEC results obtained with the higher molecular weight diamines, they are further discussed as follows.



**Scheme 5.2 - Series of products obtained from reacting the hydrophobic diamines with poly(DGC-PPG). The hydrophobic diamines are more inclined to cap poly(DGC-PPG) from both ends by reacting with its cyclic carbonate end-groups.**

However, that reasoning explains to a certain extent the drop in  $M_n$  because the  $M_w$  follows a similar trend despite the increase in dispersity. Hence, we believe that the SEC analysis might have possibly failed at quantifying the molecular weights of PDMS-5k-poly(DGC-PPG)-5k-PDMS and PDMS-7k-poly(DGC-PPG)-7k-PDMS due to the difference in the chemical structure of PPG and PDMS. This is in agreement with the WAXS data of Figure 5.3, which shows that PDMS is becoming the dominant phase in the product when using the 5k and 7k PDMS diamines. A distinct PDMS chain peak appears at  $2\theta$  of  $12.5^\circ$  and increases in intensity with an increase in the molecular weight of the PDMS blocks. Previous studies on segmented PUs with PDMS-based diols had reported a similar peak in their WAXS spectra.<sup>48-50</sup> This increase occurs with a decrease of a distinct peak at  $2\theta$  of  $17.0^\circ$  that is associated with the PPG phase of the initial PHU under study.<sup>51</sup> It actually almost completely disappears when using PDMS-5k-(NH<sub>2</sub>)<sub>2</sub> and PDMS-7k-(NH<sub>2</sub>)<sub>2</sub>, respectively, which means that the PDMS phase became dominant in the resulting PHU structure. This change in phase structure might have caused the underestimation in average molecular weights observed in the SEC results, and the PDMS and PPG non-miscible phases might have led to discrepancies in measuring the hydrodynamic volumes of the extended samples with PDMS-5k-(NH<sub>2</sub>)<sub>2</sub> and PDMS-7k-(NH<sub>2</sub>)<sub>2</sub>. Note the segmented PHU broad peak which appears at  $2\theta$  of  $21.5^\circ$  and was also reported elsewhere.<sup>48-50</sup> Moreover, since PDMS and PPG are two immiscible polymers, with the former very hydrophobic and the latter more hydrophilic, phase separation of the two species is expected. Indeed, microphase separation is confirmed from SAXS measurements for these polymers, and the SAXS data, given in Figure C.7 of Appendix C, revealed a microphase separation with no distinct pattern of the different blocks. Only one peak was observed for all the

samples with a maximum around  $q_{\max}$   $0.80 \text{ nm}^{-1}$ , which is equivalent to an interdomain spacing,  $d$ , of 7.85 nm.

On the other hand, the Priamine-poly(DGC-PPG)-Priamine had similar molecular weight distribution properties to the initial poly(DGC-PPG) because Priamine 1074 is a shorter diamine, but it had a viscosity almost three times that of the latter, as shown in Table 5.2. The viscosities of the PHUs modified with PDMS-(NH<sub>2</sub>)<sub>2</sub> could not be measured because they were excessively sticky, and not easy to handle.

**Table 5.2 - Structural and thermal properties of the extended poly(DGC-PPG) from both ends with the hydrophobic diamines of this work (2 molar equivalents of hydrophobic diamine per polymer)**

<b>Poly(DGC-PPG) and modified poly(DGC-PPG) PHUs</b>	<b>M<sub>n</sub> (g/mol)<sup>a</sup></b>	<b>Đ = M<sub>w</sub>/M<sub>n</sub><sup>a</sup></b>	<b>T<sub>g,1</sub> (°C)</b>	<b>T<sub>g,2</sub> (°C)</b>	<b>T<sub>d,10%</sub> (°C)</b>	<b>T<sub>d,50%</sub> (°C)</b>	<b>η (Pa.s)<sup>b</sup></b>
<b>Poly(DGC-PPG)</b>	4,600	2.0	-	-60	206	275	10.5
<b>PDMS-1k-poly(DGC-PPG)-1k-PDMS</b>	5,400	2.1	-92	-59	250	332	gel
<b>PDMS-3k-poly(DGC-PPG)-3k-PDMS</b>	8,300	2.5	-90	-58	287	363	gel
<b>PDMS-5k-poly(DGC-PPG)-5k-PDMS</b>	5,900	3.1	-90	-56	292	427	gel
<b>PDMS-7k-poly(DGC-PPG)-7k-PDMS</b>	5,900	2.9	-91	-52	299	456	gel
<b>Priamine-poly(DGC-PPG)-Priamine</b>	4,100	2.3	-	-59	247	325	30.5

a. Number average molecular weight and dispersities were estimated from SEC with THF eluent at 40 °C relative to poly(methyl methacrylate) standards.

b. Viscosities were measured at room temperature (~22 °C steady shear mode).

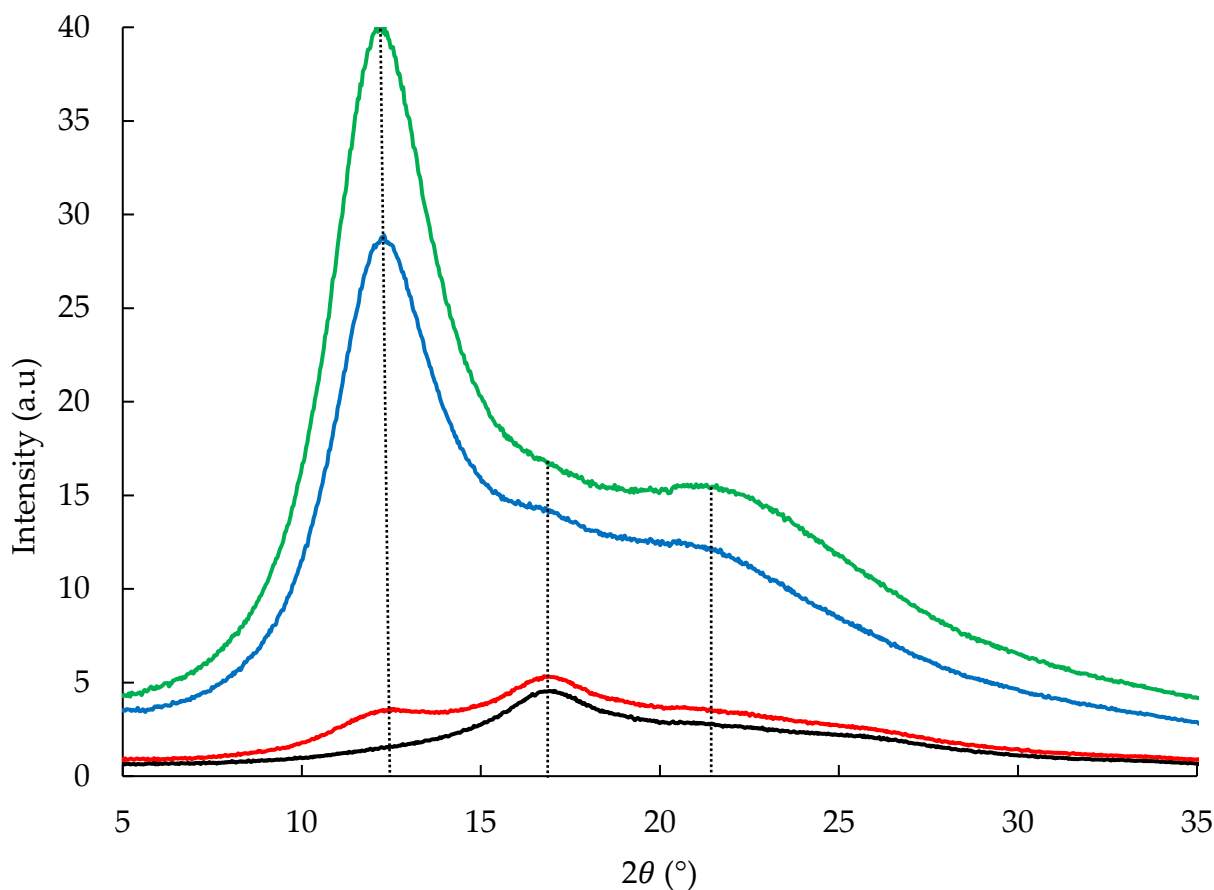


**Figure 5.3 - WAXS spectra of extended poly(DGC-PPG) from both ends with PDMS-1k-(NH<sub>2</sub>)<sub>2</sub> (black), PDMS-3k-(NH<sub>2</sub>)<sub>2</sub> (red), PDMS-5k-(NH<sub>2</sub>)<sub>2</sub> (blue), and PDMS-7k-(NH<sub>2</sub>)<sub>2</sub> (green) (2 molar equivalents of hydrophobic diamine per polymer) showing an increase of the PDMS chains peak at  $2\theta$  of  $12.5^\circ$  with increase in molecular weight of the PDMS-(NH<sub>2</sub>)<sub>2</sub> hydrophobic diamine. The intensity is given in logarithmic scale.**

In terms of thermal properties, the resulting PHUs with the different PDMS-(NH<sub>2</sub>)<sub>2</sub> showed two glass transition temperatures,  $T_g$ s, when analyzed with DSC. One  $T_g$  is that of poly(DGC-PPG),  $T_{g,2}$  around  $-60^\circ\text{C}$ , and the other is due to the attached PDMS blocks showing  $T_{g,1}$  around  $-90^\circ\text{C}$ . The former  $T_g$  slightly increased with increasing molecular weight of the PDMS blocks. The  $T_g$  of PDMS occurs usually at about  $-120^\circ\text{C}$ ; however, the PDMS blocks

herein were relatively short and lower molecular weight, and they are attached to poly(DGC-PPG) segments from both ends, which could have altered their  $T_g$ . Priamine-poly(DGC-PPG)-Priamine showed only one  $T_g$  similar to poly(DGC-PPG), and that is because Priamine 1074 is not polymeric in nature like PDMS, so the thermal behavior of the PPG component was dominant. Further, the thermal stability of poly(DGC-PPG) increased when extended on both ends with the different diamines, and the temperatures at 10 and 50 wt.% degradation,  $T_{d,10\%}$  and  $T_{d,50\%}$ , gradually increased with increasing PDMS-(NH<sub>2</sub>)<sub>2</sub> molecular weights, and with Priamine 1074. Note that  $T_{d,50\%}$  increased by almost 200 °C going from poly(DGC-PPG) to PDMS-7k-poly(DGC-PPG)-7k-PDMS due to addition of the thermally stable PDMS blocks.<sup>52</sup> This increase is more pronounced in PDMS-5k-poly(DGC-PPG)-5k-PDMS and PDMS-7k-poly(DGC-PPG)-7k-PDMS because the weights of the PDMS blocks overshadow those of the PPG segment in the PHU structure. This observation is further confirmed by taking the derivative of the weight percentage with respect to the temperature (dW/dT), as shown in Figure 5.4, where the maximum rate of degradation point shifts (first peak for the PDMS-5k-poly(DGC-PPG)-5k-PDMS and PDMS-7k-poly(DGC-PPG)-7k-PDMS cases) progressively to higher temperature values when going from poly(DGC-PPG) to PDMS-7k-poly(DGC-PPG)-7k-PDMS. The extension from both ends with PDMS-5k-(NH<sub>2</sub>)<sub>2</sub> and PDMS-7k-(NH<sub>2</sub>)<sub>2</sub> led to two maximum rate of degradation points at temperatures around 375 °C and 535 °C. As explained previously, the second peak comes from the longer PDMS blocks, due to the 5k and 7k PDMS diamines, which are responsible for increasing the weight ratio of the PDMS to PPG segment in the final PHU structure. These results are in accordance with the phase transition observed from the WAXS measurements presented above. More information related to the PHUs thermal properties can be found in Table 5.2 as well as Figure C.8 through Figure C.10.

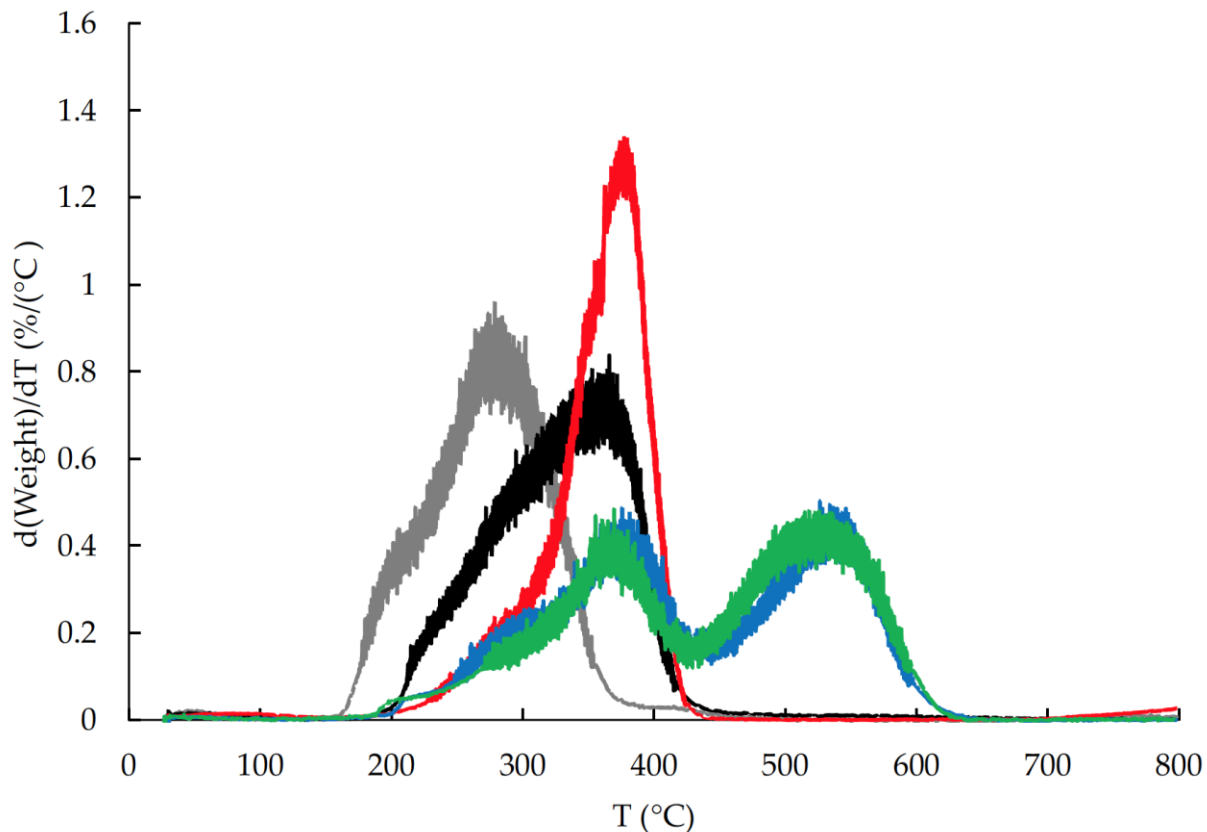


**Figure 5.4 - Derivative of weight percentage with respect to temperature traces of poly(DGC-PPG) (grey) and extended poly(DGC-PPG) from both ends with PDMS-1k-(NH<sub>2</sub>)<sub>2</sub> (black), PDMS-3k-(NH<sub>2</sub>)<sub>2</sub> (red), PDMS-5k-(NH<sub>2</sub>)<sub>2</sub> (blue), and PDMS-7k-(NH<sub>2</sub>)<sub>2</sub> (green) used in this work (2 molar equivalents of hydrophobic diamine per polymer).**

#### **5.4.2 End-capping of the modified poly(DGC-PPG)**

While the Priamine-poly(DGC-PPG)-Priamine had a viscosity that allowed the polymer to be easily end-capped, PDMS-poly(DGC-PPG)-PDMS samples, with 2 molar equivalent PDMS diamine with respect to poly(DGC-PPG), were gel-like and harder to mix with the end-cappers. Hence, less than 2 molar equivalents of the PDMS-(NH<sub>2</sub>)<sub>2</sub> had to be used per polymer to prepare the modified HPHUs and test the effect of having PDMS blocks on their water resistance.

Among all the PDMS diamines of this study, PDMS-7k-(NH<sub>2</sub>)<sub>2</sub> was chosen because it had the highest thermal stability and a dominant PDMS phase in its microstructure, as observed from the TGA and WAXS measurements, respectively. The latter reason is important because PDMS is known to be water resistant and repellent, and having it as a major component will ensure good hydrophobicity of the resulting poly(DGC-PPG) HPHU.<sup>52</sup> Poly(DGC-PPG) was reacted with only 0.5 molar equivalent of PDMS-7k-(NH<sub>2</sub>)<sub>2</sub> per polymer that provided a viscosity sufficiently low to proceed with the end-capping reaction. After 24 h, two phases were observed because not all of poly(DGC-PPG) chains were capped.

Table 5.3 summarizes the conditions at which the three PHUs were end-capped. Depending on the end-groups (carbonate or amine), different silane end-cappers were used (DAMO or GLYMO, respectively). The number of moles to be added was calculated from the estimated molecular weights which are further discussed in Appendix C. Once the PHUs were end-capped, the curing kinetics at ambient conditions (22 °C and 40-50% humidity) were followed and the results are provided in Figure 5.5 and Figure C.11 through Figure C.13 with the gel times recorded in Table 5.3. Surprisingly, Priamine-poly(DGC-PPG)-Priamine showed a dramatic increase in its storage modulus after curing, and the final value was much greater than those of PDMS-7k-poly(DGC-PPG)-7k-PDMS (four times greater) and poly(DGC-PPG) (minimum of 12 times greater) samples. The storage modulus of the other HPHUs plateaued in the 24 h window while that of Priamine-poly(DGC-PPG)-Priamine had increased further after that period of time because a plateau was not reached. The bio-based diamine added some toughness to the resulting HPHU not observed in the soft poly(DGC-PPG) and PDMS-7k-poly(DGC-PPG)-7k-PDMS HPHUs. These films were subject to swelling in different solvents,

THF, pure H<sub>2</sub>O, and toluene, to qualitatively determine their crosslinking efficacy and, most importantly, their water resistance.

**Table 5.3 - Prepolymer information necessary for end-capping the PHUs of this work to afford HPHUs. The gel times for the PDMS-7k-poly(DGC-PPG)-7k-PDMS and Priamine-poly(DGC-PPG)-Priamine were measured after addition of 0.5 wt.% of the proprietary catalyst.**

<b>PHU</b>	<b>End-group</b>	<b>Compatible end-capper</b>	<b>Estimated average molecular weight (g/mol)<sup>3</sup></b>	<b>Gel time (h)</b>
<b>Poly(DGC-PPG)</b>	Carbonate	DAMO	6,900	9
<b>PDMS-7k-poly(DGC-PPG)-7k-PDMS</b>	Carbonate and Amine	DAMO and GLYMO	10,400	0.5
<b>Priamine-poly(DGC-PPG)-Priamine</b>	Amine	GLYMO	7,900	5

---

<sup>3</sup> More information regarding the estimation of the molecular weights of the PHUs in this work is given in the supporting information of Appendix C. The values reported are rounded values of the estimated average molecular weights.

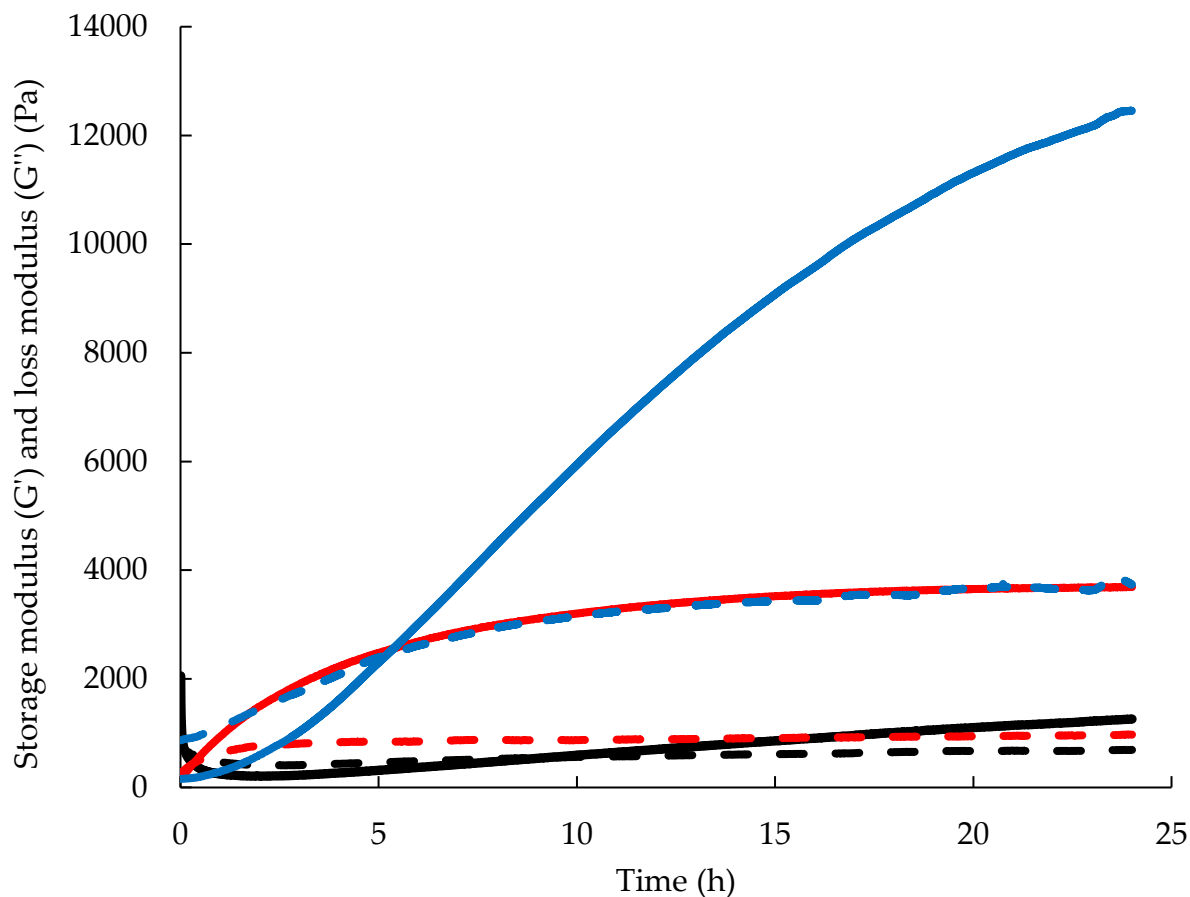


**Figure 5.5 - Curing kinetics of the end-capped poly(DGC-PPG) (black), PDMS-7k-poly(DGC-PPG)-7k-PDMS (red), and Priamine-poly(DGC-PPG)-Priamine (blue) by following the storage ( $G'$ , full lines) and loss ( $G''$ , dashed lines) moduli (Pa) at a frequency of 1 Hz and a strain of 1% for 24 h. 0.5 wt.% of the proprietary catalyst was added to accelerate the curing of PDMS-7k-poly(DGC-PPG)-7k-PDMS and Priamine-poly(DGC-PPG)-Priamine. Measurements were done at 22 °C and 40-50% humidity.**

### 5.4.3 Swelling of DGC-PPG/HydrophobicDiamine HPHUs

The swelling indexes (SI) and gel contents (GC) of the different films in THF, pure H<sub>2</sub>O, and toluene are summarized in Table 5.4. As a reminder, SI and GC were measured in THF, as one of the solvents, to qualitatively evaluate the crosslink density and the curing efficacy, respectively, of the resulting HPHUs. In fact, the original PHUs are highly soluble in THF and any uncrosslinked chains in the network will easily dissolve in it to allow for accurate measurements of the GC. By looking at Table 5.4, the SI is highest for the PDMS-7k-poly(DGC-PPG)-7k-PDMS HPHU and lowest for the Priamine-poly(DGC-PPG)-Priamine with a difference of almost 200% between the two films. This is expected since the PDMS chains are the longest ones and they create large spacing between the nodes of the crosslinked network for the solvent to penetrate. Such an observation was also made by Decostanzi et al. in their study on sol/gel HPHUs;<sup>16</sup> however, their SIs were lower than the values reported in this study because they dealt with shorter PHU chains, and hence their crosslink densities are higher, on the order of 10<sup>3</sup> mol.m<sup>-3</sup>, compared to this work which should have crosslink densities on the order of 10<sup>2</sup> mol.m<sup>-3</sup>, as measured in our previous study.<sup>21</sup> The GC measurements, on the other hand, show that around half of the PHU chains did not participate in the curing process, with the highest GC in THF reported for the Priamine-poly(DGC-PPG)-Priamine HPHU (56%). Note that the HPHUs containing hydrophobic moieties had higher GCs in THF than the poly(DGC-PPG) HPHU, so it seems that the hydrophobic portions of the chains enhanced the crosslinking process under moisture and ambient conditions of the end-capped PHUs. GC values of 70 and 90% were reported elsewhere for similar systems,<sup>16, 19</sup> but these studies crosslinked their polymers at high temperatures and did not depend on ambient conditions solely. Furthermore, the low GC values of the modified poly(DGC-PPG)-based HPHUs might also be caused by the incompleteness of

the end-capping reactions whose conditions should be further optimized and studied. The end-capping reaction conditions for poly(DGC-PPG) were already optimized in our previous study.<sup>21</sup>

In contrast, the swelling of the HPHU films in toluene reveals the presence of the hydrophobic moieties in the HPHU structure since the SI drastically increased from 129% for the poly(DGC-PPG) HPHU to 200 and 415% for the HPHUs containing Priamine 1074 and the PDMS blocks in their structure, respectively. Toluene is a hydrophobic solvent, so it is compatible with the hydrophobic moieties present in the HPHU films which favors its penetration between the crosslinking nodes of the films. The SI in toluene is the highest for the HPHU containing the PDMS blocks (almost four times higher than the SI of the poly(DGC-PPG) HPHU) because PDMS is known to be a superhydrophobic compound.<sup>52</sup> Unfortunately, we could not measure the contact angles that water would form over these films (and any of the films of this study) because they were still too soft to give accurate estimates. As for the GC values with toluene, they were close to the ones reported with THF, which reconfirms our discussion about the crosslinking efficacy of these films.

At last, the swelling in water, which is critical in environmental applications, showed a drastic decrease in the SI from 75% for the poly(DGC-PPG) HPHU to almost 4% for the Priamine-poly(DGC-PPG)-Priamine HPHU. This value is lower than the SI of 10% reported by Gomez-Lopez et al., who also worked on sol/gel HPHUs made from a blend of resorcinol and PPG dicarbonates reacted with Priamine 1074, in contrast to this work in which Primaine 1074 is added in small amounts enough to cap the ends of the poly(DGC-PPG) chains.<sup>19</sup> It is interesting how a small additive, such as Priamine 1074, was able to improve the hydrophobicity of the HPHUs to such a high extent. The PDMS-7k-poly(DGC-PPG)-7k-PDMS HPHU showed an intermediate SI of around 55% because not all chains were modified with PDMS-7k-(NH<sub>2</sub>)<sub>2</sub>.

Moreover, the GC of the poly(DGC-PPG) HPHU went from 72% to almost 100% with the hydrophobic moieties, which means that Priamine 1074 and the PDMS blocks were able to protect the poly(DGC-PPG)-based HPHU films from any hydrolysis or leaching that might occur when these films are in contact with water. In our previous study, the <sup>1</sup>H-NMR method with deuterium oxide (D<sub>2</sub>O) was used to prove that a portion of the poly(DGC-PPG) HPHU films dissolved in water,<sup>21</sup> and that is now being prevented from happening with the addition of the hydrophobic diamines, notably Primaine 1074, on both ends of the original poly(DGC-PPG) PHU. Besides, it is noticeable that there is more than one benefit for Priamine 1074 in formulating the investigated resins since it did not only increase the hydrophobicity of the HPHUs, but also increased its toughness, as observed from the curing kinetics conducted on the end-capped PHUs while the films were forming.

**Table 5.4 - Swelling experimental results of the synthesized HPHUs of this work in different solvents.**

HPHUs	THF		H <sub>2</sub> O		Toluene	
	SI (%)	GC (%)	SI (%)	GC (%)	SI (%)	GC (%)
<b>Poly(DGC-PPG)</b>	315±22	36.6±3.9	74.8±4.9	71.5±2.7	129±6.0	32.0±5.2
<b>PDMS-7k-poly(DGC-PPG)-7k-PDMS</b>	469±20	42.4±6.1	53.5±5.9	94.6±0.8	415±16	44.2±2.4
<b>Priamine-poly(DGC-PPG)-Priamine</b>	271±10	55.9±4.9	3.62±1.4	97.9±1.8	201±6.0	57.1±3.1

Finally, WAXS measurements (Figure 5.6) were conducted on the resulting HPHUs as well, and as expected the PDMS-7k-poly(DGC-PPG)-7k-PDMS HPHU had a distinct PDMS peak at  $2\theta$  of  $12.5^\circ$ , which confirms the previous arguments made for choosing PDMS-7k-( $\text{NH}_2$ )<sub>2</sub> as the PDMS diamine to make the HPHU. It is this distinct PDMS phase that brought the SI of the poly(DGC-PPG) HPHU from 75% to 55%. Nevertheless, the WAXS spectra of both the poly(DGC-PPG) and Priamine-poly(DGC-PPG)-Priamine HPHUs were similar (showing only the PHU broad peak at  $2\theta$  of  $20.5^\circ$ ), yet the latter had a lower SI (4% versus 75%). It is notable that the modification on both ends with the smaller molecule Priamine 1074, compared to other diamines, had the greatest impact on the toughness and hydrophobicity of the final poly(DGC-PPG)-based HPHU. Finally, it looks like Priamine 1074 would serve as a good additive for PHUs seeing that it improved some of the present HPHU properties, after being added in low concentrations. This study has proven that the 100% bio-sourced Priamine 1074 can replace the more expensive PDMS-( $\text{NH}_2$ )<sub>2</sub> in increasing the hydrophobicity of poly(DGC-PPG) HPHUs.

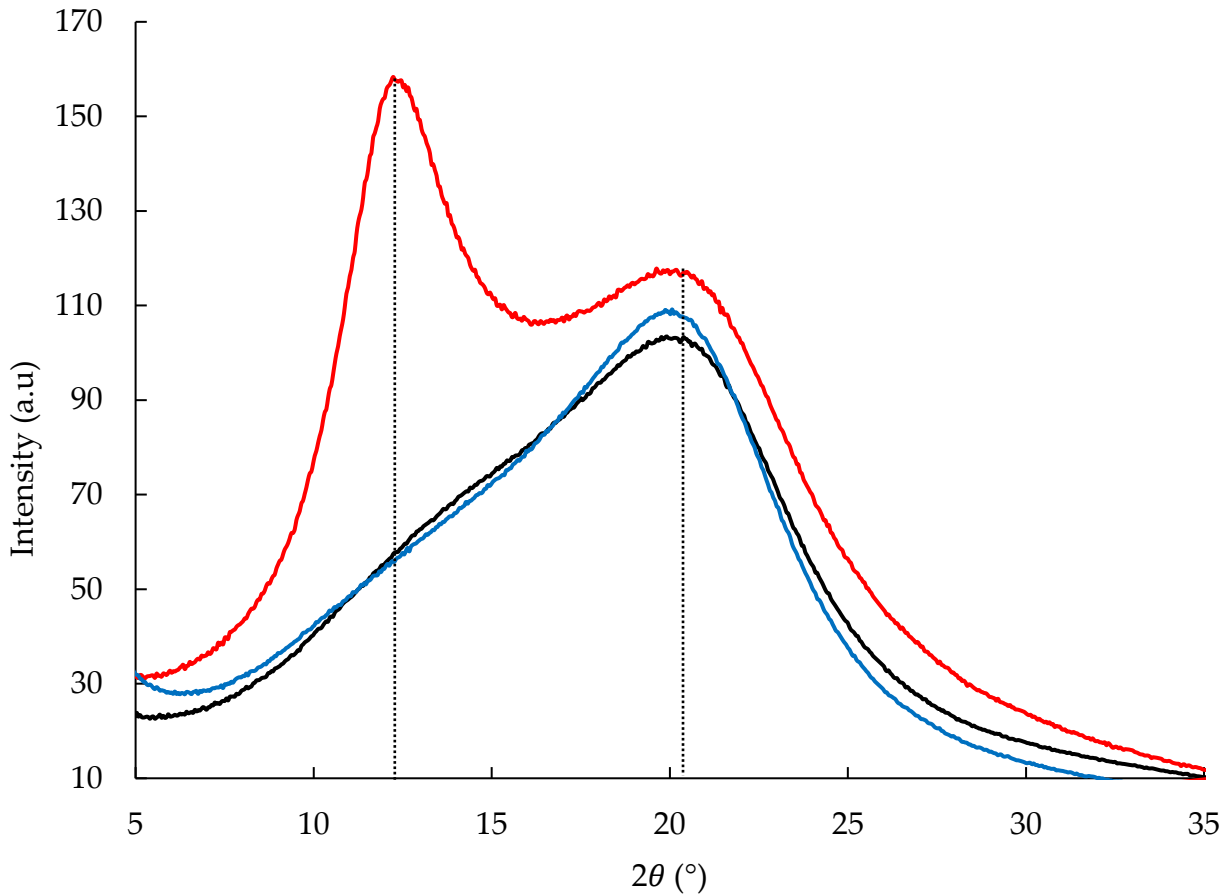


**Figure 5.6 - WAXS spectra of the poly(DGC-PPG) (black), PDMS-7k-poly(DGC-PPG)-7k-PDMS (red), and Priamine-poly(DGC-PPG)-Priamine (blue) HPHUs. The distinct sharp peak at  $2\theta$  of  $12.5^\circ$  proving the presence of a distinct PDMS phase in the microstructure of the PDMS-7k-poly(DGC-PPG)-7k-PDMS HPHU film. The intensity is given in logarithmic scale.**

## 5.5 Conclusion

In this study, the water repellency of the poly(DGC-PPG) HPHU was successfully increased by reacting the carbonate-terminated poly(DGC-PPG) PHU with PDMS-7k-(NH<sub>2</sub>)<sub>2</sub>, having hydrophobic segments of PDMS, and Priamine 1074, a bio-based dimer fatty acid derived diamine. The SI of the final HPHU dropped from 75% for the poly(DGC-PPG) HPHU to as low as 55% and 4% for the HPHU prepared from the addition of PDMS-7k-(NH<sub>2</sub>)<sub>2</sub> and Priamine 1074, respectively. The reacted PHUs were characterized by <sup>1</sup>H-NMR, FTIR, SEC, and DSC to verify the reactions targeted in this work. TGA showed that the thermal stability of the original poly(DGC-PPG) PHU prepolymer increased by at least 50 °C. The modified PHUs were then end-capped with silane agents to prepare moisture-curable HPHUs. The final products were also characterized, and while the dominant PDMS phase, providing the hydrophobicity for the end HPHU, was obvious from the WAXS spectrum of the PDMS-7k-poly(DGC-PPG)-7k-PDMS HPHU film, the presence of Priamine 1074 went undetected. However, the impact of the modification with Priamine 1074 on the toughness and the water resistance of the final HPHU was the greatest and could not be ignored. It seems that this oily substance can provide many benefits to PHUs and can eventually serve as a cheap and bio-based additive when formulating resins where some of the polymer has flexibility via poly(ether) segments, such as the poly(DGC-PPG) PHUs studied herein.

Overall, this study introduced the sequential synthesis method for preparing PHUs with tunable chemical, physical, and thermal properties which depends on the synergy between the properties of the PHU base segment and those of the chosen diamine end-cappers.

## 5.6 References

1. Guan, J.; Song, Y.; Lin, Y.; Yin, X.; Zuo, M.; Zhao, Y.; Tao, X.; Zheng, Q. Progress in Study of Non-Isocyanate Polyurethane. *Ind. Eng. Chem. Res.* **2011**, *50*, 6517-6527.
2. Kreye, O.; Mutlu, H.; Meier, M. A. R. Sustainable routes to polyurethane precursors. *Green Chem.* **2013**, *15*, 1431-1455.
3. Cornille, A.; Auvergne, R.; Figovsky, O.; Boutevin, B.; Caillol, S. A perspective approach to sustainable routes for non-isocyanate polyurethanes. *Eur. Polym. J.* **2017**, *87*, 535-552.
4. Blattmann, H.; Fleischer, M.; Bahr, M.; Mulhaupt, R. Isocyanate- and Phosgene-Free Routes to Polyfunctional Cyclic Carbonates and Green Polyurethanes by Fixation of Carbon Dioxide. *Macromol Rapid Commun.* **2014**, *35*, 1238-1254.
5. Maisonneuve, L.; Lamarzelle, O.; Rix, E.; Grau, E.; Cramail, H. Isocyanate-Free Routes to Polyurethanes and Poly(hydroxy Urethane)s. *Chem. Rev.* **2015**, *115*, 12407-12439.
6. Abitha, V. K.; Jadhav, S. A.; Rane, A. V. Non-Isocyanate Polyurethane Systems: A Review. *Moroccan J. Chem.* **2016**, *4*, 361-383.
7. Datta, J.; Wloch, M. Progress in non-isocyanate polyurethanes synthesized from cyclic carbonate intermediates and di- or polyamines in the context of structure-properties relationship and from an environmental point of view. *Polym. Bull.* **2016**, *73*, 1459-1496.
8. Bobbink, F. D.; van Muyden, A. P.; Dyson, P. J. En route to CO<sub>2</sub>-containing renewable materials: catalytic synthesis of polycarbonates and non-isocyanate polyhydroxyurethanes derived from cyclic carbonates. *Chem. Commun.* **2019**, *55*, 1360-1373.

9. Nohra, B.; Candy, L.; Blanco, J. F.; Guerin, C.; Raoul, Y.; Mouloungui, Z. From Petrochemical Polyurethanes to Biobased Polyhydroxyurethanes. *Macromolecules* **2013**, *46*, 3771-3792.
10. Błażek, K.; Datta, J. Renewable natural resources as green alternative substrates to obtain bio-based non-isocyanate polyurethanes-review. *Crit. Rev. Environ. Sci. Technol.* **2019**, *49*, 173-211.
11. Carre, C.; Ecochard, Y.; Caillol, S.; Averous, L. From the Synthesis of Biobased Cyclic Carbonate to Polyhydroxyurethanes: A Promising Route towards Renewable Non-Isocyanate Polyurethanes. *ChemSusChem* **2019**, *12*, 3410-3430.
12. Ghasemlou, M.; Daver, F.; Ivanova, E. P.; Adhikari, B. Bio-based routes to synthesize cyclic carbonates and polyamines precursors of non-isocyanate polyurethanes: A review. *Eur. Polym. J.* **2019**, *118*, 668-684.
13. Meier, M. A. R. Plant-Oil-Based Polyamides and Polyurethanes: Toward Sustainable Nitrogen-Containing Thermoplastic Materials. *Macromol. Rapid Commun.* **2019**, *40*, 1800524.
14. Lambeth, R. H. Progress in hybrid non-isocyanate polyurethanes. *Polym. Int.* **2020**, <https://doi.org/10.1002/pi.6078>.
15. Ecochard, Y.; Caillol, S. Hybrid polyhydroxyurethanes: How to overcome limitations and reach cutting edge properties? *Eur. Polym. J.* **2020**, *137*, 109915.
16. Decostanzi, M.; Ecochard, Y.; Caillol, S. Synthesis of sol-gel hybrid polyhydroxyurethanes. *Eur. Polym. J.* **2018**, *109*, 1-7.
17. Kathalewar, M.; Sabnis, A. Novel Bis-Urethane Bis-silane Precursor Prepared via Non-Isocyanate Route for Hybrid Sol-Gel Coatings. *Int. J. Sci. Eng. Res.* **2012**, *3*, 1-4.

18. Rossi de Aguiar, K. M. F.; Ferreira-Neto, E. P.; Blunk, S.; Schneider, J. F.; Picon, C. A.; Lepienski, C. M.; Rischka, K.; Rodrigues-Filho, U. P. Hybrid urethanesil coatings for inorganic surfaces produced by isocyanate-free and sol-gel routes: synthesis and characterization. *RSC Adv.* **2016**, *6*, 19160-19172.
19. Gomez-Lopez, A.; Grignard, B.; Calvo, I.; Detrembleur, C.; Sardon, H. Monocomponent Non-isocyanate Polyurethane Adhesives Based on a Sol-Gel Process. *ACS Appl. Polym. Mater.* **2020**, *2*, 1839-1847.
20. Gomez-Lopez, A.; Grignard, B.; Calvo, I.; Detrembleur, C.; Sardon, H. Synergetic Effect of Dopamine and Alkoxysilanes in Sustainable Non-Isocyanate Polyurethane Adhesives. *Macromol. Rapid Commun.* **2020**, *42*, 2000538.
21. Younes, G. R.; Price, G.; Dandurand, Y.; Maric, M. Study of Moisture-Curable Hybrid NIPUs Based on Glycerol with Various Diamines: Emergent Advantages of PDMS Diamines. *ACS Omega* **2020**, *5*, 30657-30670.
22. Günther, F.; Lima, E. F. S.; Rossi de Aguiar, K. M. F.; Bearzi, J. R.; Simões, M. B.; Schneider, R.; Bini, R. A.; Ribeiro, S. J. L.; Man, M. W. C.; Rischka, K.; Aguiar, F. H. B.; Pereira, R.; Mainardi, M. d. C. A. J.; Rocha, M. C.; Malavazi, I.; Passeti, T. A.; Santos, M. L.; Imasato, H.; Rodrigues-Filho, U. P. PDMS-urethanesil hybrid multifunctional materials: combining CO<sub>2</sub> use and sol-gel processing. *J. Sol-Gel Sci. Technol.* **2020**, *95*, 693-709.
23. Younes, G. R.; Maric, M. Moisture Curable Hybrid Polyhydroxyurethanes from Sugar-Derived Dicarbonates. *Macromol. Mater. Eng.* **2021**, *306*, 2000715.
24. Bähr, M.; Bitto, A.; Mülhaupt, R. Cyclic limonene dicarbonate as a new monomer for non-isocyanate oligo- and polyurethanes (NIPU) based upon terpenes. *Green Chem.* **2012**, *14*, 1447-1454.

25. Javni, I.; Hong, D. P.; Petrovic, Z. S. Polyurethanes from Soybean Oil, Aromatic, and Cycloaliphatic Diamines by NonIsocyanate Route. *J. Appl. Polym. Sci.* **2013**, *128*, 566-571.
26. Schmidt, S.; Ritter, B. S.; Kratzert, D.; Bruchmann, B.; Mulhaupt, R. Isocyanate-Free Route to Poly(carbohydrate-urethane) Thermosets and 100% Bio-Based Coatings Derived from Glycerol Feedstock. *Macromolecules* **2016**, *49*, 7268-7276.
27. He, X.; Xu, X.; Wan, Q.; Bo, G.; Yan, Y. Synthesis and Characterization of Dimmer-Acid-Based Nonisocyanate Polyurethane and Epoxy Resin Composite. *Polymers* **2017**, *9*, 649.
28. Ma, Z. Z.; Li, C.; Fan, H.; Wan, J. T.; Luo, Y. W.; Li, B. G. Polyhydroxyurethanes (PHUs) Derived from Diphenolic Acid and Carbon Dioxide and Their Application in Solvent- and Water-Borne PHU Coatings. *Ind. Eng. Chem. Res.* **2017**, *56*, 14089-14100.
29. Doley, S.; Dolui, S. K. Solvent and catalyst-free synthesis of sunflower oil based polyurethane through non-isocyanate route and its coatings properties. *Eur. Polym. J.* **2018**, *102*, 161-168.
30. Santiago-Medina, F. J.; Basso, M. C.; Pizzi, A.; Delmotte, L. Polyurethanes from Kraft Lignin without Using Isocyanates. *J. Renewable Mater.* **2018**, *6*, 413-425.
31. Panchireddy, S.; Grignard, B.; Thomassin, J. M.; Jerome, C.; Detrembleur, C. Bio-based poly(hydroxyurethane) glues for metal substrates. *Polym. Chem.* **2018**, *9*, 2650-2659.
32. Farhadian, A.; Ahmadi, A.; Omrani, I.; Miyardan, A. B.; Varfolomeev, M. A.; Nabid, M. R. Synthesis of fully bio-based and solvent free non-isocyanate poly (ester amide/urethane) networks with improved thermal stability on the basis of vegetable oils. *Polym. Degrad. Stab.* **2018**, *155*, 111-121.

33. Gharibi, R.; Yeganeh, H.; Kazemi, S. Green and non-leaching anti-bacterial and cytocompatible coating with build-in quaternary ammonium salt derived from methoxysilane functionalized soybean oil. *Mater. Sci. Eng., C* **2019**, *99*, 887-899.
34. Das, M.; Mandal, B.; Katiyar, V. Environment-friendly synthesis of sustainable chitosan-based nonisocyanate polyurethane: A biobased polymeric film. *J. Appl. Polym. Sci.* **2020**, *137*, 49050.
35. Ochiai, B.; Kojima, H.; Endo, T. Synthesis and Properties of Polyhydroxyurethane Bearing Silicone Backbone. *J. Polym. Sci., Part A: Polym. Chem.* **2014**, *52*, 1113-1118.
36. Panchireddy, S.; Thomassin, J. M.; Grignard, B.; Damblon, C.; Tatton, A.; Jerome, C.; Detrembleur, C. Reinforced poly(hydroxyurethane) thermosets as high performance adhesives for aluminum substrates. *Polym. Chem.* **2017**, *8*, 5897-5909.
37. Liu, G. F.; Wu, G. M.; Huo, S. P.; Jin, C.; Kong, Z. W. Synthesis and properties of non-isocyanate polyurethane coatings derived from cyclic carbonate-functionalized polysiloxanes. *Prog. Org. Coat.* **2017**, *112*, 169-175.
38. de Aguiar, K. R.; Rischka, K.; Gätjen, L.; Noeske, P.-L. M.; Cavalcanti, W. L.; Rodrigues-Filho, U. P. Biomimetic PDMS-hydroxyurethane terminated with catecholic moieties for chemical grafting on transition metal oxide-based surfaces. *Appl. Surf. Sci.* **2018**, *427*, 166-175.
39. Bossion, A.; Olazabal, I.; Aguirresarobe, R. H.; Marina, S.; Martín, J.; Irusta, L.; Taton, D.; Sardon, H. Synthesis of self-healable waterborne isocyanate-free poly(hydroxyurethane)-based supramolecular networks by ionic interactions. *Polym. Chem.* **2019**, *10*, 2723-2733.
40. Blattmann, H.; Mulhaupt, R. Multifunctional POSS Cyclic Carbonates and Non-Isocyanate Polyhydroxyurethane Hybrid Materials. *Macromolecules* **2016**, *49*, 742-751.

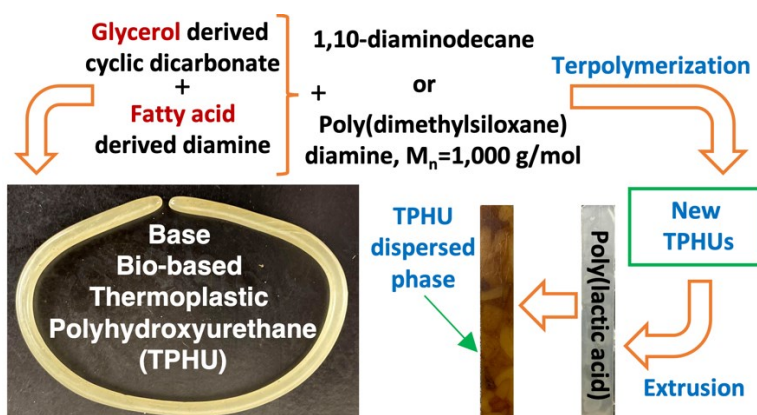
41. Ghasemlou, M.; Daver, F.; Ivanova, E. P.; Adhikari, B. Synthesis of green hybrid materials using starch and non-isocyanate polyurethanes. *Carbohydr. Polym.* **2020**, *229*, 115535.
42. Wu, Z. J.; Tang, L. Y.; Dai, J. T.; Qu, J. Q. Synthesis and properties of fluorinated non-isocyanate polyurethanes coatings with good hydrophobic and oleophobic properties. *J. Coat. Technol. Res.* **2019**, *16*, 1233-1241.
43. Hosgor, Z.; Kayaman-Apohan, N.; Karatas, S.; Gungor, A.; Menciloglu, Y. Nonisocyanate polyurethane/silica hybrid coatings via a sol-gel route. *Adv. Polym. Technol.* **2012**, *31*, 390-400.
44. Chen, X.; Li, L.; Wei, T.; Venerus, D. C.; Torkelson, J. M. Reprocessable Polyhydroxyurethane Network Composites: Effect of Filler Surface Functionality on Cross-link Density Recovery and Stress Relaxation. *ACS Appl. Mater. Interfaces* **2019**, *11*, 2398-2407.
45. Schimpf, V.; Heck, B.; Reiter, G.; Mulhaupt, R. Triple-Shape Memory Materials via Thermoresponsive Behavior of Nanocrystalline Non-Isocyanate Polyhydroxyurethanes. *Macromolecules* **2017**, *50*, 3598-3606.
46. Tryznowski, M.; Golofit, T.; Swiderska, A. Poly(hydroxyurethane)s with diethyl tartrate-based amide backbone by an isocyanate-free route: Use as adhesives. *Polymer* **2018**, *144*, 1-6.
47. Li, X. Y.; Ke, J. X.; Wang, J. W.; Kang, M. Q.; Wang, F.; Zhao, Y. H.; Li, Q. F. Synthesis of a novel CO<sub>2</sub>-based alcohol amine compound and its usage in obtaining a water- and solvent-resistant coating. *RSC Adv.* **2018**, *8*, 8615-8623.
48. Choi, T.; Weksler, J.; Padsalgikar, A.; Runt, J. Influence of soft segment composition on phase-separated microstructure of polydimethylsiloxane-based segmented polyurethane copolymers. *Polymer* **2009**, *50*, 2320-2327.

49. Choi, T.; Weksler, J.; Padsalgikar, A.; Runt, J. Microstructural organization of polydimethylsiloxane soft segment polyurethanes derived from a single macrodiol. *Polymer* **2010**, *51*, 4375-4382.
50. Hernandez, R.; Weksler, J.; Padsalgikar, A.; Runt, J. Microstructural Organization of Three-Phase Polydimethylsiloxane-Based Segmented Polyurethanes. *Macromolecules* **2007**, *40*, 5441-5449.
51. Gnanasekaran, D.; Reddy, B. S. A facile synthesis of mixed soft-segmented poly(urethane-imide)-polyhedral oligomeric silsesquioxane hybrid nanocomposites and study of their structure-transport properties. *Polym. Int.* **2014**, *63*, 507-513.
52. Jones, A.; Lamb, R. N.; Zhang, H. Hydrophobic Material. US Patent 6,743,467 B1, June 1, 2004.

## Chapter 6

### **Bio-based thermoplastic polyhydroxyurethanes synthesized from the terpolymerization of a dicarbonate and two diamines: design, rheology, and application in melt blending**

After presenting the more industrially focused aspect of the thesis in the previous chapters, this study which is published in *Macromolecules* in 2021 (Younes, G. R.; Maric, M., Bio-based Thermoplastic Polyhydroxyurethanes Synthesized from the Terpolymerization of a Dicarbonate and Two Diamines: Design, Rheology, and Application in Melt Blending. *Macromolecules* **2021**, *54* (21), 10189-10202) constitutes one of the more academic thrusts pursued in this thesis, with potential in biodegradable polymers.<sup>196</sup> This manuscript examines the terpolymerization of the bio-based monomers, DGC and Priamine 1074, with two different diamines, PDMS-based one or 1,10-diaminodecane, and the final TPHUs' rheological and microstructural properties were characterized. In addition, it studies, for the first time, the melt blending of the TPHUs into a PLA matrix. Herein, the TPHUs were blended with PLA to investigate their role as toughening agents and plasticizers, in analogy to how thermoplastic polyurethanes have been used previously. The supporting information of this manuscript are included in Appendix D.



## 6.1 Abstract

The terpolymerization of bio-based diglycerol dicarbonate (DGC) and Priamine 1074 is conducted with aminopropyl terminated polydimethylsiloxane ( $M_n = 1,000$  g/mol, PDMS) or 1,10-diaminodecane (DAD). Depending on DGC contents and PDMS/Priamine 1074 ratios, the resulting amorphous thermoplastic polyhydroxyurethanes (TPHUs) present random or block copolymer-like segmented structures. These TPHUs exhibit nanophase separation of small interdomain spacing (3-3.5 nm), mainly caused by DGC. As for DAD, it introduces crystallinity (8%) and chain ordering into the TPHU structure, as observed from X-ray measurements. Some PDMS-based TPHUs are blended with PLA, and the blends are found to be partially miscible as they exhibit two  $T_g$ s, and their estimated relative energy differences (RED), calculated from Hoftyzer-Van Krevelen's group contribution method, are nearly unity. Based on the type of hydrogen bonding interactions and the extent of immiscibility (RED) of each of the blends, the TPHUs find potential applications as toughening agents and/or plasticizers for PLA.

## 6.2 Introduction

Non-isocyanate polyurethanes (NIPUs) have been a subject of interest of many researchers, particularly in the last decade, because they are prepared without isocyanates, a dangerous and lethal main component of conventional polyurethanes (PUs).<sup>1, 2</sup> The polyaddition of cyclic (poly)carbonates with (poly)amines constitutes one pathway that leads to NIPUs with pendent hydroxyl groups in their chains, known as polyhydroxyurethanes (PHUs). PHUs are prominent materials because their polymerization does not lead to lower molecular weight byproducts and their precursors are abundant and, most importantly, can be derived from bio-based and bio-renewables sources.<sup>2-4</sup> Indeed, cyclic carbonates were previously synthesized from vegetable oils, bio-polyols (sugars) and terpenes.<sup>5-7</sup> Some of these natural materials contain double bonds

which are first epoxidized and then carbonated through the chemical fixation of carbon dioxide.<sup>8</sup> Bio-based diamines have been also synthesized from plant-based fatty acids, and some of them are commercially available, such as the Priamine family from Croda.<sup>9-11</sup> Hence, the synthesis of bio-based PHUs complies with many different green chemistry principles; the elimination of hazardous materials, such as isocyanates, the substitution of non-renewable fossil-fuels with renewable feedstocks, the reduction of organic solvent usages as reactions can be conducted in bulk, and the reduction of wastes and byproducts since the polyadditions do not generate lower molecular weight byproducts.<sup>12</sup>

An interesting renewable source for making the cyclic carbonates is diglycerol. Diglycerol dicarbonate (DGC), explored extensively in the literature for different PHU formulations,<sup>13-25</sup> is derived from glycerol, which is a byproduct obtained from the hydrolysis of biomass wastes, the methanolysis of triglycerides, and the production of biodiesel.<sup>4</sup> The worldwide annual production of glycerol has drastically increased in the past decade, and predictions showed that the production of glycerol was 6 times higher than the demand in 2020, making it an abundant raw material for the synthesis of PHUs.<sup>4, 26</sup> Furthermore, DGC has a melting point around 65 °C,<sup>13, 14</sup> so bulk polyadditions are possible at moderate temperatures.

In this study, DGC (hard segment) is combined with Priamine 1074, a bio-based diamine derived from dimer fatty acids (base of the soft segment). The reaction between DGC and Priamine 1074 leads to rubbery yellowish PHUs, as indicated previously,<sup>14, 22</sup> so this work seeks the preparation of a new family of thermoplastic PHUs (TPHUs) based on these monomers while further altering the polymer with a second diamine added to form a terpolymer. Two different diamines are considered; the aminopropyl terminated polydimethylsiloxane with  $M_n = 1,000$  g/mol (PDMS-1k-(NH<sub>2</sub>)<sub>2</sub>), which is softer than Priamine 1074, and 1,10-diaminodecane (DAD),

which is derived from castor bean oil <sup>11</sup> and enhances crystallinity more than Priamine 1074. While bio-based TPHUs have been extensively studied in the literature, <sup>27-34</sup> a similar strategy was adopted by few, <sup>23, 34</sup> mainly, those done by Mülhaupt et al. where thermoplastic and thermoset PHUs were prepared by blending two di/tricarbonates together or two diamines to tune the properties of their bio-based materials. <sup>27, 35, 36</sup>

However, blending more than one diamine draws a question about the nanophase separation and the rheological behavior of the final TPHUs. Like conventional thermoplastic polyurethanes (TPUs), the reaction between the hard segments (dicarbonates) and the soft segments (diamines) produces segmented di/triblock copolymer TPHUs whose microstructure and rheology might deviate from those of standard homopolymers. <sup>37-43</sup> Beniah et al. explored in depth the formation of nanophase separation in their segmented PHUs, notably in those prepared from poly(tetramethylene oxide)-based diamines. In their studies, the authors investigated the effects that the choice of the dicarbonates, diamines, and chain extenders as well as the functionalization of the hydroxyl groups have on tuning the nanophase separations of their TPHUs. <sup>44-49</sup> Nevertheless, there have been limited findings on the rheological behavior of such systems and their compliance to previously established models used for conventional polymers. Hence, this article tries to address these aspects, which should be interesting as PHUs exhibit additional hydrogen bonding interactions due to the presence of hydroxyl groups. <sup>10, 44-49</sup>

Moreover and to the best of our knowledge, TPHU blends with other polymers, such as poly(lactic acid) (PLA), have not been studied. PLA is a well-known bio-based and biodegradable polymer with outstanding physical and mechanical properties, but it suffers from poor ductility and impact toughness. Therefore, many TPUs were extruded with PLA with the intention to plasticize the latter and increase its toughness and ductility. <sup>50-62</sup> Hyperbranched

poly(ester amide) with a high hydroxyl functionality were also blended with PLA, and the authors found that the additive was partially miscible with the polymer matrix at high concentrations (20 wt.%).<sup>63</sup> Like these poly(ester amides), our TPHUs will have hydroxyl groups available for compatibilization and may provide some miscibility with the PLA matrix.

This study starts by examining the effects of mixing Priamine 1074 with PDMS-1k-(NH<sub>2</sub>)<sub>2</sub> or DAD in combination with DGC. The resulting TPHU's structural, thermal, rheological, and mechanical properties are studied with varying the DGC/Priamine 1074/second diamine ratios. Then, the blends of PLA with some of the TPHUs are prepared and characterized, and the application of the TPHUs as the dispersed phase in PLA blends is assessed.

## 6.3 Materials and Methods

### 6.3.1 Materials

Diglycerol (DIG, ≥80% α,α, impurities consist of mono-, α,β-di-, β,β-di-, and triglycerol) was obtained from Tokyo Chemical Industry (TCI). Dimethyl carbonate (DMC, ≥99%, anhydrous) and potassium carbonate (K<sub>2</sub>CO<sub>3</sub>, 98%, anhydrous powder) were purchased from Acros. Ethyl acetate (EthOAc, certified grade), tetrahydrofuran (THF, HPLC grade), chloroform (stabilized with ethanol), heptane, and 1,4-dioxane were purchased from Fisher Chemical. Water purified by a reverse osmosis process was provided by the McGill Chemical Engineering Department. The diamines used in this work are Priamine 1074, aminopropyl terminated polydimethylsiloxane with M<sub>n</sub> = 1,000 g/mol (PDMS-1k-(NH<sub>2</sub>)<sub>2</sub>), and 1,10-diaminodecane (DAD) which were provided by Croda, Gelest, and Sigma Aldrich, respectively. Deuterated dimethyl sulfoxide (DMSO-d<sub>6</sub>) and chloroform (CDCl<sub>3</sub>) was purchased from Sigma Aldrich. Poly(lactic acid) (PLA) was purchased from NatureWorks, Product ID Ingeo™ Biopolymer 2003D. All the

chemicals were used as received. Only PLA was dried overnight under vacuum at 40 °C before the extrusion to remove any adsorbed moisture.

### 6.3.2 Experimental methods

**DGC synthesis and purification:** The synthesis and purification of DGC were conducted following the procedure detailed in previous studies on DGC-based hybrid PHUs.<sup>22</sup> The DGC yield was 58%, based on the total amount of DIG originally loaded. The labelled <sup>1</sup>H-NMR spectrum of DGC is given as Figure D.1.

**Thermoplastic PHU (TPHU) synthesis:** The PHU terpolymers were synthesized using a one-step bulk polyaddition method with systematic alteration of the proportion of Priamine 1074 with either PDMS-1k-(NH<sub>2</sub>)<sub>2</sub> or DAD. The TPHUs were prepared by adding DGC, Priamine 1074, and one of the diamines to a 50 mL three-neck reactor. After adding a high viscosity stir bar into the mixture, the contents were purged with nitrogen for 15 min before immersing the reactor in an oil bath pre-heated to 80 °C. The reaction was allowed to proceed for 24 h, after which the reactor was removed from the oil bath to cool down and the TPHU was collected. The remaining monomers were removed by dissolving the TPHUs in chloroform and filtering them to remove the undissolved DGC. Then, a 10-fold excess of heptane was added to precipitate the polymers while removing the unreacted diamines and DGC. All terpolymers investigated herein have a hard segment content ranging between 25 and 55 wt.%. The ratio of Priamine 1074 to either PDMS-1k-(NH<sub>2</sub>)<sub>2</sub> or DAD was varied from 60/40 to 100/0 (wt.%). In subsequent discussions, these terpolymers are referred to as PDMS-2040 or DAD-2040, for example, where PDMS or DAD written before the dash refers to the second diamine used, the first two digits represent the content of these diamines in the soft segment mixture (in wt.% with respect to Priamine 1074) and the last two (40 in this case) represent the hard segment (DGC) content (in wt.%). Different

hard to soft segments concentrations were considered herein to make TPHUs of equimolar ratios and excess of hard segment.

**Extrusion:** PLA was blended with different PDMS-based TPHUs using a conical intermeshing twin-screw extruder (Haake Minilab, Thermo Electron Corporation, Beverly, MA, USA) with a screw diameter of 5/14 mm in the conical section, a screw length of 109.5 mm, and two batches equal to 3 g each. A three-step process was used to ensure homogeneity of the blends. In the first step, PLA was combined with 20 wt.% TPHU to make a batch of 3 g, and the extruder was set at 150 °C with a screw rotation speed of 30 min<sup>-1</sup>, and the resulting blend was recycled through the extruder with an additional 1.5 g of the mixture for a second step and then for a third one to ensure that the polymers were well mixed. The concentration of 20 wt.% was chosen to reflect a typical amount of plasticizer or toughening agents that is used industrially.

### 6.3.3 Characterization methods

**Proton nuclear magnetic resonance (<sup>1</sup>H-NMR) spectroscopy:** Solution-phase NMR spectra were recorded on a Bruker 500 MHz instrument (16 scans) at ambient temperature. DGC was dissolved in DMSO-d<sub>6</sub>, whereas the TPHUs were dissolved in CDCl<sub>3</sub> to be analyzed.

**Fourier transform infrared (FTIR) spectroscopy:** FTIR measurements were carried out on a Perkin Elmer instrument (Spectrum II series) equipped with a single bounce diamond attenuated transmission reflectance (ATR) for solids and zinc selenide (ZnSe) holder for liquids. 32 scans were recorded for each sample over the range 4000-500 cm<sup>-1</sup> with a normal resolution of 4 cm<sup>-1</sup>. The TPHUs were measured as is, whereas the blends were solvent cast from 1,4-dioxane.

**Size exclusion chromatography (SEC):** The TPHUs molecular weight distributions were analyzed via SEC. Number average molecular weight ( $M_n$ ) and dispersity ( $\mathcal{D} = M_w/M_n$ ) of prepolymer samples were measured using this technique on a Waters Breeze instrument with

HPLC grade THF as an eluent at a flow rate of 0.3 mL/min. The GPC has three Waters Styragel HR columns (HR1 with a molecular weight measurement range of  $10^2$  to  $5 \times 10^3$  g/mol, HR2 with a molecular weight measurement range of  $5 \times 10^2$  to  $2 \times 10^4$  g/mol, and HR4 with a molecular weight measurement range of  $5 \times 10^3$  to  $6 \times 10^5$  g/mol), a guard column, and a refractive index (RI 2414) detector. The columns were heated to 40 °C during analysis. The molecular weights were determined relative to poly(methylmethacrylate) (PMMA) calibration standards from Varian Inc. (ranging from 875 to 1,677,000 g/mol). The reported molecular weights were all relative to the PMMA standards and not adjusted with Mark-Houwink parameters.

**Thermogravimetric analysis (TGA):** TGA was performed on a Q500 system from TA Instruments. The thermal degradation of the synthesized TPHU was measured at a heating rate of 20 °C/min over the temperature range of 25 to 600 °C under a nitrogen atmosphere. The 10% degradation temperature ( $T_{d,10\%}$ ) were calculated using this method.

**Differential scanning calorimetry (DSC):** DSC was performed using a Q2500 TA Instruments calorimeter autosampler employing standard hermetic aluminum pans, calibrated with indium and nitrogen as purge gas. The instrument is equipped with a cooling unit allowing it to reach low temperatures up to -90 °C. The samples were analyzed at a heating rate of 10 °C/min, for the second heating ramp, over a temperature range of -90 °C to 100 °C (DAD TPHUs) or 150 °C (PDMS TPHUs and extruded PLA samples) under a nitrogen atmosphere after quenching the samples. Glass transition temperatures ( $T_g$ ), crystallization temperatures ( $T_c$ ), melting points ( $T_m$ ), and the associated enthalpies with the crystallization and the melting ( $\Delta H_c$  and  $\Delta H_m$ , respectively) were calculated from the second heating ramp.

**Small and Wide Angle X-ray Scattering (SAXS and WAXS):** SAXS and WAXS measurements were recorded on a SAXSpoint 2.0 (Anton Paar, Austria) equipped with a  $\text{CuK}\alpha$  radiation source (wavelength,  $\lambda = 1.54 \text{ \AA}$ ), using a detector of Eiger R 1M (Horizontal) at SAXS and WAXS distances of 1075.9 and 113.1 mm, respectively. The TPHU samples, with thickness of 1 mm, were placed on a sample holder for solids (10 by 10 mm) provided by Anton Paar, which was further secured by tape. X-ray exposure times were 30 min per frame for a total of 4 frames for every experiment. The obtained SAXS profiles were corrected and shown as function of scattering vector ( $q = (4\pi/\lambda) \sin\theta$ , where  $2\theta$  is the scattering angle in  $^\circ$  and  $q$  in  $\text{nm}^{-1}$ ). The mean interdomain spacing,  $d$  (nm), was calculated from the obtained SAXS spectra using the following formula:

$$d = 2\pi/q_{max} \quad \text{Eq. (6.1)}$$

with  $q_{max}$  ( $\text{nm}^{-1}$ ) is the value of  $q$  at maximum peak position read from SAXS spectra.

**Rheology:** For all the rheology tests, TPHU samples containing PDMS-1k-( $\text{NH}_2$ )<sub>2</sub> were cut into disks of 25 mm diameter and a thickness of 1 mm. Those samples were flexible at room temperature, so no hot pressing was required. The samples containing DAD and the blends had to be hot pressed between Teflon plates using a mold to make bars with dimensions of 50 mm length (length cut to 45 mm when running the tests), 10 mm width, 1 mm thickness, and 36 mm gauge length. Pressing, using a CARVER hydraulic unit model #3925, was performed at 80  $^\circ\text{C}$  for the DAD TPHUs and 150  $^\circ\text{C}$  for the blends using three cycles of 5, 10, and 15 metric tons for 10 min each.

Amplitude and frequency sweep measurements were conducted on the TPHU samples using different configurations on an Anton Paar Instruments rheometer (MCR 302). The parallel plates of 25 mm diameter (PP 25) configuration (gap of 1 mm) used with the samples containing

PDMS-1k-(NH<sub>2</sub>)<sub>2</sub>, whereas the torsion configuration (SRF 12) was used with the DAD-containing samples. Amplitude sweep measurements were all conducted at room temperature (~22 °C). The PDMS containing TPHUs were measured at a frequency of 10 Hz and a shear strain ranging from 0.01% to 100%. The DAD containing TPHUs measurements were done at shear strains ranging from 0.001% to 0.1% and a frequency of 10 Hz. Frequency sweeps were conducted at different temperatures, under nitrogen and using a CTD 450 convection oven, starting from room temperature (~25 °C) then 30 °C, after which the temperature was increased at 10 °C increments. All the samples were stabilized at a given temperature for 10 min before running a given test. The 10 min count started after the rheometer had reached the desired temperature. The PDMS containing TPHU samples were measured at a shear strain of 0.5%, frequency range of 0.1 to 100 rad/s, and temperatures of 25 to 120 °C.

Dynamic thermal mechanical analysis was conducted on the blends. Samples were loaded in tension and a temperature ramp was performed from 25 °C to 150 °C at a rate of 5 °C/min, with an oscillation strain of 0.5% and a frequency of 1 Hz. Amplitude and frequency sweeps were also performed on the blends in the form of bars and disks at room temperature (~22 °C) and 150 °C, respectively, with shear strains and frequency varying depending on the test and the temperature used. For all of the frequency sweeps tests conducted in this study, assurance that the experiments were operating in the viscoelastic region was achieved by performing amplitude sweeps on the samples.

**Mechanical Testing:** Tensile properties were determined at ambient temperature using an EZ Test (Shimadzu) tensile machine at speeds of 10 mm/min, on the DAD-containing TPHUs, and 20 mm/min, on films of the blends, with a load capacity of 10,000 N. Young's modulus (E), tensile strength ( $\sigma_{\max}$ ), and elongation at break (EB %) were estimated by the average of at least

three repeated samples. Free-standing dog-bone-shaped TPHU samples were prepared using Teflon plates with molds of the following dimensions: length of 50 mm, width of 3 mm, thickness of 1 mm, and gauge length of 25 mm. Pressing, using a CARVER hydraulic unit model #3925, was performed at 80 °C using three cycles of 5, 10, and 15 metric tons for 10 min each.

The extruded blends in contrast were solvent-cast using chloroform. 2.5 g of the samples were dissolved in 25 mL of chloroform and then poured into dishes of 12 cm diameter. The dishes were covered with aluminum foil perforated from four different sides to allow chloroform to evaporate slowly. After three days, the films were cut (60 mm length, gauge length of 30 mm, 10 mm width, and thickness between 0.1 and 0.2 mm). The films were dried in a vacuum oven overnight at 40 °C before running the tests. Similar film preparation methods were adopted elsewhere.<sup>64</sup> The tensile properties were monitored on WinAGS Lite software.

**Scanning Electron Microscopy (SEM):** The morphology of the prepared blends was studied with a Hitachi SU-3500 Variable Pressure SEM. The samples were immersed in liquid nitrogen for 10 min before brittle fracture. A series of samples had their surface directly treated with THF for 5 min to dissolve the TPHUs while keeping the PLA matrix, to provide contrast between the two components. Note that PLA has a low solubility in THF at cold temperatures, enabling its resistance to etching.<sup>65</sup> The fractured surfaces of all samples (treated and untreated) were tested after sputter coating them with palladium.

## 6.4 Results and Discussion

### 6.4.1 Characterization of the PDMS containing TPHUs

The polyaddition of DGC and Priamine 1074 was previously studied, and at similar reaction conditions to the ones used herein (80 °C for 24 h), the conversion of the cyclic carbonates is expected to be incomplete.<sup>14</sup> This was confirmed by performing FTIR on the TPHUs before and after purification and examining the decrease in the area of the carbonyl stretch related to the cyclic carbonate end-groups and unreacted carbonates (at 1780 cm<sup>-1</sup>) with respect to that of the carbonyl stretch of the urethane linkages (at 1695 cm<sup>-1</sup>) (Figure D.2). The TPHUs prepared from 40 wt.% hard segment content have an excess of cyclic carbonates (60-66 mol.%), whereas the ones containing 25 wt.% have a reaction mixture close to equimolar ratios (45-50 mol.% of hard segments). Hence, the amount of remaining DGC was higher in the former systems (25-35%) than in the latter (2-15%); however, after taking into consideration the diamine content participating in the reaction, the effective amount of unreacted DGC is found to be between 4 and 7%, which complies with the values reported for the equimolar systems. Besides, Carré et al. calculated a 12% residual of their dicarbonate after reacting it with Priamine 1075 at similar conditions to this study.<sup>34</sup> These results were confirmed by conducting <sup>1</sup>H-NMR on the TPHUs (Figure D.3, Figure D.4, and Table D.1) which also showed that the polyadditions with PDMS-1k-(NH<sub>2</sub>)<sub>2</sub> decreased the amount of secondary hydroxyl groups with respect to primary hydroxyl groups in the TPHU chains (please see the section on <sup>1</sup>H-NMR in Appendix D for more details on the analysis). The PDMS containing TPHUs are denoted in future discussions according to the following: PDMS-XXYY with XX represents the PDMS weight percentage in the total diamine mixture while YY represents the DGC weight percentage. For example, PDMS-2040

means that the TPHU based on DGC and Priamine 1074 is prepared from 20 wt.% PDMS-1k-(NH<sub>2</sub>)<sub>2</sub> in its soft segment mixture and 40 wt.% hard segments (DGC).

The structural and thermal properties of the TPHUs discussed in this section are summarized in Table 6.1. Depending on the hard segment content, whether it is 25 or 40 wt.%, the SEC, DSC, and TGA traces showed interesting differences. The number average molecular weights ( $M_n$ ) and the dispersity ( $\mathcal{D}$ ) of the PDMS-XX40 TPHUs were similar, with the molecular weight distribution becoming slightly broader when using 40 wt.% PDMS in the soft segment mixture (PDMS-4040). The thermal stability of these TPHUs was also similar with the degradation temperatures matching and with little difference (Figure D.5). Nevertheless, the DSC traces showed two glass transitions ( $T_{gs}$ ); one at -30 °C indicating the presence of PDMS soft segments and another one at -14 °C indicating the presence of Priamine 1074 soft segments. The first  $T_g$  was associated with PDMS segments as a PDMS-10040 TPHU was prepared, and it revealed a  $T_g$  at -35 °C. The existence of two  $T_{gs}$  suggests that PDMS-2040 and PDMS-4040 present segmented blocky structures with DGC joining the different soft segments. The soft segments might have reacted with DGC (in excess) first, which leads to two different PHUs, and then DGC bridged between one Priamine 1074 segment from one chain and another PDMS segment from a second chain by reacting with their free amines. Since the PDMS-XX25 TPHUs presented one  $T_g$ , the only factor that could be responsible of having two  $T_{gs}$  in the PDMS-XX40 TPHUs is the excess of DGC, which might have given more cyclic carbonate sites for the soft segments to react separately before they were joined by a cyclic carbonate group. Besides, these TPHUs showed interdomain spacings ( $d$ ) between their segments (DGC, PDMS-1k-(NH<sub>2</sub>)<sub>2</sub>, and Priamine 1074) of 3.2 to 3.4 nm which proves that such TPHUs exhibit nanophase separation. However, this separation is mainly between DGC and Priamine 1074, as  $d$  slightly increases with

the amount of PDMS, and  $d$  are much lower than previously measured ones in Beniah et al.'s segmented PHUs (~10 nm).<sup>44-49</sup> Hence, the soft segments of the TPHUs have a good miscibility with each other (Priamine 1074 and PDMS-1k-(NH<sub>2</sub>)<sub>2</sub>) and the hard segment (DGC) is inducing the phase separation. Although we are not totally dismissing that the observed two  $T_g$ s are caused by the presence of a mixture of two different PHU chains, it is most probable that PDMS-2040 and PDMS-4040 are made of segmented “block copolymers” of two PHUs (Priamine 1074 and PDMS-1k-(NH<sub>2</sub>)<sub>2</sub>-based) connected by a DGC unit because, the soft segments are miscible and, otherwise, the SEC traces would have been bimodal rather than monomodal, and the  $M_n$  and  $\bar{D}$  would have been higher than the values reported in Table 6.1, especially that an  $M_n$  of 15,200 g/mol was measured for a PDMS-10040 TPHU (versus 5,800 g/mol for PDMS-0040) under similar SEC experimental conditions. Figure 6.1-A illustrates the segmentalization discussed in this last section.

**Table 6.1 - Structural and thermal properties of the PDMS containing TPHUs**

TPHU	$M_n$ (g/mol) <sup>a</sup>	$\bar{D} = M_w/M_n^a$	$T_{g,1}$ (°C)	$T_{g,2}$ (°C)	$T_{d,10\%}$ (°C)	$d^b$ (nm)
<b>PDMS-0040</b>	5,800	2.6	-	-12	242	3.2
<b>PDMS-2040</b>	5,700	2.5	-32	-14	243	3.3
<b>PDMS-4040</b>	5,100	3.1	-30	-14	239	3.4
<b>PDMS-0025</b>	3,200	2.3	-16	-	256	3.1
<b>PDMS-2025</b>	4,700	3.2	-14	-	271	3.2
<b>PDMS-4025</b>	6,100	3.3	-19	-	279	3.2

a. Number average molecular weight and dispersities were estimated from SEC with THF eluent at 40 °C relative to poly(methyl methacrylate) standards.

b. The interdomain spacing ( $d$ ) was calculated from Eq. (6.1).

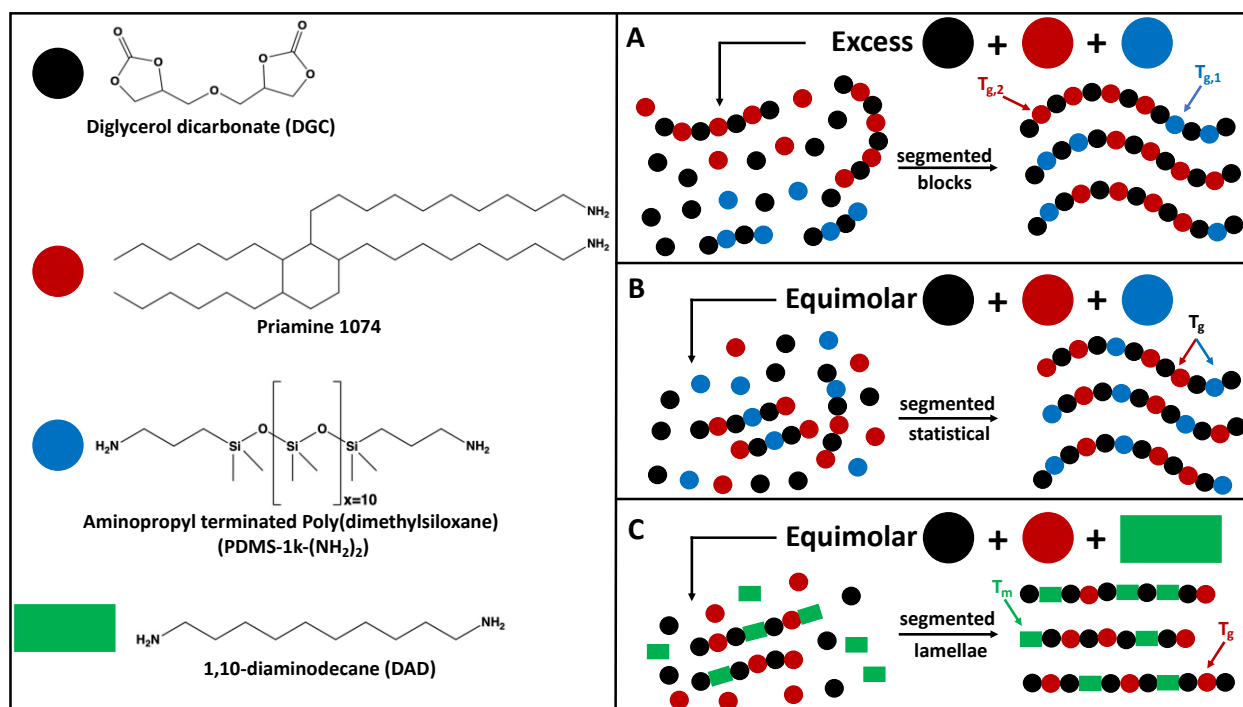


**Figure 6.1 - Summary of structural phenomena observed in this study: A and B-segmented block and statistical copolymers, respectively formed during the terpolymerization of Priamine 1074 and PDMS-1k-(NH<sub>2</sub>)<sub>2</sub> with excess and equimolar amounts of DGC, respectively, and C-segmented lamellae-like microstructure of DAD-4040 TPHU.**

To further prove that the soft segments are miscible and explain the observed two  $T_g$ s of the PDMS-XX40 TPHUs, a group contribution method, based on Hoftyzer-Van Krevelen, was conducted to estimate the Hansen solubility parameters of Priamine 1074/DGC and PDMS-1k-(NH<sub>2</sub>)<sub>2</sub>/DGC hydroxyurethane linkages.<sup>66-68</sup> In general, for liquids and amorphous polymers, the cohesive forces are dependent on the dispersion forces, polar forces, and hydrogen bonding, and hence the solubility parameter estimation is divided into three components;  $\delta_d$ ,  $\delta_p$ , and  $\delta_h$ , respectively.<sup>66</sup> The estimations, summarized in Table D.2, showed that the difference in solubility parameters ( $\Delta\delta$ ), calculated from Eq. (D.8), of Priamine 1074/DGC and PDMS-1k-(NH<sub>2</sub>)<sub>2</sub>/DGC hydroxyurethane linkages is about  $5.2 \text{ (MJ/m}^3)^{1/2}$ , which is at the limit of the good

solubility region defined at  $\Delta\delta \leq 5 \text{ (MJ/m}^3\text{)}^{1/2}$ .<sup>66</sup> The major difference between the linkages is caused by a difference in  $\delta_{ds}$  with Priamine 1074/DGC having a higher value of  $20.7 \text{ (MJ/m}^3\text{)}^{1/2}$  (versus  $15.6 \text{ (MJ/m}^3\text{)}^{1/2}$  for PDMS-1k-(NH<sub>2</sub>)<sub>2</sub>/DGC). The dispersion forces are attractive forces, and hence, could have led to the segmentalization of Priamine 1074 and PDMS-1k-(NH<sub>2</sub>)<sub>2</sub>, during the polyaddition, in the presence of an abundant quantity of DGC. Since  $\Delta\delta = 5.2 \text{ (MJ/m}^3\text{)}^{1/2} \cong 5 \text{ (MJ/m}^3\text{)}^{1/2}$ , our previous conclusion on the miscibility of the soft segments of the TPHUs is confirmed.

In contrast, the PDMS-XX25 TPHUs showed only one  $T_g$  with the lowest one exhibited by PDMS-4025 (-19 °C), which is not surprising as it contains the highest amount of PDMS-1k-(NH<sub>2</sub>)<sub>2</sub>. This suggests that, at a stoichiometric amount of DGC, the terpolymerization leads to segmented “statistical copolymers” made by Priamine 1074 and PDMS-1k-(NH<sub>2</sub>)<sub>2</sub> connected with DGC units. The  $M_n$  and  $\mathcal{D}$  increased with PDMS content, as shown in Table 6.1, and this is expected because PDMS-1k-(NH<sub>2</sub>)<sub>2</sub> has a higher molecular weight than Priamine 1074, and its addition to the PHU chains lead to higher molecular weights and broadening of the distribution. As well, there is an increase in thermal stability of these TPHUs with the PDMS content (by 20 °C in  $T_{d,10\%}$ ), and their thermal stability is higher than their PDMS-XX40 analogs (by as high as 40 °C in  $T_{d,10\%}$ ). In fact, PDMS-XX25 have randomly arranged soft segments in their structure, so the PDMS units have more possibility to interact with the Priamine 1074 segments providing better thermal stability for these TPHUs with respect to their block copolymer (PDMS-XX40) analogs, in which the different blocks are far from each other, and thermally degrade one after the other (please refer to the TGA traces provided in Figure D.5). The latter showed no improvement in thermal stability with increasing PDMS content either. The miscibility of the PDMS-1k-(NH<sub>2</sub>)<sub>2</sub> and Priamine 1074 blocks strongly influences the interaction between the soft

segments in the terpolymer structures. SAXS of these TPHUs were measured, and interdomain spacing ( $d$ ) of 3.1-3.2 nm were calculated suggesting again that the hard segments are primarily causing the phase separation. Note that  $d$  of these samples slightly increased with the PDMS content like those of the PDMS-XX40 TPHUs. Figure 6.1-A and B summarizes the main results on the PDMS-based TPHUs discussed until this point.

WAXS was conducted on the TPHUs of this section, and similar spectra were obtained for both sets of samples with differing amounts of PDMS. The WAXS spectra of the PDMS-XX25 and the PDMS-XX40 series are given as Figure 6.2 and Figure D.6, respectively, and they all present a peak at  $2\theta$  around  $14.5^\circ$ , which is that of the Priamine 1074 phase. With increasing PDMS content, a distinct shoulder peak appears at  $2\theta$  of  $9^\circ$  and increases in intensity with respect to the original peak. Previously, a distinct and sharp peak of PDMS in DGC and sugar-based dicarbonates PHUs appeared at  $2\theta$  of  $12.5^\circ$  with a broad segmented PHU peak at  $21.5^\circ$ .<sup>25</sup>  
<sup>69</sup> As well, a 1,000 g/mol  $\alpha,\omega$ -PDMS diol had a sharp PDMS phase peak at  $12.5^\circ$ ,<sup>70</sup> which is interestingly higher than the  $9^\circ$  measured herein for a similar phase. Hence, the miscibility and interactions between the coexisting phases might have caused the decrease in the scattering angle of the PDMS phase, which aligns with the previous discussion.

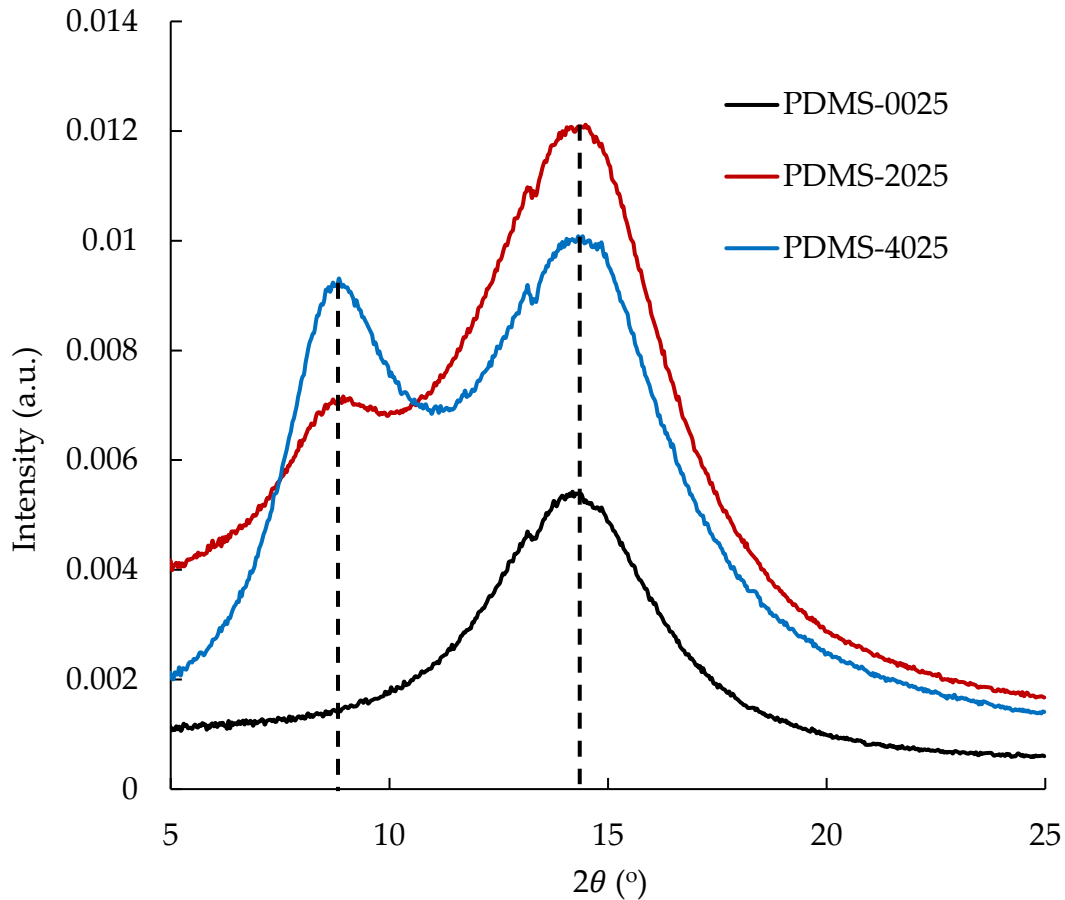


**Figure 6.2 - WAXS spectra of PDMS-0025, PDMS-2025, and PDMS-4025. The distinct shoulder peak at  $2\theta$  of  $9^\circ$  proving the presence of a PDMS phase in the microstructure of the TPHUs. The intensity is given in logarithmic scale.**

The rheology of these TPHUs was also studied, and all of the PDMS-based TPHUs (except for PDMS-0040) showed a viscous-like behavior ( $G''$ ) overcoming their elastic aspects ( $G'$ ) at room temperature. A summary of the amplitude sweeps conducted on these samples is given in Figure 6.3 (storage modulus,  $G'$ ) and Figure D.7 (loss modulus,  $G''$ ). In Figure 6.3,  $G'$  increased with DGC and Priamine 1074, and decreased with higher PDMS content, proving our initial hypothesis on blending PDMS-1k-( $\text{NH}_2$ )<sub>2</sub> with Priamine 1074. However, the decrease in  $G'$  was more significant in the PDMS-XX40 TPHUs, which might be due to the interaction of

the Priamine 1074 and the PDMS soft segments randomly organized along the polymer chain of the PDMS-XX25 TPHUs. Hence, the effect of increasing the PDMS content on  $G'$  of the latter was reduced. The same reasoning was previously applied to discuss the increase in thermal stability of the PDMS-XX25 TPHUs, which is not observed in the segmented block copolymer-like PDMS-XX40 ones. Nevertheless, to extract fundamental information about the segmented TPHUS under study, frequency sweeps at various temperatures are conducted from which time-temperature superposition curves are obtained.

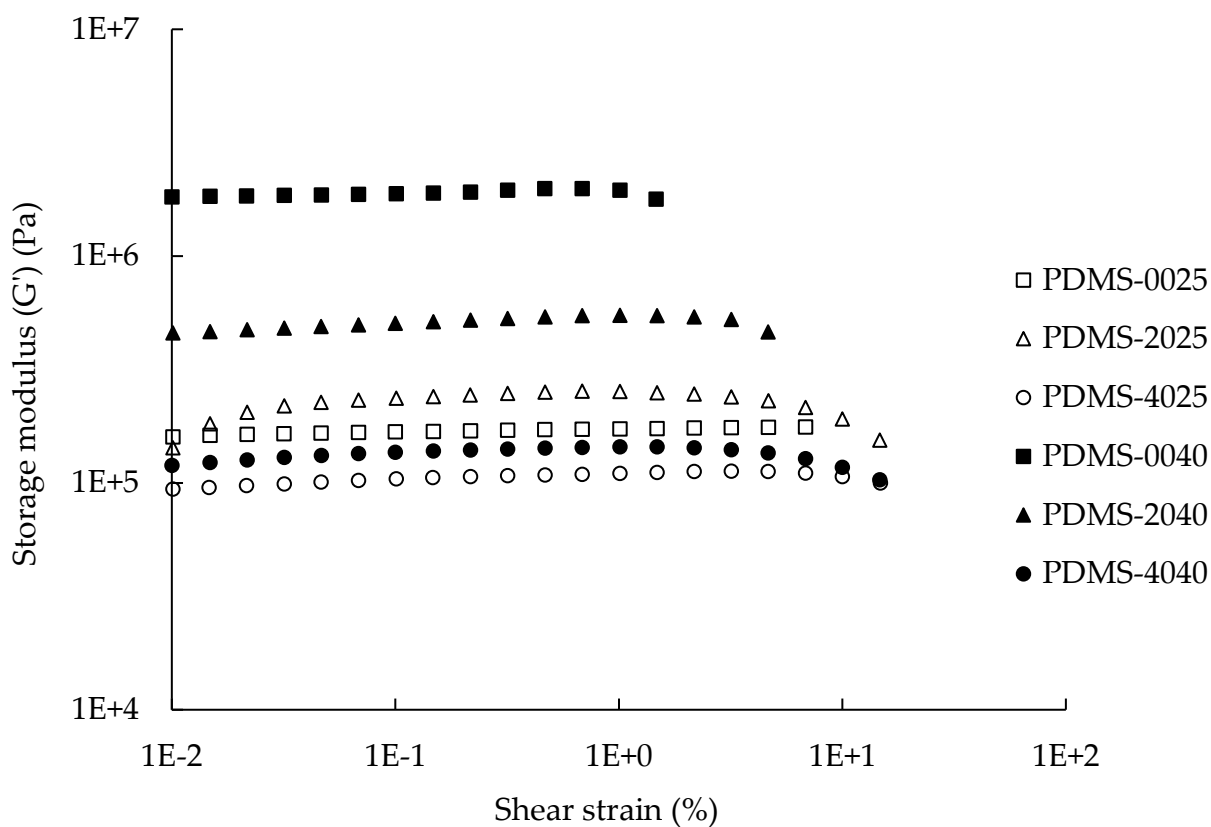


**Figure 6.3 - Storage modulus of the PDMS-based TPHUs collected from amplitude sweeps conducted at 22 °C and a frequency of 10 Hz.**

The modulus reduced frequency curves are given as Figure 6.4 to Figure 6.6 and Figure D.8 to Figure D.10. The insets show the shift factors ( $a_T$ ) used to construct the time-temperature superpositions from the frequency sweeps. The solid lines are approximate fits of the Generalized Maxwell model obtained using the least squares method and a procedure discussed elsewhere (Eqs. (3A.10) and (3A.11) of reference 71).<sup>71</sup> This model fits well the data; however, the data does not satisfy the terminal behaviour predicted by the model; slopes of 2 and 1 at low angular frequencies for  $G'$  and  $G''$ , respectively, on a log-log scale, are not observed. Indeed, the terminal slopes of the storage modulus ( $G'$ ) are between 0.9 and 1.7 with no specific trend with changes in composition of the TPHUs. The terminal slopes of the loss modulus curves vary between 0.7 and 1 for all the PDMS-based TPHUs with a decreasing slope from 1 to 0.7 with increasing PDMS content in the PDMS-XX40 series and similar values between 0.8 and 0.9 for the PDMS-XX25 series. Previously, other models, e.g. the Rouse model, were used to fit frequency sweep data collected for segmented conventional PUs with deviations also observed.<sup>40, 41</sup> The shift factors obtained were fitted with the William-Landel-Ferry (WLF) equation:<sup>72</sup>

$$\log(a_{T_g}) = -\frac{C_1(T-T_g)}{C_2+T-T_g} \quad \text{Eq. (6.2)}$$

which has been successfully used for homopolymers with universal constants  $C_1 = 17.4$  and  $C_2 = 51.6$  °C, which hold for temperatures between  $T_g$  and  $T_g + 100$  °C. The chosen reference temperature was 70 °C ( $T_{ref}$ ), from which the  $a_T$  of a given temperature was calculated as follows:

$$\log(a_T) = \log(a_{T_g}) - \log(a_{T_{ref}}) \quad \text{Eq. (6.3)}$$

In the case of two  $T_g$ s, such as for the PDMS-XX40 TPHUs, the Fox equation was used to find an equivalent  $T_g$  seeing that the phases of the different soft segments are miscible. For PDMS-

0025 and PDMS-0040, the WLF equation fits well the used shift factors; however, the insets show its limitations in predicting accurate shift factors at low temperatures (up to 50 °C) with increasing PDMS content. Valenkar et al. observed a similar pattern when increasing the length of soft segment blocks of segmented PUs.<sup>40, 41</sup> Also, their time-temperature superposition broke down at low temperatures where the storage and loss moduli plots showed branches, but only the storage modulus plots of this study exhibited branches at high temperatures (above 90 °C) with an additional relaxation at a reduced angular frequency of 10 rad/s. Hence, the latter plot cannot be the result of a breakdown of the time-temperature superposition method, and a structural phenomenon has caused it, which will be shortly discussed.

Amorphous polymers exhibit two types of relaxation; a major  $\alpha$  relaxation starting right after the  $T_g$  and minor relaxations ( $\beta$ ,  $\gamma$ ...) occurring at temperatures lower than the  $T_g$ .<sup>72</sup> The PDMS-based PHUs have  $T_{gs}$  below 0 °C, and thus the relaxations observed in the time-temperature superposition of the present  $G'$  plots can be part of the  $\alpha$  relaxations (typically known also as segmental or structural relaxations). In fact, the reduced angular frequency at 10 rad/s is spanned by temperatures ranging between 50 and 80 °C, and while DGC has a melting temperature at 65 °C, this new relaxation can be caused by the “flow” of hard segments, as it was previously indicated that DGC is the major cause of nanophase separation in the PDMS-based TPHUs. Beniah et al. observed similar trends after performing dynamic mechanical thermal analysis (DMTA) on their nanophase separated segmented PHUs.<sup>44-49</sup> Besides, the flow of the hard segments at 65 °C might have led to the branches at temperatures above 90 °C since the slopes of the curves gradually decreased when going from 80 °C to 120 °C, which is a sign of chain softening and reorganization.

The shift factors were also fitted using the Arrhenius law equation to find the activation energy:<sup>72</sup>

$$\ln(a_T) = \frac{E_A}{R} \left( \frac{1}{T} - \frac{1}{T_{ref}} \right) \quad \text{Eq. (6.4)}$$

where  $E_A$  is the activation energy for the viscoelastic relaxation,  $R$  is the gas constant (8.314 J/mol.K), and  $T_{ref}$  was previously defined as 70 °C. It is found that, contrary to the WLF equation, the Arrhenius law fits best the shift factors of the TPHUs containing PDMS ( $R^2 = 0.99$ ). The calculated activation energies decreased with PDMS content (please check Figure D.8 to Figure D.10 as well), and this is expected as a higher PDMS content softens the TPHUs and decreases the  $T_g$ , and  $E_A$  is the required energy to overcome the glass transition and achieve chain motion.

After characterizing the PDMS-based TPHUs, the next section briefly presents the impact of adding DAD on a DGC/Priamine 1074 PHU.

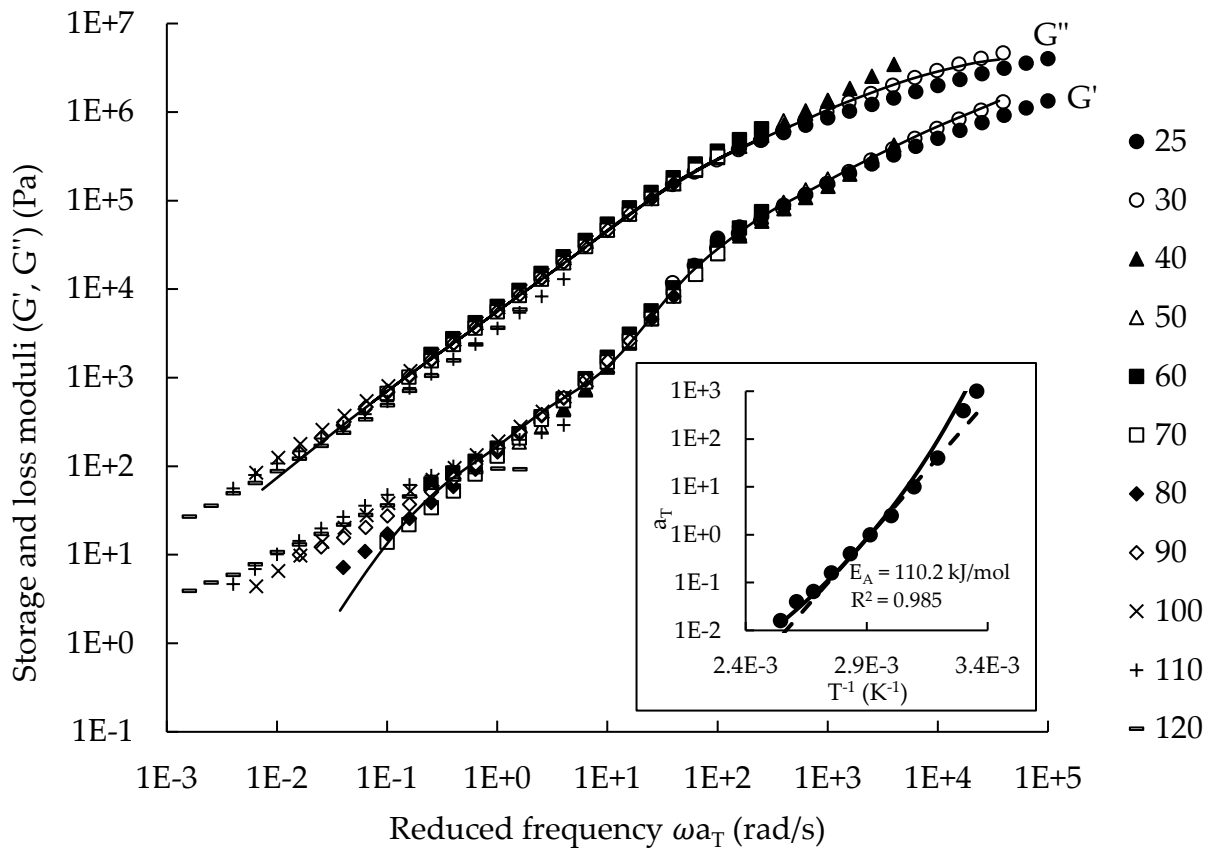


**Figure 6.4 - Dynamic mechanical frequency sweep data for PDMS-0040 ( $G''$  curve is shifted by a factor of 5) at 0.5% shear strain. The solid line is a fit to the Generalized Maxwell model. The inset shows the shift factors used for time-temperature superposition. The solid and dashed lines in the inset are the WLF and Arrhenius law fit equations, respectively.**

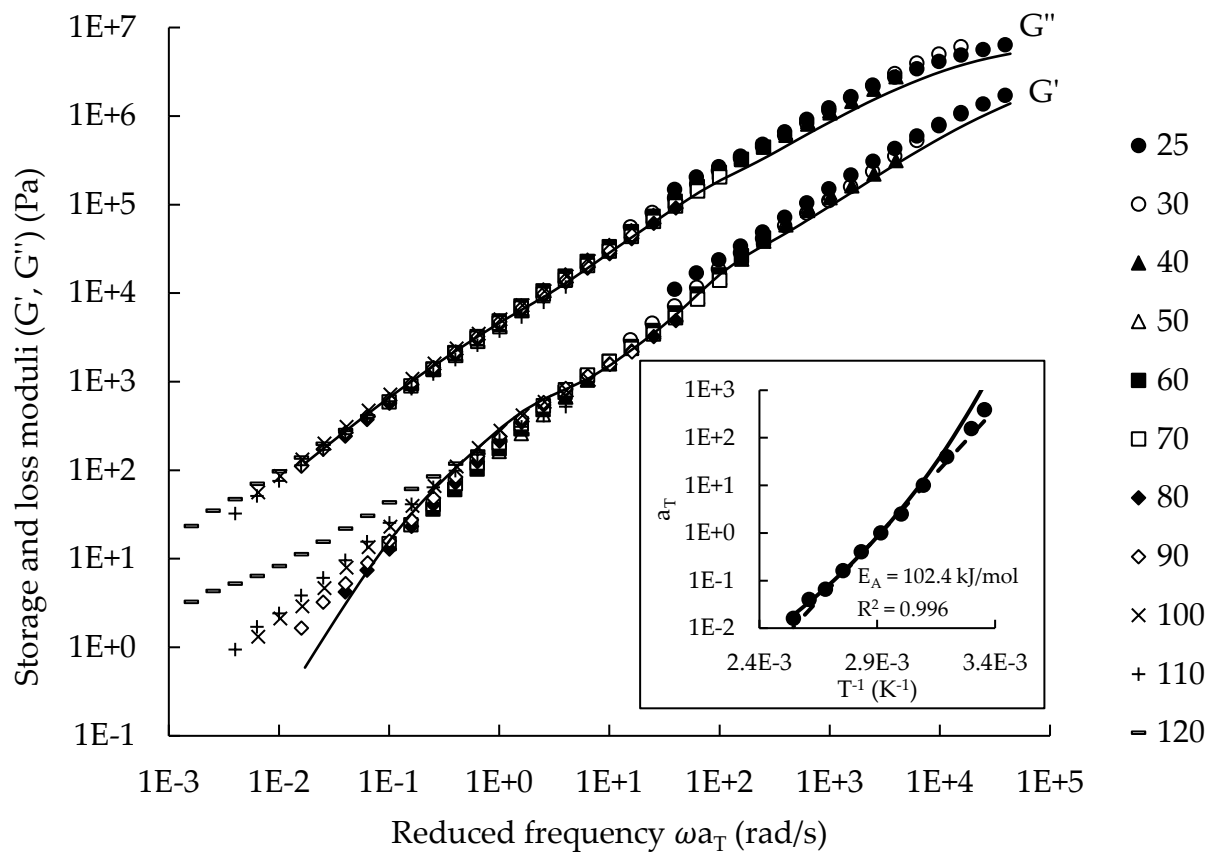


**Figure 6.5 - Dynamic mechanical frequency sweep data for PDMS-2040 ( $G''$  curve is shifted by a factor of 5) at 0.5% shear strain. The solid line is a fit to the Generalized Maxwell model. The inset shows the shift factors used for time-temperature superposition. The solid and dashed lines in the inset are the WLF and Arrhenius law fit equations, respectively.**

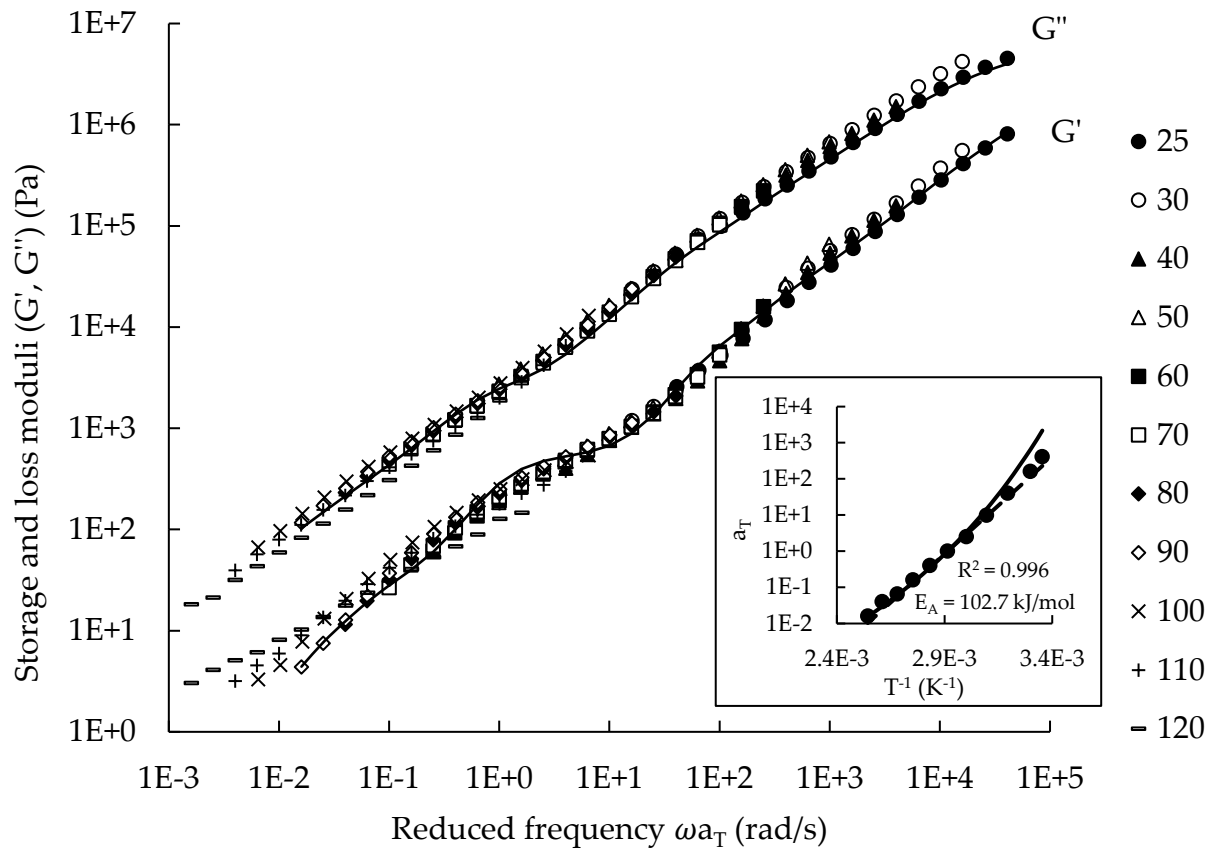


**Figure 6.6 - Dynamic mechanical frequency sweep data for PDMS-4040 ( $G''$  curve is shifted by a factor of 5) at 0.5% shear strain. The solid line is a fit to the Generalized Maxwell model. The inset shows the shift factors used for time-temperature superposition. The solid and dashed lines in the inset are the WLF and Arrhenius law fit equations, respectively.**

#### 6.4.2 Characterization of DAD containing TPHUs

Previously, it was reported by Magliozzi et al. that the equimolar reaction of DGC with DAD, after 4 h at temperatures between 80 and 95 °C using magnetic stirring, resulted in a 41% conversion of DGC.<sup>18</sup> The DAD-TPHU reactions conducted herein with 40 wt.% DGC operate at nearly equimolar ratios as well, so it is anticipated that at the applied reaction conditions (80 °C and 24 h), the conversion of DGC will be above 90%, and that was confirmed by FTIR in which the DGC carbonyl stretch (at 1790 cm<sup>-1</sup>) disappeared completely for DAD-3040 and DAD-4040 (Figure D.11). The DAD-##55 series showed a substantial fraction of unreacted monomers, mainly DGC and DAD, at the adopted reaction conditions, so the samples were disregarded from this study. The conversion of DAD-0040 was discussed previously (that of PDMS-0040). Similar to the PDMS containing TPHUs, the secondary hydroxyl groups content decreased when running the terpolymerizations with DAD, as analyzed from <sup>1</sup>H-NMR (please refer to Figure D.12 and Table D.3 for more details). Note that the naming of the TPHUs adopted herein is similar to the one used previously for the PDMS-based TPHUs.

Table 6.2 summarizes the structural and thermal properties of the DAD-based TPHUs. It is clear that blending DAD with Priamine 1074 led to higher M<sub>n</sub> with low Đ (about 2.5) with increasing DAD content. Because DAD is significantly shorter than Priamine 1074 and PDMS-1k-(NH<sub>2</sub>)<sub>2</sub>, DAD acts as a chain extender of the DGC/Priamine 1074 PHUs, as confirmed by the SEC results in Table 6.2. Besides, DAD is more rigid than Priamine 1074, so its incorporation in the TPHU structure leads to chains with lower mobility as reflected by the slightly higher T<sub>g</sub> values (-5 °C) of the DAD TPHUs versus DAD-0040 (-12 °C). The thermal stability of DAD-0040 was also improved with the addition of DAD, and T<sub>d,10%</sub> increased by 20 °C (refer to the TGA traces provided in Figure D.13). However, neither the T<sub>g</sub> nor the thermal stability were

dependent on the DAD concentrations. Interestingly, all the DAD TPHUs are semi-crystalline with a crystalline fraction ( $X_c$ ) between 7.5 and 9%, which were calculated from the WAXS spectra of Figure D.14 using the deconvolution method. However, only DAD-4040 exhibited a semi-crystalline behavior when tested on DSC with a melting temperature ( $T_m$ ) at 67 °C and heat enthalpy ( $\Delta H_m$ ) of 19.3 J/g, and its crystallinity matched the one calculated from WAXS (Table 6.2). DSC might have failed to detect the crystallinity of the other samples because of the lower content of DAD and hence lower contrast between the amorphous (Priamine 1074/DGC) and crystalline (DAD/DGC) phases. Moreover, DAD-4040 exhibited a crystallization temperature ( $T_c$ ) at 32 °C and a heat enthalpy ( $\Delta H_c$ ) of -20.5 J/g, from DSC, with an onset temperature at 19 °C, which implies that the chains of this TPHU, along with those of DAD-2040 and DAD-3040, are mobile at room temperature and rearrange into ordered microstructures. That was actually confirmed from the SAXS measurements of Figure 6.7, in which the spectra present higher order diffractions with no specific pattern for DAD-2040 and DAD-3040 and a lamellae-like pattern for DAD-4040 (ratio  $q/q^*$  of 1, 2, 3 pattern).<sup>73</sup> In fact, DAD-4040 is extremely brittle, such that its samples could not be cut out of the mold for mechanical testing as they shattered immediately (it was very glassy). This qualitative observation matches the microstructural pattern uncovered for DAD-4040, which has its chains parallelly aligned with respect to one another (Figure 6.1-C). Still, mechanical testing was carried out on the softer DAD-2040 and DAD-3040, and the results are presented in Figure 6.8. The segmentation of the DAD-based TPHUs is clearly observed from the shape of the stress-strain curves, which have two subsequent deformations: the first one for the amorphous phase followed by the deformation of the crystalline phase which yields before the sample breaks. DAD-3040, containing more DAD, broke at a lower elongation at break (EB%) of  $16\% \pm 7$  with respect to DAD-2040 ( $37\% \pm 4$ ). The DAD content also

affected the Young's modulus of the second deformation while the Young's moduli of the amorphous phase (first deformation) were close for both samples ( $0.39 \text{ MPa} \pm 0.16 \text{ MPa}$  for DAD-2040 and  $0.33 \pm 0.03 \text{ MPa}$  for DAD-3040). Actually, the effective Young's moduli for the crystalline phase were higher for DAD-3040 ( $0.12 \pm 0.02 \text{ MPa}$ ) as it comprises 10 wt.% more of DAD with respect to DAD-2040 ( $0.08 \pm 0.04 \text{ MPa}$ ). Moreover, the amplitude sweeps on these samples showed a significant increase in storage modulus ( $G'$ ) (200 to 800 times) when going from DAD-0040 to DAD-4040 as shown in Figure 6.9 and Figure D.15.

Noting the semi-crystallinity of the DAD-based TPHUs and their structural complexity, only the PDMS-based TPHUs were selected to be blended with PLA, and the results are discussed in the next section.

**Table 6.2 - Structural and thermal properties of the DAD containing TPHUs**

TPHU	$M_n$ (g/mol) <sup>a</sup>	$\bar{D} = M_w/M_n$ <sup>a</sup>	$T_g$ (°C)	$X_{c,DSC}$ <sup>b</sup> (%)	$X_{c,WAXS}$ <sup>c</sup> (%)	$T_{d,10\%}$ (°C)
<b>DAD-0040</b>	5,800	2.6	-12	-	-	242
<b>DAD-2040</b>	5,100	3.1	-5	-	7.5	260
<b>DAD-3040</b>	6,300	2.7	-7	-	8.8	266
<b>DAD-4040</b>	8,200	2.4	-4	8.8	8.4	262

a. Number average molecular weight and dispersities were estimated from SEC with THF eluent at 40 °C relative to poly(methyl methacrylate) standards.

b. The crystallinity  $X_c$  was calculated from DSC by dividing  $\Delta H_m = 19.3 \text{ J/g}$  with  $\Delta H_{m,100\%} = 219 \text{ J/g}$  of DAD as crystallinity was caused by the addition of DAD.  $\Delta H_{m,100\%}$  of DAD was estimated by interpolation from the  $\Delta H_{m,100\%}$  of 1,12-diaminododecane and 1,6-hexamethylene diamine.<sup>74</sup>

c. The crystallinity  $X_c$  was calculated from WAXS by using the deconvolution method to estimate the area of the amorphous and crystalline portions.  $X_c$  was found by taking the ratio of the crystalline area over the total area.

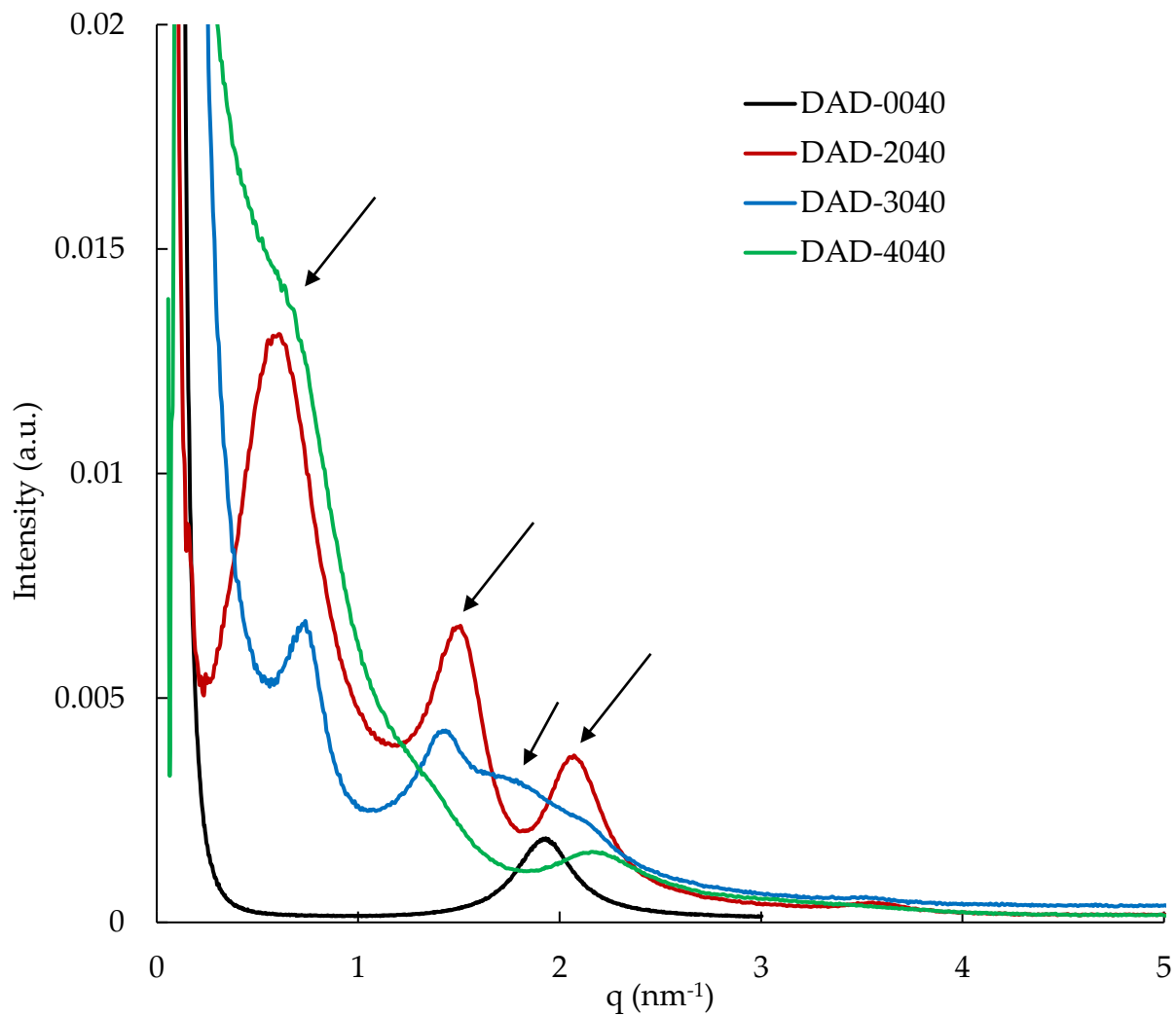


**Figure 6.7 - SAXS spectra of DAD-based TPHUs showing ordering in their microstructure.**

**The intensity is given in logarithmic scale.**

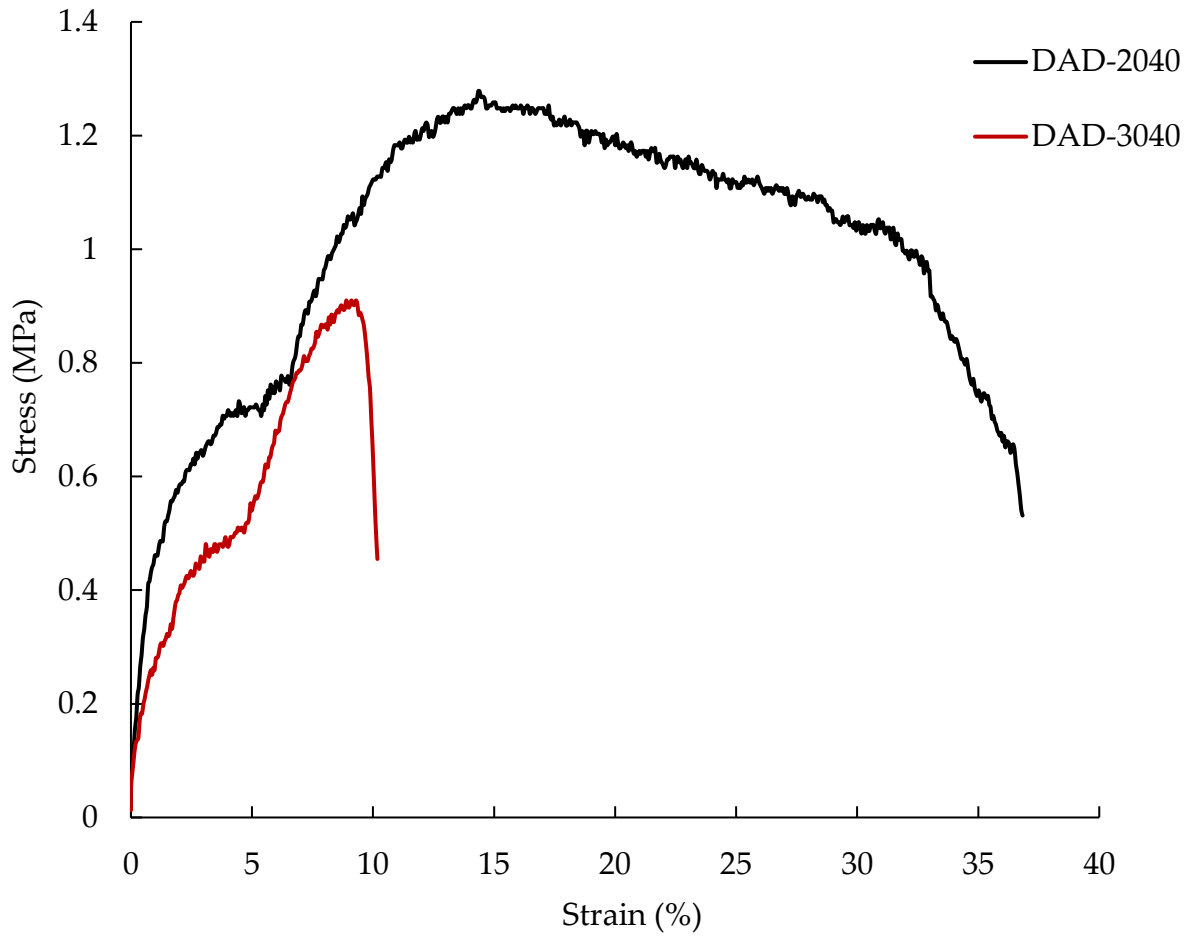


**Figure 6.8 - Tensile test results of the semi-crystalline DAD-2040 and DAD-3040 showing the stretching of the amorphous phase first followed by the crystalline phase before yielding and breaking.**

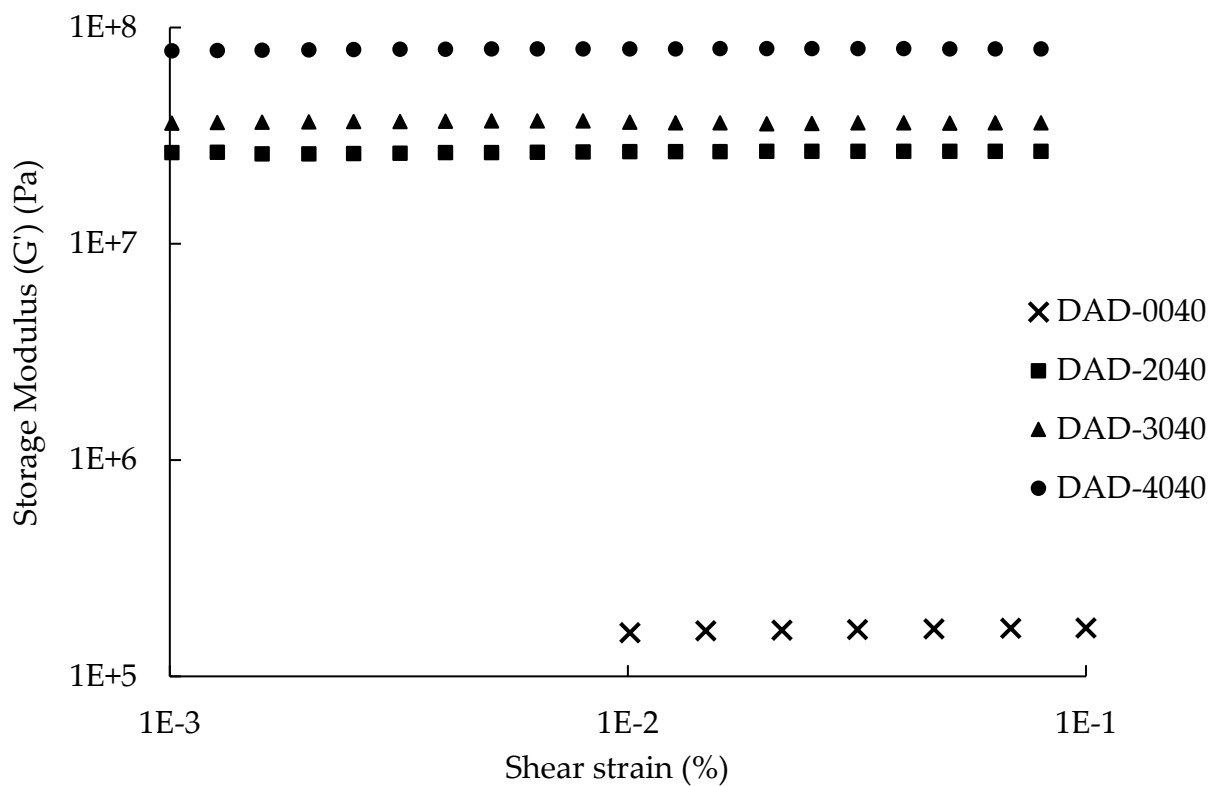


**Figure 6.9 - Storage modulus of the DAD-based TPHUs collected from amplitude sweeps conducted at 22 °C and a frequency of 10 Hz.**

### 6.4.3 Blends of PLA with bio-based TPHUs

Blending PLA with the following TPHUs; PDMS-0040, PDMS-2040, PDMS-2025, and PDMS-4025, (80/20 wt.%/wt.%) resulted in an increase in PLA flowability and viscous properties, as it was observed from the amplitude sweeps conducted on the samples at room temperature (~22 °C) and the temperature of extrusion (150 °C). Figure D.16 shows that the TPHUs did not affect the storage modulus of PLA while increasing its loss modulus and hence its viscous properties. This is more pronounced when running the amplitude sweeps at 150 °C, at which the flow point of the blends was reached at lower shear strains when compared to PLA (Figure D.17). Frequency sweeps were also conducted on the blends and their components at room temperature (shear strain of 0.01% and 0.1-100 Hz) and 150 °C (shear strain of 5% and 0.1-100 rad/s) to quantify the complex viscosities. The linear mixing rule was used to calculate the complex viscosities of the blends from the components: <sup>63</sup>

$$\eta_{1,2}^* = \phi_1 \eta_1^* + \phi_2 \eta_2^* \quad \text{Eq. (6.5)}$$

where  $\phi_1$  and  $\phi_2$  are the weight ratios of species 1 and 2, respectively, and  $\eta_1^*$  and  $\eta_2^*$  are the viscosities of the two species. Then, the calculated complex viscosities of the blends were compared to the experimental ones, and error differences between 6 and 44% were found, which suggests that the blends are partially miscible, and that is expected based on Lin et al.'s study on blending PLA with hyperbranched poly(ester amide). <sup>63</sup> This partial miscibility was observed from DSC (Table 6.3), which showed two  $T_g$ s for the blends; one for the TPHUs between -9 and -5 °C and a second for PLA between 53 and 58 °C. The component  $T_g$ s of the TPHUs were shifted more significantly with the  $T_g$ s of PDMS-2025 and PDMS-4025 shifting more, and to higher values, because they contain fewer hard segments and hence flow more easily in the PLA matrix during the extrusion process. Nevertheless, the  $T_g$  of PLA did shift to lower values, and

that in blends containing PDMS-0040 and PDMS-4040 only, as observed from the DSC and DMTA (please see Figure D.18 to Figure D.20) results of Table 6.3. This means that PDMS-0040 and PDMS-4040 are potential plasticizers/softeners of PLA, and they hold a structural feature giving them this advantage over their lower hard segment content counterparts.

**Table 6.3 - Thermal transitions of the blends of this study (80/20 wt.%/wt.%)**

Blend	DSC					DMTA <sup>a</sup>	
	T <sub>g,1</sub> <sup>b</sup> (°C)	T <sub>g,2</sub> (°C)	T <sub>m</sub> (°C)	ΔH <sub>m</sub> (J/g)	X <sub>c</sub> <sup>c</sup> (%)	T <sub>g,2</sub> <sup>(G')</sup> (°C)	T <sub>g,2</sub> <sup>(tanδ)</sup> (°C)
PLA only <sup>d</sup>	-	58	152	1.3	1.8	61	65
PLA/PDMS-0040	-9 ± 1.0	53 ± 1.6	150 ± 1.0	3.7 ± 1.4	4.9 ± 1.9	54	58
PLA/PDMS-2040	-8 ± 0.6	54 ± 1.2	-	-	-	51	57
PLA/PDMS-2025	-6 ± 0.5	57 ± 0.4	-	-	-	61	64
PLA/PDMS-4025	-5 ± 1.0	58 ± 1.0	-	-	-	60	63

a. DMTA was only capable of detecting the second T<sub>g</sub> of PLA due to equipment limitations as cooling samples to temperatures below room temperature (22 °C) were not possible.

b. T<sub>g,1</sub> for PLA/PDMS2040 had low intensity with respect to T<sub>g,2</sub> compared to other blends.

c. The crystallinity X<sub>c</sub> was calculated from DSC by dividing ΔH<sub>m</sub> with ΔH<sub>m,100%</sub> = 93.6 J/g of PLA multiplied by the weight fraction of PLA (0.8 in this case for all the blends).<sup>59</sup>

d. The PLA samples was extruded at similar conditions as the blends.

To unveil this structural feature, the FTIR spectra of the TPHUs were examined, and it was found that, in the region of 1650 to 1850 cm<sup>-1</sup>, there exists a distinct carbonyl stretch at 1790 cm<sup>-1</sup> which suggests the presence of cyclic carbonate end-groups in the chains of PDMS-0040 and PDMS-2040 (Figure D.21). This is not surprising as, at 40 wt.% DGC content, the reactions leading to these TPHUs were conducted with excess DGC. The ratios of the C=O stretches of the cyclic carbonates to those of the urethane linkages, R<sub>C=O</sub><sup>TPHU</sup>, were calculated using the

deconvolution method of the peaks, and are summarized in Table 6.4. It is possible that the abundant cyclic carbonate end-groups in PDMS-0040 and PDMS-2040 interact via hydrogen bonding with the hydroxyl end-groups of PLA. This affects the entanglements and the mobility of the PLA chains, which decreases their  $T_g$ . A similar explanation was proposed by Kuan et al., who studied multi-wall carbon nanotube/PLA composites.<sup>75</sup> Therefore, the FTIR spectra of the blends (Figure D.22 and Figure D.23) were also examined to estimate the fraction of carbonyl groups participating in hydrogen bonding,  $f_{C=O}^b$ , in each of the blends. This parameter was found from the equation below:

$$f_{C=O}^b = \frac{A_b/1.5}{\frac{A_b}{1.5} + A_f} \quad \text{Eq. (6.6)}$$

where  $A_f$  and  $A_b$  are peak areas corresponding to the free and hydrogen bonded carbonyl groups, respectively, calculated using the relative areas of the C=O stretches of PLA and the TPHUs with other distinct peaks in their structure. The deconvolution method would have been better for the purpose of these calculations, but the C=O of the urethane linkages overlapped with the rest of the carbonyl stretches, which made the deconvolution of the peaks difficult to be applied. The conversion coefficient 1.5 is the ratio of these two bands in an ester group.<sup>63</sup> The values of  $f_{C=O}^b$  are summarized in Table 6.4, and they were found to be significantly lower than those calculated in a previous study by Lin et al. (37%) on poly(ester amide)/PLA systems because these authors had more sites in their hyperbranched poly(ester amide) available for hydrogen bonding.<sup>63</sup> Indeed, the hydrogen bonding effects of the blends studied here are diluted by the structure of the soft segments used to synthesize the TPHUs.  $f_{C=O}^b$  was almost the same for all the blends except of PLA/PDMS-2025, in which the fraction of hydrogen bonded C=O is approximately half the values of the other blends. PLA/PDMS-4025 had a similar  $f_{C=O}^b$  to the PLA/PDMS-0040 and

PLA/PDMS-2040, containing TPHUs with abundant carbonate end-groups, because there exist other sites in a TPHU that can undergo hydrogen bonding with PLA, such as the NH groups of the urethane linkage and the hydroxyl groups that can interact with the carbonyl groups of PLA. The hydrogen bonding interactions were verified from FTIR by the broadening of the C=O stretch of PLA (Figure D.22) as well as the formation of a broad OH band in the 3000 to 3500  $\text{cm}^{-1}$  region (Figure D.23).

One of the main purposes of blending PLA with other additives is to increase its toughness or associated property such as impact strength; hence, the mechanical properties of the blends were measured, and they are presented in Table 6.4 and Figure 6.10. Note that the mechanical properties obtained for PLA were akin to a previous study that used a similar method for preparing the films analyzed herein.<sup>64</sup> The Young's modulus ( $E$ ) and the tensile strength ( $\sigma_{\text{max}}$ ) were not affected by the addition of the TPHUs into the PLA matrix, which confirms the amplitude sweep results discussed in the beginning of this section. Only PLA/PDMS-2040 showed a drop in  $E$  with no tensile strength, maybe due to the type of hydrogen bonding interactions occurring in this blend (discussed in the sub-section above). However, only two blends showed an increase in the toughness of PLA; PLA/PDMS-2040 and PLA/PDMS-4025, whereas the films of the other two blends broke at low elongations at break (EB%) of 40 and 60%. This suggests that some of these blends might be immiscible, so the relative energy differences (RED) of the blends were calculated (Table 6.4) using the solubility parameters estimated from the group contribution method conducted earlier (please see Table D.4 and Table D.5). An RED value less than 1 is desired for the blends to be considered miscible,<sup>76</sup> so since the RED values of the blends are around 1, it means that they are partially miscible as it was previously deduced. PLA/PDMS-0040 has the highest value of 1.2, which explains its low EB%.

PLA/PDMS-2025 has an RED at the limit of phase miscibility, and since it has the lowest  $f_{c=0}^b$ , it does not have the necessary interfacial strength, leading to the lowest EB%. The remaining two blends have the highest  $f_{c=0}^b$ , and their REDs are at the limit of phase miscibility, so they ended up slightly increasing the toughness of PLA by increasing the EB% to 300%. We expected the blending to be aided by the functional groups on the PLA and the TPHU, which could have provided the interactions needed to compatibilize the blends.

**Table 6.4 - Structural, mechanical, and miscibility properties of the blends of this study (80/20 wt.%/wt.%)**

<b>Blend</b>	$R_{C=O}^{TPHU}$	$f_{c=0}^b$ (%)	<b>E (MPa)</b>	$\sigma_{max}$ (MPa)	<b>EB (%)</b>	<b>RED<sup>a</sup></b>
<b>PLA only</b>	-	-	2.22 ± 0.32	9.50 ± 1.23	262 ± 39	-
<b>PLA/PDMS-0040</b>	0.42	8.2	2.75 ± 0.45	10.1 ± 1.00	61 ± 22	1.2
<b>PLA/PDMS-2040</b>	0.50	9.7	1.16 ± 0.09	-	305 ± 55	1.0
<b>PLA/PDMS-2025</b>	0.28	4.2	2.64 ± 0.21	11.9 ± 1.62	39 ± 9.3	1.0
<b>PLA/PDMS-4025</b>	0.06	9.6	3.09 ± 0.38	11.9 ± 1.85	297 ± 49	0.88

a. Please refer to Appendix D for more information on how to obtain the RED of the blends.

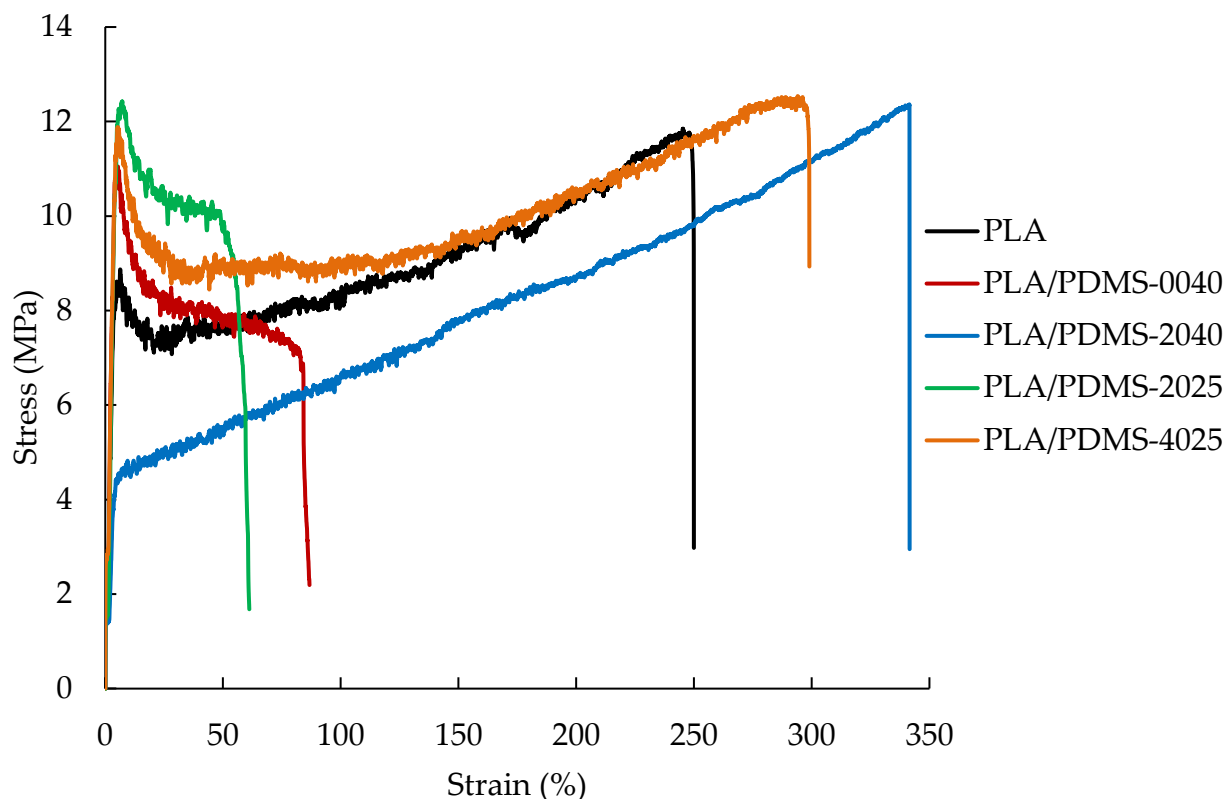


**Figure 6.10 - Stress-strain curves of the PLA/TPHU blends of this study (80/20 wt.%/wt.%).**

Finally, the blend morphologies were examined through SEM, and Figure 6.11 presents the SEM of their cryogenically fractured surfaces, untreated and treated with THF (to selectively remove one component from the other). It is seen from the SEM of the untreated surfaces that the TPUs with higher DGC content are more compatible with PLA. A similar observation was made elsewhere where the authors blended PLA with TPUs of different solid contents, and the higher solid content TPUs showed a finer phase morphology in PLA.<sup>60</sup> The TPUs droplets that got pulled out from PLA/PDMS-2025 and PLA/PDMS-4025 were slightly bigger and outnumber the ones resulting from cryo-fracturing of PLA/PDMS-0040 and PLA/PDMS-2040. Actually, all of the blends were already found to be partially miscible, and PDMS-0040 and PDMS-2040

were previously stated as being more rigid and exhibiting hydrogen bonding with PLA via end-chain interactions. However, these droplets can be misleading, as they can also result from artifacts of the fracturing process; hence, we treated the surfaces with THF to remove the TPBU phase and get more accurate information about the morphology of the blends. Interestingly, the SEM of PLA/PDMS-0040 and PLA/PDMS-2040 had better defined sphere-shaped dispersion of the TPBUs in the PLA matrix, whereas the remaining blends had TPBUs of lower hard segments forming a co-continuous-like phase with PLA. The hard segment content of the TPBUs plays a major role in forming these phases, as PDMS-0040 and PDMS-2040 are more rigid and can better disperse in the PLA matrix at the extrusion temperature of 150 °C. On the other hand, PDMS-2025 and PDMS-4025 are softer, as previously discussed from Figure 6.3, so they tend to flow more at 150 °C, and end up forming bigger droplets that coalesce, which results in co-continuous-like phases of PLA and these TPBUs.

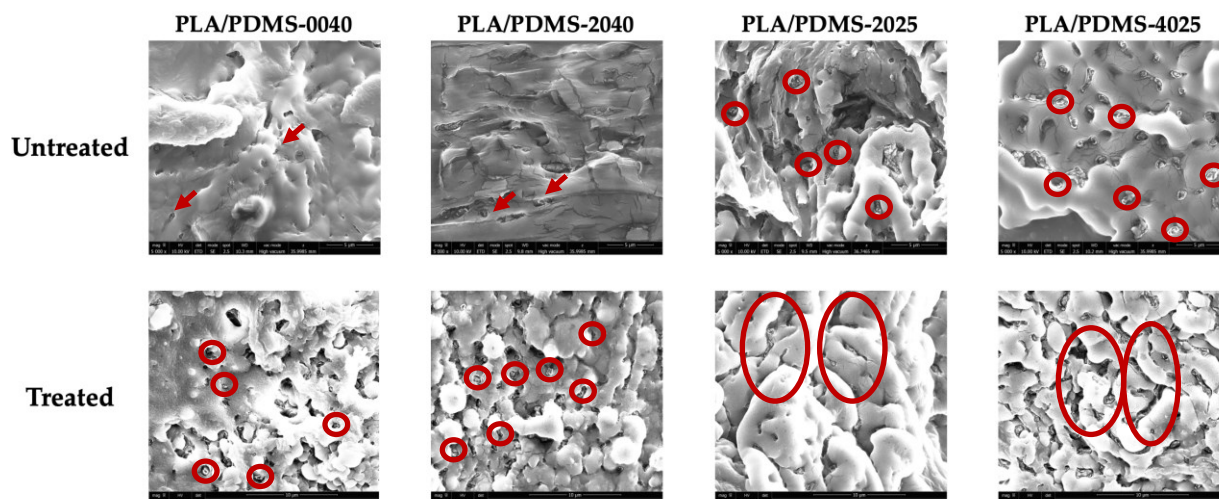


**Figure 6.11 - SEM of cryogenically fractured surfaces of PLA/TPHUs blends (80/20 wt.%/wt.%) untreated and treated with THF to remove the TPHUs phase solely (5000× magnification).**

## 6.5 Conclusion

Terpolymerizations based on DGC and Priamine 1074 were conducted by blending Priamine 1074 with PDMS-1k-(NH<sub>2</sub>)<sub>2</sub> or DAD at different ratios and with different hard segment (DGC) contents. The PDMS-based TPHUs with higher DGC content (40 wt.%) presented a block copolymer-like segmented structure and two T<sub>g</sub>s. The remaining TPHUs of lower DGC content (25 wt.%) showed an increase in thermal stability resulting from the alternation of soft segments in the TPHU structure. Additionally, Priamine 1074 and PDMS-1k-(NH<sub>2</sub>)<sub>2</sub> soft segments were fairly miscible in the TPHU microstructure, based on the Hoftyzer-Van Krevelen's group contribution method used to estimate the Hansen solubility parameters, with nanophase separation caused mainly by the presence of DGC. The rheology of these TPHUs revealed that the PDMS-based TPHUs of higher hard segment content had higher storage modulus than their lower hard segment content analogs. As well, the presence of DGC was obvious from dynamic

frequency sweeps and time-temperature superpositions, in which an additional relaxation, caused by the melting of the DGC linkages in the TPHUs at  $\sim 65$  °C, was present.

The addition of DAD into Priamine 1074, during the terpolymerization, led to a new class of fully bio-based semi-crystalline TPHUs with crystallinity fractions of about 8%. The presence of DAD introducing crystallinity was observed in the evidence of microstructural ordering of the TPHUs, as revealed by SAXS. Being a shorter diamine, DAD acted as a chain extender during the synthesis of DAD-4040, and added the rigidity needed to the DGC/Priamine 1074 matrix with the storage modulus significantly increasing with the DAD content.

At last, the blends of PLA with some of the PDMS-based TPHUs were prepared. The blends were found to be partially miscible based on different characterization techniques: rheology, DSC, Hoftzyer-Van Krevelen's group contribution method to estimate relative energy differences (RED) between PLA and the TPHUs, and SEM. PDMS-0040 and PDMS-2040 acted as plasticizers of PLA, and this is due to the type of hydrogen bonding interactions exhibited by the TPHUs/PLA systems; through the end-chain carbonate of the TPHU and hydroxyl groups of the PLA, respectively. The tensile properties of the blends revealed that PDMS-2040 and PDMS-4025 increased the toughness of PLA and that is based on different factors; highest amount of hydrogen bonding ( $f_{c=O}^b$ ) and lowest RED. The SEM presented a co-continuous morphology of the blends of PLA with the lower hard segment TPHUs, compared to a dispersed phase of the higher hard segment analogs in the PLA matrix, and that was related to the softer character of the former and their tendency of mixing better with PLA during the extrusion process.

To our knowledge, this study is the first to prepare PHUs from terpolymerizations and to investigate their rheology and blending with PLA. Our study can be used as a stepping point to

synthesize new families of fully/partially bio-based TPHUs and blend them with bio-based polymers like PLA.

## 6.6 References

1. Kathalewar, M. S.; Joshi, P. B.; Sabnis, A. S.; Malshe, V. C. Non-isocyanate polyurethanes: from chemistry to applications. *RSC Adv.* **2013**, *3*, 4110-4129.
2. Cornille, A.; Auvergne, R.; Figovsky, O.; Boutevin, B.; Caillol, S. A perspective approach to sustainable routes for non-isocyanate polyurethanes. *Eur. Polym. J.* **2017**, *87*, 535-552.
3. Kreye, O.; Mutlu, H.; Meier, M. A. R. Sustainable routes to polyurethane precursors. *Green Chem.* **2013**, *15*, 1431-1455.
4. Nohra, B.; Candy, L.; Blanco, J. F.; Guerin, C.; Raoul, Y.; Mouloungui, Z. From Petrochemical Polyurethanes to Biobased Polyhydroxyurethanes. *Macromolecules* **2013**, *46*, 3771-3792.
5. Błażek, K.; Datta, J. Renewable natural resources as green alternative substrates to obtain bio-based non-isocyanate polyurethanes-review. *Crit. Rev. Environ. Sci. Technol.* **2019**, *49*, 173-211.
6. Carre, C.; Ecochard, Y.; Caillol, S.; Averous, L. From the Synthesis of Biobased Cyclic Carbonate to Polyhydroxyurethanes: A Promising Route towards Renewable Non-Isocyanate Polyurethanes. *ChemSusChem* **2019**, *12*, 3410-3430.
7. Ghasemlou, M.; Daver, F.; Ivanova, E. P.; Adhikari, B. Bio-based routes to synthesize cyclic carbonates and polyamines precursors of non-isocyanate polyurethanes: A review. *Eur. Polym. J.* **2019**, *118*, 668-684.

8. Bobbink, F. D.; van Muyden, A. P.; Dyson, P. J. En route to CO<sub>2</sub>-containing renewable materials: catalytic synthesis of polycarbonates and non-isocyanate polyhydroxyurethanes derived from cyclic carbonates. *Chem. Commun.* **2019**, *55*, 1360-1373.
9. Meier, M. A. R. Plant-Oil-Based Polyamides and Polyurethanes: Toward Sustainable Nitrogen-Containing Thermoplastic Materials. *Macromol. Rapid Commun.* **2019**, *40*, 1800524.
10. Błażek, K.; Kasprzyk, P.; Datta, J. Diamine derivatives of dimerized fatty acids and bio-based polyether polyol as sustainable platforms for the synthesis of non-isocyanate polyurethanes. *Polymer* **2020**, *205*, 122768.
11. Froidevaux, V.; Negrell, C.; Caillol, S.; Pascault, J. P.; Boutevin, B. Biobased Amines: From Synthesis to Polymers; Present and Future. *Chem. Rev.* **2016**, *116*, 14181-14224.
12. Anastas, P.; Eghbali, N. Green chemistry: principles and practice. *Chem. Soc. Rev.* **2010**, *39*, 301-312.
13. Tryznowski, M.; Swiderska, A.; Zolek-Tryznowska, Z.; Golofit, T.; Parzuchowski, P. G. Facile route to multigram synthesis of environmentally friendly non-isocyanate polyurethanes. *Polymer* **2015**, *80*, 228-236.
14. van Velthoven, J. L. J.; Gootjes, L.; van Es, D. S.; Noordover, B. A. J.; Meuldijk, J. Poly(hydroxy urethane)s based on renewable diglycerol dicarbonate. *Eur. Polym. J.* **2015**, *70*, 125-135.
15. Bossion, A.; Aguirresarobe, R. H.; Irusta, L.; Taton, D.; Cramail, H.; Grau, E.; Mecerreyes, D.; Su, C.; Liu, G. M.; Muller, A. J.; Sardon, H. Unexpected Synthesis of Segmented Poly(hydroxyurea-urethane)s from Dicyclic Carbonates and Diamines by Organocatalysis. *Macromolecules* **2018**, *51*, 5556-5566.

16. Tryznowski, M.; Swiderska, A. Novel high reactive bifunctional five- and six-membered bicyclic dicarbonate - synthesis and characterisation. *RSC Adv.* **2018**, *8*, 11749-11753.
17. Bossion, A.; Olazabal, I.; Aguirresarobe, R. H.; Marina, S.; Martín, J.; Irusta, L.; Taton, D.; Sardon, H. Synthesis of self-healable waterborne isocyanate-free poly(hydroxyurethane)-based supramolecular networks by ionic interactions. *Polym. Chem.* **2019**, *10*, 2723-2733.
18. Magliozzi, F.; Chollet, G.; Grau, E.; Cramail, H. Benefit of the Reactive Extrusion in the Course of Polyhydroxyurethanes Synthesis by Aminolysis of Cyclic Carbonates. *ACS Sustainable Chem. Eng.* **2019**, *7*, 17282-17292.
19. Peixoto, C.; Soares, A. M. S.; Araujo, A.; Olsen, B. D.; Machado, A. V. Non-isocyanate urethane linkage formation using l-lysine residues as amine sources. *Amino Acids* **2019**, *51*, 1323-1335.
20. Magliozzi, F.; Scali, A.; Chollet, G.; Montarnal, D.; Grau, E.; Cramail, H. Hydrolyzable Biobased Polyhydroxyurethane Networks with Shape Memory Behavior at Body Temperature. *ACS Sustainable Chem. Eng.* **2020**, *8*, 9125-9135.
21. Wang, D.; Chen, S.; Zhao, J.; Zhang, Z. Synthesis and characterization of self-healing cross-linked non-isocyanate polyurethanes based on Diels-Alder reaction with unsaturated polyester. *Mater. Today Commun.* **2020**, *23*, 101138.
22. Younes, G. R.; Price, G.; Dandurand, Y.; Maric, M. Study of Moisture-Curable Hybrid NIPUs Based on Glycerol with Various Diamines: Emergent Advantages of PDMS Diamines. *ACS Omega* **2020**, *5*, 30657-30670.
23. Zhang, C.; Wang, H.; Zhou, Q. Waterborne isocyanate-free polyurethane epoxy hybrid coatings synthesized from sustainable fatty acid diamine. *Green Chem.* **2020**, *22*, 1329-1337.

24. Pronoitis, C.; Hakkarainen, M.; Odelius, K. Solubility-governed architectural design of polyhydroxyurethane-graft-poly( $\epsilon$ -caprolactone) copolymers. *Polym. Chem.* **2021**, *12*, 196-208.
25. Younes, G. R.; Maric, M. Increasing the Hydrophobicity of Hybrid Poly(propylene glycol)-Based Polyhydroxyurethanes by Capping with Hydrophobic Diamine. *Ind. Eng. Chem. Res.* **2021**, *60*, 8159-8171.
26. Christoph, R.; Schmidt, B.; Steinberner, U.; Dilla, W.; Karinen, R. Glycerol. *Ullmann's Encycl. Ind. Chem.* **2006**, *17*, 67-82.
27. Schmidt, S.; Gatti, F. J.; Luitz, M.; Ritter, B. S.; Bruchmann, B.; Mulhaupt, R. Erythritol Dicarboxylate as Intermediate for Solvent- and Isocyanate-Free Tailoring of Bio-Based Polyhydroxyurethane Thermoplastics and Thermoplastic Elastomers. *Macromolecules* **2017**, *50*, 2296-2303.
28. Poussard, L.; Mariage, J.; Grignard, B.; Detrembleur, C.; Jérôme, C.; Calberg, C.; Heinrichs, B.; De Winter, J.; Gerbaux, P.; Raquez, J. M.; Bonnaud, L.; Dubois, P. Non-Isocyanate Polyurethanes from Carbonated Soybean Oil Using Monomeric or Oligomeric Diamines To Achieve Thermosets or Thermoplastics. *Macromolecules* **2016**, *49*, 2162-2171.
29. Carre, C.; Bonnet, L.; Averous, L. Solvent- and catalyst-free synthesis of fully biobased nonisocyanate polyurethanes with different macromolecular architectures. *RSC Adv.* **2015**, *5*, 100390-100400.
30. Menard, R.; Caillol, S.; Allais, F. Chemo-Enzymatic Synthesis and Characterization of Renewable Thermoplastic and Thermoset Isocyanate-Free Poly(hydroxy)urethanes from Ferulic Acid Derivatives. *ACS Sustainable Chem. Eng.* **2017**, *5*, 1446-1456.

31. Maisonneuve, L.; More, A. S.; Foltran, S.; Alfos, C.; Robert, F.; Landais, Y.; Tassaing, T.; Grau, E.; Cramail, H. Novel green fatty acid-based bis-cyclic carbonates for the synthesis of isocyanate-free poly(hydroxyurethane amide)s. *RSC Adv.* **2014**, *4*, 25795-25803.
32. Lamarzelle, O.; Hibert, G.; Lecommandoux, S.; Grau, E.; Cramail, H. A thioglycerol route to bio-based bis-cyclic carbonates: poly(hydroxyurethane) preparation and post-functionalization. *Polym. Chem.* **2017**, *8*, 3438-3447.
33. Duval, C.; Kebir, N.; Charvet, A.; Martin, A.; Burel, F. Synthesis and Properties of Renewable Nonisocyanate Polyurethanes (NIPUs) from Dimethylcarbonate. *J. Polym. Sci., Part A: Polym. Chem.* **2015**, *53*, 1351-1359.
34. Carré, C.; Zoccheddu, H.; Delalande, S.; Pichon, P.; Avérous, L. Synthesis and characterization of advanced biobased thermoplastic nonisocyanate polyurethanes, with controlled aromatic-aliphatic architectures. *Eur. Polym. J.* **2016**, *84*, 759-769.
35. Schmidt, S.; Goppert, N. E.; Bruchmann, B.; Mulhaupt, R. Liquid sorbitol ether carbonate as intermediate for rigid and segmented non-isocyanate polyhydroxyurethane thermosets. *Eur. Polym. J.* **2017**, *94*, 136-142.
36. Schimpf, V.; Ritter, B. S.; Weis, P.; Parison, K.; Mulhaupt, R. High Purity Limonene Dicarboxylate as Versatile Building Block for Sustainable Non-Isocyanate Polyhydroxyurethane Thermosets and Thermoplastics. *Macromolecules* **2017**, *50*, 944-955.
37. Rueda-Larraz, L.; d'Arlas, B. F.; Tercjak, A.; Ribes, A.; Mondragon, I.; Eceiza, A. Synthesis and microstructure–mechanical property relationships of segmented polyurethanes based on a PCL–PTHF–PCL block copolymer as soft segment. *Eur. Polym. J.* **2009**, *45*, 2096-2109.

38. Sánchez-Adsuar, M.; Papon, E.; Villenave, J.-J. Rheological characterization of thermoplastic polyurethane elastomers. *Polym. Int.* **2000**, *49*, 591-598.
39. Heydarnezhad, H. R.; Mohammadi, N.; Arbe, A.; Alegria, A. How Does Microstructural Design Affect the Dynamics and Rheology of Segmented Polyurethanes?. *Macromolecules* **2020**, *53*, 5381-5398.
40. Velankar, S.; Cooper, S. L. Microphase Separation and Rheological Properties of Polyurethane Melts. 3. Effect of Block Incompatibility on the Viscoelastic Properties. *Macromolecules* **2000**, *33*, 395-403.
41. Velankar, S.; Cooper, S. L. Microphase Separation and Rheological Properties of Polyurethane Melts. 1. Effect of Block Length. *Macromolecules* **1998**, *31*, 9181-9192.
42. Arun, A.; Baack, K. K. J.; Gaymans, R. J. Polyurethane tri-block copolymers-Synthesis, mechanical, elastic, and rheological properties. *Polym. Eng. Sci.* **2010**, *50*, 747-755.
43. Mourier, E.; David, L.; Alcouffe, P.; Rochas, C.; Méchin, F.; Fulchiron, R. Composition effects of thermoplastic segmented polyurethanes on their nanostructuring kinetics with or without preshear. *J. Polym. Sci., Part B: Polym. Phys.* **2011**, *49*, 801-811.
44. Beniah, G.; Chen, X.; Uno, B. E.; Liu, K.; Leitsch, E. K.; Jeon, J.; Heath, W. H.; Scheidt, K. A.; Torkelson, J. M. Combined Effects of Carbonate and Soft-Segment Molecular Structures on the Nanophase Separation and Properties of Segmented Polyhydroxyurethane. *Macromolecules* **2017**, *50*, 3193-3203.
45. Beniah, G.; Fortman, D. J.; Heath, W. H.; Dichtel, W. R.; Torkelson, J. M. Non-Isocyanate Polyurethane Thermoplastic Elastomer: Amide-Based Chain Extender Yields Enhanced Nanophase Separation and Properties in Polyhydroxyurethane. *Macromolecules* **2017**, *50*, 4425-4434.

46. Beniah, G.; Heath, W. H.; Jeon, J.; Torkelson, J. M. Tuning the properties of segmented polyhydroxyurethanes via chain extender structure. *J. Appl. Polym. Sci.* **2017**, *134*, 44942.
47. Beniah, G.; Heath, W. H.; Torkelson, J. M. Functionalization of hydroxyl groups in segmented polyhydroxyurethane eliminates nanophase separation. *J. Polym. Sci., Part A: Polym. Chem.* **2017**, *55*, 3347-3351.
48. Beniah, G.; Uno, B. E.; Lan, T.; Jeon, J.; Heath, W. H.; Scheidt, K. A.; Torkelson, J. M. Tuning nanophase separation behavior in segmented polyhydroxyurethane via judicious choice of soft segment. *Polymer* **2017**, *110*, 218-227.
49. Leitsch, E. K.; Beniah, G.; Liu, K.; Lan, T.; Heath, W. H.; Scheidt, K. A.; Torkelson, J. M. Nonisocyanate Thermoplastic Polyhydroxyurethane Elastomers via Cyclic Carbonate Aminolysis: Critical Role of Hydroxyl Groups in Controlling Nanophase Separation. *ACS Macro Lett.* **2016**, *5*, 424-429.
50. Chen, H.; Yu, X.; Zhou, W.; Peng, S.; Zhao, X. Highly toughened polylactide (PLA) by reactive blending with novel polycaprolactone-based polyurethane (PCLU) blends. *Polym. Test.* **2018**, *70*, 275-280.
51. Feng, F.; Ye, L. Morphologies and mechanical properties of polylactide/thermoplastic polyurethane elastomer blends. *J. Appl. Polym. Sci.* **2011**, *119*, 2778-2783.
52. Feng, L.; Bian, X.; Li, G.; Chen, Z.; Chen, X. Compatibility, mechanical properties and stability of blends of polylactide and polyurethane based on poly(ethylene glycol)-b-polylactide copolymers by chain extension with diisocyanate. *Polym. Degrad. Stab.* **2016**, *125*, 148-155.
53. Han, J.-J.; Huang, H.-X. Preparation and characterization of biodegradable polylactide/thermoplastic polyurethane elastomer blends. *J. Appl. Polym. Sci.* **2011**, *120*, 3217-3223.

54. Jašo, V.; Cvetinov, M.; Rakić, S.; Petrović, Z. S. Bio-plastics and elastomers from polylactic acid/thermoplastic polyurethane blends. *J. Appl. Polym. Sci.* **2014**, *131*, 41104.
55. Liu, T.; Huang, R.; Qi, X.; Dong, P.; Fu, Q. Facile preparation of rapidly electro-active shape memory thermoplastic polyurethane/polylactide blends via phase morphology control and incorporation of conductive fillers. *Polymer* **2017**, *114*, 28-35.
56. Mo, X.-Z.; Wei, F.-X.; Tan, D.-F.; Pang, J.-Y.; Lan, C.-B. The compatibilization of PLA-g-TPU graft copolymer on polylactide/thermoplastic polyurethane blends. *J. Polym. Res.* **2020**, *27*, 33.
57. Zhang, L.; Xiong, Z.; Shams, S. S.; Yu, R.; Huang, J.; Zhang, R.; Zhu, J. Free radical competitions in polylactide/bio-based thermoplastic polyurethane/ free radical initiator ternary blends and their final properties. *Polymer* **2015**, *64*, 69-75.
58. Suthapakti, K.; Molloy, R.; Punyodom, W.; Nalampang, K.; Leejarkpai, T.; Topham, P. D.; Tighe, B. J. Biodegradable Compatibilized Poly(l-lactide)/Thermoplastic Polyurethane Blends: Design, Preparation and Property Testing. *J. Polym. Environ.* **2017**, *26*, 1818-1830.
59. Kahraman, Y.; Özdemir, B.; Kılıç, V.; Goksu, Y. A.; Nofar, M. Super toughened and highly ductile PLA/TPU blend systems by in situ reactive interfacial compatibilization using multifunctional epoxy-based chain extender. *J. Appl. Polym. Sci.* **2021**, *138*, 50457.
60. Nofar, M.; Mohammadi, M.; Carreau, P. J. Effect of TPU hard segment content on the rheological and mechanical properties of PLA/TPU blends. *J. Appl. Polym. Sci.* **2020**, *137*, 49387.
61. Dogan, S. K.; Reyes, E. A.; Rastogi, S.; Ozkoc, G. Reactive compatibilization of PLA/TPU blends with a diisocyanate. *J. Appl. Polym. Sci.* **2014**, *131*, 40251.

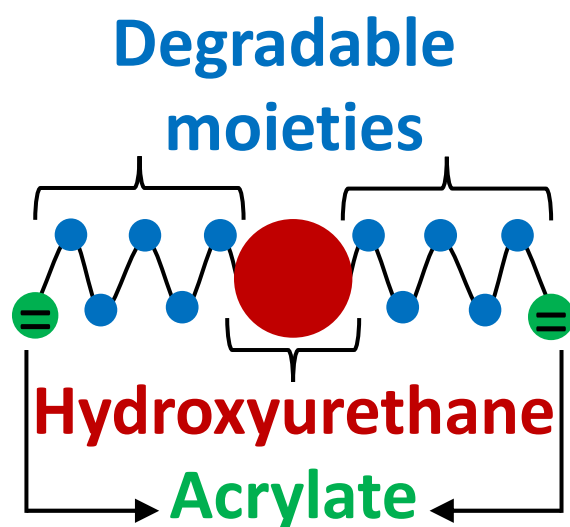
62. Kratochvíl, J.; Kelnar, I. Non-isothermal kinetics of cold crystallization in multicomponent PLA/thermoplastic polyurethane/nanofiller system. *J. Therm. Anal. Calorim.* **2017**, *130*, 1043-1052.
63. Lin, Y.; Zhang, K.-Y.; Dong, Z.-M.; Dong, L.-S.; Li, Y.-S. Study of Hydrogen-Bonded Blend of Polylactide with Biodegradable Hyperbranched Poly(ester amide). *Macromolecules* **2007**, *40*, 6257-6267.
64. Yang, X.; Hakkarainen, M. Migration resistant glucose esters as bioplasticizers for polylactide. *J. Appl. Polym. Sci.* **2015**, *132*, 41928.
65. Casalini, T.; Rossi, F.; Castrovinci, A.; Perale, G. A Perspective on Polylactic Acid-Based Polymers Use for Nanoparticles Synthesis and Applications. *Front. Bioeng. Biotechnol.* **2019**, *7*, 259.
66. Van Krevelen, D. W.; Te Nijenhuis, K., Cohesive Properties and Solubility. In *Properties of Polymers*, Fourth ed.; Elsevier: New York, 2009; pp 189-227.
67. Ashworth, A. J.; Price, G. J. Comparison of Static with Gas Chromatographic Interaction Parameters and Estimation of the Solubility Parameter for Poly(dimethylsiloxane). *Macromolecules* **1986**, *19*, 362-363.
68. Elif Hamurcu, E.; Baysal, B. M. Solubility Parameter of a Poly (dimethylsiloxane) Network. *J. Polym. Sci., Part B: Polym. Phys.* **1994**, *32*, 591-594.
69. Younes, G. R.; Maric, M. Moisture Curable Hybrid Polyhydroxyurethanes from Sugar-Derived Dicarbonates. *Macromol. Mater. Eng.* **2021**, *306*, 2000715.
70. Hernandez, R.; Weksler, J.; Padsalgikar, A.; Runt, J. Microstructural Organization of Three-Phase Polydimethylsiloxane-Based Segmented Polyurethanes. *Macromolecules* **2007**, *40*, 5441-5449.

71. Macosko, C. W., Linear Viscoelasticity. In *Rheology Principles, Measurements and Applications*, VCH-Wiley: New York, 1994; pp 109-133.
72. Rudin, A.; Choi, P., *The Elements of Polymer Science & Engineering*. Third ed.; Academic Press: Oxford, United Kingdom, 2013.
73. Hamley, I.; Castelletto, V., Small-Angle Scattering of Block Copolymers. In *Soft Matter Characterization*; R., B., R., P., Eds. Springer: New York, 2008; Vol. 725, pp 1021-1081.
74. Shi, R.; Jiang, S.; Cheng, H.; Wu, P.; Zhang, C.; Arai, M.; Zhao, F. Synthesis of Polyurea Thermoplastics through a Nonisocyanate Route Using CO<sub>2</sub> and Aliphatic Diamines. *ACS Sustainable Chem. Eng.* **2020**, *8*, 18626-18635.
75. Kuan, C.-F.; Kuan, H.-C.; Ma, C.-C. M.; Chen, C.-H. Mechanical and electrical properties of multi-wall carbon nanotube/poly(lactic acid) composites. *J. Phys. Chem. Solids* **2008**, *69*, 1395-1398.
76. Stefanis, E.; Panayiotou, C. Prediction of Hansen Solubility Parameters with a New Group-Contribution Method. *Int. J. Thermophys.* **2008**, *29*, 568-585.

## Chapter 7

### Bio-based and hydrolytically degradable hydroxyurethane acrylates as photocurable thermosets

This chapter is the last of the experimental results provided in this thesis. It also represents the second new area risen from the PHU studies, and it got published in *Journal of Applied Polymer Science* end of 2021 (Younes, G. R.; Maric, M., Bio-based and Hydrolytically Degradable Hydroxyurethane Acrylates as Photocurable Thermosets. *Journal of Applied Polymer Science* **2021**, 52044).<sup>223</sup> This manuscript presents the step-wise synthesis of hydrolytically degradable photocurable films from bio-based hydroxyurethane acrylates (HUA), and hence is the first in making such materials comparable to previous studies on HUAs and hydroxyurethane methacrylates (HUMA). The photocured films and their degradation, through accelerated hydrolysis, are also carefully examined. The supporting information of this chapter is provided in Appendix E.



## 7.1 Abstract

This study focuses on the synthesis of bio-based and hydrolytically degradable photocurable thermosets made from hydroxyurethane acrylates (HUA). The hydroxyurethanes (HUs) are prepared from the reaction between ethylene carbonate and a bio-based diamine, Priamine 1074. Subsequently, the HU initiates the ring opening polymerization of  $\epsilon$ -caprolactone (CL), resulting in telechelic groups of 5 CL units at both ends of the HU. The resulting HU-CL<sub>5</sub> is finally acrylated to prepare the degradable HUA (HU-CL<sub>5</sub>-A) with transformations confirmed following each step via proton nuclear magnetic resonance (<sup>1</sup>H-NMR) and Fourier-transform infrared (FTIR) spectroscopies. HU-CL<sub>5</sub>-A is photocured with 4-acryloylmorpholine (ACMO) as a photosensitive reactive diluent. The photocurable thermosets exhibit slight water swelling (swelling index of 46%), as Priamine 1074 and ACMO are hydrophobic and hydrophilic, respectively, leading to the slow and partial degradation of the films in water at 85 °C for 14 days. The cleavage of the CL units from the film networks is proven via <sup>1</sup>H-NMR and FTIR, which demonstrates the main objective of this study in synthesizing photocurable and degradable HUA resins.

## 7.2 Introduction

With the increased awareness of the toxicity of isocyanates in the formulation of conventional polyurethanes (PUs), routes towards preparing non-isocyanate polyurethanes (NIPUs) have been achieved.<sup>1</sup> One interesting route lies in the aminolysis reaction between an amine and a cyclic carbonate group which opens the carbonate ring leading to a urethane group containing a pendent hydroxyl group (-OH), known also as a hydroxyurethane (HU). Hence, linear polyhydroxyurethanes (PHUs) are obtained from the polyaddition reaction between cyclic

dicarbonates and diamines,<sup>1</sup> with the final polymeric product containing primary and secondary -OH which can be post-functionalized. The study by Ochiai et al. successfully acetylated, benzoylated, and silylated the hydroxyl groups of their investigated PHUs, and the functionalized polymers showed a lower glass transition temperature,  $T_g$ , than the original PHU due to a decrease in intermolecular interactions exhibited through hydrogen bonding of the hydroxyl groups.<sup>2</sup> He et al. reacted the hydroxyl groups of their HUs with pyridine to make bifunctional couplers and ATRP initiators, and they used them, alternatively, to grow poly( $\epsilon$ -caprolactone) (PCL) chains,<sup>3</sup> a similar chemistry that was recently studied by Pronoitis et al. in designing their PHU-graft-PCL copolymers.<sup>4</sup>

In contrast, the post-functionalization of the -OH of HUs and PHUs with methacrylic anhydride led to hydroxyurethane methacrylates (HUMA) and PHU methacrylates which were thermally crosslinked<sup>5</sup> or UV-cured.<sup>6</sup> Also, methacrylic and acrylic acids were used to impart vinyl groups into the HU structures which served to make polyurethane acrylate polymers.<sup>7</sup> Michael addition and epoxy/amine reactions led, as well, to UV-curable PHU acrylates and methacrylates from amine-terminated prepolymers,<sup>6, 8, 9</sup> whose formulations were optimized to make coatings with high-end properties, such as good chemical resistance, hardness, flexibility, and impact resistance. Interestingly, the Mülhaupt group made several HUMAs from glycerol carbonate methacrylate, which was prepared from glycidyl methacrylate, and different diamines. The resulting HUMAs were mixed with 4-aryloylmorpholine (ACMO), which is a photosensitive monomer, to obtain photocurable thermosets used in 3D-printing.<sup>10, 11</sup> They even functionalized the -OH in their HUMAs with methacrylic and acetic anhydrides as well as 2-isocyanatoethyl methacrylate to replace them with vinyl groups.<sup>11</sup> These different methods targeted the synthesis of non-toxic photocurable thermosets, and the final HUMA or hydroxyurethane acrylate (HUA)

materials proved to be capable of replacing conventional UV-curable PU (meth)acrylate coatings.

Unlike the previous studies on photocurable HUMAs and HUAs,<sup>10, 11</sup> the objective of this work is to synthesize photocurable films that are hydrolytically degradable and prepared from largely bio-based HUA. This is achieved by, first, reacting Priamine 1074, a bio-derived diamine from dimer fatty acids, with ethylene carbonate (EC) to prepare the HU which is, then, used as a macroinitiator to grow short degradable PCL chains of five  $\epsilon$ -caprolactone (CL) units on average. The resulting HU-CL<sub>5</sub> is acrylated with acryloyl chloride (ACI) to finally obtain the photocurable macromonomer diacrylates, HU-CL<sub>5</sub>-A. However, the photocuring was achieved by diluting the diacrylates with ACMO, similar to Mülhaupt et al.'s studies,<sup>10, 11</sup> to prepare the final biodegradable films which can be used not only as coatings and materials for 3D-printing, like previously reported, but also as patches and films for biomedical applications. The following study is divided into two main parts: a synthesis section focusing mainly on the ring-opening polymerization (ROP) of CL followed by the examination of the final film after degradation and identifying the degradation products.

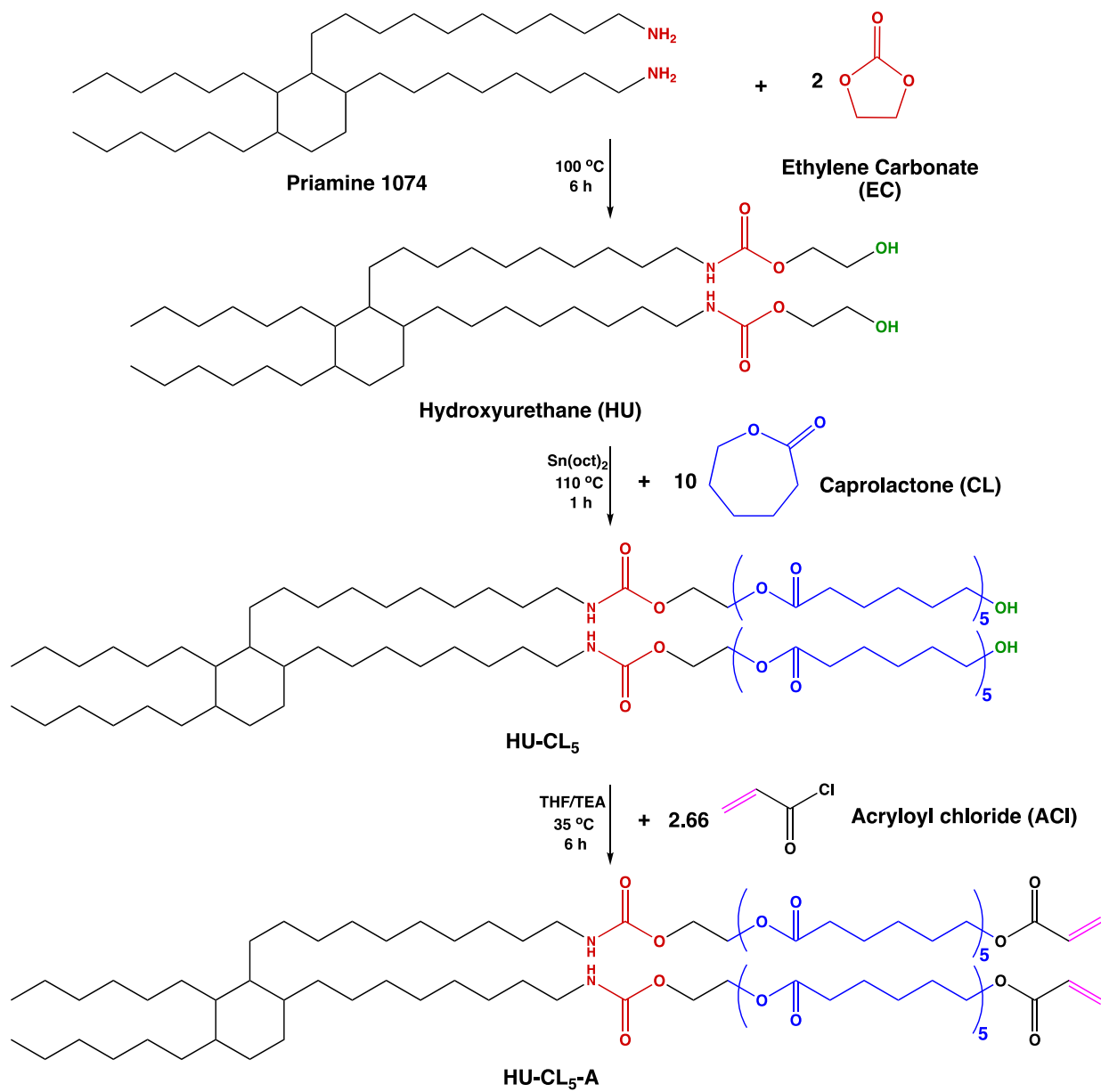
## **7.3 Results and Discussion**

### **7.3.1 Synthesis of HU-CL<sub>5</sub>-A**

Scheme 7.1 summarizes the step-wise synthesis pathway followed to prepare the bio-based and hydrolytically degradable macromonomer diacrylate of this work, HU-CL<sub>5</sub>-A. The first step consists of preparing the HU made from the aminolysis reaction of the bio-based Priamine 1074 and EC. 6 h at 100 °C were enough to achieve the same conversion of monomers as conducting the reaction for 24 h at 100 °C. The conversions of Priamine 1074 and EC were found to be 98%

based on the  $^1\text{H-NMR}$  spectrum presented as Figure E.1 of the Appendix E. Briefly, the peak corresponding to the protons ( $-\text{CH}_2$ ) of EC at 4.50 ppm decreases with two other peaks appearing at 3.75 and 4.15 ppm due to the opening of the cyclic carbonate. As for Priamine 1074, the signal at 2.65 ppm of the protons linked to the primary amine groups decreases, and it is replaced by another one at 3.13 ppm, proving the formation of amide groups in the hydroxyurethanes.

The next step uses the bio-based HU as a macroinitiator to grow short degradable PCL chains of 5 units from both ends. However, this reaction was not necessarily straightforward and the conditions had to be optimized by probing different formulations. Information about the trials is provided in Table 7.1 along with the SEC results of each of the final products obtained. With the initial HU macroinitiator having a number average molecular weight ( $M_n$ ) of  $1,100 \text{ g mol}^{-1}$  and a dispersity ( $D$ ) of 1.1, the final HU-CL<sub>5</sub>-A was expected to have a higher molecular weight, but with a low dispersity ( $\sim 1.2$ ) seeing that the ROPs are generally classified as living polymerizations. Table 7.1 provides insights on optimizing the ROP reaction of this work that is described subsequently.



**Scheme 7.1 - Reaction pathway for the preparation of bio-based and hydrolytically degradable hydroxyurethane acrylates (HUAs)**

**Table 7.1 - Trials of ROP of CL using bio-based HU macroinitiator and SEC results**

<b>Trial</b>	<b>CL:OH:Sn(oct)<sub>2</sub><sup>a</sup></b>	<b>Temperature (°C)</b>	<b>Times (h)</b>	<b>M<sub>n</sub> (g mol<sup>-1</sup>)<sup>b</sup></b>	<b>D = M<sub>w</sub>/M<sub>n</sub><sup>b</sup></b>
<b>1</b>	5:1:1	130	6	3,200	2.6
<b>2</b>	5:1:0.1	130	6	6,100	2.5
<b>3</b>	5:1:0.01	130	6	5,000	2.4
<b>4</b>	5:1:0.01	110	6	2,600	1.6
<b>5</b>	5:1:0.01	110	1	2,800 ± 100 <sup>c</sup>	1.2 ± 0.05 <sup>c</sup>

a. Molar ratio of reactants CL with respect to the hydroxyl groups (-OH) found in the HU structure (total of two -OH/HU) and the added catalyst (Sn(oct)<sub>2</sub>).

b. Number average molecular weight ( $M_n$ ) and dispersities ( $D$ ) were estimated from SEC with THF eluent at 40 °C relative to poly(methyl methacrylate) (PMMA) standards.

c. The reported values are the average of three trials to confirm the reproducibility of trial 5.

Regardless of the catalyst loading, the ROP reactions conducted at 130 °C (trials 1, 2, and 3) led to gelled final products having broad molecular weight distributions (MWDs). At these conditions, CL was consumed in less than 10 min, as found from the conducted kinetic studies during which aliquots were withdrawn to be analyzed using <sup>1</sup>H-NMR. The broadening of the MWD, and hence the increase in  $D$  at high monomer conversions, was also observed in Pronoitis et al.'s work, who grafted PCL chains from their PHU backbone using Sn(oct)<sub>2</sub> as the catalyst.<sup>4</sup> This is attributed to different inter and intramolecular side reactions with the transesterification reactions being prominent during the ROP of lactones and highly dependent on the time, temperature, and type of catalyst used. Indeed, transesterification reactions were identified in Sn(oct)<sub>2</sub> catalyzed ROPs elsewhere,<sup>4, 12-16</sup> and their rates were found to be competitive from the onset of the ROP and to overcome the rates of polymerization at high monomer conversions. Besides, a potential reason for the lower  $M_n$  measured for trial 1 compared to trials 2 and 3, also observed in Pronoitis et al.'s study,<sup>4</sup> is the formation of octanoic acid when Sn(oct)<sub>2</sub>, present in

higher quantities in trial 1, is heated above 100 °C. The acid can undergo an esterification reaction with the hydroxyl groups of the HU which forms water that can eventually hydrolyze the ester groups in the chains causing the observed decrease in  $M_n$  of the final product. Water can also react with  $\text{Sn}(\text{oct})_2$  to form stannoxanes and tin hydroxides that can initiate side polymerizations, making it difficult to control the molecular weight of the oligomers.<sup>16</sup> Therefore, it was necessary to decrease the catalyst loading from 1/5 to 1/500 with respect to CL (trials 1, 2, and 3), then decrease the temperature from 130 to 110 °C (trial 4) followed by the time of reaction from 6 to 1 h (trial 5) to limit the side reactions by tracking the conversion of CL.

The CL and HU conversions in trial 4 were tracked using  $^1\text{H-NMR}$  and plotted in Figure 7.1. Detailed calculations of these parameters are provided in Appendix E (Figure E.2 along with Eq. (E.3) through Eq. (E.6)). Usually in living polymerizations, the initiation step is quick enough to provide all the active species for the chain propagation step to occur. This makes the dependence of  $\ln\left(\frac{1}{1-X}\right)$ , with  $X$  being the monomer conversion, linearly dependent on the time of reaction since the rate of propagation,  $k_p$ , and the concentration of active species,  $[P^*]$ , are constant (Eq. (E.7)).<sup>17</sup> However, Figure 1 shows that the HU macroinitiator is progressively consumed with CL conversion up to 45 min of the start of the reaction, which means that the initiation step was slow and  $[P^*]$  increased with time. Hence,  $\ln\left(\frac{1}{1-X}\right)$  does not linearly depend on time, as shown in Figure E.3. Besides, it was observed from  $^1\text{H-NMR}$  that, after  $t = 60$  min (~90 % CL conversion), side reactions occurred with the peak at 3.65 ppm decreasing from a maximum integral value close to 4 (4 protons), and the difference appearing downfield at 4.27 ppm. This decreasing signal represents the protons attached to the hydroxyl groups of the last CL

unit in HU-CL<sub>5</sub>, proving that the hydroxyl groups engage in side reactions, after t =60 min, which broadens the MWDs of the final products and leads to their gelation, as previously discussed. This point was further verified by conducting the SEC analysis on the aliquots withdrawn during the kinetic study of trial 4 (Figure E.4). Therefore, the reaction time of trial 4 was limited to only 60 min leading to trial 5 whose conditions were confirmed by running the ROP three times. The averaged conversions (%) of CL and HU were found to be  $87 \pm 4$  and  $97 \pm 1$ , respectively, with an expected CL degree of polymerization ( $DP_n$ ) or number of CL units/ per OH equal to  $4.7 \pm 0.3$ .

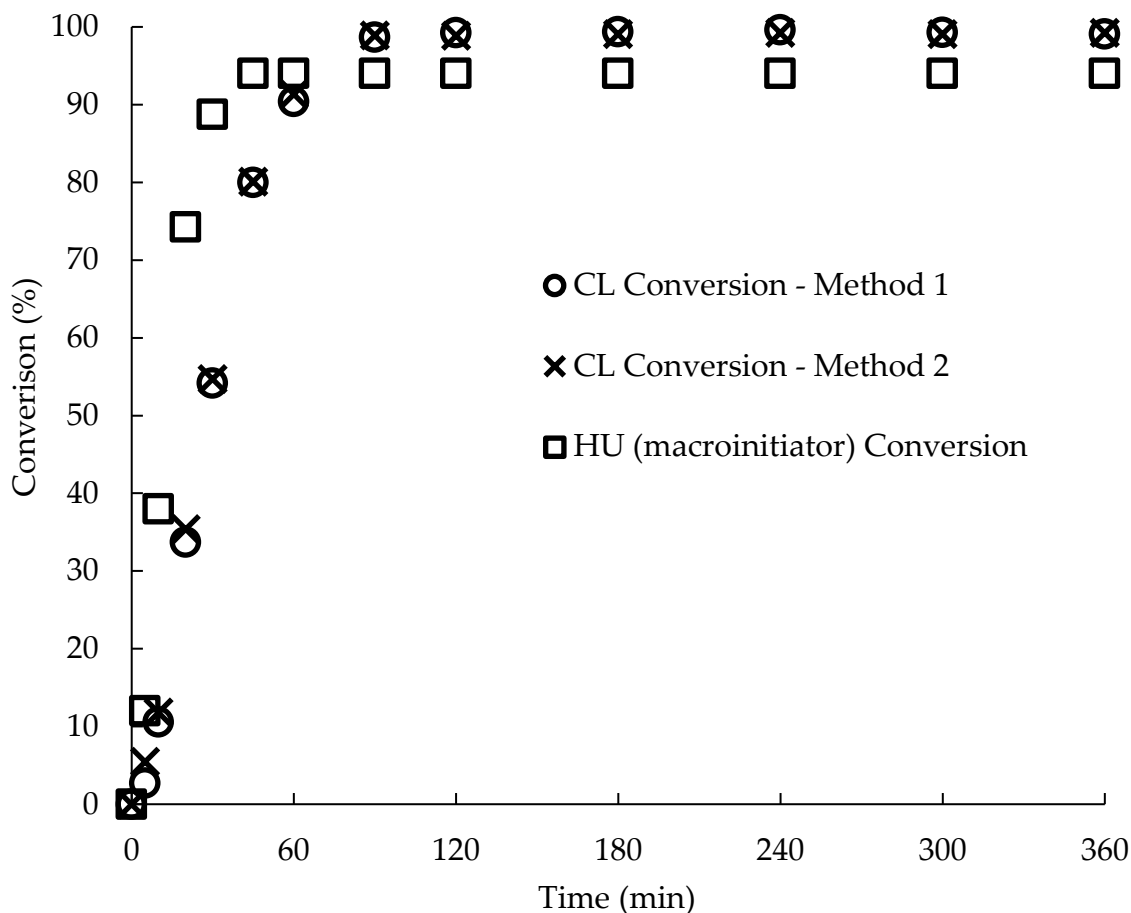


**Figure 7.1 - Conversion of CL tracked from  $^1\text{H-NMR}$  using signals of two different proton sets (the disappearance and appearance of protons at 4.23 and 3.65/4.07 ppm (Method 1), respectively, and those of 2.64 and 2.33 ppm (Method 2), respectively). Conversion of HU tracked using the disappearance of the signal at 3.79 ppm with the signal at 3.17 ppm being the reference (Figure E.2).**

Moreover, ROP was conducted to target a lower number of CL units of 2 ( $\text{HU-CL}_2$ ), but only 79% of the OH groups in the HUs were functionalized with CL units seeing the slow initiation of the macroinitiator. Afterwards,  $\text{HU-CL}_5$  was purified, as discussed in Section 7.5, to remove any unreacted species (EC, Priamine 1074, CL, and HU), and its  $^1\text{H-NMR}$  spectrum is

presented as Figure E.5. The acrylation reaction was then carried with an excess of ACl, which was removed along with the salt composed of TEA scavenging the produced hydrochloric acid (HCl). The  $^1\text{H-NMR}$  of the bio-based and hydrolytically degradable HU-A-CL<sub>5</sub> is given as Figure 7.2, in which the  $DP_n$  is equal to 5.07 on average (Eq. (E.6)), which is expected based on the initial formulation. Also, the number of vinyl groups per HU-CL<sub>5</sub>-A is  $\sim 2$  based on the integrals of i, j, and k.

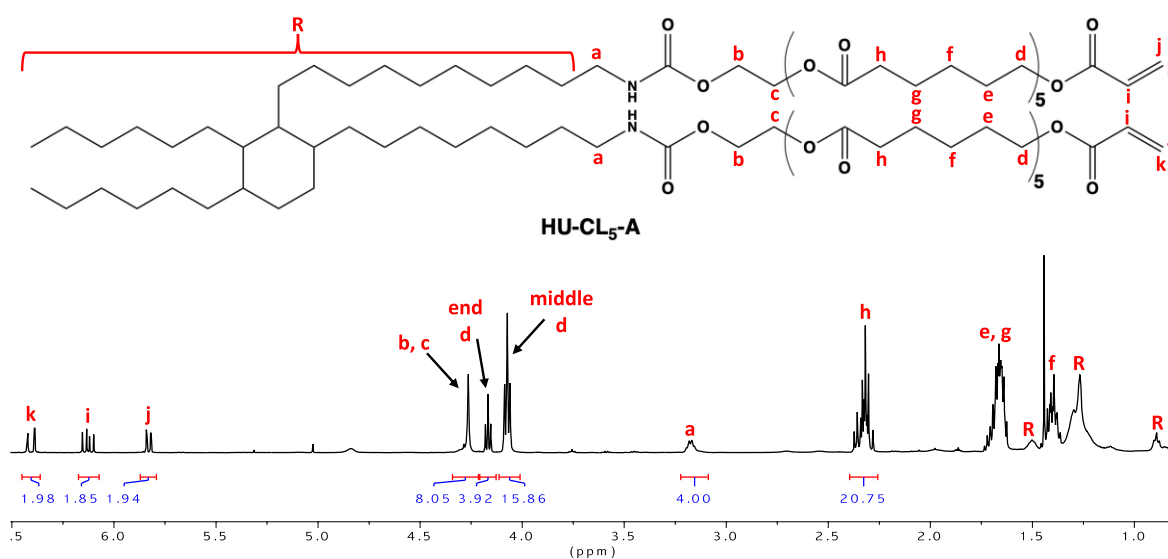


**Figure 7.2 - Labeled  $^1\text{H-NMR}$  of the bio-based HU-CL<sub>5</sub>-A of this work in  $\text{CDCl}_3$  at 25 °C. (500 MHz,  $\text{CDCl}_3$ ,  $\delta$ ): 6.4 (k), 6.13 (i), 5.83 (j), 4.26 (b, c), 4.17 (end d), 4.07 (middle d), 3.17 (a), 2.32 (h), 1.66 (e, g), 1.40 (f), 1.50/1.27/0.89 (R).**

The FTIR spectra in Figure 7.3 of the sub-products, starting from Priamine 1074 to HU-A-CL<sub>5</sub>, complement the  $^1\text{H-NMR}$  analysis while underlining the appearance and disappearance of main functional groups. Notably, we observed the evolution of the signals between 3200 and 3600  $\text{cm}^{-1}$  where the NH stretches of Priamine 1074 were measured first, which then were replaced by a broad OH stretch when forming the HU. This broad stretch persisted in HU-CL<sub>5</sub>,

which had a C=O ester stretch at 1724  $\text{cm}^{-1}$  overlapping the C=O urethane stretch of HU at 1685  $\text{cm}^{-1}$ . With the formation of HU-CL<sub>5</sub>-A, the -OH groups react to form acrylate vinyl groups on both ends of the final macromonomer, which is confirmed by the disappearance of the broad OH stretch leaving behind the NH stretch of the secondary amide groups.

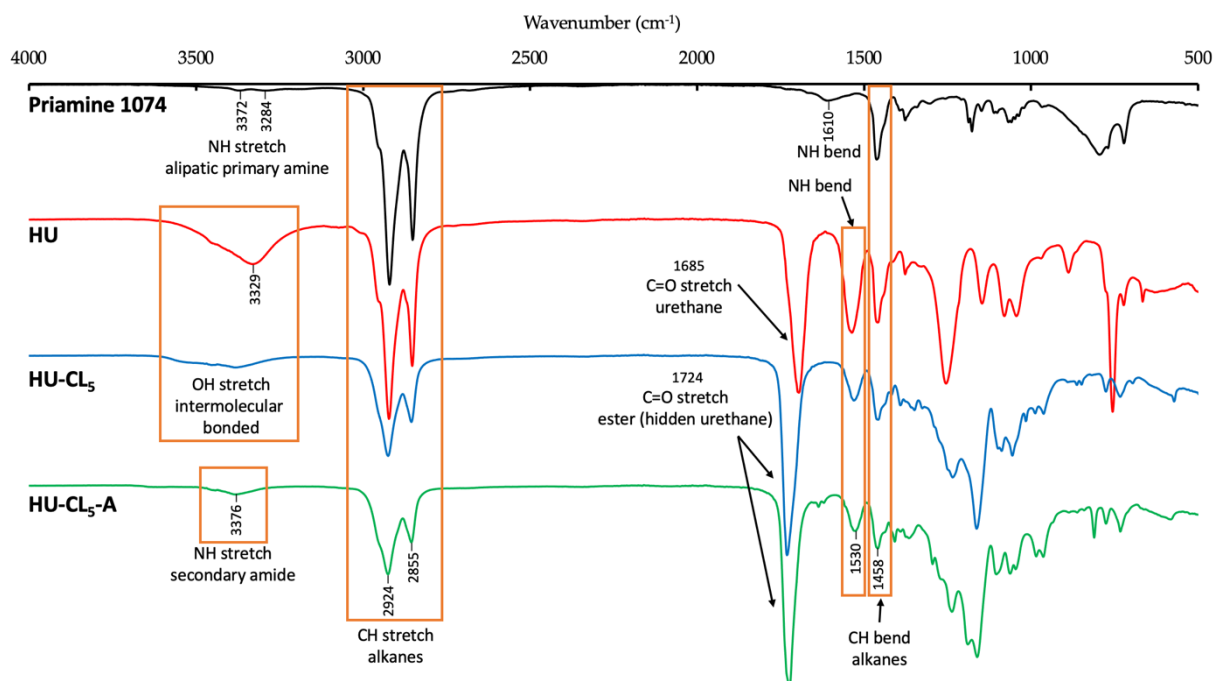


**Figure 7.3 - FTIR spectra showing the changes in the functional groups during the step-wise synthesis of bio-based and degradable HU-CL<sub>5</sub>-A of this work.**

### 7.3.2 Photocurable Thermosets and Degradation Study

The curing of HU-CL<sub>5</sub>-A was done by diluting the diacrylate with ACOMO, a photosensitive monomer.<sup>10, 11</sup> The UV curing was conducted at  $\lambda = 254 \text{ nm}$ , as the wavelength, which activated the photoinitiator, Irgacure 819, to statistically copolymerize the ACOMO/HU-CL<sub>5</sub>-A mixture via free radical polymerization. The crosslinking occurred because HU-CL<sub>5</sub>-A has two vinyl groups, thus permitting branching. Despite HU-CL<sub>5</sub>-A being an acrylate, it could not be cured as the sole

monomer because of its relatively high viscosity and restricted chain mobility. Hence, mixing it with ACMO as a reactive diluent at a proportion of 40/60 (wt./wt.) was successful in getting a cured film, similar to previous studies,<sup>10, 11</sup> whose swelling index (*SI*) and gel content (*GC*) in THF were found to be  $79.7\% \pm 1.3$  and  $87.4\% \pm 1.2$ , respectively. Since ACMO and HU-CL<sub>5</sub>-A dissolves in THF, the high *GC* denotes an effective photocuring process in which most of the vinyl groups in the diacrylate and ACMO (87 wt.%) reacted to form photocurable networks. The low *SI*, on the other hand, is a sign of high crosslink density, and it is much lower than values reported elsewhere for thermo-curable HUMA systems.<sup>5</sup> The *SI* in H<sub>2</sub>O was calculated as  $45.8\% \pm 2.7$  higher than previously reported values for films containing Priamine 1074.<sup>18</sup> Since Priamine 1074 is derived from fatty acids, it provides hydrophobicity to the films in which it is present, but in this case, ACMO is water-soluble,<sup>19, 20</sup> so the final photocurable thermosets show a water resistance balance between their hydrophobic and hydrophilic components. The *GC* in H<sub>2</sub>O was also high with a value of  $94.7\% \pm 1.8$ , meaning that 5 wt.% of the unreacted species during the photocuring process are ACMO, which leaves the remaining 8 wt.% to uncured HU-CL<sub>5</sub>-A (based on the *GC* value of 87% found after film swelling in THF). Table E.1 provides the data of the swelling experiments conducted in this work. Besides, a similar wt.% of unreacted species was also observed when running TGA. In fact, the TGA trace showed a continuous initial decrease of 13.4 wt.% from 25 °C up to 265 °C, after which the wt.% stabilizes before starting to sharply decrease at 300 °C (Figure E.6). The initial decrease could be caused by the thermal degradation of HU-CL<sub>5</sub>-A and the volatility of ACMO. Hence, the TGA results were adjusted, by disregarding this initial decrease, before calculating the  $T_{d,10\%}$  which was found to be equal to 363 °C with a  $T_{max}$  at 422 °C (Figure E.7). However, the DSC technique did not detect any  $T_g$  for the thermosets seeing that their complex structure is made of Priamine 1074,

short PCL chains, and ACMO. This was previously observed in some samples of Schimpf et al.'s study on polyfunctional acrylic HUs.<sup>10</sup>

The main objective of this work was to synthesize HU (meth)acrylates that, once polymerized, can degrade to make photocurable and hydrolytically degradable thermosets. Hence, the films were immersed in H<sub>2</sub>O and set at a temperature of 85 °C for 14 days. In previous studies, the water-soluble degradable polymers were set at a similar temperature for a shorter period of time,<sup>21, 22</sup> but seeing that the films contain hydrophobic components (Priamine 1074), as discussed above, it was necessary to adopt a longer period so that the accelerated hydrolysis is more effective. As expected, the film partially degraded with small film parts cleaving out of the original film sample, as shown in Figure 7.4.

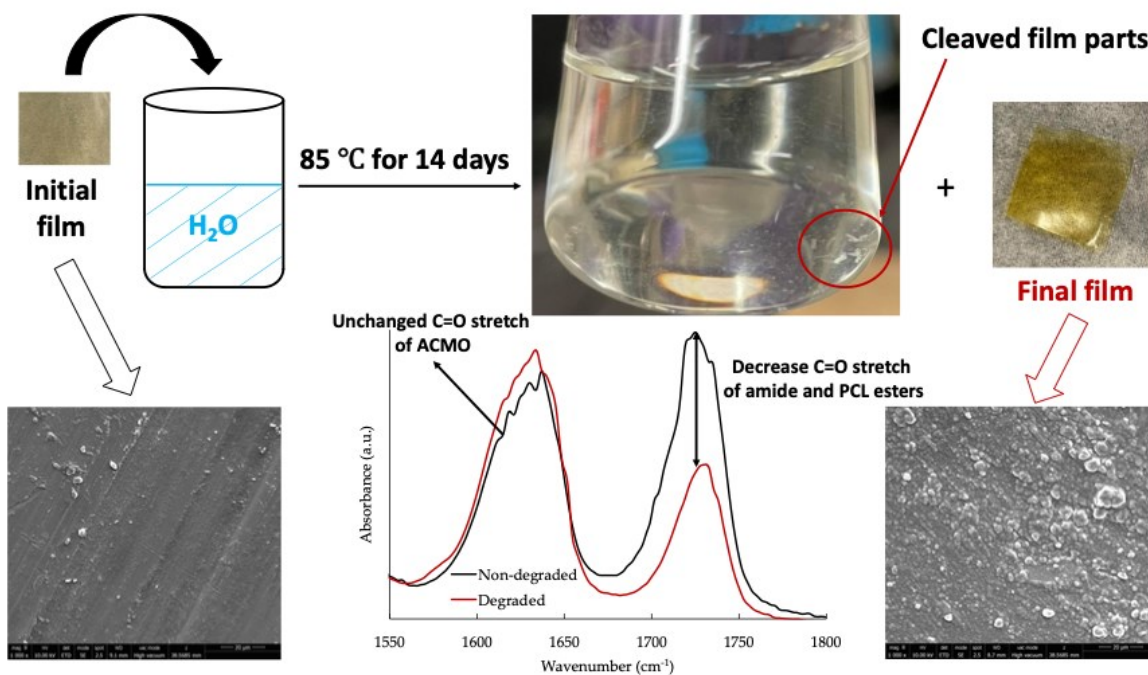


**Figure 7.4 - Photocurable films accelerated degradation study with initial and final films SEM images (1000 magnification) and their FTIR spectra in the range of 1800 and 1550 cm<sup>-1</sup> proving the hydrolysis of CL units resulting in the cleaving of film parts.**

The hydrolysis of the ester groups of the CL units and their cleaving was assessed using SEM and FTIR. The SEM images show the change in the surface morphology before and after the degradation. The initial film had a smooth surface morphology while that of the final film was irregular due to the cleaving of some film parts to the water medium following the accelerated hydrolysis study (Figure 7.4). After looking at the FTIR spectra of the initial and final films, it was found that the C=O stretch of the ACMO units ( $1635\text{ cm}^{-1}$ ) was almost unchanged, whereas that of the CL esters ( $1724\text{ cm}^{-1}$ ) and the amides (hidden  $1635\text{ cm}^{-1}$ ) decreased after the degradation. However, the hydroxyurethane and the CL units C=O stretches overlap, as it was observed from the FTIR spectra of Figure 3 (HU and HU-CL<sub>5</sub> spectra). Thus, it was necessary to quantify the percentage of each of the stretches to confirm the cleaving of the CL moieties, which was done by using the relative area method. The area of the NH bend peak at  $1530\text{ cm}^{-1}$  of the hydroxyurethane amide groups was found, and the area of the amide C=O stretch was concluded using the relative area between both signals found from the FTIR spectra of HU of Figure 7.3. The deconvolution method would have been also appropriate, but the results would have been less accurate seeing the overlapping C=O stretches of the CL esters and amide groups. At the end of the analysis, the percentage area of C=O stretches attributed to each of ACMO, CL, and amides were  $49.3 \pm 1.5$ ,  $41.9 \pm 1.4$ , and  $8.8 \pm 0.1$ , respectively, for the initial film, and  $66.2 \pm 2.2$ ,  $28.6 \pm 1.4$ , and  $5.2 \pm 0.9$ , respectively, for the final degraded film. With a decrease in the area of the CL units C=O stretches from 42 to 29%, it was confirmed that the change in the surface morphology of the films and the splitting of some film parts to the water medium were caused by the degradation of CL units that got cleaved out from the film networks. Moreover, a TGA was conducted on the final film and a  $20\text{ }^{\circ}\text{C}$  decrease in  $T_{d,10\%}$  ( $343\text{ }^{\circ}\text{C}$ ) was observed (no changes in  $T_{max}$ ), as shown in Figure E.7, demonstrating that the film became less

thermally stable because its network became weaker after the CL degradation. Note that the TGA trace of the final degraded film was also adjusted, as some water was still left in the film even after drying it under vacuum for 24 h, and that was shown by a slight initial decrease of 4 wt.% from 25 °C up to 120 °C (Figure E.6) due to the evaporation of water. The adjustment was done by neglecting this initial decrease after which the  $T_{d,10\%}$  was found.

To further confirm the cleaving of the CL units, the water medium of the hydrolysis was dried, after the degradation study, to collect the water-soluble products that were dissolved in D<sub>2</sub>O to be analyzed using <sup>1</sup>H-NMR. This analysis revealed interesting information about the degradation mechanism occurring during the accelerated hydrolysis, as presented in Figure 7.5. As it is already known, the ester groups are sensitive to water which causes their splitting from the main network chain and the release of CL units along with the species attached to them. Once in the water medium, the hydrolysis continues leading to four different water-soluble degradation products, as shown in the different stages of Figure 7.5. These products were detected in the <sup>1</sup>H-NMR spectrum of Figure E.8, and they were examined, as detailed in Table E.2 and Eq. (E.8), to deduce that approximately 3 CL units per ACMO unit are cleaved from the film network, which confirms the results of the FTIR analysis conducted earlier on the initial and final films of the degradation study (Figure 7.4). Additionally, two of the products contain double bonds coming from either unreacted vinyl groups of HU-CL<sub>5</sub>-A or chain termination by disproportionation of terminal ACMO units during the free radical polymerization process initiated by the UV light ( $\lambda = 254$  nm) and the photoinitiator (Irgacure 819). The percentage of CL units cleaving with unreacted vinyl groups is estimated as 11% of the total cleaved CL units (Eq. (E.9)), and that of terminal ACMO units is calculated to be 54% of the total ACMO units cleaved (Eq. (E.10)). Figure E.8 shows also unreacted ACMO as previously discussed for the water swelling results.

While only the water-soluble degradation products are revealed during the previous  $^1\text{H}$ -NMR analysis, water insoluble HU units are cleaving from the network as well, occurring when CL units from both sides break from the film network. Going back to the FTIR analysis of Figure 4, the ratio of CL to amide C=O stretches are calculated to be  $4.8 \pm 0.1$  and  $5.6 \pm 0.8$  for the initial and final films, respectively, of the degradation study. The degraded film shows a slight increase in the number of CL units per HU in its network, meaning that 1 HU unit was cleaving with 8 to 10 CL units equivalent to 4 to 5 CL units per side.

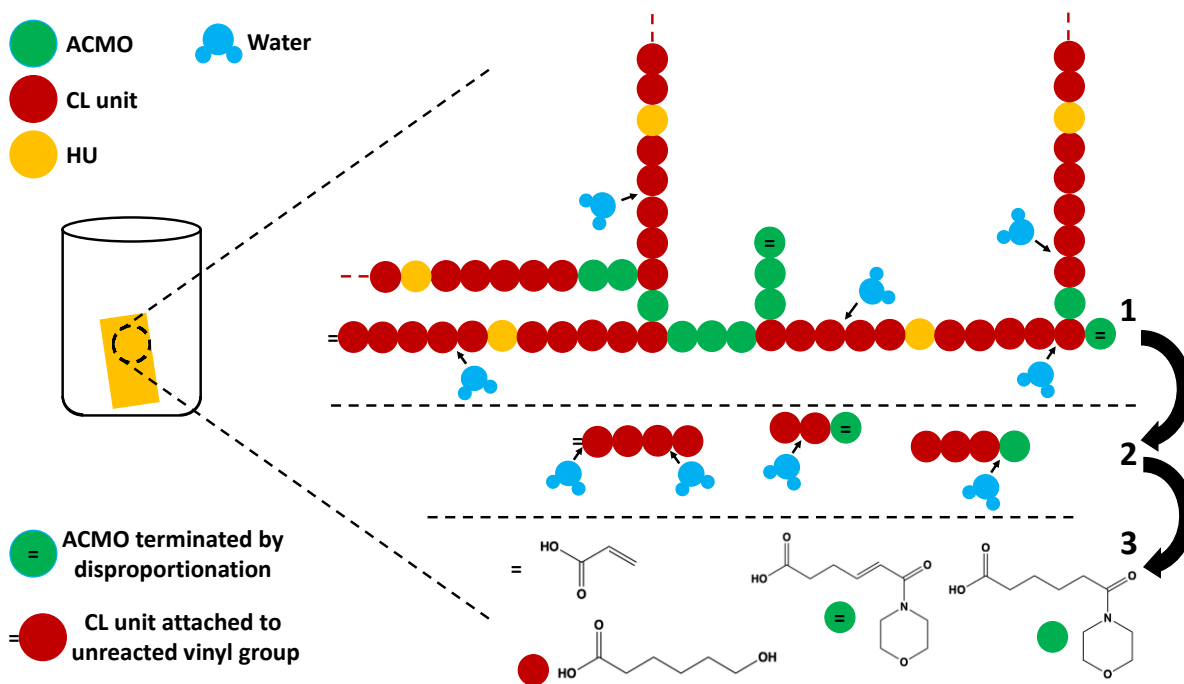


**Figure 7.5 - Proposed degradation mechanism of accelerated hydrolysis of the photocurable thermosets of this work leading to the final water-soluble degradation products detected from  $^1\text{H}$ -NMR (Figure E.8).**

## 7.4 Conclusion

This study demonstrated the successful synthesis of bio-based and hydrolytically degradable photocurable thermosets, using hydroxyurethanes as the main building block, that could be used in 3D-printing, coatings, and biomedical applications. The dimer fatty acid derived diamine, Priamine 1074, was first reacted with EC to obtain a HU that was, then, used as a macroinitiator for the ROP of CL. The ROP was optimized to get ~5 CL units per -OH with a low  $D$  of 1.2. The living polymerization was identified to be slowly initiated by the HU to prepare HU-CL<sub>5</sub>. The ROP product was acrylated on both chain ends to get the hydroxyurethane diacrylate, HU-CL<sub>5</sub>-A, confirmed by <sup>1</sup>H-NMR and FTIR. The photocuring of HU-CL<sub>5</sub>-A with ACMO as a photosensitive comonomer was conducted, and the process was found to be highly effective with a high  $GC$  value of the films obtained after swelling in THF (~88%). The resulting thermosets were found to be thermally stable ( $T_{d,10\%} = 363$  °C) and their hydrophobic and hydrophilic components (Priamine 1074 and ACMO, respectively) exhibited a balance making the film slightly water swellable ( $SI$  of ~46%). This rendered the degradation of the films slower, which makes it an ideal candidate when such a feature is sought.

The accelerated hydrolysis conducted in H<sub>2</sub>O at 85 °C for 14 days partially degraded the films. The final film exhibited an irregular surface morphology, compared to the initial smooth morphology, caused by the breaking of film parts following the cleavage of CL units from the crosslinked networks. Besides, the film became less thermally stable ( $T_{d,10\%} = 343$  °C) due to the weakening of its network caused by the cleavage as well. The latter was verified using FTIR, and the water-soluble degradation products were identified via <sup>1</sup>H-NMR. The <sup>1</sup>H-NMR analysis detected that ~3 CL units per ACMO unit cleaved from the film network, while the calculations of the FTIR study showed that ~8 to 10 CL units cleaved per HU unit. Finally, this study is the

first to integrate biodegradable moieties in the structure of HUMA/HUA and indicates the versatility of the non-toxic isocyanate-free HU materials compared to their conventional urethane counterparts.

## 7.5 Experimental Section

*Materials:* Ethylene carbonate (EC, 98%),  $\epsilon$ -caprolactone (CL, 97%), stannous octoate ( $\text{Sn}(\text{oct})_2$ , 92.5-100.0%), triethylamine (TEA,  $\geq 99.5\%$ ), basic alumina (Brockmann Type 1), acryloyl chloride (ACl,  $\geq 97\%$ ), were purchased from Sigma Aldrich. Tetrahydrofuran (THF, HPCL grade), chloroform (stabilized with ethanol), and heptane were purchased from Fischer Chemical. Priamine 1074 was provided by Croda. Deuterated chloroform ( $\text{CDCl}_3$ ) and deuterium oxide ( $\text{D}_2\text{O}$ ) were purchased from Sigma Aldrich and Cambridge Isotope Laboratories, respectively. 4-Acryloylmorpholine (ACMO, 97%) and bis(2,4,6-trimethylbenzoyl)-phenylphosphineoxide (Irgacure 819), which is the photoinitiator with  $\lambda_{\text{max}} = 295$  and 370 nm, were purchased from Sigma Aldrich. All chemicals were used as received. Water ( $\text{H}_2\text{O}$ ) purified by a reverse osmosis process was provided by the McGill Chemical Engineering Department.

*Synthesis of HU-CL<sub>5</sub>-A:* Priamine 1074 has an amine hydrogen equivalent weight (AHEW) of 270 g eq<sup>-1</sup> provided by Croda and a molecular weight of 534.58 g mol<sup>-1</sup> measured from electrospray ionization mass spectroscopy (ESI-MS)  $m/z$ :  $[\text{M}]^{2+}$  calculated for  $\text{C}_{36}\text{H}_{74}\text{N}_2$ , 267.29 g mol<sup>-1</sup>. EC has a carbonate equivalent weight (CEW) equal to its molecular weight 88.06 g eq<sup>-1</sup>. Hence, the mass of Priamine 1074 was calculated using the following equation to get 2 M of EC equivalent:

$$m_{\text{Priamine 1074}} = \frac{\text{AHEW} \times m_{\text{EC}}}{\text{CEW}} = \frac{270 \times m_{\text{EC}}}{88.06} \quad \text{Eq. (7.1)}$$

The reactants (7.52 g of EC and 23.06 g of Priamine 1074) were added into a 50 mL round bottom flask reactor having a magnetic stirrer, and the mixture was purged with nitrogen (N<sub>2</sub>) for 15 min before immersing the reactor in an oil bath pre-heated to 100 °C. The reaction was allowed to proceed for 6 h, after which the reactor was removed from the oil bath to cool down and the HU was obtained with conversions of Priamine 1074 and EC of 98%. The molecular weight of the HU was analyzed by ESI-MS *m/z*: [M+Na]<sup>+</sup> calculated for 731.59 and 733.60 g mol<sup>-1</sup>. This leaves the HU with a molecular weight of 710 g mol<sup>-1</sup>, which was expected.

The HU was used as a macroinitiator for the ROP of CL, and the reaction with CL:OH:Sn(oct)<sub>2</sub> of 5:1:0.01 at 110 °C for 1 h is used as a representative example since it represents the optimized conditions of this step confirmed by conducting three trials. In a 50 mL round bottom flask, 5.0 g (43.8 mmol) of CL were mixed with 3.11 g (4.38 mmol) of HU (equivalent to 5 CL monomers per -OH), and the HU was allowed to dissolve in CL with a magnetic stirrer. Then, the mixture was purged with N<sub>2</sub> for 15 min and placed in an oil bath pre-heated to 110 °C after which 0.036 g of Sn(oct)<sub>2</sub> was added. Time zero was set as the time when all of the catalyst had been added, and the N<sub>2</sub> flow kept for the entire reaction. After 1 h, the crude product was cooled down to room temperature and crude HU-CL<sub>5</sub> was collected with an average number of CL units equal to 4.7 ± 0.3 and percentage conversions of CL and HU of 87 ± 4 and 97 ± 1, respectively. The product was then purified twice by precipitations from chloroform in a 10-fold excess of cold heptane. The solvent was filtered out and pure HU-CL<sub>5</sub> was dried under vacuum at room temperature and stored for the acetylation reaction. In the case of kinetic studies, samples were withdrawn at regular times with glass pipettes and dissolved in CDCl<sub>3</sub> and THF for <sup>1</sup>H-NMR and SEC analysis, respectively, presented in the next sections. The other trials are presented in Table 7.1.

For the acetylation reaction, it was followed using the procedure presented in Younes et al.'s work on hydrolytically degradable polymeric flocculants.<sup>22</sup> Briefly, HU-CL<sub>5</sub> (7.0 g, 3.78 mmol) was dissolved in 40 mL of THF ([OH] = 0.2 mol L<sup>-1</sup>) in a three neck 100 mL round bottom flask reactor. TEA (30 mL) was added, and the solution was warmed to 35 °C using an oil bath. The flask was purged with N<sub>2</sub> before slowly adding 1.0 mL of AcI (2.7 molar equivalent of HU-CL<sub>5</sub>) diluted in 5 mL of THF via syringe over 2 h. The reaction mixture was kept at 35 °C for another 4 h after which the TEA salt was filtered and the residual AcI was removed using a column of basic alumina. THF and the remaining TEA were evaporated under vacuum to yield the hydrolytically degradable hydroxyurethane acrylate, HU-CL<sub>5</sub>-A.

*Resin formulation and curing:* The resin formulations consisted of 60 wt.% ACMO and 40 wt.% HU-CL<sub>5</sub>-A. In addition, 0.5 wt.% of the photoinitiator Irgacure 819 was added. The corresponding components were mixed until a homogeneous resin mixture was obtained. The test specimen were cured in a Spectrolinker, 1000 XL UV crosslinker (254 nm, LED) for 5 min, as it was previously done.<sup>11</sup>

*Degradation study:* A portion of the film (2 by 2 cm) was placed in H<sub>2</sub>O present in a 20 mL vial. The vial was placed in an oil bath pre-heated to 85 °C for 14 days to allow for the accelerated degradation of the “initial” film by hydrolysis. After 14 days, the “final” film was collected and dried under vacuum oven at room temperature for 24 h. The water insoluble degradation product was filtered, collected, and dried in the vacuum oven under similar conditions. The water-soluble products were collected after removing the water and they were dissolved in D<sub>2</sub>O for <sup>1</sup>H-NMR analysis. The temperature of the accelerated degradation study was chosen between the melting temperature of PCL (60 °C) and the boiling point of water (100 °C).

*Proton Nuclear Magnetic Resonance (<sup>1</sup>H-NMR) Spectroscopy:* Solution phase NMR spectra were recorded on a Bruker 500 MHz instrument (16 scans) at ambient temperature. All samples of this study were dissolved in CDCl<sub>3</sub> to be analyzed except of the water-soluble degradation products which were dissolved in D<sub>2</sub>O.

*Fourier Transform infrared (FTIR) Spectroscopy:* FTIR measurements were carried out on a Perkin Elmer instrument (Spectrum II series) equipped with a single bounce diamond attenuated transmission reflectance (ATR) for solids and zinc selenide (ZnSe) holder for liquids. 32 scans were recorded for each sample over the range 4000-500 cm<sup>-1</sup> with a normal resolution of 4 cm<sup>-1</sup>. The products of the step-wise synthesis as well as the initial and final degradation films were analyzed on FTIR.

*Electrospray Ionization Mass Spectroscopy (ESI-MS):* Mass spectra analysis on Priamine 1074 and HU were performed on an LCQ-API (Atmospheric pressure ionization) Ion Trap (THERMO) in a positive ionization mode.

*Size Exclusion Chromatography (SEC):* The ROP products (of all the trials) molecular weight distributions were analyzed via SEC. Number average molecular weight ( $M_n$ ) and dispersity ( $\mathcal{D} = M_w/M_n$ ) of prepolymer samples were measured using this technique on a Waters Breeze instrument with HPLC grade THF as an eluent at a flow rate of 0.3 mL min<sup>-1</sup>. The GPC has three Waters Styragel HR columns (HR1 with a molecular weight measurement range of 10<sup>2</sup> to 5 × 10<sup>3</sup> g mol<sup>-1</sup>, HR2 with a molecular weight measurement range of 5 × 10<sup>2</sup> to 2 × 10<sup>4</sup> g mol<sup>-1</sup>, and HR4 with a molecular weight measurement range of 5 × 10<sup>3</sup> to 6 × 10<sup>5</sup> g mol<sup>-1</sup>), a guard column, and a refractive index (RI 2414) detector. The columns were heated to 40 °C during analysis. The molecular weights were determined relative to poly(methylmethacrylate) (PMMA) calibration standards from Varian Inc. (ranging from 875 to 1,677,000 g mol<sup>-1</sup>). The reported molecular

weights were all relative to the PMMA standards and not adjusted with Mark-Houwink parameters.

*Thermogravimetric Analysis (TGA)*: TGA was performed on a Q500 system from TA Instruments. The thermal degradation of the initial and final degradation films was measured at a heating rate of 20 °C min<sup>-1</sup> over the temperature range of 25 to 800 °C under a nitrogen atmosphere. The 10% and maximum degradation temperatures ( $T_{d,10\%}$  and  $T_{max}$ , respectively) were calculated using this method.

*Differential Scanning Calorimetry (DSC)*: DSC was performed using a Q2500 TA Instruments calorimeter autosampler employing standard hermetic aluminum pans, calibrated with indium and N<sub>2</sub> as purge gas. The instrument is equipped with a cooling unit allowing it to reach low temperatures up to -90 °C. The photocurable thermoset was analyzed at a heating rate of 10 °C min<sup>-1</sup>, for the second heating ramp, over a temperature range of -90 °C to 280 °C to check for any glass transition temperature ( $T_g$ ).

*Scanning Electron Microscopy (SEM)*: The surface morphology of the initial and final degradation films was studied with a Hitachi SU-3500 Variable Pressure SEM at 5kV. Before imaging the films, the samples were sputter coated with palladium to make the sample conductive.

*Swelling*: The cured film was allowed to sit for 24 h before conducting their swelling tests in THF and H<sub>2</sub>O. Film samples of 10-20 mg were immersed in 7 mL of solvent at room temperature for 72 h, after which the swelling index ( $SI$ ) was calculated using Eq. (7.2), after which the samples were dried in a vacuum oven overnight at 40 °C to find their gel content ( $GC$ ) by applying Eq. (7.3).

$$SI (\%) = \left( \frac{W_s - W_d}{W_d} \right) \times 100 \quad \text{Eq. (7.2)}$$

$$GC (\%) = \left(\frac{W_f}{W_i}\right) \times 100 \quad \text{Eq. (7.3)}$$

Here,  $W_s$  is the weight of the swollen sample,  $W_d$  is the weight of the dry sample,  $W_i$  is the initial weight (same as  $W_d$  in this case), and  $W_f$  is the final weight of the dried sample.

## 7.6 References

1. O. Kreye, H. Mutlu, M. A. R. Meier, *Green Chem.* **2013**, *15*, 1431.
2. B. Ochiai, S. Inoue, T. Endo, *J. Polym. Sci., Part A: Polym. Chem.* **2005**, *43*, 6613.
3. Y. He, H. Keul, M. Möller, *Eur. Polym. J.* **2011**, *47*, 1607.
4. C. Pronoitis, M. Hakkarainen, K. Odelius, *Polym. Chem.* **2021**, *12*, 196.
5. M. Decostanzi, C. Bonneaud, S. Caillol, *J. Polym. Sci., Part A: Polym. Chem.* **2019**, *57*, 1224.
6. F. Zareanshahraki, H. R. Asemani, J. Skuza, V. Mannari, *Prog. Org. Coat.* **2020**, *138*, 105394.
7. A. Filip, O. V. Badulescu, P. Dan Sirbu, B. Valiceasa, B. Puha, I. A. Pascal, L. Andrusca, S. Oprea, C. Filip, O. Alexa, *Mater. Plast. (Bucharest, Rom.)* **2019**, *56*, 559.
8. J. Z. Hwang, S. C. Wang, P. C. Chen, C. Y. Huang, J. T. Yeh, K. N. Chen, *J. Polym. Res.* **2012**, *19*, 1.
9. F. Zareanshahraki, V. Mannari, *J. Coat. Technol. Res.* **2021**, *18*, 695.
10. V. Schimpf, A. Asmacher, A. Fuchs, B. Bruchmann, R. Mülhaupt, *Macromolecules* **2019**, *52*, 3288.
11. H. Buchheit, B. Bruchmann, K. Stoll, R. Mülhaupt, *J. Polym. Sci.* **2021**, *59*, 882.
12. A. Kowalski, A. Duda, S. Penczek, *Macromol. Rapid. Commun.* **1998**, *19*, 567.
13. R. F. Storey, A. E. Taylor, *J. Macromol. Sci., Part A* **1998**, *35*, 723.

14. M. Bero, B. Czaplá, P. Dobrzyński, H. Janeczek, J. Kasperczyk, *Macromol. Chem. Phys.* **1999**, *200*, 911.
15. R. F. Storey, J. W. Sherman, *Macromolecules* **2002**, *35*, 1504.
16. A. Albertsson, I. K. Varma, *Biomacromolecules* **2003**, *4*, 1466.
17. J. Qiu, B. Charleux, K. Matyjaszewski, *Prog. Polym. Sci.* **2001**, *26*, 2083.
18. G. R. Younes, M. Maric, *Ind. Eng. Chem. Res.* **2021**, *60*, 8159.
19. P. Kulal, V. Badalamoole, *J. Environ. Chem. Eng.* **2020**, *8*, 104207.
20. X. Zhai, C. Ruan, J. Shen, C. Zheng, X. Zhao, H. Pan, W. W. Lu, *J. Mater. Chem. B* **2021**, *9*, 2394.
21. T. R. Rooney, S. P. Gumfekar, J. B. P. Soares, R. A. Hutchinson, *Macromol. Mater. Eng.* **2016**, *301*, 1248.
22. G. R. Younes, A. R. Proper, T. R. Rooney, R. A. Hutchinson, S. P. Gumfekar, J. B. P. Soares, *Ind. Eng. Chem. Res.* **2018**, *57*, 10809.

## Chapter 8

### Conclusions and future work

This work proves the versatility of PHUs as safer and potentially greener materials that can eventually replace their conventional PU analogs made from toxic isocyanates. It underlines the synthesis of different types of PHUs, thermoplastics, thermosets, hybrids, and smart materials, from bio-sourced building blocks, that can be used in various fields, such as adhesives, sealants, 3D-printing, coatings, plasticizers, toughening agents, and biomedical applications. The bio-based sources used throughout this work were glycerol, sugars, and plant-derived dimer fatty acids to make the respective monomers, which are the five-membered cyclic dicarbonates and the diamines, and a wide range of PHU materials were prepared starting with moisture-curable hybrid thermosets (HPHU), thermoplastics designed using terpolymerizations (TPHU), and photocurable hydroxyurethane acrylates (HUA).

The first three studies described in this thesis dealt with the preparation of partially sustainable moisture-curable HPHUs. The PDMS-based HPHUs exhibited properties, such as hydrophobicity, mechanical strength, and elasticity, that made their films promising for different applications, like adhesives, sealants, and coatings, similarly to moisture-curable conventional PUs. However, the PDMS-(NH<sub>2</sub>)<sub>2</sub> is more expensive compared to Jeffamine D-2000, the PPG-based diamine, which makes the former HPHU economically unfeasible. Hence, the PPG-based prepolymer had to be extended with hydrophobic diamines, the bio-sourced Priamine 1074 and PDMS-(NH<sub>2</sub>)<sub>2</sub> of different chain lengths, from both ends, and the final HPHUs showed an increase in hydrophobicity, thermal stability, and storage modulus, especially with Priamine 1074. Therefore, there is a potential in commercializing these materials as adhesives and sealants, but before, their properties still need to be examined, using the lap shear tests for

example, to verify if they meet the standards set for such applications while comparing them to commercialized PU sealants and adhesives.

The first academic study used a terpolymerization system to make new TPHUs. The base bio-sourced TPHU was made of DGC and Priamine 1074. The third monomer consisted of two different diamines; a PDMS-1k-(NH<sub>2</sub>)<sub>2</sub> softer than Priamine 1074 and DAD inducing crystallinity into the base PHU structure. The study revealed significant insights on the nanophase separation exhibited in TPHUs as well as the rheological properties presented by such polymeric materials. The study applied TPHUs in polymer blends for the first time, and it served as a stepping stone to optimize the design of appropriate TPHUs as toughening agents and plasticizers for brittle biopolymers, such as PLA. Hence in the future, the effects of the TPHUs on the PLA matrix can be improved by making higher molecular weight TPHUs with shorter di/triblocks. This would make the hydrogen bonding interactions, between the hydroxyl groups of the TPHUs and the carbonyls of PLA, stronger leading to more pronounced plasticizing and toughening of PLA even with small amounts of TPHUs (< 20wt.%).

The next study of this second phase of the research, which is also the last one of this work, cleanly synthesizes HUAs from bio-sourced Priamine 1074 while incorporating degradable CL moieties. This is the first study making bio-based and biodegradable HUAs that are photocurable using UV-light. The final partially hydrolytically degradable films can be potentially used as patches, for example, in the biomedical field; however, the cytotoxicity of those films and their degradation products must be investigated. In the future, the CL units can be replaced by lactide (LA) units, which degrade quicker than CL seeing that the former is more hydrophilic than the latter, and hence, is more susceptible to cleavage through hydrolysis. Besides, the films formulation can be optimized by varying the ratio of ACMO to HUA to reach

higher degradable contents while keeping the viscosity of the mixture low enough to get successful photocuring of the resins.

## References

1. Akindoyo, J. O.; Beg, M. D. H.; Ghazali, S.; Islam, M. R.; Jeyaratnam, N.; Yuvaraj, A. R., Polyurethane types, synthesis and applications – a review. *RSC Advances* **2016**, *6* (115), 114453-114482.
2. Engels, H. W.; Pirkl, H. G.; Albers, R.; Albach, R. W.; Krause, J.; Hoffmann, A.; Casselmann, H.; Dormish, J., Polyurethanes: versatile materials and sustainable problem solvers for today's challenges. *Angewandte Chemie International Edition in English* **2013**, *52* (36), 9422-9441.
3. Kreye, O.; Mutlu, H.; Meier, M. A. R., Sustainable routes to polyurethane precursors. *Green Chemistry* **2013**, *15* (6), 1431-1455.
4. Bayer, O.; Siefken, W.; Rinke, H.; Orthner, L.; Schild, H. A process for the production of polyurethanes and polyureas. German Patent DRP 728981, 1937.
5. Sharma, A. K.; Kumar, N., Phosgene: Risk assessment, environmental, and health hazard. In *Hazardous Gases*, 2021; pp 313-325.
6. Peters, J. M., Studies of Isocyanate Toxicity: Cumulative Pulmonary Effects in Workers Exposed to Toluene Diisocyanate. *Journal of the Royal Society of Medicine* **1970**, *73*, 372-375.
7. Liu, Y.; Stowe, M. H.; Bello, D.; Woskie, S. R.; Sparer, J.; Gore, R.; Youngs, F.; Cullen, M. R.; Redlich, C. A., Respiratory protection from isocyanate exposure in the autobody repair and refinishing industry. *Journal of Occupational and Environmental Hygiene* **2006**, *3* (5), 234-249.
8. Bello, D.; Herrick, C. A.; Smith, T. J.; Woskie, S. R.; Streicher, R. P.; Cullen, M. R.; Liu, Y.; Redlich, C. A., Skin exposure to isocyanates: reasons for concern. *Environmental Health Perspectives* **2007**, *115* (3), 328-335.

9. Stocks, S. J.; Jones, K.; Piney, M.; Agius, R. M., Isocyanate exposure and asthma in the UK vehicle repair industry. *Occupational Medicine (Lond)* **2015**, *65* (9), 713-718.
10. Shelby, M. D.; Allen, J. W.; Caspary, W. J.; Haworth, S.; Ivett, J.; Kligerman, A.; Luke, C. A.; Mason, J. M.; Myhr, B.; Tice, R. R.; Valencia, R.; Zeiger, E., Results of In Vitro and In Vivo Genetic Toxicity Tests on Methyl Isocyanate. *Environmental Health Perspectives* **1987**, *72*, 183-187.
11. Varma, D. R.; Ferguson, J. S.; Alarie, Y., Reproductive toxicity of methyl isocyanate in mice. *Journal of Toxicology and Environmental Health, Part A Current Issues* **1987**, *21* (3), 265-75.
12. Ganguly, B. B.; Mandal, S.; Kadam, N. N., Genotoxic and Carcinogenic Effects of Methyl Isocyanate (MIC) Reviewed on Exposed Bhopal Population and Future Perspectives for Assessment of Long-Term MIC-Effect. *Journal of Environmental & Analytical Toxicology* **2017**, *7* (3), 2161-0525.
13. Paabo, M.; Levin, B. C., A Review of the Literature on the Gaseous Products and Toxicity Generated from the Pyrolysis and Combustion of Rigid Polyurethane Foams. *Fire and Materials* **1987**, *11* (1), 1-29.
14. McKenna, S. T.; Hull, T. R., The fire toxicity of polyurethane foams. *Fire Science Reviews* **2016**, *5* (1), 1-27.
15. Guan, J.; Song, Y.; Lin, Y.; Yin, X.; Zuo, M.; Zhao, Y.; Tao, X.; Zheng, Q., Progress in Study of Non-Isocyanate Polyurethane. *Industrial & Engineering Chemistry Research* **2011**, *50* (11), 6517-6527.
16. Kathalewar, M. S.; Joshi, P. B.; Sabnis, A. S.; Malshe, V. C., Non-isocyanate polyurethanes: from chemistry to applications. *RSC Advances* **2013**, *3* (13), 4110-4129.

17. Maisonneuve, L.; Lamarzelle, O.; Rix, E.; Grau, E.; Cramail, H., Isocyanate-Free Routes to Polyurethanes and Poly(hydroxy Urethane)s. *Chemical Reviews* **2015**, *115* (22), 12407-12439.
18. Rokicki, G.; Parzuchowski, P. G.; Mazurek, M., Non-isocyanate polyurethanes: Synthesis, properties, and applications. *Polymers for Advanced Technologies* **2015**, *26* (7), 707-761.
19. Abitha, V. K.; Jadhav, S. A.; Rane, A. V., Non-Isocyanate Polyurethane Systems: A Review. *Moroccan Journal of Chemistry* **2016**, *4* (2), 361-383.
20. Cornille, A.; Auvergne, R.; Figovsky, O.; Boutevin, B.; Caillol, S., A perspective approach to sustainable routes for non-isocyanate polyurethanes. *European Polymer Journal* **2017**, *87*, 535-552.
21. Suryawanshi, Y.; Sanap, P.; Wani, V., Advances in the synthesis of non-isocyanate polyurethanes. *Polymer Bulletin* **2019**, *76* (6), 3233-3246.
22. Datta, J.; Wloch, M., Progress in non-isocyanate polyurethanes synthesized from cyclic carbonate intermediates and di- or polyamines in the context of structure-properties relationship and from an environmental point of view. *Polymer Bulletin* **2016**, *73* (5), 1459-1496.
23. Hahn, C.; Keul, H.; Möller, M., Hydroxyl-functional polyurethanes and polyesters: synthesis, properties and potential biomedical application. *Polymer International* **2012**, *61* (7), 1048-1060.
24. Nohra, B.; Candy, L.; Blanco, J. F.; Guerin, C.; Raoul, Y.; Mouloungui, Z., From Petrochemical Polyurethanes to Biobased Polyhydroxyurethanes. *Macromolecules* **2013**, *46* (10), 3771-3792.

25. Desroches, M.; Auvergne, R.; Boutevin, B.; Caillol, S., Synthesis of bio-based building blocks from vegetable oils: a platform chemicals approach. *Ocl-Oilseeds and Fats Crops and Lipids* **2013**, *20* (1), 16-22.
26. Desroches, M.; Benyahya, S.; Besse, V.; Auvergne, R.; Boutevin, B.; Caillol, S., Synthesis of bio-based building blocks from vegetable oils: A platform chemicals approach. *Lipid Technology* **2014**, *26* (2), 35-38.
27. de la Cruz-Martínez, F.; Martínez de Sarasa Buchaca, M.; Martínez, J.; Fernández-Baeza, J.; Sánchez-Barba, L. F.; Rodríguez-Diéguez, A.; Castro-Osma, J. A.; Lara-Sánchez, A., Synthesis of Bio-Derived Cyclic Carbonates from Renewable Resources. *ACS Sustainable Chemistry & Engineering* **2019**, *7* (24), 20126-20138.
28. Błażek, K.; Datta, J., Renewable natural resources as green alternative substrates to obtain bio-based non-isocyanate polyurethanes-review. *Critical Reviews in Environmental Science and Technology* **2019**, *49* (3), 173-211.
29. Carre, C.; Ecochard, Y.; Caillol, S.; Averous, L., From the Synthesis of Biobased Cyclic Carbonate to Polyhydroxyurethanes: A Promising Route towards Renewable Non-Isocyanate Polyurethanes. *ChemSusChem* **2019**, *12* (15), 3410-3430.
30. Ghasemlou, M.; Daver, F.; Ivanova, E. P.; Adhikari, B., Bio-based routes to synthesize cyclic carbonates and polyamines precursors of non-isocyanate polyurethanes: A review. *European Polymer Journal* **2019**, *118*, 668-684.
31. Mhd Haniffa, M. A. C.; Munawar, K.; Ching, Y. C.; Illias, H. A.; Chuah, C. H., Bio-based Poly(hydroxy urethane)s: Synthesis and Pre/Post-Functionalization. *Chemistry – An Asian Journal* **2021**, *16* (11), 1281-1297.

32. Wang, G.; Lopez, L.; Coile, M.; Chen, Y.; Torkelson, J. M.; Broadbelt, L. J., Identification of Known and Novel Monomers for Poly(hydroxyurethanes) from Biobased Materials. *Industrial & Engineering Chemistry Research* **2021**, *60* (18), 6814-6825.
33. Tomczyk, K. M.; Guńka, P. A.; Parzuchowski, P. G.; Zachara, J.; Rokicki, G., Intramolecular etherification of five-membered cyclic carbonates bearing hydroxyalkyl groups. *Green Chemistry* **2012**, *14* (6), 1749.
34. Dannecker, P. K.; Meier, M. A. R., Facile and Sustainable Synthesis of Erythritol bis(carbonate), a Valuable Monomer for Non-Isocyanate Polyurethanes (NIPUs). *Scientific Reports* **2019**, *9* (1), 9858.
35. Magliozzi, F.; Scali, A.; Chollet, G.; Grau, E.; Cramail, H., Enantioselective Crystallization of Diglycerol Dicarboxylate: Impact of the Microstructure on Polyhydroxyurethane Properties. *Macromolecular Rapid Communications* **2021**, *42* (3), 2000533.
36. Cai, X. S.; Aissa, K. A.; Estel, L.; Leveneur, S., Investigation of the Physicochemical Properties for Vegetable Oils and Their Epoxidized and Carbonated Derivatives. *Journal of Chemical and Engineering Data* **2018**, *63* (5), 1524-1533.
37. Charbonneau, L.; Foster, X.; Kaliaguine, S., Ultrasonic and catalyst free epoxidation of limonene and other terpenes using dimethyl dioxirane in semi-batch conditions. *ACS Sustainable Chemistry & Engineering* **2018**, *6* (9), 12224-12231.
38. Chen, J.; de Liedekerke Beaufort, M.; Gyurik, L.; Dorresteyn, J.; Otte, M.; Klein Gebbink, R. J. M., Highly efficient epoxidation of vegetable oils catalyzed by a manganese complex with hydrogen peroxide and acetic acid. *Green Chemistry* **2019**, *21* (9), 2436-2447.
39. Mahamat Ahmat, Y.; Madadi, S.; Charbonneau, L.; Kaliaguine, S., Epoxidation of Terpenes. *Catalysts* **2021**, *11* (7), 847.

40. Blattmann, H.; Fleischer, M.; Bahr, M.; Mulhaupt, R., Isocyanate- and Phosgene-Free Routes to Polyfunctional Cyclic Carbonates and Green Polyurethanes by Fixation of Carbon Dioxide. *Macromolecular Rapid Communications* **2014**, *35* (14), 1238-1254.
41. Martinez, J.; Fernandez-Baeza, J.; Sanchez-Barba, L. F.; Castro-Osma, J. A.; Lara-Sanchez, A.; Otero, A., An Efficient and Versatile Lanthanum Heteroscorpionate Catalyst for Carbon Dioxide Fixation into Cyclic Carbonates. *ChemSusChem* **2017**, *10* (14), 2886-2890.
42. Longwitz, L.; Steinbauer, J.; Spannenberg, A.; Werner, T., Calcium-Based Catalytic System for the Synthesis of Bio-Derived Cyclic Carbonates under Mild Conditions. *ACS Catalysis* **2018**, *8* (1), 665-672.
43. Bobbink, F. D.; van Muyden, A. P.; Dyson, P. J., En route to CO<sub>2</sub>-containing renewable materials: catalytic synthesis of polycarbonates and non-isocyanate polyhydroxyurethanes derived from cyclic carbonates. *Chemical Communications* **2019**, *55* (10), 1360-1373.
44. Yadav, N.; Seidi, F.; Crespy, D.; D'Elia, V., Polymers Based on Cyclic Carbonates as Trait d'Union Between Polymer Chemistry and Sustainable CO<sub>2</sub> Utilization. *ChemSusChem* **2019**, *12* (4), 724-754.
45. Wulf, C.; Reckers, M.; Perehodjuk, A.; Werner, T., Catalytic Systems for the Synthesis of Biscarbonates and Their Impact on the Sequential Preparation of Non-Isocyanate Polyurethanes. *ACS Sustainable Chemistry & Engineering* **2019**, *8* (3), 1651-1658.
46. Motokucho, S.; Morikawa, H., Poly(hydroxyurethane): catalytic applicability for the cyclic carbonate synthesis from epoxides and CO<sub>2</sub>. *Chemical Communications* **2020**, *56* (73), 10678-10681.

47. Schmitt, M.; Strehmel, V., Chemical Reaction of Carbon Dioxide with Bisepoxides for Synthesis of Organic Cyclic Dicarbonates at Ambient Pressure for Polyhydroxy Urethane Synthesis. *Organic Process Research & Development* **2020**, *24* (11), 2521-2528.
48. North, M.; Pasquale, R.; Young, C., Synthesis of cyclic carbonates from epoxides and CO<sub>2</sub>. *Green Chemistry* **2010**, *12* (9), 1514.
49. Martín, C.; Fiorani, G.; Kleij, A. W., Recent Advances in the Catalytic Preparation of Cyclic Organic Carbonates. *ACS Catalysis* **2015**, *5* (2), 1353-1370.
50. Buttner, H.; Longwitz, L.; Steinbauer, J.; Wulf, C.; Werner, T., Recent Developments in the Synthesis of Cyclic Carbonates from Epoxides and CO<sub>2</sub>. *Topics in Current Chemistry* **2017**, *375* (3), 1-56.
51. Verma, S.; Kumar, G.; Ansari, A.; Kureshy, R. I.; Khan, N. U., A nitrogen rich polymer as an organo-catalyst for cycloaddition of CO<sub>2</sub> to epoxides and its application for the synthesis of polyurethane. *Sustainable Energy & Fuels* **2017**, *1* (7), 1620-1629.
52. Verma, S.; Nazish, M.; Kureshy, R. I.; Khan, N. U., Bi-functional heterogeneous iron complexes for catalytic conversion of epoxides to cyclic carbonates and their application in the synthesis of polyurethane. *Sustainable Energy & Fuels* **2018**, *2* (6), 1312-1322.
53. Liang, H.; Wang, J.; Wang, F.; Feng, Y.; Kang, M.; Wang, Z., An efficient heterogeneous LiBr/-Al<sub>2</sub>O<sub>3</sub> catalyst for the cycloaddition of CO<sub>2</sub> with diglycidyl ethers. *Journal of Chemical Technology and Biotechnology* **2018**, *93* (8), 2271-2280.
54. Ngassam Tounzoua, C.; Grignard, B.; Brege, A.; Jerome, C.; Tassaing, T.; Mereau, R.; Detrembleur, C., A Catalytic Domino Approach toward Oxo-Alkyl Carbonates and Polycarbonates from CO<sub>2</sub>, Propargylic Alcohols, and (Mono- and Di-)Alcohols. *ACS Sustainable Chemistry & Engineering* **2020**, *8* (26), 9698-9710.

55. Mesías-Salazar, Á.; Yepes, Y. R.; Martínez, J.; Rojas, R. S., Highly Active CO<sub>2</sub> Fixation into Cyclic Carbonates Catalyzed by Tetranuclear Aluminum Benzodiiimidazole-Diylidene Adducts. *Catalysts* **2020**, *11* (1), 2.
56. Lahkar, S.; Borah, R.; Deori, N.; Brahma, S., (L)-phenylalanine derived Schiff base ligated vanadium(IV) complex as an efficient catalyst for a CO<sub>2</sub> fixation reaction. *Polyhedron* **2020**, *192*, 114848.
57. Hu, Y.; Wei, Z.; Frey, A.; Kubis, C.; Ren, C. Y.; Spannenberg, A.; Jiao, H.; Werner, T., Catalytic, Kinetic, and Mechanistic Insights into the Fixation of CO<sub>2</sub> with Epoxides Catalyzed by Phenol-Functionalized Phosphonium Salts. *ChemSusChem* **2021**, *14* (1), 363-372.
58. Grollier, K.; Vu, N. D.; Onida, K.; Akhdar, A.; Norsic, S.; D'Agosto, F.; Boisson, C.; Duguet, N., A Thermomorphic Polyethylene-Supported Imidazolium Salt for the Fixation of CO<sub>2</sub> into Cyclic Carbonates. *Advanced Synthesis & Catalysis* **2020**, *362* (8), 1696-1705.
59. Fernandez-Baeza, J.; Sanchez-Barba, L. F.; Lara-Sanchez, A.; Sobrino, S.; Martinez-Ferrer, J.; Garces, A.; Navarro, M.; Rodriguez, A. M., NNC-Scorpionate Zirconium-Based Bicomponent Systems for the Efficient CO<sub>2</sub> Fixation into a Variety of Cyclic Carbonates. *Inorganic Chemistry* **2020**, *59* (17), 12422-12430.
60. Pescarmona, P. P., Cyclic carbonates synthesised from CO<sub>2</sub>: Applications, challenges and recent research trends. *Current Opinion in Green and Sustainable Chemistry* **2021**, *29*, 100457.
61. Rehman, A.; Saleem, F.; Javed, F.; Ikhlaiq, A.; Ahmad, S. W.; Harvey, A., Recent advances in the synthesis of cyclic carbonates via CO<sub>2</sub> cycloaddition to epoxides. *Journal of Environmental Chemical Engineering* **2021**, *9* (2), 105113.

62. Froidevaux, V.; Negrell, C.; Caillol, S.; Pascault, J. P.; Boutevin, B., Biobased Amines: From Synthesis to Polymers; Present and Future. *Chemical Reviews* **2016**, *116* (22), 14181-14224.
63. Meier, M. A. R., Plant-Oil-Based Polyamides and Polyurethanes: Toward Sustainable Nitrogen-Containing Thermoplastic Materials. *Macromolecular Rapid Communications* **2019**, *40* (1), 1800524.
64. Tomita, H.; Sanda, F.; Endo, T., Self-polyaddition of six-membered cyclic carbonate having Fmoc-protected amino group: Novel synthetic method of polyhydroxyurethane. *Macromolecules* **2001**, *34* (22), 7601-7607.
65. Tomita, H.; Sanda, F.; Endo, T., Structural analysis of polyhydroxyurethane obtained by polyaddition of bifunctional five-membered cyclic carbonate and diamine based on the model reaction. *Journal of Polymer Science Part a-Polymer Chemistry* **2001**, *39* (6), 851-859.
66. Tomita, H.; Sanda, F.; Endo, T., Polyaddition behavior of bis(five- and six-membered cyclic carbonate)s with diamine. *Journal of Polymer Science Part a-Polymer Chemistry* **2001**, *39* (6), 860-867.
67. Tomita, H.; Sanda, F.; Endo, T., Model reaction for the synthesis of polyhydroxyurethanes from cyclic carbonates with amines: Substituent effect on the reactivity and selectivity of ring-opening direction in the reaction of five-membered cyclic carbonates with amine. *Journal of Polymer Science Part a-Polymer Chemistry* **2001**, *39* (21), 3678-3685.
68. Tomita, H.; Sanda, F.; Endo, T., Polyaddition of bis(seven-membered cyclic carbonate) with diamines: A novel and efficient synthetic method for polyhydroxyurethanes. *Journal of Polymer Science Part a-Polymer Chemistry* **2001**, *39* (23), 4091-4100.

69. Benyahya, S.; Boutevin, B.; Caillol, S.; Lapinte, V.; Habas, J. P., Optimization of the synthesis of polyhydroxyurethanes using dynamic rheometry. *Polymer International* **2012**, *61* (6), 918-925.
70. Nohra, B.; Candy, L.; Blanco, J. F.; Raoul, Y.; Mouloungui, Z., Aminolysis Reaction of Glycerol Carbonate in Organic and Hydroorganic Medium. *Journal of the American Oil Chemists Society* **2012**, *89* (6), 1125-1133.
71. Lambeth, R. H.; Henderson, T. J., Organocatalytic synthesis of (poly)hydroxyurethanes from cyclic carbonates and amines. *Polymer* **2013**, *54* (21), 5568-5573.
72. Blain, M.; Jean-Gerard, L.; Auvergne, R.; Benazet, D.; Caillol, S.; Andrioletti, B., Rational investigations in the ring opening of cyclic carbonates by amines. *Green Chemistry* **2014**, *16* (9), 4286-4291.
73. Levina, M. A.; Krasheninnikov, V. G.; Zabalov, M. V.; Tiger, R. P., Nonisocyanate polyurethanes from amines and cyclic carbonates: Kinetics and mechanism of a model reaction. *Polymer Science Series B* **2014**, *56* (2), 139-147.
74. Lombardo, V. M.; Dhulst, E. A.; Leitsch, E. K.; Wilmot, N.; Heath, W. H.; Gies, A. P.; Miller, M. D.; Torkelson, J. M.; Scheidt, K. A., Cooperative Catalysis of Cyclic Carbonate Ring Opening: Application Towards Non-Isocyanate Polyurethane Materials. *European Journal of Organic Chemistry* **2015**, *2015* (13), 2791-2795.
75. Alves, M.; Mereau, R.; Grignard, B.; Detrembleur, C.; Jerome, C.; Tassaing, T., DFT investigation of the reaction mechanism for the guanidine catalysed ring-opening of cyclic carbonates by aromatic and alkyl-amines. *RSC Advances* **2017**, *7* (31), 18993-19001.

76. Cornille, A.; Blain, M.; Auvergne, R.; Andrioletti, B.; Boutevin, B.; Caillol, S., A study of cyclic carbonate aminolysis at room temperature: effect of cyclic carbonate structures and solvents on polyhydroxyurethane synthesis. *Polymer Chemistry* **2017**, *8* (3), 592-604.
77. Lambeth, R. H.; Mathew, S. M.; Baranoski, M. H.; Housman, K. J.; Tran, B.; Oyler, J. M., Nonisocyanate polyurethanes from six-membered cyclic carbonates: Catalysis and side reactions. *Journal of Applied Polymer Science* **2017**, *134* (45), 44941.
78. Levina, M. A.; Zabalov, M. V.; Krashennnikov, V. G.; Tiger, R. P., Green chemistry of polyurethanes: The catalytic n-butylaminolysis of ethylene carbonate as a model chain-growth reaction in the formation of nonisocyanate polyurethanes. *Polymer Science, Series B* **2017**, *59* (5), 497-505.
79. Perez-Sena, W. Y.; Cai, X. S.; Kebir, N.; Vernieres-Hassimi, L.; Serra, C.; Salmi, T.; Leveneur, S., Aminolysis of cyclic-carbonate vegetable oils as a non-isocyanate route for the synthesis of polyurethane: A kinetic and thermal study. *Chemical Engineering Journal* **2018**, *346*, 271-280.
80. Levina, M. A.; Zabalov, M. V.; Krashennnikov, V. G.; Tiger, R. P., Comparative Reactivity of Cyclocarbonate Groups of Oligomeric Triglycerides Based on Soybean Oil and Model Compounds in the Reactions of Nonisocyanate Urethane Formation. *Polymer Science, Series B* **2018**, *60* (5), 563-570.
81. Tryznowski, M.; Swiderska, A., Novel high reactive bifunctional five- and six-membered bicyclic dicarbonate - synthesis and characterisation. *Rsc Advances* **2018**, *8* (21), 11749-11753.
82. Günther, F.; Batista Simões, M.; Imasato, H.; Pereira Rodrigues-Filho, U., Experimental and theoretical assessment of the aminolysis of cyclo carbonate to form polyhydroxyurethanes. *Materials Today Communications* **2019**, *21*, 100604.

83. Levina, M. A.; Zabalov, M. V.; Krashennnikov, V. G.; Tiger, R. P., Kinetics and quantum chemical aspects of the mechanism of the guanidine (TBD) catalyzed aminolysis of cyclocarbonate containing soybean oil triglycerides as the model process of green chemistry of polyurethanes. *Reaction Kinetics, Mechanisms and Catalysis* **2019**, *129* (1), 65-83.
84. Felipe Guzmán Agudelo, A.; Pérez-Sena, W. Y.; Kebir, N.; Salmi, T.; Alberto Ríos, L.; Leveneur, S., Influence of steric effects on the kinetics of cyclic-carbonate vegetable oils aminolysis. *Chemical Engineering Science* **2020**, *228*, 115954.
85. Dong, W.; Yoshida, Y.; Endo, T., Synthesis of poly(hydroxyurethane) from 5-membered cyclic carbonate under mild conditions in the presence of bicyclic guanidine and their reaction process. *Journal of Polymer Science* **2021**, *59* (6), 502-509.
86. Quienne, B.; Poli, R.; Pinaud, J.; Caillol, S., Enhanced aminolysis of cyclic carbonates by  $\beta$ -hydroxylamines for the production of fully biobased polyhydroxyurethanes. *Green Chemistry* **2021**, *23* (4), 1678-1690.
87. Dong, T.; Dheressa, E.; Wiatrowski, M.; Pereira, A. P.; Zeller, A.; Laurens, L. M. L.; Pienkos, P. T., Assessment of Plant and Microalgal Oil-Derived Nonisocyanate Polyurethane Products for Potential Commercialization. *ACS Sustainable Chemistry & Engineering* **2021**, *9* (38), 12858-12869.
88. Ecochard, Y.; Caillol, S., Hybrid polyhydroxyurethanes: How to overcome limitations and reach cutting edge properties? *European Polymer Journal* **2020**, *137*, 109915.
89. Lambeth, R. H., Progress in hybrid non-isocyanate polyurethanes. *Polymer International* **2020**, *70* (6), 696-700.
90. Bizet, B.; Grau, É.; Cramail, H.; Asua, J. M., Water-based non-isocyanate polyurethane-ureas (NIPUUs). *Polymer Chemistry* **2020**, *11* (23), 3786-3799.

91. Gomez-Lopez, A.; Elizalde, F.; Calvo, I.; Sardon, H., Trends in non-isocyanate polyurethane (NIPU) development. *Chemical Communications* **2021**, 57 (92), 12254-12265.
92. Besse, V.; Camara, F.; Mechin, F.; Fleury, E.; Caillol, S.; Pascault, J. P.; Boutevin, B., How to explain low molar masses in PolyHydroxyUrethanes (PHUs). *European Polymer Journal* **2015**, 71, 1-11.
93. Blain, M.; Cornille, A.; Boutevin, B.; Auvergne, E.; Benazet, D.; Andrioletti, B.; Caillol, S., Hydrogen bonds prevent obtaining high molar mass PHUs. *Journal of Applied Polymer Science* **2017**, 134 (45), 44958.
94. Khatoon, H.; Iqbal, S.; Irfan, M.; Darda, A.; Rawat, N. K., A review on the production, properties and applications of non-isocyanate polyurethane: A greener perspective. *Progress in Organic Coatings* **2021**, 154, 106124.
95. Gomez-Lopez, A.; Panchireddy, S.; Grignard, B.; Calvo, I.; Jerome, C.; Detrembleur, C.; Sardon, H., Poly(hydroxyurethane) Adhesives and Coatings: State-of-the-Art and Future Directions. *ACS Sustainable Chemistry & Engineering* **2021**, 9 (29), 9541-9562.
96. Tai, N. L.; Ghasemlou, M.; Adhikari, R.; Adhikari, B., Starch-based isocyanate- and non-isocyanate polyurethane hybrids: A review on synthesis, performance and biodegradation. *Carbohydrate Polymers* **2021**, 265, 118029.
97. Stachak, P.; Lukaszewska, I.; Hebda, E.; Pielichowski, K., Recent Advances in Fabrication of Non-Isocyanate Polyurethane-Based Composite Materials. *Materials (Basel)* **2021**, 14 (13), 3497.
98. Tamami, B.; Sohn, S.; Wilkes, G. L., Incorporation of carbon dioxide into soybean oil and subsequent preparation and studies of nonisocyanate polyurethane networks. *Journal of Applied Polymer Science* **2004**, 92 (2), 883-891.

99. Baumann, H.; Bühler, M.; Fochem, H.; Hirsinger, F.; Zobelein, H.; Falbe, J., Natural Fats and Oils-Renewable Raw Materials for the Chemical Industry. *Angewandte Chemie International Edition in English* **1988**, *27* (1), 41-62.
100. Javni, I.; Hong, D. P.; Petrovic, Z. S., Soy-based polyurethanes by nonisocyanate route. *Journal of Applied Polymer Science* **2008**, *108* (6), 3867-3875.
101. Li, Z.; Zhao, Y.; Yan, S.; Wang, X.; Kang, M.; Wang, J.; Xiang, H., Catalytic synthesis of carbonated soybean oil. *Catalysis Letters* **2008**, *123* (3-4), 246-251.
102. Turunc, O.; Kayaman-Apohan, N.; Kahraman, M. V.; Menciloglu, Y.; Gungor, A., Nonisocyanate based polyurethane/silica nanocomposites and their coating performance. *Journal of Sol-Gel Science and Technology* **2008**, *47* (3), 290-299.
103. Boyer, A.; Cloutet, E.; Tassaing, T.; Gadenne, B.; Alfos, C.; Cramail, H., Solubility in CO<sub>2</sub> and carbonation studies of epoxidized fatty acid diesters: towards novel precursors for polyurethane synthesis. *Green Chemistry* **2010**, *12* (12), 2205-2213.
104. Bähr, M.; Mülhaupt, R., Linseed and soybean oil-based polyurethanes prepared via the non-isocyanate route and catalytic carbon dioxide conversion. *Green Chemistry* **2012**, *14* (2), 483-489.
105. Javni, I.; Hong, D. P.; Petrovic, Z. S., Polyurethanes from Soybean Oil, Aromatic, and Cycloaliphatic Diamines by NonIsocyanate Route. *Journal of Applied Polymer Science* **2013**, *128* (1), 566-571.
106. Hambali, R. A.; Mohd, A. F.; Samsuri, A. In *Synthesis and characterization of non-isocyanate polyurethane from epoxidized linoleic acid - A preliminary study*, International Polymer Technology Conference and Exhibition 2013, IPTCE 2013, April 16, 2013 - April 18, 2013, Selangor, Malaysia, Trans Tech Publications Ltd: Selangor, Malaysia, 2013; pp 73-79.

107. Camara, F.; Benyahya, S.; Besse, V.; Boutevin, G.; Auvergne, R.; Boutevin, B.; Caillol, S., Reactivity of secondary amines for the synthesis of non-isocyanate polyurethanes. *European Polymer Journal* **2014**, *55*, 17-26.
108. Carre, C.; Bonnet, L.; Averous, L., Original biobased nonisocyanate polyurethanes: solvent- and catalyst-free synthesis, thermal properties and rheological behaviour. *Rsc Advances* **2014**, *4* (96), 54018-54025.
109. Kathalewar, M.; Sabnis, A.; D'Mello, D., Isocyanate free polyurethanes from new CNSL based bis-cyclic carbonate and its application in coatings. *European Polymer Journal* **2014**, *57*, 99-108.
110. Mahendran, A. R.; Aust, N.; Wuzella, G.; Müller, U.; Kandelbauer, A., Bio-Based Non-Isocyanate Urethane Derived from Plant Oil. *Journal of Polymers and the Environment* **2012**, *20* (4), 926-931.
111. Mahendran, A. R.; Wuzella, G.; Aust, N.; Muller, U., Synthesis, characterization, and properties of isocyanate-free urethane coatings from renewable resources. *Journal of Coatings Technology and Research* **2014**, *11* (3), 329-339.
112. Maisonneuve, L.; More, A. S.; Foltran, S.; Alfos, C.; Robert, F.; Landais, Y.; Tassaing, T.; Grau, E.; Cramail, H., Novel green fatty acid-based bis-cyclic carbonates for the synthesis of isocyanate-free poly(hydroxyurethane amide)s. *RSC Advances* **2014**, *4* (49), 25795-25803.
113. Maisonneuve, L.; Wirotius, A. L.; Alfos, C.; Grau, E.; Cramail, H., Fatty acid-based (bis) 6-membered cyclic carbonates as efficient isocyanate free poly(hydroxyurethane) precursors. *Polymer Chemistry* **2014**, *5* (21), 6142-6147.
114. Jalilian, S.; Yeganeh, H., Preparation and properties of biodegradable polyurethane networks from carbonated soybean oil. *Polymer Bulletin* **2015**, *72* (6), 1379-1392.

115. Bigot, S.; Daghrir, M.; Mhanna, A.; Boni, G.; Pourchet, S.; Lecamp, L.; Plasseraud, L., Undecylenic acid: A tunable bio-based synthon for materials applications. *European Polymer Journal* **2016**, *74*, 26-37.
116. Carré, C.; Zoccheddu, H.; Delalande, S.; Pichon, P.; Avérous, L., Synthesis and characterization of advanced biobased thermoplastic nonisocyanate polyurethanes, with controlled aromatic-aliphatic architectures. *European Polymer Journal* **2016**, *84*, 759-769.
117. Duval, C.; Kebir, N.; Jauseau, R.; Burel, F., Organocatalytic synthesis of novel renewable non-isocyanate polyhydroxyurethanes. *Journal of Polymer Science Part a-Polymer Chemistry* **2016**, *54* (6), 758-764.
118. Poussard, L.; Mariage, J.; Grignard, B.; Detrembleur, C.; Jérôme, C.; Calberg, C.; Heinrichs, B.; De Winter, J.; Gerbaux, P.; Raquez, J. M.; Bonnaud, L.; Dubois, P., Non-Isocyanate Polyurethanes from Carbonated Soybean Oil Using Monomeric or Oligomeric Diamines To Achieve Thermosets or Thermoplastics. *Macromolecules* **2016**, *49* (6), 2162-2171.
119. Samanta, S.; Selvakumar, S.; Bahr, J.; Wickramaratne, D. S.; Sibi, M.; Chisholm, B. J., Synthesis and Characterization of Polyurethane Networks Derived from Soybean-Oil-Based Cyclic Carbonates and Bioderivable Diamines. *ACS Sustainable Chemistry & Engineering* **2016**, *4* (12), 6551-6561.
120. Cheng, C. J.; Li, Y. P.; Zhang, X.; Li, J., Eugenol-based non-isocyanate polyurethane and polythiourethane. *Iranian Polymer Journal* **2017**, *26* (11), 821-831.
121. Haniffa, M. A. C. M.; Ching, Y. C.; Chuah, C. H.; Kuan, Y. C.; Liu, D.-S.; Liou, N.-S., Synthesis, characterization and the solvent effects on interfacial phenomena of jatropha curcas oil based non-isocyanate polyurethane. *Polymers* **2017**, *9* (5), 162.

122. Doley, S.; Agarwal, V.; Bora, A.; Borah, D.; Dolui, S. K., Development of sunflower oil-based nonisocyanate polyurethane/multiwalled carbon nanotube composites with improved physico-chemical and microwave absorption properties. *Polymer Composites* **2018**, *40* (S2), E1120-E1130.
123. Doley, S.; Dolui, S. K., Solvent and catalyst-free synthesis of sunflower oil based polyurethane through non-isocyanate route and its coatings properties. *European Polymer Journal* **2018**, *102*, 161-168.
124. Doley, S.; Sarmah, A.; Sarkar, C.; Dolui, S. K., In situ development of bio-based polyurethane-blend-epoxy hybrid materials and their nanocomposites with modified graphene oxide via non-isocyanate route. *Polymer International* **2018**, *67* (8), 1062-1069.
125. Farhadian, A.; Ahmadi, A.; Omrani, I.; Miyardan, A. B.; Varfolomeev, M. A.; Nabid, M. R., Synthesis of fully bio-based and solvent free non-isocyanate poly (ester amide/urethane) networks with improved thermal stability on the basis of vegetable oils. *Polymer Degradation and Stability* **2018**, *155*, 111-121.
126. He, X.; Wu, G.; Xu, L.; Yan, J.; Yan, Y., Lipase-catalyzed synthesis, properties characterization, and application of bio-based dimer acid cyclocarbonate. *Polymers* **2018**, *10* (3), 262.
127. Malik, M.; Kaur, R., Synthesis of NIPU by the carbonation of canola oil using highly efficient 5,10,15-tris(pentafluorophenyl)corrolato-manganese(III) complex as novel catalyst. *Polymers for Advanced Technologies* **2018**, *29* (3), 1078-1085.
128. Panchireddy, S.; Grignard, B.; Thomassin, J. M.; Jerome, C.; Detrembleur, C., Bio-based poly(hydroxyurethane) glues for metal substrates. *Polymer Chemistry* **2018**, *9* (19), 2650-2659.

129. Farid, M. E.; El-Sockary, M. A.; El-Saeed, A. M.; Hashem, A. I.; Abo Elenien, O. M.; Selim, M. S.; Park, S. E., An eco-friendly non-isocyanate polyurethane treated by CO<sub>2</sub> as flame retardant nanocomposite coating/ZrO<sub>2</sub>@SiO<sub>2</sub>. *Materials Research Express* **2019**, *6* (6), 065042.
130. Gharibi, R.; Yeganeh, H.; Kazemi, S., Green and non-leaching anti-bacterial and cytocompatible coating with build-in quaternary ammonium salt derived from methoxysilane functionalized soybean oil. *Materials Science and Engineering: C* **2019**, *99*, 887-899.
131. Hu, S.; Chen, X.; Torkelson, J. M., Biobased Reprocessable Polyhydroxyurethane Networks: Full Recovery of Crosslink Density with Three Concurrent Dynamic Chemistries. *ACS Sustainable Chemistry & Engineering* **2019**, *7* (11), 10025-10034.
132. Mokhtari, C.; Malek, F.; Manseri, A.; Caillol, S.; Negrell, C., Reactive jojoba and castor oils-based cyclic carbonates for biobased polyhydroxyurethanes. *European Polymer Journal* **2019**, *113*, 18-28.
133. Quérette, T.; Fleury, E.; Sintès-Zydowicz, N., Non-isocyanate polyurethane nanoparticles prepared by nanoprecipitation. *European Polymer Journal* **2019**, *114*, 434-445.
134. Bizet, B.; Grau, E.; Cramail, H.; Asua, J. M., Volatile Organic Compound-Free Synthesis of Waterborne Poly(hydroxy urethane)–(Meth)acrylic Hybrids by Miniemulsion Polymerization. *ACS Applied Polymer Materials* **2020**, *2* (9), 4016-4025.
135. Das, M.; Mandal, B.; Katiyar, V., Environment-friendly synthesis of sustainable chitosan-based nonisocyanate polyurethane: A biobased polymeric film. *Journal of Applied Polymer Science* **2020**, *137* (36), 49050.
136. Gomez-Lopez, A.; Grignard, B.; Calvo, I.; Detrembleur, C.; Sardón, H., Monocomponent Non-Isocyanate Polyurethane Adhesives Based on a Sol-Gel Process. *ACS Applied Polymer Materials* **2020**, *2* (5), 1839-1847.

137. Laprise, C. M.; Hawboldt, K. A.; Kerton, F. M.; Kozak, C. M., Synthesis of a Renewable, Waste-Derived Nonisocyanate Polyurethane from Fish Processing Discards and Cashew Nutshell-Derived Amines. *Macromolecular Rapid Communications* **2021**, *42* (3), 2000339.
138. Mokhtari, C.; Malek, F., New bio-based polyhydroxyurethane material. *Materials Today: Proceedings* **2020**, *31*, S12-S15.
139. Doley, S.; Bora, A.; Saikia, P.; Ahmed, S.; Dolui, S. K., Blending of cyclic carbonate based on soybean oil and glycerol: a non-isocyanate approach towards the synthesis of polyurethane with high performance. *Journal of Polymer Research* **2021**, *28* (5), 1-9.
140. Gholami, H.; Yeganeh, H., Soybean oil-derived non-isocyanate polyurethanes containing azetidinium groups as antibacterial wound dressing membranes. *European Polymer Journal* **2021**, *142*, 110142.
141. Hambali, R. A.; Faiza, M. A.; Zuliahani, A., Non-Isocyanate Polyurethane (NIPU) based on Rubber Seed Oil Synthesized via Low-Pressured Carbonization Reaction. *Sains Malaysiana* **2021**, *50* (8), 2407-2417.
142. Liu, X.; Yang, X.; Wang, S.; Wang, S.; Wang, Z.; Liu, S.; Xu, X.; Liu, H.; Song, Z., Fully Bio-Based Polyhydroxyurethanes with a Dynamic Network from a Terpene Derivative and Cyclic Carbonate Functional Soybean Oil. *ACS Sustainable Chemistry & Engineering* **2021**, *9* (11), 4175-4184.
143. Ren, F.-Y.; You, F.; Gao, S.; Xie, W.-H.; He, L.-N.; Li, H.-R., Oligomeric ricinoleic acid synthesis with a recyclable catalyst and application to preparing non-isocyanate polyhydroxyurethane. *European Polymer Journal* **2021**, *153*, 110501.
144. Sessini, V.; Thai, C. N.; Amorín, H.; Jiménez, R.; Samuel, C.; Caillol, S.; Cornil, J.; Hoyas, S.; Barrau, S.; Dubois, P.; Leclère, P.; Raquez, J.-M., Solvent-Free Design of Biobased

Non-isocyanate Polyurethanes with Ferroelectric Properties. *ACS Sustainable Chemistry & Engineering* **2021**, 9 (44), 14946-14958.

145. Yang, X.; Ren, C.; Liu, X.; Sun, P.; Xu, X.; Liu, H.; Shen, M.; Shang, S.; Song, Z., Recyclable non-isocyanate polyurethanes containing a dynamic covalent network derived from epoxy soybean oil and CO<sub>2</sub>. *Materials Chemistry Frontiers* **2021**, 5 (16), 6160-6170.

146. Yang, X.; Wang, S.; Liu, X.; Huang, Z.; Huang, X.; Xu, X.; Liu, H.; Wang, D.; Shang, S., Preparation of non-isocyanate polyurethanes from epoxy soybean oil: dual dynamic networks to realize self-healing and reprocessing under mild conditions. *Green Chemistry* **2021**, 23 (17), 6349-6355.

147. Bähr, M.; Bitto, A.; Mülhaupt, R., Cyclic limonene dicarbonate as a new monomer for non-isocyanate oligo- and polyurethanes (NIPU) based upon terpenes. *Green Chemistry* **2012**, 14 (5), 1447-1454.

148. Liu, G. F.; Wu, G. M.; Chen, J.; Huo, S. P.; Jin, C.; Kong, Z. W., Synthesis and properties of POSS-containing gallic acid-based non-isocyanate polyurethanes coatings. *Polymer Degradation and Stability* **2015**, 121, 247-252.

149. Liu, G.; Wu, G.; Chen, J.; Kong, Z., Synthesis, modification and properties of rosin-based non-isocyanate polyurethanes coatings. *Progress in Organic Coatings* **2016**, 101, 461-467.

150. Janvier, M.; Ducrot, P. H.; Allais, F., Isocyanate-Free Synthesis and Characterization of Renewable Poly(hydroxy)urethanes from Syringaresinol. *ACS Sustainable Chemistry & Engineering* **2017**, 5 (10), 8648-8656.

151. Menard, R.; Caillol, S.; Allais, F., Chemo-Enzymatic Synthesis and Characterization of Renewable Thermoplastic and Thermoset Isocyanate-Free Poly(hydroxy)urethanes from Ferulic Acid Derivatives. *ACS Sustainable Chemistry & Engineering* **2017**, 5 (2), 1446-1456.

152. Schimpf, V.; Ritter, B. S.; Weis, P.; Parison, K.; Mulhaupt, R., High Purity Limonene Dicarboxylate as Versatile Building Block for Sustainable Non-Isocyanate Polyhydroxyurethane Thermosets and Thermoplastics. *Macromolecules* **2017**, *50* (3), 944-955.
153. Esmacili, N.; Zohuriaan-Mehr, M. J.; Salimi, A.; Vafayan, M.; Meyer, W., Tannic acid derived non-isocyanate polyurethane networks: Synthesis, curing kinetics, antioxidizing activity and cell viability. *Thermochimica Acta* **2018**, *664*, 64-72.
154. Santiago-Medina, F. J.; Basso, M. C.; Pizzi, A.; Delmotte, L., Polyurethanes from Kraft Lignin without Using Isocyanates. *Journal of Renewable Materials* **2018**, *6* (4), 413-425.
155. Mimini, V.; Amer, H.; Hettegger, H.; Bacher, M.; Gebauer, I.; Bischof, R.; Fackler, K.; Potthast, A.; Rosenau, T., Lignosulfonate-based polyurethane materials via cyclic carbonates: preparation and characterization. *Holzforschung* **2019**, *74* (2), 203-211.
156. Błażek, K.; Kasprzyk, P.; Datta, J., Diamine derivatives of dimerized fatty acids and bio-based polyether polyol as sustainable platforms for the synthesis of non-isocyanate polyurethanes. *Polymer* **2020**, *205*, 122768.
157. Capar, Ö.; Tabatabai, M.; Klee, J. E.; Worm, M.; Hartmann, L.; Ritter, H., Fast curing of polyhydroxyurethanes via ring opening polyaddition of low viscosity cyclic carbonates and amines. *Polymer Chemistry* **2020**, *11* (43), 6964-6970.
158. Chen, X.; Xi, X.; Pizzi, A.; Fredon, E.; Zhou, X.; Li, J.; Gerardin, C.; Du, G., Preparation and Characterization of Condensed Tannin Non-Isocyanate Polyurethane (NIPU) Rigid Foams by Ambient Temperature Blowing. *Polymers (Basel)* **2020**, *12* (4), 750.
159. Chen, X.; Li, J.; Xi, X.; Pizzi, A.; Zhou, X.; Fredon, E.; Du, G.; Gerardin, C., Condensed tannin-glucose-based NIPU bio-foams of improved fire retardancy. *Polymer Degradation and Stability* **2020**, *175*, 109121.

160. Chen, H.; Chauhan, P.; Yan, N., “Barking” up the right tree: biorefinery from waste stream to cyclic carbonate with immobilization of CO<sub>2</sub> for non-isocyanate polyurethanes. *Green Chemistry* **2020**, *22* (20), 6874-6888.
161. Sternberg, J.; Pilla, S., Materials for the biorefinery: high bio-content, shape memory Kraft lignin-derived non-isocyanate polyurethane foams using a non-toxic protocol. *Green Chemistry* **2020**, *22* (20), 6922-6935.
162. Zhang, C.; Huang, K.-C.; Wang, H.; Zhou, Q., Anti-corrosion non-isocyanate polyurethane polysiloxane organic/inorganic hybrid coatings. *Progress in Organic Coatings* **2020**, *148*, 105855.
163. Chen, X.; Pizzi, A.; Essawy, H.; Fredon, E.; Gerardin, C.; Guigo, N.; Sbirrazzuoli, N., Non-Furanic Humins-Based Non-Isocyanate Polyurethane (NIPU) Thermoset Wood Adhesives. *Polymers (Basel)* **2021**, *13* (3), 372.
164. Zhao, W.; Liang, Z.; Feng, Z.; Xue, B.; Xiong, C.; Duan, C.; Ni, Y., New Kind of Lignin/Polyhydroxyurethane Composite: Green Synthesis, Smart Properties, Promising Applications, and Good Reprocessability and Recyclability. *ACS Applied Materials & Interfaces* **2021**, *13* (24), 28938-28948.
165. Benyahya, S.; Desroches, M.; Auvergne, R.; Carlotti, S.; Caillol, S.; Boutevin, B., Synthesis of glycerin carbonate-based intermediates using thiol-ene chemistry and isocyanate free polyhydroxyurethanes therefrom. *Polymer Chemistry* **2011**, *2* (11), 2661-2667.
166. Fleischer, M.; Blattmann, H.; Mülhaupt, R., Glycerol-, pentaerythritol- and trimethylolpropane-based polyurethanes and their cellulose carbonate composites prepared via the non-isocyanate route with catalytic carbon dioxide fixation. *Green Chemistry* **2013**, *15* (4), 934-942.

167. Carre, C.; Bonnet, L.; Averous, L., Solvent- and catalyst-free synthesis of fully biobased nonisocyanate polyurethanes with different macromolecular architectures. *RSC Advances* **2015**, *5* (121), 100390-100400.
168. Tryznowski, M.; Swiderska, A.; Zolek-Tryznowska, Z.; Golofit, T.; Parzuchowski, P. G., Facile route to multigram synthesis of environmentally friendly non-isocyanate polyurethanes. *Polymer* **2015**, *80*, 228-236.
169. van Velthoven, J. L. J.; Gootjes, L.; van Es, D. S.; Noordover, B. A. J.; Meuldijk, J., Poly(hydroxy urethane)s based on renewable diglycerol dicarbonate. *European Polymer Journal* **2015**, *70*, 125-135.
170. Blattmann, H.; Lauth, M.; Mulhaupt, R., Flexible and Bio-Based Nonisocyanate Polyurethane (NIPU) Foams. *Macromolecular Materials and Engineering* **2016**, *301* (8), 944-952.
171. Blattmann, H.; Mulhaupt, R., Multifunctional POSS Cyclic Carbonates and Non-Isocyanate Polyhydroxyurethane Hybrid Materials. *Macromolecules* **2016**, *49* (3), 742-751.
172. Blattmann, H.; Mulhaupt, R., Multifunctional beta-amino alcohols as bio-based amine curing agents for the isocyanate- and phosgene-free synthesis of 100% bio-based polyhydroxyurethane thermosets. *Green Chemistry* **2016**, *18* (8), 2406-2415.
173. Lamarzelle, O.; Durand, P. L.; Wirotius, A. L.; Chollet, G.; Grau, E.; Cramail, H., Activated lipidic cyclic carbonates for non-isocyanate polyurethane synthesis. *Polymer Chemistry* **2016**, *7* (7), 1439-1451.
174. Hibert, G.; Lamarzelle, O.; Maisonneuve, L.; Grau, E.; Cramail, H., Bio-based aliphatic primary amines from alcohols through the Nitrile route towards non-isocyanate polyurethanes. *European Polymer Journal* **2016**, *82*, 114-121.

175. Nohra, B.; Candy, L.; Blanco, J. F.; Raoul, Y.; Mouloungui, Z., Synthesis of High-Molecular-Weight Multifunctional Glycerol Polyhydroxyurethanes PHUs. *Molecules* **2016**, *21* (9), 1220.
176. Rix, E.; Grau, E.; Chollet, G.; Cramail, H., Synthesis of fatty acid-based non-isocyanate polyurethanes, NIPUs, in bulk and mini-emulsion. *European Polymer Journal* **2016**, *84*, 863-872.
177. Schmidt, S.; Ritter, B. S.; Kratzert, D.; Bruchmann, B.; Mulhaupt, R., Isocyanate-Free Route to Poly(carbohydrate-urethane) Thermosets and 100% Bio-Based Coatings Derived from Glycerol Feedstock. *Macromolecules* **2016**, *49* (19), 7268-7276.
178. He, X.; Xu, X.; Wan, Q.; Bo, G.; Yan, Y., Synthesis and Characterization of Dimmer-Acid-Based Nonisocyanate Polyurethane and Epoxy Resin Composite. *Polymers (Basel)* **2017**, *9* (12), 649.
179. Karami, Z.; Zohuriaan-Mehr, M. J.; Rostami, A., Bio-based thermo-healable non-isocyanate polyurethane DA network in comparison with its epoxy counterpart. *Journal of CO2 Utilization* **2017**, *18*, 294-302.
180. Lamarzelle, O.; Hibert, G.; Lecommandoux, S.; Grau, E.; Cramail, H., A thioglycerol route to bio-based bis-cyclic carbonates: poly(hydroxyurethane) preparation and post-functionalization. *Polymer Chemistry* **2017**, *8* (22), 3438-3447.
181. Bossion, A.; Aguirresarobe, R. H.; Irusta, L.; Taton, D.; Cramail, H.; Grau, E.; Mecerreyes, D.; Su, C.; Liu, G. M.; Muller, A. J.; Sardon, H., Unexpected Synthesis of Segmented Poly(hydroxyurea-urethane)s from Dicyclic Carbonates and Diamines by Organocatalysis. *Macromolecules* **2018**, *51* (15), 5556-5566.

182. Bossion, A.; Olazabal, I.; Aguirresarobe, R. H.; Marina, S.; Martín, J.; Irusta, L.; Taton, D.; Sardon, H., Synthesis of self-healable waterborne isocyanate-free poly(hydroxyurethane)-based supramolecular networks by ionic interactions. *Polymer Chemistry* **2019**, *10* (21), 2723-2733.
183. Karami, Z.; Kabiri, K.; Zohuriaan-Mehr, M. J., Non-isocyanate polyurethane thermoset based on a bio-resourced star-shaped epoxy macromonomer in comparison with a cyclocarbonate fossil-based epoxy resin: A preliminary study on thermo-mechanical and antibacterial properties. *Journal of CO2 Utilization* **2019**, *34*, 558-567.
184. Magliozzi, F.; Chollet, G.; Grau, E.; Cramail, H., Benefit of the Reactive Extrusion in the Course of Polyhydroxyurethanes Synthesis by Aminolysis of Cyclic Carbonates. *ACS Sustainable Chemistry & Engineering* **2019**, *7* (20), 17282-17292.
185. Peixoto, C.; Soares, A. M. S.; Araujo, A.; Olsen, B. D.; Machado, A. V., Non-isocyanate urethane linkage formation using l-lysine residues as amine sources. *Amino Acids* **2019**, *51* (9), 1323-1335.
186. Schimpf, V.; Asmacher, A.; Fuchs, A.; Bruchmann, B.; Mülhaupt, R., Polyfunctional Acrylic Non-isocyanate Hydroxyurethanes as Photocurable Thermosets for 3D Printing. *Macromolecules* **2019**, *52* (9), 3288-3297.
187. Magliozzi, F.; Scali, A.; Chollet, G.; Montarnal, D.; Grau, E.; Cramail, H., Hydrolyzable Biobased Polyhydroxyurethane Networks with Shape Memory Behavior at Body Temperature. *ACS Sustainable Chemistry & Engineering* **2020**, *8* (24), 9125-9135.
188. Wang, D.; Chen, S.; Zhao, J.; Zhang, Z., Synthesis and characterization of self-healing cross-linked non-isocyanate polyurethanes based on Diels-Alder reaction with unsaturated polyester. *Materials Today Communications* **2020**, *23*, 101138.

189. Wang, D. w.; Chen, S.; Zhao, J. b.; Zhang, Z. y.; Zhang, J. y., Synthesis and properties of self-healing cross-linked nonisocyanate polyurethanes from biobased diglycerol bis(cyclic carbonate). *Polymer Engineering & Science* **2020**, *61* (2), 497-505.
190. Younes, G. R.; Price, G.; Dandurand, Y.; Maric, M., Study of Moisture-Curable Hybrid NIPUs Based on Glycerol with Various Diamines: Emergent Advantages of PDMS Diamines. *ACS Omega* **2020**, *5* (47), 30657-30670.
191. Zhang, C.; Wang, H.; Zhou, Q., Waterborne isocyanate-free polyurethane epoxy hybrid coatings synthesized from sustainable fatty acid diamine. *Green Chem.* **2020**, *22* (4), 1329-1337.
192. Błażek, K.; Beneš, H.; Walterová, Z.; Abbrent, S.; Eceiza, A.; Calvo-Correas, T.; Datta, J., Synthesis and structural characterization of bio-based bis(cyclic carbonate)s for the preparation of non-isocyanate polyurethanes. *Polymer Chemistry* **2021**, *12* (11), 1643-1652.
193. Buchheit, H.; Bruchmann, B.; Stoll, K.; Mülhaupt, R., Functionalized acrylic polyhydroxy urethanes as molecular tool box for photocurable thermosets and 3D printing. *Journal of Polymer Science* **2021**, *59* (10), 882-892.
194. Pronoitis, C.; Hakkarainen, M.; Odelius, K., Solubility-governed architectural design of polyhydroxyurethane-graft-poly( $\epsilon$ -caprolactone) copolymers. *Polymer Chemistry* **2021**, *12* (2), 196-208.
195. Younes, G. R.; Maric, M., Increasing the Hydrophobicity of Hybrid Poly(propylene glycol)-Based Polyhydroxyurethanes by Capping with Hydrophobic Diamine. *Industrial & Engineering Chemistry Research* **2021**, *60* (22), 8159-8171.
196. Younes, G. R.; Marić, M., Bio-based Thermoplastic Polyhydroxyurethanes Synthesized from the Terpolymerization of a Dicarboxylate and Two Diamines: Design, Rheology, and Application in Melt Blending. *Macromolecules* **2021**, *54* (21), 10189-10202.

197. Besse, V.; Auvergne, R.; Carlotti, S.; Boutevin, G.; Otazaghine, B.; Caillol, S.; Pascault, J. P.; Boutevin, B., Synthesis of isosorbide based polyurethanes: An isocyanate free method. *Reactive & Functional Polymers* **2013**, *73* (3), 588-594.
198. Mazurek-Budzyska, M. M.; Rokicki, G.; Drzewicz, M.; Guka, P. A.; Zachara, J., Bis(cyclic carbonate) based on D-mannitol, D-sorbitol and di(trimethylolpropane) in the synthesis of non-isocyanate poly(carbonate-urethane)s. *European Polymer Journal* **2016**, *84*, 799-811.
199. Ma, Z. Z.; Li, C.; Fan, H.; Wan, J. T.; Luo, Y. W.; Li, B. G., Polyhydroxyurethanes (PHUs) Derived from Diphenolic Acid and Carbon Dioxide and Their Application in Solvent- and Water-Borne PHU Coatings. *Industrial & Engineering Chemistry Research* **2017**, *56* (47), 14089-14100.
200. Schmidt, S.; Gatti, F. J.; Luitz, M.; Ritter, B. S.; Bruchmann, B.; Mulhaupt, R., Erythritol Dicarboxylate as Intermediate for Solvent- and Isocyanate-Free Tailoring of Bio-Based Polyhydroxyurethane Thermoplastics and Thermoplastic Elastomers. *Macromolecules* **2017**, *50* (6), 2296-2303.
201. Schmidt, S.; Goppert, N. E.; Bruchmann, B.; Mulhaupt, R., Liquid sorbitol ether carbonate as intermediate for rigid and segmented non-isocyanate polyhydroxyurethane thermosets. *European Polymer Journal* **2017**, *94*, 136-142.
202. Zhang, L.; Luo, X. L.; Qin, Y. S.; Li, Y. B., A novel 2,5-furandicarboxylic acid-based bis(cyclic carbonate) for the synthesis of biobased non-isocyanate polyurethanes. *RSC Advances* **2017**, *7* (1), 37-46.

203. Clark, J. H.; Farmer, T. J.; Ingram, I. D. V.; Lie, Y.; North, M., Renewable Self-Blowing Non-Isocyanate Polyurethane Foams from Lysine and Sorbitol. *European Journal of Organic Chemistry* **2018**, *2018* (31), 4265-4271.
204. Furtwengler, P.; Averous, L., From D-sorbitol to five-membered bis(cyclo-carbonate) as a platform molecule for the synthesis of different original biobased chemicals and polymers. *Scientific Reports* **2018**, *8* (1), 9134.
205. Wu, Z.; Dai, J.; Tang, L.; Qu, J., Sorbitol-based aqueous cyclic carbonate dispersion for waterborne nonisocyanate polyurethane coatings via an environment-friendly route. *Journal of Coatings Technology and Research* **2018**, *16* (3), 721-732.
206. Xi, X. D.; Pizzi, A.; Delmotte, L., Isocyanate-Free Polyurethane Coatings and Adhesives from Mono- and Di-Saccharides. *Polymers* **2018**, *10* (4), 402.
207. Yu, A. Z.; Setien, R. A.; Sahouani, J. M.; Docken Jr, J.; Webster, D. C., Catalyzed non-isocyanate polyurethane (NIPU) coatings from bio-based poly(cyclic carbonates). *Journal of Coatings Technology and Research* **2018**, *16* (1), 41-57.
208. Xi, X.; Pizzi, A.; Gerardin, C.; Du, G., Glucose-Biobased Non-Isocyanate Polyurethane Rigid Foams. *Journal of Renewable Materials* **2019**, *7* (3), 301-312.
209. Xi, X.; Pizzi, A.; Gerardin, C.; Lei, H.; Chen, X.; Amirou, S., Preparation and Evaluation of Glucose Based Non-Isocyanate Polyurethane Self-Blowing Rigid Foams. *Polymers (Basel)* **2019**, *11* (11), 1802.
210. Xi, X.; Wu, Z.; Pizzi, A.; Gerardin, C.; Lei, H.; Zhang, B.; Du, G., Non-isocyanate polyurethane adhesive from sucrose used for particleboard. *Wood Science and Technology* **2019**, *53* (2), 393-405.

211. Choong, P. S.; Chong, N. X.; Wai Tam, E. K.; Seayad, A. M.; Seayad, J.; Jana, S., Biobased Nonisocyanate Polyurethanes as Recyclable and Intrinsic Self-Healing Coating with Triple Healing Sites. *ACS Macro Letters* **2021**, *10* (5), 635-641.
212. Jana, S.; Seayad, J.; Seayad, A. M.; Choong, P. S. A Crosslinked Polymer and Related Methods Thereof. US Patent Application 17/043,448, 2021.
213. Younes, G. R.; Maric, M., Moisture Curable Hybrid Polyhydroxyurethanes from Sugar-Derived Dicarbonates. *Macromolecular Materials and Engineering* **2021**, *306* (4), 2000715.
214. Lee, A.; Deng, Y., Green polyurethane from lignin and soybean oil through non-isocyanate reactions. *European Polymer Journal* **2015**, *63*, 67-73.
215. Rehman, A.; López Fernández, A. M.; Gunam Resul, M. F. M.; Harvey, A., Highly selective, sustainable synthesis of limonene cyclic carbonate from bio-based limonene oxide and CO<sub>2</sub>: A kinetic study. *Journal of CO<sub>2</sub> Utilization* **2019**, *29*, 126-133.
216. Stadler, B. M.; Wulf, C.; Werner, T.; Tin, S.; de Vries, J. G., Catalytic Approaches to Monomers for Polymers Based on Renewables. *ACS Catalysis* **2019**, *9* (9), 8012-8067.
217. Maltby, K. A.; Hutchby, M.; Plucinski, P.; Davidson, M. G.; Hintermair, U., Selective Catalytic Synthesis of 1,2- and 8,9-Cyclic Limonene Carbonates as Versatile Building Blocks for Novel Hydroxyurethanes. *Chemistry* **2020**, *26* (33), 7405-7415.
218. Rehman, A.; Russell, E.; Saleem, F.; Javed, F.; Ahmad, S.; Eze, V. C.; Harvey, A., Synthesis of trans-limonene bis-epoxide by stereoselective epoxidation of (R)-(+)-limonene. *Journal of Environmental Chemical Engineering* **2021**, *9* (1), 104680.
219. Mosquera, M. E. G.; Jiménez, G.; Taberner, V.; Vinuesa-Vaca, J.; García-Estrada, C.; Kosalková, K.; Sola-Landa, A.; Monje, B.; Acosta, C.; Alonso, R.; Valera, M. Á., Terpenes and

- Terpenoids: Building Blocks to Produce Biopolymers. *Sustainable Chemistry* **2021**, 2 (3), 467-492.
220. Christoph, R.; Schmidt, B.; Steinberner, U.; Dilla, W.; Karinen, R., Glycerol. *Ullmann's Encyclopedia of Industrial Chemistry* **2006**, 17, 67-82.
221. Xiang, J.; Yang, S.; Zhang, J.; Wu, J.; Shao, Y.; Wang, Z.; Yang, M., The preparation of sorbitol and its application in polyurethane: a review. *Polymer Bulletin* **2021**, 1-18.
222. Decostanzi, M.; Ecochard, Y.; Caillol, S., Synthesis of sol-gel hybrid polyhydroxyurethanes. *European Polymer Journal* **2018**, 109, 1-7.
223. Younes, G. R.; Maric, M., Bio-based and hydrolytically degradable hydroxyurethane acrylates as photocurable thermosets. *Journal of Applied Polymer Science* **2021**, 52044.

## Appendix A

### Supporting information for “Study of moisture-curable hybrid NIPUs based on glycerol with various diamines: emergent advantages of PDMS-diamines”

- DGC synthesis

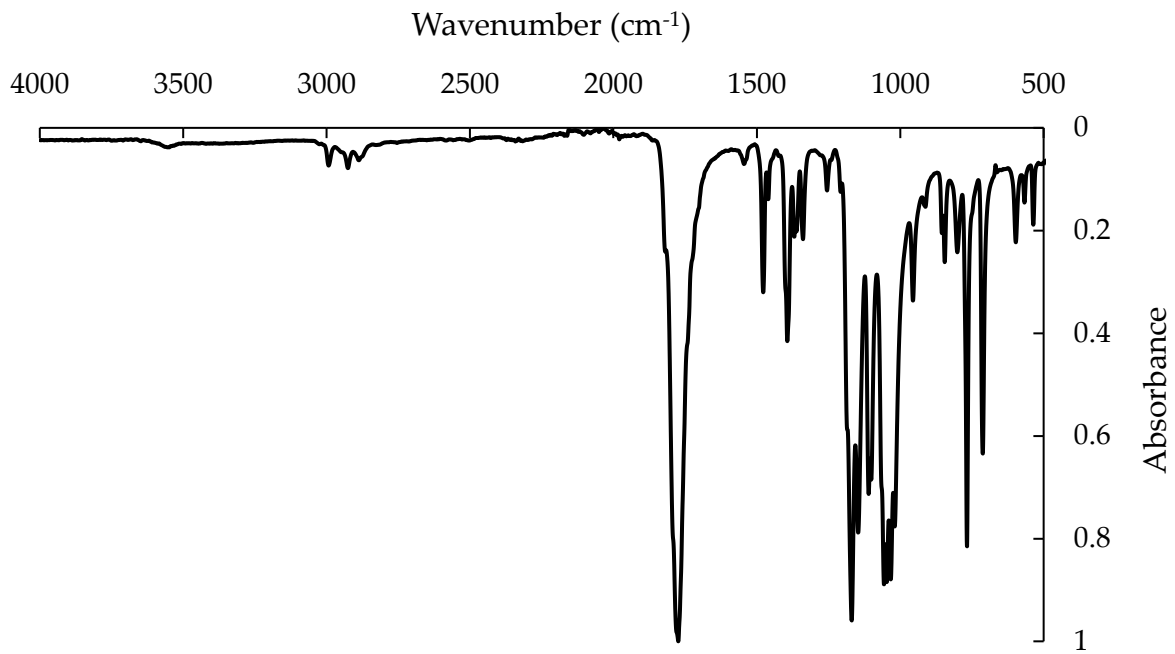


Figure A.1 - FTIR spectra of DGC molecule at room temperature (C=O stretch is at 1780  $\text{cm}^{-1}$ )

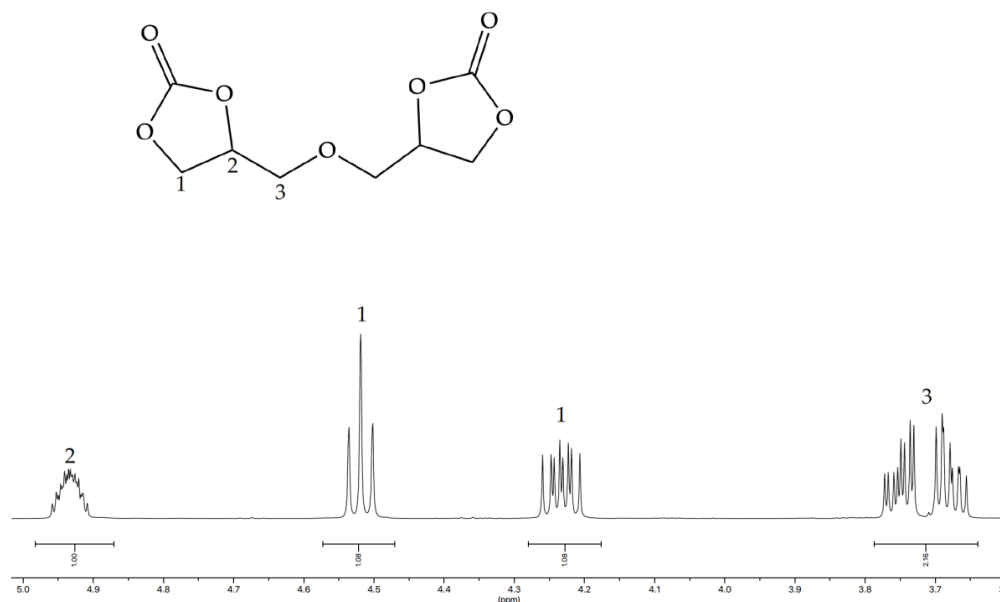


Figure A.2 - Labelled DGC  $^1\text{H}$ -NMR spectrum in DMSO- $\text{d}_6$  at 25 °C

- PHU prepolymer characterization

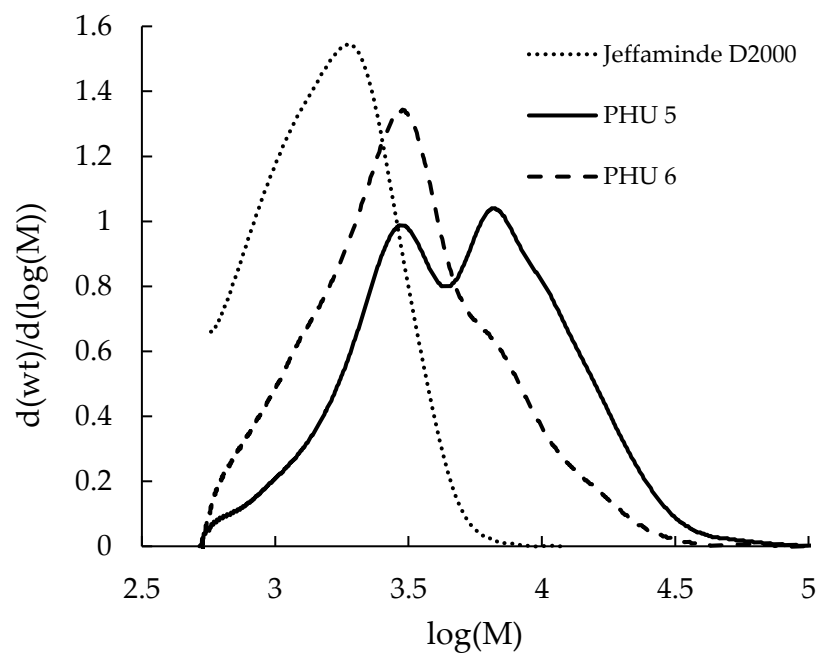


Figure A.3 - GPC signals showing chain scission occurring after 18 h of PHU 6 polymerization reaction at 140 °C

**Table A.1 - Data of molecular weight and dispersity evolution during PHU 6 polymerization at 140 °C (the initial data is that of Jeffamine D-2000)**

<b>Time (h)</b>	<b>M<sub>n</sub> (g/mol)</b>	<b>D = M<sub>w</sub>/M<sub>n</sub></b>
<b>0</b>	1,100	1.36
<b>1</b>	1,300	1.55
<b>3</b>	1,500	1.62
<b>5</b>	1,600	1.73
<b>10</b>	2,500	2.55
<b>15</b>	3,200	2.14
<b>18</b>	3,300	2.15
<b>21</b>	3,200	2.11
<b>24</b>	3,100	2.02
<b>43</b>	2,100	2.01
<b>48</b>	2,000	1.94

**Table A.2 - Data of molecular weight and dispersity evolution during PHU 11 polymerization at 80 °C (the initial data is that of PDMS-(NH<sub>2</sub>)<sub>2</sub>, M<sub>n</sub> = 5,000 g/mol)**

<b>Time (h)</b>	<b>M<sub>n</sub> (g/mol)</b>	<b>D = M<sub>w</sub>/M<sub>n</sub></b>
0	2,800	2.68
2	4,100	2.44
4	4,200	2.38
6	4,100	2.45
8	3,500	2.53
10	4,400	2.86
12	4,500	2.78
14	4,400	2.72
16	6,300	2.43
24	7,600	2.81
26	9,900	2.86
28	24,600	1.79
30	28,100	1.77
32	26,600	1.89
48	31,300	1.74

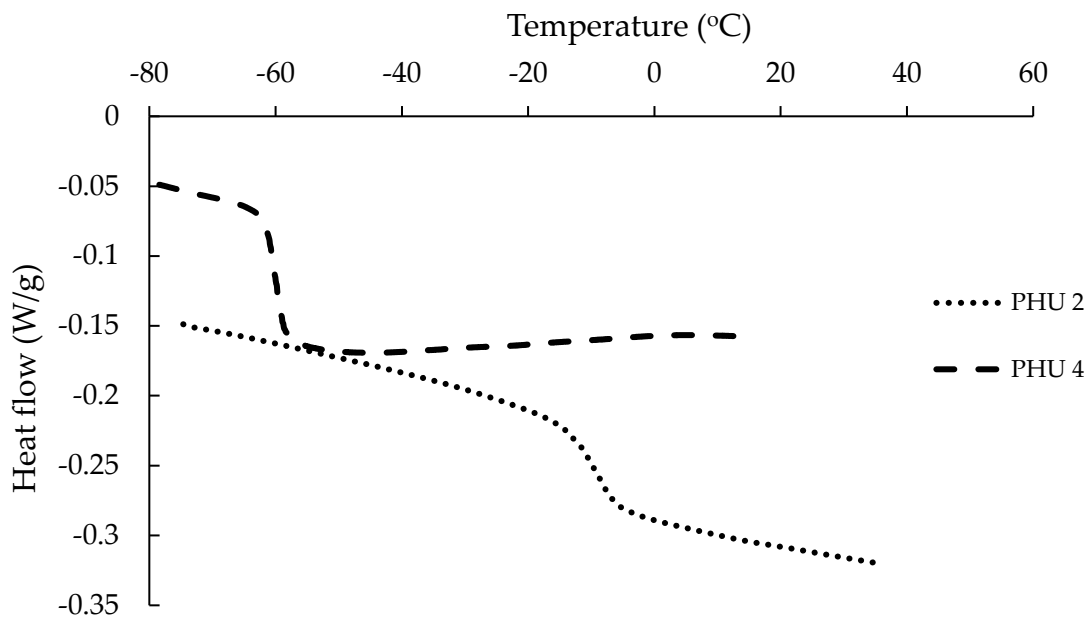


**Figure A.4 - DSC traces of the second heating run of PHUs 2 and 4**

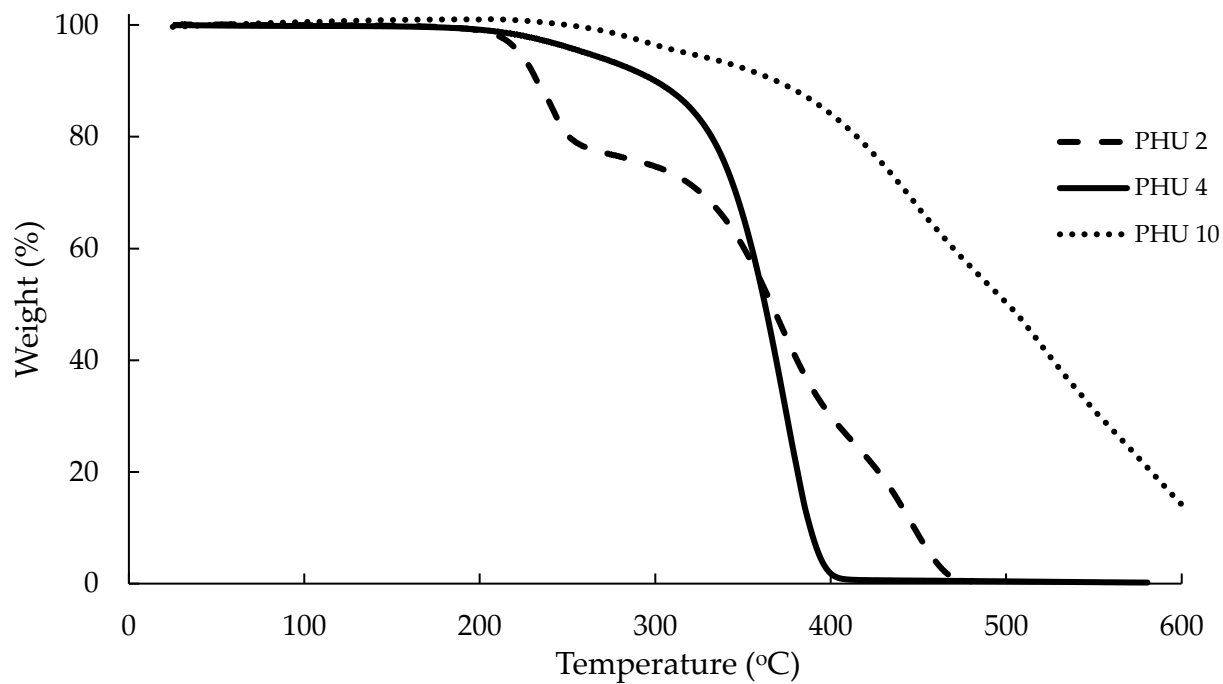


**Figure A.5 - TGA traces of PHUs 2, 4, and 10**

- **Estimation of the prepolymer absolute molecular weight**

This section takes the case of PHU 4 to illustrate the calculations done to estimate the absolute molecular weights of the PHU prepolymers of this work.

From the GPC data, the average number molecular weight,  $M_n$ , of SBC-PHU 4, with respect to PS standards, is:

$$M_n = 3,200 \text{ g/mol}$$

The average number molecular weight of Jeffamine D-2000 measured by GPC using PS standards is:

$$M_n^{\text{Jeffamine D-2000}} = 900 \text{ g/mol}$$

Dividing the molecular weight of the prepolymer by that of Jeffamine D-2000, gives:

$$\# \text{ of diamine molecules incorporated into the prepolymer chain} = 3.56 \approx 3$$

Assuming that the prepolymers have on average 3 amine units and that carbonates are the end-groups, as shown by the FTIR spectrum of PHU 4, gives:

$$\# \text{ of dicarbonate molecules incorporated into the prepolymer chain} = 4$$

As there are two dicarbonate units that have to link the three diamine units and two dicarbonate units have to be on both ends of the oligomers. Knowing that the molecular weight of DGC is 218 g/mol and that of Jeffamine D-2000 is 2,000 g/mol, the absolute average number molecular weight of PHU 4 can be estimated as:

$$M_n^{\text{absolute}} = 3 \times 2,000 + 4 \times 218 = 6,872 \text{ g/mol}$$

This is equivalent to an average of 6 hydroxyurethane linkages in the given oligomer chains.

The same calculation procedure applies to PHU 10 with the average number molecular weight of PDMS-5k-(NH<sub>2</sub>)<sub>2</sub> with respect to PS standards is:

$$M_n^{\text{PDMS-5k-(NH}_2)_2} = 2,800 \text{ g/mol}$$

the absolute molecular weight of PDMS-5k-(NH<sub>2</sub>)<sub>2</sub> is 5,000 g/mol, and the average number molecular weights of PHU 10, with respect to PS standards, can be found in Table 3.1. Besides, PHU 10 has amines as end groups, which helps in estimating the number of diamines and dicarbonates reacted to form this PHU.

- **Curing kinetics**

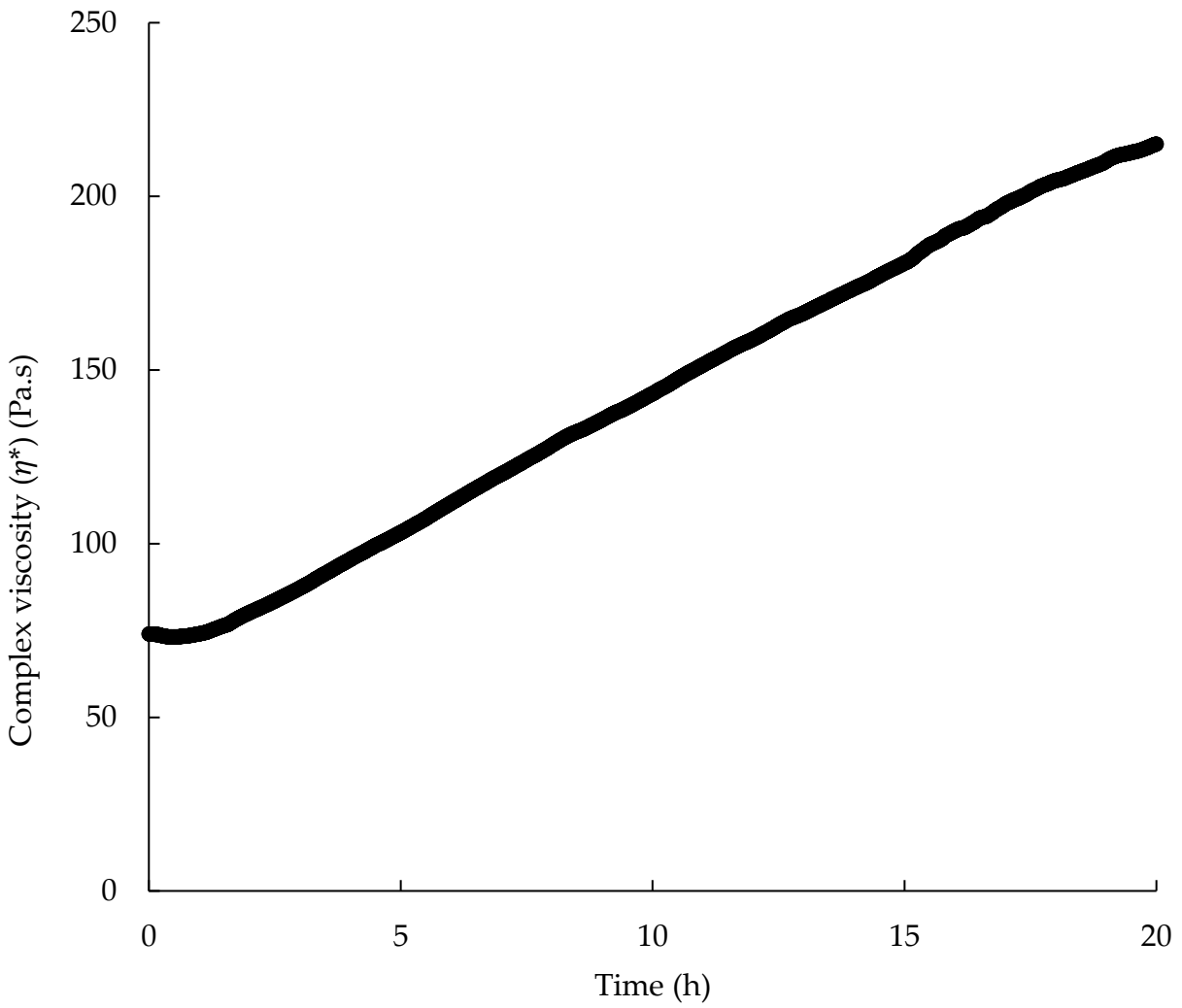


**Figure A.6 - Curing kinetics of PHU 4 by following the complex viscosity ( $\eta^*$ ) (Pa.s) at a frequency of 1 Hz and a strain of 1% for 20 h. Measurements were done at 22 °C and 40-50% humidity.**

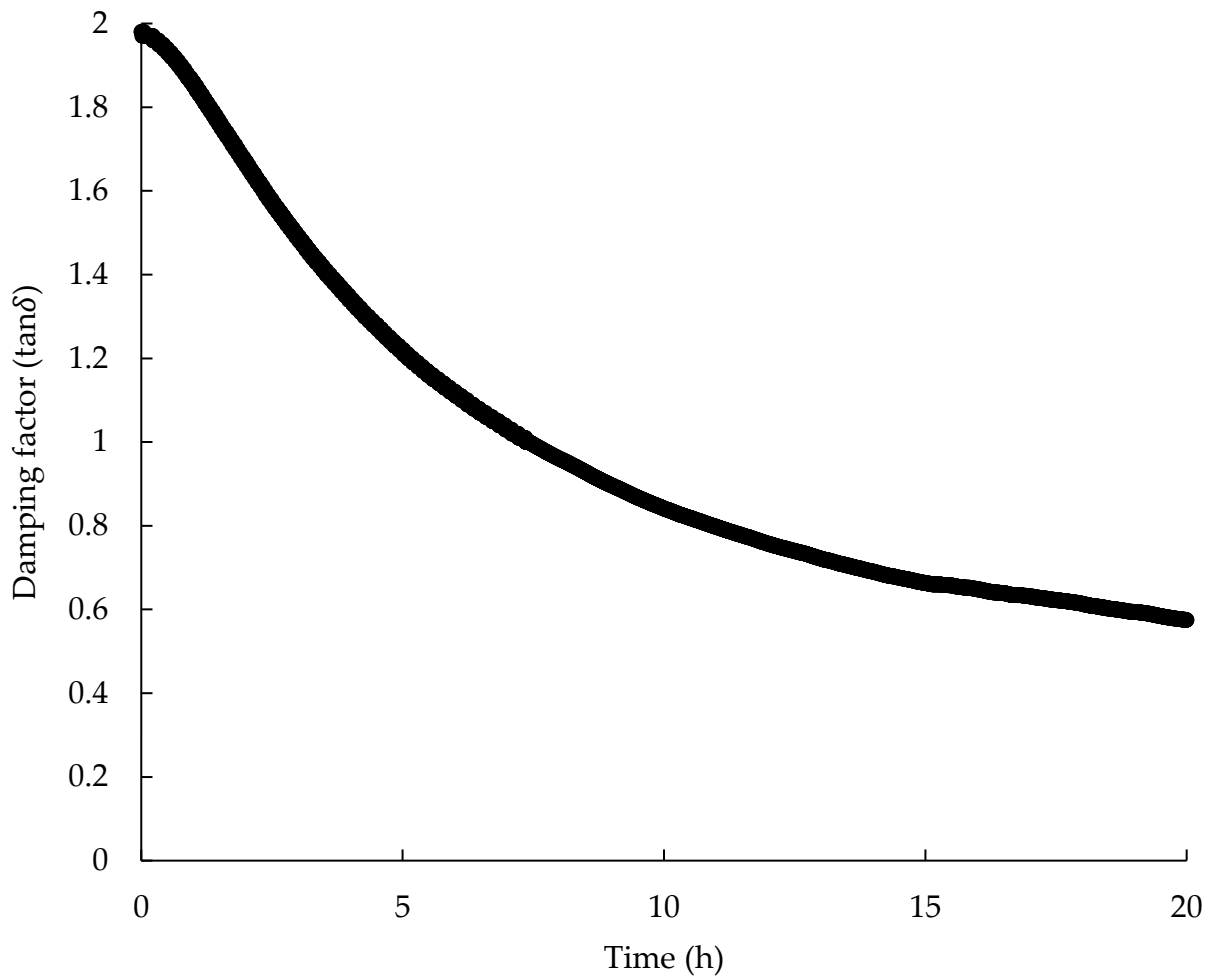


**Figure A.7 - Curing kinetics of PHU 4 by following the damping factor ( $\tan\delta$ ) at a frequency of 1 Hz and a strain of 1% for 20 h. Measurements were done at 22 °C and 40-50% humidity.**

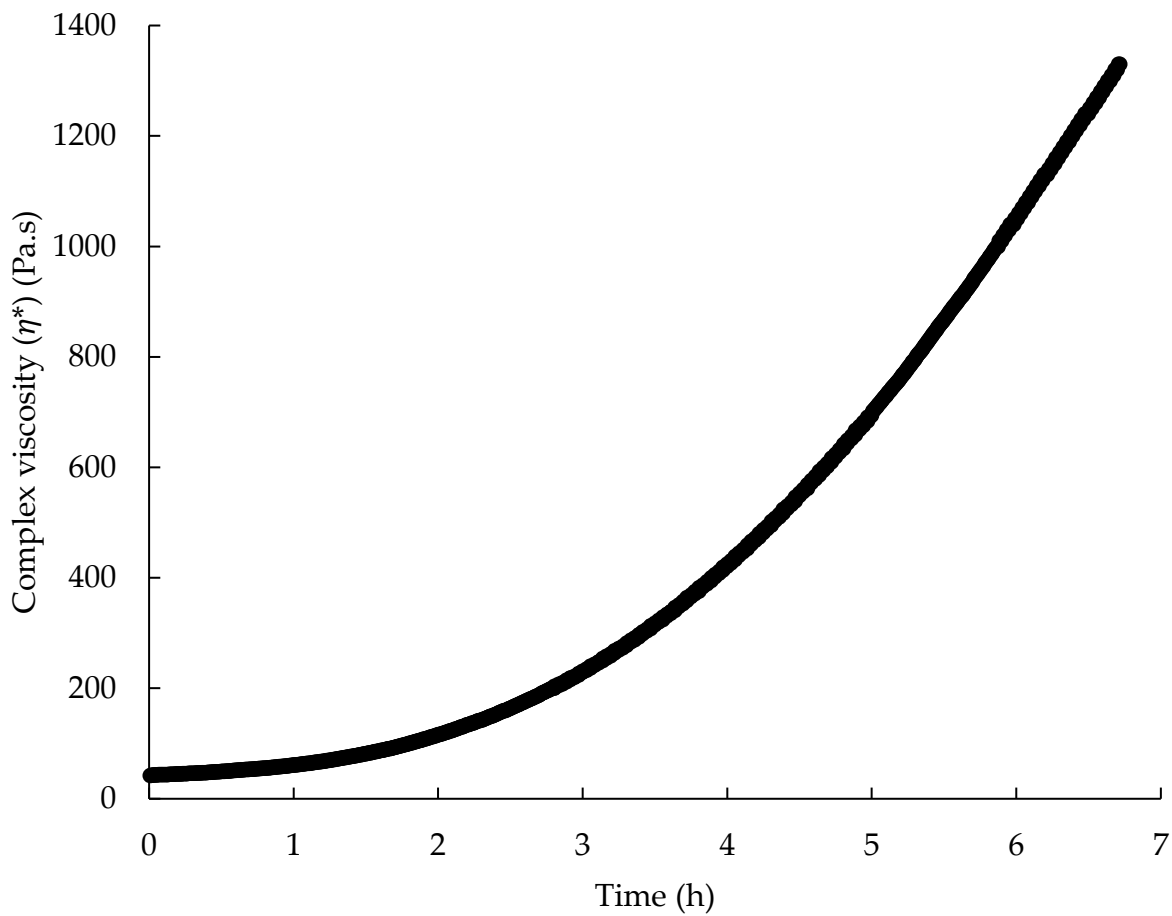


**Figure A.8 - Curing kinetics of PHU 10 by following the complex viscosity ( $\eta^*$ ) (Pa.s) at a frequency of 1 Hz and a strain of 1% for 7 h. Measurements were done at 22 °C and 40-50% humidity.**

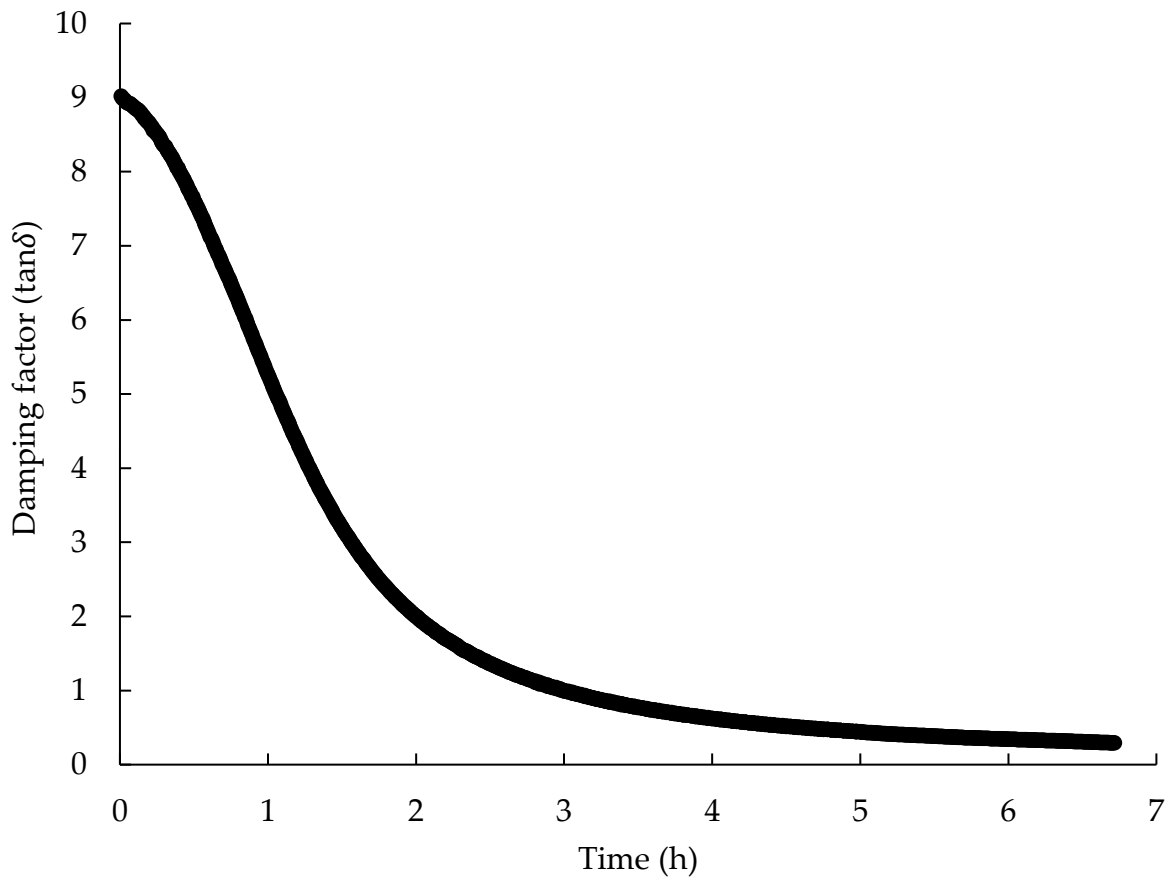


**Figure A.9 - Curing kinetics of PHU 10 by following the damping factor ( $\tan\delta$ ) at a frequency of 1 Hz and a strain of 1% for 7 h. Measurements were done at 22 °C and 40-50% humidity.**

- **HPHU characterization**

**Table A.3 - Swelling experiment data HPHU 4 samples in pure H<sub>2</sub>O**

<b>Samples</b>	<b>1</b>	<b>2</b>	<b>3</b>
<b>Mass initial (g)</b>	0.0105	0.0232	0.0169
<b>Mass 24 h (g)</b>	0.0143	0.03	0.021
<b>Mass 5 days (g)</b>	0.0167	0.0385	0.0277
<b>Mass 1 week (g)</b>	0.0162	0.0379	0.0284
<b>EWC (%)</b>	59.05	65.95	63.91
<b>EWA (%)</b>	37.13	39.74	38.99
<b>Dried mass (g)</b>	0.0071	0.0155	0.0111
<b>GC (%)</b>	67.62	66.81	65.68

**Table A.4 - Swelling experiment data of HPHU 10 samples in pure H<sub>2</sub>O**

<b>Samples</b>	<b>1</b>	<b>2</b>	<b>3</b>
<b>Mass initial (g)</b>	0.0714	0.043	0.0383
<b>Mass 1 week (g)</b>	0.0713	0.0433	0.038
<b>Mass 2 weeks (g)</b>	0.0712	0.0433	0.0384

**Table A.5 - Sessile drop tests of Milli-Q water on HPHU 10 films**

<b>Measurement</b>	<b>Contact angle left (°)</b>	<b>Contact angle right (°)</b>	<b>Average (°)</b>
<b>1</b>	103.7	109.2	106.45
<b>2</b>	101.4	121.9	111.65
<b>3</b>	111.9	108.3	110.1
<b>4</b>	107	111.9	109.45
<b>5</b>	105.6	111.5	108.55
<b>6</b>	107.1	111.9	109.5
<b>7</b>	100.2	112.5	106.35
<b>8</b>	112.4	111.7	112.05

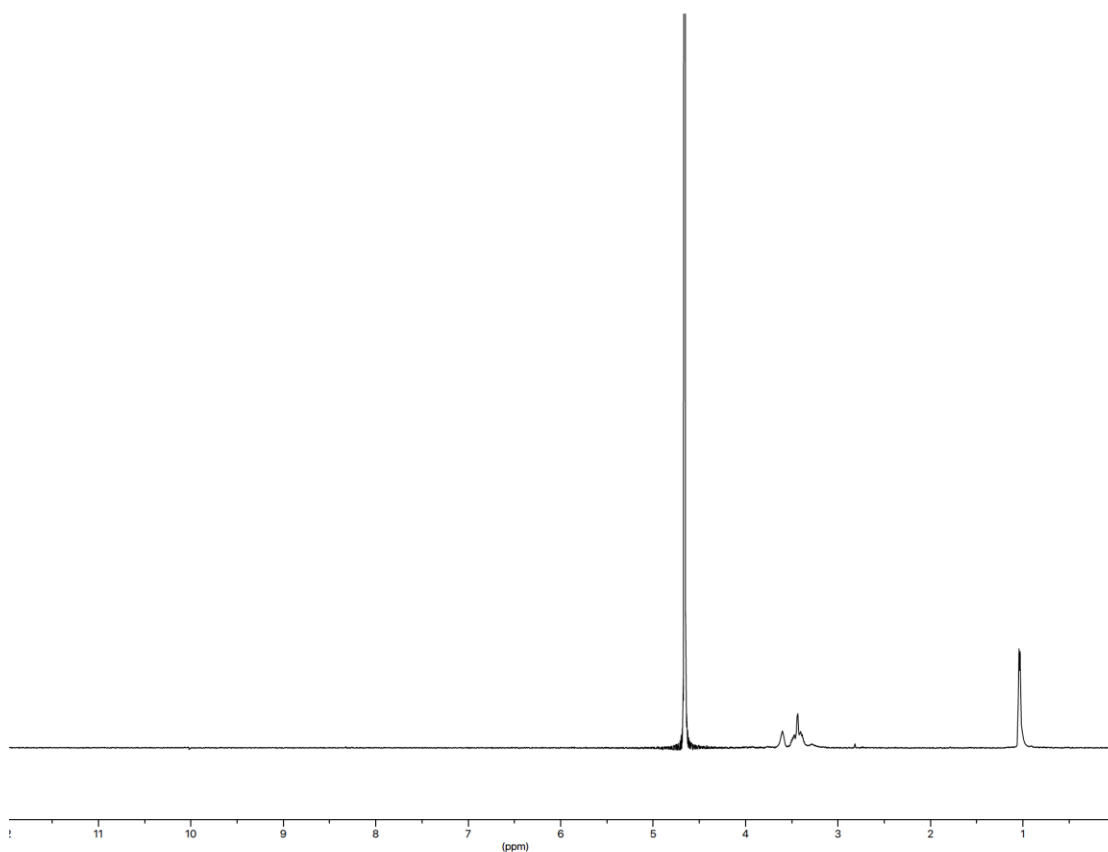


**Figure A.10 -  $^1\text{H}$ -NMR spectrum on HPHU 4 degradation residuals in  $\text{D}_2\text{O}$  at  $25\text{ }^\circ\text{C}$  showing possible leaching occurring from HPHU 4 films in pure  $\text{H}_2\text{O}$**

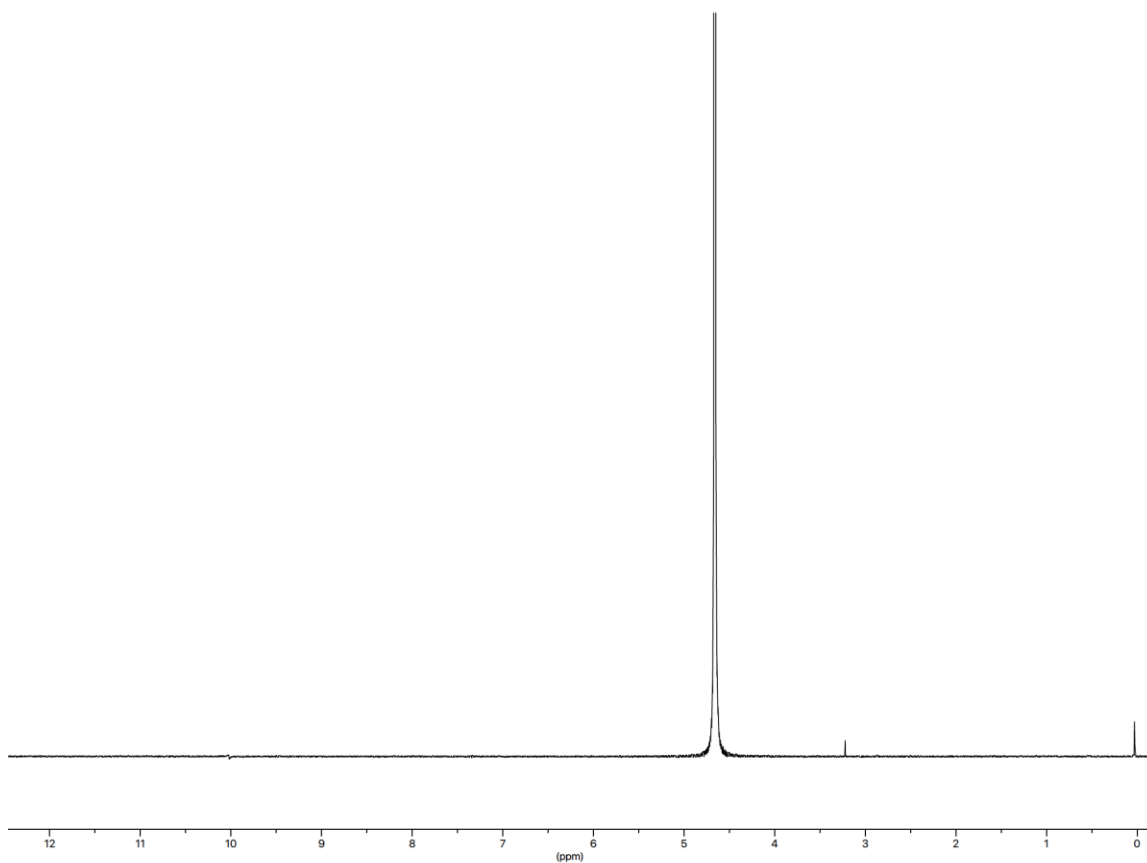


**Figure A.11 - <sup>1</sup>H-NMR spectrum on HPHU 10 degradation residuals in D<sub>2</sub>O at 25 °C showing no leaching occurring from HPHU 10 films in pure H<sub>2</sub>O**

**Table A.6 - Degradation experiment data of HPHU 10 films in acid medium pH = 3**

<b>Samples</b>	<b>1</b>	<b>2</b>	<b>3</b>
<b>Mass initial (g)</b>	0.0453	0.0414	0.038
<b>Mass 1 week (g)</b>	0.045	0.041	0.0379
<b>Mass 2 weeks (g)</b>	0.045	0.0412	0.0381

**Table A.7 - Tensile properties for the dog-bone samples cured for one week under moisture at ambient conditions**

Samples	E (MPa)	EB%	$\sigma_{\max}$ (MPa)
1	1.3	54.1	0.29
2	1.5	70.0	0.39
3	1.0	56.5	0.33
4	1.0	42.9	0.19
5	1.3	44.4	0.28

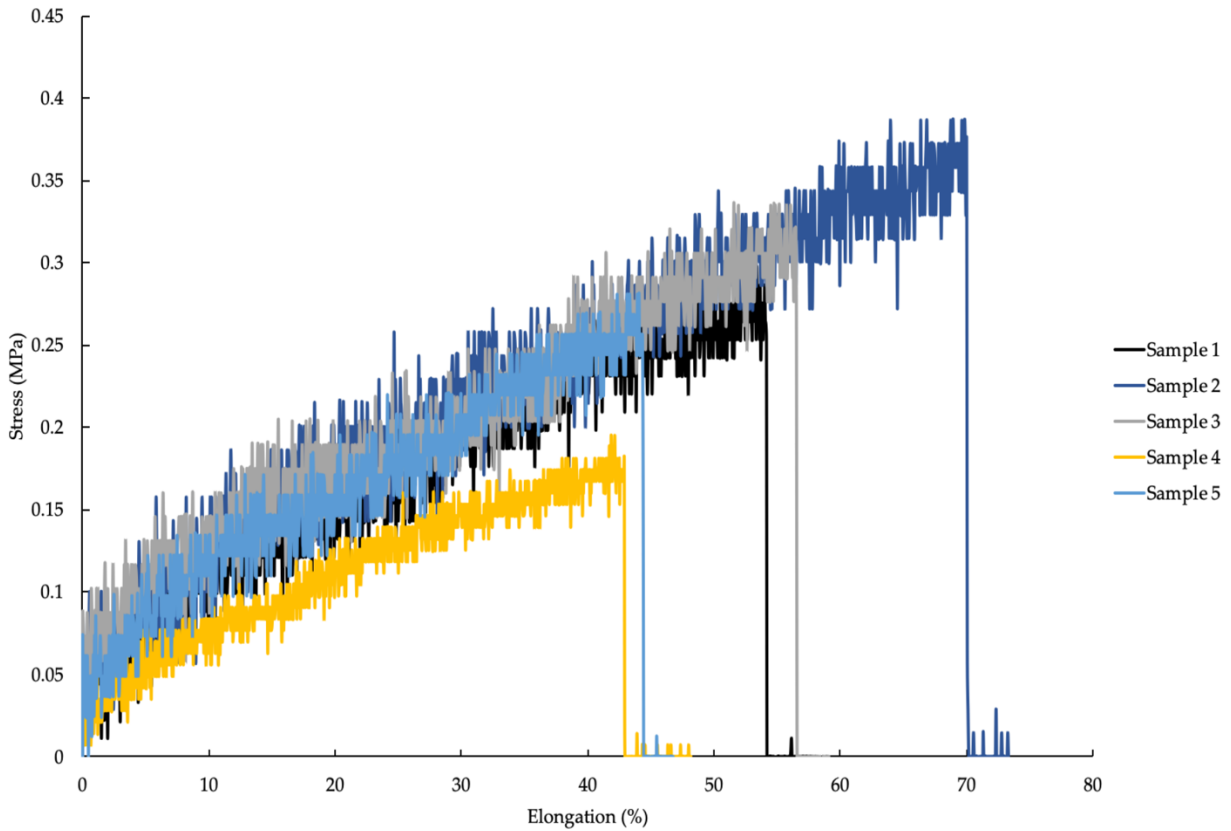


**Figure A.12 - Tensile tests data for the dog-bone samples cured for one week under moisture at ambient conditions**

**Table A.8 - Tensile properties for the dog-bone samples cured for one week at ambient conditions and another week in pure H<sub>2</sub>O**

Samples	E (MPa)	EB%	$\sigma_{\max}$ (MPa)
1	0.75	92.4	0.44
2	0.50	108	0.44
3	1.0	100	0.37

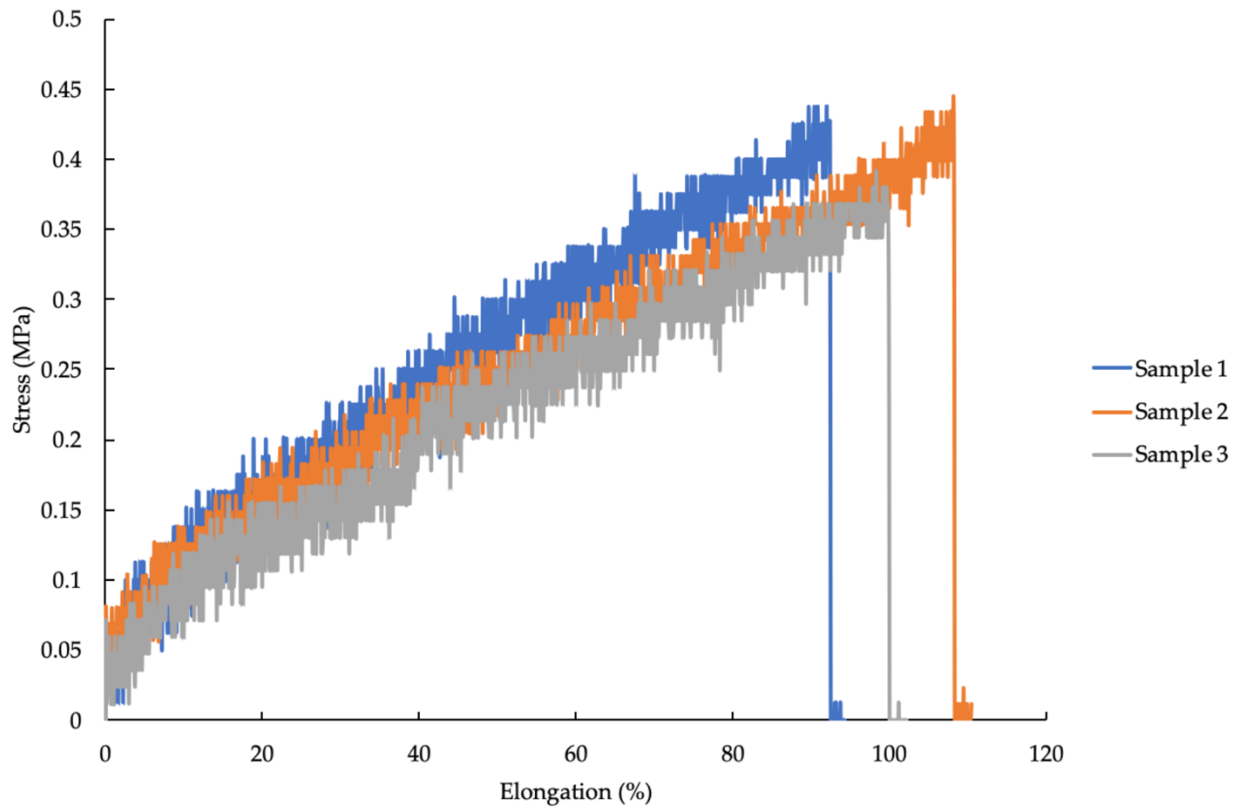


**Figure A.13 - Tensile tests data for the dog-bone samples cured for one week at ambient conditions and another week in pure H<sub>2</sub>O**

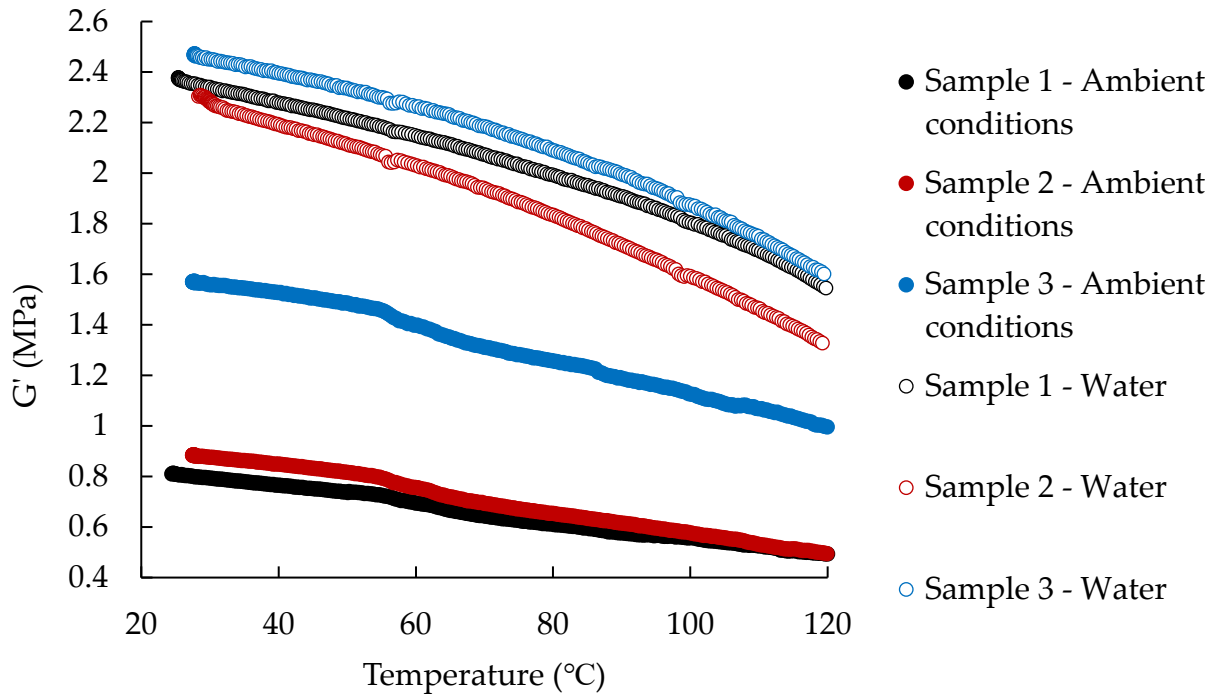


**Figure A.14 - Dynamic mechanical thermal analysis on the sample cured at ambient conditions for one week and the ones cured at ambient conditions for one week and in water for an extra week at a strain of 0.5% and a frequency of 1 Hz from 25 °C to 120 °C at a rate of 5 °C/min**

## Appendix B

### Supporting information for “Moisture-curable hybrid polyhydroxyurethanes from sugar-derived dicarbonates”

- SBC and MBC synthesis

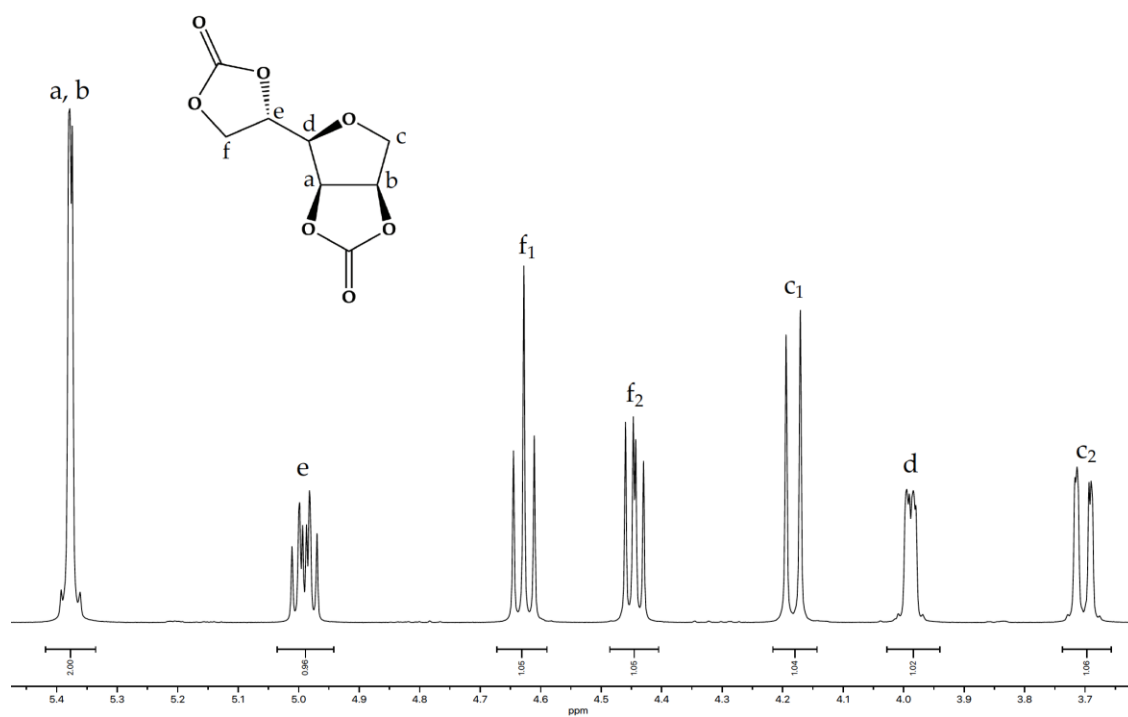


Figure B.1 - Labelled SBC <sup>1</sup>H-NMR spectrum in DMSO-d<sub>6</sub> at 25 °C

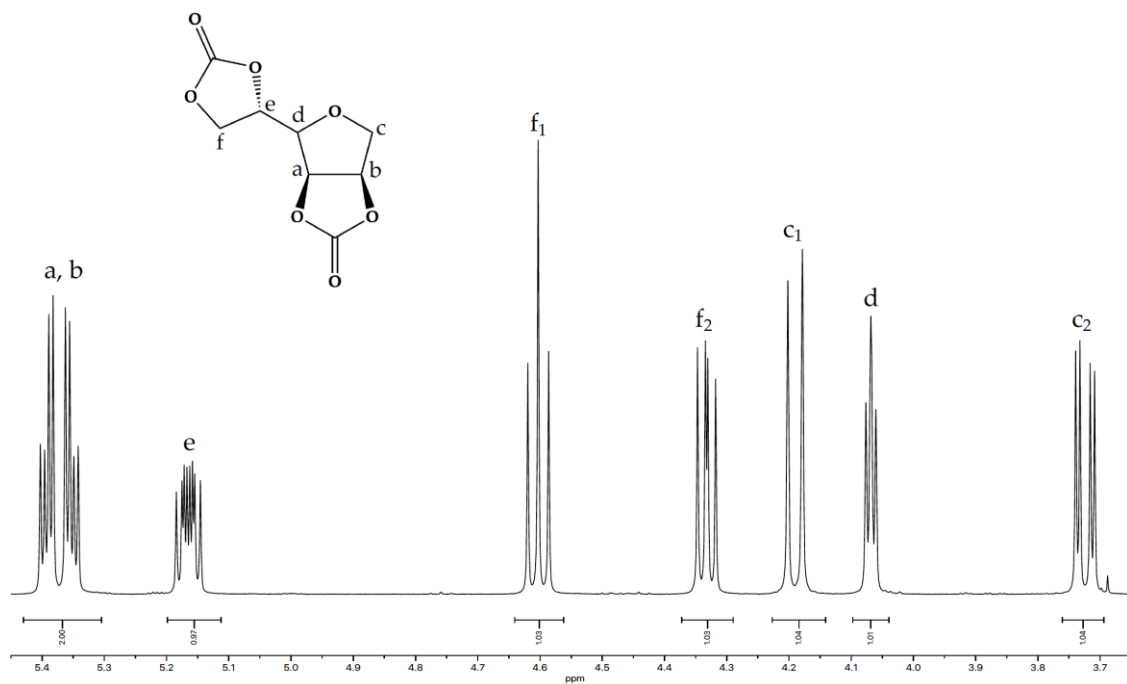


Figure B.2 - Labelled MBC  $^1\text{H-NMR}$  spectrum in  $\text{DMSO-d}_6$  at  $25\text{ }^\circ\text{C}$

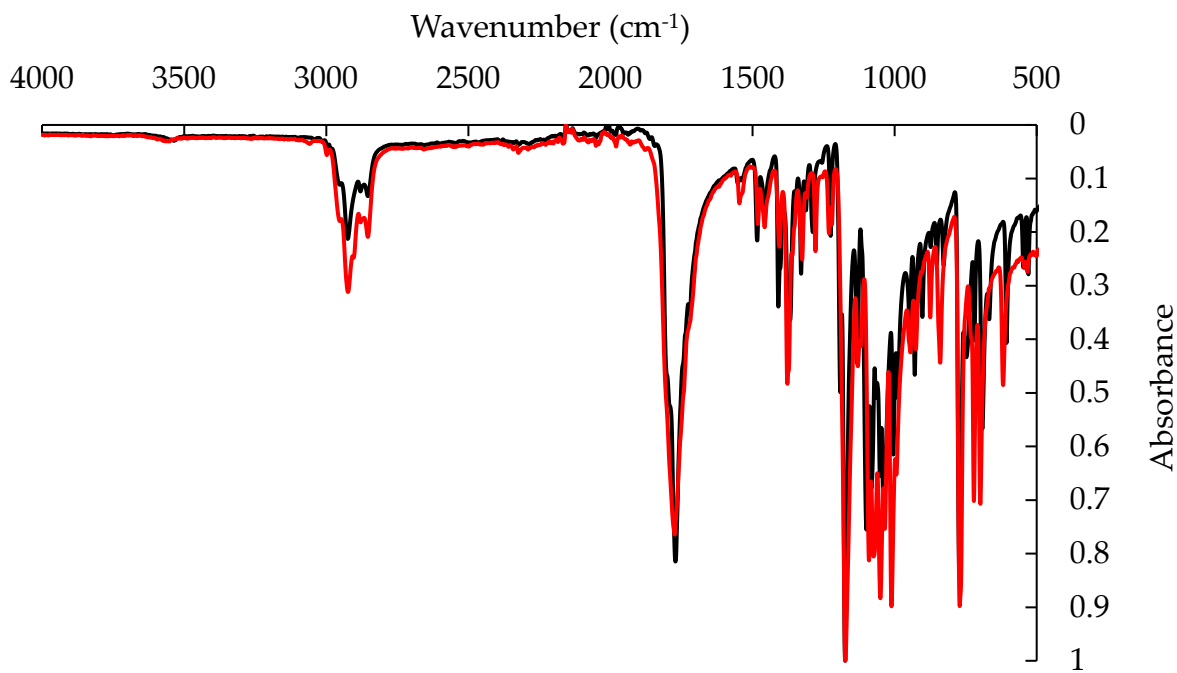
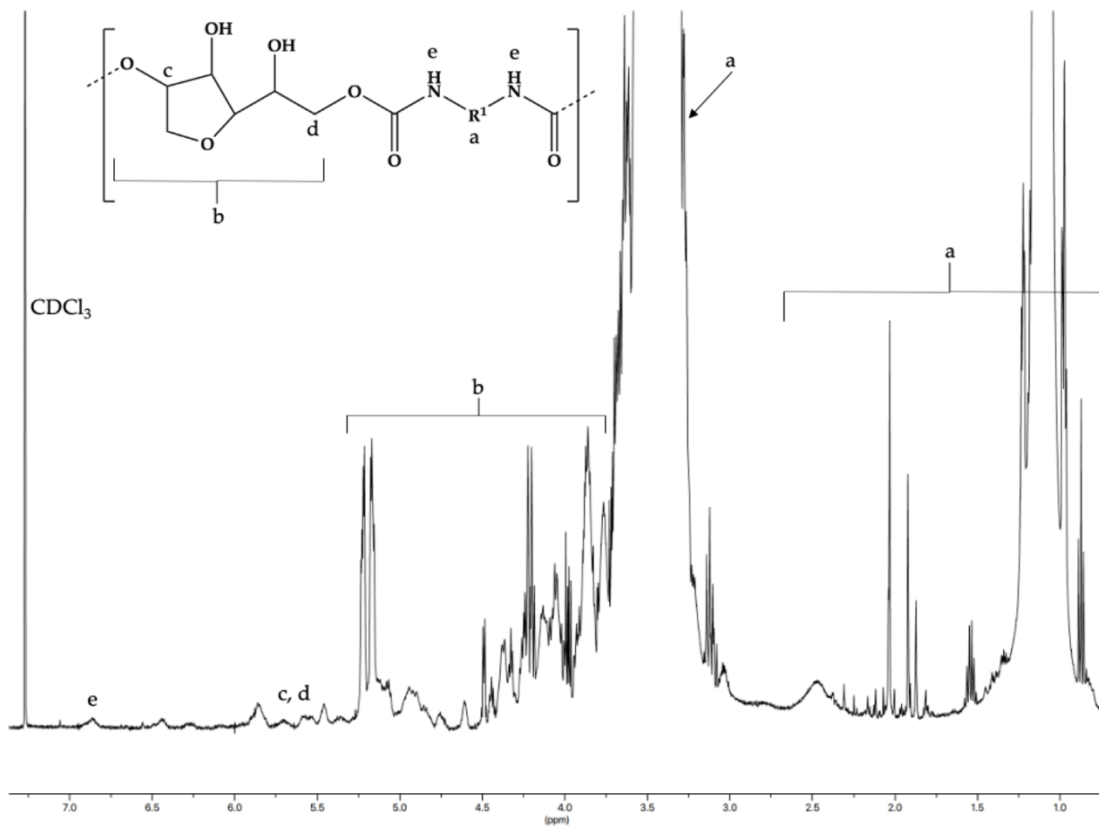
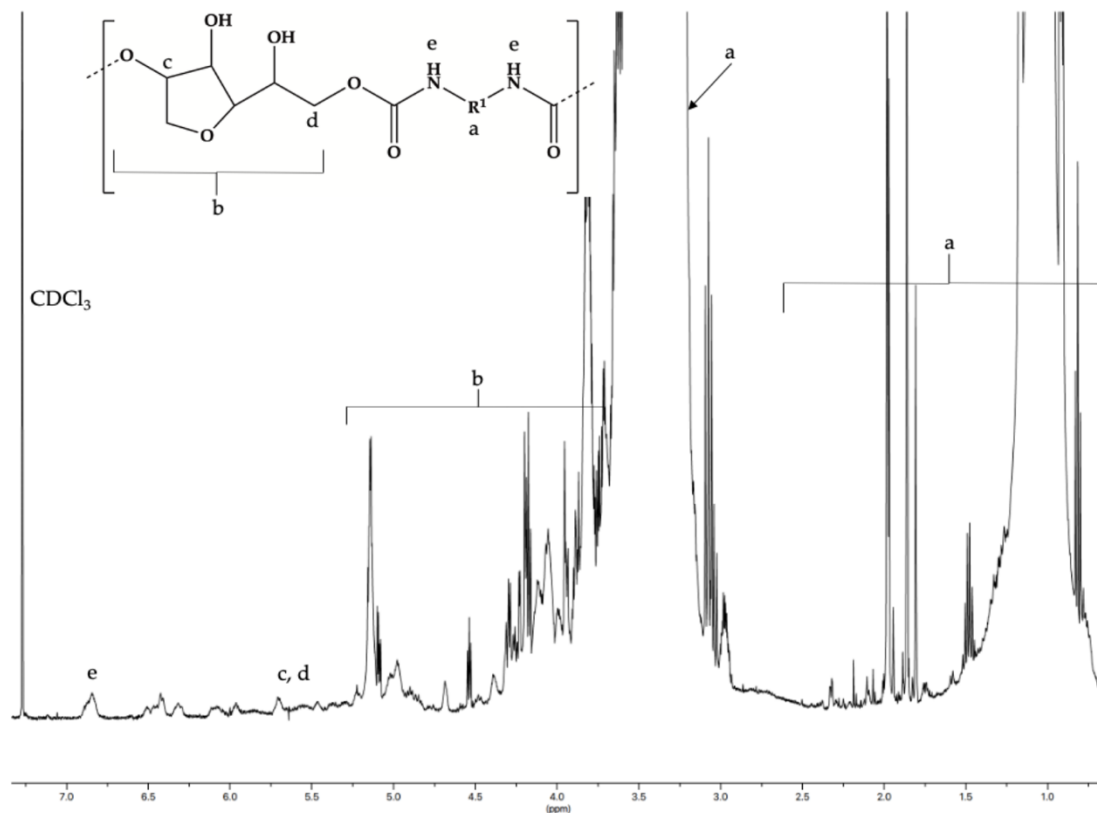


Figure B.3 - FTIR spectra of SBC or MBC molecule at room temperature ( $\text{C=O}$  stretch is at  $1780\text{ cm}^{-1}$ )

- PHU prepolymer characterization



**Figure B.4 - <sup>1</sup>H-NMR spectrum of SBC-PHU 1 (SBC + Jeffamine D-2000) in CDCl<sub>3</sub> at 25°C. Protons denoted by c belong to the diamine backbone (R<sup>1</sup>) whereas protons denoted by e belong to the opened cyclic carbonate ring and what belonged to SBC. The rest of the peaks are predicted.**



**Figure B.5 - <sup>1</sup>H-NMR spectrum of MBC-PHU 1 (MBC + Jeffamine D-2000) in CDCl<sub>3</sub> at 25°C. Protons denoted by c belong to the diamine backbone (R<sup>1</sup>) whereas protons denoted by e belong to the opened cyclic carbonate ring and what belonged to MBC. The rest of the peaks are predicted.**

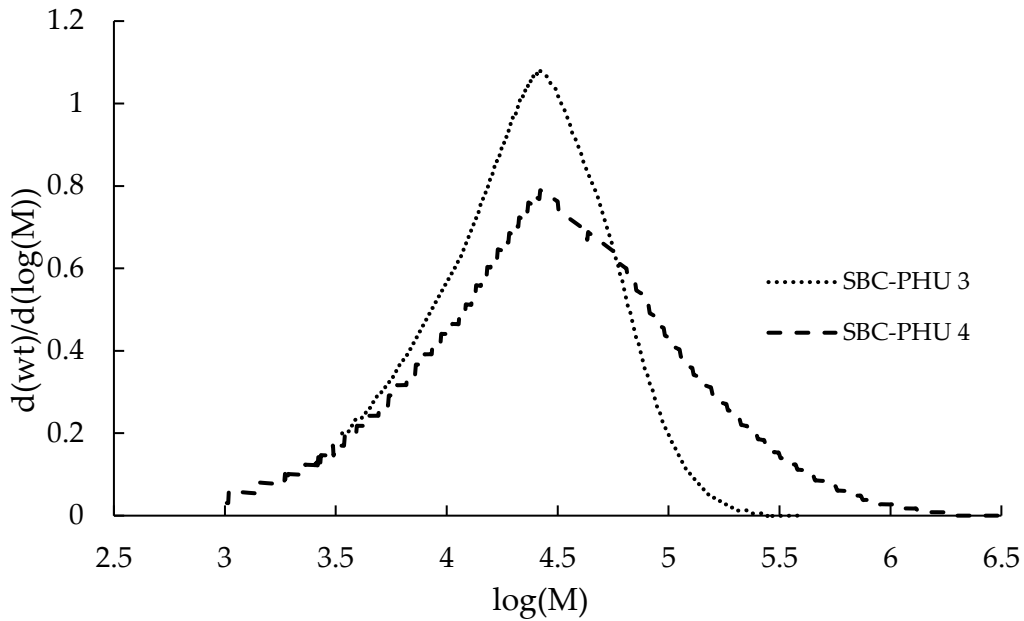


**Figure B.6 - GPC traces of SBC-PHU 3 and SBC-PHU 4 showing the broad distribution of the latter compared to the former**

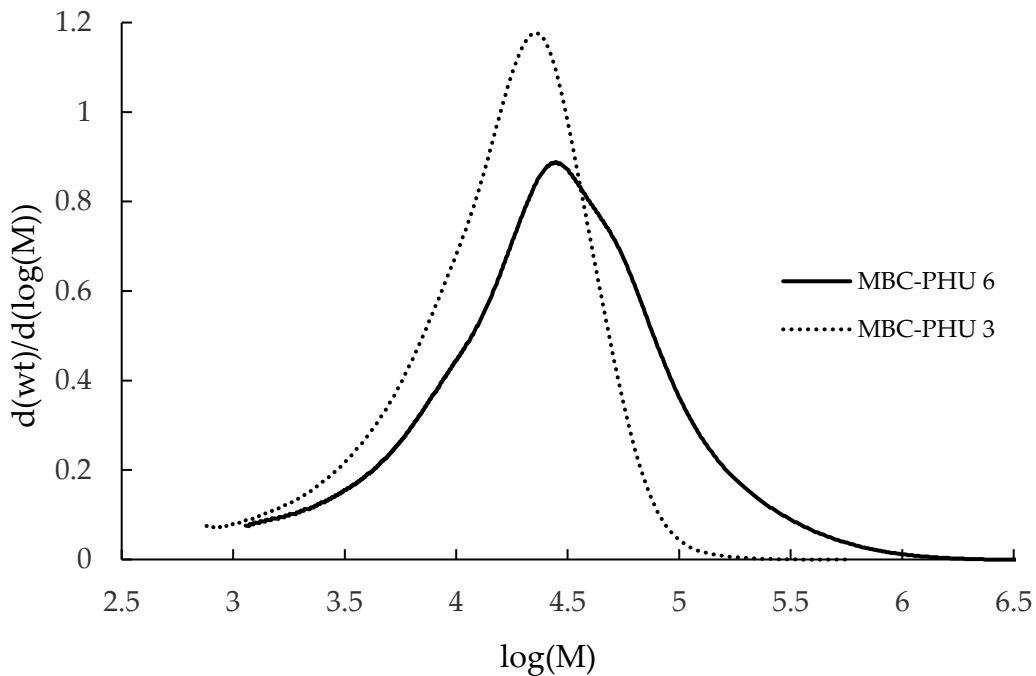


**Figure B.7 - GPC traces of MBC-PHU 3 and MBC-PHU 6 showing the broad distribution of the latter compared to the former**



**Figure B.8 -  $^1\text{H-NMR}$  spectrum of SBC-PHU 3 (SBC + PDMS-5k- $(\text{NH}_2)_2$ ) in  $\text{CDCl}_3$  at  $25^\circ\text{C}$  (note that the signal shown at 0 ppm is the proton from the  $-\text{O-Si}(\text{CH}_3)_2$  groups). Protons denoted by c belong to the diamine backbone ( $\text{R}^1$ ) whereas protons denoted by e belong to the opened cyclic carbonate ring and what belonged to SBC. The rest of the peaks are predicted.**

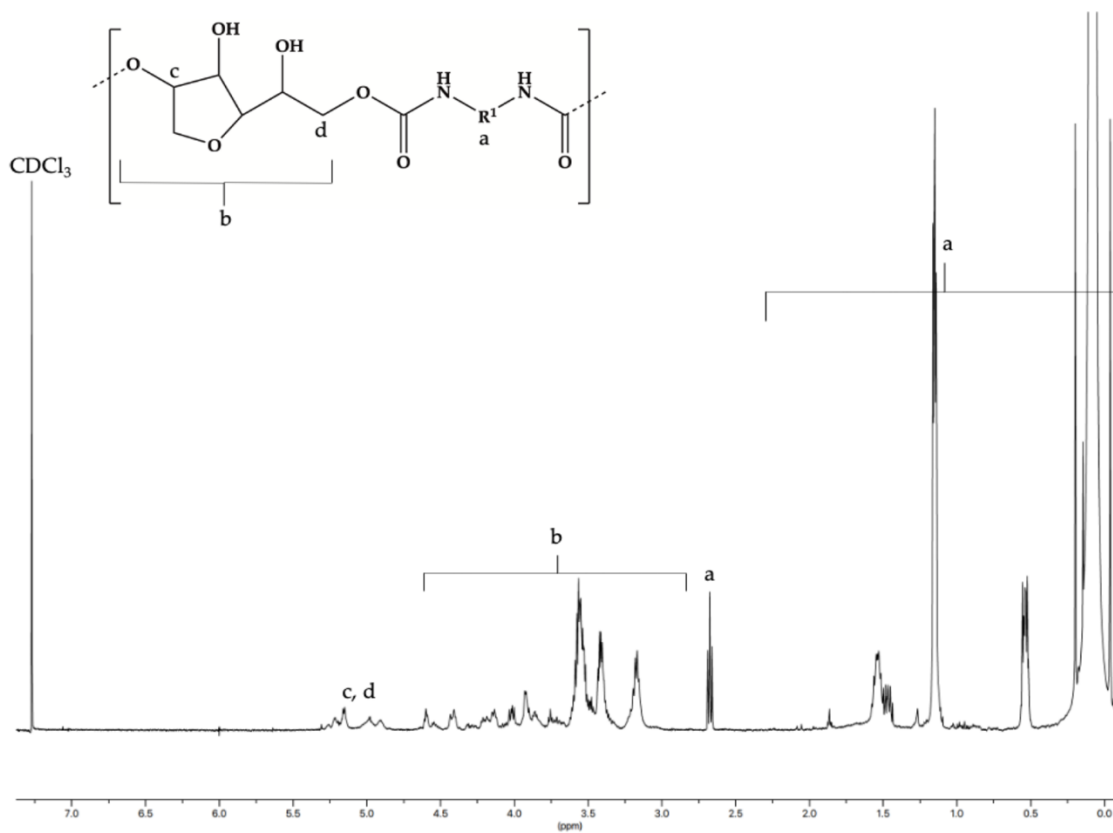


**Figure B.9 - <sup>1</sup>H-NMR spectrum of MBC-PHU 3 (MBC + PDMS-5k-(NH<sub>2</sub>)<sub>2</sub>) in CDCl<sub>3</sub> at 25°C (note that the signal shown at 0 ppm is the proton from the -O-Si(CH<sub>3</sub>)<sub>2</sub> groups). Protons denoted by c belong to the diamine backbone (R<sup>1</sup>) whereas protons denoted by e belong to the opened cyclic carbonate ring and what belonged to MBC. The rest of the peaks are predicted.**

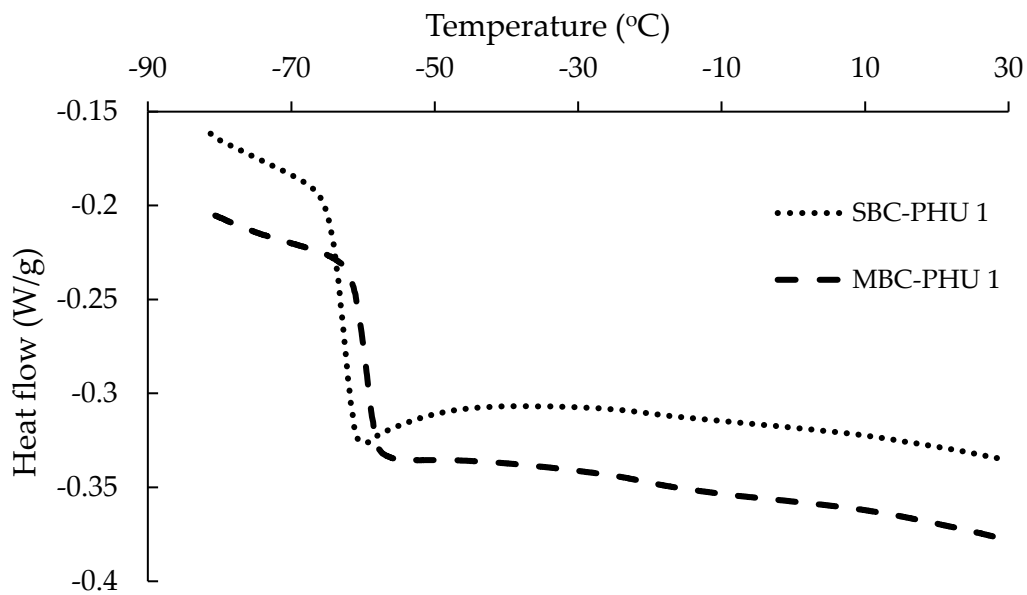


**Figure B.10 - DSC traces of the second heating run of SBC-PHU 1 and MBC-PHU 1**

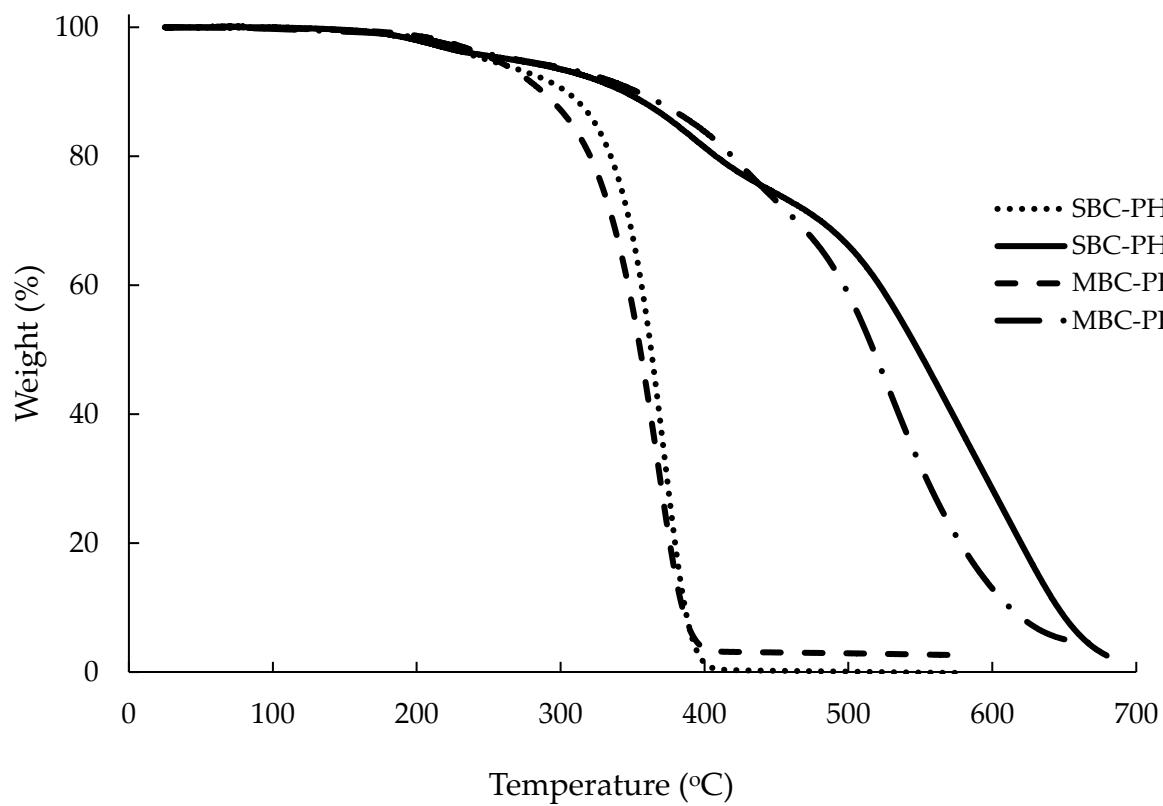


**Figure B.11 - TGA traces of selected sugar-based PHUs**

- **Estimation of the prepolymers absolute molecular weights**

This section takes the case of SBC-PHU 1 to illustrate the calculations done to estimate the average molecular weights of the PHU prepolymers of this work.

From the GPC data, the average number molecular weight,  $M_n$ , of SBC-PHU 1, with respect to PS standards, is:

$$M_n = 3,400 \text{ g/mol}$$

The average number molecular weight of Jeffamine D-2000 measured by GPC using PS standards is:

$$M_n^{\text{Jeffamine D-2000}} = 1,300 \text{ g/mol}$$

Dividing the molecular weight of the prepolymer by that of Jeffamine D-2000, gives:

$$\# \text{ of diamine molecules incorporated into the prepolymer chain} = 2.61 \approx 2$$

Assuming that the prepolymers have on average 2 amine units and that carbonates are the end-groups, as shown by the FTIR spectrum of SBC-PHU 1, gives:

$$\# \text{ of dicarbonate molecules incorporated into the prepolymer chain} = 3$$

As there is one dicarbonate unit that has to link the two diamine units and two dicarbonate units have to be on both ends of the oligomers. Knowing that the molecular weight of SBC is 216 g/mol and that of Jeffamine D-2000 is 2,000 g/mol, the average molecular weight of SBC-PHU 1 can be estimated as:

$$MW^{\text{Average}} = 2 \times 2,000 + 3 \times 216 = 4,614 \text{ g/mol}$$

This is equivalent to an average of 4 hydroxyurethane linkages in the given oligomer chains.

The same calculation procedure applies to the other sugar-based prepolymers with the average number molecular weight of PDMS-5k-(NH<sub>2</sub>)<sub>2</sub> with respect to PS standards is:

$$M_n^{\text{PDMS-5k-(NH}_2)_2} = 3,300 \text{ g/mol}$$

the molecular weight and average molecular weight of MBC and PDMS-5k-(NH<sub>2</sub>)<sub>2</sub> are 216 and 5,000 g/mol, respectively, and the average number molecular weights of the PHUs, with respect to PS standards, can be found in Table 4.1. Besides, the MBC-PHU 1 and the PDMS-5k-(NH<sub>2</sub>)<sub>2</sub>-based PHUs have carbonates and amines as end groups, respectively, which helps in estimating the number of diamines and dicarbonates reacted to form these PHU oligomers.

- **Curing kinetics**

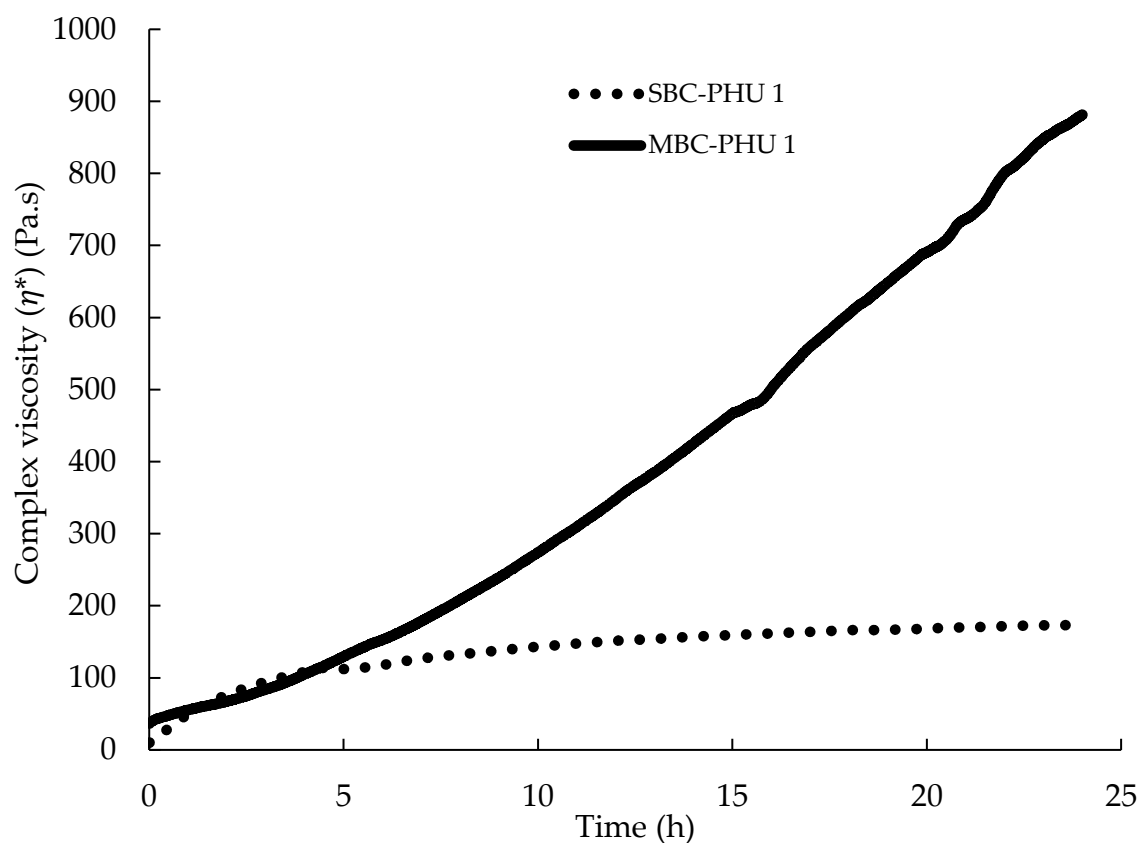


**Figure B.12 - Curing kinetics of SBC-PHU 1 and MBC-PHU 1 by following the complex viscosity ( $\eta^*$ ) (Pa.s) at a frequency of 1 Hz and a strain of 1% for 24 h. 0.5 wt.% of the proprietary catalyst was added to end-capped SBC-PHU 1 to accelerate the curing.**

**Measurements were done at 22 °C and 20-30% humidity.**

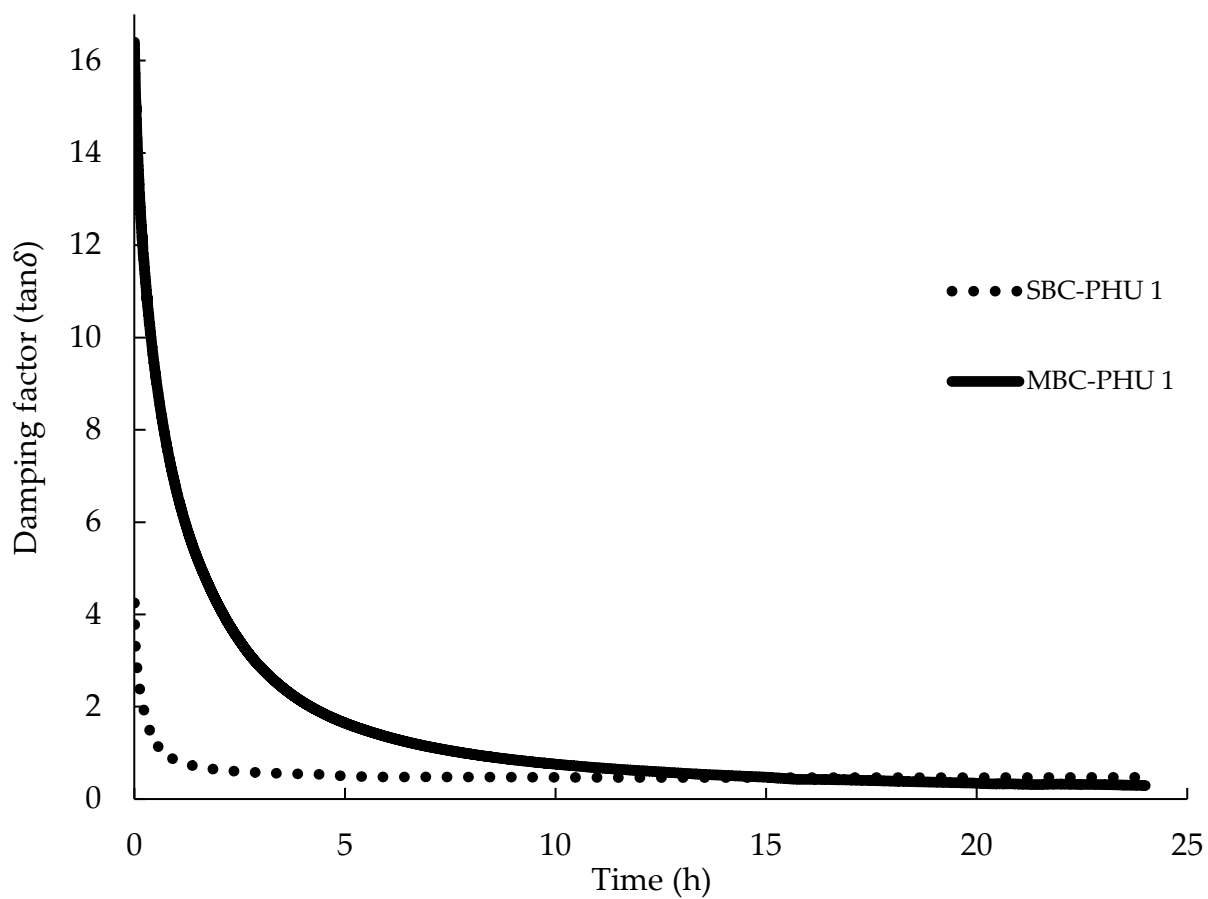


**Figure B.13 - Curing kinetics of SBC-PHU 1 and MBC-PHU 1 by following the damping factor ( $\tan\delta$ ) at a frequency of 1 Hz and a strain of 1% for 24 h. 0.5 wt.% of the proprietary catalyst was added to end-capped SBC-PHU 1 to accelerate the curing. Measurements were done at 22 °C and 20-30% humidity.**

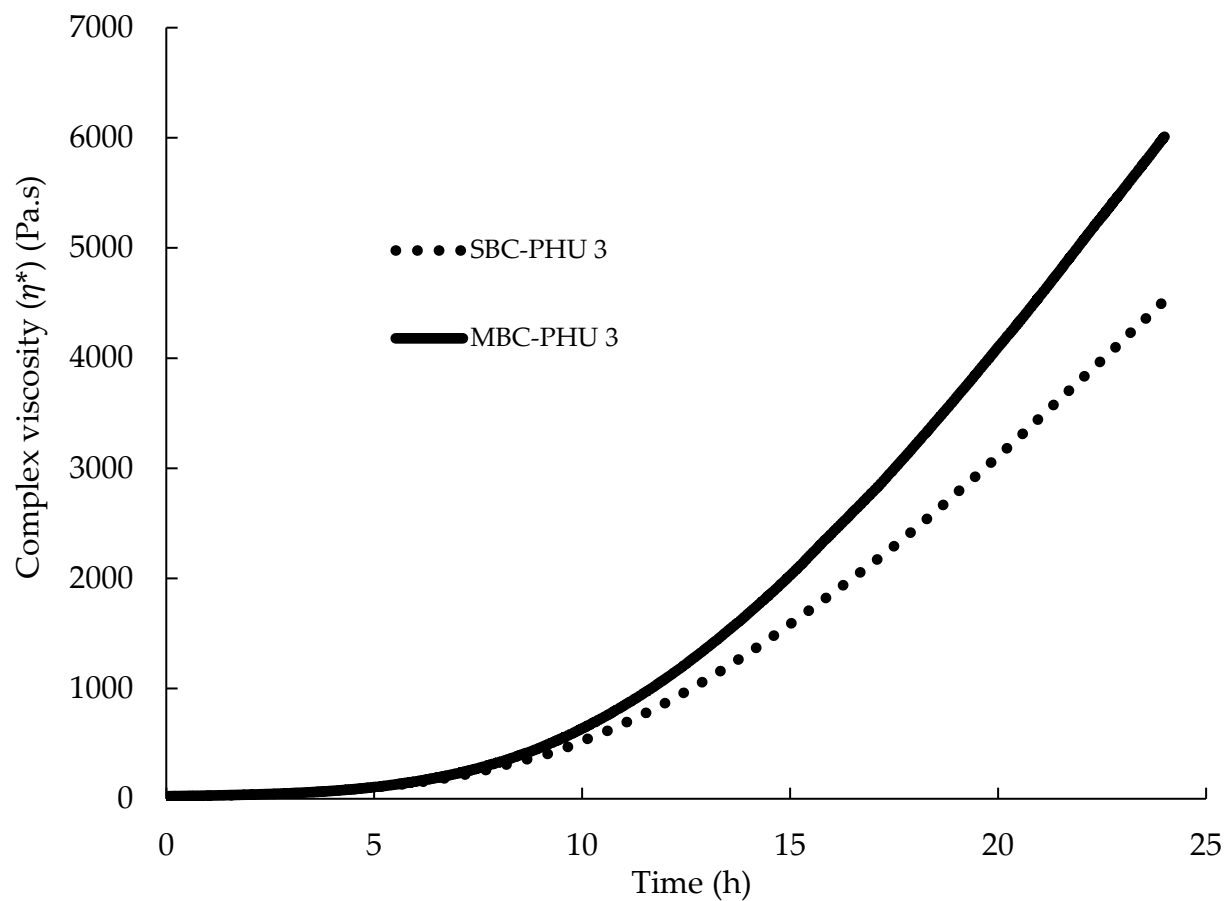


**Figure B.14 - Curing kinetics of SBC-PHU 3 and MBC-PHU 3 by following the complex viscosity ( $\eta^*$ ) (Pa.s) at a frequency of 1 Hz and a strain of 1% for 24 h. Measurements were done at 22 °C and 20-30% humidity.**

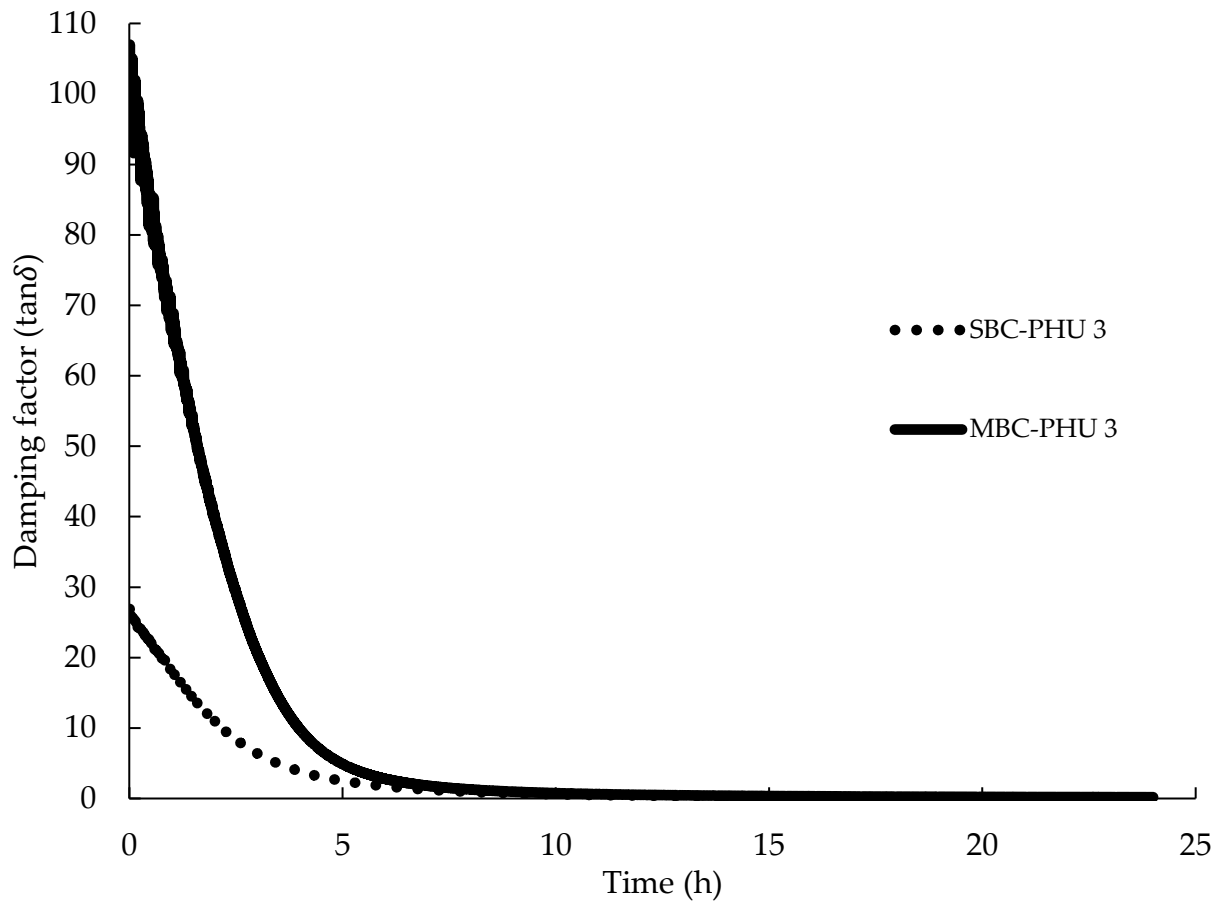


**Figure B.15 - Curing kinetics of SBC-PHU 3 and MBC-PHU 3 by following the damping factor ( $\tan\delta$ ) at a frequency of 1 Hz and a strain of 1% for 24 h. Measurements were done at 22 °C and 20-30% humidity.**

- **HPHU characterization**

**Table B.1 - Swelling experiment data of SBC-HPHU 1 samples in THF and pure H<sub>2</sub>O**

<b>Samples</b>	<b>THF-1</b>	<b>THF-2</b>	<b>THF-3</b>	<b>H<sub>2</sub>O-1</b>	<b>H<sub>2</sub>O-2</b>	<b>H<sub>2</sub>O-3</b>
<b>Mass initial (g)</b>	0.0179	0.0235	0.0131	0.0156	0.0361	0.0339
<b>Mass 1 week (g)</b>	-	-	-	-	-	-
<b>SI (%)</b>	-	-	-	-	-	-
<b>Dried mass (g)</b>	0.0044	0.0067	0.0028	0.0054	0.0148	0.0141
<b>GC (%)</b>	24.58	28.51	21.37	34.62	41.00	41.59

**Table B.2 - Swelling experiment data of MBC-HPHU 1 samples in THF and pure H<sub>2</sub>O**

<b>Samples</b>	<b>THF-1</b>	<b>THF-2</b>	<b>THF-3</b>	<b>H<sub>2</sub>O-1</b>	<b>H<sub>2</sub>O-2</b>	<b>H<sub>2</sub>O-3</b>
<b>Mass initial (g)</b>	0.0158	0.0278	0.0168	0.0124	0.0111	0.0169
<b>Mass 1 week (g)</b>	0.0704	0.110	0.0690	-	-	-
<b>SI (%)</b>	346	296	311	-	-	-
<b>Dried mass (g)</b>	0.0040	0.0062	0.0047	0.0071	0.0056	0.0096
<b>GC (%)</b>	25.32	22.30	27.98	57.26	50.45	56.80

**Table B.3 - Swelling experiment data of SBC-HPHU 3 samples in THF and pure H<sub>2</sub>O**

<b>Samples</b>	<b>THF-1</b>	<b>THF-2</b>	<b>THF-3</b>	<b>H<sub>2</sub>O-1</b>	<b>H<sub>2</sub>O-2</b>	<b>H<sub>2</sub>O-3</b>
<b>Mass initial (g)</b>	0.0172	0.0188	0.0148	0.0985	0.1035	0.0673
<b>Mass 24 h (g)</b>	-	-	-	0.1015	0.1057	0.0689
<b>Mass 3 days (g)</b>	-	-	-	0.104	0.1055	0.0692
<b>Mass 1 week (g)</b>	0.0782	0.0923	0.0695	0.1045	0.1064	0.0701
<b>SI or EWC (%)</b>	355	391	370	6.09	2.80	4.16
<b>EWA (%)</b>	-	-	-	5.74	2.73	3.99
<b>Dried mass (g)</b>	0.0093	0.0124	0.0094	0.0982	0.1024	0.0671
<b>GC (%)</b>	59.88	65.96	63.51	99.70	98.94	99.70

**Table B.4 - Swelling experiment data of MBC-HPHU 3 samples in THF and pure H<sub>2</sub>O**

<b>Samples</b>	<b>THF-1</b>	<b>THF-2</b>	<b>THF-3</b>	<b>H<sub>2</sub>O-1</b>	<b>H<sub>2</sub>O-2</b>	<b>H<sub>2</sub>O-3</b>
<b>Mass initial (g)</b>	0.0154	0.0155	0.0185	0.0772	0.0642	0.0907
<b>Mass 24 h (g)</b>	-	-	-	0.0811	0.0664	0.0931
<b>Mass 3 days (g)</b>	-	-	-	0.0791	0.0685	0.0955
<b>Mass 1 week (g)</b>	0.0624	0.063	0.0733	0.0802	0.0671	0.0948
<b>SI or EWC (%)</b>	305	306	296	3.89	4.52	4.52
<b>EWA (%)</b>	-	-	-	3.74	4.32	4.32
<b>Dried mass (g)</b>	0.0119	0.012	0.014	0.076	0.0633	0.0894
<b>GC (%)</b>	77.27	77.42	75.68	98.45	98.60	98.57

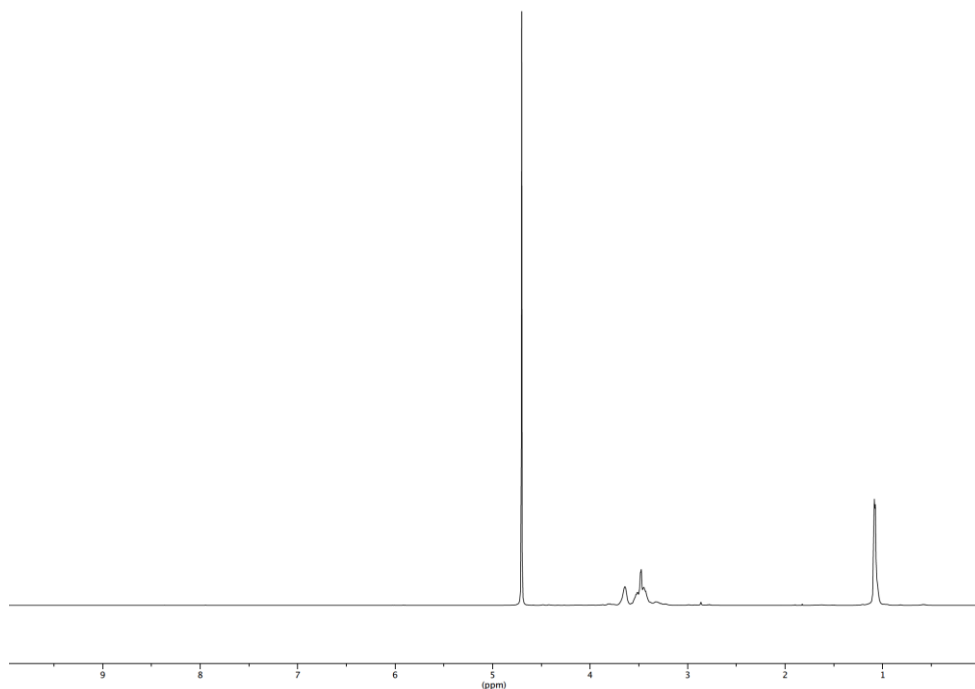


**Figure B.16 - <sup>1</sup>H-NMR spectrum on SBC-HPHU 1 degradation residuals in D<sub>2</sub>O at 25 °C showing possible leaching occurring from SBC-HPHU 1 films in pure H<sub>2</sub>O**

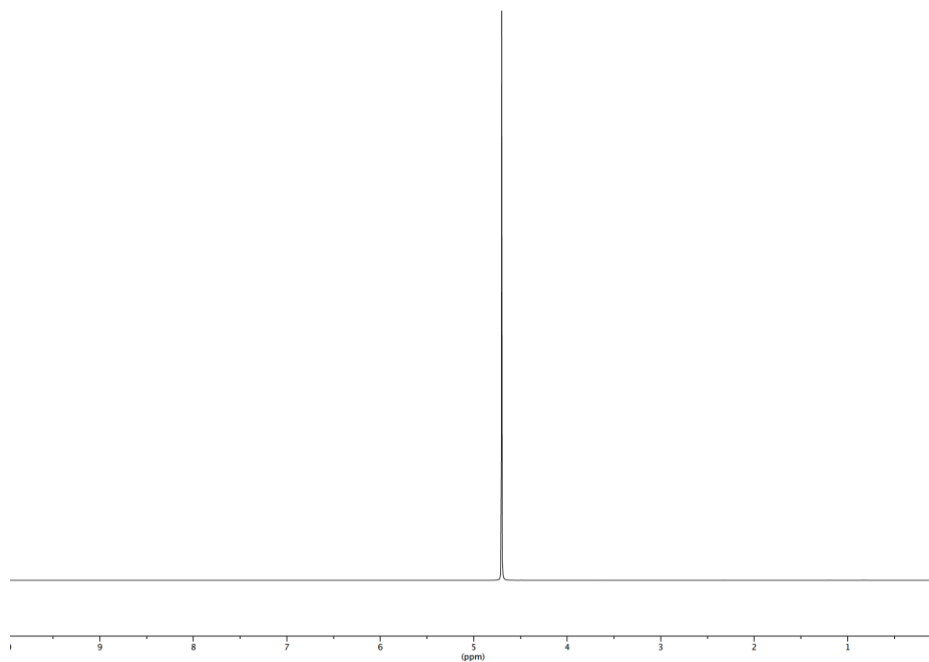


**Figure B.17 - <sup>1</sup>H-NMR spectrum on MBC-HPHU 3 degradation residuals in D<sub>2</sub>O at 25 °C showing no leaching occurring from MBC-HPHU 3 films in pure H<sub>2</sub>O**

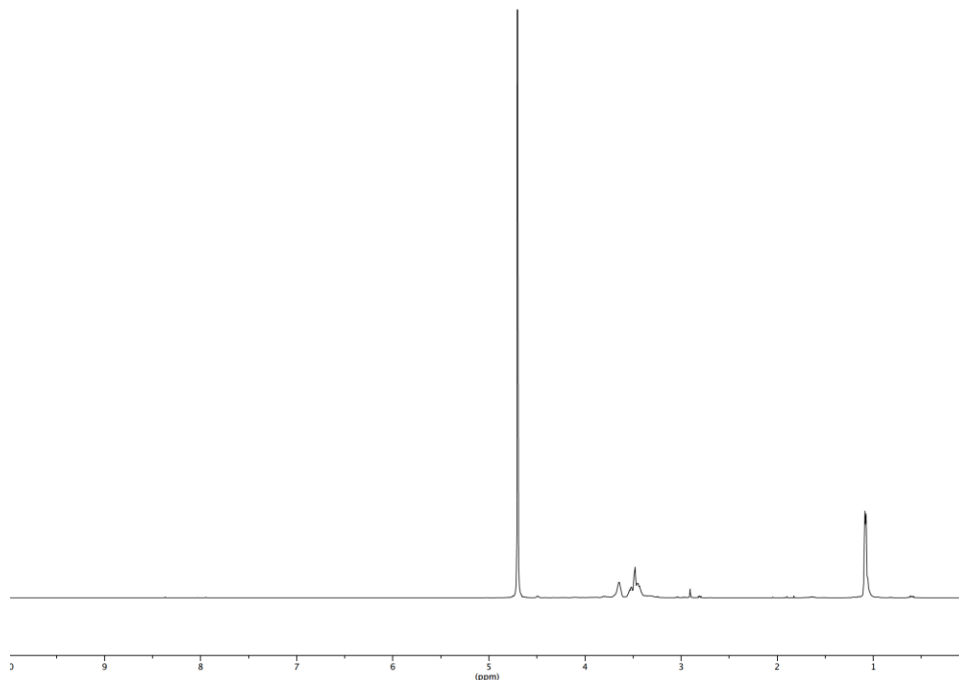


**Figure B.18 -  $^1\text{H}$ -NMR spectrum on MBC-HPHU 1 degradation residuals in  $\text{D}_2\text{O}$  at  $25\text{ }^\circ\text{C}$  showing possible leaching occurring from MBC-HPHU 1 films in pure  $\text{H}_2\text{O}$**

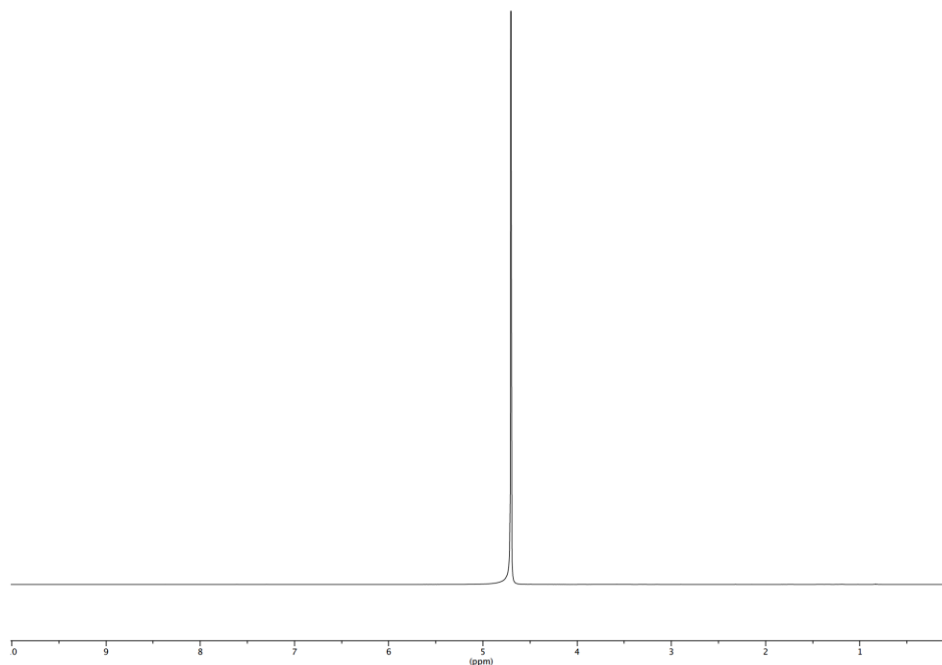


**Figure B.19 -  $^1\text{H}$ -NMR spectrum on MBC-HPHU 3 degradation residuals in  $\text{D}_2\text{O}$  at  $25\text{ }^\circ\text{C}$  showing no leaching occurring from MBC-HPHU 3 films in pure  $\text{H}_2\text{O}$**

**Table B.5 - Degradation experiment data of SBC-HPHU 3 films in acid medium pH = 3**

<b>Samples</b>	<b>1</b>	<b>2</b>	<b>3</b>
<b>Mass initial (g)</b>	0.6681	0.3441	0.2111
<b>Mass 24 h (g)</b>	0.6816	0.3510	0.2153
<b>Mass 3 days (g)</b>	0.6907	0.3569	0.2182
<b>Mass 1 week (g)</b>	0.6928	0.3608	0.2219
<b>EWC (%)</b>	3.70	4.85	5.12
<b>EWA (%)</b>	3.57	4.63	4.87
<b>Dried mass (g)</b>	0.6688	0.3425	0.2111
<b>Initial mass recovery (%)</b>	100	99.54	100

**Table B.6 - Degradation experiment data of MBC-HPHU 3 films in acid medium pH = 3**

<b>Samples</b>	<b>1</b>	<b>2</b>	<b>3</b>
<b>Mass initial (g)</b>	0.4552	0.2697	0.3136
<b>Mass 24 h (g)</b>	0.4683	0.2808	0.3205
<b>Mass 3 days (g)</b>	0.4691	0.2849	0.3243
<b>Mass 1 week (g)</b>	0.4665	0.2820	0.3274
<b>EWC (%)</b>	2.48	4.56	4.40
<b>EWA (%)</b>	2.42	4.36	4.22
<b>Dried mass (g)</b>	0.4443	0.2619	0.3084
<b>Initial mass recovery (%)</b>	97.61	97.11	98.34

**Table B.7 - Sessile drop tests of Milli-Q water on SBC-HPHU 3 films**

<b>Measurement</b>	<b>Contact angle left (°)</b>	<b>Contact angle right (°)</b>	<b>Average (°)</b>
<b>1</b>	102.8	106.8	104.8
<b>2</b>	115.2	98.6	116.9
<b>3</b>	110.4	112.9	111.65
<b>4</b>	102.5	97.7	100.1
<b>5</b>	104.3	99.4	101.85

**Table B.8 - Sessile drop tests of Milli-Q water on MBC-HPHU 3 films**

<b>Measurement</b>	<b>Contact angle left (°)</b>	<b>Contact angle right (°)</b>	<b>Average (°)</b>
<b>1</b>	116.5	100.9	108.7
<b>2</b>	107.6	110.1	108.85
<b>3</b>	105.7	113.2	109.45
<b>4</b>	104.7	112.9	108.8
<b>5</b>	115.8	107.1	111.45

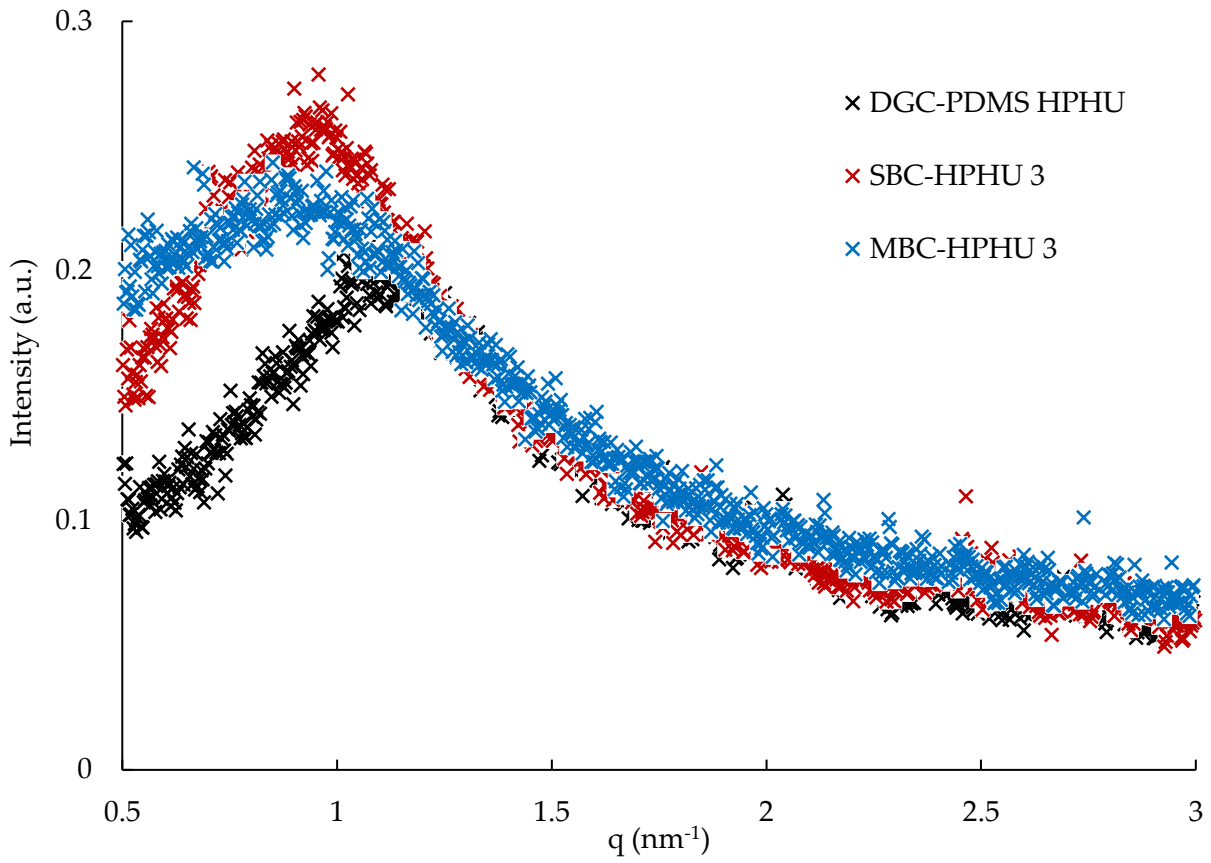


**Figure B.20 - SAXS spectra of DGC- PDMS-5k-(NH<sub>2</sub>)<sub>2</sub> HPHU, SBC-HPHU 3, and MBC-HPHU 3 showing peaks at  $q_{\max}$  used to calculate the mean interdomain spacing of the films.**

**The intensity is given in logarithmic scale.**

**Table B.9 - SBC and MBC experimental trials for reaction optimization<sup>4</sup>**

<b>Trial</b>	<b>Catalyst</b>	<b>Catalyst/sugar alcohol mol%</b>	<b>DMC/sugar alcohol molar ratio</b>	<b>Reaction time (h)</b>	<b>Yield (%)</b>
<b>SBC-1</b>	DBU	5	10	24	18
<b>SBC-2</b>	TBD	5	7	16	42
<b>SBC-3</b>	DBU	5	7	16	41
<b>SBC-4</b>	TBD	5	5	16	7
<b>SBC-5</b>	TBD	1	7	24	17
<b>SBC-6</b>	TBD	3	7	16	39
<b>SBC-7</b>	TBD	3	7	19	41
<b>MBC-1</b>	TBD	5	7	16	55
<b>MBC-2</b>	TBD	3	7	19	32
<b>MBC-3</b>	TBD	5	10	16	56

---

<sup>4</sup>Reactions with DBU (1,8-Diazabicyclo[5.4.0]undec-7-ene) led to dark brown and black final product solutions compared to those with TBD (1,5,7,5-triazabicyclo[4.4.0]dec-5-ene) that lead to light yellow or orange final reaction solutions.

## Appendix C

### Supporting information for “Increasing the hydrophobicity of hybrid poly(propylene glycol)-based polyhydroxyurethanes by capping with hydrophobic diamine”

- DGC synthesis

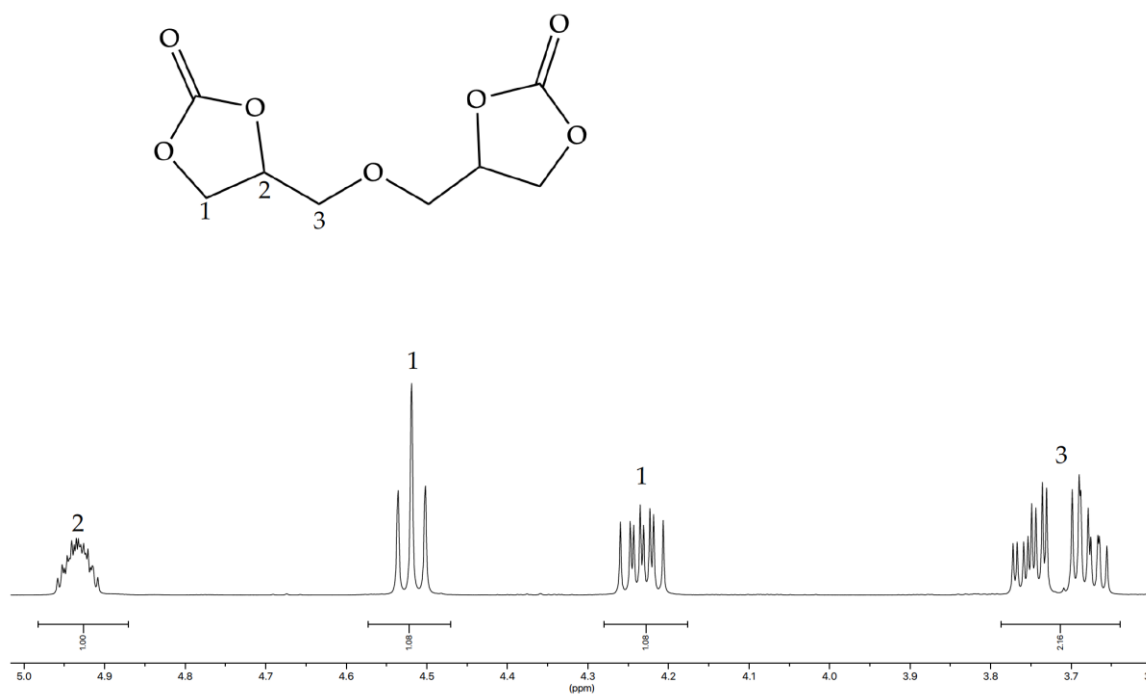
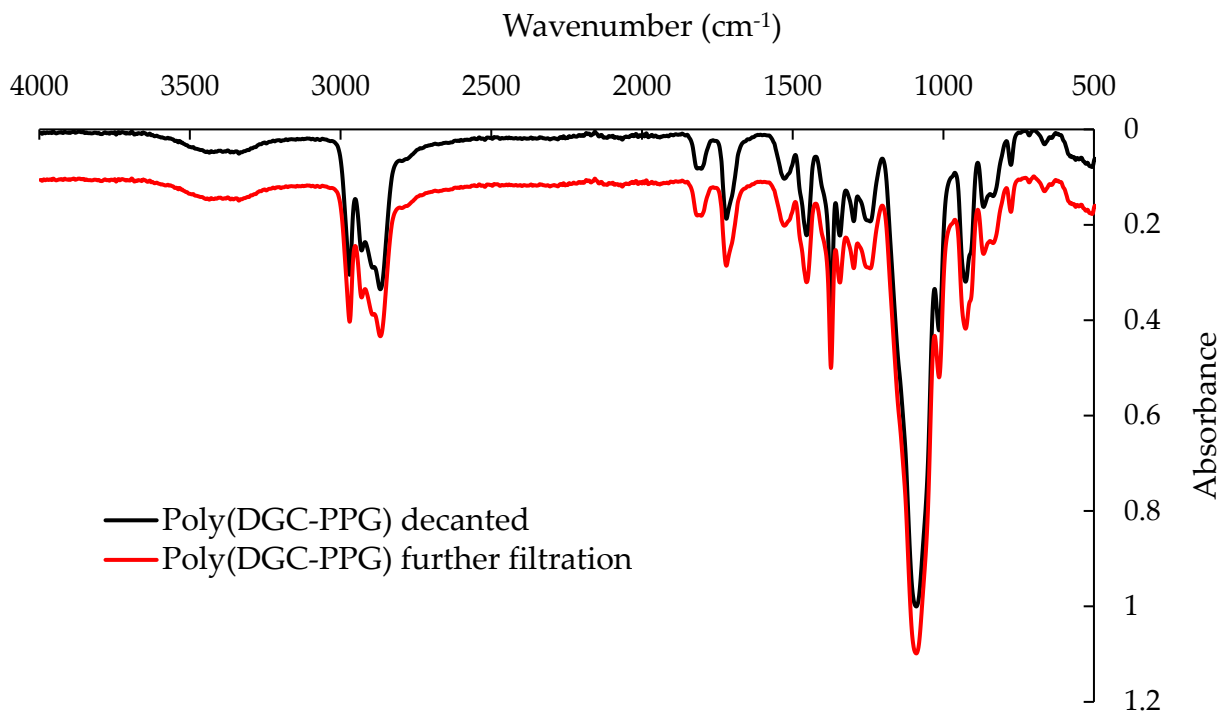


Figure C.1 - Labelled DGC <sup>1</sup>H-NMR spectrum in DMSO-d<sub>6</sub> at 25 °C.  $\delta$  (ppm): 4.93 (m, 2H, H<sub>2</sub>), 4.52 (t, 2H, H<sub>1</sub><sup>cis or trans</sup>), 4.25 (ddd, 2H, H<sub>1</sub><sup>cis or trans</sup>), 3.79-3.65 (m, 4H, H<sub>3</sub>).

- **Poly(DGC-PPG) synthesis**



**Figure C.2 - FTIR spectra of decanted poly(DGC-PPG) (black) and filtered poly(DGC-PPG) to verify that the DGC monomer was fully removed from the polymer medium. The carbonyl stretch 1800 cm<sup>-1</sup> area remained unchanged relatively to that of the carbonyl stretch of the urethane linkage at 1720 cm<sup>-1</sup>. DGC has a carbonyl stretch at 1780 cm<sup>-1</sup> that would have overlapped with the one at 1800 cm<sup>-1</sup> and increased its intensity if it were present in the PHU medium.**

- **Extended poly(DGC-PPG) PHU characterization**

**<sup>1</sup>H-NMR:**

To calculate the number *n* for every PDMS-(NH<sub>2</sub>)<sub>2</sub>, a molecular weight calculation was conducted by first finding the molecular weight of every unit inside the brackets (74 g/mol) and the molecular weight of the part outside of the brackets (248 g/mol). Then, the following formula was applied:

$$n = \frac{(MW^{\text{Diamine}} - 248)}{74}$$

To compare the <sup>1</sup>H-NMR to the predicted values, the following formula was applied to calculate the ratio of the number of siloxane units with respect to the propylene glycol ones:

$$\frac{\text{Si} - (\text{CH}_3)_2 - \text{O units}}{\text{PPG} - \text{CH}_3 \text{ units}} = \frac{(n + 2) \times 4}{34.1 \times 3.07}$$

where, (n+2) is multiplied by 4 because there are two methyl groups and two PDMS-(NH<sub>2</sub>)<sub>2</sub> chains are reacting with the cyclic carbonates on each side of the prepolymer, 34.1 is the number of repeating units in Jeffamine D-2000 containing the methyl group being studied herein, and 3.07 is the average number of Jeffamine D-2000 units in the prepolymer chains calculated following the procedure discussed under “Estimation of prepolymer absolute molecular weight”.

**FTIR:**

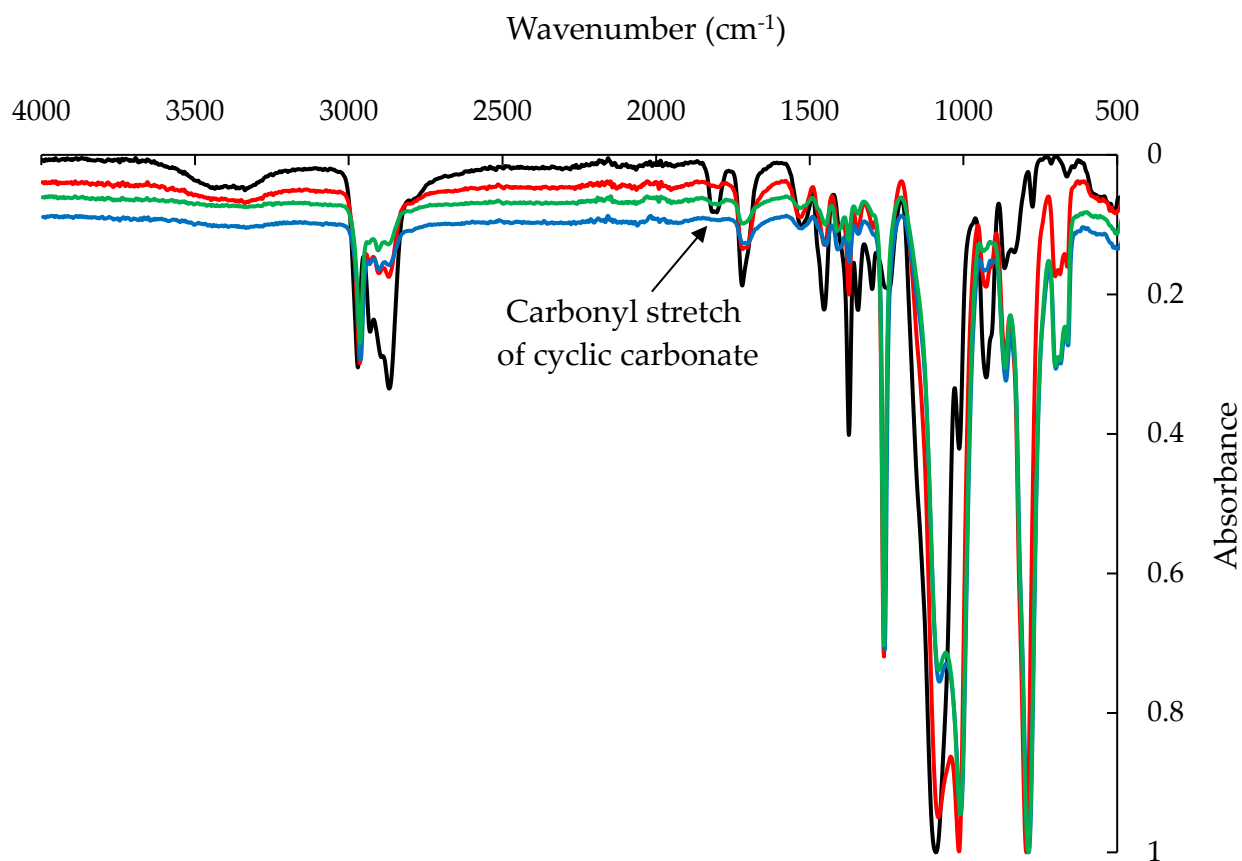


**Figure C.3 - FTIR spectra of poly(DGC-PPG) (black) and extended poly(DGC-PPG) with PDMS-3k-(NH<sub>2</sub>)<sub>2</sub> (red), PDMS-5k-(NH<sub>2</sub>)<sub>2</sub> (blue), and PDMS-7k-(NH<sub>2</sub>)<sub>2</sub> (green) (2 molar equivalents of hydrophobic diamine per polymer) showing the disappearance of the carbonyl stretch at 1800 cm<sup>-1</sup> for the extended polymers from both ends compared to poly(DGC-PPG) FTIR spectrum.**

SEC:

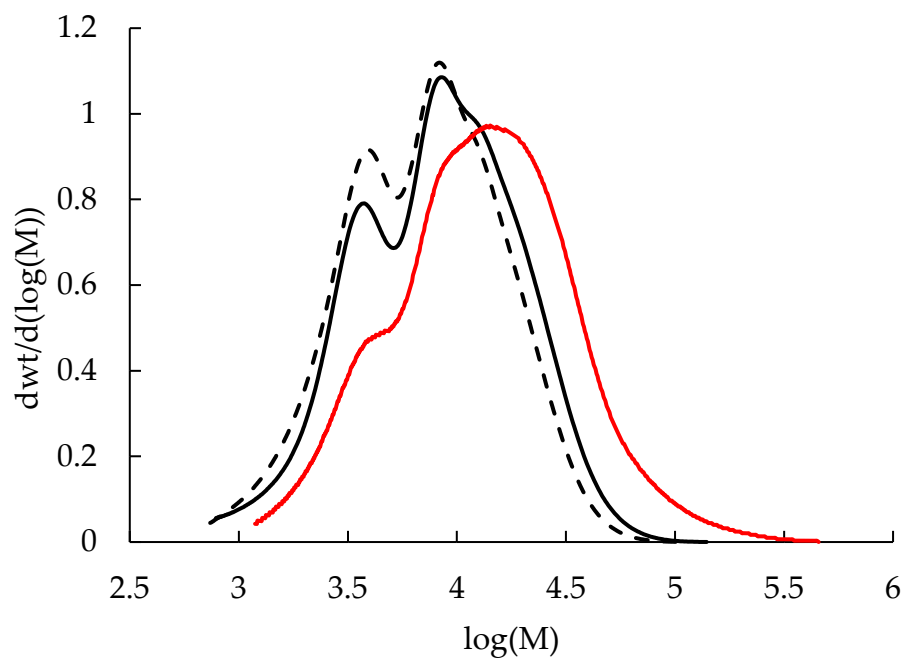


**Figure C.4 - SEC traces of poly(DGC-PPG) (black-discontinuous) and extended poly(DGC-PPG) with PDMS-1k-(NH<sub>2</sub>)<sub>2</sub> (black) and PDMS-3k-(NH<sub>2</sub>)<sub>2</sub> (red) (2 molar equivalents of hydrophobic diamine per polymer)**

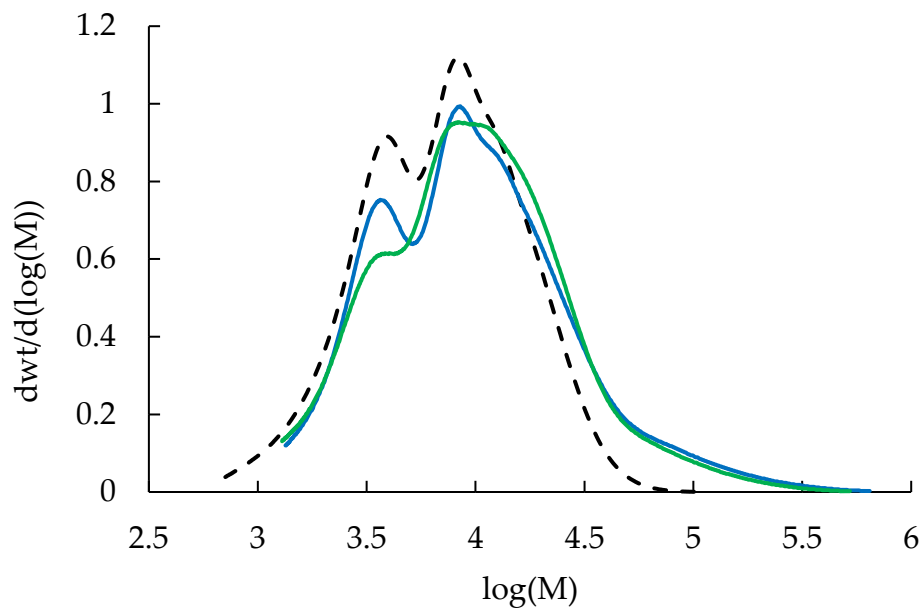


**Figure C.5 - SEC traces of poly(DGC-PPG) (black-discontinuous) and extended poly(DGC-PPG) with PDMS-5k-(NH<sub>2</sub>)<sub>2</sub> (blue) and PDMS-7k-(NH<sub>2</sub>)<sub>2</sub> (green) (2 molar equivalents of hydrophobic diamine per polymer)**

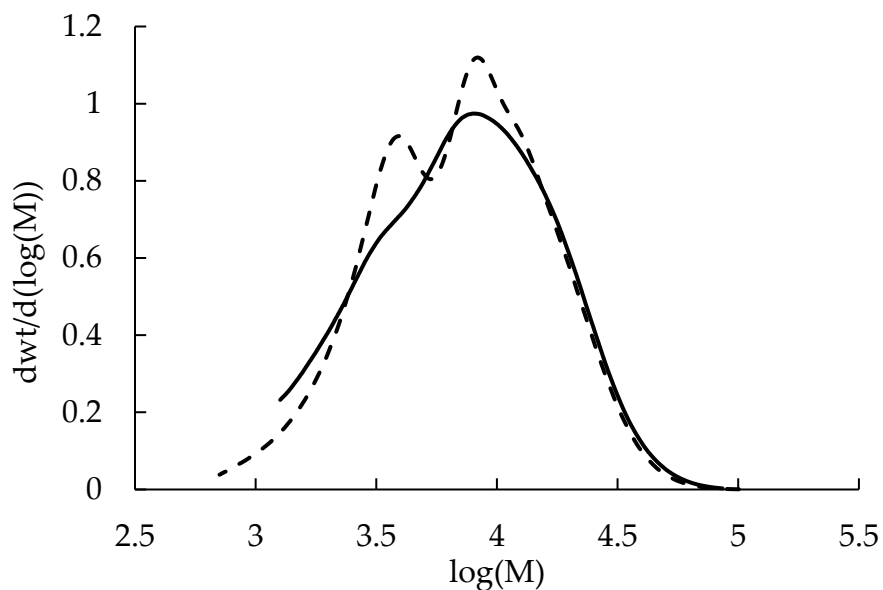


**Figure C.6 - SEC traces of poly(DGC-PPG) (black-discontinuous) and Priamine-poly(DGC-PPG)-Priamine (black)**

**SAXS:**

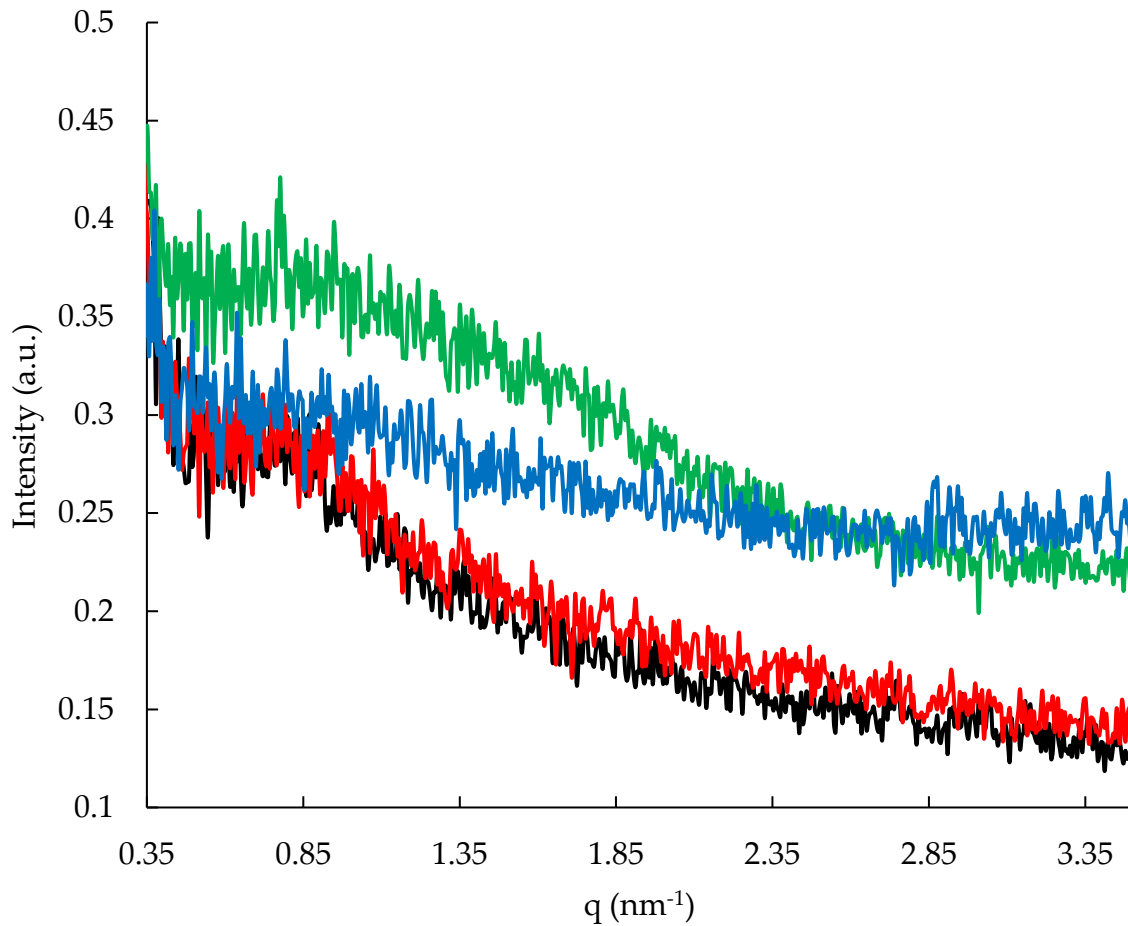


**Figure C.7 - SAXS spectra of extended poly(DGC-PPG) from both ends with PDMS-1k-(NH<sub>2</sub>)<sub>2</sub> (black), PDMS-3k-(NH<sub>2</sub>)<sub>2</sub> (red), PDMS-5k-(NH<sub>2</sub>)<sub>2</sub> (blue), and PDMS-7k-(NH<sub>2</sub>)<sub>2</sub> (green) (2 molar equivalents of hydrophobic diamine per polymer) showing peaks at  $q_{\max}$  used to calculate the mean interdomain spacing of the gel-like samples. The intensity is given in logarithmic scale.**

**TGA:**

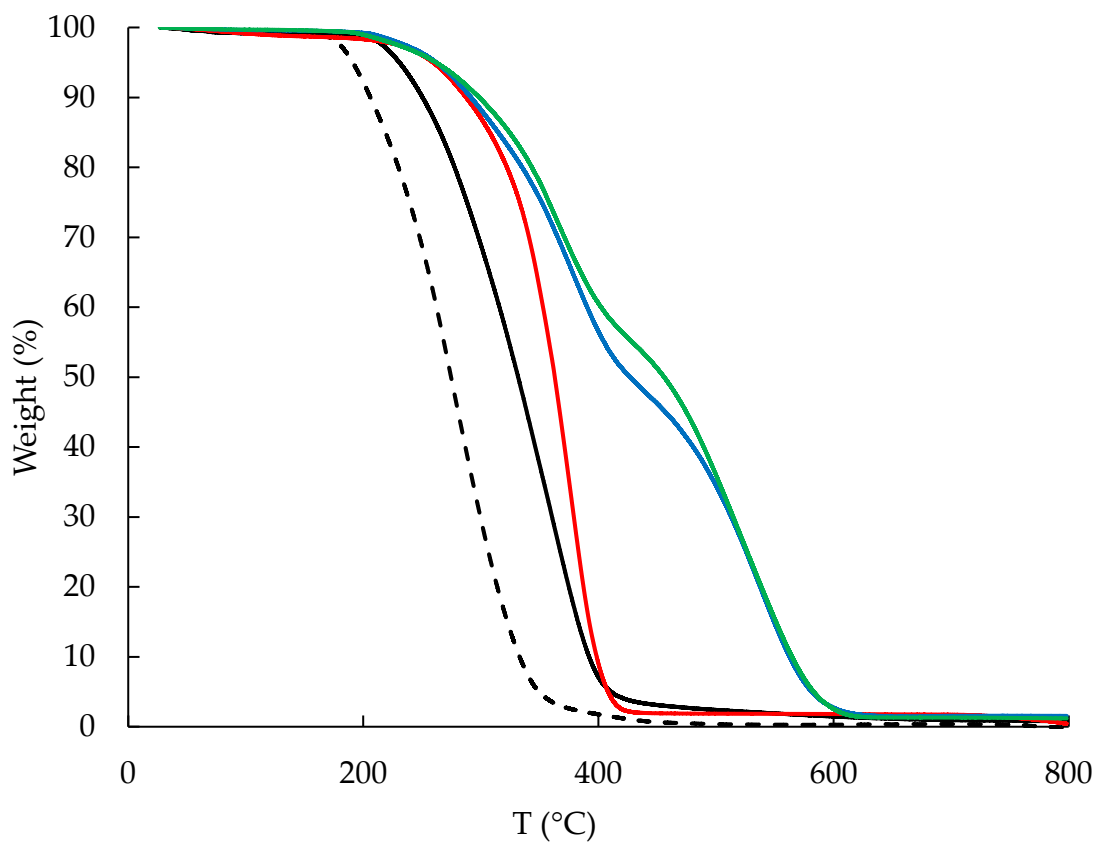


**Figure C.8 - TGA traces of poly(DGC-PPG) (black-discontinued) and extended poly(DGC-PPG) from both ends with PDMS-1k-(NH<sub>2</sub>)<sub>2</sub> (black), PDMS-3k-(NH<sub>2</sub>)<sub>2</sub> (red), PDMS-5k-(NH<sub>2</sub>)<sub>2</sub> (blue), and PDMS-7k-(NH<sub>2</sub>)<sub>2</sub> (green) used in this work (2 molar equivalents of hydrophobic diamine per polymer)**

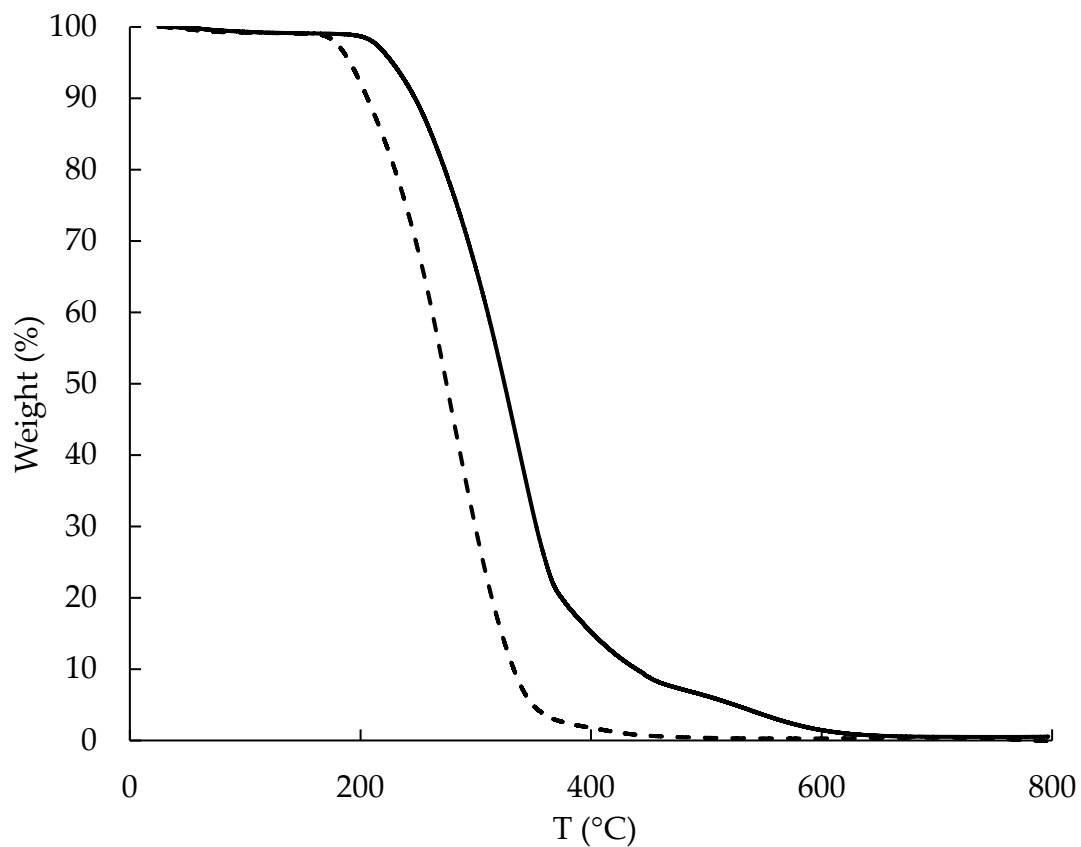


**Figure C.9 - TGA traces of poly(DGC-PPG) (black-discontinuous) and Priamine-poly(DGC-PPG)-Priamine (black)**

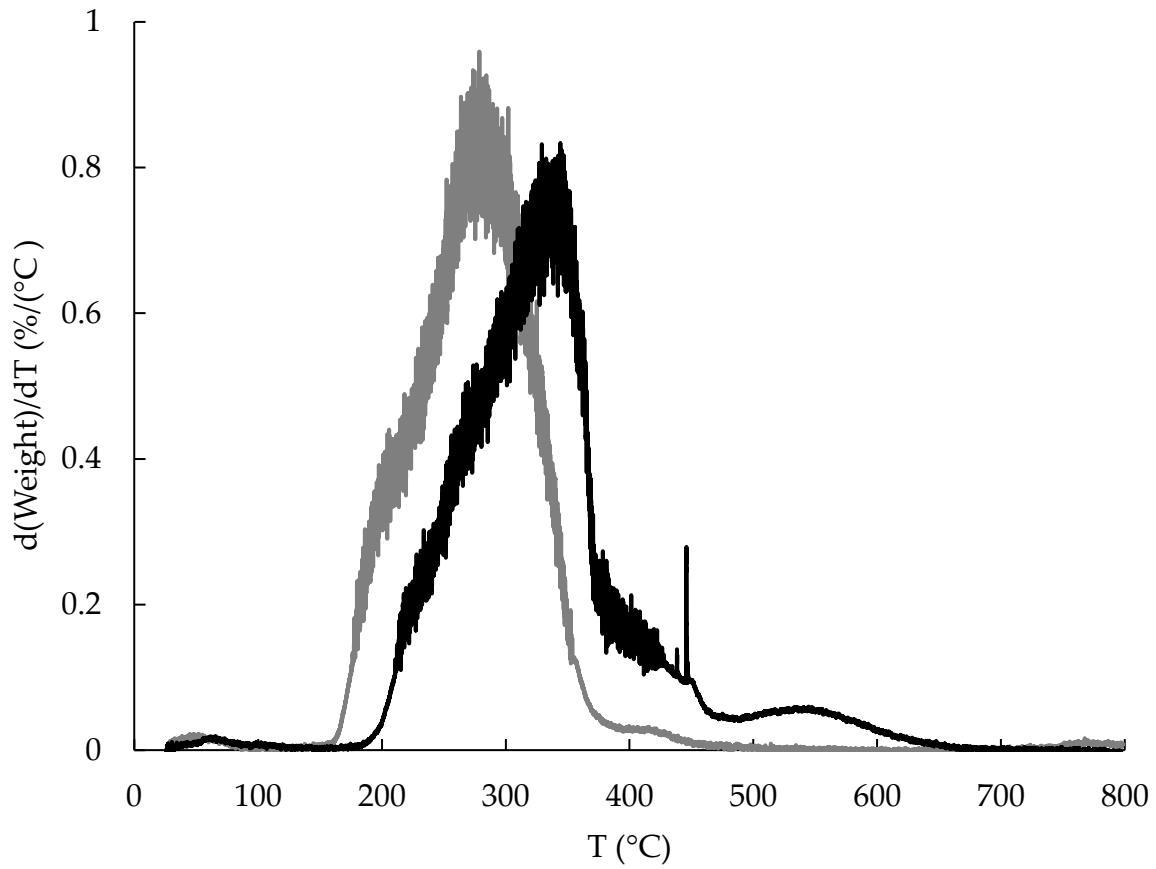


**Figure C.10 - Derivative of weight percentage with respect to temperature traces of poly(DGC-PPG) (grey) and Priamine-poly(DGC-PPG)-Priamine (black)**

- **Estimation of prepolymer absolute molecular weight**

This section discusses the steps taken to estimate the molecular weight of poly(DGC-PPG). From the SEC data, the average number molecular weight,  $M_n$ , of this prepolymer, with respect to PMMA standards, is:

$$M_n = 4,600 \text{ g/mol}$$

The average number molecular weight of Jeffamine D-2000 measured by GPC using PMMA standards is:

$$M_n^{\text{Jeffamine D-2000}} = 1,500 \text{ g/mol}$$

Dividing the molecular weight of the prepolymer by that of Jeffamine D-2000, gives:

$$\# \text{ of diamine molecules incorporated into the prepolymer chain} = 3.07 \approx 3$$

Assuming that the prepolymers have on average 3 amine units and that carbonates are the end-groups, as shown by the FTIR spectrum of poly(DGC-PPG), gives:

$$\# \text{ of dicarbonate molecules incorporated into the prepolymer chain} = 4$$

as there are two dicarbonate units that have to link the three diamine units and two dicarbonate units have to be on both ends of the oligomers. Knowing that the molecular weight of DGC is 218 g/mol and that of Jeffamine D-2000 is 2,000 g/mol, the average number molecular weight of poly(DGC-PPG) can be estimated as:

$$M_n = 3 \times 2,000 + 4 \times 218 = 6,872 \text{ g/mol}$$

This is equivalent to an average of 6 hydroxyurethane linkages in the given oligomer chains.

To calculate the molecular weights of the modified polymers to be end-capped, the molecular weight of the diamines was added to that of poly(DGC-PPG), as follows:

For PDMS-7k-poly(DGC-PPG)-7k-PDMS, the absolute molecular weight becomes:

$$M_n^{\text{absolute}} = 6,872 + 0.5 \times 7,000 = 10,372 \text{ g/mol}$$

For -Priamine-poly(DGC-PPG)-Priamine, the absolute molecular weight becomes:

$$M_n^{absolute} = 6,872 + 2 \times 534 = 7,940 \text{ g/mol}$$

- **Curing kinetics and FTIR of cured samples**

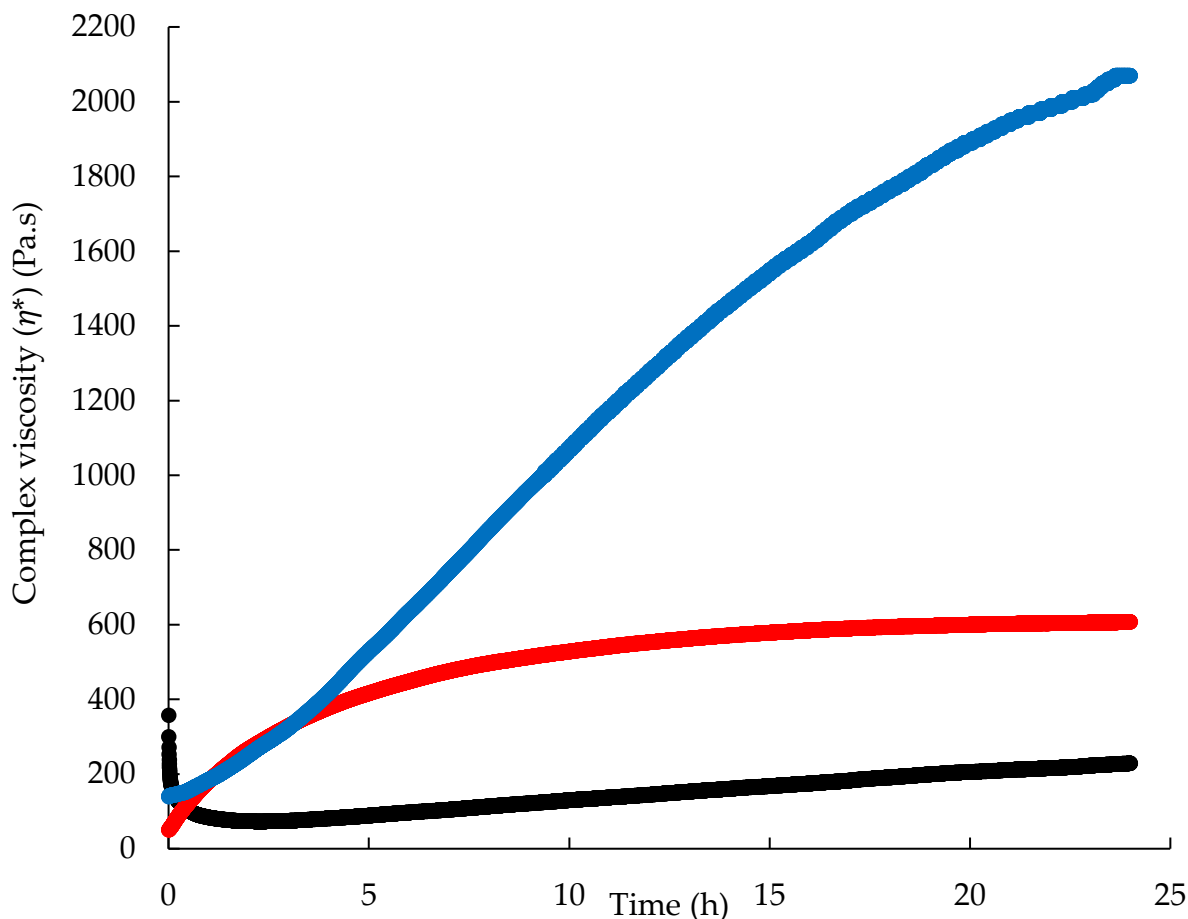


**Figure C.11 - Curing kinetics of the end-capped poly(DGC-PPG) (black), PDMS-7k-poly(DGC-PPG)-7k-PDMS (red), and Priamine-poly(DGC-PPG)-Priamine (blue) by following the complex viscosity ( $\eta^*$ ) (Pa.s) at a frequency of 1 Hz and a strain of 1% for 24 h. 0.5 wt.% of the proprietary catalyst was added to accelerate the curing of PDMS-7k-poly(DGC-PPG)-7k-PDMS, and Priamine-poly(DGC-PPG)-Priamine. Measurements were done at 22 °C and 40-50% humidity.**

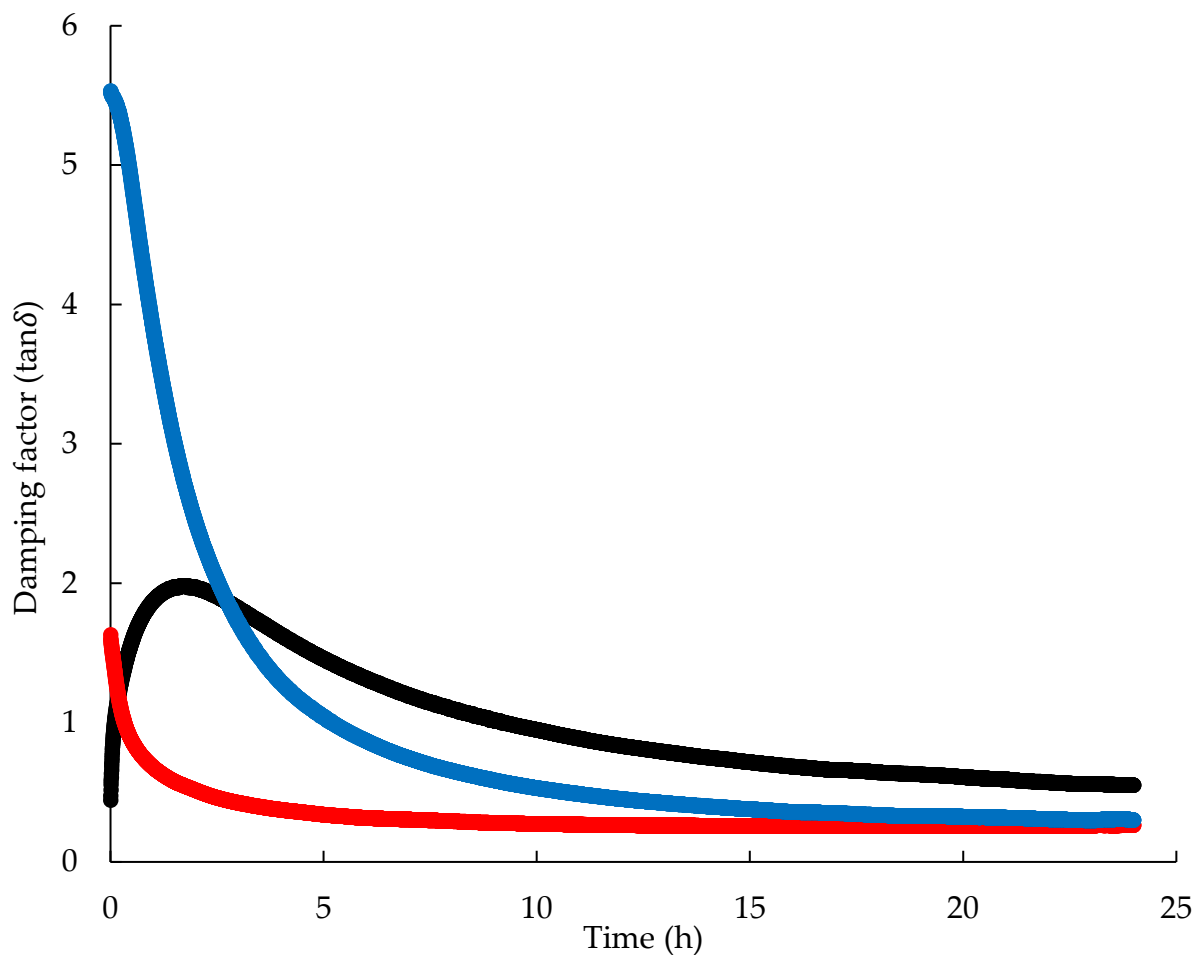


**Figure C.12 - Curing kinetics of the end-capped poly(DGC-PPG) (black), PDMS-7k-poly(DGC-PPG)-7k-PDMS (red), and Priamine-poly(DGC-PPG)-Priamine (blue) by following the damping factor ( $\tan\delta$ ) at a frequency of 1 Hz and a strain of 1% for 24 h. 0.5 wt.% of the proprietary catalyst was added to accelerate the curing of PDMS-7k-poly(DGC-PPG)-7k-PDMS, and Priamine-poly(DGC-PPG)-Priamine. Measurements were done at 22 °C and 40-50% humidity.**

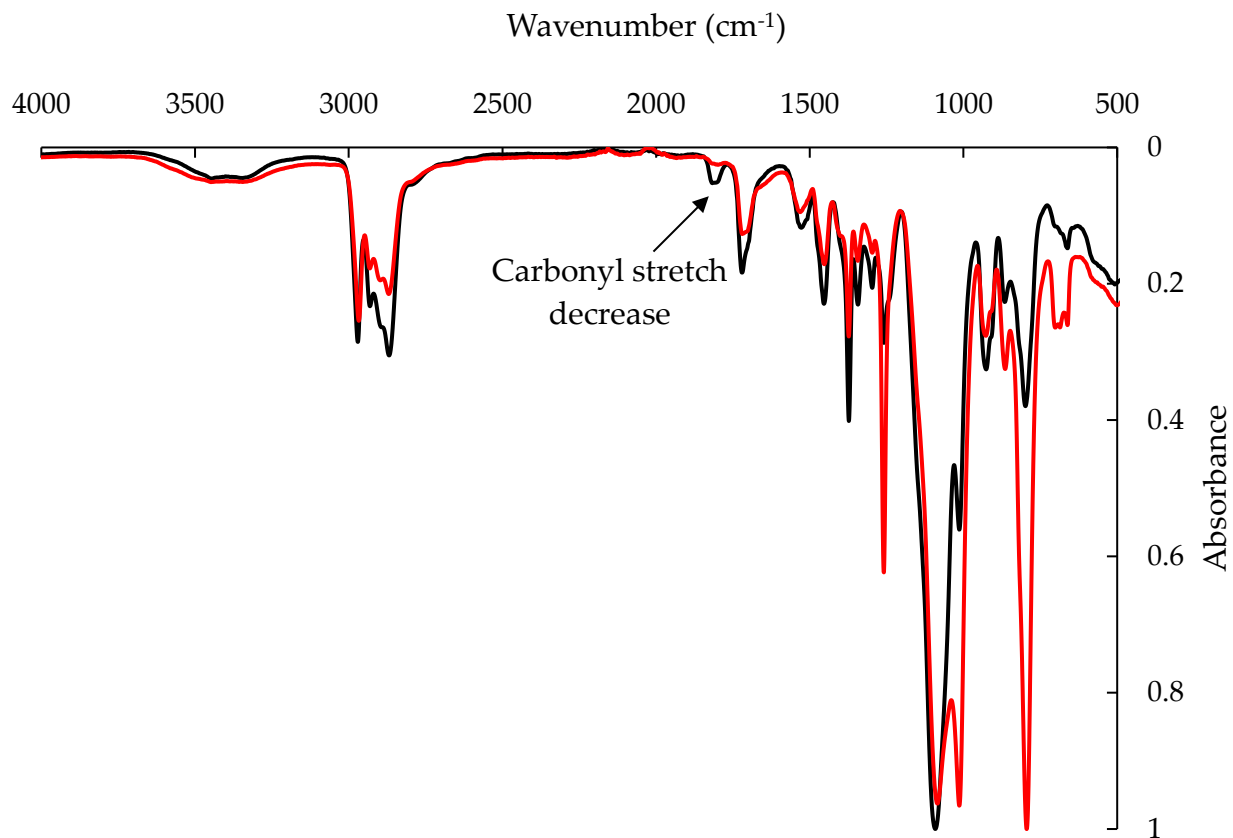


**Figure C.13 - FTIR spectra of PDMS-7k-poly(DGC-PPG)-7k-PDMS-7k before (black) and after (red) end-capping showing the decrease of the carbonyl stretch at 1800 cm<sup>-1</sup> in the end-capped prepolymer spectrum.**

- **HPHU characterization**

**Table C.1 - Swelling experiment data of the poly(DGC-PPG) HPHU samples in different solvents**

<b>Samples</b>	<b>THF-1</b>	<b>THF-2</b>	<b>THF-3</b>	<b>H<sub>2</sub>O-1</b>	<b>H<sub>2</sub>O-2</b>	<b>H<sub>2</sub>O-3</b>	<b>Toluene-1</b>	<b>Toluene-2</b>	<b>Toluene-3</b>
<b>Mass initial (mg)</b>	21.5	21.8	10.2	11.2	15.5	22.5	17.6	22.5	14.0
<b>Mass 1 week (mg)</b>	89.6	95.1	40.1	19.5	26.4	40.5	41.2	50.0	32.1
<b>SI (%)</b>	317	336	293	74.1	70.1	80.0	134	122	129
<b>Dried mass (mg)</b>	6.90	8.60	3.90	7.70	11.1	16.7	5.30	6.30	5.30
<b>GC (%)</b>	32.1	39.4	38.2	68.8	71.6	74.2	30.1	28.0	37.9

**Table C.2 - Swelling experiment data of the PDMS-7k-poly(DGC-PPG)-7k-PDMS HPHU samples in different solvents**

<b>Samples</b>	<b>THF-1</b>	<b>THF-2</b>	<b>THF-3</b>	<b>H<sub>2</sub>O-1</b>	<b>H<sub>2</sub>O-2</b>	<b>H<sub>2</sub>O-3</b>	<b>Toluene-1</b>	<b>Toluene-2</b>	<b>Toluene-3</b>
<b>Mass initial (mg)</b>	19.4	18.4	13.8	11.1	23.6	10.7	13.8	17.8	12.2
<b>Mass 1 week (mg)</b>	108.2	102.6	81.8	17.4	34.6	16.8	69.1	94.7	62.6
<b>SI (%)</b>	458	458	493	56.8	46.6	57.0	401	432	413
<b>Dried mass (mg)</b>	7.30	7.40	6.80	10.4	22.4	10.2	5.80	7.80	5.70
<b>GC (%)</b>	37.6	40.2	49.3	93.7	94.9	95.3	42.0	43.8	46.7

**Table C.3 - Swelling experiment data of the Priamine-poly(DGC-PPG)-Priamine HPHU samples in different solvents**

<b>Samples</b>	<b>THF- 1</b>	<b>THF- 2</b>	<b>THF- 3</b>	<b>H<sub>2</sub>O -1</b>	<b>H<sub>2</sub>O -2</b>	<b>H<sub>2</sub>O -3</b>	<b>Toluene -1</b>	<b>Toluene -2</b>	<b>Toluene -3</b>
<b>Mass initial (mg)</b>	14.3	19.0	10.1	15.4	15.0	20.8	18.4	17.7	13.4
<b>Mass 1 week (mg)</b>	54.3	70.9	36.3	16.1	15.3	21.7	56.7	52.6	40.0
<b>SI (%)</b>	280	273	259	4.55	2.00	4.33	208	197	199
<b>Dried mass (mg)</b>	8.20	11.4	5.10	15.4	14.5	20.2	10.4	9.60	8.10
<b>GC (%)</b>	57.3	60.0	50.5	100	96.7	97.1	56.5	54.2	60.4

## Appendix D

### Supporting information for “Bio-based thermoplastic polyhydroxyurethanes synthesized from the terpolymerization of a dicarbonate and two diamines: design, rheology, and application in melt blending”

- DGC synthesis

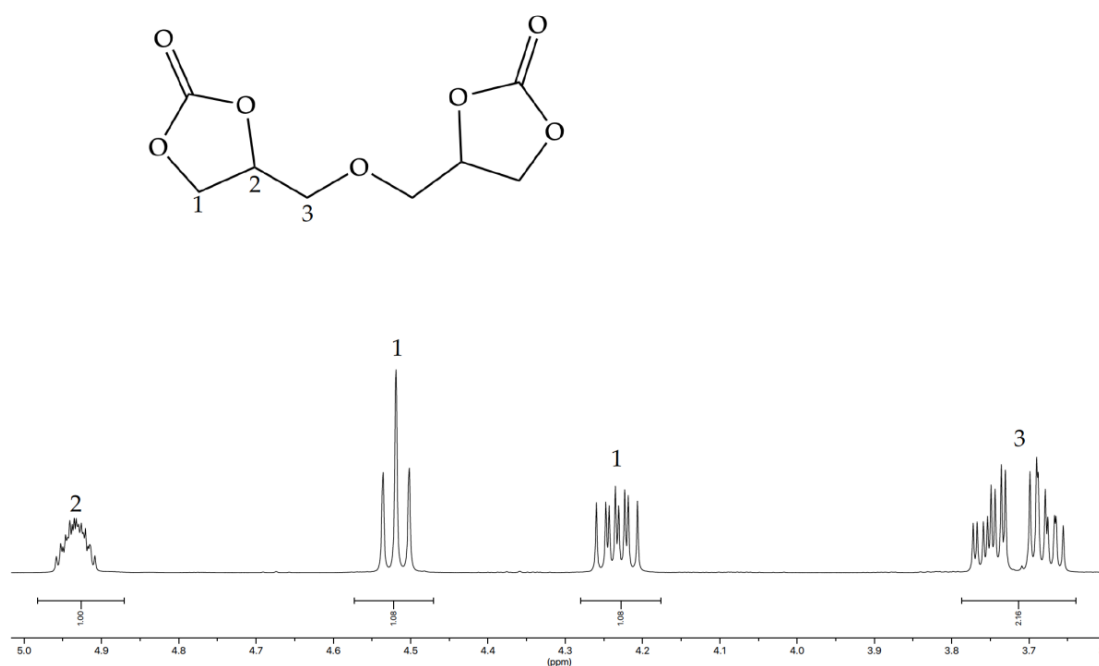
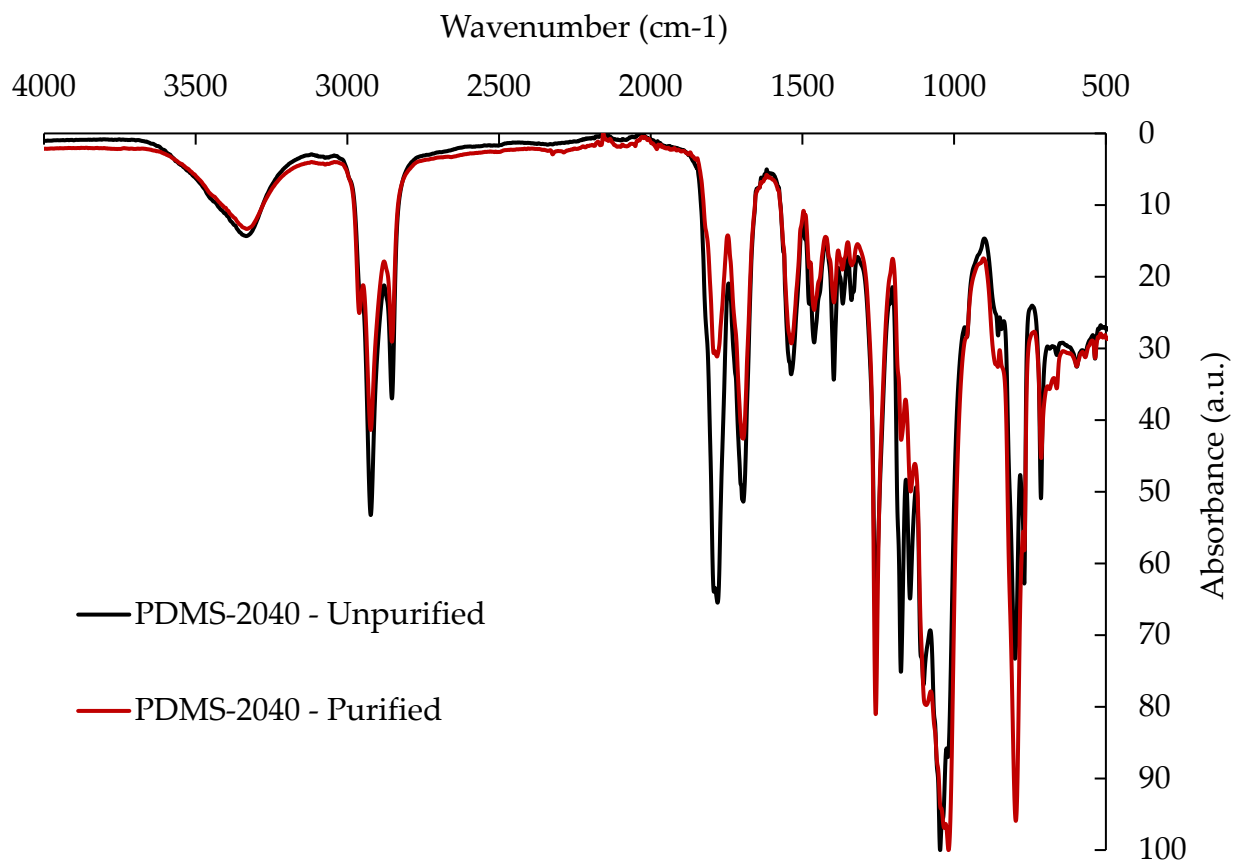


Figure D.1 - Labelled DGC <sup>1</sup>H-NMR spectrum in DMSO-d<sub>6</sub> at 25 °C. δ (ppm): 4.93 (m, 2H, H<sub>2</sub>), 4.52 (t, 2H, H<sub>1</sub><sup>cis or trans</sup>), 4.25 (ddd, 2H, H<sub>1</sub><sup>cis or trans</sup>), 3.79-3.65 (m, 4H, H<sub>3</sub>).

- **Characterization of PDSM containing TPHUs**

**FTIR:**



**Figure D.2 - FTIR spectra showing the decrease in the carbonyl stretch related to the cyclic carbonate end-groups and unreacted carbonates (at 1780 cm<sup>-1</sup>) with respect to that of the carbonyl stretch of the urethane linkages (at 1695 cm<sup>-1</sup>) after purifying PDMS-2040.**

**<sup>1</sup>H-NMR:**

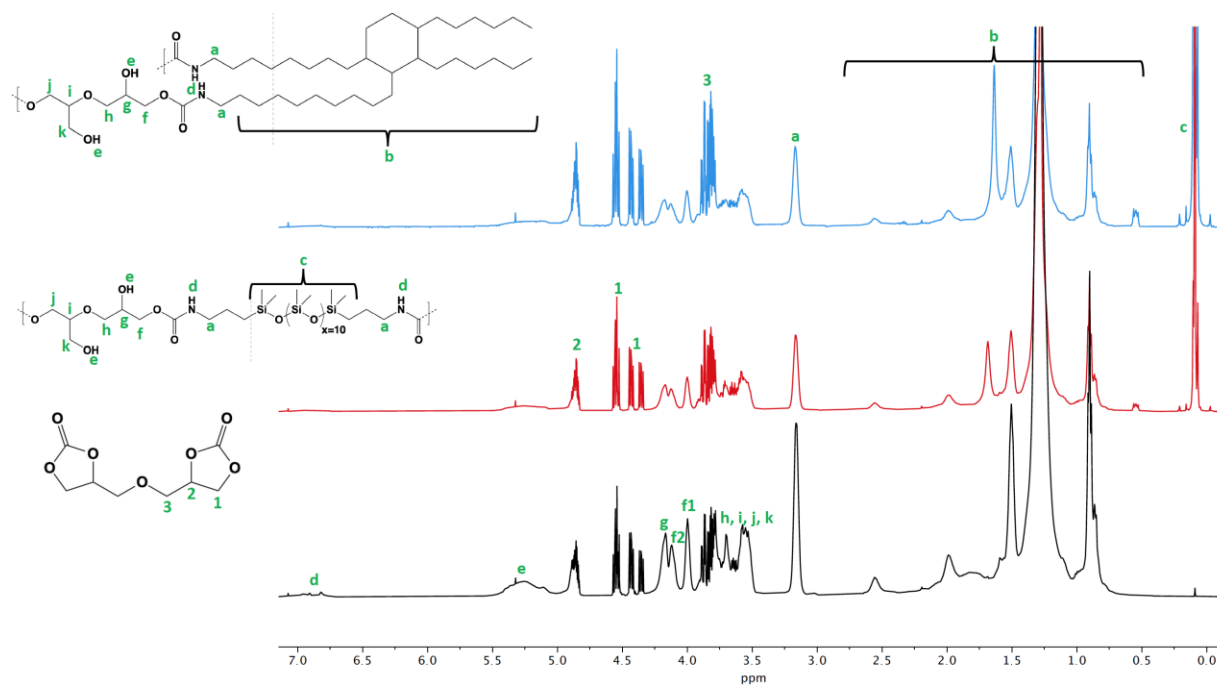


**Figure D.3 - Stacked <sup>1</sup>H-NMR spectra of unpurified PDMS-0040 (black), PDMS-2040 (red), and PDMS-4040 (blue) in CDCl<sub>3</sub> at 25 °C.**

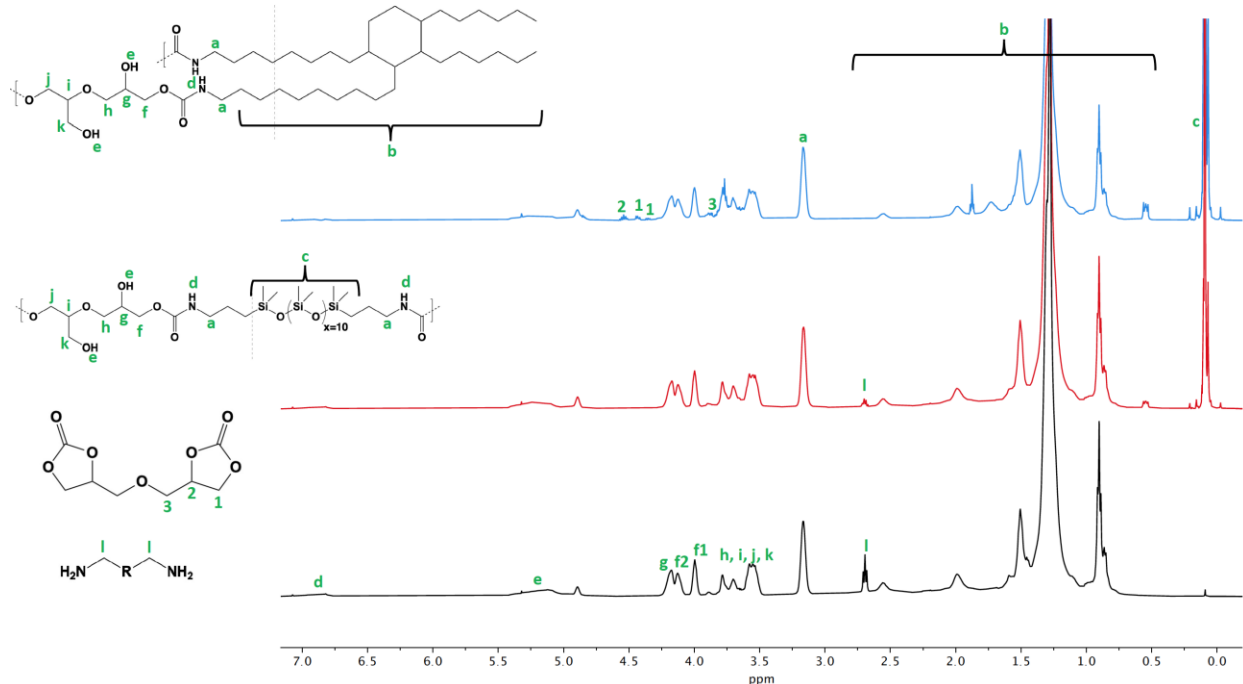


**Figure D.4 - Stacked  $^1\text{H-NMR}$  spectra of unpurified PDMS-0025 (black), PDMS-2025 (red), and PDMS-4025 (blue) in  $\text{CDCl}_3$  at  $25\text{ }^\circ\text{C}$ .**

The  $^1\text{H-NMR}$  spectra were analyzed and the ratio of secondary to primary hydroxyl groups as well as the cyclic carbonate and diamine conversions were calculated. The former is calculated as follows:

$$\text{secondary OH (\%)} = \frac{\int g + \int f + \int h}{\int g + \int f + \int h + \int i + \int j + \int k} \times 100 \quad \text{Eq. (D.1)}$$

The integrations of  $f$  and  $g$  can be found and that of  $h$  is equal to that of  $f$ . Hence, the sum of the integrations of  $i$ ,  $j$ , and  $k$  can be found. In the case where carbonate end-groups are present, the integration of 3 can be deduced from those of 1, and then it is subtracted from the total integrated value to end up with the sum of the integrations of  $h$ ,  $i$ ,  $j$ , and  $k$ .

The cyclic carbonate conversion was found through (DGC dissolves partially in  $\text{CDCl}_3$ ):

$$\text{CC (\%)} = \frac{\int g + \int i}{\int g + \int i + \int 2} \quad \text{Eq. (D.2)}$$

The integration of peak 2 can be deduced from that of peak 1 by dividing the latter by 2. The integration of  $i$  can be found by dividing the sum of the integrations of peaks  $i, j$ , and  $k$  by 5.

The diamine conversion was found through:

$$\text{Diamine (\%)} = \frac{f_a}{f_{a+fl}} \quad \text{Eq. (D.3)}$$

All the calculated values are summarized below:

**Table D.1 - Parameters analyzed from the  $^1\text{H-NMR}$  of PDMS containing TPHUs**

TPHU	Sec OH/prim OH	CC (%)	CC (%) from FTIR	Diamine (%)
<b>PDMS-0040</b>	65/35	77	72	100
<b>PDMS-2040</b>	59/41	64	65	100
<b>PDMS-4040</b>	60/40	54	NA	100
<b>PDMS-0025</b>	70/30	100	100	72
<b>PDMS-2025</b>	66/34	100	91	89
<b>PDMS-4025</b>	63/37	92	98	100

**Group contribution method:**

**Table D.2 - Calculation of solubility parameters using the Hoftyzer-Van Krevelen group contribution method of the PDMS containing TPHUs**

Component	MW (g/mol)	Density (g/cm <sup>3</sup> )	Molar Volume (cm <sup>3</sup> /mol)	Number of group	Group Contribution	F <sub>di</sub> (MJ/m <sup>3</sup> ) <sup>1/2</sup>	F <sub>pi</sub> <sup>2</sup> (MJ/m <sup>3</sup> )/mol <sup>2</sup>	E <sub>hi</sub> (J/mol)	δ <sub>d</sub> (MJ/m <sup>3</sup> ) <sup>1/2</sup>	δ <sub>p</sub> (MJ/m <sup>3</sup> ) <sup>1/2</sup>	δ <sub>h</sub> (MJ/m <sup>3</sup> ) <sup>1/2</sup>	δ (MJ/m <sup>3</sup> ) <sup>1/2</sup>
Priamine 1074				1	Cyclic aliphatic	1620	0	0				
+				2	-NH-	160	44100	3100				
				28	-CH <sub>2</sub> -	270	0	0				
Hard Segment DGC				1	-O-	100	160000	3000				
=				4	-CH <sub>2</sub> -	270	0	0				
				2	>CH-	80	0	0				
				2	-OH	210	250000	20000				
				2	-COO-	390	240100	7000				
<b>Priamine linkage</b>	<b>534</b>	<b>0.92</b>	<b>580</b>						<b>20.7</b>	<b>1.91</b>	<b>10.4</b>	<b>23.3</b>
PDMS Diamine				24	-CH <sub>3</sub>	420	0	0				
+				11	-O-	100	160000	3000				
				12	>Si<	20	0	0				
				6	-CH <sub>2</sub> -	270	0	0				
				2	-NH-	160	44100	3100				
Hard Segment DGC				1	-O-	100	160000	3000				
=				4	-CH <sub>2</sub> -	270	0	0				
				2	>CH-	80	0	0				
				2	-OH	210	250000	20000				
				2	-COO-	390	240100	7000				
<b>PDMS linkage</b>	<b>1000</b>	<b>0.98</b>	<b>1020</b>						<b>15.6</b>	<b>1.70</b>	<b>9.71</b>	<b>18.4</b>

To calculate the Hansen solubility parameters were calculated for the hydroxyurethane linkages by taking the diamines molecular weights and densities to find the molar volume (V). The following equations were applied to find the corresponding solubility parameters:

$$\delta_d = \frac{\sum F_{di}}{V} \quad \text{Eq. (D.4)}$$

$$\delta_p = \frac{\sqrt{\sum F_{pi}^2}}{V} \quad \text{Eq. (D.5)}$$

$$\delta_h = \sqrt{\frac{\sum E_{hi}}{V}} \quad \text{Eq. (D.6)}$$

$$\delta = \sqrt{\delta_d^2 + \delta_p^2 + \delta_h^2} \quad \text{Eq. (D.7)}$$

With  $\delta_d$  the contribution of dispersion forces,  $\delta_p$  the contribution of polar forces, and  $\delta_h$  the contribution of hydrogen bonding.

To determine the solubility of two polymers in one another, the following equations is applied:

$$\Delta\delta = \sqrt{(\delta_{d,P_1} - \delta_{d,P_2})^2 + (\delta_{p,P_1} - \delta_{p,P_2})^2 + (\delta_{h,P_1} - \delta_{h,P_2})^2} \quad \text{Eq. (D.8)}$$

For a value of  $\Delta\delta \leq 5 \left(\frac{MJ}{m^3}\right)^{1/2}$ , the polymers are considered to be miscible.

**TGA:**

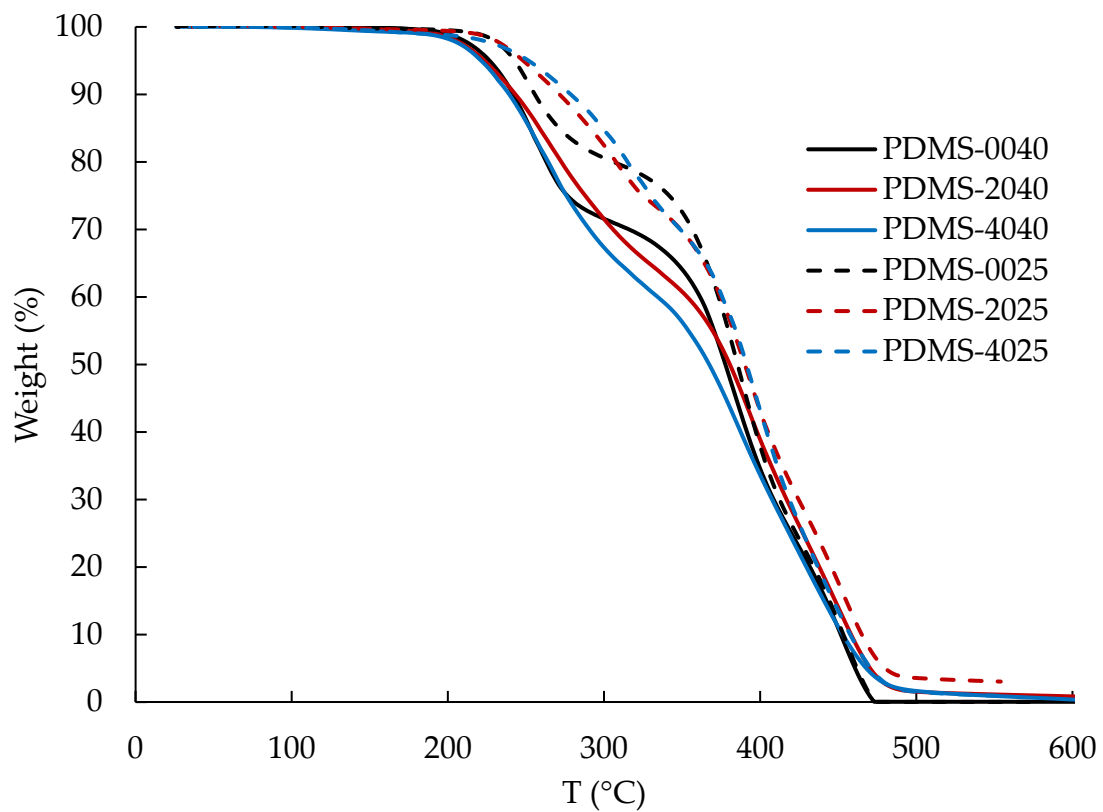


**Figure D.5 - TGA traces of the PDMS containing TPHUs**

**WAXS:**

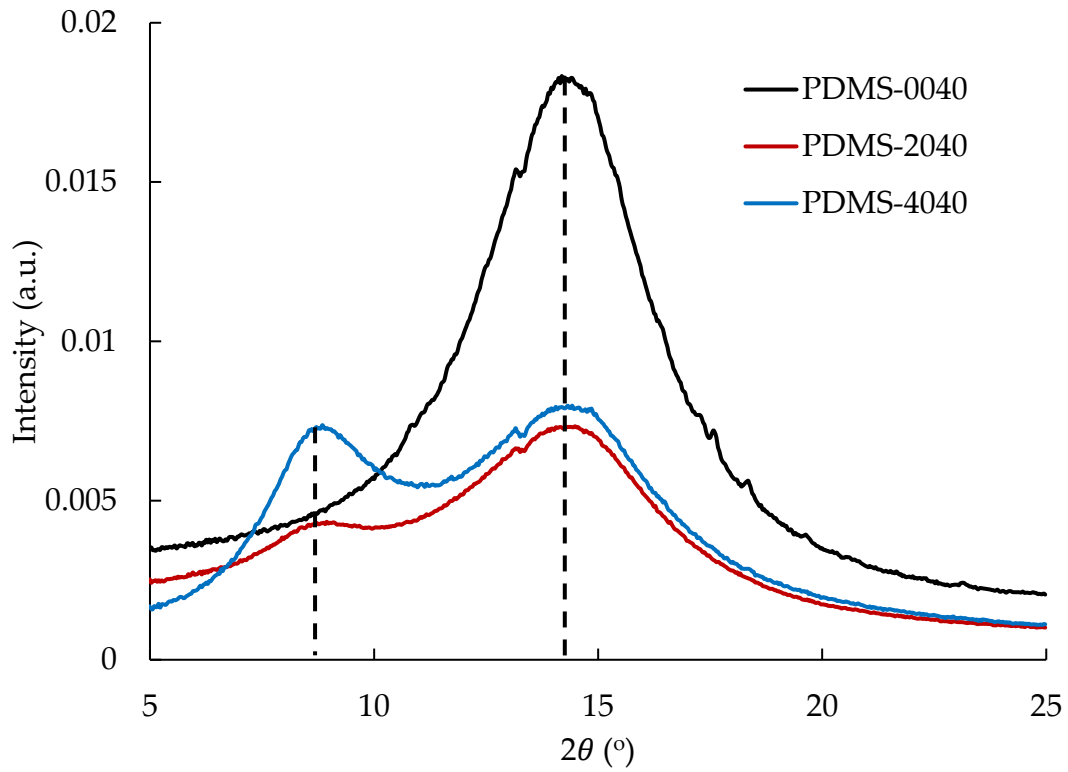


**Figure D.6 - WAXS spectra of PDMS-0040, PDMS-2040, and PDMS-4040. The distinct shoulder peak at  $2\theta$  of  $9^\circ$  proving the presence of a PDMS phase in the microstructure of the TPHUs. The intensity is given in logarithmic scale.**

**Rheology:**

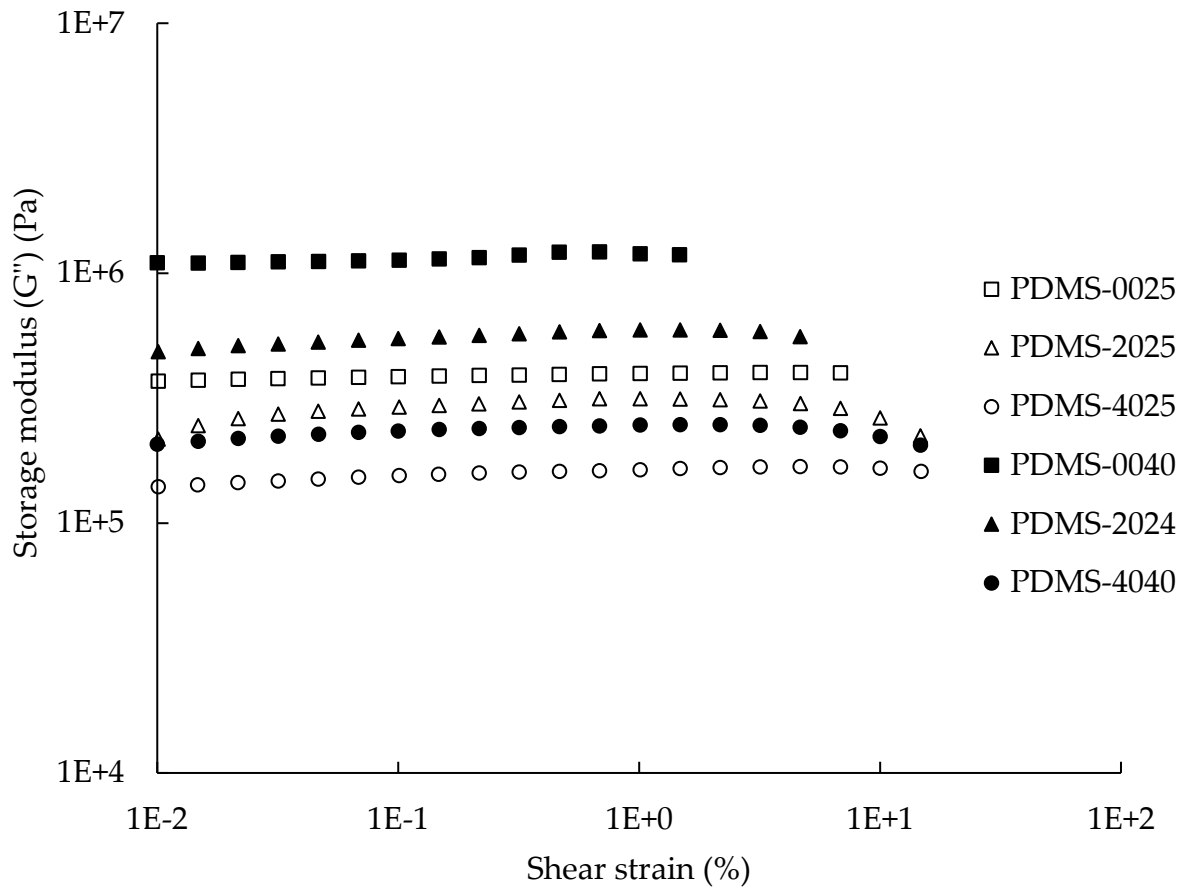


**Figure D.7 - Loss modulus of the PDMS containing TPHUs collected from amplitude sweeps conducted at 22 °C and a frequency of 10 Hz.**

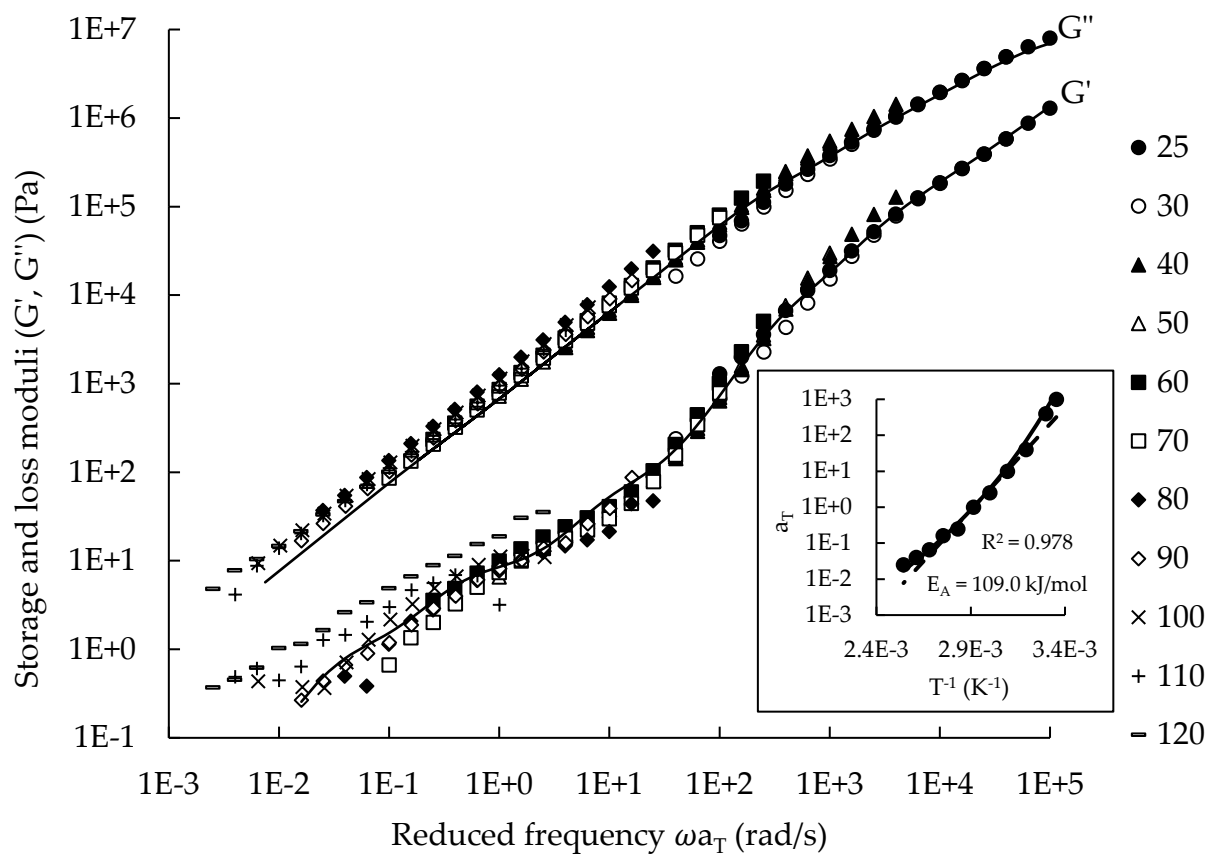


**Figure D.8 - Dynamic mechanical frequency sweep data for PDMS-0025 ( $G''$  curve is shifted by a factor of 5) at 0.5% shear strain. The solid line is a fit to the Generalized Maxwell model. The inset shows the shift factors used for time-temperature superposition. The solid and dashed lines in the inset are the WLF and Arrhenius law fit equations, respectively.**

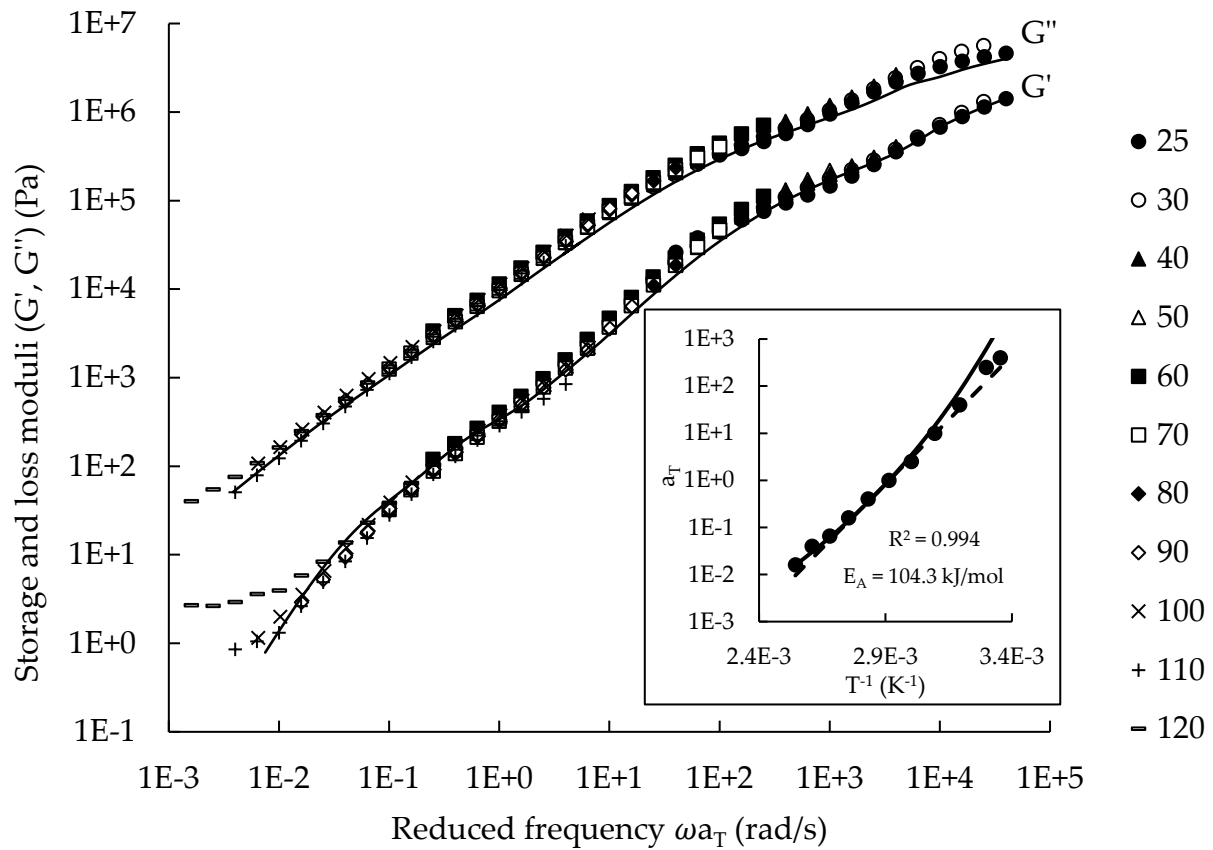


**Figure D.9 - Dynamic mechanical frequency sweep data for PDMS-2025 ( $G''$  curve is shifted by a factor of 5) at 0.5% shear strain. The solid line is a fit to the Generalized Maxwell model. The inset shows the shift factors used for time-temperature superposition. The solid and dashed lines in the inset are the WLF and Arrhenius law fit equations, respectively.**

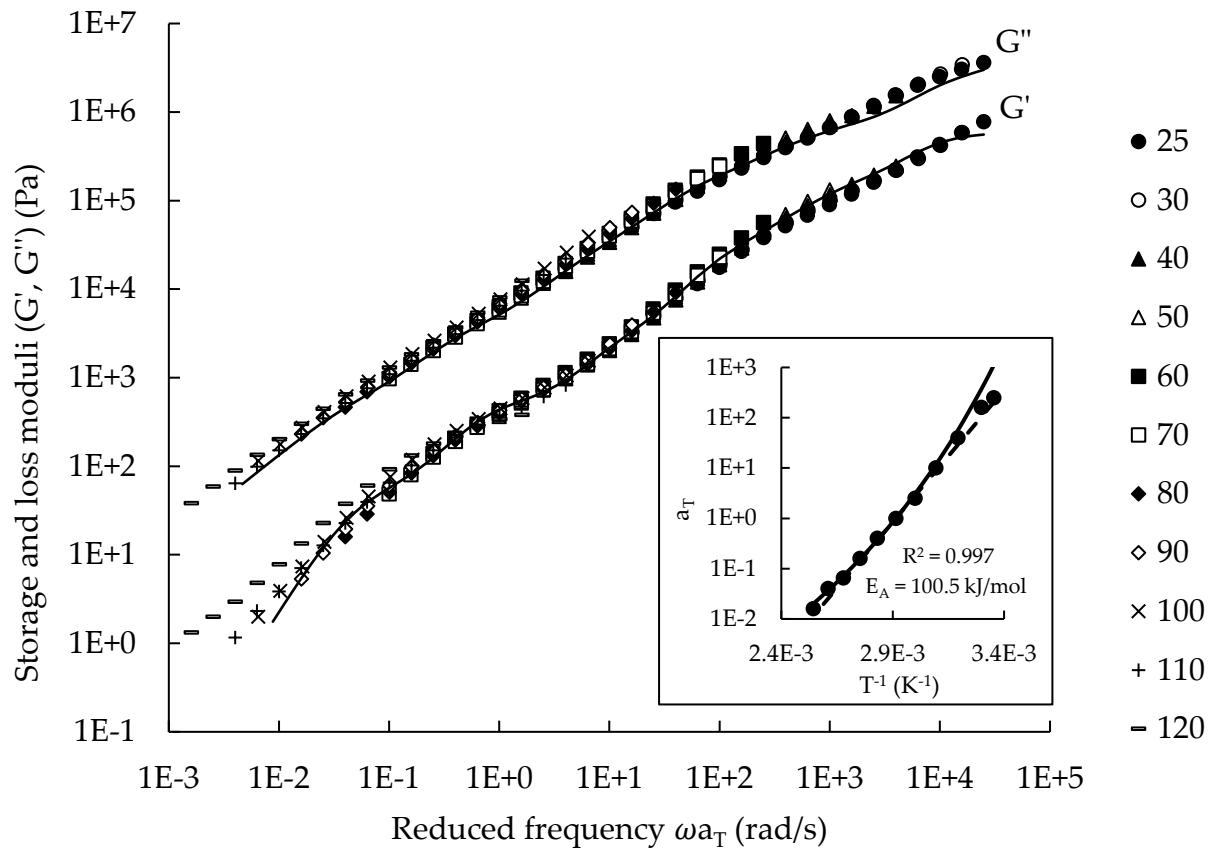


**Figure D.10 - Dynamic mechanical frequency sweep data for PDMS-4025 ( $G''$  curve is shifted by a factor of 5) at 0.5% shear strain. The solid line is a fit to the Generalized Maxwell model. The inset shows the shift factors used for time-temperature superposition. The solid and dashed lines in the inset are the WLF and Arrhenius law fit equations, respectively.**

- **Characterization of DAD containing TPHUs**

**FTIR:**

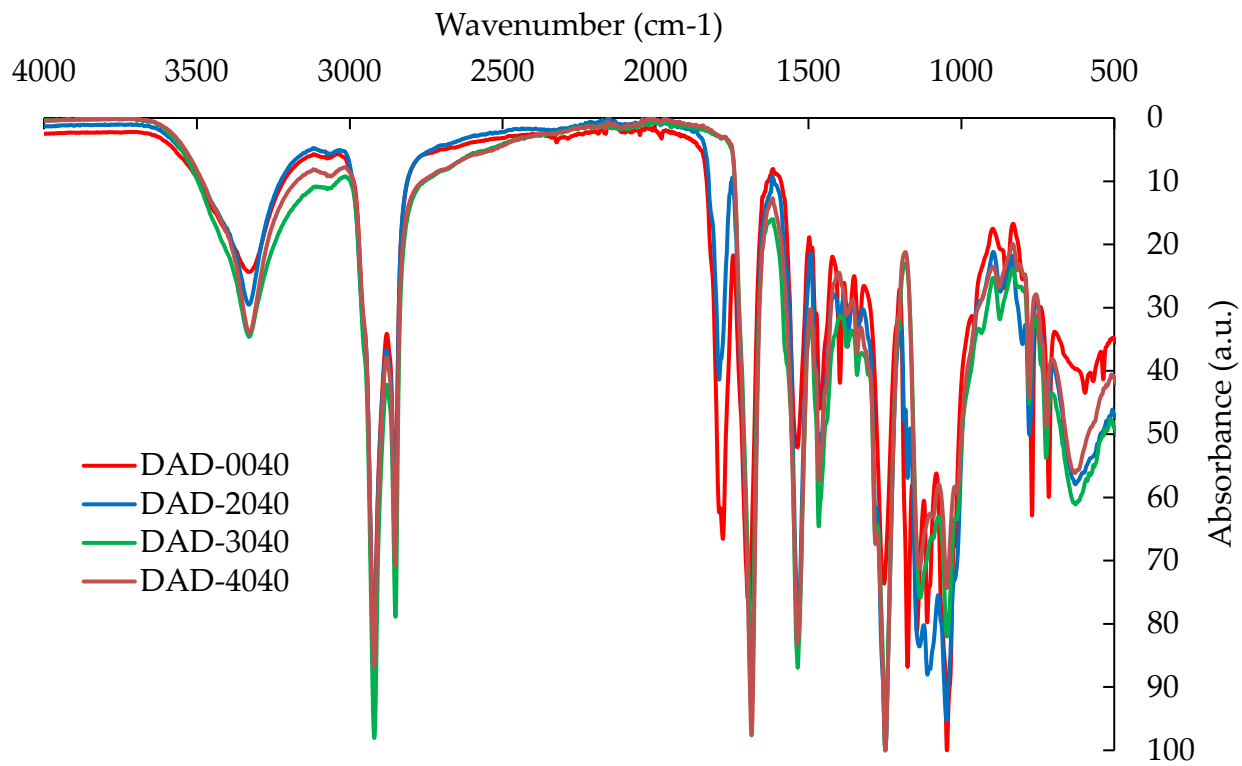


**Figure D.11 - FTIR spectra of the unpurified DAD containing TPHUs.**

## <sup>1</sup>H-NMR:

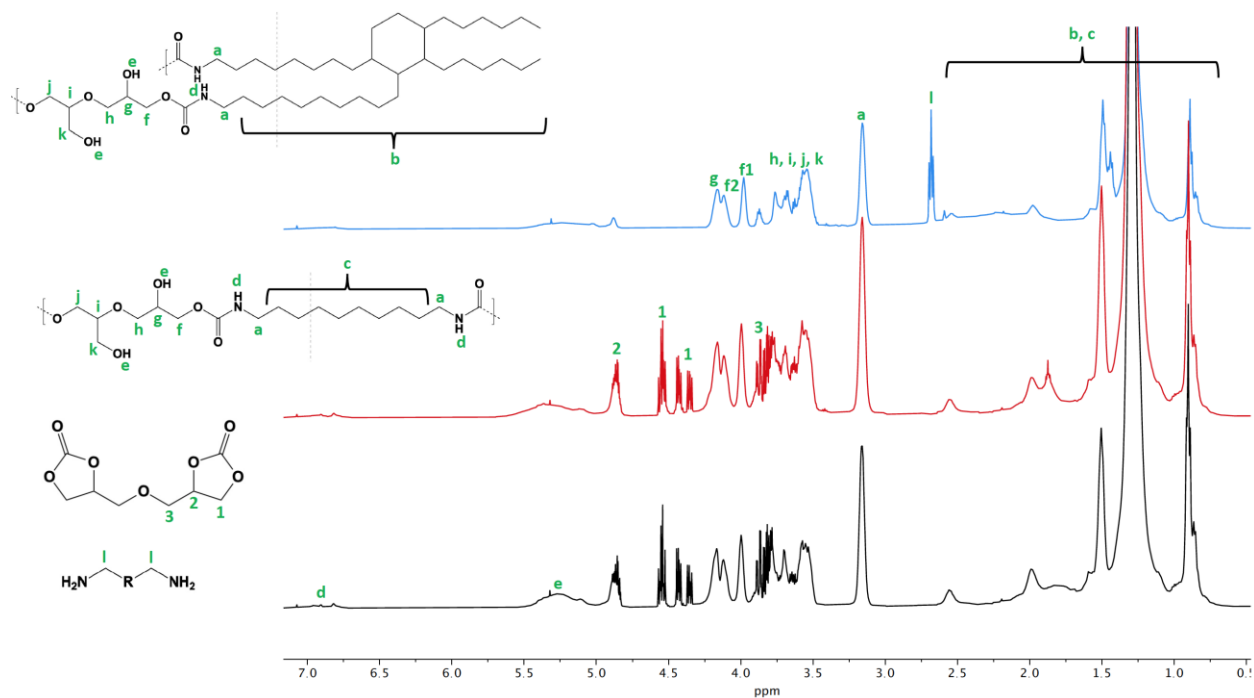


Figure D.12 - Stacked <sup>1</sup>H-NMR spectra of unpurified DAD-0040 (black), DAD-2040 (red), and DAD-4040 (blue) in CDCl<sub>3</sub> at 25 °C.

The method described in the previous <sup>1</sup>H-NMR section was also used to find the parameters summarized below.

Table D.3 - Parameters analyzed from the <sup>1</sup>H-NMR of DAD containing TPHUs

TPHU	Sec OH/prim OH	CC (%)	CC (%) from FTIR	Diamine (%)
DAD-0040	65/35	77	72	100
DAD-2040	68/32	75	NA	100
DAD-3040	56/44	100	100	80
DAD-4040	57/43	100	100	65

**TGA:**

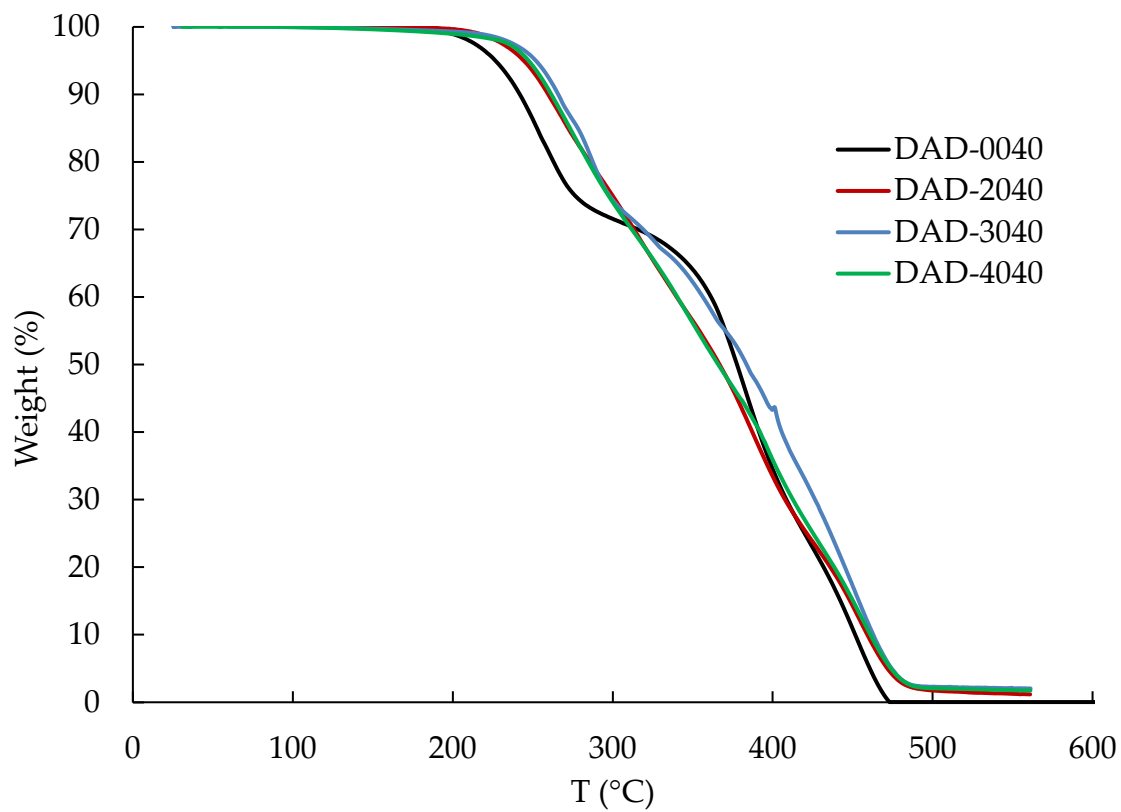


**Figure D.13 - TGA traces of the DAD containing TPHUs**

**WAXS:**

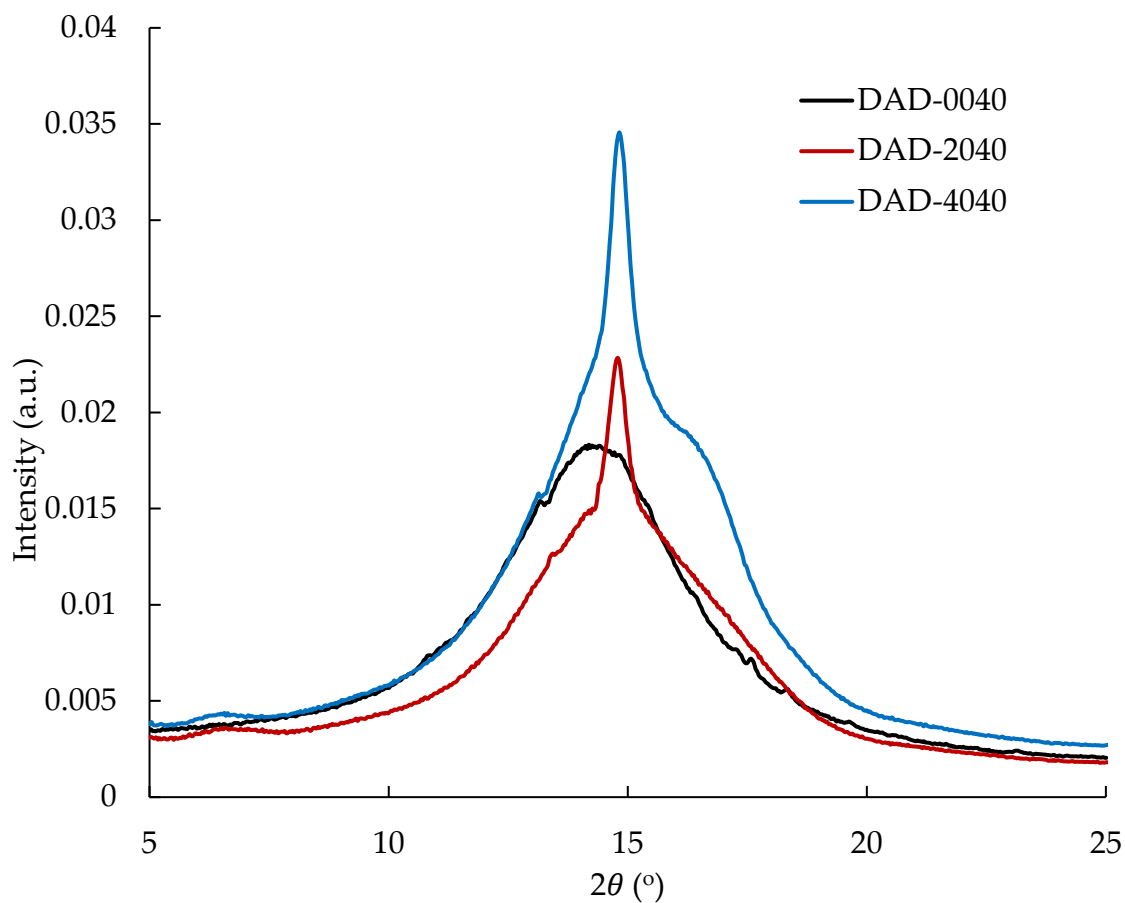


**Figure D.14 - WAXS spectra of DAD-0040, DAD-2040, and DAD-4040. The distinct sharp peak at  $2\theta$  of  $14.8^\circ$  proving the presence of crystallinity in the microstructure of the TPHUs having an amorphous phase constituted of Priamine 1074. The intensity is given in logarithmic scale.**

**Rheology:**

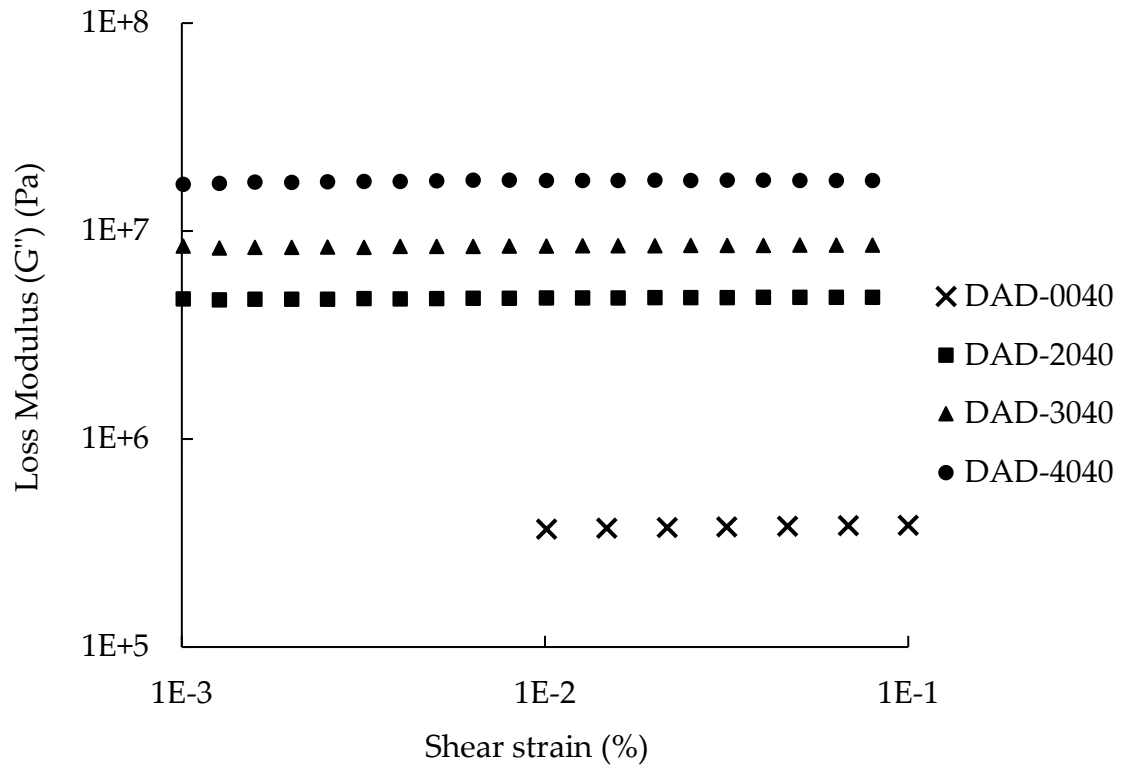


**Figure D.15 - Loss modulus of the DAD containing TPHUs collected from amplitude sweeps conducted at 22 °C and a frequency of 10 Hz.**

- Blends of PLA with bio-based TPHUs

**Rheology:**

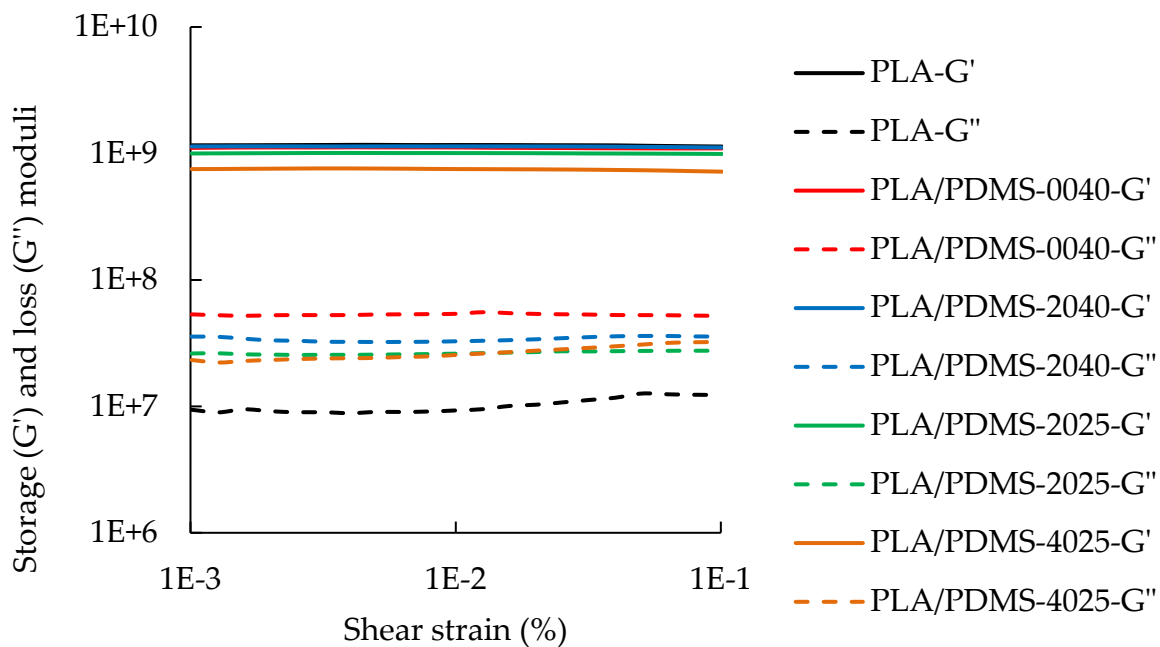


**Figure D.16 - Storage and loss moduli of the PLA/TPHUs blends (80/20 wt.%/wt.%) collected from amplitude sweeps conducted at 22 °C and a frequency of 1 Hz.**

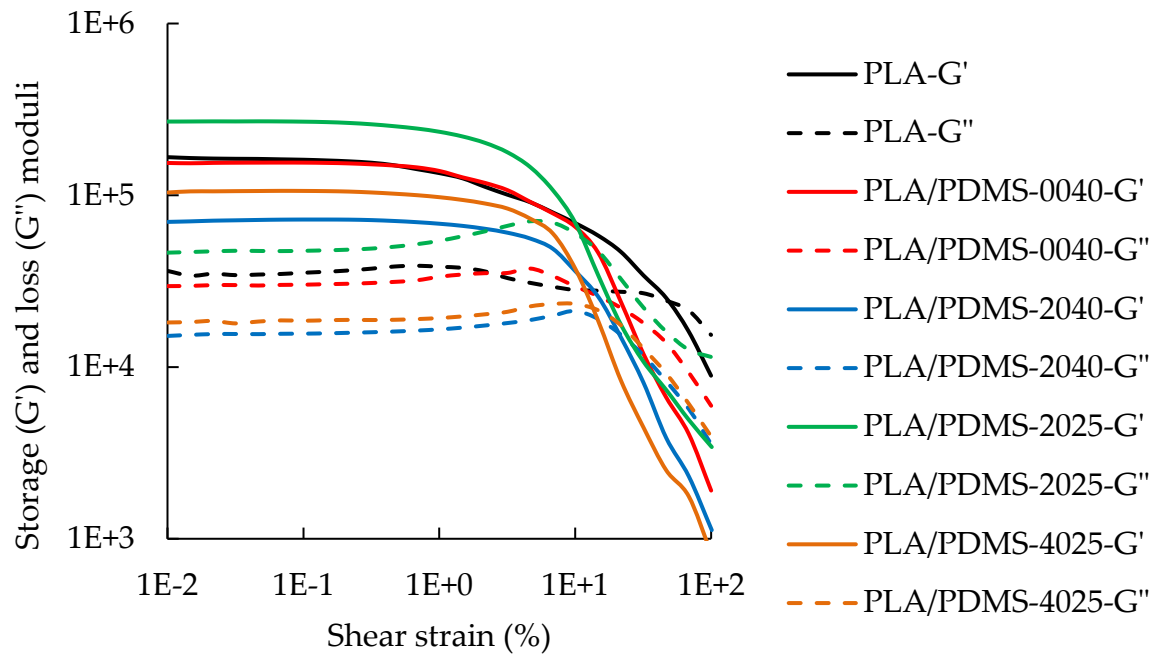


**Figure D.17 - Storage and loss moduli of the PLA/TPHUs blends (80/20 wt.%/wt.%) collected from amplitude sweeps conducted at 150 °C and a frequency of 1 Hz.**

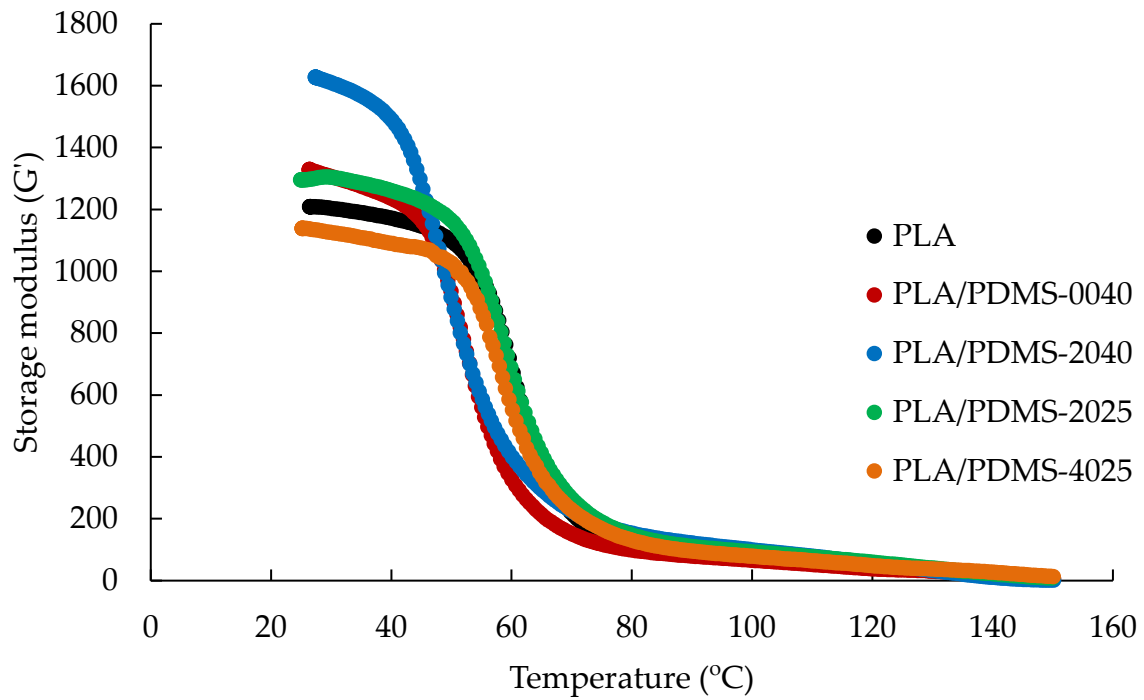


**Figure D.18 - Storage modulus data of the PLA/TPHUs blends (80/20 wt.%/wt.%) collected from dynamic mechanical thermal analysis conducted at frequency of 1 Hz and 0.01% shear strain.**

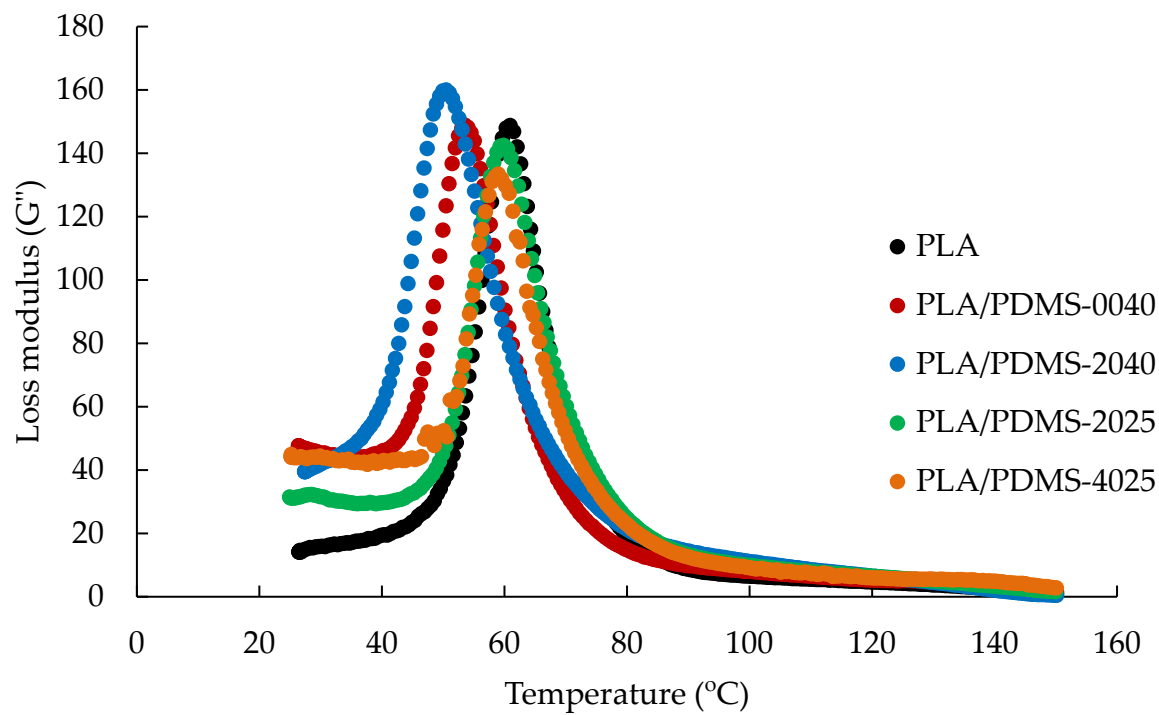


**Figure D.19 - Loss modulus data of the PLA/TPHUs blends (80/20 wt.%/wt.%) collected from dynamic mechanical thermal analysis conducted at frequency of 1 Hz and 0.01% shear strain.**

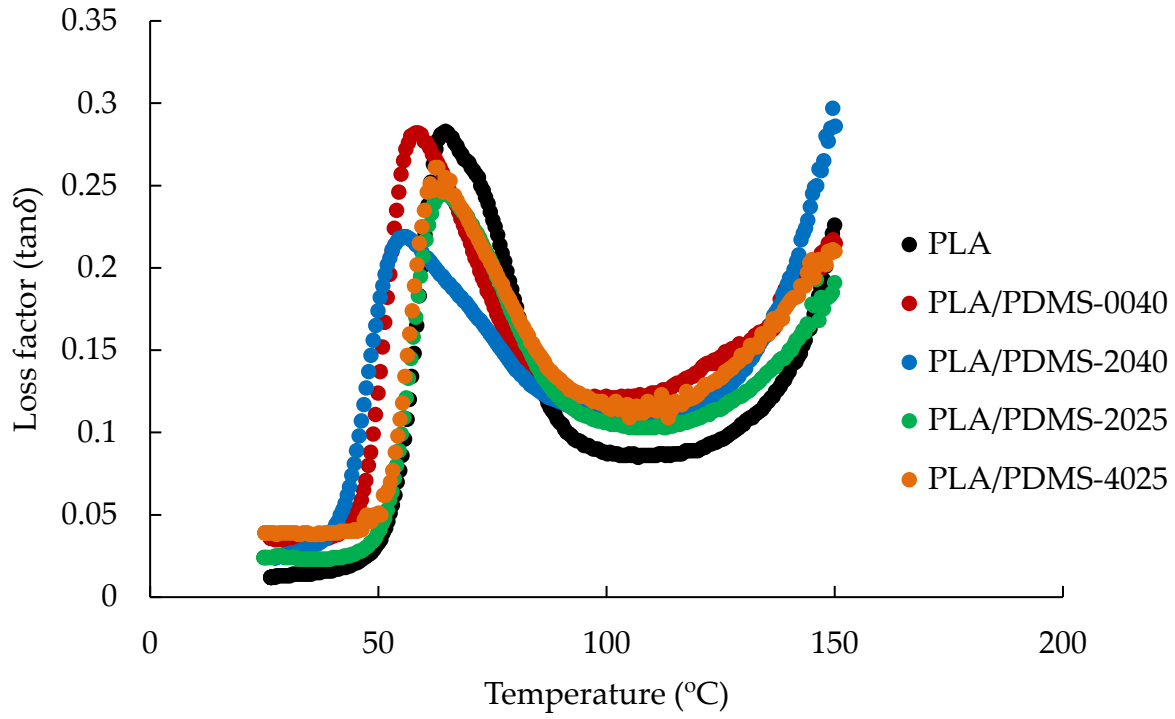


**Figure D.20 - Loss factor data of the PLA/TPHUs blends (80/20 wt.%/wt.%) collected from dynamic mechanical thermal analysis conducted at frequency of 1 Hz and 0.01% shear strain.**

**FTIR:**

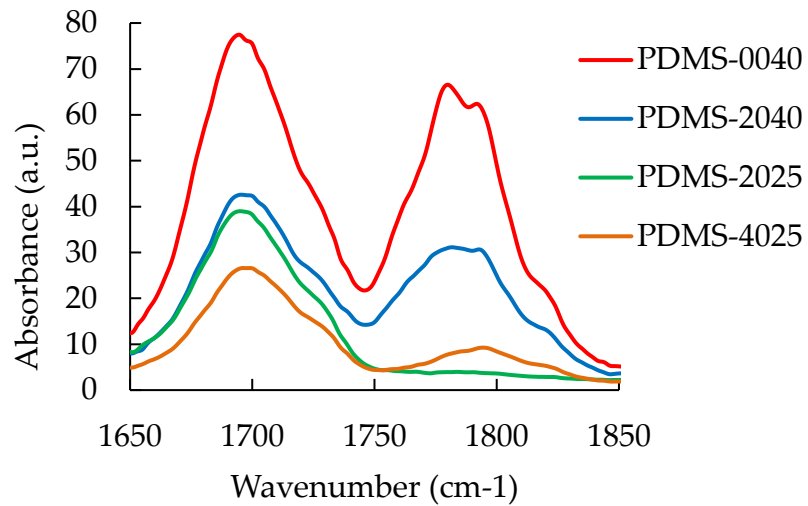


**Figure D.21 - Portion of the FTIR spectra of some TPHUs showing the distinct C=O stretch at 1790 cm<sup>-1</sup> proving the abundance of carbonate end-groups in the chains of PDMS-0040 and PDMS-2040.**

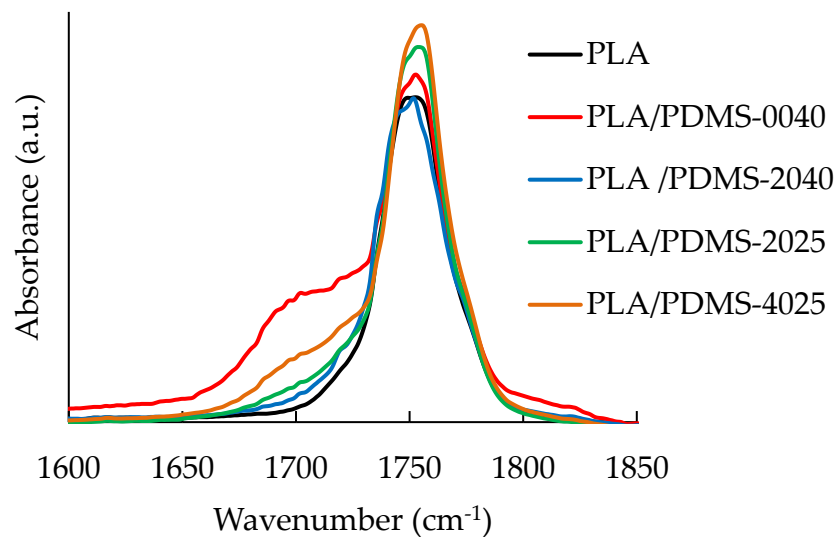


**Figure D.22 - Portion of the FTIR spectra of the blends (80/20 wt.%/wt.%) showing the broadening of the C=O stretch of PLA at 1760 cm<sup>-1</sup> proving the presence of hydrogen bonding.**

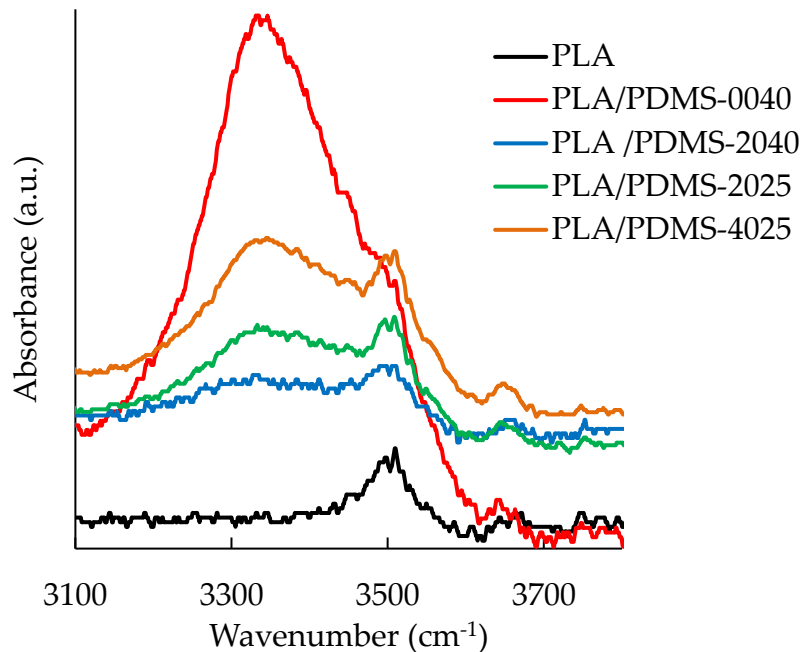


**Figure D.23 - Portion of the FTIR spectra of the blends (80/20 wt.%/wt.%) showing the appearance of the broad hydroxyl groups band proving the presence of hydrogen bonding (intermolecular interactions).**

**Group contribution method and calculation of relative energy difference (RED):**

**Table D.4 - Calculation of solubility parameters using the Hoftyzer-Van Krevelen group contribution method of PLA (those of the TPHUs found in the previous sections)**

Component	MW (g/mol)	Density (g/cm <sup>3</sup> )	Molar Volume (cm <sup>3</sup> /mol)	Number of group	Group Contribution	F <sub>di</sub> (MJ/m <sup>3</sup> ) <sup>1/2</sup> /mol	F <sub>pi</sub> <sup>2</sup> (MJ/m <sup>3</sup> ) / mol <sup>2</sup>	E <sub>hi</sub> (J/mol)	δ <sub>d</sub> (MJ/m <sup>3</sup> ) <sup>1/2</sup>	δ <sub>p</sub> (MJ/m <sup>3</sup> ) <sup>1/2</sup>	δ <sub>h</sub> (MJ/m <sup>3</sup> ) <sup>1/2</sup>	δ (MJ/m <sup>3</sup> ) <sup>1/2</sup>
Priamine linkage	534	0.92	580						20.7	1.91	10.4	23.3
PDMS linkage	1000	0.98	1020						15.6	1.70	9.71	18.4
PLA	72.06	1.24	58	1	>CH-	80	0	0	15.3	8.43	11.0	20.6
				1	-CH <sub>3</sub>	420	0	0				
				1	-COO-	390	240100	7000				

The solubility parameters of PLA were found using Eq. (D.4) to Eq. (D.7). The solubility parameters of the TPHUs were calculated from the solubility parameters of the Priamine and PDMS hydroxyurethane linkages in Table D.4 by using the linear mixing rule, as the Priamine and the PDMS phases were found to be miscible. Therefore, the solubility parameters to calculate the relative energy difference (RED) of the blends are as follows:

**Table D.5 - Solubility parameters used to calculate the RED. The solubility parameters of the TPHUs were calculated from the linear mixing rule based on the ones estimated for the Priamine and PDMS hydroxyurethane linkages.**

<b>Component</b>	$\delta_d$ (MJ/m <sup>3</sup> ) <sup>1/2</sup>	$\delta_p$ (MJ/m <sup>3</sup> ) <sup>1/2</sup>	$\delta_h$ (MJ/m <sup>3</sup> ) <sup>1/2</sup>	$\delta$ (MJ/m <sup>3</sup> ) <sup>1/2</sup>	<b>RED</b>
<b>PLA</b>	15.3	8.43	11.0	20.6	-
<b>PDMS-0040</b>	20.7	1.91	10.4	23.3	1.2
<b>PDMS-2040</b>	19.7	1.87	10.3	22.3	1.0
<b>PDMS-2025</b>	19.7	1.87	10.3	22.3	1.0
<b>PDMS-4025</b>	18.7	1.82	10.1	21.3	0.88

$$RED = \frac{\sqrt{4(\delta_{d,TPHU}-\delta_{d,PLA})^2 + (\delta_{p,TPHU}-\delta_{p,PLA})^2 + (\delta_{h,TPHU}-\delta_{h,PLA})^2}}{R_a} \quad \text{Eq. (D.9)}$$

Where  $R_a$  is the radius of PLA given as 10.7.<sup>1,2</sup>

- **References**

1. Abbott, S., Chemical Compatibility Of Poly(lactic acid): A Practical Framework Using Hansen Solubility Parameters. In *Poly(lactic acid): Synthesis, Structures, Properties, Processing, and Applications*, Auras, R., L.-T., L., Selke, S. E. M., Tsuji, H., Eds. John Wiley & Sons, Inc.: New Jersey, 2010; pp 83-95.
2. Stefanis, E.; Panayiotou, C. Prediction of Hansen Solubility Parameters with a New Group-Contribution Method. *Int. J. Thermophys.* **2008**, *29*, 568-585.

## Appendix E

### Supporting information for “Bio-based and hydrolytically degradable hydroxyurethane acrylates as photocurable thermosets”

- Synthesis of HU-CL<sub>5</sub>-A

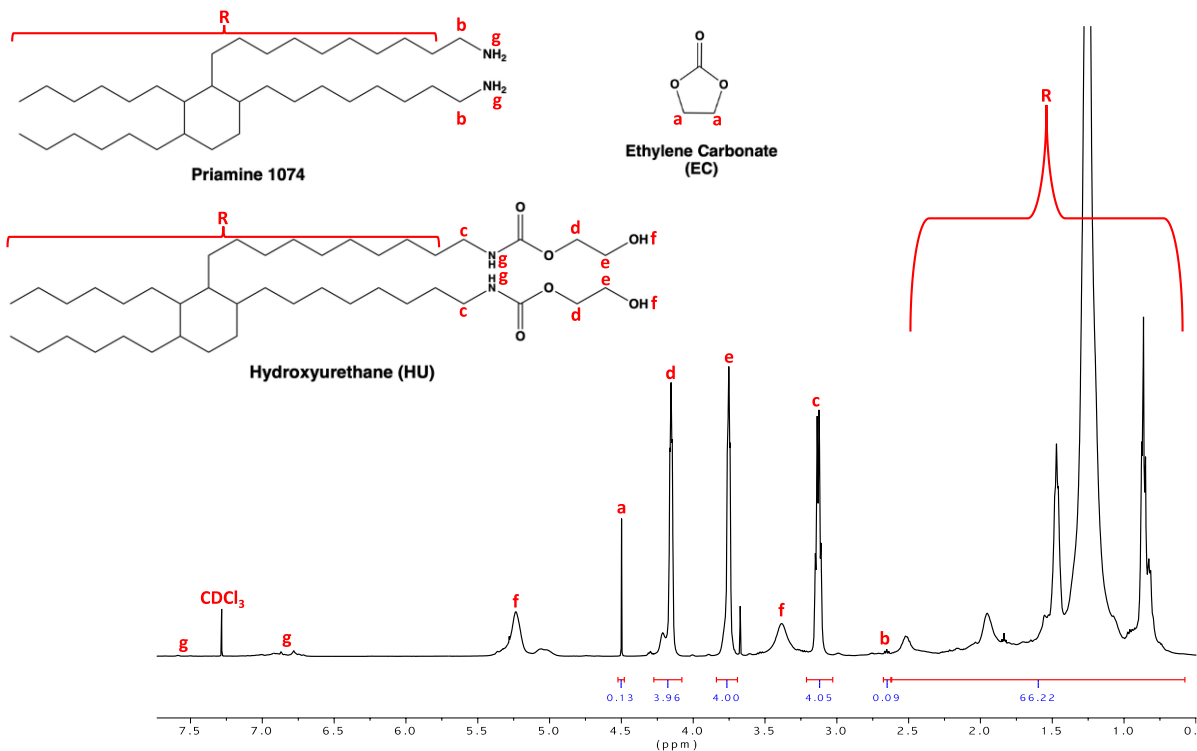


Figure E.1 - Labeled <sup>1</sup>H-NMR of the bio-based HU of this work in CDCl<sub>3</sub> at 25 °C.

(500 MHz, CDCl<sub>3</sub>, δ): 7.58 (g), 6.87/6.78 (g), 5.23 (f), 4.50 (a), 4.15 (d), 3.75 (e), 3.39 (f), 3.13 (c), 2.65 (b), 2.6-0.6 (R).

The conversions of EC and Priamine 1074 are calculated as follows:

$$\text{Conversion}_{EC}(\%) = \frac{\int d + \int e}{\int a + \int d + \int e} \times 100 \approx 98 \quad \text{Eq. (E.1)}$$

$$\text{Conversion}_{\text{Priamine } 1074}(\%) = \frac{\int c}{\int b + \int c} \times 100 \approx 98 \quad \text{Eq. (E.2)}$$

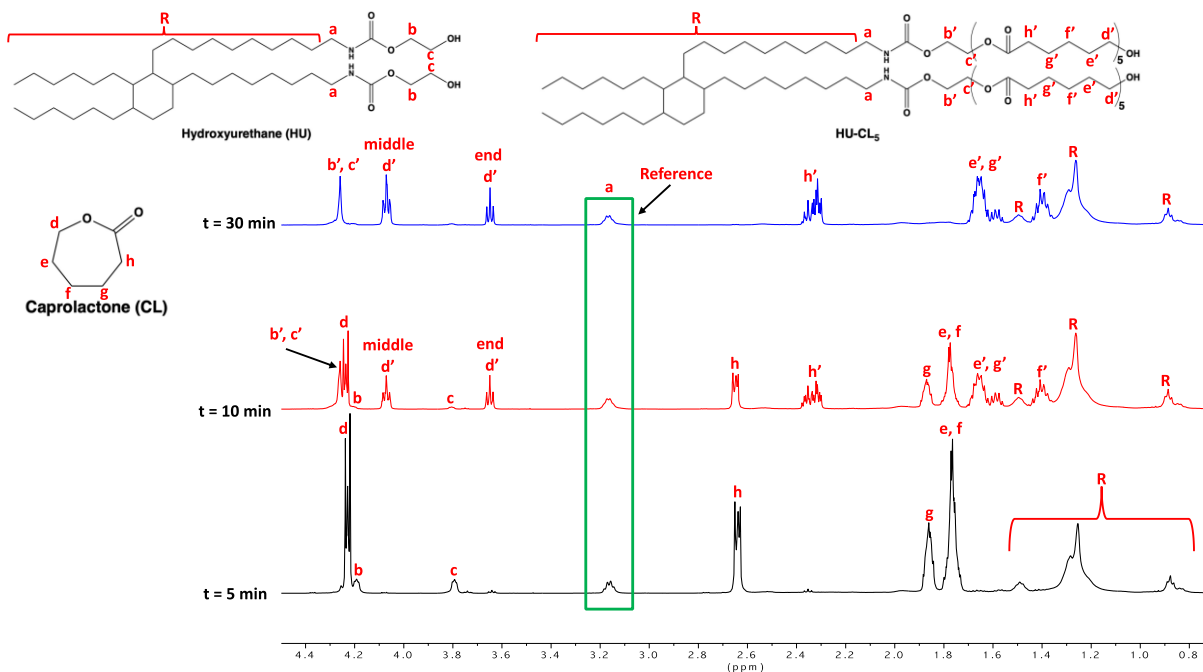


**Figure E.2 - Labeled  $^1\text{H}$ -NMR of the kinetic study of trial 4 (Table 7.1) at  $t = 5, 30,$  and  $90$  min of forming the bio-based and degradable  $\text{HU-CL}_5$  of this work in  $\text{CDCl}_3$  at  $25^\circ\text{C}$ .**

**(500 MHz,  $\text{CDCl}_3$ ,  $\delta$ ): 4.26 ( $b', c'$ ), 4.24 ( $d$ ), 4.19 ( $b$ ), 4.07 (middle  $d'$ ), 3.79 ( $c$ ), 3.65 (end  $d'$ ), 3.17 ( $a$ ), 2.64 ( $h$ ), 2.33 ( $h'$ ), 1.86 ( $g$ ), 1.77 ( $e, f$ ), 1.66/1.59 ( $e', g'$ ), 1.40 ( $f'$ ), 1.49/1.28/0.88 ( $R$ ).**

Signal  $a$  was used as the reference peak because it is unchanged throughout the reaction of  $\text{HU}$  to  $\text{HU-CL}_5$ . Its integration was set to 4, and the integrations of the other peaks were found with respect to it. The conversion of  $\text{CL}$  using Method 1 was found using the following equation:

$$\text{Conversion}_{\text{CL}_1} (\%) = \frac{f_{\text{end } d'} + f_{\text{middle } d'}}{f_{d} + f_{\text{end } d'} + f_{\text{middle } d'}} \times 100 \quad \text{Eq. (E.3)}$$

The value of the integral of  $d$  was found by integrating the whole area of signals  $b, d, b',$  and  $c'$ . Then, the summation of the integrals of  $b$  and  $b'$  is 4 because the integral of  $b$  is equal to that of  $a$  in the  $\text{HU}$ . The integral of  $c'$  was found by subtracting that of  $c$  from 4 since the initial integral of  $c$  is 4, as shown in Figure E.1.

The conversion of CL using Method 2 was found using the following equation:

$$\text{Conversion}_{\text{CL}_2}(\%) = \frac{f_{h'}}{f_h + f_{h'}} \times 100 \quad \text{Eq. (E.4)}$$

The conversion of HU was found as follows:

$$\text{Conversion}_{\text{HU}}(\%) = \frac{f_a - f_c}{f_a} \times 100 \quad \text{Eq. (E.5)}$$

The integral of a was used because the initial integral of c was 4.

Side reactions were observed starting  $t = 60$  min, the integral of the end d' proton at 3.65 ppm decreased from its maximum value (close to 4), and the difference appeared at 4.27 ppm. Hence, the integrals were adjusted accordingly to find the CL conversion using Method 1, and the values matched those of Method 2. The conversions were found using unpurified aliquots and final products. The degree of polymerization ( $\text{DP}_n$ ) or number of CL units per OH is found as follows:

$$\text{DP}_n = \frac{\# \text{CL}}{\text{OH}} = \frac{f_{\text{end d'}} + f_{\text{middle d'}}}{f_a} = \frac{f_{h'}}{f_a} \quad \text{Eq. (E.6)}$$

This parameter can be found before or after purifying the final product.

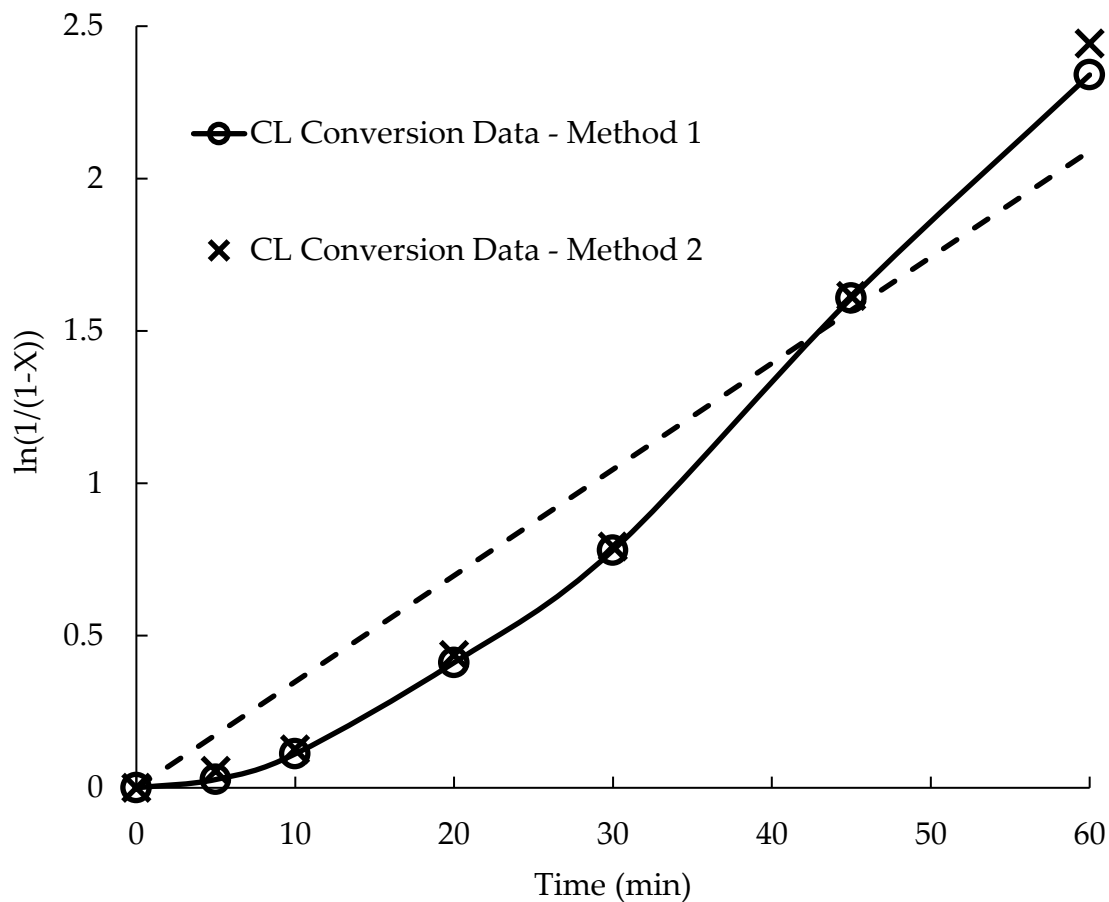


**Figure E.3 - Plot of  $\ln(1/(1-X))$  using the CL conversion data of trial 4 (Table 7.1) with the linear fitting of Eq. (E.7) and the smooth fitting of the data (dashed and solid, respectively) added.**

$$\ln\left(\frac{1}{1-X}\right) = k_p[P^*]t \quad \text{Eq. (E.7)}$$

where  $X$  is the monomer conversion,  $k_p$  is the rate of propagation,  $[P^*]$  is the concentration of active species, and  $t$  is the time of reaction at a given  $X$ . Knowing that  $k_p$  is constant, then if  $[P^*]$  is constant,  $\ln\left(\frac{1}{1-X}\right)$  linearly depends on  $t$ , which is not the case of the ROP studied herein.

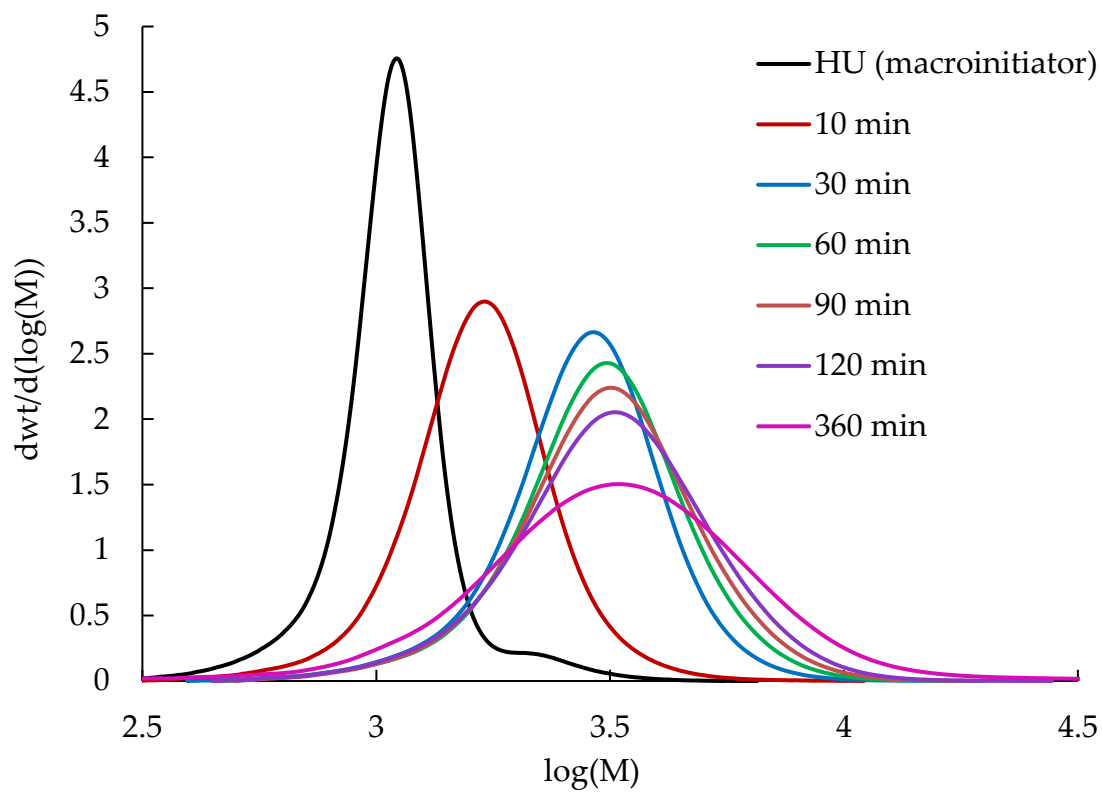


**Figure E.4 - SEC traces of aliquots withdrawn during the kinetic study of trial 4 (Table 7.1) at specific time intervals**

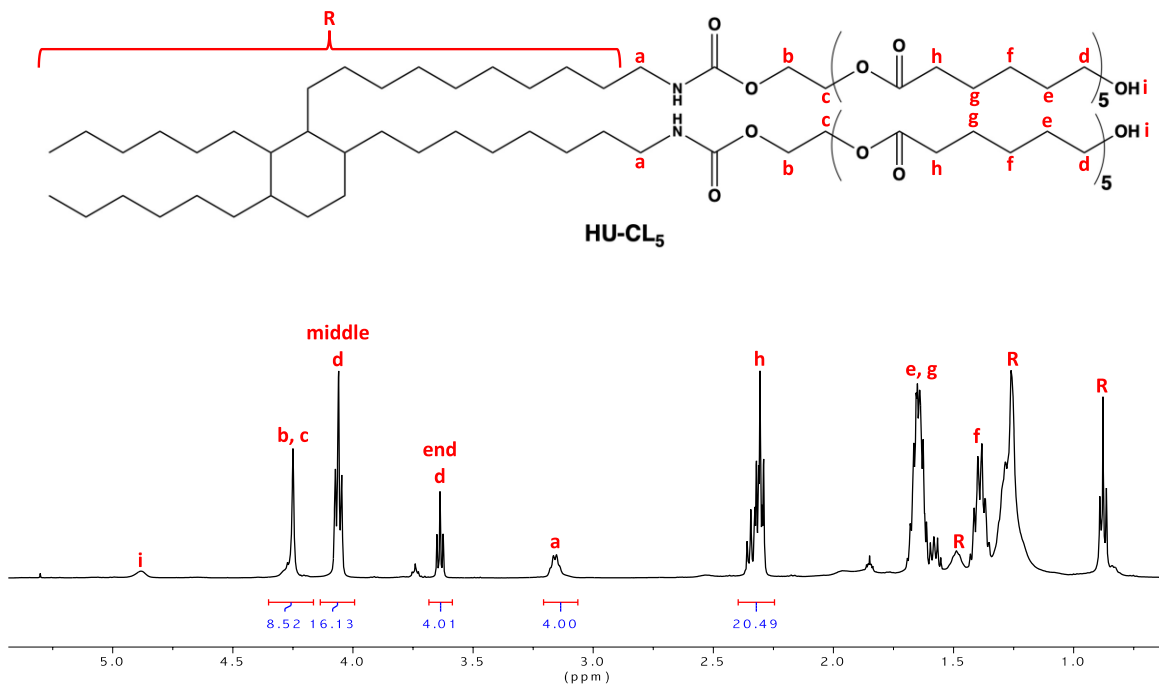


**Figure E.5 - Labelled <sup>1</sup>H-NMR of the bio-based and degradable HU-CL<sub>5</sub> of this work in CDCl<sub>3</sub> at 25 °C. (500 MHz, CDCl<sub>3</sub>, δ): 4.88 (i), 4.25 (b, c), 4.06 (middle d), 3.64 (end d), 3.16 (a), 2.31 (h), 1.65/1.58 (e, g), 1.39 (f), 1.49/1.26/0.87 (R).**

- Photocuring of Thermosets and Degradation Study

Table E.1 - Swelling experiment data of the photocurable thermoset in different solvents

Samples	THF-1	THF-2	THF-3	H <sub>2</sub> O-1	H <sub>2</sub> O-2	H <sub>2</sub> O-3
Mass initial (mg)	21.6	19.3	13.7	16.3	15.0	18.0
Mass 72 h (mg)	39.0	34.4	24.7	24.1	22.0	25.7
SI (%)	80.6	78.2	80.3	47.9	46.7	42.8
Dried mass (mg)	19.1	16.9	11.8	15.7	13.9	17.1
GC (%)	88.4	87.6	86.1	96.3	92.7	95.0

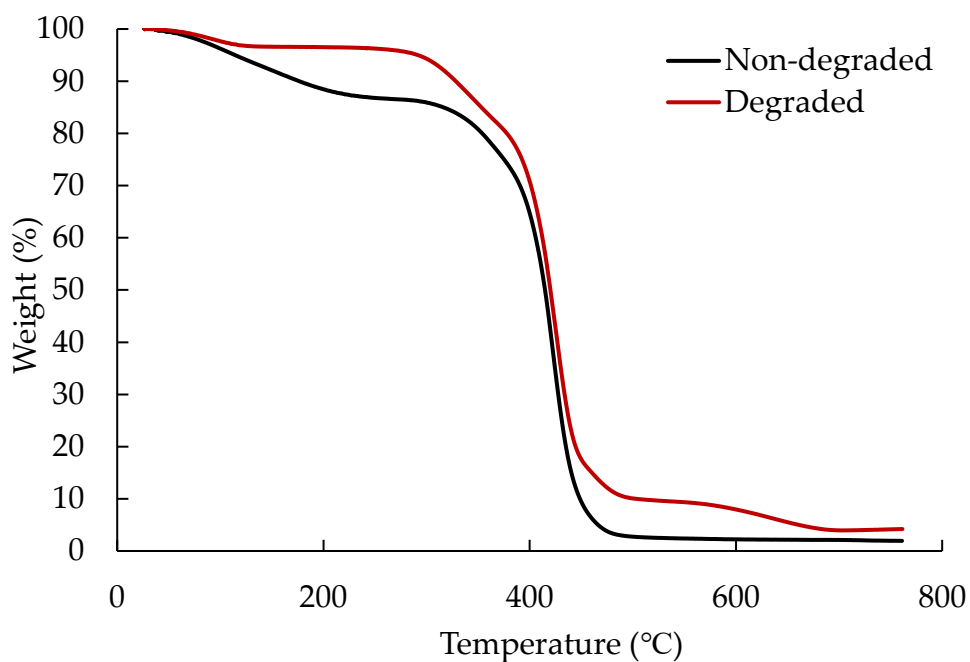
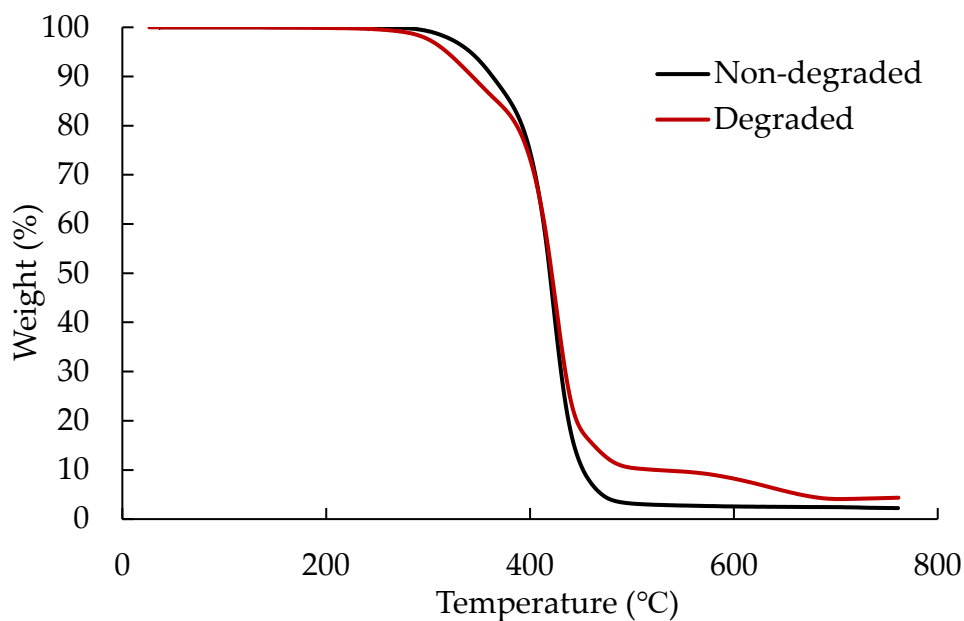
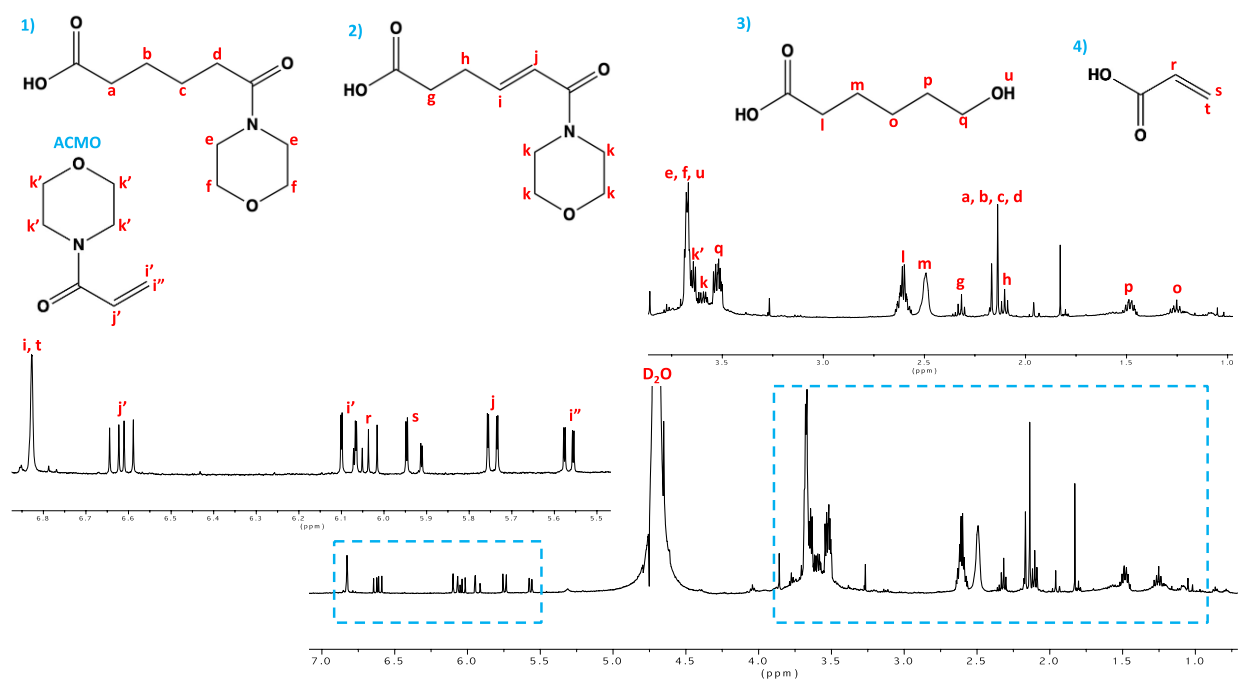


Figure E.6 - Unadjusted TGA traces of photocurable thermosets before and after degradation



**Figure E.7 - Adjusted TGA traces of photocurable thermosets before and after degradation**



**Figure E.8 - Water-soluble degradation products caused by the accelerated hydrolysis of the degradable photocurable thermosets (details about the peaks given in Table E.2).**

**Table E.2 - Information of the peak assignments of the water-soluble degradation products complementing Figure E.8.**

Compound	Peak	$\delta$ (ppm)	Integral
1)	a, b, c, d	2.14/2.17	10.7
	e, f	3.67	10.7
2)	g	2.32	2.96
	h	2.10	4.13
	i	6.83	1.56
	j	5.73/5.76	1.56
	k	3.56/3.62	12.58
	ACMO	i'	6.07/6.10
	i''	5.56/5.58	1.35
	j'	6.59/6.64	1.44
	k'	3.63/3.65	12.37
3)	l	2.61	19.06
	m	2.49	18.34
	o	1.24	15.40
	p	1.48	16.62
	q	3.52	22.28
	u	3.67	24.60
4)	r	6.02/6.07	0.87
	s	5.91/5.95	1.00
	t	6.83	1.00

From Table E.2, the number of CL units cleaved with respect to ACMO can be found from the equation below:

$$\frac{\#CL_{cleaved}}{ACMO} = \frac{[(\int l + \int m + \int o + \int p + \int q)/5]/2}{(\int e + \int f + \int k)/8} = \frac{9.17}{2.91} \approx 3 \quad \text{Eq. (E.8)}$$

The percentage of cleaved end-chain CL units is calculated from:

$$\%CL_{cleaved\ end-chain} = \frac{f_s}{[(f_l + f_m + f_o + f_p + f_q)/5]/2} \times 100 = \frac{100}{9.17} \approx 11 \quad \text{Eq. (E.9)}$$

The percentage of cleaved end-chain ACMO units is calculated from:

$$\%ACMO_{cleaved\ end-chain} = \frac{f_k}{f_e + f_f + f_k} \times 100 = \frac{1258}{23.28} \approx 54 \quad \text{Eq. (E.10)}$$